INFORMATION TO USERS

This manuscript has been reproduced from the microfilm master. UMI films the text directly from the original or copy submitted. Thus, some thesis and dissertation copies are in typewriter face, while others may be from any type of computer printer.

The quality of this reproduction is dependent upon the quality of the copy submitted. Broken or indistinct print, colored or poor quality illustrations and photographs, print bleedthrough, substandard margins, and improper alignment can adversely affect reproduction.

In the unlikely event that the author did not send UMI a complete manuscript and there are missing pages, these will be noted. Also, if unauthorized copyright material had to be removed, a note will indicate the deletion.

Oversize materials (e.g., maps, drawings, charts) are reproduced by sectioning the original, beginning at the upper left-hand corner and continuing from left to right in equal sections with small overlaps. Each original is also photographed in one exposure and is included in reduced form at the back of the book.

Photographs included in the original manuscript have been reproduced xerographically in this copy. Higher quality 6" x 9" black and white photographic prints are available for any photographs or illustrations appearing in this copy for an additional charge. Contact UMI directly to order.

UMI

A Bell & Howell Information Company
300 North Zeeb Road, Ann Arbor MI 48106-1346 USA
313/761-4700 800/521-0600

Gasification of Rice Husk
in a Fluidized Bed Reactor

by

Kelleh Gbawuru Mansaray

A Thesis Submitted to the
Faculty of Engineering
in Partial Fulfillment of the Requirements
for the Degree of

DOCTOR OF PHILOSOPHY

Major Subject: Biological Engineering

APPROVED:

[redacted]
Dr. A. E. Ghaly, Supervisor

[redacted]
Dr. K. C. Watts

[redacted]
Dr. A. M. Al-Taweel

[redacted]
Dr. B. Hamdullahpur

[redacted]
Dr. V. I. Ugursal

[redacted]
Dr. J. Chaouki, Ecole Polytechnique, External Examiner

DALHOUSIE UNIVERSITY - DALTECH

Halifax, Nova Scotia 1998

DALTECH LIBRARY

"AUTHORITY TO DISTRIBUTE MANUSCRIPT"

TITLE:

GASIFICATION OF RICE HUSK IN A FLUIDIZED BED GASIFIER

The above library may make available or authorize another library to make available individual photo/microfilm copies of this thesis without restrictions.

Full Name of Author: Kelleh Gbawuru Mansaray

Signature of Author: [redacted]

Date: May 11, 1998

DEDICATION

To My Late Father

Paramount Chief Gbawuru Mansaray II

TABLE OF CONTENTS

LIST OF TABLES

LIST OF FIGURES

LIST OF ABBREVIATIONS, SYMBOLS AND DERIVATIVES

Abbreviations

BH Static Bed height.

CC Carbon Conversion.

CSTR Continuous stirred tank reactor.

CV Coefficient of variation.

DTG Derivative thermogravimetry.

DW Dry weight of rice husk sample.

ER Equivalence ratio.

ESEM Environmental scanning electron microscope.

FB Fluidized bed.

FRZ First reaction zone.

FV Fluidization velocity.

GC Gas chromatograph.

HHV Higher heating value.

HHV_{EB} Higher heating value from Boie's equation.

HHV_{rh} Higher heating value of rice husks.

LG Long grain.

LHV Lower heating value.

MC Moisture content of the fuel.

RH Rice husk.

SCXI Signal conditioning extentions for instrumentation.

SRZ Second reaction zone.

STD Standard deviation.

TDH Transport disengaging height.

TG Thermogravimetry.

TGA Thermogravimetric analysis.

WW Wet weight of rice husk sample.

English Symbols

A Pre-exponential or frequency factor (1/min.).

A_C Percent ash by weight on a dry basis (%).

a_{ik} Number of atoms of the k_{th} element present in each molecule of a chemical species i (-).

A_k Total number of atomic weights of the k_{th} element present in the system, as determined by its initial constituents (-).

A_o Cross-sectional area of the orifice plate (m^2).

Ar Archimedes number (-).

A_t Bed cross-sectional area (m^2).

C Mass fraction of carbon (-).

C_{ic} Predicted concentration of gas component i (%).

C_{ie} Measured concentration of gas component i (%).

C_s Segregation coefficient (-).

d_b Bubble diameter (m).

d_{bm} Maximum attainable bubble diameter (m).

d_{bo} Initial bubble diameter (m).

d_{eq} Volume-equivalent bubble diameter (m).

d_{or} Jet orifice diameter (m).

d_p Particle diameter (m).

d_t Average bed diameter (m).

E Activation energy (kJ/mol).

E_{ei} Elutriation rate of particles of size d_{pi} (kg/m^2s).

E_o Particle entrainment flux at bottom of freeboard (kg/m^2s).

f_1 Fitting Parameter (-).

f_2 Fitting Parameter (-).

f_o Char reactivity (-).

f_{wg} Water-gas shift reactivity (-).

g Gravitational acceleration (m/s^2).

G_{air} Air flow rate (kg/min.).

G_{ch} Char flow rate (kg/min.).

G_g Gas flow rate (kg/min.).

$G^o_{f,i}$ Free energy of formation of compound i at temperature T (kJ/kg).

G_{rh} Rice husk flow rate (kg/min.).

h Vertical distance from the bottom of the bed (m).

H Mass fraction of hydrogen (-).

K Equilibrium temperature (K).

K'_1 Equilibrium constant (-).

k = 1 - 3 represents the three equations for carbon, hydrogen and oxygen (-).

K_{bc} Mass transfer coefficient between bubble and cloud phases (m/s).

K_{be} Mass transfer coefficient between bubble and emulsion phases (m/s).

K_{ec} Mass transfer coefficient between emulsion and cloud phases (m/s).

$K_{i\infty}$ Elutriation rate constant for particles of size d_{pi} (kg/m^2s).

K_o Orifice coefficient (-).

L Number of moles of oxygen in 100 kg of fuel (-).

L_j Jet penetration depth from the nozzle (m).

M Number of moles of hydrogen in 100 kg of fuel (-).

M_i Molecular weight of a specie (kJ/kmol.K).

M_I Mixing index (-).

N Number of moles of carbon in 100 kg of fuel (-).

n Order of reaction (-).

n_i Number of moles of i_{th} species in the system (-).

N_i Total number of moles of the final gas (-).

N_{io} Total number of moles of the initial gas (-).

n_{or} Total number of orifices in distributor (-).

n_T	Total number of moles of the species (-).
O	Mass fraction of oxygen (-).
P	Pressure of the system (atm).
P_A	Adjustable parameter (-).
q	Volumetric gas flow rate (m^3/min.).
Q	Enthalpy flow of a stream (kJ/kmol).
Q_b	Volumetric bubble flow rate (m^3/s).
Q_{loss}	Heat loss through the gasifier walls (MJ/kg).
R	Universal gas constant (kJ/mol.K).
R_b	Bubble radius (m).
Re	Reynolds number (-).
R_j	Number of moles of the reacting gas (-).
S	Mass fraction of sulphur (-).
T	Absolute temperature (K).
t	Time (min.).
U_A	Average velocity of a bubble in a freely bubbling bed (m/s).
U_b	Rise velocity of an isolated bubble (m/s).
U_e	Gas velocity in the emulsion phase (m/s).
U_F	Fluidization velocity of particles having larger minimum fluidization velocity (m/s).
U_{mf}	Minimum fluidization velocity (m/s).
U_o	Superficial gas velocity (m/s).
U_{or}	Jet nozzle velocity (m/s).
U_P	Fluidization velocity of particles having smaller minimum fluidization velocity (m/s).
V_B	Bubble volume (m^3).
w	Weight of sample at time t (min.).
w_f	Weight of residue at the end of a reaction (kg).
w_i	Weight fraction of particles of size d_{pi} in the bed (-).
w_o	Initial weight of sample (kg).

x Concentration of the material under scrutiny at some level in the bed (-).

X Weight of sample undergoing reaction (kg).

x_B Concentration of the material in the bottom half of the bed (-).

$\bar{x}$ Average concentration (-).

X_F Weight fraction having larger minimum fluidization velocity (-).

x_i Amount of carbon in the rice husk ($i = C_{rh}$), gas ($i = C_g$) and char ($i = C_{ch}$).

X_i Volume percentage of gas species i in the dry gas (%).

x_T Concentration of the material in the top half of the bed (-).

y_i Number of moles of species produced (-).

Greek Symbols

α Wake fraction associated with the bubbles (-).

δ Bubble phase fraction of the bed (-).

$\Delta h_{ch_{chem}}$ Chemical energy out with the char (MJ/kg).

$\Delta h_{g_{chem}}$ Chemical energy out with the gas (MJ/kg).

$\Delta h_{ch_{sen}}$ Sensible heat out with the char (MJ/kg).

$\Delta h_{g_{sen}}$ Sensible heat out with the gas (MJ/kg).

$\Delta G_{f_i}^{o}$ Standard Gibbs free energy of formation of compound i from its constituent elements at temperature T (kJ/kmole).

ΔP Pressure drop across the orifice plate (Pa).

ε Void fraction of the bed at minimum fluidization velocity (-).

ε_{mf} Bed voidage at minimum fluidization (-).

λ Latent heat of vaporization of water (KJ/kg).

λ_k Langrangian multiplier corresponding to the k_{th} atomic balance constraints (-).

μ Gas viscosity (Ns/m^2).

ρ Average bed density (kg/m^3).

ρ_b Bulk density of the rice husk sample (kg/m^3).

ρ_F Density of particles having larger minimum fluidization velocity (kg/m^3).

ρ_g Gas density (kg/m^3).

ρ_{mix} Density of gas mixture (kg/m^3).

ρ_P Density of particles having smaller minimum fluidization velocity (kg/m^3).

ρ_s Particle density (kg/m^3).

θ_w Bubble wake angle (°).

v_{ij} Mole fraction of the species (-).

v_t Particle terminal velocity (m/s).

$\hat{\phi}_i$ Fugacity coefficient (-).

Φ Equivalence ratio (-).

Derivatives

$\frac{dx}{dt}$ Decomposition rate (kg/min.).

$\frac{\partial(nG)}{\partial n_i}$ Standard chemical potential of species i (function of T and P).

ACKNOWLEDGEMENTS

I wish to express my sincere gratitude to my thesis supervisor, Dr. A. E. Ghaly, Professor, Biological Engineering Department, for providing technical guidance, suggestions and assistance in writing this thesis.

Special thanks go to Dr. A. M. Al-Taweel, Professor, Department of Chemical Engineering, for his help and guidance, especially with the mathematical model. I also wish to thank the other committee members, Drs. K. C. Watts, Professor, Biological Engineering Department, F. Hamdullahpur, Professor, Mechanical Engineering Department, and V. I. Ugursal, Professor, Mechanical Engineering Department for their suggestions and contributions. They made the project both educational and enjoyable.

I am thankful to Dr. J. L. Tommy (deceased), former University Planning Officer, Dr. A. B. Rashid-Noah, Agricultural Engineering Department, Dr. I. Palmer, Acting Director of University R & D Services Bureau, Dr. J. G. M. Massaquoi, Mechanical Engineering Department, University of Sierra Leone, for their support and personal interest that resulted in my pursing this study.

I am very grateful for the assistance and contributions of Dr. A. O. Ongiro, Research Associate, Chemical Engineering Department. Thanks are due Mr. J. B. Pyke, Research Scientist, Biological Engineering Department, for his contributions in many ways throughout the course of this work. I extend my appreciation to Dr. K. Moran and Mr. F. C. Thomas of the Geological Survey Laboratory of the Atlantic Canada, Bedford Institute of Oceanography, Dartmouth, Nova Scotia, for their instructions on scanning electron microscopy and energy dispersive x-ray analyses. Frequent and stimulating discussion with Mr. R. Eagle of the Research Services of DalTech - Dalhousie University is gratefully acknowledged.

Numerous friends and colleagues assisted in obtaining the material presented in this work. I am especially grateful to all the Sierra Leonean students of Dalhousie University (Miss R. Laverley and Messrs. M. Swaray, J. Cole, H. Tommy and M. Bundu) for providing friendship and for their help on performing some experiments in this study. I am also thankful to fellow graduate students in the Biological Engineering Department (Miss B. Campbell and Messrs. M. Tango, I. Husseini, M. Elshafei, A. Bahnasawy and D. Ramkumar) for their friendship and help during the experimental work and preparation of the thesis.

Special gratitude is expressed to Messrs. J. Vissers and A. Murphy, Technicians, Biological Engineering Department, for their effort in the modification of the gasifier and the fabrication of the gas and particle sampling probes. The assistance provided by Mr. Greg Jollimore, Electronic Technician, Biological Engineering Department, with the electrical aspects of experimental apparatus is gratefully appreciated. Special thanks to the visiting technician from the National Power Authority in Sierra Leone, Mr. C. French, who also contributed to the modification of the gasifier.

The financial assistance provided by the Canadian International Development Agency (CIDA) through the University of Sierra Leone and DalTech - Dalhousie University Energy Conversion and Management Project, Contract Number 011356 S-45003, under the directorship of Dr. V. I. Ugursal, is gratefully acknowledged. I am also grateful to my employer, University of Sierra Leone, for granting me study leave to pursue this program. The rice husk was supplied through the courtesy of Broussard Rice Mills Ltd., Mermentau, Louisiana, USA.

Heartfelt thanks go to my children, Kelleh and Kondeh, my parents, family and friends for their constant support and love. Finally, a most special thanks goes to the Almighty God for giving me the strength and ability to undertake, perform and complete this work.

ABSTRACT

Gasification of rice husks in a dual distributor fluidized bed gasifier using air as the sole gasifying agent was investigated. The study was conducted in four stages: (a) modification of existing fluidized bed gasifier and data acquisition system, (b) preliminary experimentation to assess the suitability of rice husks for gasification, to determine the feasible range of operating conditions for fluidized bed gasification of rice husks and to obtain data for proper design of thermochemical conversion systems, (c) development of mathematical models to predict the performance of the fluidized bed gasification system and (d) experimentation to investigate the effects of various operating variables on the performance of the gasifier and provide data to evaluate the validity of the models.

The modified feeding system handled rice husks efficiently and the upgraded data acquisition and measurement system was trouble free. The developed gas and solid sampling probes performed satisfactorily. The dual distributor fluidized bed rice husk gasifier performed very well (steady operating conditions, a uniform temperature distribution in the dense bed, a consistent pressure drop, slug free operation and good mixing of solids and gases).

The physical and chemical properties of rice husks, agglomeration characteristics of inert bed materials in the presence of rice husk ash, and thermal degradation and kinetics of rice husks were determined. Moisture content ranged from 8.68 to 10.44% (w. b.), bulk density ranged from 86 to 114 kg/m^3, ash content ranged from 15.30 to 24.60% and the ash silica content ranged from 90 to 97%. The lower heating value range ranged from 13.24 to 16.20 MJ/kg and the volatile matter contents were in excess of 60%. The very low concentrations of nitrogen (0.38 to 0.51%), sulphur (0.014 to 0.034%) and chlorine (0.01 to 0.13%) offer environmentally more desirable fuel properties. The initial deformation temperature of the rice husk ash in the oxidizing and the reducing atmospheres ranged from 1349 to 1486°C and 1330 to 1460°C, respectively.

The agglomeration tests conducted on silica and alumina sand particles in the presence of rice husk ash showed that rice husk ash particles treated at higher

temperatures (850-1000°C) formed weak bonds at the surface of the Si or Al sand particles resulting in soft and friable agglomerates. A possible mechanism of formation considers that the condensation of low melting temperature mineral oxides (K_2O, Na_2O and P_2O_5), present in rice husk ash, upon the Si or Al particles provides an initial sticky surface to which ash particles adhere.

The thermogravimetric analyses (TGA) performed on rice husks at three heating rates (10, 20, and 50°C/min) in air, oxygen and nitrogen atmospheres from ambient temperature to 700°C showed two distinct reaction zones. The kinetic parameters (activation energy, pre-exponential factor and order of reaction) determined for each zone separately at the heating rate of 20°C/min under air, nitrogen and oxygen atmospheres showed higher thermal degradation rates in the first reaction zone due to rapid release of volatiles as compared to those in the second reaction zone. The kinetic parameters were influenced principally by the gas phase atmosphere imposed on the samples. In the first reaction zone, the activation energies were in the range of 29.0 to 35.4 kJ/mol, 37.0 to 54.7 kJ/mol and 142.7 to 188.5 kJ/mol under nitrogen, air and oxygen atmospheres, respectively.

Gasification experiments carried out at three bed heights (19.5, 25.5 and 31.5 cm), three fluidization velocities (0.22, 0.28 and 0.33 m/s) and three equivalence ratios (0.25, 0.30 and 0.35) showed that both the fluidization velocity and equivalence ratio have a major influence on the distribution and yield of products. The fluidization velocity of 0.22 m/s and equivalence ratio of 0.25 appeared to be the optimum conditions with respect to the quality of gas. The mole fractions of the combustible components reached their maximum values at these conditions. A typical gas composition at the fluidization velocity of 0.22 m/s and equivalence ratio of 0.25 was 4% H_2, 5% hydrocarbons (CH_4, C_2H_2, C_2H_4 and C_2H_6), 15% CO_2, 20% CO and 57% N_2. The higher heating value of the gas obtained at these fluidization velocity and equivalence ratio (3.2-5.0 MJ/Nm^3) compared very well with published data from air-biown biomass gasifiers of similar scale of operation. The gas yield increased with increasing equivalence ratio and/or decreasing fluidization velocity but at the conditions of interest it was 1.5 Nm^3/kg feedstock. On the contrary, increasing the

equivalence ratio and/or decreasing the fluidization velocity decreased the char yield. The particle size distributions of char samples withdrawn from the dense bed were similar to each other and much coarser than those captured by the cyclone collector. Also, variations in elemental composition between char samples withdrawn from the dense bed were relatively small, indicating that the solids were well mixed and distributed. The carbon conversion spanned from 55.0 to 84.0% and the cold gas thermal efficiency was found to range from 56.0 to 87.6% under all conditions investigated. Using the results obtained, it was estimated that operating the gasifier at a bed height of 31.5 cm, fluidization velocity of 0.22 m/s and an equivalence ratio of 0.25 with a feed rate of 1.02 kg/min can produce enough gas (127.5 kW) to operate a 32 kW internal combustion engine operating at 25% efficiency.

Two mathematical models were developed to simulate the performance of the dual distributor fluidized bed gasifier. The first model has a single parameter (overall carbon conversion) that can be used to improve the fit between predicted and experimental gas compositions. On the other hand, the second model has two parameters (carbon conversion in the core and annular regions) that can be independently adjusted to account for the effect of various operating and design conditions on the composition of the gasification products. The mean error between the predicted and measured product gas composition ranged from 2.45 to 3.05% when the one-compartment model was used. The use of the two-compartment model resulted in 4-fold reduction in the mean error (0.61-0.76%). The sensitivity analysis performed on the two-compartment model showed that changes in bed height had a significant effect on the reactor temperatures, but only a small effect on the gas composition, higher heating value and overall carbon conversion. The fluidization velocity, equivalence ratio, oxygen concentration in fluidizing gas and moisture content in rice husks had dramatic effects on the gasifier performance. The results of computation from the two-compartment model were compared with the experimental data. The model gave reasonable predictions of the core, annulus and exit temperatures as well as the mole fractions of the combustible gas components and product gas higher heating value, except for the overall carbon conversion which was overestimated.

CONTRIBUTIONS TO KNOWLEDGE

The following are the contributions of this study to the general understanding of fluidized bed biomass gasification:

1. Gas and solid sampling probes were designed, fabricated and used successfully to withdraw gas samples from different axial positions in the gasifier and solids (for the first time) from different axial positions in the dense bed of the gasifier, respectively. These samplers contain several unique features that allow accurate sampling of the high temperature gases and solids from the gasifier. The analyses of gas and solids samples withdrawn from the dense bed provide an indication of the progress of local reactions and solids distribution. In the past, no investigator attempted to collect and analyze gas and solids samples from the dense bed of the dual distributor fluidized bed gasifier.

2. The suitability of rice husks as a gasification fuel was experimentally established by characterizing the physical and chemical properties (moisture content, bulk density, particle size, heating values, proximate analysis, ultimate analysis, ash composition and ash fusibility) of six varieties of rice husks obtained from Africa and North America. This information is necessary for the proper design and operation of thermochemical conversion systems.

3. The conditions at which the gasifier can be operated without agglomeration of the bed materials (silica or alumina sand) when using a low density biomass fuel with high silica content in the ash (rice husk) were established.

4. The thermal degradation characteristics (thermal degradation rates, initial degradation temperatures and residual weights) and kinetic parameters (activation energy, pre-exponential factor and order of reaction) of four varieties of rice husks were determined. This information can be used in the modeling and design of thermochemical conversion systems.

5. The quality of the gas produced was observed and quantified at various operating parameters.

6. A two-compartment model was developed and used to predict the performance of the rice husk gasification system. The model accounts for the complex hydrodynamic conditions prevailing in the dual distributor fluidized bed gasifier. This approach allows for complete qualitative description of the operation. It also has the ability of generating concentration and temperature profiles. The temperature profile is most useful in providing information regarding possible agglomeration at hot spots within the bed.

1. INTRODUCTION

Most of the energy requirements of a majority of the developing countries are provided by petroleum-related products, the import of which imposes a major drain on already depleted foreign exchange reserves. Sierra Leone is one such developing country where a high percentage of the scarce foreign exchange earnings are spent on petroleum imports (World Bank, 1996). This has left the country in serious debt to international lending organizations, and investment in various development plans has been suppressed. Most developing countries are, therefore, taking effective measures to improve their economy by reducing the great dependence on oil imports through the development of alternative energy technologies using various biomass fuels.

Biomass fuels are organic materials derived from living plants and animals. They include wood and wood wastes, crop residues such as straw, shells, residues from food processing operations such as refining of sugarcane, milling of rice, and residues from livestock production such as excreta and slaughterhouse residues. Others include crops raised specifically for energy such as fast growing trees, sugar crops and other plants (Jenkins and Summer, 1986). The most important merits of biomass fuels as energy carriers are their sustainability and renewability, unlike fossil based fuels which have a finite supply. There is also the fact that biomass fuels contain very low levels of sulphur, chlorine or heavy metals, in contrast to most fossil fuels (Ebeling and Jenkins, 1985; and Mansaray and Ghaly, 1997a). In addition, energy conversion of biomass does not contribute to CO_2 emissions or global warming because the CO_2 released during the conversion of biomass is equivalent to that which has been absorbed by the biomass from the atmosphere through the process of photosynthesis. Thus, biomass materials, unlike fossil based fuels, is a CO_2 neutral energy resource.

A biomass material that could be utilized in a large number of developing countries for the recovery of energy because of its reasonably high energy content (~ 15 MJ/kg) is rice husk.

Large quantities of rice husks are generated annually as the major by-product in the rice milling industry. The total annual rice production worldwide is about 500 million tonnes with a rice husk production of about 100 million tonnes (FAO, 1996), assuming 20% rice husk recovery rate from rice grains (Beagle, 1978). This contains a total energy potential of about 1.5×10^{12} MJ. Over 90% of these husks can be used for energy recovery with no serious consequences on their alternative uses (World Bank, 1996).

Despite the increasing trend of the rice husk surplus, proper methods of disposal and/or utilization of rice husks have yet to be developed. Today, most of the surplus rice husks is disposed by direct burning in open heaps, which results in loss of energy as well as emission of various pollutants to the atmosphere. However, in the last decade, many countries imposed new regulations to restrict field burning of rice husks, primarily for environmental reasons. Consequently, this increased the interest in the utilization of rice husks as a renewable source of energy (Beagle, 1978; Hamad, 1981; Kaupp, 1984; and Luan and Chou, 1990). Converting rice husks (in solid form) into gaseous or liquid fuels will be beneficial to developing countries which have no conventional energy resources and whose economies are tied to agriculture and local industries. Apart from energy generation, the proper use of fuel derived from rice husks will help eliminate the waste disposal problem and reduce the existence of environmentally hazardous conditions.

The conversion of biomass fuels into more useful forms of energy such as liquid and gaseous products has centered on biochemical (anaerobic digestion and alcohol fermentation) and thermochemical (pyrolysis, combustion and gasification) processes (Beagle, 1978). Thermochemical processes have the advantage of compact equipment due to relatively short residence times (1-1000 seconds), easy start-up and stable operation (van Swajj, 1981). Amongst the thermochemical processes, gasification of rice husks has been proposed by several researchers as a potential energy recovery and waste disposal method (Beagle, 1978; van den Aarsen et al., 1982; Kaupp, 1984; and Rei et al., 1986). The process of gasification

involves the conversion of organic matter to combustible gas through thermal decomposition in a limited air environment, followed by secondary reactions of the resulting volatiles. Combustible char and tar are also produced in the process, which can be burned with air to provide the necessary heat for processing (Reed, 1981).

Gasification can be carried out using air, oxygen, steam, a mixture of air and steam, or a mixture of oxygen and steam (Reed, 1981; and Narváez et al., 1996). Oxygen or steam gasification produces a high calorific value gas. On the contrary, air gasification produces a low calorific value gas due to the dilution of nitrogen in air. However, air gasification seems to have a feasible application in many scenarios since there is not the cost or hazard of oxygen production; nor the cost and complexity of multiple reactors required in steam gasification (Narváez et al., 1996). The gas produced from the process of gasification has many advantages over solid fuels: gases are easy to clean, transport and combust with a low excess of air and there is little pollution resulting from the process. Furthermore, gases can be used to provide fuel for internal combustion engines (gas turbines, reciprocating engines) and can be easily applied in combined cycles (Bernard, 1984). Gasification of rice husks at moderate temperatures also offers the prospect of providing silica containing ash suitable for making cement (Boateng, 1989).

Gasification of rice husks is strongly affected by its physical, chemical and thermochemical properties. Despite the fact that many studies on the rice husk physical, chemical and thermochemical properties have been done (Beagle, 1978; Hamad, 1981; van den Aarsen et al., 1982; Kaupp, 1984 and Ebeling and Jenkins, 1985), little is known about the effect of these properties on the gasification process. Full understanding of these properties of rice husk is essential in order to accomplish the gasification process in a better, safe and environmentally acceptable manner.

Apart from the influence of the gasifying agent and rice husk properties, the gas quality is also dependent on the reactor type used in the gasification process. The systems of present gasifiers are complicated and there are several problems in these gasifiers such as the size distribution of solid particles in the feed as well as in the products, quality of gas produced, types of feed materials and energy consumption of gasification (van den Aarsen et al., 1982; Kaupp, 1984; Ghaly et al., 1986; and Boateng, 1989). To find more efficient and economical gasification system to produce gases from biomass is, therefore, of paramount importance.

The reactors that can convert biomass into product gas of low tar concentrations include the entrained flow gasifier, the fixed bed downdraft gasifier and the fluidized bed gasifier. Although conversion in entrained beds effectively approaches 100%, there is little experience with biomass in such systems (van den Aarsen, 1985; and Bridgwater, 1995). Low bulk density and high ash containing biomass materials such as rice husks cause flow and sintering problems in fixed bed downdraft gasifiers. Fluidized bed gasifiers have been proposed as the technology with promise because of their many inherent advantages, such as excellent gas-solid contact, enhanced reaction rate and heat transfer due to very high percentage of inert bed material (such as silica or alumina sand). Another important feature of fluidized bed gasifiers is that the temperature can be easily controlled and maintained below the fusion temperature of most ashes by varying the air and/or feed inputs (Ghaly et al., 1986; Boateng et al., 1991; Ergudenler and Ghaly, 1991; and Mleczko and Marschall, 1997). As a result, the gasification reactions can be adjusted to provide optimum conversion efficiency.

A major problem associated with the development of fluidized bed gasification technologies is the agglomeration of inert bed material (such as silica and alumina sand particles) in the presence of biomass ash at relatively low temperatures, resulting in serious channelling and defluidization (Salour et al., 1989; and Ergudenler and Ghaly, 1993a, b). The operation of a fluidized bed gasifier at elevated temperatures and the composition and

concentration of ash in biomass materials are the major factors causing the bed particles to agglomerate (Kaupp, 1984; Siegell, 1984; Arastoopour et al., 1989; Mansaray and Ghaly, 1997b; and Steenari and Lindqvist, 1997). Kaupp (1984) reported a significant decrease in the melting temperature of biomass ash in the presence of large amounts of low melting temperature mineral oxides such as sodium oxide (Na_2O) and potassium oxide (K_2O). Groeneveld and Hos (1983) stated that rice husk ash is highly prone to slagging due to its high silica content and low mineral melting temperature (800-1000°C). Luan and Chou (1990) found that feeding coal along with rice husks to a fluidized bed gasification process significantly reduced the agglomerating phenomena that occurred often in the process. These studies suggest the pressing need for better understanding the high-temperature agglomeration characteristics of inert bed materials in the presence of high ash containing materials such as rice husk for proper design and efficient operation of fluidized bed gasifiers.

The operational variables considered in the present study include bed height, fluidization velocity and equivalence ratio. The temperature distribution in the reactor, pressure drop across the reactor, and char production rate were also measured. Optimization of these variables is required in order to be able to provide data for operational and design studies. A very precise research and development effort is, therefore, necessary before rice husk fluidized bed gasifiers are competitive to traditional plants fired with fossil fuels, as to operation, safety and economy.

2. OBJECTIVES

The primary aim of this study was to investigate the feasibility of gasifying rice husks using a dual-distributor type fluidized bed reactor with air as the sole fluidizing agent. The specific objectives were:

1. to modify an existing fluidized bed straw gasifier:

   (a) modification of the feeding system to handle and utilize rice husk, and
   (b) design, fabrication and installation of solid sampling system to allow solids withdrawal from the dense bed.

2. to investigate the physical and thermochemical properties of rice husk related to handling, thermochemical conversion processes and agglomeration.

3. to study the effects of bed height, fluidization velocity and equivalence ratio on the performance of the fluidized bed gasifier in terms of gasification temperature, bed pressure drop, product gas composition, product gas heating value, product gas yield, carbon conversion and energy recovery.

4. to develop a simple predictive mathematical model to describe the fluidized bed rice husk gasifier.

5. to validate the model using experimental data to ensure that known limitations are not exceeded.

3. SCOPE OF STUDY

A fluidized bed gasifier developed at the Biological Engineering Department of DalTech, Dalhousie University, Halifax, Nova Scotia, was used in this study. This gasifier is more suited to low density and non free-flowing biomass materials.

The study was conducted in four stages: (a) modification of existing fluidized bed gasifier and data acquisition system, (b) preliminary experimentation to assess the suitability of rice husk for gasification, define conditions beyond which it is not safe to operate the fluidized bed gasifier and provide design data for thermochemical conversion systems, (c) development of mathematical models to predict the performance of the fluidized bed gasification system and (d) experimentation to investigate the effects of various operating variables on the performance of the gasifier and to provide the necessary data to evaluate the validity of the models.

The first stage of this study involved modification of the existing fluidized bed gasifier to improve its overall efficiency. Problems of bridging in the hopper and compaction in the auger of the feeding system were experienced with rice husks. Rice husks tend to rotate with the metering screw without actually being transported. The auger housing was, therefore, modified to overcome this problem. Gas sampling probes were fabricated and installed to withdraw gas samples from different locations in the dense bed, freeboard and exit of the gasifier. Solid sampling probes were added to withdraw solids as needed from the dense bed to maintain the solids inventory. A computer based data acquisition and measurement system capable of detecting temperature and pressure distributions within the gasifier was upgraded.

The second stage was devoted to exploratory experiments to determine the feasible range of operating conditions for fluidizied bed gasification of rice husk. The physical and thermochemical properties of rice husks were determined. Physical analysis included

determination of moisture content, bulk density and particle size distribution. Chemical analysis included heating values, proximate analysis, ultimate analysis, ash composition and ash fusibility characteristics. Thermochemical analysis (Thermogravimetric Analysis) was done to determine thermal degradation characteristics and, therefore, kinetic parameters. Agglomeration characteristics of inert bed materials (silica and alumina sand particles) in the presence of rice husk ash were also investigated at elevated temperatures.

In the third stage, a mathematical model was developed and used to predict the steady state performance of the fluidized bed gasifier based on chemical equilibrium considerations, and material and energy balances.

Finally, in the fourth stage, gasification experiments were conducted using rice husks as fuel. The effects of operating variables such as bed height, fluidization velocity and equivalence ratio on the gasifier performance were investigated. The data obtained from these experiments were used to test the capability of the model to predict the gasification temperatures, product gas composition, higher heating value and overall carbon conversion.

4. REVIEW OF LITERATURE

4.1 Biomass Residues

Biomass fuels are solid carbonaceous materials derived from plants and animals. These fuels include wastes from processing wood into lumber, plywood, and pulp; manure from cattle, poultry, and hogs; crop wastes such as straws; and wastes from food processing operations such as the milling of rice, the refining of cane sugar, and the canning of fruits and vegetables. Biomass fuels also include crops grown specifcally for energy such as fast growing trees, sugar crops and other plants (Tillman, 1987). The scope of this study considers only agricultural residues from crop production such as straws, husks and herbs.

4.1.1 Potential of Crop Residues

The development of biomass as an energy source should always start with an assessment of the available quantity of the particular material. Such an assessment will provide guidance to policy makers on the type of biomass to be developed and the direction in which it should be developed.

Although production of some crops in Sierra Leone has been decreasing over the years as Table 4.1 indicates, probably due to the low level of mechanization and the rebel incursion into the country in 1991, significant amounts of crop residues are generated annually in the country. The present and potential supply of agricultural by-products from crops has not been systematically inventoried; as a result, the quantity has to be calculated via estimates of the ratio of by-products to main crop yields for each crop type and the relation between main crop and by-product as shown in Table 4.2.

Table 4.1 The Production of Major Crops in Sierra Leone (FAO, 1996).

	Harvested Area (1000 Ha)					Crop Production (1000 Mt)				
Crop	1992	1993	1994	1995	Mean	1992	1993	1994	1995	Mean
Rice	354	382	328	230	324	479	486	405	284	414.0
Maize	12	12	12	12	12	11	10	11	11	10.8
Millet	28	26	30	30	29	22	21	28	28	24.8
Cocoa beans	6	6	6	6	6	10	10	10	10	10.0
Coffee	11	11	15	15	13	26	25	25	25	25.3
Sorghum	37	35	43	43	40	22	21	25	25	23.3
Dry peas	2	2	2	2	2	2	2	2	2	2.0
Broad beans	1	1	1	1	1	1	1	1	1	1.0
Sugar cane	1	1	1	1	1	45	70	70	70	63.8

Table 4.2 Relation of Main Product to By-product for Some Crops (Anon., 1978).

Product	Main-product	By-product	Ratio main-product to by-product
Rice[1]	Grain	Husk	1:0.2
Rice	Grain	Straw	1:1.4
Maize	Grain	Straw	1:1
Millet	Grain	Straw	1:1.4
Wheat	Grain	Straw	1:1.3
Sorghum	Grain	Straw	1:1.4
Dry peas	Grain	Straw	1:1.5
Broad beans	Grain	Straw	1:2.1
Cocoa	Nut	Shell/outer fibre	1:0.2
Peanut	Nut	Stalk	1:1
Potatoes	Tuber	Stalk	1:0.4
Sugar cane	Sugar	Bagasse	1:1.16

[1] Beagle (1978).

The residue potential shown in Table 4.3 was calculated by multiplication of the mean crop production in 1992-1995 presented in Table 4.1 by the residue ratios presented in Table 4.2. As Table 4.3 shows, rice production and processing generates the most important residues. Additionally, there are important residues from sugar cane, millet, sorghum, dry peas and broad beans. It is probable that a large amount of crop residue is already utilized in some way, but the potential is so high, that there may still be large surpluses which could be utilized in the future as an energy supply or raw material for industry.

The quantity of usable residues for energy generation is a function of demand, economics, and the availability of necessary technology (Strehler, 1985; and Jenkins, 1997). All residues, shown in Table 4.3 can be best utilized for heat generation since that is the application for which the conversion efficiency is the highest. A high heat demand is to be found mainly in cooler areas of the world. However, in the tropics and subtropics, heat will be utilized mainly for drying agricultural crops. In warm areas power generation (mechanical and electrical) is probably more appropriate, despite the lower efficiency (18-25%) with gasifiers (Tillman, 1987).

Rice husk, one of the principal by-products in the rice milling industry, is the agricultural residue of interest in this study. Rice is the main staple food in Sierra Leone and is grown by more than 80% of rural families. Rice production, which represents 85% of national cereal output, fell from 670 000 t in 1976 to 284 000 t in 1995 (FAO, 1996). Low producer prices and an unfavourable market situation have restricted domestic rice production. The past civil war, also, seriously affected rice production. Extensive and continuous population displacement has left large tracts of agricultural land deserted. Insecurity in settled areas has made it difficult for farmers to store seed for planting, and most are depending on emergency seed distribution programmes. The last year of rice export was 1953 and imported rice in 1991 was estimated to represent an average of 20% of total consumption of 120 000 t.

Table 4.3 Estimated Production of Major Crop Residues in Sierra Leone.

Crop Residue	Production* (1000 Mt)
Rice straw	579.60
Rice husk	82.80
Maize straw	10.80
Millet straw	37.72
Cocoa shell/outer fibre	2.00
Sorghum straw	32.62
Dry pea straw	30.00
Broad bean straw	2.10
Bagasse	74.00

* Estimated from Tables 4.1 and 4.2.

Land preparation for planting of rice is underway in the relatively secure areas. Current estimates point to substantially larger plantings of rice in 1998, compared to 1996. However, the expected recovery in production in 1998 will not materialize because the cease fire declared in 1996 has not been observed to date. Rehabilitation programmes which include distribution of planting materials, farm tools and agrochemicals, and technical support, would also be affected.

4.1.2 Rice Milling Facilities and By-products

Rice milling basically involves the removal of the outer coat (husk) and the underlying bran layers from rice (paddy). This process is currently carried out at different scales using different techniques in Sierra Leone. In the simplest level, the husk is removed by hand pounding. This process is performed using a mortar and pestle made of wood. Mortars are of various sizes and the pestles are usually about six feet in length. After pounding, the rice is winnowed and the operation repeated several times depending on the degree of milling desired. The rate of processing is slow, generally in the range of 4-12 kg per hour. The actual time spent pounding by each household depends on the household size, the total output of rice, the total proportion which is marketed as well as the proportion marketed as clean rice (Spencer, 1967).

The next level of milling uses mechanically driven equipment. The types in operation in Sierra Leone are the small steel cylinder mills, small rubber roller mills and large disc-sheller mills. In the steel cylinder and rubber roller mills, the husks are removed and the rice is simultaneously polished. In the disc-sheller the grains are dehusked but are not polished. The steel cylinder and rubber roller mills are powered by 10 to 15 hp engines and are rated to process about 250 kg of clean rice per hour. The average throughput of the disc-sheller mills is about 500 kg per hour (Spencer, 1967; and BTG, 1990). Estimates for the current total number and the distribution by size of mills in Sierra Leone are not available.

The three main by-products of rice milling are: the grains, rice meal (consisting of broken rice and bran) and rice husk, which may also include a certain amount of straw. The rice meal and bran are usually used as a feed for cattle or poultry. Rice husks have virtually no nutritional value. The proportions of these by-products vary depending on the variety of rice, the method of milling and other local factors. BTG (1990) assumed that each tonne of raw rice produces 600 kg of grain, 200 kg of rice meal and bran and 200 kg of husks.

Rice may be dehusked raw (i.e., rough rice) or it may be parboiled before dehusking. Parboiling is a hydro-thermal treatment which basically involves the soaking of rice in water overnight and raising the temperature to that required to gelatinize the starchy endosperm. It is then dried and milled in the normal manner. In small mills, drying is usually done by spreading the parboiled rice so that it can be dried by the sun. Hot air driers are normally used in larger mills. Rice husk is a major source of energy for rice drying as well. Only when the required quantity of husk is not available is the use of other fuels like coal and furnace oil resorted to. The advantages of parboiling are that it increases the milling and nutritional qualities of rice. It also increases its resistance to fungal and insect attack and improves its mechanical strength. The efficiency of the milling operation is also increased from 60 to 70% (Gariboldi, 1984). For complete parboiling of the rice grain, the moisture content should not be less than 30% (Gariboldi, 1984), but for milling the required moisture content is 14-16% (Kapur et al., 1997), thus necessitating the drying of rice before milling. About 20% of the world's total rice production is parboiled but the proportion is considerebly higher in some Asian and African countries (Mahin, 1990).

4.1.3 Rice Milling Energy Requirements

The type and scale of the process employed has a significant influence on the energy requirements of rice milling. At the household level, the energy is supplied entirely by hand. Small village rice mills are almost exclusively powered by 10-25 kW diesel engines. Medium scale rice mills, with a processing capacity of 1-3 tonnes per hour, are powered by diesel

engines, steam engines or by electric motors with output capacities in the range of 40 to 80 kW. Large scale industrial rice mills with capacities up to 24 tonnes per hour are generally powered by electric motors, steam engines or steam turbines with output capacities in the range of 80 to 500 kW (Gariboldi, 1974; Beagle, 1978; Terdyothin and Wilbulswas, 1989; and BTG, 1990).

In rice milling, shaft or motive power is required for dehusking, polishing, conveyors, sieves, and separators. Additional energy is required in the form of heat for parboiling (where it is carried out) and drying. The energy required for parboiling depends on the efficiency and sophistication of the plant. Studies show a range from 130 MJ per tonne of rice (BTG, 1990) to about 2000 MJ per tonne of rice (Beagle, 1978). Terdyothin and Wilbulswas (1989) quoted 532 MJ per tonne of rice for a mill with a combined heat and power system.

The energy needs of rice milling thus vary widely. In principle, however, the energy contained in rice husks can generally meet these needs. In an energy-efficient operation, and particularly where parboiling is not carried out, there will be a significant surplus of rice husks for other uses.

4.2 Physical and Chemical Properties of Crop Residues

The evaluation of the physical and chemical properties of crop residues is an essential prerequisite to their utilization as energy sources. These properties include moisture content, bulk density, ultimate analysis, proximate analysis, heating value and ash composition.

4.2.1 Physical Properties

Moisture content and bulk density are the major physical properties that influence the design of a biomass conversion unit (Ghaly and Al-Taweel, 1990).

4.2.1.1 Moisture content. The moisture content of the biomass feedstock has a marked effect on the efficiency of the conversion process and is directly proportional to the gas yield and composition. High moisture content biomass fuel lowers the conversion efficiency of the process. In addition, substantial amount of the heating value of the biomass fuel is considerably lost in the form of irrecoverable heat of evaporation when the moisture content of the fuel is high (Ebeling and Jenkins, 1985). Table 4.4 shows the moisture content of some crop residues used as biomass fuels. Kaupp (1984) reported that the variation in the moisture of rice husk (8-12%) depends on harvesting and handling procedures as well as the local storage and climate. Black et al. (1980) achieved reliable operation using fuels with moisture contents of 30-50%. However, the recommended moisture value for biomass should be below 20-30% but not necessarily very low, because moisture is required in the reaction and part of the water is broken down, yielding hydrogen (Beagle, 1978).

The moisture content also directly affects the handling, storage and transportation of biomass fuels. High moisture biomass is difficult to store because of the dangers of spontaneous ignition. Decomposition and the resulting energy loss and increase in ash content of high moisture fuels during storage is also a problem. Transportation of high moisture fuels is generally undesirable because of the high costs involved (Ebeling and Jenkins, 1985).

4.2.1.2 Bulk density. Typical bulk densities of some biomass materials are presented in Table 4.5. Gasification velocity and residence time of a biomass fuel in a reactor are directly affected by the fuel bulk density, which is in turn influenced by its pre-processing, handling and moisture content. A low density fuel decreases the residence time of the fuel in the reactor resulting in lower conversion efficiency (Black et al., 1980; and Kaupp, 1984). These authors also reported that a low density fuel necessitates either a very large hopper or a mechanism for continuous feeding and, a high density fuel facilitates the design of systems with very small hoppers that could operate for close to four hours without refuelling. A low density fuel material may also lead to poor mixing characteristics and non-uniform temperature distribution

Table 4.4 Moisture Content of Some Crop Residues.

Crop Residue	Moisture Content (% w.b.)	Source
Rice husk	3-5	Mendis (1989)
Rice husk	8	Beagle (1978)
Rice straw	12-22	Strehler (1985)
Maize straw	50-70	Strehler (1985)
Wheat straw	12-22	Strehler (1985)
Wheat straw	10-13	Ghaly and Al-Taweel (1990)
Barley straw	11-15	Ghaly and Al-Taweel (1990)
Oats straw	10-12	Ghaly and Al-Taweel (1990)
Rye straw	17-18	Ghaly and Al-Taweel (1990)
Coconut shell/fibre	10-20	La Nauze (1986)
Potato plant	40-70	Strehler (1985)
Bagasse	40-60	Strehler (1985)

Table 4.5 Bulk Density of Some Crop Residues (Dry Basis).

Crop Residue	Bulk Density (kg/m^3)	Source
Rice husk:		
Loose	150	Mahin (1990)
Loose	83-125	Kaupp (1984)
Briquetted	550-750	Kaupp (1984)
Straw:		
Loose	20-40	Jenkins (1989)
Chopped	40-80	Jenkins (1989)
Baled	60-70	Ghaly et al. (1989a)
Baled	100-200	Jenkins (1989)
Cubed	320-640	Jenkins (1989)
Pelleted	450-600	Wilen et al. (1985)
Pelleted	560-720	Jenkins (1989)
Briquetted	300-450	Jenkins (1989)
Coconut shell/fibre	430	Peel and Santos (1980)
Bagasse	80	Peel and Santos (1980)

in the conversion system (Bilbao et al., 1988).

High investments of energy to collect, compact, transport or process low density crop residues could cause the overall energy output to approach zero or even become negative (Beagle, 1978). Warehouse storage of low density crop residues is also expensive and usually excessive considering the benefit to be derived from their use.

Kaupp (1984) suggested briquetting and pelletization of low density crop residues to solve the problem of high transport costs. Briquetting of rice husks was found to increase their bulk density from 120 to 750 kg/m^3 (Beagle, 1978). However, these are expensive technologies due to the need for a suitable binder and extra energy to bind the residues (Bento, 1989).

4.2.2 Chemical Properties

The most important chemical properties of biomass fuels are the ultimate analysis, proximate analysis, heating value and ash composition. These properties greatly influence the design criteria of biomass conversion systems (Ebeling and Jenkins, 1985; Ghaly and Al-Taweel, 1990; and Demirbas, 1997).

4.2.2.1 Ultimate analysis. The ultimate analysis of a biomass fuel involves determining the percentage of carbon, hydrogen, nitrogen, sulphur, chlorine and ash and calculating the percentage of oxygen by difference (Jenkins, 1989). The ultimate analysis of a fuel material is essential in determining the theoretical air-to-feed ratio and in assessing the pollution potential of the feedstock.

Carbon, oxygen and hydrogen are the main elements of biomass materials. These elements are important in assessing the potential of biomass as an energy source. Nitrogen, sulphur and chlorine are normally included in the analysis to assess whether their

concentrations in the biomass residue are high enough to cause environmental pollution (Graboski and Bain, 1981; and Ebeling and Jenkins, 1985). Ultimate analysis data can also be used to evaluate the heat of formation and heating value of biomass materials (Ebeling and Jenkins, 1985).

The ultimate analyses of some biomass materials are given in Table 4.6. The table reveals that crop residues have considerably lower carbon and higher bound oxygen content compared to that of coal (Graboski and Bain, 1981). The low concentrations of nitrogen, sulphur and chlorine in crop residues indicate their insignificant contribution to environmental pollution.

4.2.2.2 Proximate analysis. Proximate analysis is a common laboratory method for determining the percentage of volatile matter, ash and fixed carbon (by difference). The results of these heating tests highly depend on the rate of heating, final temperature and type of furnace (Kaupp, 1984).

Volatile matter evolves in the form of gases, light hydrocarbons and tars; fixed carbon burns slowly in the solid state; and ash, which has a variable composition depending on the species and the nature of the soil on which the biomass was grown, is the inert residue left behind after combustion of the volatile and fixed carbon fractions (Graboski and Bain 1981; and Schiefelbein, 1989). Table 4.7 gives proximate analyses of some biomass materials and solid fuels. The results of these tests can be affected by the presence of even minute amounts of water (Kaupp, 1984). This could be a possible reason for the existence of a wide range of proximate analysis data for a given biomass fuel. Varietal characteristics and processing variables can also cause differences to occur. The volatile matter content of biomass fuels is higher than that of solid fuels such as lignite and coal. Comparing the feedstock potential of biomass and solid fuels in terms of their volatile matter content, Graboski and Bain (1981) noted that the high volatile matter content of biomass fuels makes them more readily

Table 4.6 Ultimate Analysis of Some Crop Residues (Dry Basis).

Crop Residue	Weight Percentage						Source
	C	H	O	N	S	Ash	
Rice Husk	38.30	4.36	35.45	0.83	0.06	21.00	Rossi (1984)
Rice straw	41.80	4.60	36.60	0.70	0.08	15.90	Jenkins (1989)
Maize straw	47.09	5.54	39.79	0.81	0.12	5.77	Strehler (1985)
Wheat straw	44.3-46.0	5.0-5.9	43.8-44.8	0.3-1.2	0.08-0.13	2.9-5.0	Ghaly and Al-Taweel (1990)
Wheat straw	47.20	6.20	42.00	0.80	0.13	3.70	Chornet et al. (1980)
Barley straw	44.5-46.0	5.1-5.6	41.6-44.6	0.2-0.8	0.10-0.19	4.0-7.4	Ghaly and Al-Taweel (1990)
Barley straw	47.50	6.30	41.70	0.60	0.07	3.80	Chornet et al. (1980)
Bagasse	46.95	6.10	42.65	0.30	0.10	3.90	Strehler (1985)

The range covers the results of multiple varieties of straws analyzed.

Table 4.7 Proximate Analysis of Some Crop Residues (Dry Basis).

Crop Residue	Volatile Matter (%)	Fixed Carbon (%)	Ash (%)	Source
Rice husk	56.4-69.3	12.7-17.4	15.8-23.0	Beagle (1978)
Rice husk	63.6	15.8	20.6	Rossi (1984)
Rice straw	69.3	17.3	13.4	Jenkins (1989)
Wheat straw	71.3	19.8	8.9	Jenkins (1989)
Wheat straw	77.0-79.9	16.8-18.2	3.1-4.8	Ghaly and Al-Taweel (1990)
Barley straw	68.8	20.9	10.3	Jenkins (1989)
Barley straw	73.8-82.4	13.3-18.8	4.2-7.3	Ghaly and Al-Taweel (1990)
Oats straw	75.7-81.5	17.0-19.3	1.8-5.1	Ghaly and Al-Taweel (1990)
Rye straw	82.4-83.9	14.6-15.0	2.0-3.1	Ghaly and Al-Taweel (1990)
Coconut shell/fibre	81.8	17.6	0.6	Rossi (1984)

The range covers the results of multiple varieties of rice husks and straws analyzed.

devolatilized than solid fuels, liberating considerably less fixed carbon, and hence making them useful fuels for pyrolysis and gasification processes.

4.2.2.3 Heating value. Heating value is the amount of energy released upon combustion of a unit mass of fuel. It is a significant thermal property for modeling thermochemical conversion systems (Jenkins, 1989). The two major factors affecting the heating value of biomass materials are ash composition and moisture content. High values of these two components lower the heating value of biomass materials.

The higher heating value is the amount of heat liberated from the combustion of a unit mass of fuel if all the water in the products exit at a steady flow in a condensed state. The lower heating value measures the amount of heat liberated from the combustion of a unit mass of fuel if all the products including water exit at a steady flow in a gaseous state (Chandra and Payne, 1986). The higher heating value can be measured using an adiabatic, constant volume bomb calorimeter. Boie (1952) developed the following formula for estimating the higher heating value of fuels using 16 biomass fuels, 66 coal, coke and char fuels and 67 liquid fuels:

$$HHV = 35.160C + 116.225H - 11.090O + 6.28N + 10.465S \qquad (4.1)$$

where:

HHV is the higher heating value (KJ/kg)

C is the mass fraction of carbon (-)

H is the mass fraction of hydrogen (-)

O is the mass fraction of oxygen (-)

N is the mass fraction of Nitrogen (-)

S is the mass fraction of sulphur (-)

Oxygen has a negative coefficient because it ties up some of the carbon and hydrogen in the form of CO, H_2O and phenols (OH).

Annamalia et al. (1987) used equation (4.1) to estimate the higher heating value of some biomass fuels and compared the calculated values with measured values. They concluded that equation (4.1) can be accurately used to estimate the higher heating value of biomass fuels from their ultimate analyses. The accuracy is expected to be within ± 5.0% of the measured higher heating values for most biomass materials. The authors also used equation (4.1) to develop a formula for estimating HHV using 47 fuels. Linear regression was used to determine the line of best fit which yielded an error less than 2 MJ/kg. The following relationship was obtained ($r^2 = 0.906$):

$$HHV = 0.913 HHV_{EB} + 2.04 \qquad (4.2)$$

where:

HHV_{EB} is the estimated HHV from Boie's equation (MJ/kg)

Because proximate analysis is relatively easy to perform, an estimate of the higher heating value based on it would be very useful. Ebeling and Jenkins (1985) performed a multiple regression analysis on 9 different field crops (alfalfa straw, barley straw, bean straw, corn cobs, corn stovers, cotton stalks, rice straw, sudan grass and wheat straw). The highest correlation coefficient ($r^2 = 0.911$) was found for the relationship between the heating value and ash content with the following regression equation:

$$HHV[KJ / kg] = 18980 - 183.4 * A_C \qquad (4.3)$$

where:

A_C is the percent ash by weight on a dry basis

The lower heating value is calculated by subtracting the latent heat of vaporization of water from the higher heating value as follows (Ebeling and Jenkins, 1985):

$$LHV = [HHV(1 - MC) - (\lambda)(MC) - (1 - MC)]\left(\frac{18H}{200}\right) \qquad (4.4)$$

where:

LHV is the lower heating value (KJ/kg)

MC is the moisture content of the fuel, wet basis (%)

λ is the latent heat of vaporization of water (KJ/kg)

H is the hydrogen percentage by weight (%)

Table 4.8 gives the lower and higher heating values of some biomass materials. In general, the ranges of the lower and higher heating values were from 2.9 to 17.0 MJ/kg and from 12.8 to 18.0 MJ/kg, respectively.

4.2.2.4 Ash composition. Ash is the mineral material remaining as a residue after complete combustion. The mineral elements composition of ashes from crop residues are: Si, Ca,K, P, Mg, Al, Fe, Na, S, and Zn and the mineral oxides include SiO_2, K_2O, CaO, P_2O_5, MgO, Al_2O_3, Fe_2O_3, Na_2O, and ZnO (Ghaly et al., 1990).

The percentage of ash a biomass fuel contains, and its composition and fusing temperature, strongly influence the thermochemical conversion of biomass fuels. The higher the ash content of the biomass fuel the greater the chances of impeding the chemical reactions or clogging the equipment due to its accumulation in the reactor (Wilen et al., 1985). Ash

Table 4.8 Heating Value of Some Crop Residues.

Crop Residue	Lower Heating Value (MJ/kg)	Higher Heating Value (MJ/kg)	Source
Rice husk	-	12.8	Cruz (1984)
Rice Husk	-	14.9	Rossi (1984)
Rice straw	15.3	16.3	Jenkins (1989)
Wheat straw	16.5	17.5	Jenkins (1989)
Wheat straw	19.4-19.9	18.3-18.7	Ghaly and Al-Taweel (1990)
Barley straw	16.2	17.3	Jenkins (1989)
Barley straw	18.2-19.4	17.1-18.2	Ghaly and Al-Taweel (1990)
Oats straw	18.9-19.5	17.8-18.2	Ghaly and Al-Taweel (1990)
Rye straw	19.3-19.4	17.9-18.2	Ghaly and Al-Taweel (1990)

The range covers the results of multiple varieties of straws analyzed.

composition indicates the potential for the formation of undesirable bonded deposits on combustor/gasifier surfaces and possible disposal problems of the ash. Biomass ashes with low fusion temperature tend to create more severe problems. The ash melts when the combustion temperature exceeds the melting temperature of the eutectic mixtures in the ash. The molten ash resolidifies on leaving the combustion zone, forming slag and causing severe operational problems. Ash analysis for some representative biomass fuels are presented in Table 4.9.

4.3 Utilization of Crop Residues

Crop residues contain organic and combustible solids and liquids that can be tapped for a number of uses. Crop residues are mostly used in the agricultural, industrial and energy sectors as shown in Figure 4.1.

4.3.1 Agricultural Uses

Organic fertilizers in the form of crop residues placed in the soil are a major source of plant nutrients. Groundnut leaves, for example, contain nutrient values of about 1.9% nitrogen, 0.2% phosphorus and 2.1% potassium on dry basis (Barnard and Kristoferson, 1985). These residues will decay if left in the field, enriching the soil with nutrients essential for increased crop production. They also enhance soil and water conservation and improve the physical properties of the soil, thereby reducing the susceptibility to both wind and water erosion.

In as much as the use of crop residues plays a vital role in maintaining soil fertility, some detrimental effects of large quantities of crop residues in the soil have been identified. Staniforth (1982) reported on the reduction of soil temperature, which depresses germination rates and delays plant maturity; a reduction in nitrate formation; production of substances that are toxic to germination; increased need for pesticides; and creation of substances that increase the potential for plant disease.

Table 4.9. Ash Analysis of Some Crop Residues (Ebeling and Jenkins, 1985; Ghaly et al., 1990; and Mansaray and Ghaly, 1997a).

Crop Residue	Mineral Oxide Analysis (dry basis)											Fusion Temperature (°C)	
	SiO_2	Al_2O_3	Fe_2O_3	CaO	MgO	Na_2O	K_2O	P_2O_5	TiO_2	SO_3	ZnO	IDT[1]	FT[2]
Rice Husk	90.34	0.75	0.72	0.90	0.78	0.34	3.26	0.96	0.04	0.15	-	1440	1650
Rice straw	79.78	3.25	0.27	2.00	2.82	1.11	7.95	1.12	0.17	0.44	-	1026	1500
Wheat straw	56.80	-	0.50	5.80	2.00	6.00	14.80	2.60	-	7.60	-	700	-
Barley straw	44.70	-	2.60	3.22	4.84	5.25	8.01	11.56	-	1.80	0.13	925	1100
Bean straw	32.70	-	3.93	6.30	3.65	0.82	25.30	7.30	-	2.28	0.15	900	1150
Corn cobs	40.30	-	4.06	1.27	2.49	1.19	2.04	6.87	-	8.74	0.22	900	1020
Corn stovers	70.71	-	7.10	0.46	2.70	0.33	10.28	0.66	-	2.20	0.02	820	1091
Cotton stalks	33.00	-	2.80	3.56	6.05	1.37	21.40	6.40	-	6.50	0.07	1110	1275
Cotton gin trash	23.20	-	1.93	7.18	2.87	1.59	13.00	10.00	-	4.24	0.19	1010	1380

[1]Initial Deformation Temperature

[2]Fluid Temperature

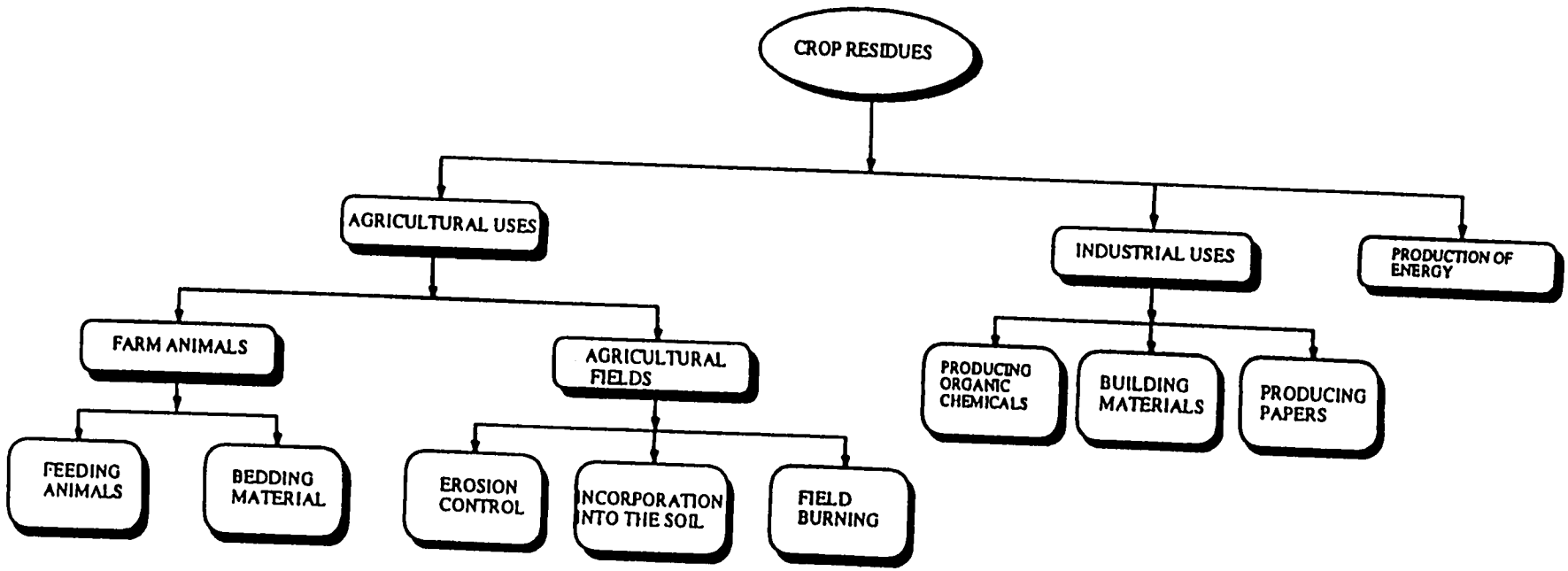

Figure 4.1 Competing Uses of Crop Residues (Sadaka, 1994).

Most farmers prefer burning residues to recycling them to the fields, especially where multi-cropping is being carried out demanding the quick disposal of the residues. This will impair crop yields considerably as virtually all the nitrogen is lost, along with 20-25% of the phosphorus and potassium and significant quantities of sulphur (Jenkinson, 1981). Temperature rise in the soil, resulting from field burning, may kill useful organisms living in the soil. The most distinguished problem in the field burning of crop residues is the influence it has on the environment (Langille and Ghaly, 1991).

The composition of most crop residues plays a major role in their suitability as animal feed. The high protein content and easily digestible crop residues like most green plant residues, green sugar cane tops and groundnut residues are normally fed to animals. Despite its minerals and vitamins deficiency, very low metabolizable energy and protein contents, straw is used to provide bulk to a ration (Staniforth, 1982). Straw is also widely used as bedding material for animals (Jenkins et al., 1984).

The products of rice milling are the grains or kernels, rice meal, which consists of broken rice and bran, and rice husk. The rice meal and bran are used as feed for cattle or poultry. Rice husks are used as bedding materials for animals, litter and nesting for poultry. Although rice husks have virtually no nutritional value, small amounts have been ground for use as animal feed adjunt (Mahin, 1990). The rice grains are usually polished after milling to produce the white rice used for human consumption.

4.3.2 Industrial Uses

Crop residues can be used as industrial raw materials for the production of organic chemicals because of their cellulose and hemicellulose content. Rice husks, corn cobs, cotton seed husks, oat hulls and sugarcane bagasse can be used as raw materials for the production of furfural, activated carbon and other chemical derivatives (Staniforth, 1979). Crop residues can, also, be used to make writing papers, printing papers and corrugated media. Rice husk ash,

which is left after gasification or burning the husks in a boiler, is used in the manufacture of portland cement (Mahin, 1990). Efforts are being made for manufacturing solar grade silicon materials from rice husk. The silica present in rice husks, being biogenic in origin, is inherently amorphous. This silica is an attractive source for manufacturing high purity silicon. Ultrapure silicon is used for the production of photovoltaic cells (Chakraverty and Kaleemullah, 1991). Because of its open porous structure, rice husk ash is highly absorbent and can, therefore, be used as an additive for the manufacture of hand soap powder (Jenkinson, 1981). Straw is widely used as a binding ingredient in the manufacture of mud blocks used for constructing low cost buildings. Straw bales have been used for thatching roofs and constructing barns (Staniforth, 1979).

It is important to note, however, that the use of agricultural biomass in construction is labour intensive and requires frequent maintenance in comparison to modern building materials. Modern construction techniques based on mass production of inexpensive building materials have significantly reduced the use of crop residues as building materials in developing countries.

4.3.3 Energy Production

Crop residues have always been an important source of energy in the less developed economies of the world, and they have become an increasingly important energy source in the industrialized world. Crop residues are used to supply process heat, electricity, and a combination of the two to biomass industries such as food processing and other agri-businesses. Rice and sugar mills can be largely self-sufficient in fuels as a result of using their own wastes and by-products.

Most crop residues have reasonably good energy content and their conversion to cleaner energy forms such as liquid, gaseous or high energy content solid fuels through biological and thermochemical conversion processes is usually preferred (Walawender et al.,

1982). This will not only help reduce the huge quantities of solid wastes currently facing disposal problems, but can also play a major role in controlling environmental pollution.

4.4 Thermochemical Conversion of Crop Residues to Energy

Generally, energy production from crop residues can be via biological and thermochemical conversion processes (Figure 4.2). Biological conversion processes, which include anaerobic digestion and alcoholic fermentation, involve the anaerobic decomposition of biomass to yield methane from bacterial fermentation or ethanol from yeast fermentation. This technology preserves the nutrient components of the feedstock in a form that can be used as animal feed or fertilizer. Thermochemical conversion processes include pyrolysis, combustion and gasification (Figure 4.3). The thermochemical conversion processes have been recommended by a number of authors for energy recovery from biomass (Ebeling and Jenkins, 1985; Ghaly et al., 1986; and Corrella et al., 1989).

4.4.1 Pyrolysis

Pyrolysis is the destructive distillation of carbonaceous materials in the absence of oxygen, resulting in char, condensable liquids or tars and gaseous products. The char may be useful as a fuel either directly, as activated carbon, or as char oil or char water slurries (Bridgwater, 1989). In addition, the liquid product may be upgraded to refined fuels, added to petroleum refinery feedstocks or may contain chemicals in economically recoverable concentrations (Font et al., 1989; and Bridgwater, 1989). The heating value of the product gas is sufficiently high to be used for the total energy requirements of a biomass waste pyrolysis plant (Bridgwater, 1989).

The relative proportions of the three main pyrolysis products depend on the chemical composition of the biomass used and on the operational conditions (Deglise and Magne, 1987).

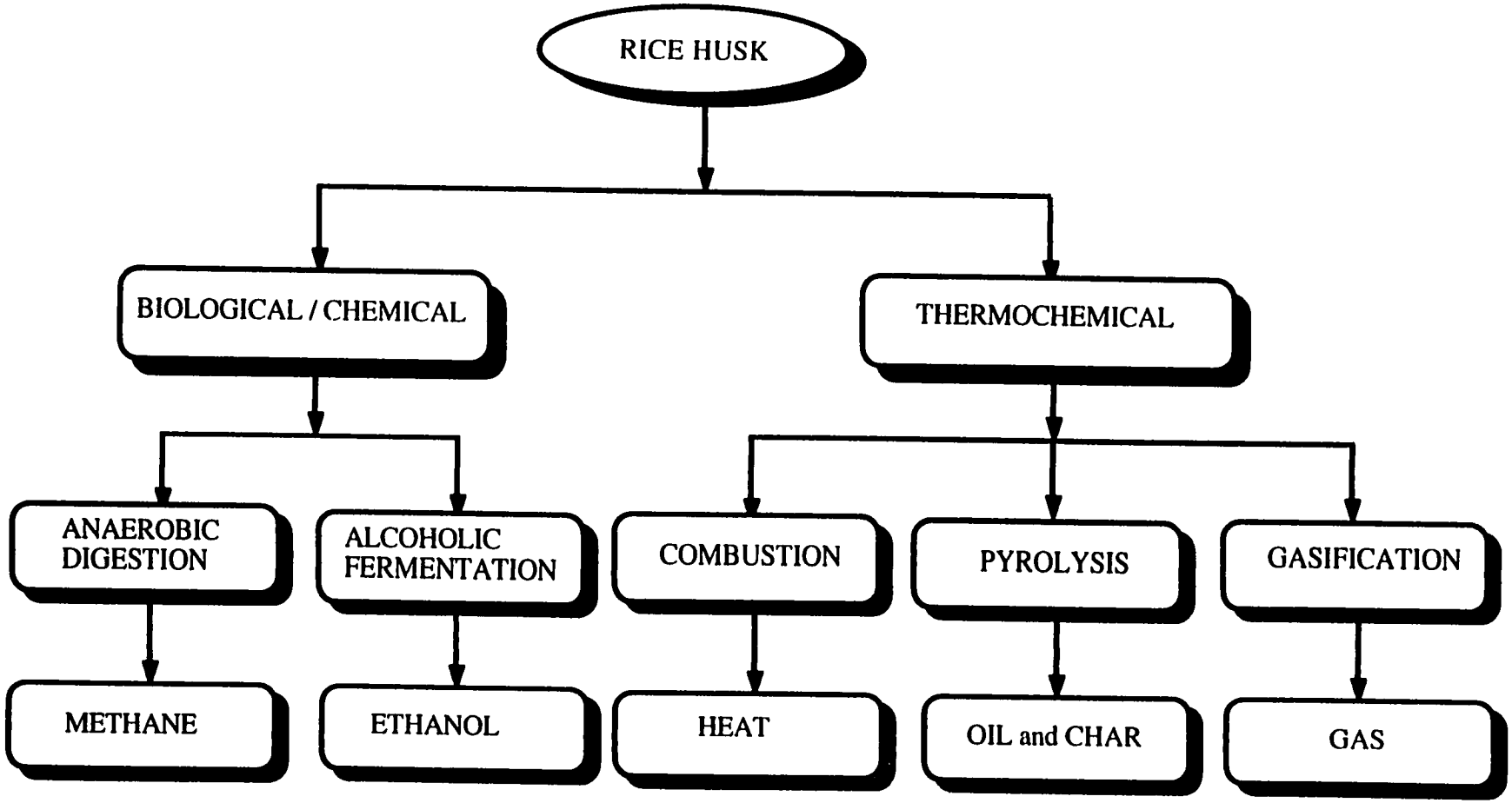

Figure 4.2. Routes of Energy Recovery from Rice Husk.

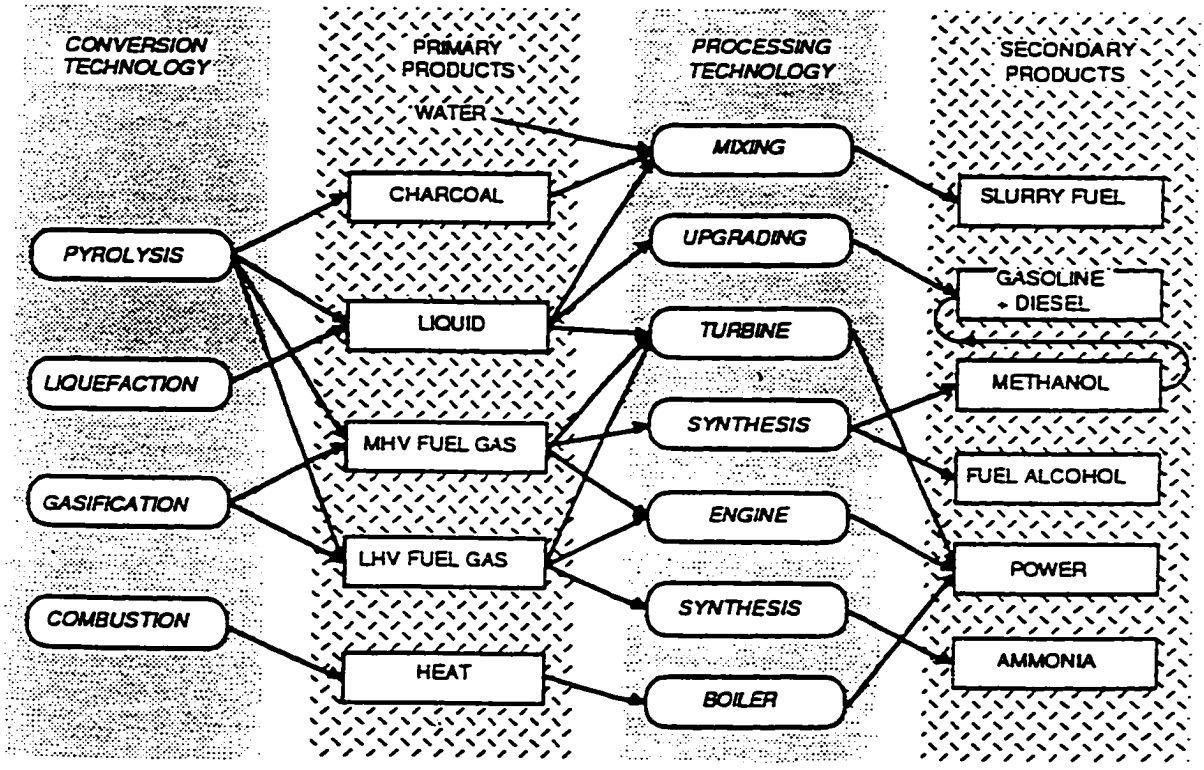

Figure 4.3 Products of Biomass Thermochemical Conversion Processes (Beenackers and Bridgwater, 1989).

As biomass is a mixture of three main components (cellulose, hemicellulose and lignin) and of some other minor ones (extractives and inorganic compounds), its pyrolysis proceeds through a series of complex, concurrent and consecutive reactions. Shafizadeh (1985) reported that at temperatures above 300°C, the polysaccharides break down at the glycosic linkage to provide tarry pyrolyzates containing lower molecular weight anhydro sugar derivatives and relatively little char, whereas the lignin is mainly condensed to a carbonaceous char and gives smaller amount of pyrolyzates containing phenolic compounds. It is then reasonable to conclude that the operational conditions have a great influence on the proportion and even the composition of the three major reaction products: char, tar and gas.

The operational conditions acting on the yield of the reaction products are: heating rate (thermal flux), residence time of the reaction products, highest temperature used and pressure (Deglise and Magne, 1987). The yield of volatiles increases with the heating rate, but for the highest temperatures, the condensables (tar) are cracked and the gas content is increased. The char yield is maximized at low heating rates, low temperatures, and long residence times (Capart et al., 1989).

Flash pyrolysis (heating rate of 100-10 000°C/s) occurs at moderate temperatures (400-600°C) and aims to maximize the yield of liquid tar and oil products at the expense of char and gas with vapour residence times less than 2 seconds. In fast pyrolysis, extremely high heating rates (1 000-20 000°C/s) are used at temperatures higher than 600°C and very short vapour residence times (less than 0.5 s) in order to produce gas at the expense of char and tar/oil (Font et al., 1989; and Maniatis et al., 1989).

The pyrolysis of biomass materials have been successfully carried out in several systems. Lucchesi and Maschio (1982) used an updraft reactor to pyrolyze crop residues. They showed that the amount of gas produced increased and the yield of liquid decreased with increases in pyrolysis temperature. However, many unanswered questions related to continuous

plant operations versus batch loading, moisture control in the pyrolysis zone, most efficient system design and economics of scale, place the economics of pyrolysis in question. The pyrolysis of crop residues yield products which are more suited to chemical industries. But, most of the research and development efforts in the utilization of crop residues for energy recovery are directed towards combustion and gasification.

4.4.2 Combustion

Combustion can be defined as a series of free radical reactions whereby carbon and hydrogen in the fuel react with oxygen to form CO_2 and H_2O while liberating useful heat according to the following equation (Tillman, 1987):

$$C_xH_y + \left(x + \frac{y}{4}\right)O_2 \rightarrow xCO_2 + \frac{y}{2}H_2O + HEAT \qquad (4.5)$$

The oxygen is often supplied in excess to ensure complete combustion of the fuel. In so doing, production of CO is minimized while the heat released in the process is maximized. According to Shafizadeh and DeGroot (1976), general combustion mechanisms for solid fuels include particle heating and drying, pyrolysis, gas-phase reactions (combustion of volatiles), and gas-solid reactions (char oxidation). A thorough understanding of these mechanisms is essential in order to efficiently manipulate the combustion process for maximum thermal efficiency and minimum pollution production. Figure 4.4 shows the reaction stages of heating and drying, solid particle pyrolysis, gas phase reactions and char oxidation reactions.

When the wet biomass fuel enters the combustion unit, it is heated to the point where pyrolysis begins. These heating and drying stages are dominated by physical reactions. Fuel particle heating is heavily influenced by particle moisture content, due to the dominating physical phenomena (Tillman, 1987). Tillman (1987), also, showed that the energy required for

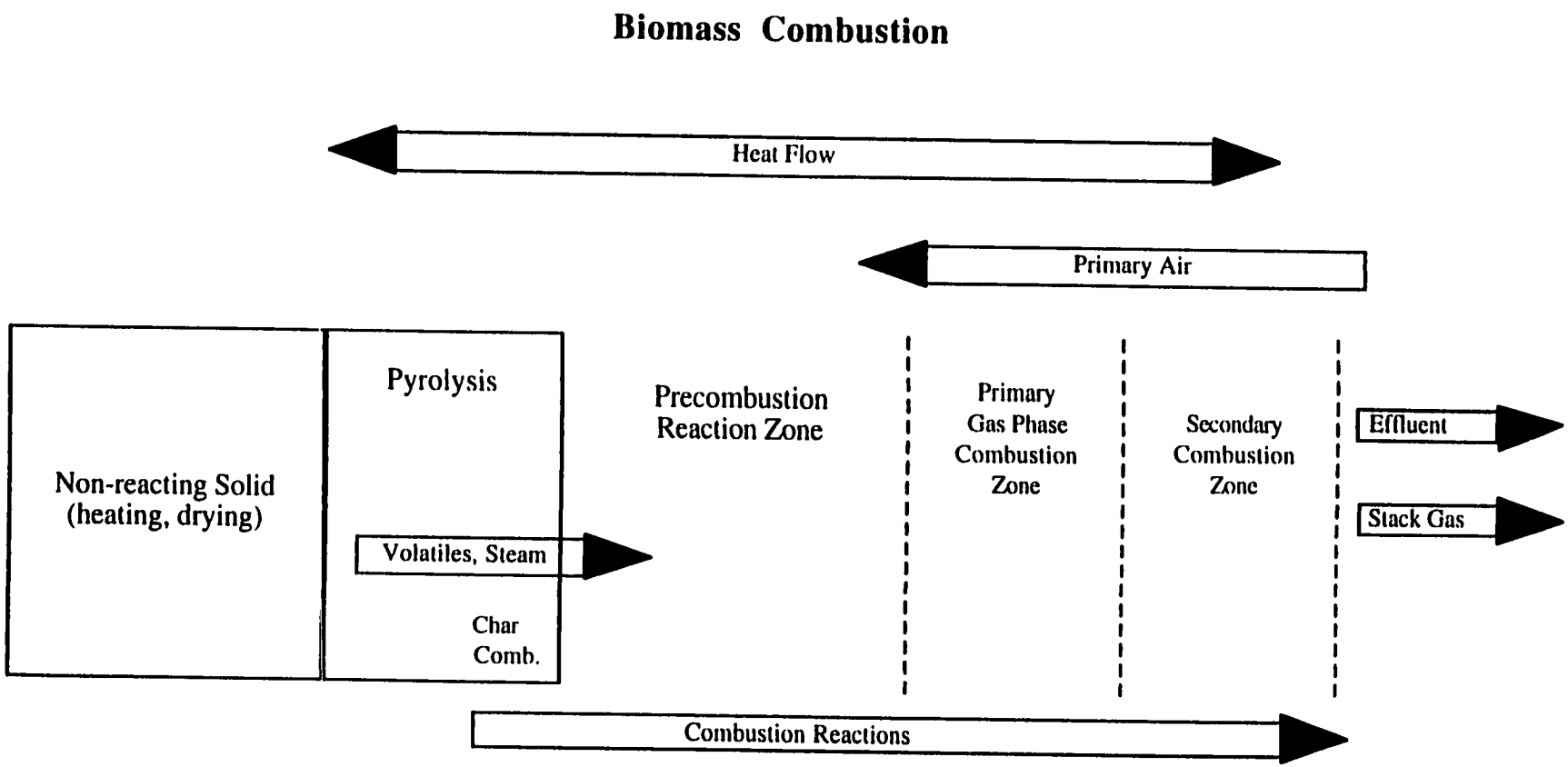

Figure 4.4 A Representation of the Combustion Mechanism for Biomass Fuels (Adapted from Tillman, 1987)

heating and drying is increased by the presence of moisture, but that the ability to conduct heat to the center of the fuel particle is enhanced by the presence of moisture.

Low combustion efficiencies due to high flue gas temperatures and problems of high levels of particulate emissions during the combustion of biomass in boilers and furnaces have been reported with biomass materials (Kraus, 1985; and Strehler, 1985). Kraus (1985) observed slagging of biomass ash at higher temperatures which clogged the grate resulting in serious operational problems. He also observed that through-burning boilers generate relatively low CO_2, high CO and high solids emission whereas bottom-burning boilers generate lower solids emission but still above the legally accepted limit of 300 mg/m^3.

4.4.3 Gasification

Biomass gasification is a thermochemical process that involves the conversion of the carbonaceous material in biomass by partial combustion using different gasifying agents such as air, oxygen, steam, hydrogen or a combination of these agents to produce a mixture of gases (Kaupp, 1984; Mendis, 1989; BTG, 1990; and Mahin, 1990). The main combustible components of the resulting gas, usually referred to as producer gas, are CO and H_2. Small amounts of CH_4, C_2H_2, C_2H_4 and other hydrocarbons also frequently occur. The incombustible gas products include N_2 from the air, and CO_2. Tars and ashes are other products of biomass gasification. The gas can be used directly to run furnaces, boilers or kilns or it can be cleaned of all solid particulate, tars and moisture and cooled to as close as possible to ambient conditions if it is to be used in internal combustion engines or gas turbines as substitute fuel. The conversion of biomass into fuel gas is an old but promising technology. Nevertheless, much remains to be done to fully realize its potential.

The final products of biomass gasification depend on the type of gasification process employed as shown in Figure 4.5. Using air to gasify, the gas generated is of low energy value

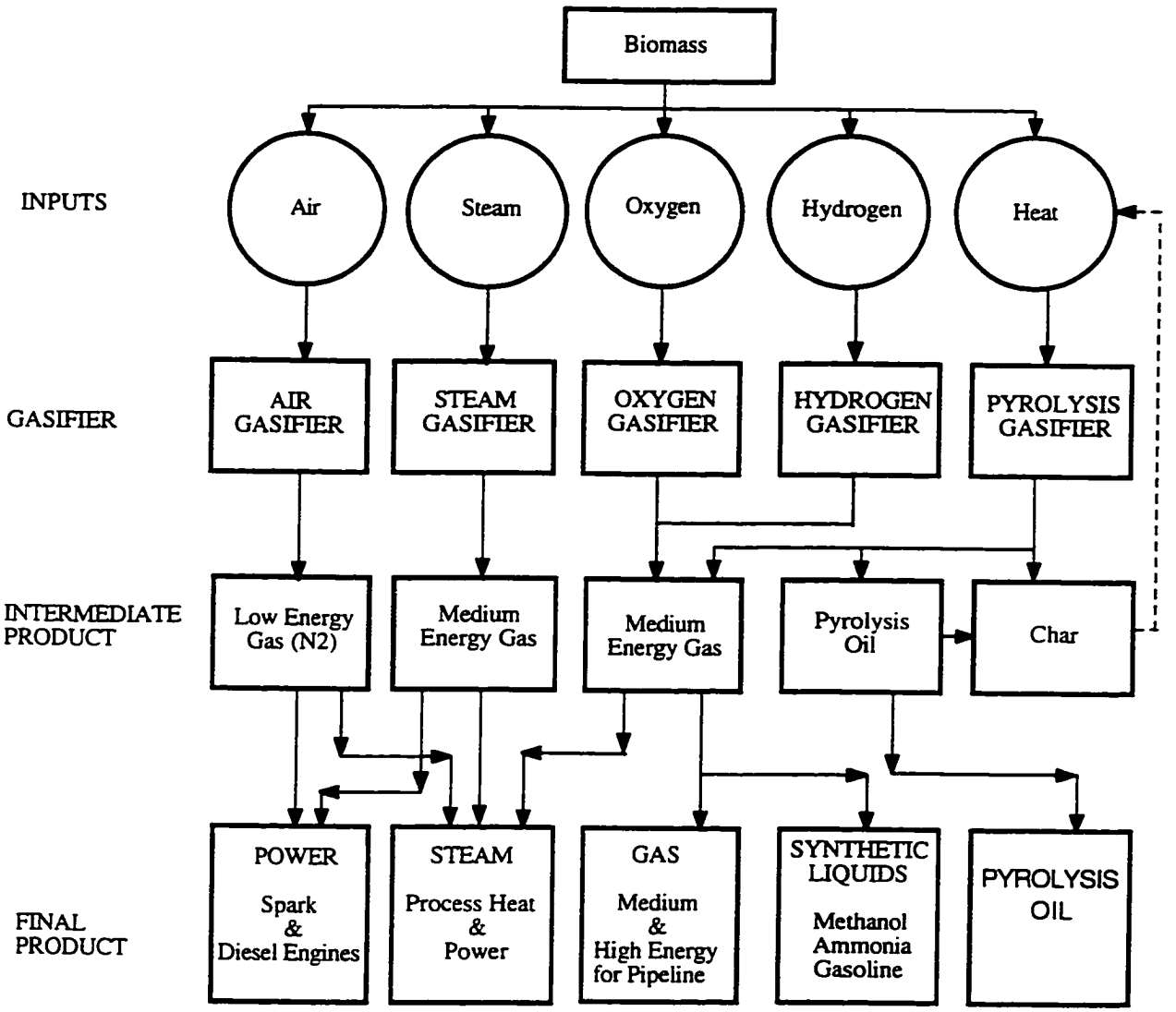

Figure 4.5 Gasification Processes and Their Products (Adapted from Reed, 1981).

(about 3.0 to 7.0 MJ/Nm^3) due to nitrogen dilution and this gas cannot, therefore, be economically transported over long distances (Walawender et al., 1985). However, it is suitable for operating boilers, engines and turbines. Gasifying the biomass with oxygen gives relatively nitrogen free gas of higher energy content (about 10-18 MJ/Nm^3) which is suitable for limited pipeline distribution and as synthesis gas for conversion to ammonia, methanol and gasoline (Reed, 1981). However, such a technology requires an expensive, energy consuming air separation plant and additional safety precautions. When oxygen is used, it represents 25 to 35% of the cost of the gas (von Fredersdorff and Elliott, 1963). This factor has stimulated development work on continuous gasification processes using air but producing a gas containing low concentrations of nitrogen. These developments have not as yet led to commercial processes. Recently, investigations into fluidized bed steam gasification have grown with the majority of them focusing on the analysis of the produced gas from various biomass feedstocks. This process also includes steam reforming into a hydrogen-rich gas which can be utilized as a raw material for ammonia and methanol synthesis or in fuel cells (Boateng et al., 1991). Although, biomass has a low hydrogen to carbon ratio compared to most liquid and gaseous fuels, biomass can be converted to liquid or gaseous fuels under pressure with hydrogen (Reed, 1981). This process is known as hydrogasification.

4.5 Chemistry of Biomass Gasification

The chemistry of biomass gasification can be described by assuming biomass as carbon and by listing the several well-known solid-gas and gas-phase reactions involved as shown in Table 4.10. The combustion reaction (Equation 4.6), which is highly exothermic, supplies most of the thermal energy for the gasification process. The water-gas (Equation 4.8) and Boudouard (Equation 4.9) reactions are endothermic and represent the conversion of carbon into combustible gases. These are driven by the heat energy supplied by the combustion reaction. The hydrogen and carbon monoxide produced by the gasification reaction react with

Table 4.10 The Main Chemical Reactions in Gasification Processes.

Reaction	Reaction Heat (kJ/kg.mol)	Process	Equation Number
	Heterogeneous (gas-solid) reactions		
$C + O_2 \rightarrow CO_2$	-393,800	Combustion	(4.6)
$C + 2H_2 \rightarrow CH_4$	-74,930	Hydrogasification	(4.7)
$C + H_2O \rightarrow CO + H_2$	+131,400	Water-gas	(4.8)
$C + CO_2 \rightarrow 2CO$	+172,600	Boudouard	(4.9)
	Homogeneous (gas-phase) reactions		
$CO + H_2O \rightarrow H_2 + CO_2$	-41.2	Water-gas shift	(4.10)
$CO + 3H_2 \rightarrow CH_4 + H_2O$	-201,900	Methanation	(4.11)

each other and with carbon. The reaction of hydrogen with carbon (Equation 4.7) is exothermic and can contribute heat energy. Similarly, the methanation reaction (Equation 4.11) can contribute heat energy to the gasification process. These equations are interrelated by the water-gas shift reaction (Equation 4.10), the equilibrium of which controls the extent of the water-gas and Boudouard reactions.

High temperatures favour, thermodynamically and kinetically, the endothermic water-gas and Boudouard reactions (Desrosiers, 1981). Hence, a decreased yield of CH_4 and C_2-hydrocarbons is expected as the hydrogasification and methanation reactions will proceed at a lower rate, H_2 and CO production will be favoured, and all reaction rates will increase in the direction in which heat absorption takes place. The main objective of biomass gasification is its conversion into a combustible gas containing the maximum remaining heating value. This is primarily achieved in low temperature gasification to produce CH_4 as the primary gaseous component according to the following overall reaction:

$$2C + 2H_2O \rightarrow CH_4 + CO_2 \qquad (4.12)$$

Liinanki et al. (1985) observed an increasing yield of CH_4 at low temperatures (< 800°C) with a maximum yield reached at about 800°C and then decreases with increasing temperature. This was explained as due to the considerable decrease in the yield of tars at reforming temperatures up to 800°C.

4.6 Biomass Gasifiers

The three types of gasifiers commonly used for biomass gasification are the updraft (or countercurrent), downdraft (or cocurrent) and fluidized bed.

4.6.1 Updraft Gasifier

In an updraft gasifier, the fuel is fed from the top, the air is introduced from the bottom through a grate and the gas is drawn out at the top (Figure 4.6.). The downward moving fuel is first dried by the upflowing hot product gas. The solid fuel is then pyrolyzed giving char which continues to descend through the different reaction zones to be gasified, and pyrolysis vapours which are carried upward by the upflowing hot product gas. The tars in the vapour either condense on the descending fuel or are carried out of the gasifier with the product gas contributing to its high tar content (Bridgwater and Evans, 1993). This tar contains about 30% of the energy content of the biomass fuel (Overend, 1982). The condensed tars are recycled back to the reaction zones where they are further cracked to gas and char. The solid char from pyrolysis and tar cracking is partially oxidized with the incoming air or oxygen (Bridgwater and Evans, 1993). Updraft gasifier product gas thus contains a significant proportion of tars and hydrocarbons which contributes to its high heating value.

The principle advantages of updraft gasifiers are their simplicity in construction and high thermal efficiency; the sensible heat of the gas produced is recovered by direct heat exchange with the entering feed, which is thus dried, preheated and pyrolyzed prior to entering the gasification zone. In principle, there is little scaling up limitation (Brink, 1981).

The major drawback of an updraft gasifier is that most of the tars and other pyrolysis products are drawn out with the gas, producing dirty gas (Foley and Barnard, 1985). The fuel gas requires substantial clean up if further processing is to be performed. Another serious disadvantage of this type of gasifier is the high temperature in the oxidation zone (about 500°C) that may melt the ash in the case where the reaction temperature is higher than the ash melting temperature. Steam, as an endothermic agent, and exhaust gas recirculation have been common approaches for controlling the oxidation zone temperature of updraft gasifiers (Payne and Alphin, 1983).

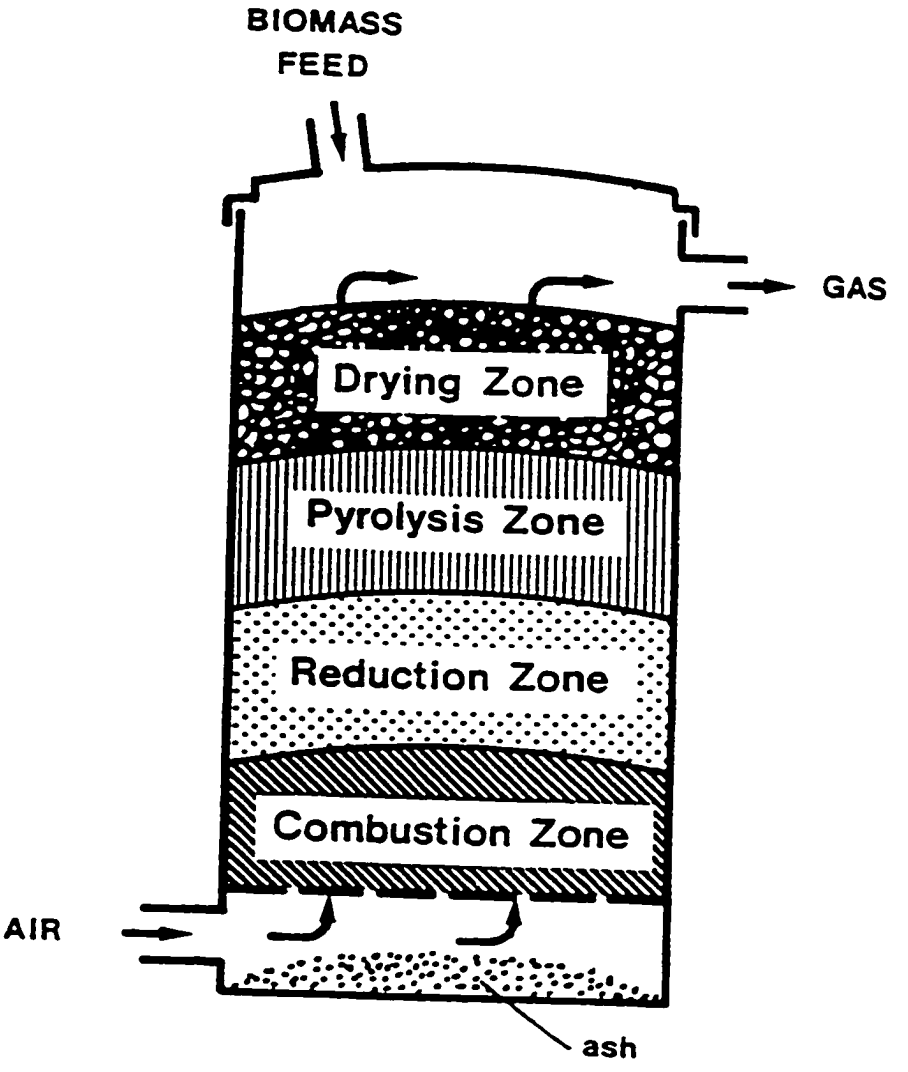

Figure 4.6. Updraft Gasifier (Foley and Barnard, 1985).

4.6.2 Downdraft Gasifier

This gasifier is a refinement of the updraft gasifier to solve the problem of tar in the gas. The fuel, air and vapour flow in the same direction and the gas is drawn out through a grate (Figure 4.7). There is a constriction or throat in the combustion zone where most of the gasification reactions occur. Air is injected through nozzles into the combustion zone and then drawn down through the char bed along with the pyrolysis products. The reaction products are intimately mixed in the turbulent high temperature region around the throat which aids tar cracking. Some tar cracking also occurs below the throat on the residual char bed where the gasification process is completed (Reed, 1981; and Foley and Barnard, 1985). Biomass fuels containing a lot of tar after gasification are usually gasified in downdraft gasifiers to produce gas with low tar content requiring less cleaning if it is to be used in internal combustion engines (Manurung and Beenackers, 1985).

A homogeneous fuel bed that is free from channels and caves is a major design and operating parameter of a downdraft gasifier. This type of gasifier requires a biomass fuel of uniform size and size distribution (not smaller than about 1 cm and not bigger than about 30 cm in the longest dimension), with moisture content of up to about 30% dry basis and a low ash content (below 1%). Fines and fluffy (low density) fuels create a pressure drop in the fuel bed that is too high for efficient performance (Hos and Groeneveld, 1987). Due to the low tar content in the gas produced, the downdraft gasifier is generally favoured for small scale electricity generation (about 500 kW_{el}) with an internal combustion engine.

4.6.3 Fluidized Bed Gasifier

Three typical fluidized bed gasifiers with the temperature and solid conversion profiles are given in Figure 4.8. The conventional fluidized bed gasification process (Figure 4.8a) is generally carried out by continuously feeding solid fuel into a bed of some inert materials such as silica sand, alumina or ashes supported by a distributor floor. The inert bed materials help maintain the operating temperature steady at the desired level. Catalysts have also been used to

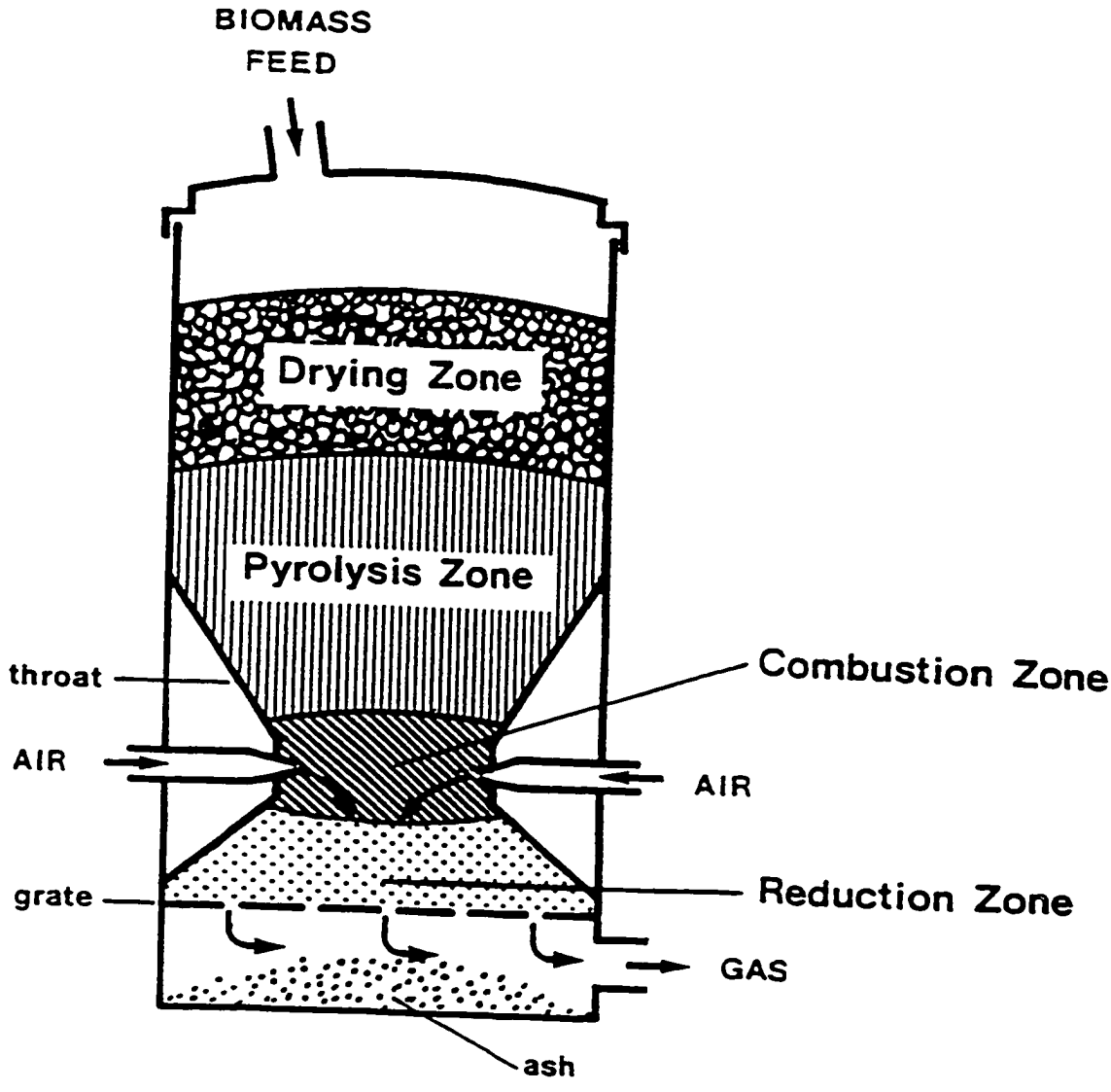

Figure 4.7. Downdraft Gasifier (Foley and Barnard, 1985).

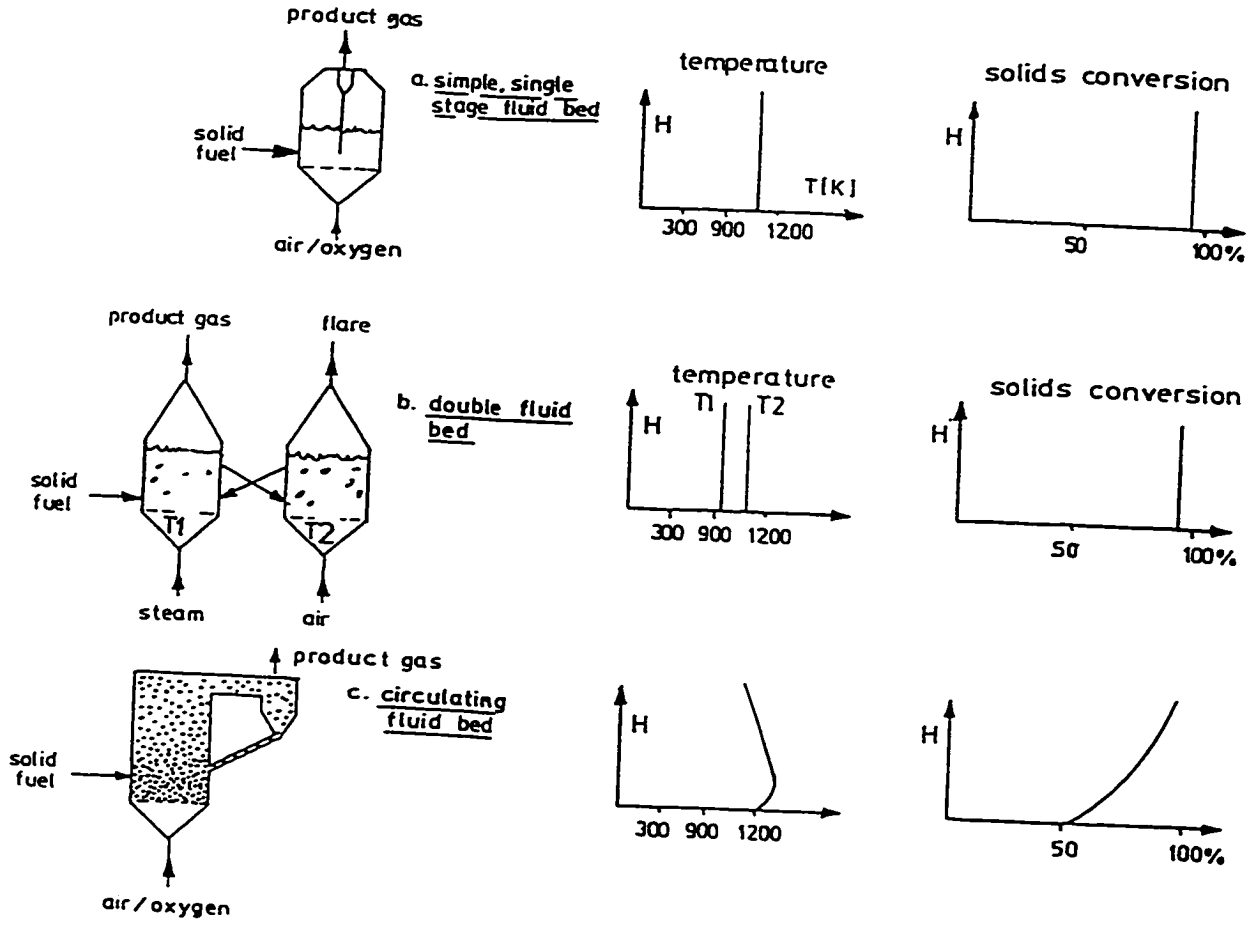

Figure 4.8. Fluidized Bed Reactor Types (van den Aarsen, 1985).

reduce tars and modify product gas composition (Bridgwater, 1995). A typical operating temperature for biomass gasification is 750-850°C. The bed temperature is controlled by means of the air-fuel ratio. The bed is initially heated from an external source to a sufficiently high temperature and the fuel is then introduced either by a continuous mechanical feed directly into the dense bed or by gravity from the top of the fluidized bed.

The fuel-sand mixture is subjected to an upward flow of air through a distributor plate at sufficient velocity such that the mixture becomes fluidized. On entering the bed, the solid fuel is rapidly heated to the reactor bed temperature and pyrolyzed, releasing char, volatile high molecular compounds and gas as the initial products. The pyrolysis gases are then thermally cracked and/or gasified by steam, while the char particles are gasified via reactions with carbon dioxide and steam. The product gas can be directed into a cyclone to remove solid particulate as they rise upward and then cooled and cleaned to reduce or eliminate unwanted tars (Overend, 1982; and Foley and Barnard, 1985).

The double fluidized bed gasifier (Figure 4.8b) is designed to give a gas of higher energy content from reaction with air than is obtained from a single air-blown gasifier. The gasifier is heated with hot sand from the second fluidized bed, which is heated by burning the product char in air before recirculation to the first reactor. Steam is also usually added to encourage the shift reaction to generate hydrogen and to encourage carbon-steam reactions. Product quality is good as far as the heating value is concerned, but poor in terms of tar loading (Bridgwater, 1995). The circulating fluidized bed gasifier (Figure 4.8c) is developed so that the entrained materials are recycled back to the fluidized bed to improve the carbon conversion efficiency compared with the single fluidized bed design. A hot raw gas is produced which is used in boilers to recover the sensible heat in the gas (Bridgwater and Evans, 1993). This gasifier has been extensively developed for woodwaste conversion for firing lime and cement kilns and steam-raising for electricity generation (Bridgwater, 1995).

Defluidization due to bed sintering is one of the commonly encountered problems depending on the thermal characteristics of the ash. Oxides of alkali metals from the biomass ash (such as Na_2O and K_2O) form low melting temperature eutectics with the silica in the sand which is the usual fluidizing medium. This results in agglomeration and bed sintering with eventual loss of fluidization (Arastoopour et al., 1989; and Ergudenler and Ghaly, 1993a). However, the inherently low operating temperature of a fluidized bed and its inherently better temperature control provide an acceptable control measure for many biomass materials. With biomass of high ash/inerts content it may be better to use alumina or even metallic sand such as chromate sand (Bridgwater and Evans,1993).

In contrast to fixed bed reactors there are no reaction zones developed in a fluidized bed gasifier during gasification. Drying, pyrolysis and gasification occur simultaneously over the whole reactor volume, which is almost perfectly mixed and thus isothermal (Overend, 1982; and Buekens and Schoeters, 1985). Fluidized bed gasifiers also have the advantage that they can be readily scaled up with considerable confidence. Only the fuel distribution becomes problematical in large beds, although multiple feeding is an acceptable solution (Buekens and Schoeters, 1985; Bridgwater, 1989; and Bridgwater and Evans,1993). Fluidized beds provide many features that are lacking in the fixed bed types. These include high rates of heat and mass transfer, good mixing of the solid phase and uniform temperature in the bed.

4.7 Gasifier Applications

The gas produced by gasification can be used in direct combustion systems, powering a specially adapted engine and production of methanol.

4.7.1 Direct Heating

Gasifiers can be used to fuel external combustion systems such as those found in boilers, kilns or ovens. These gasifiers, usually referred to as heat gasifiers, have an efficiency ranging from 50 to 70%. Coupled to a steam engine or turbine, the burner to which a heat gasifier is directly connected can be used to generate motive power or electricity. Potential industries for direct heat applications include food processing, crop drying, cement manufacturing, brick making, ceramics and pottery.

The use of heat gasifiers in external burners has a number of advantages. Heat gasifiers are simple to design, fabricate and operate as a result of the less critical gas quality requirements, and can utilize a wide range of fuels. In most cases, little or no modification to the existing oil-fired equipment is necessary, unlike converting the same equipment to use raw biomass fuels. Corrosion of the boiler and air pollution can be reduced through better gasifier designs so that the gas is free from hydrochloric acid and sulphur dioxide. The hydrocarbon pollutants emitted from the external burner can also be drastically reduced by increasing the temperature in the gasification process. The fact that the volume of producer gas is only about one third that generated by the direct combustion of the fuel makes it considerably easier and cheaper to clean. Because heat gasifiers tend to utilize the sensible heat and tars in the producer gas, they can be twice as energy-efficient as burning the biomass fuel directly in a combustion system (Foley and Barnard, 1985; and Mendis, 1989).

Updraft and fluidized bed gasifiers are commonly used for direct heat applications. Updraft gasifiers are preferred in systems rated below 1 MW thermal power while fluidized bed gasifiers are appropriate above this value (Beagle, 1978).

4.7.2 Power Generation

An attractive application of a gasification system is an internal combustion engine coupled to a generator or pump set to generate shaft power. This type of system is referred to

as power gasifier. The shaft power can be used in electricity generation, irrigation, vehicular power and milling. For reliable and efficient operation of internal combustion engines on producer gas, the gas should be cleaned of all particulate matter, tars and moisture and cooled to near ambient conditions. Also, the concentration of acetic acid should not be too high (van den Aarsen et al., 1982).

Producer gas has been extensively used in diesel (compression ignition) and otto (spark ignition) engines but its combustion in gas turbines, though possible, has not been adequately demonstrated (Mendis, 1989). Spark ignition engines designed to operate on natural gas are available up to 1 MW_{el} output and have compression ratios up to 12:1 with engine speeds of 750-1500 rpm and full load thermal efficiencies of 28-32% (Mendis, 1989). The carburettor of these engines can be modified to operate entirely on producer gas. The gas-air mixture is taken into the cylinder instead of the normal gasoline-air mixture (Hos and Groeneveld, 1987). Ignition is provided in the normal way. Diesel engines (often referred to as compression ignition engines) operated on producer gas consume a certain percentage of diesel fuel (about 5-10% of the total energy input at full load) for ignition (Foley and Barnard, 1985; and Hos and Groeneveld, 1987). This has an advantage in that the engine can revert to full diesel oil operation in case of lack of biomass. The maximum power output of engines running on producer gas is affected by the engine characteristics, the heating value of the gas, the proportion of diesel fuel injected and other factors. Results of field evaluation of practical biomass gasifiers in developing countries show the producer gas to have a heating value of 4-5 MJ/m^3 and an overall energy efficiency in the range 10-15% (Foley and Barnard, 1985; and BTG, 1990). The low heating value of the producer gas causes a 30-40% derating of spark ignition engines and 10-20% derating of diesel engines (Hos and Groeneveld, 1987).

Internal combustion engines are designed to run on clean high quality gas. This means that if these engines are to be fuelled by producer gas, the power gasification systems must incorporate elaborate systems for cleaning the gas of the particules, tars and moisture it

contains when it emerges from the gasifier. It was agreed at the 1989 International Pyrolysis and Gasification Conference that the maximum tar and dust content of producer gas to be used in internal combustion engines should be about 20 and 100 mg/m^3, respectively (Maniatis et al., 1989).

4.7.3 Methanol Production

The first step in the production of methanol from biomass is a gasification process. The product gas is then subjected to an extensive treatment to remove tars, acids and particulates. Carbon dioxide is also removed and a catalyst is used to promote the production of methane/hydrocarbon syngas (H_2/CO). The resulting syngas is then converted to methanol by the methanol synthesis reaction:

$$CO + 2H_2 \rightarrow CH_3OH \tag{4.13}$$

Methanol is a clean-burning material that may find widespread future uses such as: (i) an automotive fuel, (ii) a fuel for industrial or utility boilers, gas turbines, or fuel cells, (iii) a chemical intermediate, and (iv) a biological feedstock for protein production (Kohan, 1980).

4.8 Rice Husk Gasification

A wide variety of crop residues such as cereal straw, coffee husk, coconut shell, palm oil shell, corn stover, cotton gin trash, cocoa hull, and rice husk/hull have beeen used for gasification in fixed bed and fluidized bed gasifiers (Lepori, 1982; van den Aarsen et al., 1982; Kaupp, 1984; Walawender et al., 1986; Rei et al., 1986; Maniatis, 1990; Boateng et al., 1992; Ergudenler, 1993; and Sadaka, 1994). However, rice husk has been comparatively regarded as a difficult fuel to gasify and have, therefore, been used to a very limited extent (Beagle, 1978; Kaupp and Goss, 1981; and Mahin, 1990). A number of studies have been done on steam

gasification of rice husks (Chen and Rei, 1980; Maniatis, 1990; and Boateng et al., 1992). Relatively speaking, air gasification of rice husks in fluidized bed gasifiers is sparsely reported in the literature.

van den Aarsen et al. (1982) gasified rice husk in an air-blown 50 kg/h fluidized bed pilot-scale gasifier using an electrical heat source and compared their results with those obtained for beech wood. They observed that the tar level in the produced gas from the rice husk was two to six times higher than that from beech wood. In an attempt to reduce the tar content of the produced gas in rice husk gasification, Rei et al. (1986) resorted to catalytic gasification and steam reforming. Their results revealed that continuous steam reforming in a fluidized bed reactor of Ni catalyst increased the gas yield; hydrogen reached 65% of the produced gas composition at reaction temperatures between 600 and 700°C. Although these results are encouraging, Boateng et al. (1992) commented that the economic viability of such a process is questionable because of the high cost of the Ni-based catalyst. In addition, these catalysts are not availlable in developing countries which are usually the major rice producers.

In their study of rice hull steam gasification in a bench-scale fluidized bed, Boateng et al. (1992) found that the produced gas was rich in hydrogen and had a heating value ranging between 12.1 and 11.1 MJ/m^3 at the respective reactor temperatures of 700°C and 800°C; energy recovery varying between 35 and 59%. In their study, the reactor section was heated externally by means of electrical resistance heaters capable of delivering up to 1200 W of power. Thus, the quality of the generated gas may be deceiving.

Maniatis (1990) investigated the air-steam gasification of three types of agricultural residues (rice husk, coconut shell and palm oil shell) in a laboratory scale fluidized bed pilot plant gasifier. The steady state temperature varied in the range of 555-970°C but optimum performance was found in the range of 650-750°C. The higher heating value of the gas and the thermal efficiency varied in the ranges of 1.5 to 6.2 MJ/Nm^3 and 20 to 85%, respectively, rice

husks giving consistently lower values under comparable experimental conditions. The author also employed a continuous external energy input to the system in the form of electrical resistance heating elements.

Chen and Rei (1980) gasified rice husks over a temperature range of 873 to 973 K using super heated steam as fluidizing gas in an electrically heated 0.05 m I.D. fluidized bed gasifier. They produced 0.38-0.55 m^3/kg DAF gas, consisting of 51.1-52.2% carbon monoxide, 3.6-13.1% hydrogen, 13.5-14.4% methane, 14.6-23.0% carbon dioxide with a heating value of 16.8-18.5 MJ/m^3. The super heated steam used and the external energy input resulted in higher than expected heating values.

A rice husk fuelled fluidized bed gasifier was developed to the prototype stage in the USA (BTG, 1990). This gasifier operates on high pressure steam at a temperature between 600 and 740°C to produce a gas with an energy content of 13.6 MJ/m^3. As of 1995, the design was still being tested.

There are a series of problems associated with any consideration of rice husk utilization as a gasification fuel. These include rice husk handling and storage, feeding characteristics and ash composition (Beagle, 1978; Kaupp and Goss, 1981; van den Aarsen et al., 1982; Cruz, 1984; Jenkins et al., 1984; Kaupp, 1984; Manurung and Beenackers, 1985; Foley and Barnard, 1985; BTG, 1990; and Mahin, 1990).

4.8.1 Rice Husk Handling and Storage

The low bulk density of rice husks (100-150 kg/m^3) imposes problems in volume handling and increases transportation costs. On the other hand rice husk does not require any pre-treatment other than keeping it dry (Mendis, 1989). Rice husks are easily drifted by wind when stored in outdoor piles due to their low bulk density. The storage of rice husks in a warehouse requires large volumes also due to their low density, which makes them expensive

to store and their use uneconomical when compared to the value to be derived from their commercial utilization (Beagle, 1978).

To be economically competitive as an energy source, the handling, transportation and storage of large quantities of the fuel at a processing site must be accomplished at low costs (Jenkins et al., 1984). BTG (1990) suggested the utilization of rice husks at the rice mill where it is produced or its immediate vicinity. Briquetting and pelletization of rice husk to provide a cleaner, more easily handled, denser fuel have been attempted (Kaupp, 1984). However, the abrasive nature of rice husk and the need for a binding component (eg. wood resin) which is lacking in rice husks increases the net cost of the process. In addition, the extra energy needed for pressing the husks have so far prevented the commercial use of briquettes and pellets (Bento, 1989).

4.8.2 Rice Husk Feeding Characteristics

The feeding mechanism of a fuel is affected by its size, shape, bulk density, moisture content and composition (Kaupp, 1984). Rice husks are normally fed into small gasifiers by hand from sacks; medium sized gasifiers are fed manually or by means of a conveyor through a hopper; and larger gasifiers are usually fed continuously using conveyors, screw feeders or pneumatic conveying equipment (BTG, 1990).

Overhead feeding of rice husks produces a dirty gas as a direct result of particle entrainment which in turn increases the costs of gas cleaning and fuel loss (Manurung and Beenackers, 1985; and Maniatis et al., 1989). This feeding method is, therefore, limited to high density fuels which are less likely to be entrained out of the gasifier with the exiting gases (Maniatis et al., 1989). Direct feeding to the bed require the feeding system to be isolated from the gasifier otherwise back-flow of the tars can easily occur. If this happens on a significant scale, the tars can condense on the feeding mechanism and cause excessive wear (Corella et al., 1989). Feeding fuel from the bottom of the gasifier by means of a pneumatic conveying

equipment results in good mixing and better fuel distribution within the bed (Ghaly et al., 1989d). The adaptability of rice husks to pneumatic conveying is an important feature used in most rice husk handling systems (Beagle, 1978).

It has been reported that low density fuels must be fed directly into the bed to avoid instant escape from the gasifier (Ghaly et al., 1989e). In order to ensure uniformity of fuel and temperature distribution, especially in fluidized bed gasifiers, Ergudenler and Ghaly (1991) recommended direct feeding from the bottom centre of the distributor plate.

4.8.3 Rice Husk Ash Composition

Rice husks have a hard silica skeleton with a series of minute projections which interlock with those of adjacent husk and prevent free flow of fuel. This increases the tendency for bridging of the fuel to occur across the gasifier. Hot spots can also form in the fuel bed resulting in dome-like structures of fused material which may block the gasifier (Kaupp and Goss, 1981; and Foley and Barnard, 1985). Normally, a high proportion of the carbon, about 50% by weight of the total residue, remains behind supported by the silica and making rice husks extremely difficult to gasify completely (Foley and Barnard, 1985; and BTG, 1990). Rice husks have a high ash content of 15-24% by weight in comparison with 1-2% for wood (Kaupp, 1984). Processing rice husks at temperatures higher than the melting point of the ash (~ 1600°C) can result in the fusion of the ash to form slag or clinker. This can reduce or block the free flow of air, rice husks and gas in the reactor (Kaupp, 1984; Manurung and Beenackers, 1985; and Maniatis et al., 1989).

4.9 Fluidized Bed Hydrodynamics

Fluidization is defined as the process by which fine solid particles are transformed into a fluidlike state through contact with a gas or liquid (Grace and Clift, 1974). When a fluid is passed through a bed of particles at low velocity, a drag force is exerted on the particles by the fluid flowing through the interstitial or void spaces between the stationary particles. As the velocity of the fluid is increased, the pressure drop across the bed increases while the bed remains stationary. Increasing the velocity to a point such that the particles are kept in suspension, i.e., their weight is balanced by the buoyancy and the drag due to the fluid, the particles start behaving like a dense liquid and the bed is considered to be just fluidized. This state is usually referred to as an incipiently fluidized bed or a bed at minimum fluidization, and the corresponding fluid velocity is the minimum fluidization velocity. The ability to have solid particles behave as a liquid has been exploited in a number of technologies such as fluidized bed gasifiers (Ghaly et al., 1986; Grace, 1986; Grace and Lim, 1987; BTG, 1990).

Increasing the fluid flow rate above that for incipient fluidization produces expansion of the suspension. This additional expansion may occur uniformly, and is called homogeneous or particulate fluidization, or through the appearance of instabilities with the formation of bubbles and channels, and is called bubbling, aggregative or heterogeneous fluidization (Sun and Grace, 1992). The bubbles are relatively stable structures which rise through the bed, have sharp boundaries and are almost completely free of particles. Further increase in the fluid flow produces larger bubbles, which coalesce and grow as they rise, spanning the entire cross section of the bed and culminating into a slugging state. Further increases can eventually lead to the transport of the whole bed out of the column.

However, fluidized beds are often operated in the bubbling regime and rarely in the particulate regime. The motion of bubbles through the fluidized bed effectively stirs the bed. The large surface area of the suspension provides good transfer of heat and mass between the

fluid and the particles. The stirring action of the bubbles provides a nearly uniform temperature. However, fluid passing through the bubbles can bypass some of the solids. The split of fluid flow between the bubbles and the suspension, and the exchange of fluid between bubbles and suspension, determine the behaviour of a fluidized bed reactor (Grace, 1986; Geldert and Rhodes, 1992; and Gogolek and Grace, 1995).

The operation and behaviour of a fluidized bed system is strongly influenced by the system hydrodynamics, which, in turn, is a function of bubble dynamics within the bed. The particulate phase motion caused by the rising bubbles is the primary source of solids mixing in bubbling fluidized beds. This particulate motion, in turn, causes temperature uniformity and high bed/surface heat transfer coefficients which is characteristic of fluidized beds.

4.9.1 Bubble Characteristics

Bubbles in a fluidized bed are rising gas voids that may be followed by some solid particles. An idealized bubble is shown in Figure 4.9. The general shape of the bubble has been identified using fast photography techniques (Grace and Clift, 1974) and x-rays (Rowe and Masson, 1980). The upper surface of a bubble is approximately spherical in shape and the slightly indented base occupied by solids moving upward together with the bubble is known as the wake. Studies by Clift (1986) showed that the wake angle ranged from 90° to 134°. The wake is measured either by the angle from the nose to the start of the indentation or the wake volume relative to the bubble volume. Rowe and Patridge (1965) measured the wake fraction for several different solids and found that the wake fraction decreases with increasing particle size and increases with particle roughness or angularity. For particles from 100 to 600 μm the wake fraction was from 0.22 to 0.28. This is one of the causes of the change in particle mixing characteristics between different group of particles.

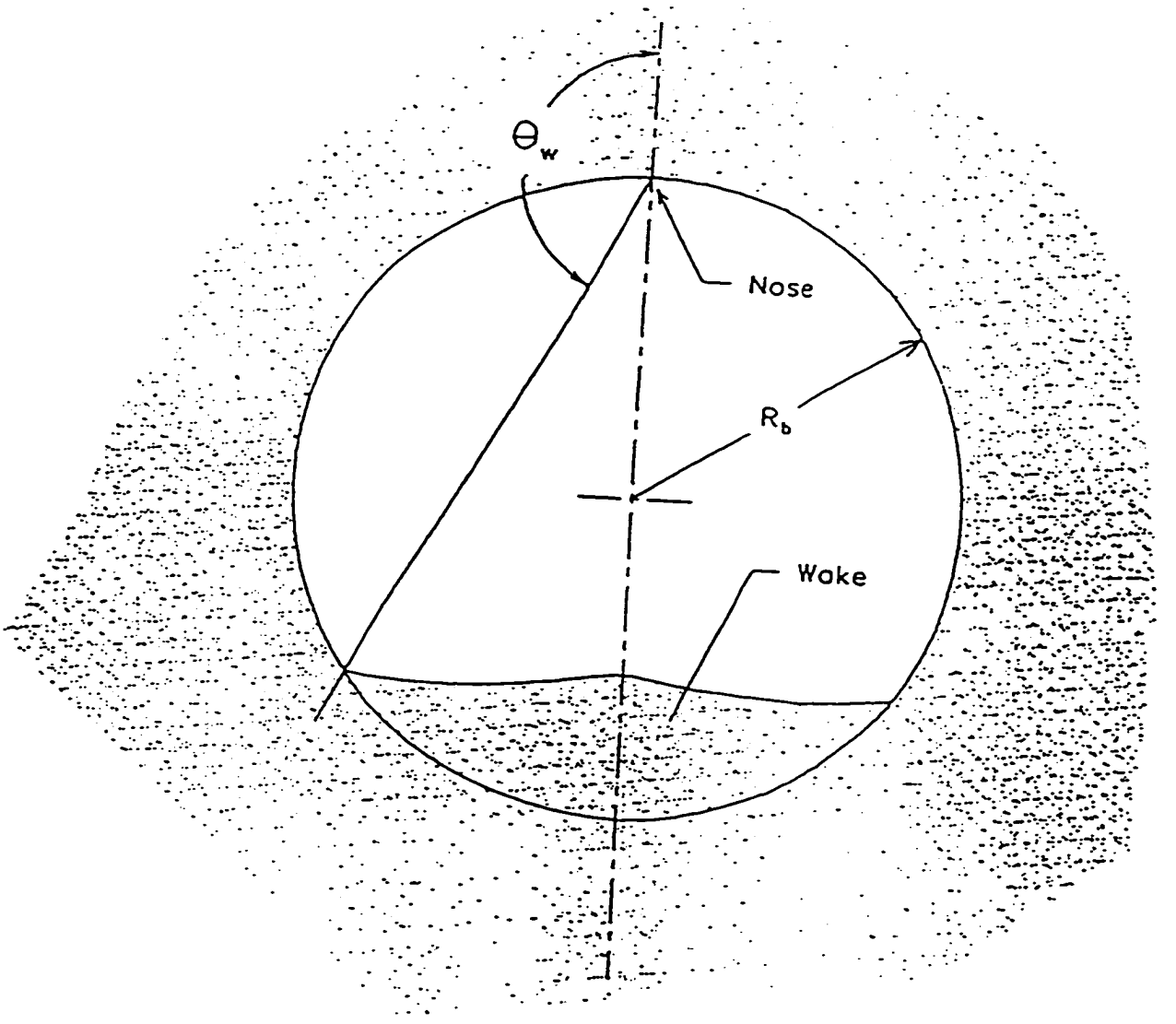

θ_w = Wake Angle

R_b = Bubble Radius

Figure 4.9 Bubble Structure (Gogolek and Grace, 1995).

The visible flowrate in a fluidized bed (Q_b) is defined as the rate at which bubble volume crosses any level in the bed. The flow of gas in the bubble phase is greater than the visible bubble flowrate because of the bulk throughflow of gas into and out of each bubble. The two-phase theory of fluidization proposed by Toomey and Johnstone (1952) and developed by Davidson and Harrison (1963) is used to give a first estimate of the visible flowrate in a fluidized bed. This theory models a fluidized bed as consisting of two phases: a particulate phase in which the flowrate is equal to the flowrate for incipient fluidization (i.e. the voidage is essentially constant at minimum fluidization voidage); and a bubble phase which carries the additional flow of fluidizing fluid. Applying this model, the visible bubble flowrate can be estimated as the excess gas flow above that required for minimum fluidization as follows:

$$Q_b = A_t\left(U_o - U_{mf}\right) \tag{4.14}$$

where:

Q_b is the volumetric bubble flow rate (m^3/s)

A_t is the bed cross-sectional area (m^2)

U_o is the superficial gas velocity (m/s)

U_{mf} is the minimum fluidization velocity (m/s)

The rise velocity of an isolated bubble is given by Cranfield and Geldart (1974) as follows:

$$U_b = 0.711\sqrt{gd_{eq}} \tag{4.15}$$

where:

U_b is the rise velocity of an isolated bubble (m/s)

g is the gravitational acceleration (m/s^2)

d_{eq} is the volume-equivalent bubble diameter (m)

Clift (1986) conveniently expressed bubble size as its 'volume-equivalent diameter', i.e. the diameter of the sphere whose volume is equal to that of the bubble, as follows:

$$d_{eq} = \left(\frac{6V_B}{\pi} \right)^{\frac{1}{3}} \tag{4.16}$$

where:

V_B is the bubble volume (m^3)

The rise velocity for an isolated bubble, Eq. (4.15), is relative to stationary solids. In regions of solids flow, the absolute bubble velocity needs to be adjusted. Coalescence also changes bubble rise velocity and direction. A common adjustment to account for the changes in a freely bubbling bed was given by Davidson and Harrison (1963) as follows:

$$U_A = \left(U_o - U_{mf}\right) + U_b \tag{4.17}$$

where:

U_A is the average velocity of a bubble in a freely bubbling bed (m/s)

4.9.2 Bubble Formation and Jetting

Bubbles form as the gas enters the bed and the formation process depends on the configuration of the distributor (Miwa et al., 1972). For a porous distributor plate, bubbles were assumed to form according to a dense packing on a triangular pitch and the volumetric flow of the bubbles accounts for the gas in excess of minimum fluidization. This gives the following expression (Miwa et al., 1972):

$$d_{bo} = 3.69\left(\frac{U_o - U_{mf}}{g}\right)^2 \tag{4.18}$$

where:

d_{bo} is the initial bubble diameter (m)

For a perforated distributor plate, bubble formation at an orifice in a liquid was adopted, with detachment occuring when the rise velocity exceeds the expansion due to the filling by the gas giving the following expression (Davidson and Schuler, 1960):

$$d_{bo} = 1.38\left(\frac{(U_o - U_{mf})A}{n_{or}}\right)^{0.4} \tag{4.19}$$

where:

n_{or} is the total number of orifices in distributor (-)

Addis et al. (1991) investigated bubble formation at a bolt distributor with four horizontal orifices. At low velocities, bubbles form at each of the orifices. At high velocities the four streams coalesced at the top of the bolt to form a single bubble. For high velocities employed in combustors and gasifiers the overlapping condition is generally met and Eq. (4.18) then applies.

Depending on the momentum of the fluidizing gas forced into the fluidized bed, a permanent jet may or may not form at the orifice. When a permanent jet forms, it may penetrate right to the bed surface, or it may form a void from the top of which bubbles break away in an almost periodic manner. When a jet is not formed, elongated bubbles tend to develop and break away from the orifice itself, with a frequency in the range 5-20 Hz (Roach, 1993). Knowledge of which types of behaviour will occur is of considerable importance for

applications of fluidized beds. Understanding the fluid mechanics and transfer processes in the distributor region is critical to the successful modeling of fluidized bed reactors.

Grace and Lim (1987) showed that a permanent jet forms only if the following condition is satisfied:

$$\frac{d_{or}}{d_p} \leq 25.4 \tag{4.20}$$

where:

d_{or} is the jet nozzle or orifice diameter (m)

d_p is the particle diameter (m)

Equation (4.20), which is shown to delineate quite effectively between jets and bubbles for a wide range of data, is also the criterion for spouting (Grace and Lim, 1987). Massimilla (1985) suggested that jet formation is more likely with coarser and lighter particles, low superficial gas velocity, increased fluid density and increased orifice velocity.

In their study of vertical jets at the walls of a cylindrical bed, Markhevka et al. (1971) observed that the bottom region of a jet is conical and that bubbles form in a regular pattern at the end of the jet. Since the sand blasting effect of a high velocity jet will likely cause extreme erosion on the vessel internals (Baldyga et al., 1994), knowledge of jet penetration depth into the bed is important for design purposes.

Several correlations have been proposed to relate the jet penetration length to bed hydrodynamics and physical parameters. However, all the correlations are derived from jets at low temperatures and near atmospheric pressures except that of Yang (1981) which covers a wide range of pressures. Observing erosion marks on reactor walls caused by jets, Clift et al.

(1991) compared several correlations for jet penetration depth and suggested that only the correlation of Merry (1975) gave reasonable predictions of jet penetration depth at high temperature conditions. This correlation is given as follows:

$$\frac{L_j}{d_{or}} = 5.2\left(\frac{\rho_g d_{or}}{\rho_s d_p}\right)^{0.3}\left[1.3\left(\frac{U_{0r}^2}{g d_{or}}\right)^{0.2} - 1\right] \qquad (4.21)$$

where:

L_j is the jet penetration depth from the nozzle (m)

ρ_g is the fluid density (kg/m^3)

ρ_s is the particle density (kg/m^3)

U_{or} is the jet nozzle velocity (m/s)

Gas jets are regions of very high gas and solids velocity. Solid surfaces in the jet region are, therefore, subject to rapid erosion as a direct result of this property of gas jets (Clift et al., 1991). For distributor plates which introduce gas vertically into the bed, the jet penetration determines the lowest level at which surfaces such as heat exchange tubes should be located, and imposes a lower limit on operating bed depth. In addition, the jet region provides enhanced mass and heat transfer between phases.

4.9.3 Bubble Growth and Coalescence

Bubbles interact as they rise in the bed after detachment from the distributor (Gogolek and Grace, 1995). Several researchers have investigated the coalescence of a pair of bubbles (Clift and Grace, 1985; and Clift et al., 1991). In the coalescence process, the leading bubble spreads horizontally as the trailing bubble elongates and accelerates into the wake of the leader. The volume of the two bubbles increases by 20-30% during coalescence, followed by a 10% decrease during consolidation after wake entry, giving a net volume increase of 10-20%. There is increased gas flow through the emulsion between the bubbles, which has implications for

interphase transfer and reactor modeling. For bubbles with moderately large clouds, the clouds can join even while the bubbles are significantly separated (Gogolek and Grace, 1995).

Bed hydrodynamics are closely related to the bubble diameter in the bubbling region. It is assumed that bubbles are uniform in size at any cross section of the bed but grow by coalescence with other bubbles while rising through the bed. Mori and Wen (1975) proposed a semi-empirical correlation for bubble growth using the initial and maximum bubble sizes as follows:

$$d_b = d_{bm} - (d_{bm} - d_{bo})\exp\left(-\frac{0.3z}{d_t}\right) \tag{4.22}$$

where:

d_b is the bubble diameter (m)

d_t is the average bed diameter (m)

d_{bm} is the maximum attainable bubble diameter (m)

z is the bed height (m)

The initial bubble diameter (d_{bo}) is given in Equations 4.18 and 4.19 and the maximum bubble diameter (d_{bm}) is given as follows:

$$d_{bm} = 2.34\left[d_t^2 \frac{(U_o - U_{mf})}{\sqrt{g}}\right]^{0.4} \tag{4.23}$$

The size of bubbles in a gas fluidized bed affects bed expansion, solids entrainment, in-bed heat transfer, solids mixing as well as the conversion and selectivity of chemical reactions (Gogolek and Grace, 1995; and Gogolek and Becker, 1992). This means a thorough

knowledge of bubble size in a fluidized bed is necessary for its design, operation and simulation.

In their review of literature on particle size correlations, Gogolek and Becker (1992) found that the assumption of the bubble size being proportional either to the excess gas velocity ($U - U_{mf}$) or to the ratio (U/U_{mf}) is common to all the correlations reviewed. They reported that U_{mf} decreased with increasing bed temperature. The temperature influence on the size and growth of bubbles in a fluidized bed is a consequence of the effect on the U_{mf}, which affects bubble stability in systems such as fine catalyst beds with appreciable splitting (Clift and Grace, 1985). This also influences the coalescence mechanism of small bubbles in fluidized beds (Clift, 1986). An increase in bed temperature will, therefore, result in a decrease in bubble size.

Jaraiz et al. (1992) found that increasing pressure decreased bubble size in beds of group A particles and has no effect on the bubble size in beds of group B particles. Weimer and Quarderer (1983) explained the decrease in bubble size in beds of group A particles with pressure to be strongly influenced by particle size, the decrease being greatest with small particles.

4.9.4 Bed Particle Characteristics

Fluidized bed reactors contain solid particles of inert material which act as a store house for heat and which transfer heat to the fuel particles during contact. The most widely used inert material is sand. Mixtures of sand and alumina, sand and gravel, and sand and limestone have also been used as bed materials in some cases (Baeyens et al., 1992). Different mixtures of bed material are used to avoid agglomeration of the bed due to formation of alkali salts during the gasification of certain fuels, or to enhance the conversion process due to the catalytic effect of the bed material (Arastoopour et al., 1989). The major bed particle characteristics affecting the quality of fluidization in a fluidized bed are particle size, particle size distribution, particle density, particle shape and surface roughness (Baeyens et al., 1992).

Geldart (1986) classified solids fluidized by gases into four principal groups according to their fluidization behaviour at atmospheric temperature and pressure. These groups, usually characterized by density difference and mean particle size, are presented in Table 4.11 in order of increasing particle size (C, A, B and D). Group C powders are small particles (<20μm), having irregular shape, strong electrostatic charges and sticky surfaces. These properties of group C powders give rise to significant interparticle forces resulting in extreme fluidization difficulties. Group A powders have low particle density (<1400 kg/m^3) in the size range of 20-100μm. These powders are characterized by considerable stable bed expansion beyond the point of minimum fluidization before bubbling starts and, therefore, flow freely in the fluidized state. With group B powders having large (40-500μm) and dense particles (1400-4000 kg/m^3), bubbling starts at or slightly above the minimum fluidization velocity. Group D powders consist of large (usually > 600μm) and/or dense particles which give rise to an unstable bed behaviour as a result of the largest bubbles rising at lower rate than the interstitial fluidizing gas.

Sun and Grace (1992) investigated the effect of particle size distribution on the performance of fluidized bed reactors in different fluidization regimes using three particle size distributions (narrow, wide and bimodal) with the same mean diameter (d_p = 60μm), about the same density and surface area. The results indicated that the wide particle size distribution gave smaller voids and earlier transition from bubbling or slugging to turbulent or fast fluidization which significantly improved the reactor performance. The results further revealed that as the particle size distribution broadened, the aeration capacity increased and the dense-phase viscosity decreased. The lower the bed viscosity, the more likely voids will split (Yates et al., 1994). Zhao et al. (1994) also reported that a wide particle size distribution gave a greater air retention capacity than narrow or bimodal distribution.

De Grooth (1967) measured particle diffusivities with catalyst material of two size distributions in beds of diameter up to 1.5 m, and found that the beds of wider size distribution catalyst displayed better mixing and less sensitivity to the scale of the equipment. For reliable

Table 4.11. Classification of Powders (Geldart, 1986).

Group	C	A	B	D
Most obvious characteristic	Cohesive, difficult to fluidize	Bubble-free range of fluidization	Starts bubbling at U_{mf}	Coarse solids
Typical solids	Flour cement	Cracking catalyst	Bubbling sand, table salt	Crushed limestone, coffee beans
Properties				
1. Bed expansion	Low when bed channels (can be high when fluidized)	High	Moderate	Low
2. Deaeration rate	Initially fast (exponential)	Slow (linear)	Fast	Fast
3. Bubble properties	No bubbles, Channels, cracks	Splitting/recoalescence predominate, maximum size exists and large wake	No limit on size	No known upper size, small wake
4. Solids mixing	Very low	High	Moderate	Low
5. Gas backmixing	Very low	High	Moderate	Low
6. Slug properties	Solids slugs	Axisymmetric	Axisymmetric, asymmetric	Horizontal voids, solids slugs, wall slugs
7. Spouting	No	No (except in very shallow beds)	Shallow beds only	Yes (even in deep beds)
effect on properties 1 to 7 Mean particle size within group	Cohesiveness increases as d_p decreases	Properties improve as size decreases	Properties improve as size decreases	Not known
Particle size distribution	Not known	increasing < 45 μm fraction improves properties	None	Increased segregation
Increasing pressure, temperature, viscosity and density of gas	Probably improve	Definitely improve	Uncertain, some possibly improve	Uncertain, some possibly improve

fluidization, the average particle size should be in the range of 50 to 60μm and the relative densities of the gas and solid should be very close (Volk et al., 1962). The shape of the particles influences the mixing characteristics of the sand and fuel particles mixture. In a study of a bed containing a mixture of non-uniform particles, Nienow et al. (1978) found that the segregation of the particles is affected by their shape.

4.9.5 Particle Mixing and Circulation

A thorough knowledge of particles mixing characteristics and circulation patterns resulting from bubble behaviour in the bed is essential for maximum bed utilization. Particle circulation is essential where bed homogeneity is required and of particular interest when solid feed streams must be rapidly and totally dispersed in order to avoid localized accumulations (Baeyens and Geldart, 1986; and Rowe, 1993).

Bubbles enhance solids mixing in a number of ways. Clift (1986) reported that solids move in a net horizontal direction largely by being (a) carried up to the surface where they are dispersed sideways by bursting bubbles and (b) carried down to, and across, the distributor by bubble-free flows of dense phase material. Fan et al. (1979) stated that coalescing of non-aligned bubbles causes radial mixing; larger rising bubbles enhancing lateral mixing more than smaller bubbles. In a model study, Pereira et al. (1981) found that bubbles coalescence to enhance interphase mass transfer.

As a bubble rises, the solids in the wake are intermittently shed and replaced by solids from the surrounding emulsion phase (Clift and Grace, 1985). This cross-flow of solids in the bubble-wake contributes significantly to solids mixing, which in turn causes the high rates of heat transfer and temperature uniformity found in fluidized beds. No gas-solid interactions are considered to take place in a bubble since it contains no solids; only homogeneous gas-phase reactions are considered to take place.

In their study of mixing mechanisms, Rowe and Partridge (1965) disturbed layers of coloured and colourless particles by injected bubbles and observed the movement of particles in two-dimensional beds. They observed that particles move upwards in the wake of the bubble and in the drift. The particles appear to be pulled into the wake or drift, carried up the bed for a distance (where bubbles are present) and then downwards where there are no bubbles.

Grace and Lim (1987) reported that the directional probability of bubble coalescence causes non-uniform bubble distribution patterns in freely bubbling fluidized beds. They observed that areas close to the wall region have fewer bubbles, and bubbles which are initiated in this wall region at the distributor are attracted towards other bubbles close to the centre but can themselves attract only a limited number. As a consequence of an almost bubble free zone near the wall, particles flow downwards near the wall. Once established, this return flow of solids tends to maintain the tendency for bubbles to move inward from the walls.

Baeyens and Geldart (1986) stated that at equal excess gas velocities the flow patterns and solids downflow velocities are similar in different bed sizes having the same aspect ratio. They also reported that at low velocities bubble-rich regions occur close to the corners leaving bubble-free regions close to the walls and in the centre. The bubble-rich region was found to increase at higher velocities and further increases in velocity led to a reversed pattern; an upward flow in the centre and a downward flow at the walls.

4.9.6 Segregation in Multicomponent Systems

Segregation occurs when there is a substantial difference in shape, size and/or in density between different particles. It is more pronounced at low gas velocities especially when there is an appreciable particle density difference. Even a strongly segregating system, however, can be fairly well mixed if the gas velocity is increased sufficiently although it can be difficult to remove the last traces of segregation (Beeckmans and Yu, 1992; and Rowe, 1993).

Nienow et al. (1978) have done a considerable amount of work on segregation caused by density differences and have called the component that tends to sink 'jetsam' and that which tends to float 'flotsam'. When fluidized, the upper part of the bed will attain a fairly uniform composition, while the component that tends to sink forms a concentrated bottom layer. It is possible for a defluidized jetsam layer to form at the bottom of the bed, leading to catastrophic failure in the reactor. This also has implications for experimental procedures, such as the determination of minimum fluidization (Gogolek and Grace, 1995).

Multicomponent fluid beds at steady state are flotsam-rich on top and jetsam-rich at the bottom. The overlaying of solids at the top by bubbles bursting and the downflow regions act to take the flotsam back into the bed; particles descend until swept upwards by a bubble. The mean penetration depth of the flotsam particles is a good measure of the quality of mixing in the bed, deeper penetration indicating better mixing (Rowe and Nienow, 1976).

Baeyens and Geldart (1986) proposed the following two parameters to describe a quantitative measure of segregation:

(a) The coefficient of segregation is defined as follows:

$$C_s = \left(\frac{x_B - x_T}{x_B + x_T} \right) X 100 \qquad (4.24)$$

where:

C_s is the segregation coefficient

x_B is the concentration of the material in the bottom half of the bed (-)

x_T is the concentration of the material in the top half of the bed (-)

$-100 < C_S < +100$ per cent, 0 per cent being perfect mixing.

(b) The degree of mixing is described by the mixing index, M_I, as follows:

$$M_I = \frac{x}{\bar{x}} \tag{4.25}$$

where:

M_I is the mixing index (-)

x is the concentration of the material under scrutiny at some level in the bed (-)

$\bar{x}$ is its average concentration (-)

The mixing index can have values between 0, for complete horizontal segregation, and 1, for complete mixing. At low gas velocities (but greater than U_{mf}) a layer of pure jetsam forms at the bottom with some remaining uniformly dispersed in the upper part of the bed contaminating the pure flotsam. Increasing the gas velocity (or decreasing the particle density difference) causes the proportion of jetsam in the upper region to increase and the bottom layer becomes thinner. The concentration of jetsam in the upper region compared with its overall value is a good measure of the degree of mixing achieved.

Rowe and Nienow (1976) showed that the mechanism by which mixing and segregation occurs in fluidized beds can be revealed mainly through observations of two differently coloured components pre-arranged in some particular pattern. Arranging the bed with pure jetsam in the upper part, it is found to be undisturbed until approached by a bubble. With the arrival of a bubble, jetsam collapses into it partly because the gas velocity needed to move flotsam particles is inadequate to move jetsam particles which are larger and denser. A certain amount of unsteady-state also occurs in the path just before the bubbles particles recover hydrodynamic equilibrium. The net result is that an area of jetsam particles, approximately equal to the frontal area of the bubble, descend an average distance of about a bubble diameter. With pure jetsam at the bottom and pure flotsam above, some mixing is

observed to occur. As a bubble forms, within the jetsam if it is fluidized or at the interface if it is not, it develops a wake wholly or partially composed of jetsam. This jetsam ascends with spillage and is dispersed in the upper region. An overall circulation of the particles then occurs in a manner similar to natural convection if the bed is vigorously bubbling. Rowe and Nienow (1976) explained the mechanism by which large and dense particles move downwards in the bed as the fall of particles through the free space of bubbles.

Segregation is affected by a number of factors. It is well known that particle density is a much stronger factor affecting the degree of segregation in a gas fluidized bed than particle size and shape. A wide range of particle size can be tolerated in a gas fluidized bed which will remain homogeneous whereas quite small density differences make separation possible (Rowe and Nienow, 1976). Other factors that affect the degree of segregation in a gas fluidized bed are mixture composition, superficial gas velocity and increasing jetsam fraction (Rowe and Nienow, 1976; and Gera and Guatam, 1994).

Gas velocity is the most important and complex factor in determining segregation. It is clear from mixing and segregation studies that the important quantity is the excess flow over the minimum fluidization value ($U - U_{mf}$), which in turn depends on the composition of any mixture and on the ratio of particle diameter and density. Nienow et al. (1978) showed that the degree of mixing varies with gas velocity. Considering a fully segregated system, mixing at first increases only slowly with increasing gas velocity, the rate of increase rises to a maximum and then decreases again as the mixture approaches perfection.

Studies by Rowe and Nienow (1976) showed that when jetsam is present in abundance complete stratification becomes unusual except at velocities near minimum fluidization velocity. They observed that it is not really different in kind from the case where the proportions are reversed but the range of gas velocity and density ratio over which appreciable segregation

occurs is much reduced. The reason given for this change is that under moderate bubbling conditions the bulk of jetsam develops the characteristic convective motion.

4.9.7 Minimum Fluidization Velocity

The minimum fluidization velocity (U_{mf}) is a very important variable in the design of fluidized bed reactors and can generally be defined as the minimum superficial gas velocity at which the pressure drop through the bed is equal to the weight of the bed per unit cross-sectional area (Clift et al., 1991). It can be estimated experimentally by measuring and plotting the pressure drop across the bed at different fluid velocities and finding the intersection of the two lines as shown in Figure 4.10.

The minimum fluidization velocity sets the gas flowrate to the fluidized bed, and it is useful in the prediction of many of the hydrodynamic properties of fluidized beds. Clift et al. (1991) showed that the bed may bubble due to channelling at lower gas velocities or may even remain unfluidized due to the extra force required to overcome inertia at velocities higher than the minimum fluidization velocity. The minimum fluidization velocity is reported to increase with the square of particle size (Sun and Grace, 1992), and to be a function of bed height (Bai, 1992). The minimum fluidization velocity of fine powders decreases as temperature increases and is not affected by pressure changes, whereas that of coarse particles increases with temperature and decreases as pressure increases (Geldart, 1986).

Geldart (1986) gave the following correlations to estimate the minimum fluidization velocity, U_{mf}:

(a) For particles greater than 100 μm:

$$U_{mf} = \left(\frac{\mu}{\rho_g d_p}\right)\sqrt{1135.7 + 0.0408Ar} - 33.7 \qquad (4.26)$$

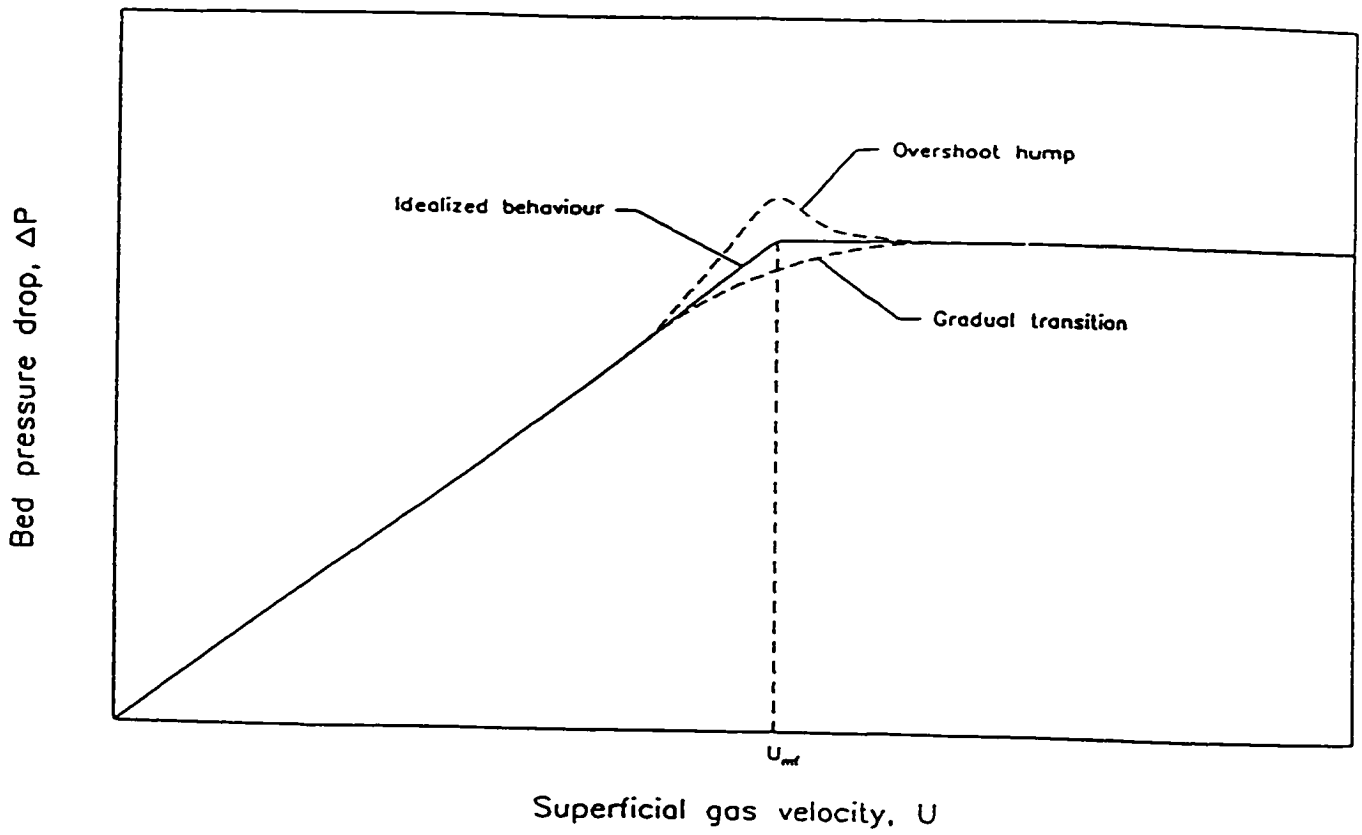

Figure 4.10. Pressure Drop-Superficial Gas Velocity Relationship (Gogolek and Grace, 1995)

where:

μ is the gas viscosity (Ns/m^2)

ρ_g is the gas density (kg/m^3)

Ar is the Archimedes number (-) given as follows:

$$Ar = \frac{d_p^3 \rho_g (\rho_s - \rho_g) g}{\mu^2} \tag{4.27}$$

where:

ρ_s is the sand particle density (kg/m^3)

(b) For particles less than 100 μm:

$$U_{mf} = \frac{(\rho_s - \rho_g)^{0.934} g^{0.934} d_p^{1.8}}{1111 \mu^{0.87} \rho_g^{0.066}} \tag{4.28}$$

Relating the force owing to the pressure drop to that arising from the bed weight and using Ergun's equation (Ergun, 1952), U_{mf} for a single component gas fluidized bed of spherical particles can be estimated as follows:

$$U_{mf} \propto \frac{\varepsilon_{mf}}{1 - \varepsilon_{mf}} \rho d_t^2 \tag{4.29}$$

where:

ε_{mf} is the bed voidage at minimum fluidization (-)

ρ is the average bed density (kg/m^3)

Assuming a constant voidage, Chiba et al. (1979) gave the following general equation to determine the minimum fluidization velocity of binary mixtures of different particle densities or sizes:

$$U_{mf} = U_F\left[f_{VF} + (1 - f_{VF})\frac{\rho_P}{\rho_F}\right]^{0.95}\left[X_F + \left(\frac{\rho_P U_F}{\rho_F U_P}\right)^{0.54}(1 - X_F)\right]^{-1.85} \qquad (4.30)$$

where:

U_F is the fluidization velocity of particles having larger minimum fluidization velocity (m/s)

U_P is the fluidization velocity of particles having smaller minimum fluidization velocity (m/s)

ρ_F is the density of particles having larger minimum fluidization velocity (kg/m^3)

ρ_P is the density of particles having smaller minimum fluidization velocity (kg/m^3)

X_F is the weight fraction having larger minimum fluidization velocity (-)

The term f_{VF} is determined as follows:

$$f_{VF} = \frac{1}{\left[1 + \left(\frac{1}{X_F}\right)\left(\frac{\rho_F}{\rho_P}\right)\right]} \qquad (4.31)$$

Defluidization may occur at any point in the bed if the operating gas velocity is less than the velocity of complete fluidization of particles of mixed densities or sizes (Rowe and Nienow, 1976). Defluidization is undesirable because a defluidized portion of the bed is like a fixed bed with poor mass and heat transfer, hence the exothermic fuel-oxygen reactions will cause high local temperatures and could lead to sintering of the bed material. Poor mixing could also lead to low conversion and carbon build-up in the reactor.

4.9.8 Particle Elutriation and Entrainment

Elutriation and entrainment are terms used interchangeably to describe the ejection of particles from the surface of a bubbling fluidized bed and their eventual removal from the unit in the gas stream (Geldart, 1986b). Elutriation accounts for the major loss of combustible material in fluidized bed combustion/gasification systems. Prediction of the solids loading in the exiting gas stream is helpful in designing the cyclone and other gas-cleaning equipment (Gogolek and Grace, 1995).

Many suggestions have been put forward to explain the mechanism by which particles are carried into the freeboard of fluidized beds. It has been postulated that bursting bubbles at the bed surface eject particles into the freeboard as intermittent jets. The ejection of particles becomes more vigorous if coalescence occurs as the leading bubble is bursting. Particles are then ejected from the wake of the leading bubble (Fung and Hamdullahpur, 1993). But, observations made by Geldart (1986c) at the surface of two-dimensional beds indicated that, in general, it is the nose of the bubble which ejects the particles. He maintained, however, that ejection from the wake can occur when a bubble bursts through the base of another which is itself about to break at the surface.

The rate of particle entrainment from a fluidizing column depends on a number of factors including bed diameter, size of particles, fluidizing gas velocity, freeboard height, internal surfaces and operating pressure. Lewis et al. (1962) carried out studies using beds of diameters ranging from 0.019 to 0.146 m and 0.1 m deep, and found that the carryover rate increased with decreasing diameter for diameters smaller than 0.04 m, but that there was minimal change above 0.1 m. Geldart (1986c) reported that the carryover fluxes in both 0.46 m and 1 m beds are approximately equal at equal velocities and distances above the bed.

The freeboard region significantly contributes into the reduction of particle entrainment from the bed by providing a space for particles, depending on their terminal and gas velocities,

to be disengaged from the exiting gas stream. Particles having a terminal velocity larger than the gas velocity move upwards and then fall back, thereby reducing the flux of the entrained particles. This decrease continues until a certain height above the bed is reached where the solids flux remains constant, i.e. the solids disengagement has been completed. This height is called the transport disengaging height (TDH). Above the TDH are found fines (particles with terminal velocities less than the superficial gas velocity and the most likely to be carried over).

Various correlations have been suggested to estimate the TDH. One such correlation is given by Fournol et al. (1973) as follows:

$$TDH = 1000\frac{U^2}{g} \tag{4.32}$$

Horio et al. (1980) gave the following correlation:

$$TDH = 4.47\sqrt{d_{eq}} \tag{4.33}$$

The freeboard region allows favourable gas and solids contacting with little or no tendency of the gas to separate into two phases and near plug flow for the gas. Hence, there is a low hold-up of solids in the freeboard above the dense bed surface due to this effective gas-solids contacting and lack of backmixing, coupled with the fact that entrained particles tend to be finer than those in the bed (Grace, 1986).

Geldart (1986b) postulated four phases in the freeboard region. Phase 1 is a gas stream carrying dispersed solids upwards. Phase 2 consists of agglomerates ejected upwards by the action of bubbles. Phase 3 consists of agglomerates falling downwards. Phase 4 is an emulsion, more concentrated than Phase 1, moving downwards at the wall. The mass transfer rates

between these phases depend on the gas velocity, bubble action, bed diameter, particle size and particle size distribution.

Grace (1986) postulated that three zones can be identified in the freeboard region: (a) the splash zone immediately above the bed surface, (b) the disengagement zone which extends up to the TDH level, and (c) the region beyond TDH. Particles in zones (a) and (b) move upwards and downwards amid periodic bursts of bubbles. Zone (c) is usually neglected or considered absent if the TDH is equal to the freeboard height.

Horio et al. (1980) reported that in the freeboard of a bed of group B particles, the effect of splashing is considerable and the concentration of fines is low, whereas diffusion becomes predominant at higher heights above the bed. They identified two zones, in the freeboard region: the splash and diffusion zones.

It has also been reported that in the freeboard region a dense phase layer of solids descends close to the column walls while particles move upwards away from the wall at a velocity similar to that of the gas velocity (Horio et al, 1980). Ismail and Chen (1984) have shown that solid distribution in the freeboard alternates between bursts of fairly packed packets and regions of essentially purely gas. Using a fluidized bed with immersed tubes, Andersson and Leckner (1989) showed that particle flux across the freeboard is relatively constant except near the wall where it is about twice as large as the average. In the vertical direction, the flux was found to decrease exponentially with height, except close to the bed where the decay rate was less than that at higher elevations.

The main source of turbulence in the freeboard of bubbling fluidized beds is from bubbles generated at the bed surface. Turbulence in the freeboard increases with increasing fluidizing gas velocity, increasing bed height, and decreasing particle size. Hamdullahpur and Mackay (1986) reported that turbulence is very intense in the lower section of the freeboard

because of bubble eruptions at the bed surface. It decays with distance from the bed surface until it reaches a level that is characteristic of flow at minimum fluidization velocity.

Hamdullahpur and Mackay (1986) reported that velocity fluctuations caused by bursting bubbles at the bed surface leads to highly turbulent gas motion in the freeboard. There is a fast decay of gas local mean velocity, and root-mean-square velocity profiles with freeboard height. Close to the bed surface, the horizontal gas velocity profile shows a maximum at the centre of the fluidizing column. They also reported that turbulence intensity increases as the bed depth and bubble diameter increase. Freeboard turbulence intensities of 5 to 40% have been recorded by Horio et al. (1980).

Since particle ejection from the bed results from bubble bursts, the ejection flux (E_o) can be estimated as being proportional to the volumeric bubble flow as follows (Gogolek and Grace, 1995):

$$E_o \propto (1-\varepsilon_{mf})\rho_p \frac{Q_b}{A} \tag{4.34}$$

where:

E_o is the particle entrainment flux at the bottom of the freeboard (kg/m^{2}s)

Geldart (1986c) recommended a value of 0.1 for the proportionality constant, the ratio of volume of ejected emulsion to the bubble volume.

Considering the particle flux decay with height above the bed to be exponential and approaching an equilibrium flux E_∞, Wen and Chen (1982) proposed a flux profile of the following form:

$$E_h = E_\infty + (E_o - E_\infty)\exp(-ah) \tag{4.35}$$

Values of a from 3.5 to 6.4 m^{-1} (Wen and Chen, 1982) and 1.3 to 2.5 m^{-1} (Andersson and Leckner, 1989) have been reported.

Elutriation from a fluidized bed is generally described by the following equation:

$$E_{\infty i} = K_{i\infty} w_i \tag{4.36}$$

where:

$E_{\infty i}$ is the elutriation rate of particles of size d_{pi} (kg/m^2s)

$K_{i\infty}$ is the elutriation rate constant for particles of size d_{pi} (kg/m^2s)

w_i is the weight fraction of particles of size d_{pi} in the bed (kg)

The elutriation rate constant is primarily a function of the fluidizing gas, the gas velocity, and the particle size and density.

Geldart (1986) tabulated a number of correlations for elutriation rate constant and recommended using the following equation:

$$\frac{K_{i\infty}}{\rho_g U} = 23.7\exp\left(-5.4\frac{v_t}{U}\right) \tag{4.37}$$

where:

v_t is the particle terminal velocity (m/s)

The particle terminal velocity is calculated from the following equations (Kunni and Levenspiel, 1990):

$$v_t = \frac{(\rho_s - \rho_g) g d_p^2}{18\mu} \qquad \text{Re} < 0.4 \qquad (4.38)$$

$$v_t = d_p \left[\frac{4}{225} \frac{(\rho_s - \rho_g)^2 g^2}{\rho_g \mu} \right]^{\frac{1}{3}} \qquad 0.4 < \text{Re} < 500 \qquad (4.39)$$

$$v_t = \left[\frac{3.1(\rho_s - \rho_g) g d_p}{\rho_g} \right]^{\frac{1}{2}} \qquad 500 < \text{Re} < 2\text{x}10^5 \qquad (4.40)$$

where:

Re is the Reynolds number given as follows:

$$\text{Re} = \frac{d_p \rho_g v_t}{\mu} \qquad (4.41)$$

4.10 Fluidized Bed Gasification Models

Modeling of fluidized bed reactors involve the identification and mathematical description of the most important features of the process to simplify and obtain deeper understanding. Models should be tested for sensitivity to values of various parameters. Modeling, also, requires validation against experimental data to gain acceptance (Gogolek and Grace, 1995; and Puchyr et al., 1997).

Models of fluidized bed gasifiers have several possible applications among which are: design, scale-up, evaluation of experimental data, simulation of existing units under changed

operating conditions or inputs, and process control. The fluidized bed reactor is a hydrodynamically complex system, with a large number of reactions and a wide range of time scales. Ideally, account needs to be taken of the partial oxidation of the fuel, fast pyrolysis of the fuel, gasification of pyrolysis char by means of reaction with CO_2 and H_2O, and combustion in the gas phase of volatiles and carbon monoxide. The associated fluid mechanical and thermal processes further complicate the modeling problem. For example, radiation heat transfer from the bed needs to be included when calculating temperature profiles in the freeboard.

The basis of gasification models are the material balance, energy balance, chemical reaction rates, equilibrium relationships, process kinetics and hydrodynamic features of the system. In addition, other assumptions such as steady state conditions, uniform particle temperatures, insignificant temperature gradient, isothermicity and disregarding of some reactions as not very significant, are required. The number of assumptions used determines the number of degrees of freedom in the system.

Models of fluidized bed gasification can be classified into: (a) equilibrium models, (b) single phase models, (c) two or three phase models, (d) grid models and (e) transient or dynamic models (Grace and deLasa, 1978; Raman et al., 1981; Wen and Chen, 1982; Buekens and Schoeters, 1985; and Double et al., 1989). Most of the fluidized bed models available in the literature are based on coal. The underlaying assumptions of the different models are extremely varied and the kinetics of gas-solid reactions have different origins, which makes the evaluation of these models very complex.

4.10.1 Equilibrium Models

Equilibrium models compute the generated gas composition at equilibrium. There are three cases of chemical equilibrium: (a) when there is excess carbon present in the system and char appears in the solid residue; (b) all the carbon is gasified in an excess of gasifying agent; and (c) the point between (a) and (b) usually referred to as the carbon boundary where the

carbon is completely gasified without an excess of gasifying agent (Double et al., 1989). A set of solvable equations consisting the definitions of the equilibrium constants of the reactions involved in the gasification process, material balance equations and partial pressure summation law (i.e. Dalton's law) can be derived for the cases either side of the carbon boundary or on the carbon boundary itself. The heat balance equation is also required in a case where the reaction temperature is unknown.

Double and Bridgwater (1985) developed a carbon boundary equilibrium model as a "target" against which to compare the results of real gasifiers. The gas composition and reaction temperatures predicted by the carbon boundary model were far lower than those achieved in real gasifiers. According to Buekens and Schoeters (1985), the major equilibrium models are based on heterogeneous and homogeneous equilibrium reactions.

Gumz (1950) stated that the generated gas composition can be computed on the basis of the equilibrium of the heterogeneous reactions of carbon with steam (water-gas), carbon dioxide (Boudouard) and hydrogen (methane formation) It is assumed that (a) these reactions attain equilibrium, and (b) sufficient carbon is available for reaction with those gases. However, heterogeneous chemical equilibrium is hardly attained in a fluidized bed gasifier due to low temperatures (750-850°C). It can only serve to set the trend of the variations in gas composition with operating parameters. Also, the flow of carbon and that of blast gas in a fluidized bed gasifier can be varied independently to avoid an excess of carbon under all operating conditions. Therefore, assumption (b) is, also, not completely valid.

Homogeneous equilibrium models involve mainly the two gas-phase reactions (water-gas shift and methanation). The homogeneous chemical equilibrium is likely to be attained since these reactions are generally accepted to be in equilibrium above 800-850°C (Bacon et al., 1985; and Buekens and Schoeters, 1985). A theoretical gas composition can, therefore, be derived from the feed rate and elementary composition of the solid fuel, and the flow rate and

composition of the blast gas, using a mass balance together with homogeneous reaction equilibria (Buekens and Schoeters, 1985). The operating temperature can either be varied as an independent parameter (which supposes that heat is either delivered to or possibly withdrawn from the system), or derived from an energy balance over the system, supposed to operate adiabatically.

Bacon et al. (1985) developed a mathematical model as a basis for assessing the performance of a fluidized bed wood gasifier. The authors considered the following three gasification reactions identified by Desrosiers (1981):

$$C + CO_2 \rightarrow 2CO \tag{4.42}$$

$$C + H_2O \rightarrow CO + H_2 \tag{4.43}$$

$$C + 2H_2 \rightarrow CH_4 \tag{4.44}$$

Due to the lack of kinetic information on wood pyrolysis and gasification, assigned degrees of approach to equilibrium were used to describe the overall gasification process. A modified free energy term was used and a modified equilibrium constant (K') was defined as the true equilibrium constant multiplied by the degree of approach to equilibrium (ε) as follows:

$$\ln\left(\frac{K_j'}{\varepsilon_j}\right) = -\sum_j \Delta \frac{G_{f,j}^o}{RT} \tag{4.45}$$

where:

$G_{f,j}^o$ is the free energy of formation of compound i at temperature T (kJ/kg)

R is the gas constant (kJ/kg.K)

K is the equilibrium temperature (K)

Defining

$$a = 1 - \left(\frac{RT}{\Delta G^{o}_{f,k}} \right) \tag{4.46}$$

the equilibrium constants for the three reactions were written as follows:

$$K_1 = \exp\left[- \frac{\left(a_{CH_4} \Delta G^{o}_{f.CH_4} \right)}{RT} \right] \tag{4.47}$$

$$K_2 = \exp\left[- \frac{\left(2\Delta G^{o}_{f.CO} - a_{CO_2} \Delta G^{o}_{f.CO_2} \right)}{RT} \right] \tag{4.48}$$

$$K_3 = \exp\left[- \frac{\left(\Delta G^{o}_{f.CO} a_{H_2O} \Delta G^{o}_{f.H_2O} \right)}{RT} \right] \tag{4.49}$$

The thermodynamic data needed in the equilibrium calculations were obtained from JANAF thermodynamic tables compiled by Stull and Prophet (1971).

The Modified Bubble Assemblage Model of Mori and Wen (1975) was applied to their model for the bed hydrodynamics. Since the quantitative distribution of wood in the bed is unknown, the following empirical distribution function was used:

$$f(n) = 2.2576 P_A^{1.5} \exp\left[-P_A (P_B - h)\right]^2 (P_B - h)^2 \qquad (4.50)$$

where:

h is the vertical distance from the bottom of the bed (m)

P_A is an adjustable parameter (-)

P_B is a parameter equal to $P_B^{'}(U_o - U_{mf})$

$P_B^{'}$ is a constant (-)

The bed was considered to be composed of a number of compartments. It was assumed that most of the wood pyrolysis occurred at the level of the feed nozzle and that the wood feed was instantly distributed. Wood devolatilization was considered to be instantaneous and the resulting char, together with the wood particles, were assumed to be only in the emulsion phase. Mass and energy balances were done for each compartment and the resulting equations were solved starting with a temperature for the first compartment. Simulation runs were made using industrial operating conditions. The effects of various model parameters, operating and design variables on the model performance were investigated. The results showed that the gas composition, with the exception of CH_4, was almost entirely dependent on the assigned degree of approach to equilibrium. The calorific value of the product gas was strongly dependent on air/dry wood ratio, but not the moisture content of wood. Using O_2 enriched gas increased the calorific value of the product gas but did not improve the overall thermal efficiency. The results for the composition and calorific value of the product gas and the temperature difference across the fluidized bed were in good agreement with the limited amount of industrial data available.

The authors emphasized that additional data are needed before the model can be adequately tested.

Watkinson et al. (1991) formulated a simple equilibrium model for gas composition and yield from entrained, moving and fluidized bed coal gasifiers. The model basically consists of elemental mass balances for C, H, O, N and S, equilibra for four key reactions (water-gas shift, methanation, H_2S-H_2O and H_2S-COS), a statement of Dalton's law, and an optional energy balance. It requires as input the ultimate analysis of the solid fuel, the composition of the blast, the ratio of fuel to blast and the pressure of operation. The major components of the produced gas (H_2, CO, CO_2, CH_4, N_2, H_2O) as well as the sulphurous species H_2S, COS and SO_2 were predicted. Gas compositions reported in the literature for nine commercial and semicommercial gasifier designs were found to be in reasonable agreement with predictions of the model. Predictions were best for entrained bed systems, and were slightly poorer for fluidized bed gasifiers, and more uncertain for moving bed gasifiers.

4.10.2 Single-Phase Models

The fluidized bed gasifier is treated as a well mixed reactor in single-phase models. The gas and solids are considered to be intimately mixed without segregation into the dilute (or lean) phase and the emulsion (or dense) phase. Single-phase models are also referred to as homogeneous models. It is assumed that the reactor performance can be determined from the residence time distribution of gas elements (Grace, 1986). This assumption is only valid for beds with small bubbles. For beds with large bubbles (high superficial gas velocity), reactor performance is more likely to be affected by the contact time distribution (i.e. the distribution of times that gas elements spend in the vicinity of, and in effective contact with, solid particles) (Kunii and Levenspiel, 1991).

It has been shown that the resulting mass balances in a well mixed reactor can be written for both the reacting gas and the carbon in the form of simple algebraic equations as follows (Buekens and Schoeters, 1985):

(a) Gas:

$$N_i - N_{io} = \sum_j \upsilon_{ij} R_j \tag{4.51}$$

(b) Carbon:

$$N_{carbon} = \sum_j R_j + N_{overflow} + N_{elutriated} \tag{4.52}$$

where:

N is the total number of moles (-)

N_i is the total number of moles of the final gas (-)

N_{io} is the total number of moles of the initial gas (-)

υ_{ij} is the mole fraction of the species (-)

R_j is the number of moles of the reacting gas (-)

Equations 4.51 and 4.52 can be readily solved with specific rate equations and, when desirable, a population balance incorporated. A heat balance can, also, be considered.

Sundaresan and Amundson (1979a) developed a perfectly mixed single-phase model for fluidized bed coal char gasification in a steam-oxygen medium. The char gasification reactions were assumed to occur over the entire bed. The following three gasification reactions were considered in the model:

$$C + H_2O \rightarrow CO + H_2 \tag{4.53}$$

$$C + 2H_2 \rightarrow CH_4 \tag{4.54}$$

$$CO + H_2O \rightarrow CO_2 + H_2 \tag{4.55}$$

Thus, the gaseous products considered were CO, CO_2, H_2, H_2O and CH_4 plus O_2 (which was in the gasifying medium). The water-gas shift reaction was assumed to be in equilibrium. The model development was based on mass balance for the gaseous products, carbon balance and heat balance. Kinetic parameters and expressions were adopted from the complex kinetics of Johnson (1974) and other simpler kinetic schemes in the literature. It was also assumed that the bed was isothermal. The model was used to study the effect of residence time on total carbon conversion as a function of oxygen in the feed and also to study the influence of kinetics type on the performance of the gasifier. Analysis of the model using the two kinetics schemes led the authors to conclude that, for reliability in predicting reactor performance over a wide range of operating conditions (pressure and residence time), the complex Johnson kinetics must be used. However, no comparison with experimental data was done.

Purdy et al. (1981) proposed a single-phase model to predict the performance of a pressurized fluidized bed coal gasifier. Steam and oxygen mixture was used as the gasifying medium. Assumptions made were a perfectly mixed bed and instantaneous devolatilization and combustion. The kinetic scheme developed by Johnson (1974) was used for the steam gasification and hydrogasification reactions. The combustion product distribution was assumed to be governed by the following equation:

$$C + aO_2 \rightarrow 2(1-a)CO + (2a-1)CO_2 \tag{4.56}$$

The stoichiometric coefficient, 'a' was used as an adjustable model parameter. Other adjustable model parameters are the char reactivity (f_o) and the water-gas shift reactivity (f_{wg}). The optimum values of the model parameters estimated using experimental and predicted values of gasifier performance were used to compute values of carbon conversion, dry product gas flow rate and gas higher heating value. These were compared with experimental data obtained in a 15.2 cm I.D. pressurized fluidized bed gasifier. In general, the agreement between model predictions and measured variables were reasonable. The model was also used to predict the ratio $(CO_2)(H_2)/(CO)(H_2O)$. In this case, the agreement between model predictions and experimental data were rather poor and the authors ascribed this to a departure from isothermicity in the bed, with deviations in the axial temperature as high as 50°C. Another possible cause of this discrepancy could be the negligence of the C/CO_2 reaction which occurs in the presence of CO_2, a product of several of the gasification reactions considered.

A major drawback of single-phase models is their inability to account for the true flow and mixing behaviour of bubbling fluidized beds. This is as a result of the gas elements in the bubbles being in poor contact with solids and those in the emulsion phase being in intimate contact (Purdy et al., 1981; and Grace, 1986). This drawback of single-phase models can be overcome by considering more complex two or more phase models.

4.10.3 Two-Phase Models

In the two-phase model, the bubble cloud-wake is lumped with either the emulsion phase or the bubble phase. Gogolek and Grace (1995) classified the two phases in different ways. One classification is made according to the local solids concentration, with a dilute phase and a dense (or aggregated) phase. This classification is useful in reactor modeling. Another is according to the topology of the phases, with a dispersed and a continuous phase. This classification is useful in hydrodynamic modeling.

Sundaresan and Amundson (1979b) modified their single-phase model by considering the bed to be in two phases: bubble phase and emulsion phase. The authors assumed no flow in the emulsion phase (i.e., gas flow is stagnant) and the bubble size was taken as a model parameter. The modified two-phase model and the single-phase model (CSTR) were compared by calculating the total carbon conversion as a function of oxygen in the feed. For small bubble sizes there is practically no difference between the results of the two models. For large bubbles, however, the two models were significantly different, the two-phase model predicted lower carbon conversion. There was no experimental data to compare these observations.

Purdy (1983) developed a two-phase bubbling fluidized bed model to describe a coal gasifier. The model divided the bed into two main sections: a bed region, and a freeboard region. The bed region was assumed to consist of an incipiently fluidized emulsion phase and a solid-free phase. The solids were assumed to be well-mixed, but plug flow of the gases was assumed. No gas phase reactions were considered in the freeboard. Model options include: consideration of a jetting region, elutriation of fines and water-gas shift kinetics. The results revealed that jetting and elutriation have no significant effect on model predictions. He concluded that despite its complexity, the two-phase model offers no significantly better correlations of run data than does the simple perfectly mixed model.

Raman et al. (1981) developed a two-phase model to describe the gasification of biomass in a fluidized bed reactor. A well-mixed emulsion phase and the flow of gas in the bubble phase in plug flow were assumed. A simplified bubble-emulsion mass interchange coefficient was used. The devolatilization step in the biomass gasification process was considered to be instantaneous. So only secondary char gasification reactions and the water-gas shift reaction were considered. Cracking and reforming of heavy volatiles (such as tars) were disregarded. Rate of generation of i_{th} species in the emulsion phase included the rate of production by devolatilization reactions as well as by other chemical reactions. Devolatilization data were obtained from thermogravimetric analyses as well as from slow heating experiments

in a packed bed (heated from ambient to 500°C). Other kinetic parameters were obtained from the literature for coal gasification. The model was used to simulate gas composition and gasification product distribution. These were compared with experimental data obtained from a 23 cm I.D. fluidized bed gasifier. The model predicted gas composition and gas, char and liquid yields deviated from the experimentally measured values. The authors gave two possible reasons for the discrepancy: (a) the omission of the volatile cracking and reforming reactions, and (b) the use of initial weight fractions of char obtained by TGA technique. Deglise and Magne (1987) showed that less char is produced under rapid heating conditions (typical of fluidized beds) than slow heating conditions (as in TGA).

An extended two-phase model for a fluidized bed wood gasifier was developed by van den Aarsen et al. (1986) to predict the product gas composition, the char hold-up in the reactor, bed temperature and bed height. The hydrodynamics of a bubbling fluidized bed and the specific processes occurring in wood gasification were considered in this model. They assumed that: (a) the gas in both the bubble and emulsion phases was in plug flow; (b) no solids in the bubble phase; and (c) interfacial area and bubble hold-up were a function of bed height but not of the radial position in the bed. They also assumed in their model calculations the establishment of the homogeneous water-gas shift equilibrium in both the bubble phase and the emulsion phase, and included the tar cracking which occurs in both the bubble and emulsion phases. The model was subdivided into two stages: the oxidation stage which occurs in the lower part of the bed, immediately above the distributor plate, and the gasification stage which occurs in the upper part of the bed after the oxidation stage where pyrolysis, char gasification and tar conversion occur. The gas composition at the oxidation stage was determined by complete combustion of the pyrolysis gas (including tar) resulting from the wood fraction that was assumed to be combusted. Comparison of predicted model values with experimental values from a pilot scale fluidized bed gasifier showed that the mass transfer rate between the bubble phase and emulsion phase was not of significant importance in a fluidized bed gasifier. The results further revealed that the gas composition and the product gas heating value

predicted by the model were relatively insensitive to the operating temperature and bed height, but in perfect agreement with experimental values.

Ergudenler (1993) developed a generalized steady state mathematical model for a fluidized bed straw gasifier. The model was based on homogeneous chemical equilibrium, material and energy balances and the two-phase theory. The model has the capability of predicting the gas production rate, gas composition, higher heating value of the gas and the reactor temperature under a wide range of parameters (equivalence ratio, fluidization velocity, bed height, nitrogen-oxygen ratio, solid circulation ratio and fuel distribution function). The gasification process was represented by the following sub-stoichiometric equation:

$$C_N H_M O_L + \Phi\left(N + \frac{M}{4} - \frac{L}{2}\right)(O_2 + 3.711 N_2) \rightarrow$$

$$aCO_2 + bCO + dCH_4 + eH_2O + fH_2 + gO_2 + hN_2 + jNO \qquad (4.57)$$

where:

a,b,d,e,f,g,h,j	are the number of moles of carbon dioxide, carbon monoxide, methane, water, hydrogen, oxygen, nitrogen and nitrogen oxide, respectively.
N, M and L	are the number of moles of carbon, hydrogen and oxygen in the fuel, respectively
Φ	is the equivalence ratio (-)

The model was used to simulate a pilot scale dual-distributor type fluidized bed straw gasifier, and its predictions verified using experimental data. The model gave reasonable predictions of the mole fractions of the species, the gas higher heating value, the bed temperatures and the gas production rate. This model neglected the pyrolysis or devolatilization process which is very important especially in biomass gasification because of the high volatile matter content.

Bilodeau et al. (1993) developed a mathematical model for biomass gasification in a fluidized bed gasifier. They considered axial variations of concentrations and temperature in the bubble and emulsion phases. The mass balance involved instantaneous oxidation and equilibrium devolatilization of the biomass, kinetics of gas-solid gasification reactions as well as of gaseous phase reactions and interphase mass transfer and gas convection. The energy balance was solved locally for each vertical volume element, and globally on the reactor by iteration on the temperature at the bottom of the bed. Three parameters were adjusted based on the experimental results: (a) the heat transfer coefficient at the wall, (b) the weighting of the kinetics of the water-gas shift reaction, and (c) the fraction of biomass carbon remaining as char after devolatilization. The model was used to simulate a pilot-scale fluidized bed biomass gasifier, and its predictions compared to experimental measurements. The temperature and gaseous concentrations were estimated with good accuracy.

4.10.4 Three-Phase Models

Three distinct phases can be identified in a fast bubbling bed, (a) the emulsion phase with uniformly distributed (assumed) bed particles and gases in the interstices, (b) the bubble phase containing a negligible small fraction of solids, and (c) the cloud-wake phase comprising of the bubble wake and the bubble cloud. A good example of a three phase model is the K-L model developed by Kunii and Levenspiel (1990). The K-L model assumptions are: (a) no solid particles in the bubble phase, (b) the bubble size is constant throughout, (c) the emulsion and cloud phases are stagnant while the bubble phase is in plug flow, (d) the emulsion phase is at minimum fluidization conditions, (e) no axial dispersion in the emulsion phase, and (f) the void fraction of the wake is similar to that of the emulsion phase. The two mass transfer boundary resistances taken into account in the K-L model are the resistance at the bubble-cloud boundary and the resistance at the cloud-emulsion boundary. The superficial gas velocity was given as follows:

$$U_o = (1-\delta-\alpha\delta)\varepsilon_{mf}U_e + (\delta+\alpha\delta\varepsilon_{mf})U_b \qquad (4.58)$$

where:

U_o is the superficial gas velocity (m/s)

δ is the bubble phase fraction of the bed (-)

α is the wake fraction associated with the bubbles (-)

ε is the void fraction of the bed at minimum fluidization velocity (-)

U_e is the gas velocity in the emulsion phase (m/s)

The gas velocity in the emulsion phase (U_e) was given as follows:

$$U_e = \frac{U_{mf}}{\varepsilon_{mf}} - \left(\frac{\alpha U_o}{(1-\alpha-\alpha\delta)-\alpha U_{mf}} \right) \tag{4.59}$$

The bubble fraction in the bed was given as follows:

$$\delta = \frac{(U_o - U_{mf})}{(U_b - U_{mf} - \alpha U_{mf})} \tag{4.60}$$

The authors approximated typical values of the wake of the bubble (α) to range from 0.2 to 0.4. The K-L model has been widely applied with some modifications in the flow assignments and/or correlations for evaluation of various quantities as more data based on recent experimental evidence become available.

The K-L model was simplified by Caram and Amundson (1979) by neglecting the volume of the cloud-wake phase and using the overall bubble-emulsion interphase mass transfer coefficient proposed by Kunii and Levenspiel (1990):

$$\frac{1}{K_{bc}} = \frac{1}{K_{be}} + \frac{1}{K_{ec}} \tag{4.61}$$

where:

K_{bc} is the mass transfer coefficient between bubble and cloud phases (m/s)

K_{be} is the mass transfer coefficient between bubble and emulsion phases (m/s)

K_{ec} is the mass transfer coefficient between emulsion and cloud phases (m/s)

The authors compared the D-H model developed by Davidson and Harrison (1963), the simplified K-L model and the single phase (or CSTR) model by applying them to the gasification of coal. They used the simple first order kinetics and the complex empirical expressions of Johnson (1974). They investigated the influence of operating pressure, oxygen molefraction in the feed gas and particle residence time on the conversion behaviour of a char particle. Their results revealed that for very small bubbles the two-phase D-H model approaches the CSTR model. The K-L model was found to behave like a plug flow reactor. They concluded that: (a) use of empirical correlations for the exchange coefficient, which do not account for the effect of temperature and pressure on gas diffusivity, could lead to erroneous results at high temperatures and pressures, and (b) the predictions were more sensitive to the bubble size and to the structure of the diffusional resistances between the bubble and the emulsion phases than to the assumed flow patterns in the bed.

4.10.5 Grid Models

Yang et al. (1984) observed that large conversions are possible in the region near the distributor and that bubble models underestimate the conversion in this region. This implies much better contact between gas and solids in the grid zone. Two mechanisms have been proposed to explain this phenomenon: (a) enhanced transfer from permanent jets, which may also entrain particles, (b) and gas leakage during bubble formation. These are not competing mechanisms but different modes of operation for a distributor (Grace and Lim, 1987).

In jetting grid modeling, the jets which form the dilute phase are assumed to be in plug flow. The aggregated phase is the surrounding emulsion, which may be shared with the

bubbling bed region or assigned a separate compartment. The usual assumption about the flow division is that all the inlet gas flow is in the jets, while the gas in the emulsion is stagnant, or well mixed with no net flow. At the top of the jets, the jet gas is split between the bubble and emulsion phases according to the flow divisions in the bubbling bed (Grace and deLasa, 1978). As a quantitative measure of the effect of the jetting region on model predictions, Purdy (1983) evaluated a fluidized bed coal gasifier model for the cases of jetting and no jetting. The results indicated that inclusion of a jetting region has little effect on model predictions. Consideration of a jetting region yielded slightly higher carbon conversion and gas production rate predictions. The differences observed were small and show that little is gained from the added complexity of consideration of a jetting region.

Kimura et al. (1993) developed a grid model and combined it with the K-L bubbling bed model (Kunii and Levenspiel, 1990) to analyse local contribution of individual reaction and predict local concentration profile in the grid and bubbling zones of a laboratory scale fluidized bed coal gasifier. In the model, fluidized bed is supposed to be divided into two zones: bubbling zone and grid zone. Both zones consist of two regions: (a) bubble region and emulsion region in the bubbling zone, and (b) jet region and annulus region in the grid zone. The acts of particles and gas were explicated as follows: particles initially entering the jet at velocity of zero are accelerated by the jetting gas and then begin to slow down at some height. Part of the particles in the annulus region is descending around the jet edge, some of them, entering the jet region. Gases introduced from the nozzle ascend rapidly along the jet region with lateral gas exchange between the jet and annulus. Gases introduced from the distributor ascend with a velocity of U_{mf}, simultaneously, with a radial dispersion in the annulus region. In the bubbling zone, the Kunii-Levenspiel bubbling bed model (Kunii and Levenspiel, 1990) for intermediate particles was employed. In this simulation, three reactions were considered: (a) steam gasification, (b) CO_2 gasification, and (c) CO_2 combustion. The scheme of the steam gasification was given as follows:

$$C + f_1 H_2O \rightarrow (2 - f_1)CO + (f_1 - 1)CO_2 + f_1 H_2 \qquad (4.62)$$

where:

f_1 is a fitting parameter given to be 1.2 at 1173 K (-)

The CO_2 combustion scheme was given as follows:

$$C + \frac{2 - f_2}{2} O_2 \rightarrow f_2 CO + (1 - f_2)CO_2 \qquad (4.63)$$

where:

f_2 is a fitting parameter determined from experiments without steam (-)

The CO_2 gasification rate by Matsui et al. (1987) was employed in the model.

The effects of lateral temperature and bed height on H_2, CO and CO_2 concentration were discussed by comparison with experimental results. The results showed that the model predictions corresponded to the experimental values. However, the model CO concentration was lower than the experimental values. The difference is possibly explained by the higher reaction rate in experiment than the assumed rate employed in the numerical simulation.

4.10.6 Transient or Dynamic Models

A model capable of describing the dynamic behaviour and steady state performance of a fluidized bed for biomass gasification was developed by Chang et al. (1980). The dynamic devolatilization of biomass, cracking and other volatile and char reactions were considered in the development of this model. Significant disagreement was observed when they compared their results with experimental data obtained from a pilot scale fluidized bed feedlot manure gasifier under steady state conditions. The only agreement observed was in the concentrations

of hydrogen, nitrogen and methane at a temperature of about 596°C. The agreement was found to be very poor at higher temperatures (710°C) for all gas components owing to the inclusion of the coal char gasification kinetics. Transient results revealed that the gas production rate reached a steady state in less than 5 seconds, indicating that the product gases attained equilibrium before exiting the reactor. However, char production was observed to increase with time since the bed did not reach steady state. This was attributed to low operating temperatures resulting in low char gasification rates.

Weimer and Clough (1981) developed a comprehensive dynamic fluidized bed model for the gasification of coal. The model accounted for the jetting region, fines elutriation, homogeneous dilute phase reactions including the oxidation of CO and H_2, coal devolatilization, the water-gas shift reaction and coalescence and growth of bubbles in the bed. The reactions of C/H_2O, C/ CO_2, CO/H_2O, C/ O_2, CO/O_2 and H_2/O_2 were considered. A modified D-H two-phase model was used to describe the bubbling bed region. Simulation results indicated that the dilute phase homogeneous reactions have considerable influence on carbon conversion, bed temperature and product gas composition. The jet-emulsion mass and heat interchanges had a substantial effect on overall bed performance and on the temperature of the bed close to the inlet gas distributor. It is important to note that they did not account for the change in number of moles due to reaction.

Sadaka (1994) developed a two stage (devolatilization and combustion/gasification) dynamic model for a fluidized bed straw gasifier using finite element approximation. The jetting, bubbling and slugging zones were incorporated. The model also incorporated the minimization of the free energy technique, physical and chemical transformation processes as well as the hydrodynamic factors affecting these processes. The transformations and transport of seven gas components (CH_4, H_2, CO, CO_2, O_2, N_2 and H_2O) were considered. The model predicted the gasifier performance during dynamic operation as well as steady state operation. A sensitivity analysis was performed on the model to test its ability to respond to variations in

the bed temperature, bed pressure drop, product gas composition in both the bubble and emulsion phases, gas production rate, gas higher heating value and char yield under various aspect ratios, fluidization velocities, steam flow rates, biomass/steam ratio, inlet gas temperature and biomass type. A base case was used for each variable and this was independently changed around its base value. The results showed that the model is not only capable of predicting the gasifier performance but was, also, very sensitive to changes in these conditions. The model results were compared to the experimental results obtained from a 25.5 cm I.D. dual-distributor fluidized bed gasifier. An excellent agreement between model predictions and experimental data was obtained under all operating conditions studied. A limitation of this model is that it was developed to describe a specific system and may not well represent other systems differing in design and operating features due to the complicated nature of fluidized bed behaviour. Also, the numerical (finite element approximation) approach used in this model may result in stability and convergence problems.

5. MODELING OF FLUIDIZED BED RICE HUSK GASIFICATION

5.1 Background

The efficient operation of a fluidized bed rice husk gasifier is dependent on a number of complex chemical reactions, including fast pyrolysis of the rice husks, partial oxidation of pyrolysis products, gasification of the resulting char, conversion of tar and lower hydrocarbons, and the water-gas shift reaction (van den Aarsen et al., 1982). These complicated processes, coupled with the sensitivity of the product distribution to the rate of heating and residence time in the reactor, call for the development of a mathematical model capable of predicting the effects of process variables on the performance and dimensions of the gasifier.

Various models with widely differing complexity have been proposed to describe fluidized bed biomass gasification. These models range from complex kinetic models incorporating bed hydrodynamics and particle distributions (Gururajan et al., 1992; and Wang and Kinoshita, 1993) to simple thermodynamic models based on reaction stoichiometry, chemical equilibrium, and mass and energy balances (Bacon et al., 1985; Double and Bridgwater, 1985; Maniatis, 1986; and Double et al., 1989). Although kinetic models have the capability of predicting both the overall gasifier performance and the behaviour inside the gasifier, there are many problems involved in making use of kinetic data. First, the kinetics of biomass pyrolysis is mainly based on measurements of weight loss, which is of no help in estimating product distribution (Bacon et al., 1985; and Liou et al., 1997). Second, the experimental conditions under which the kinetic data are obtained are usually different from those expected in a fluidized bed gasifier (Bacon et al., 1985; Double et al., 1989; and Cozzani et al., 1997). Third, the intensive char circulation between the oxidizing and reducing zones present within the gasifier might affect the reactivity of the fuel char surface (Squires, 1973). Thus, the direct application of the thermogravimetrically obtained kinetic parameters to the analysis of fluidized bed

gasification may not be always justified. According to Grace (1986) the hydrodynamics of fluidized beds are far too complex to be used for deriving reaction kinetics.

These process complexities dictate the formulation of the simplest possible model which incorporates the principal gasification reactions and the gross physical characteristics of the reactor to determine the degree to which the gasifier performance could be correlated by this model. Chern and Walawender (1989) reported that at operating temperatures above 600°C, the gaseous mixtures leaving many types of gasifiers were found to approach equilibrium. These authors also reported very little difference in predicted product gas composition obtained by kinetic and thermodynamic-based models. Consequently, thermodynamic studies can be used to provide data for designing and assessing the performance of gasifiers. The results of thermodynamic equilibrium calculations can also be used to guide in the planning of experimental programs aimed at identifying the effect of various design and operating variables (such as bed height, fluidization velocity, equivalence ratio, oxygen enrichment and moisture content) on gasifier performance.

A thermodynamic model, based on chemical equilibrium and material and energy balances was, therefore, developed and used to assess the performance of the fluidized bed rice husk gasification system in this study. Although various attempts have been made to develop thermodynamic models to predict the performance of fluidized bed biomass gasification systems, calculation of the equilibrium composition encountered in fluidized bed gasification systems is a difficult and time consuming task (Bacon et al., 1985; Double and Bridgwater, 1985; Maniatis, 1986; Double et al., 1989; and Ergudenler et al., 1997) because of the need to simultaneously solve the mass and energy balances as well as the many chemical equations involved in equilibrium calculations through minimization of free energy. Prior methods resorted to complex numerical solutions in which stability and convergence problems are often involved. In this study, the modeling is done in ASPEN PLUS shell to take advantage of the extensive thermal and property data base and built in convergence algorithms. The ease of application is greatly enhanced and the computing

time is drastically reduced, as compared to prior approaches.

The dual distributor type fluidized bed gasifier simulated in this work is a further development of a spout-fluidized bed in which a bubbling fluidized bed is maintained towards the outer region of the bed (the annulus) while the active spout is maintained at the center. The basic physical difference between the two, however, is the presence of a secondary distributor plate in the spout (or secondary column). By virtue of its design, the dual distributor fluidized bed ensures a more homogeneous mixture since the biomass is pneumatically introduced through the bottom center of the reactor by the secondary column. The uniform biomass distribution in the dual distributor fluidized bed is assured by the expected spout which entrains bed particles from the bottom of the bed, mixing them with biomass and secondary air, then transporting the mixture in the upper region of the bed. From here, bed particles and the unreacted biomass proceed in a three dimensional fashion; i. e., their direction is determined by the movement of bubbles in the bed. A systematic pattern of solids movement is, thus, established, giving rise to a unique hydrodynamic system which is more suitable for the gasification of low density biomass materials than other conventional fluid-solid configurations. These unique features of the dual distributor fluidized bed gasifier are considered in developing the ASPEN PLUS simulation flow diagrams to simulate the actual operating conditions.

5.2 Model Development

Fluidized bed gasification involves a sequence of physico-chemical transformations as well as mass transport induced by bed hydrodynamics. The two models developed in this study (the one-compartment and the two-compartment models) are based on the use of mass and energy balances and chemical equilibrium relationships to predict the product gas composition from a dual distributor fluidized bed rice husk gasifier. They, however, differ in the extent to which the hydrodynamic conditions encountered in the gasifier are taken into account.

The fuel fed into a gasifier undergoes the following physical and chemical changes (which cannot be entirely dissociated from each other): drying/pyrolysis (leading to gas and char formation) and the partial combustion/gasification of the resulting char with O_2, CO_2, H_2O, and H_2. As far as the drying step is concerned, the fuel moisture is assumed to flash instantaneously. Consequently, drying is lumped with pyrolysis. In the equilibrium calculations the following species were considered as possible products: CO, CO_2, H_2O, H_2 and CH_4. According to Desrosiers (1981), no hydrocarbon other than CH_4 is thermodynamically stable under gasification conditions. Although C_2H_2, C_2H_4 and C_2H_6 as well as oils and tars are produced in the gasifier, they are accepted as non-equilibrium products. Therefore, in this study, CH_4 is the only hydrocarbon taken into consideration in the equilibrium calculations. No attempt was made to model char or tar yields. Cho and Joseph (1981) reported that more than 50% of N_2 in the fuel is released in the devolatilization process and the rest which may be chemically bonded with carbon is slowly released during combustion and gasification. However, the impact of this on the gasifier performance is small due to the low percentage of the nitrogen compounds (0.38%) present in the rice husk. The chemical reactions considered in the model development are pyrolysis, partial combustion and gasification.

5.2.1 Pyrolysis (Devolatilization)

The pyrolysis reaction can be represented as follows:

$$CH_{\alpha h}O_{\beta h}(SiO_2)_{\delta h} \xrightarrow{\Delta} CH_{\alpha}O_{\beta}(SiO_2)_{\delta} + Volatiles \qquad (5.1)$$

where:

$CH_{\alpha h}O_{\beta h}(SiO_2)_{\delta i}$	is the chemical formula for rice husk
$CH_{\alpha}O_{\beta}(SiO_2)_{\delta}$	is the chemical formula for devolatilized char
αh, βh, δh	are determined from the ultimate analyses of rice husk
α, β, δ	are determined from the ultimate analyses of char

The volatiles include CO, CO_2, H_2, H_2O, CH_4, low molecular weight hydrocarbons, char and tars. It is noted that silicon (Si) is already in its oxidized form in the rice husk and will not be oxidized by the combustion air. The representation as SiO_2 only serves to indicate that there will be no oxygen consumed by this material in rice husk. In previous investigations, the ash was usually neglected in the equilibrium computations, a factor which can introduce additional errors in the case of rice husk which has a large ash content of about 15-24 % (Mansaray and Ghaly, 1997a).

5.2.2 Combustion and Gasification

The devolatilized char first undergoes partial combustion by oxygen to produce CO and CO_2 as follows:

$$CH_\alpha O_\beta (SiO_2)_\delta + \gamma O_2 \rightarrow \left(2 - 2\gamma - \beta + \left(\frac{\alpha}{2}\right)\right)CO + \left(2\gamma + \beta - \left(\frac{\alpha}{2}\right)\right)CO_2 + \left(\frac{\alpha}{2}\right)H_2O + Ash \quad (5.2)$$

and the rest undergoes several gasification reactions , some of which are shown below:

$$CH_\alpha O_\beta (SiO_2)_\delta + (1-\beta)H_2O \Leftrightarrow CO + \left(1 - \beta + \left(\frac{\alpha}{2}\right)\right)H_2 + Ash \quad (5.3)$$

$$CH_\alpha O_\beta (SiO_2)_\delta + CO_2 \Leftrightarrow 2CO + \beta H_2O + \left(\left(\frac{\alpha}{2}\right) - \beta\right)H_2 + Ash \quad (5.4)$$

$$CH_\alpha O_\beta (SiO_2)_\delta + \left(\frac{(4 - \alpha + 2\beta)}{2}\right)H_2 \Leftrightarrow CH_4 + \beta H_2O + Ash \quad (5.5)$$

$$H_2 + \frac{1}{2}O_2 \rightarrow H_2O \quad (5.6)$$

$$CO + \frac{1}{2}O_2 \rightarrow CO_2 \quad (5.7)$$

$$CO + H_2O \Leftrightarrow CO_2 + H_2 \quad (5.8)$$

$$CH_4 + H_2O \Leftrightarrow CO + 3H_2 \quad (5.9)$$

5.2.3 Transport and Thermodynamic Properties

Each of the chemical components involved in this study is included in the ASPEN PLUS Pure Component Data Base. For each component, this data base contains the following transport and thermodynamic data as a function of temperature (ASPEN PLUS Users Guide, 1994), i.e.:

- viscosity (Chapman-Enskog-Brokaw Viscosity Model)
- diffusivity (Wilke-Chang Diffusion Coefficients Model)
- thermal conductivity (Stiel-Thodos Thermal Conductivity Model)
- Gibbs free energy of formation (BARIN Equation for Gibbs Energy)
- standard enthalpy of formation (BARIN Equation for Enthalpy)
- heat capacity (BARIN Equation for Heat Capacity)

That information is required to calculate energy balances and determine equilibrium compositions by minimizing the total Gibbs free energy of the system.

5.2.4 Material Balance

Using the principle of conservation of mass, the mass balances can be generally given as follows:

$$\sum_{i}(y_i a_{ik}) = A_k / \sum_{i} n_i \qquad (5.10)$$

where:

k = 1 - 3 represents the three equations for carbon, hydrogen and oxygen (-)

y_i is the number of moles of the species produced (-)

a_{ik} is the number of atoms of the k_{th} element present in each molecule of the chemical species i (-)

A_k is the total number of atomic weights of the k_{th} element present in the system, as determined by its initial constituents (-)

n_i is the number of moles of i_{th} species in the system (-)

In addition, one more equation is required. This is provided by Dalton's law,

$$\sum_i y_i = 1 \tag{5.11}$$

which can be written as,

$$y_{CO} + y_{CO_2} + y_{CH_4} + y_{H_2} + y_{H_2O} + y_{N_2} = 1 \tag{5.12}$$

which states that the sum of the mole fractions of all gaseous species which exit the gasifier is unity. Nitrogen is considered to be an inert gas and, therefore, does not affect the chemical behaviour of the system.

5.2.5 Energy Balance

The enthalpy exchanged as heat amongst the different components/processes taking place in the fluidized bed gasifier and the surroundings is given in Figure 5.1. The corresponding energy balance equation is given as follows:

$$\begin{aligned} Q_c(T, P)\big|_{combustion} = &- Q_l(T, P)\big|_{heat\ loss} + Q_{rh}(T, P)\big|_{rice\ husk} + Q_o(T, P)\big|_{oxidant} \\ &+ Q_d(T, P)\big|_{drying} + Q_{dv}(T, P)\big|_{devolatilization} + Q_g(T, P)\big|_{gasification} \\ &- Q_e(T, P)\big|_{elutnation} - Q_p(T, P)\big|_{product\ gas} \end{aligned} \tag{5.13}$$

where:

Q is the enthalpy flow of a stream (kJ)

c, l, rh, o, d, dv, g, e and p refer to the various streams of enthalpy (-)

T is the temperature of the process (K)

P is the pressure of the system (atm)

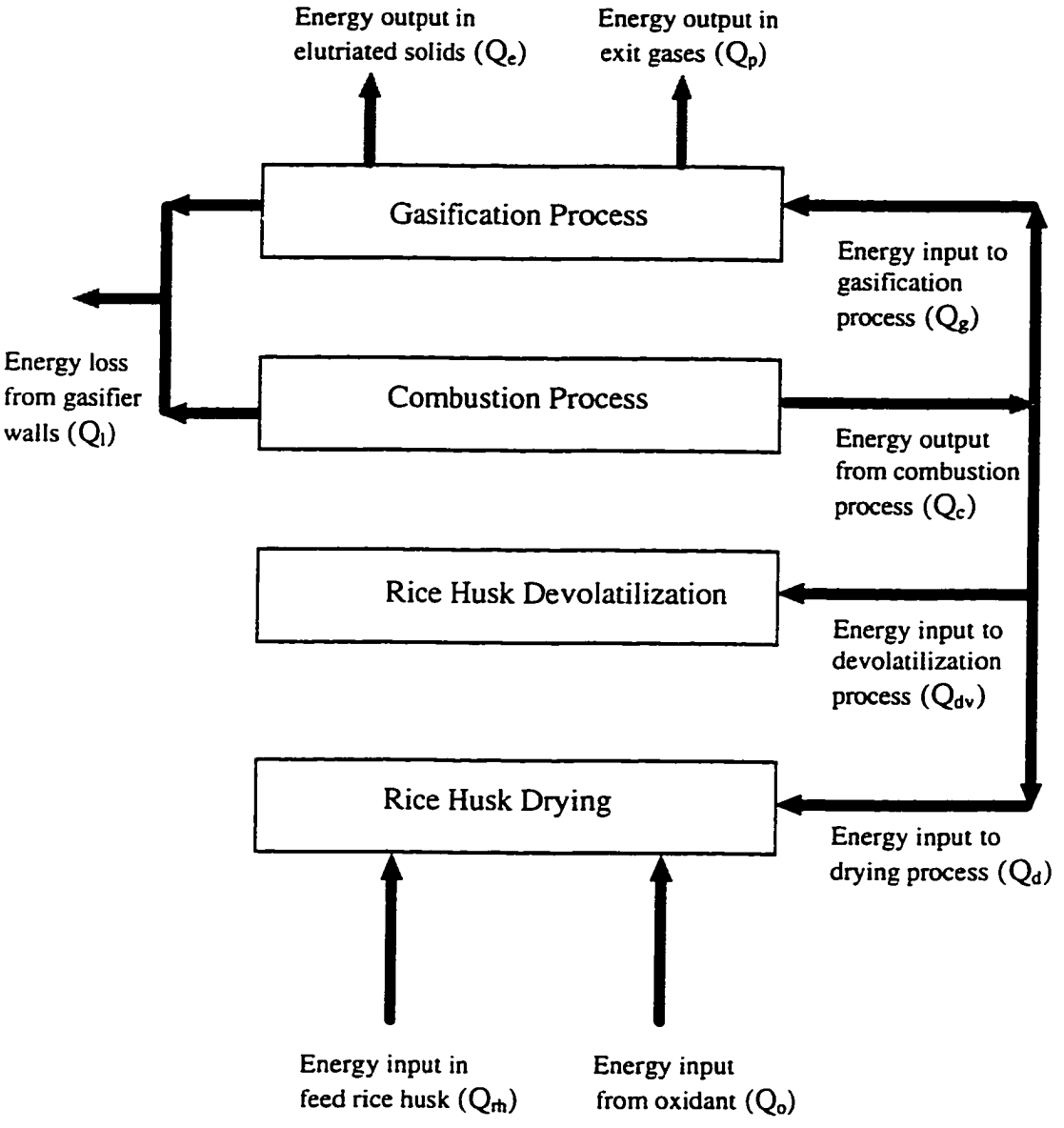

Figure 5.1 Schematic diagram of energy flow in fluidized bed gasifier processes.

Since there is a high level of mixing in the fluidized bed, drying, devolatilization, combustion and gasification processes all occur at very high rates at approximately the same temperature, which is equal to that of the reactor operating temperature. The specific heat of ash was taken as that of silica since rice husk ash has 90-97 % SiO_2.

5.2.6 Calculating Equilibrium Gas Compositions

In order to find the equilibrium composition for a given initial feed to the gasifier and a particular temperature and pressure the gas-phase chemical reaction equilibrium criterion can be applied. It can be expressed as follows (Lin et al., 1984):

$$\left(dG_{system}\right)_{T,P} = 0 \tag{5.14}$$

The total Gibbs function for the system is given as follows (Lin et al., 1984):

$$nG = \sum\left(n_i \Delta G_{f_i}^{o}\right) + \left(\sum n_i\right) RT \ln P + RT \sum\left(n_i \ln y_i\right) + RT \sum\left(n_i \ln \hat{\phi}_i\right) \tag{5.15}$$

where:

$\Delta G_{f_i}^{o}$ is the standard Gibbs free energy of formation of compound i from its constituent elements at temperature T (kJ/kmole)

R is the gas constant (kJ/moleK)

y_i is the molar fraction of compound j (-)

$\hat{\phi}_i$ is the fugacity coefficient (-)

It is the total Gibbs function, nG, that is to be minimized with respect to the composition of the individual species at the specified temperature and pressure. This is subject to the restraints imposed by atomic balances written for a closed system. The standard solution to this type of problem is through the method of Langrangian undetermined multipliers. This requires that the restraints imposed by the atomic balance be incorporated in the

expression for nG.

For each element k, the atomic balance is given as follows:

$$\sum_i (n_i a_{ik}) = A_k \tag{5.16}$$

which can be rearranged as follows:

$$\sum_i (n_i a_{ik}) - A_k = 0 \tag{5.17}$$

This is multiplied by the Langrangian undetermined multiplier and the expression is then summed over all k, giving the following expression:

$$\sum_k \left\{ \lambda_k \left[\sum_i (n_i a_{ik}) - A_k \right] \right\} = 0 \tag{5.18}$$

where:

λ_k is the Langrangian multiplier corresponding to the k_{th} atomic balance constraints (-)

Adding this equation to the right-hand side of the equation (5.15) for nG yields the following expression:

$$nG = \sum_i \left(n_i \Delta G_{f_i}^o\right) + \left(\sum_i n_i\right) RT \ln P + RT \sum_i \left(n_i \ln \frac{n_i}{\sum_i n_i} \right) + RT \sum_i \left(n_i \ln \hat{\phi}_i \right)$$
$$+ \sum_k \left\{ \lambda_k \left[\sum_i (n_i a_{ik}) - A_k \right] \right\} \tag{5.19}$$

where y_i has been replaced by $n_i / \sum_i n_i$.

Differentiating equation (5.19) partially with respect to n_i to form the derivatives

$$\left[\partial(nG)/\partial n_i\right]_{T,P,n_j} \tag{5.20}$$

and setting each derivative equal to zero leads to the following equation:

$$\Delta G^o_{f_i} + RT\left(\ln P + \ln y_i + \ln \hat{\phi}\right) + \sum_k (\lambda_k a_{ik}) = 0 \tag{5.21}$$

For an ideal gas, $\hat{\phi}_i = 0$. When the gas is nonideal, the Peng-Robinson equation (ASPEN PLUS Users Guide, 1994) is used to describe the system.

The five chemical compounds considered (CO, CO_2, H_2O, H_2 and CH_4) lead to five equations of the form (5.21). These compounds in turn are composed of three elements (C, H and O) which add three further equations of the form (5.11). In principle, the composition under equilibrium conditions can be determined by simultaneously solving this set of eight algebraic equations. However, when multiple reaction equilibria and/or phase equilibria are involved, it is easier to solve for the equilibrium composition of the system by using mathematical techniques that minimize the total Gibbs free energy of the system, subject to the constraints of the elemental balances. The equilibrium compositions in this study were calculated using the Gibbs free energy minimization module entitled RGIBBS in the ASPEN PLUS software for chemical process flowsheet simulation.

5.2.7 Hydrodynamics of the Dual Distributor Fluidized Bed Gasifier

The hydrodynamics of the dual distributor fluidized bed gasifier have been extensively investigated by Swan (1993). From those findings it is possible to consider the gasifier as composed of two distinct hydrodynamic regions; a core region in which the rice

husk feed is introduced into a fast moving central gas jet which moves upwards through the bed of sand particles (Figure 5.2), and an annular region which is fluidized by the slower annular gas flow. There is a continuous exchange of gases and solid particles (both sand and char) between the regions as shown in Figure 5.3. Most of the solids carried over to the freeboard region fall back to the annular region through the action of gravity and/or the centrifugal forces generated by the de-entrainment device. Solids escaping the gasification chamber are removed by a low pressure drop cyclone.

Although good mixing is expected to prevail in each region, different reaction conditions are expected to prevail in both the core and annular regions. These complex hydrodynamics can either be ignored (resulting in a relatively simple model) or taken into account (in which case a somewhat more complex model is encountered). Those two approaches were evaluated using ASPEN PLUS shell to facilitate the solution of the resulting model equations.

5.2.8 ASPEN PLUS Simulation

ASPEN PLUS is a problem-oriented input language that is used to facilitate the calculation of physical, chemical, and biological processes. It can be used for describing processes involving solids in addition to vapour and liquid streams. Use of ASPEN PLUS leads to an easier way of model creation and updating since small sections of complex and integrated systems can be created and tested as separate modules before they are integrated. This process simulator is equipped with a large property databank where the diverse stream properties required to model the material streams in a gasification plant are all available with an allowance for addition of in-house property data. Where more sophisticated block abilities are required, they can be developed as FORTRAN subroutines and added to the plant model, or entirely new user blocks can be created.

For a multi-phase multi-reaction system (such as rice husk gasification which involves numerous dissociation, recombination and elementary reactions) it is recommended to use the Gibbs reactor module (RGIBBS) present in ASPEN PLUS for

(a) (b) (c)

Figure 5.2 Photographs Showing (a) Bubble Formation, (b) Core Penetration and (c) Solids Recirculation in the Dual Distributor Fluidized Bed Gasifier.

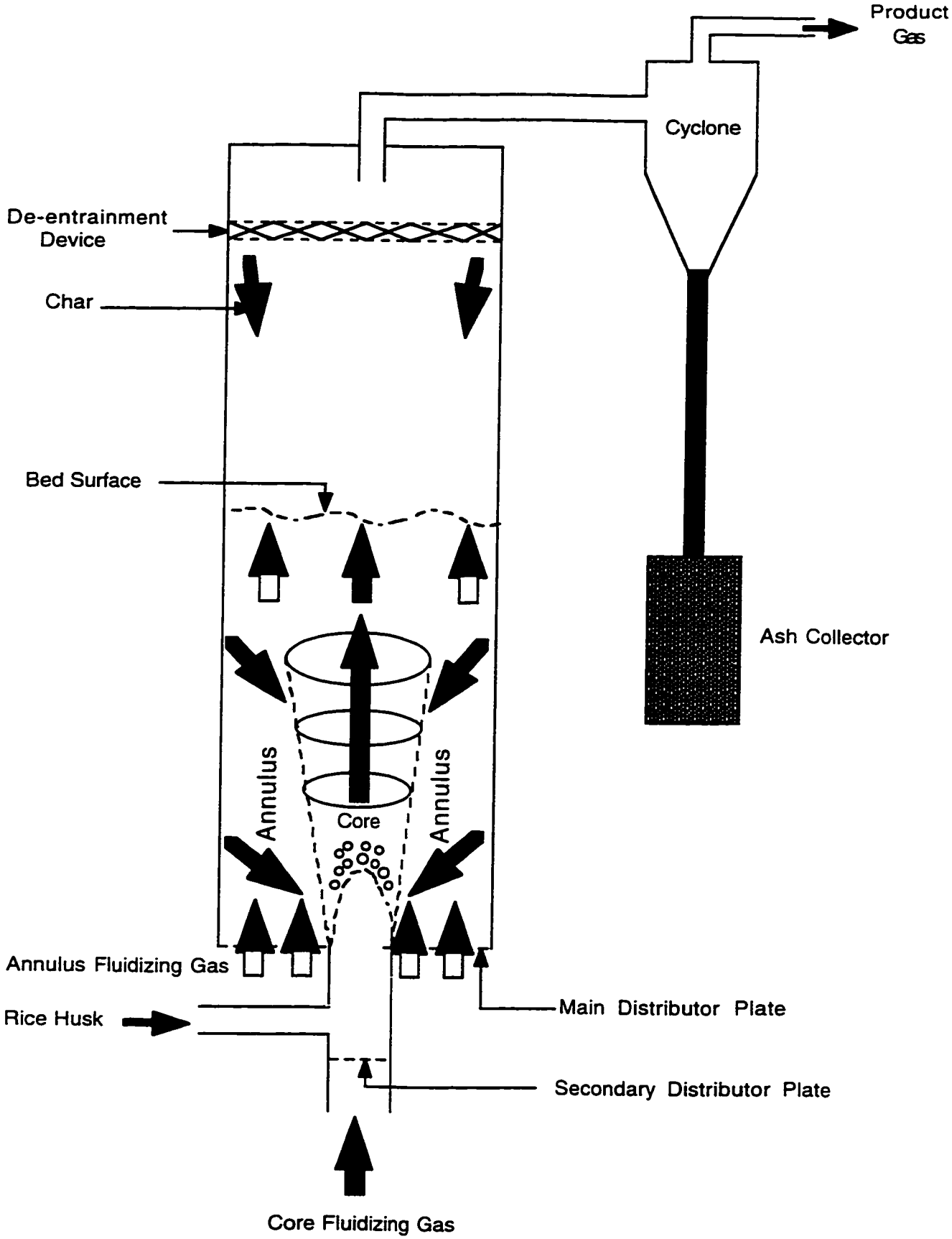

Figure 5.3 Schematic drawing of the dual distributor fluidized bed gasifier hydrodynamics.

solving the set of equations needed to predict equilibrium compositions (Equations 5.14 to 5.21). This module is preferred because it is based on the minimization of the total Gibbs free energy of the product mixture and allows for controlling the conversion of certain specified components.

Two models were developed in an attempt to simulate the performance of the dual distributor fluidized bed gasifier. In the first model the hydrodynamic complexity of the gasifier was neglected and an overall equilibrium approach similar to that adopted by many investigators (Double and Bridgwater, 1985; Maniatis, 1986; Double et al., 1989; Gururajan et al., 1992; and Ergudenler et al., 1997) was used. The second model takes into account the complex hydrodynamic conditions present within the gasification chamber.

5.2.8.1 <u>One-Compartment model.</u> In this model, the fluidized bed reactor is treated as a well mixed reactor with no distinction neither between the dense and dilute phases nor between the core and annular regions present in the reactor. The whole bed is considered to be made up of the dense phase, with the solids and the gas in the interstices being well mixed. The ASPEN PLUS simulation flow diagram developed to model the fluidized bed gasifier based on the single-compartment approach is shown in Figure 5.4.

Since RGIBBS can not handle non-conventional components such as rice husks, the feed stream is introduced into an RYIELD block which converts it into equivalent elemental components at the same enthalpy level. This stream as well as that for the air needed for partial combustion and gasification, are directed into an RGIBBS block and the products of the gasification reactions are specified. The RGIBBS module calculates the adiabatic reaction temperatures as well as the equilibrium product composition (estimated using the Gibbs free energy minimization method). The calculation module RGIBBS can also be used when one or more of the reactants is not fully involved in the equilibrium conditions. This is accomplished by specifying the extent of equilibrium for these components.

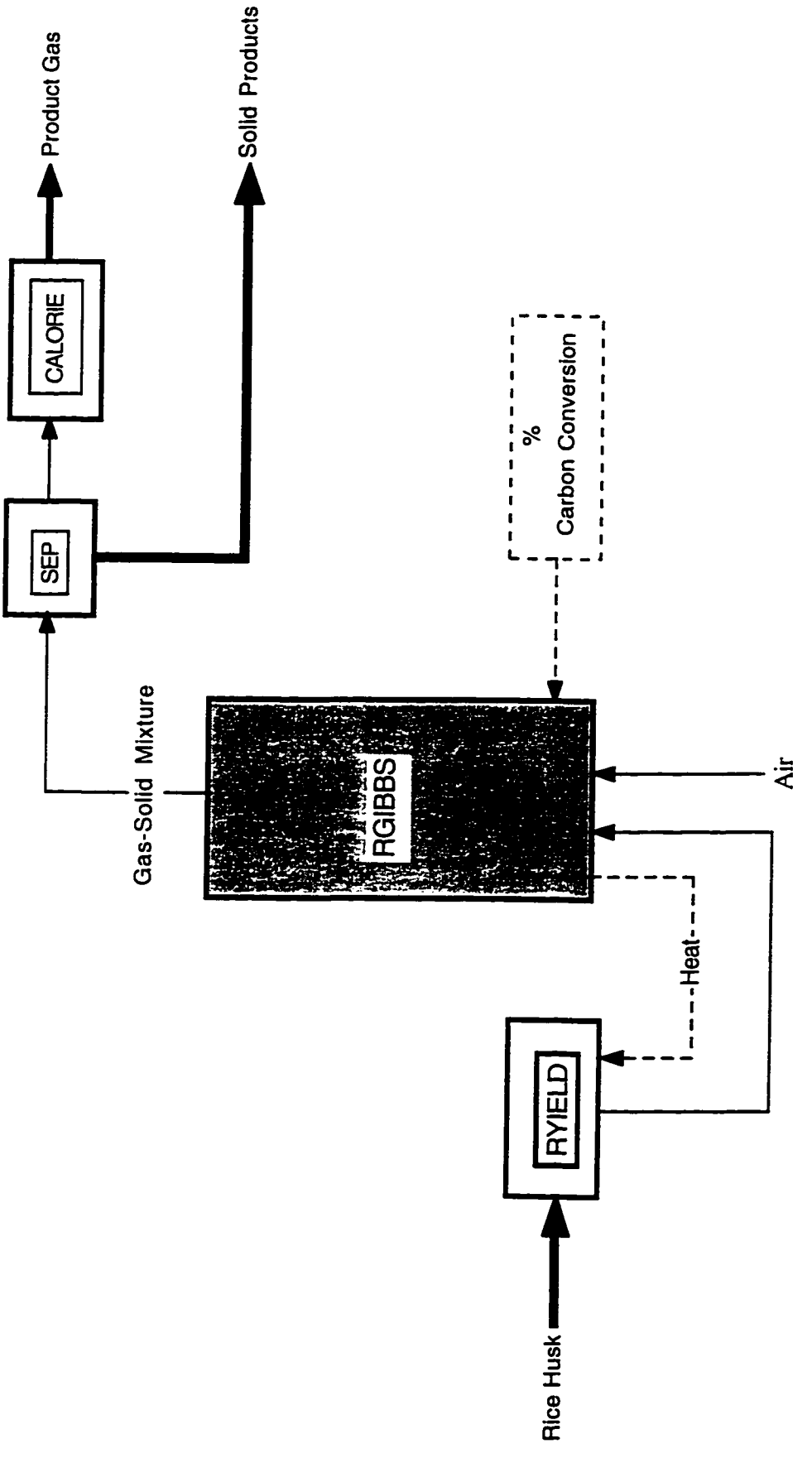

Figure 5.4 Schematic drawing of the single-compartment model ASPEN PLUS simulation flowsheet.

In the case of rice husk gasification under adiabatic conditions, the equilibrium product composition predicted by RGIBBS depends on the flowrates, composition, and feed temperatures of the material fed to the gasifier (rice husk and air) as well as the extent to which the carbon present in the feed was converted into gaseous products. The latter was used as an adjustable parameter to fit the predicted dry gas compositions to those experimentally obtained. The components of the gas considered are the combustible gases CO, H_2 and CH_4 that contribute to the heating value of the gas. As already mentioned, contents of C_2H_2, C_2H_4 and C_2H_6 are accepted as non-equilibrium products so that, for equilibrium calculations at atmospheric pressure, their presence can be ignored. Exit gas compositions, obtained at carbon conversions varying between 50-99%, were computed and the carbon conversion that minimizes the following residual sum of squares criterion (based on dry solid-free mole fractions) was identified:

$$RSS = \sum_{i}^{N} \left(\frac{C_{ie} - C_{ic}}{C_{ie}} \right)^2 \qquad (5.22)$$

where:

C_{ie} is the measured concentration of component i

C_{ic} is the predicted concentration of component i

N is the number of data points

The mean residual sum of squares was then calculated as follows:

$$MRSS = \frac{RSS}{n} \qquad (5.23)$$

where:

n is the number of gaseous components (3 in this case)

and the mean error between predicted and experimental product gas compositions was

calculated from the mean residual sum of squares as follows:

$$\text{Mean Error} = \sqrt{\text{MRSS}} \tag{5.24}$$

The module SEP was used to separate the solids from the gasification products. The higher heating value of the gaseous product was calculated using the CALORIE module.

5.2.8.2 Two-Compartment model. In this model, the complex hydrodynamic conditions prevailing in the dual distributor fluidized bed gasifier were taken into account. The fluidized bed reactor is, thus, treated as two separate and distinct compartments, one representing the core region where the feed is introduced in conjunction with most of the gasification air whereas the other compartment represents the annular fluidized bed region where much of the char is gasified. Both regions are treated as well-mixed reactors with no distinction between the dense and dilute phases present in either region. Each region is, thus, considered to be made up of a dense phase, with all the solids and the gas in the interstices being well mixed. The ASPEN PLUS simulation flow diagram developed to model the fluidized bed gasifier based on the two-compartment approach is shown in Figure 5.5.

In a fashion similar to that used in the one-compartment model, the rice husk feed stream is introduced into an RYIELD block which converts it into equivalent elemental components at the same enthalpy level. This stream, as well as the air stream fed to the core region, are directed into an RGIBBS block for which the gasification products are specified. The RGIBBS module calculates the adiabatic reaction temperatures in the core region as well as the equilibrium product composition achieved in this region. The extent to which the carbon present in the feed was converted into gaseous products in this region was adjusted between 70-95%. Some of the unconverted carbon, present in the gases, issuing from the core region is separated in the freeboard and in the de-entrainment device. This was simulated using an SEP module that completely separates solids from the gasification products.

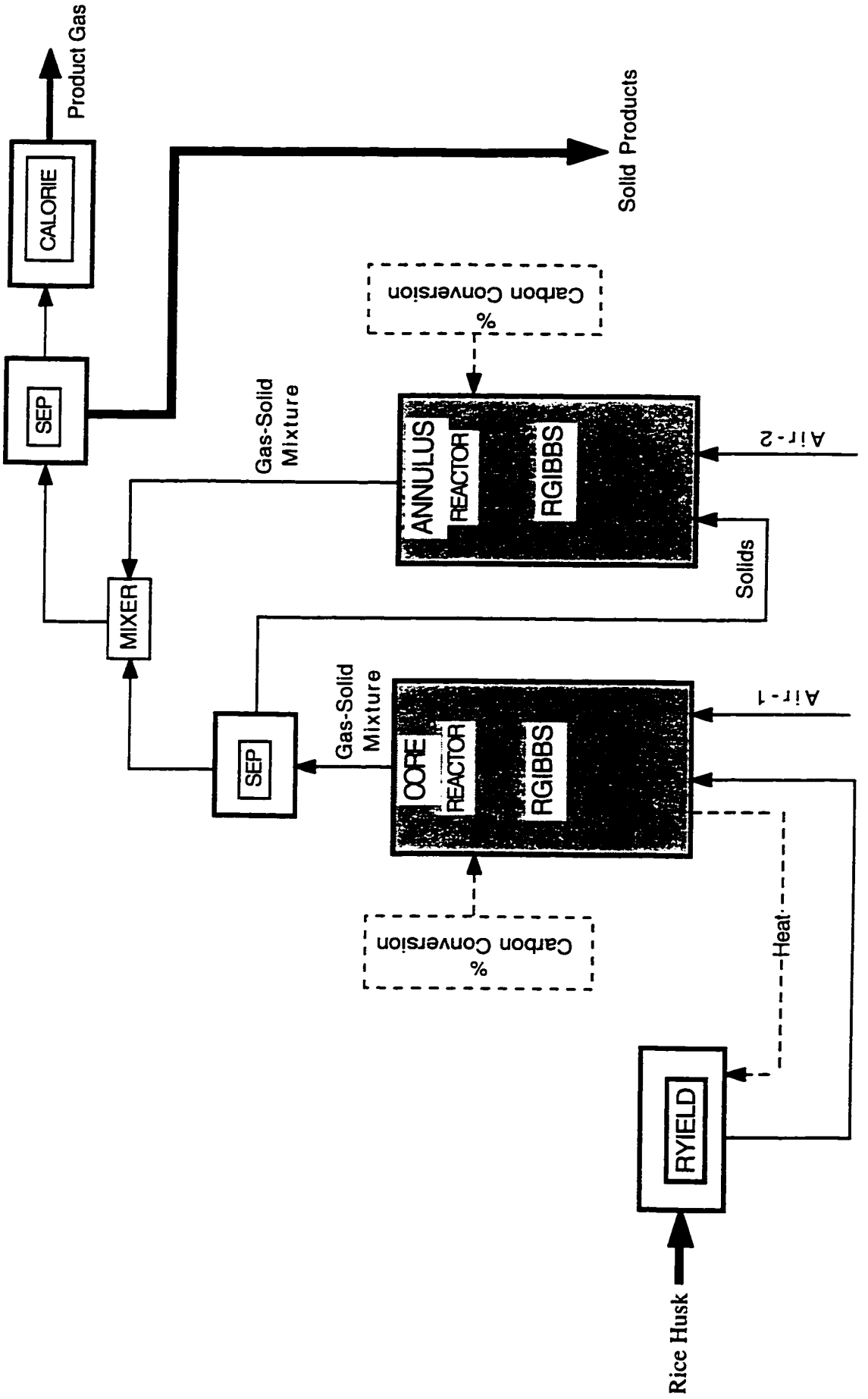

Figure 5.5 Schematic drawing of the two-compartment model ASPEN PLUS simulation flowsheet.

The remaining unconverted solids removed from the core region are fed into the annular region where they undergo gasification reactions with the annular air. The adiabatic reaction temperatures achieved in the annular region, as well as the equilibrium product composition, are calculated using RGIBBS block for which the gasification products are specified. The extent to which the carbon present in the recycled solids was converted into gaseous products in this region was adjusted between 50-99% (of the annular carbon) for each carbon conversion in the core region.

The gasification products of the two regions are combined and the solids were removed from the combined stream using an SEP module. The solid-free gas was directed to the CALORIE module in which the higher heating value of the gas was calculated. The extent to which the predicted gasification composition fits the experimental one was determined by applying Equation 5.22 to the dry, solid-free combined gasification stream.

The overall carbon conversion was calculated using the best fit core and annulus carbon conversions as follows:

$$CC_{Overall} = CC_{Core} + \left(\frac{100 - CC_{Core}}{100}\right) \times CC_{Annulus} \tag{5.25}$$

where:

$CC_{Overall}$ is the overall carbon conversion (%)

CC_{Core} is the carbon conversion in the core region (%)

$CC_{Annulus}$ is the carbon conversion in the annulus region (%)

6. EXPERIMENTAL APPARATUS

The fluidized bed gasification system is shown in Figure 6.1. It consisted of a fuel feeder, a fluidized bed reactor, and measurement and data acquisition systems.

6.1 Fuel Feeder

Figure 6.2 shows the feeding system developed by Ghaly et al. (1989b) for biomass materials. It consisted of a frame, a hopper, two agitators, an auger and a drive system consisting of an electric motor and a speed controller.

The frame was made of 50.8 mm angle iron (mild steel) used to position the hopper over the auger and to support and align the auger and the agitators. The base of the frame was 500 mm x 610 mm and the height was 1210 mm. It was designed in such a way that the hopper can slide in and out for easy evaluation and modifications. The angle iron of the main frame section, which formed the rectangular housing portion of the hopper, was single fillet arc welded. The hopper is a funnel shaped reservoir into which rice husks were fed and discharged into an auger located at its base. It was made of 6 pieses of 18 gauge galvanized sheet metal. The agitators help loosen and mix the fuel to keep its supply homogeneous and consistent. They were made of 25.5 mm diameter steel shafts with wire wrapped around them four turns and extended to form spikes. The auger system consisted of the auger screw and housing. The auger screw was made of 8.5 mm thick stainless steel flighting tig welded to a 1200 mm long, 316 stainless steel shaft of 30 mm outer diameter and 10 mm inner diameter. A copper tubing of 6 mm in diameter was fitted inside the steel cylinder and served as a water cooling system. This was necessary since one end of the auger housing was exposed to high temperatures generated in the secondary column of the fluidized bed gasifier. The auger screw is a 1000 mm

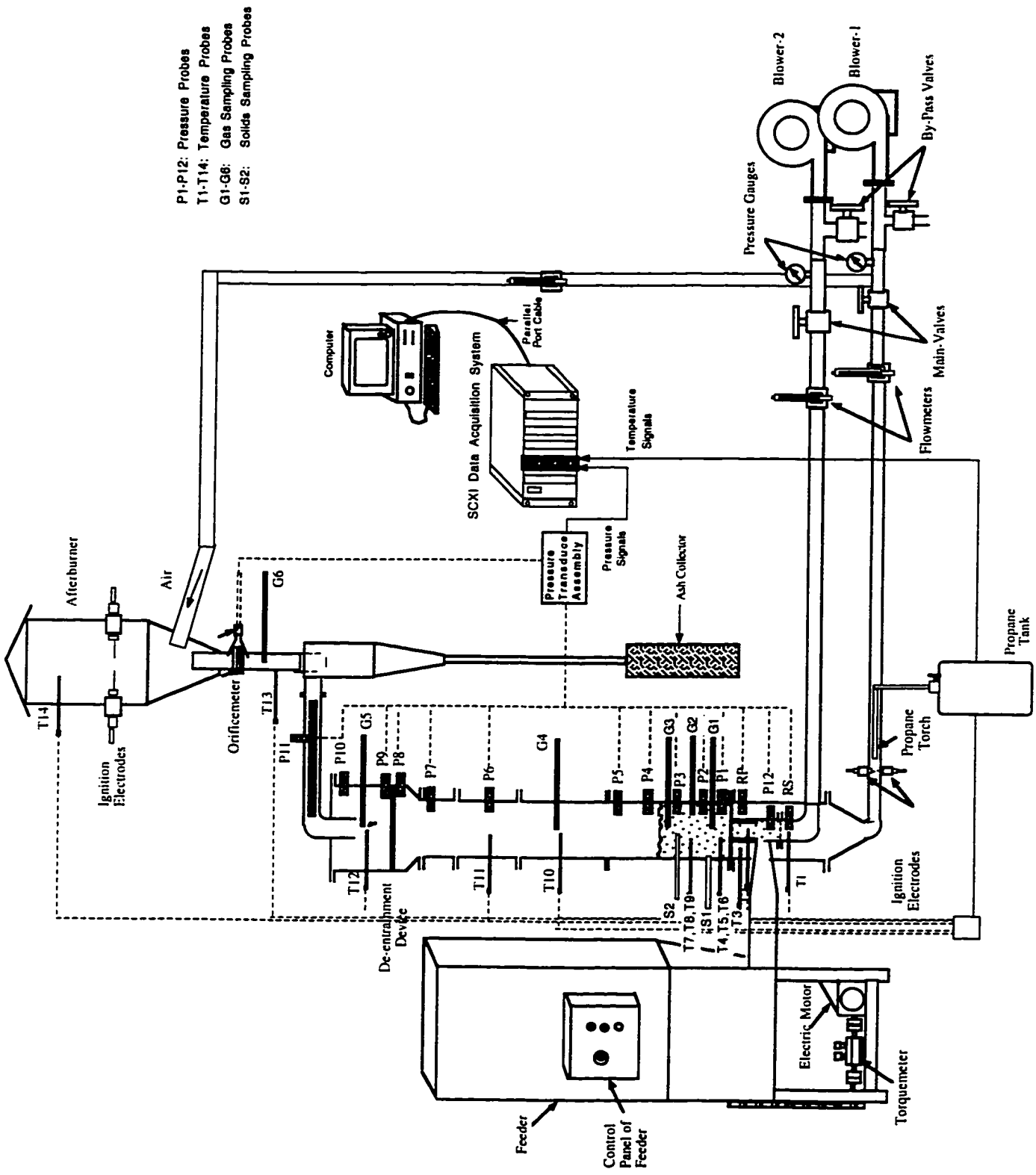

Figure 6.1 Experimental Apparatus.

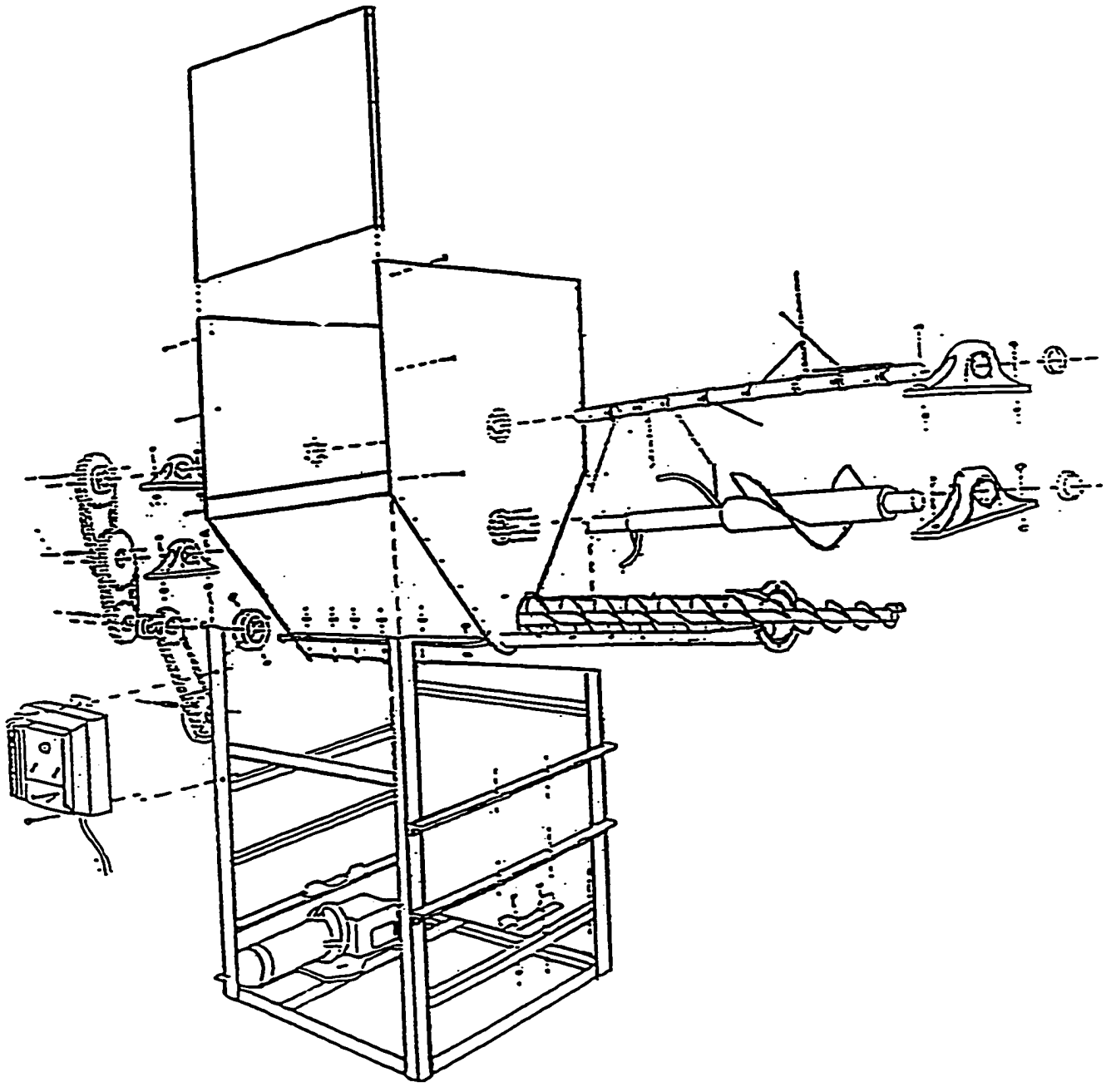

Figure 6.2 Fuel Feeding System (Ghaly et al., 1989b).

long single threaded right-hand design. The auger housing was made of stainless steel cylinder of 10 mm thick wall and 95 mm inner diameter (Figure 6.3).

Attempts to feed rice husks through an auger system designed for straw were faced with some problems. The rice husks tended to rotate with the auger metering screw without actually being transported. This resulted in problems of blockage in the auger housing due to the accumulation and compression of rice husk in that section. These problems were attributed to the physical nature of rice husk (smaller particle size and lower bulk density) compared to straw. To facilitate mixing and transportation of the rice husks, the diameter of the auger housing was increased from 60 to 66 mm. This diameter also provided a very good compaction of rice husk at the auger exit which is necessary to avoid hot gas backflow into the feeder.

The fuel feed rate was controlled by varying the speed of the auger through a variable speed electric motor. The rice husk feed rate was calibrated against the auger speed (Figure 6.4) and the feeder operated at the pre-selected speed to obtain the desired feed rate of rice husk to the gasifier. In general, the feeding system performed well.

6.2 Fluidized Bed Reactor

The fluidized bed reactor, which consisted of an air supply system, a start-up unit, a dual-distributor type feeding mechanism, a fluidizing column, a disengagement section, a deentrainment device, a cyclone, and an afterburner, is shown in Figure 6.5.

6.2.1 Air Supply Unit

The primary air (fluidizing), secondary air (for feeding) and the air required for the afterburner were supplied to the fluidized bed reactor by two air supply units. Each unit (Figure 6.6) consisted of a blower, a pressure gauge having a pressure range of 0-690 kPa, a main

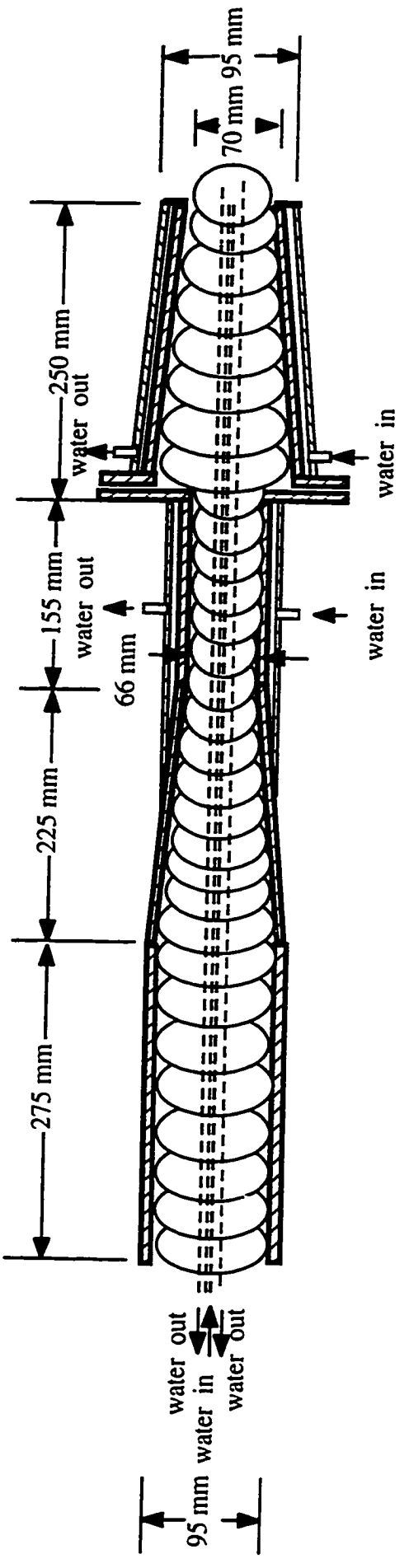

Figure 6.3 Auger Housing of the Feeding System.

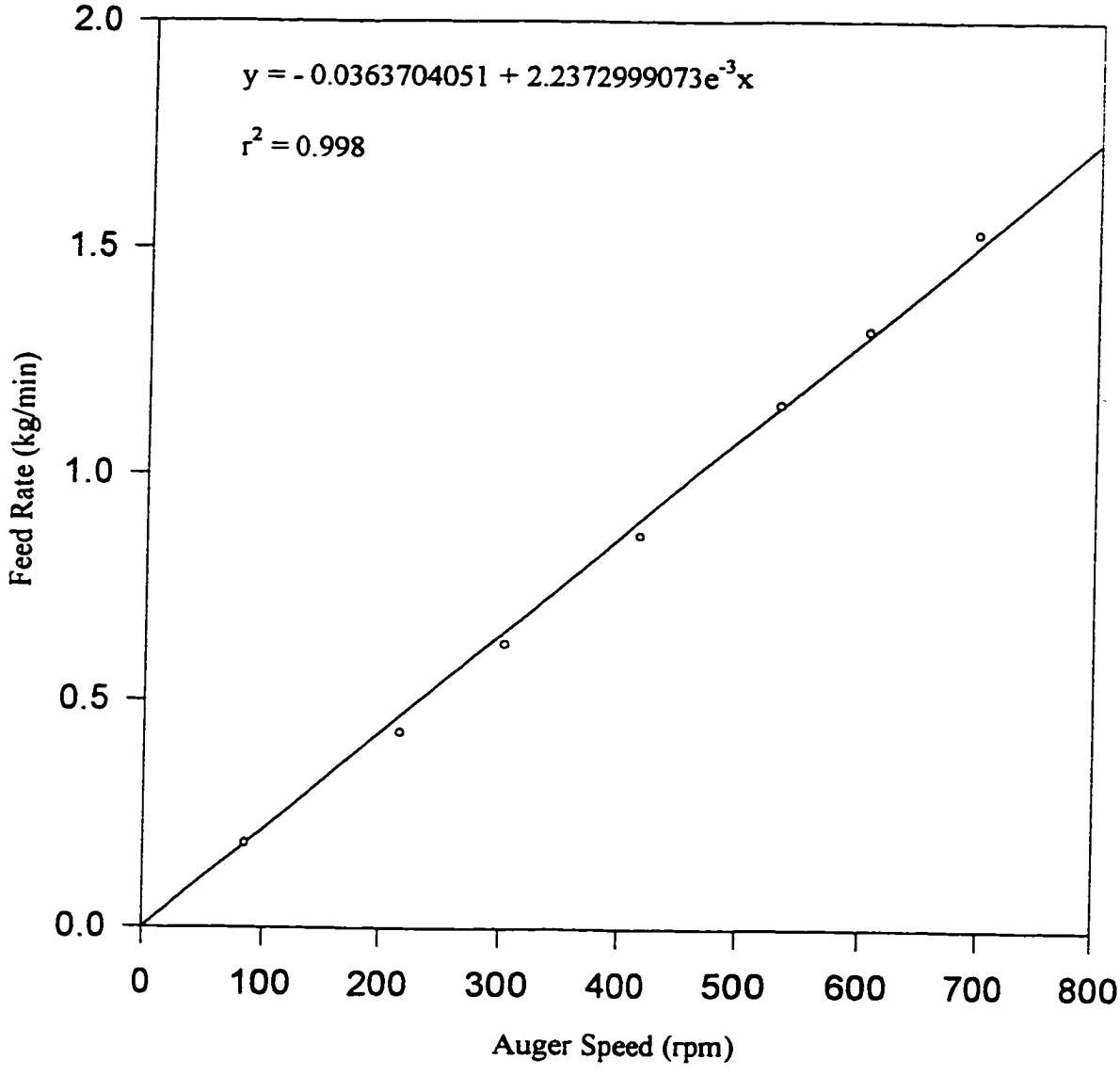

Figure 6.4 Calibration Curve for the Rice Husk Feeder.

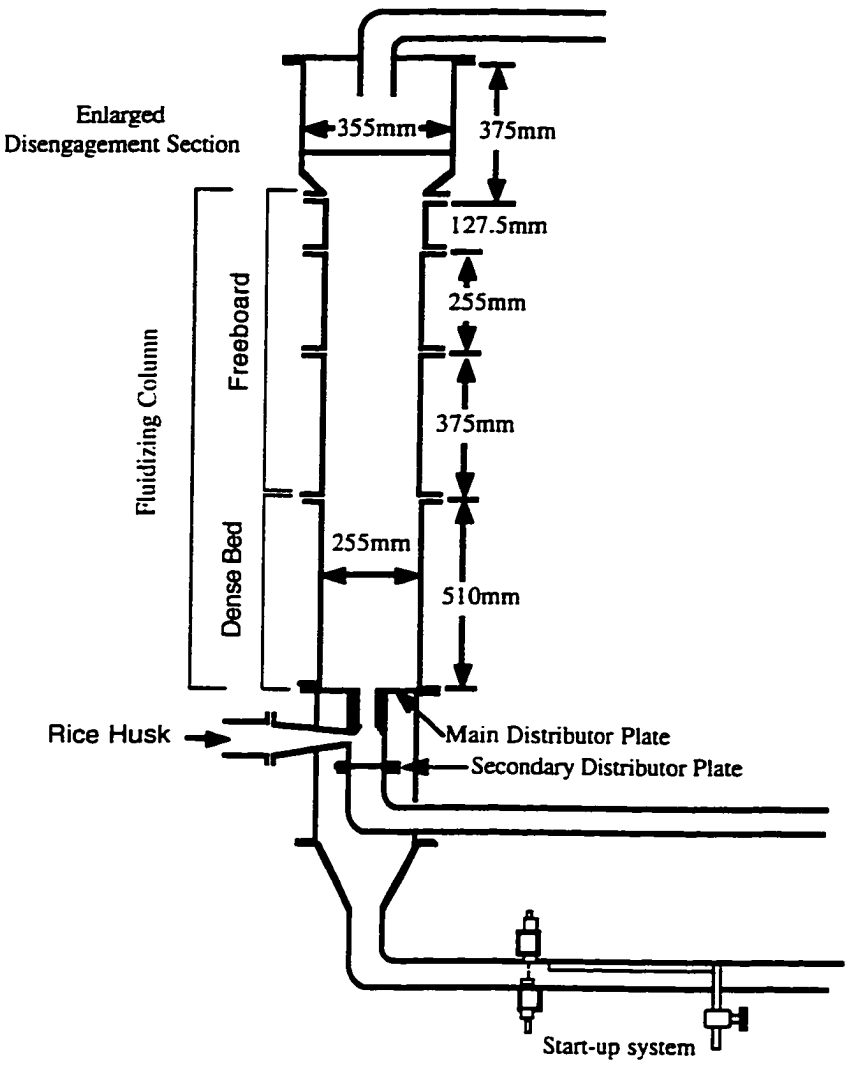

Figure 6.5 Fluidized Bed Reactor.

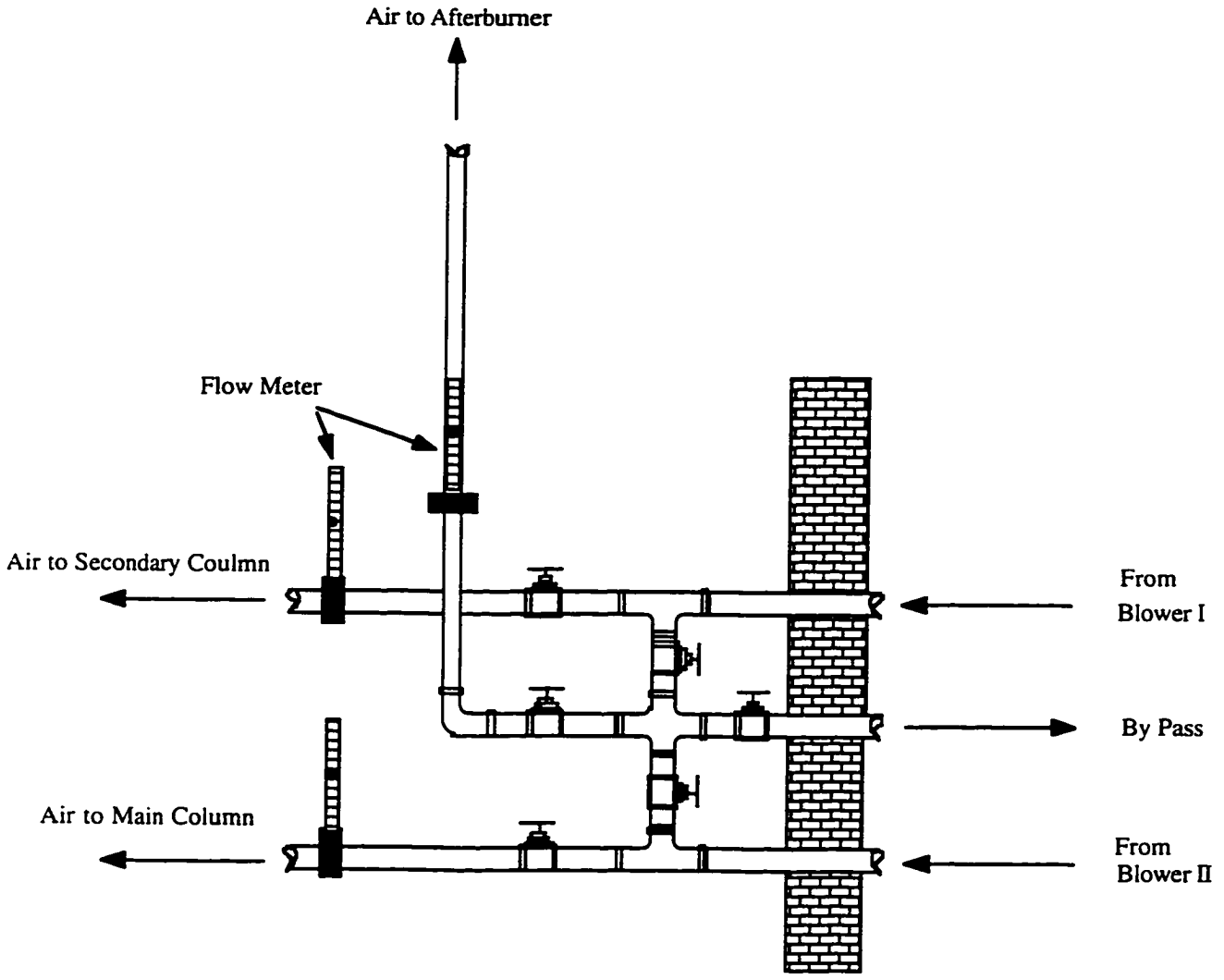

Figure 6.6. Air Supply System (Sadaka, 1994).

valve to control the air flow rate, a by-pass valve to prevent overheating of the electric motor, a 50 mm inner diameter steel pipe serving as an air supply line and a flowmeter. The blower (Model ENGENAIR R4310A-2, Benton Harbour, Michigan), driven by a 4.8 hp (three-phase 220 volts and 13.4 amps) electric motor (Baldor Industrial Motor, Benton Harbour, Michigan), had a maximum flow capacity of 4.87 m^3/min and maximum pressure of 20 kPa. Each blower inlet had a filter with a micron rating of 25 and a maximum flow of 7.08 m^3/min to clean the incoming air of contaminants such as dust particles and water. Flow Cell Bypass flowmeters (Metal FLT-type, Cole Parmar Catalog No. N-03251-60, Chicago, Illinois) were used to measure the air supply rates. Each flowmeter was accurate to 2.5% of full scale and could be used up to maximum temperature and pressure of 60°C and 1035 kPa, respectively. The air supply from blower-1 was used to fluidize the bed material within the main fluidizing column and to supply air to the after burner, while that from blower-2 was used to create a jet of air within the secondary column which carried the bed material and rice husk into the main fluidizing column.

6.2.2 Start-up Burner

The start-up burner was used to preheat the bed before commencement of fuel feeding. After the bed temperature required to sustain the operation of the system was reached, the start-up burner was shut off and the feeder was simultaneously started. The start-up burner consisted of a 350 mm long stainless steel propane torch, two electric arc electrodes and a high voltage ignition transformer mounted to the primary air supply line (Figure 6.7). The propane gas was supplied to the torch from the propane vessel through a pipeline at a pressure of 140 kPa. A safety mechanism made of a solenoid valve (Cat. No. CG 8215-G20, Brantford, Ontario) was incorporated into the start-up unit to prevent the supply of propane to the system until both the air supply and the ignition systems were on. The air was detected through a pressure tap connected to a pressure switch (Honeywell Model No. C 7027 A, MPLS, Minesota) and the flame was detected by an ultraviolet detector (Honeywell Model No. C 7027 A 0232, MPLS, Minesota).

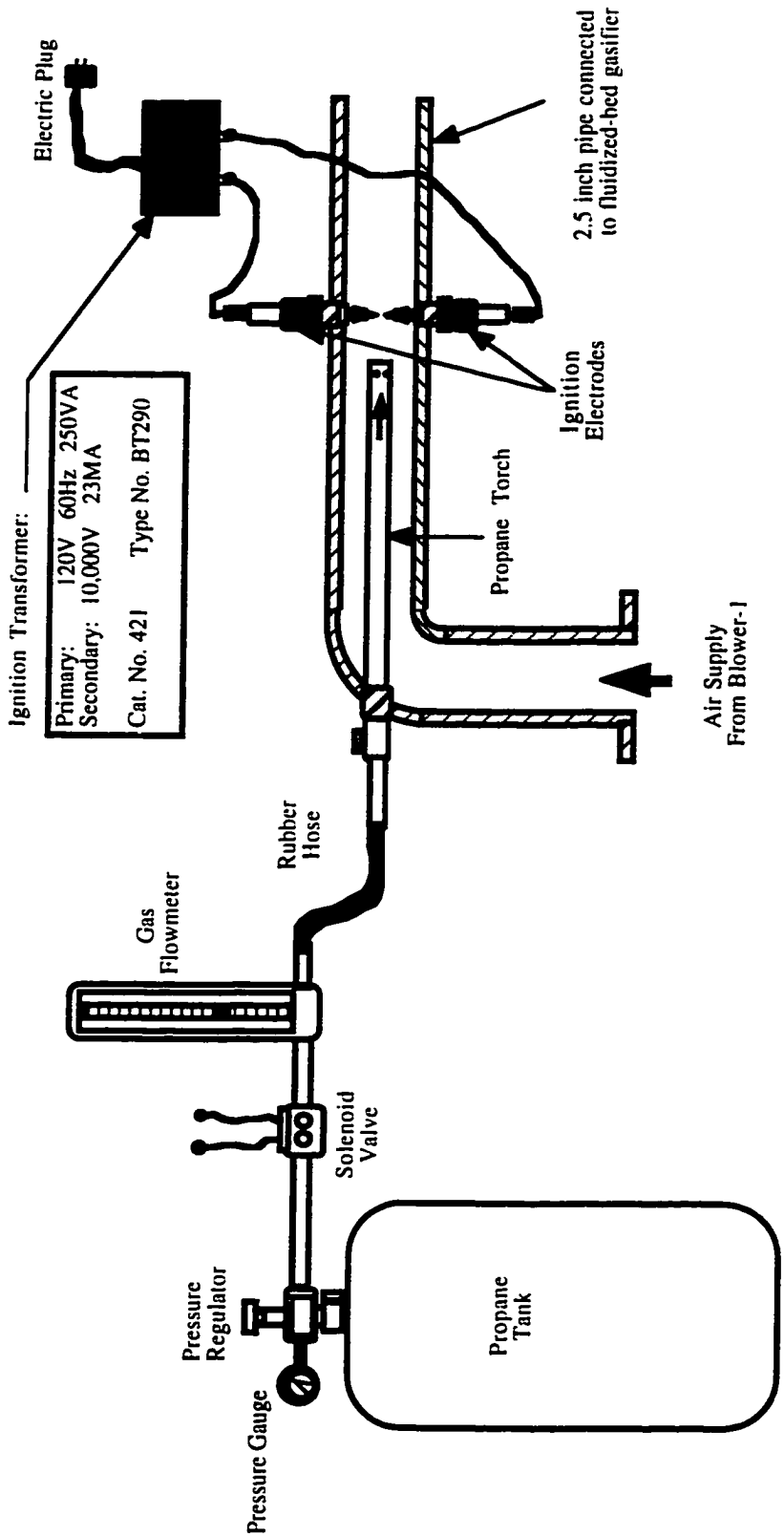

Figure 6.7 Start-Up Burner (Ergudenler, 1993).

6.2.3 Dual-Distributor-Plate Type Feeding Mechanism

The dual-distributor type feeding system consisted of the main distributor plate, the secondary distributor plate, secondary column and the feeding tube (Figure 6.8). Figure 6.9 shows the cross-sectional view of the dual-distributor type feeding system. It was designed to feed low density biomass fuels directly into the bed from the bottom centre of the main distributor plate. Both distributor plates were perforated in circular patterns as shown in Figure 6.10. The main distributor plate had a circular opening of 75 mm diameter at the centre, surrounded by 267 circular holes of 2 mm diameter each. The holes were drilled in circular patterns with a pitch of 11.2 mm, resulting in a perforated area of 1.65 %. The secondary column which is 200 mm long and 75 mm diameter was connected to the bottom centre of the main distributor plate. The secondary distributor plate (with 127 holes of 2 mm diameter each and 9.0 % perforated area with circular pitch of 6 mm) supported the bed material within the secondary column. The surface of each distributor plate was point welded with a 140 stainless steel mesh size screen to prevent the bed material from falling through the distributor holes. The primary air supply was used to fluidize the bed material within the main fluidizing column, whereas the secondary air supply created a jet of air within the secondary column which forced all the bed material out of this narrow column to the main fluidizing column. The fuel fed into the secondary column by the auger system above the secondary distirbutor plate was also carried up by the air jet into the main fluidizing column. This section is subject to high temperatures and was, therefore, cooled using a water jacket to avoid the danger of burning the rice husk in the auger.

6.2.4 Fluidizing Column

The fluidized bed gasifier was made of 8 mm thick, 310 stainless steel. The diameter and total height of the gasifier are 255 mm and 2700 mm, respectively. The main fluidizing column consisted of four circular steel sections of different lengths (12.8, 25.5, 38.3 and 51.0 cm), bolted to each other with good gasket sealing between them. Two rectangular view windows (7.5 mm X 150 mm) made of vitrosil quartz glasses (TAFCO Thermal American

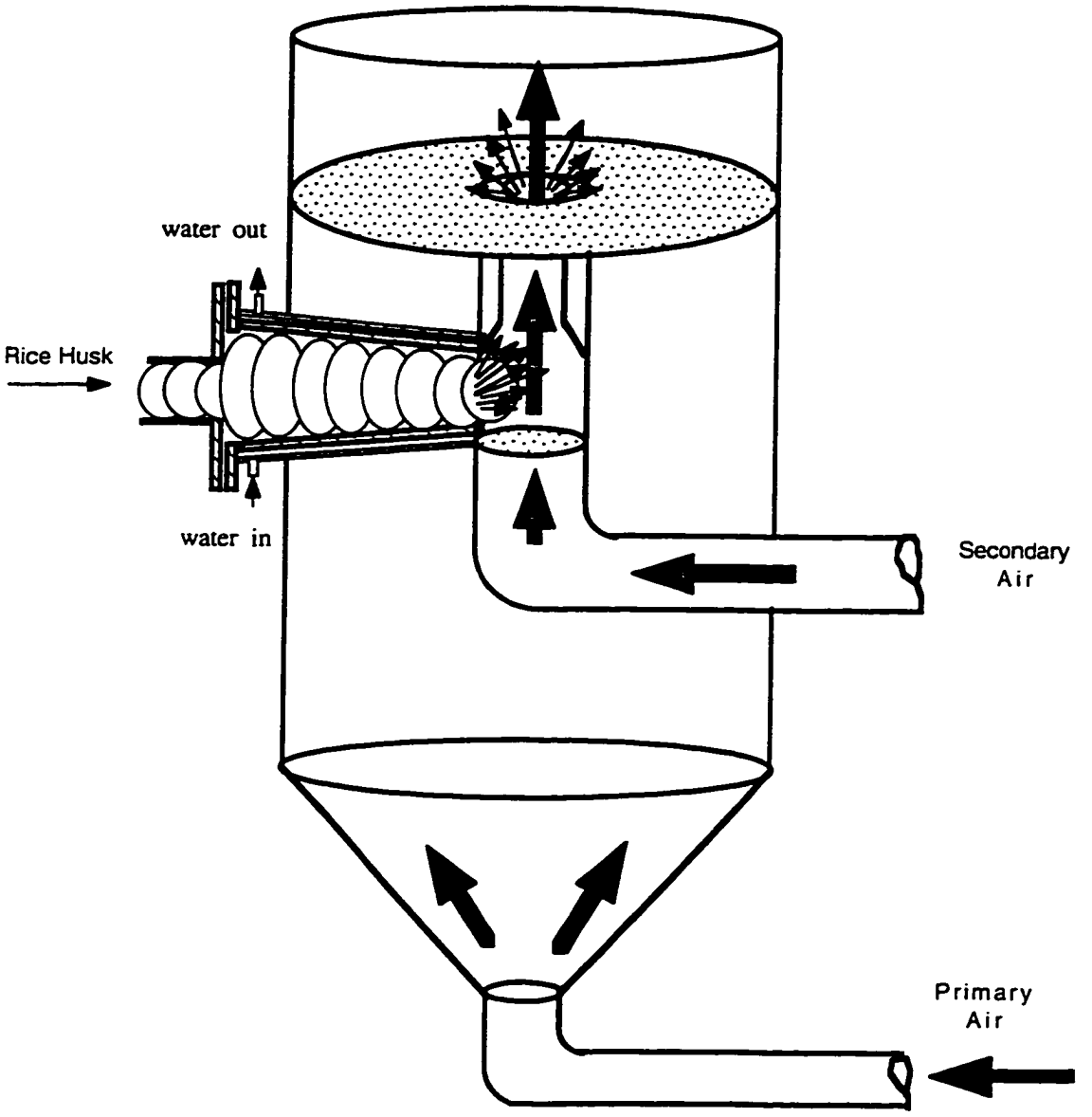

Figure 6.8 Feeding Mechanism.

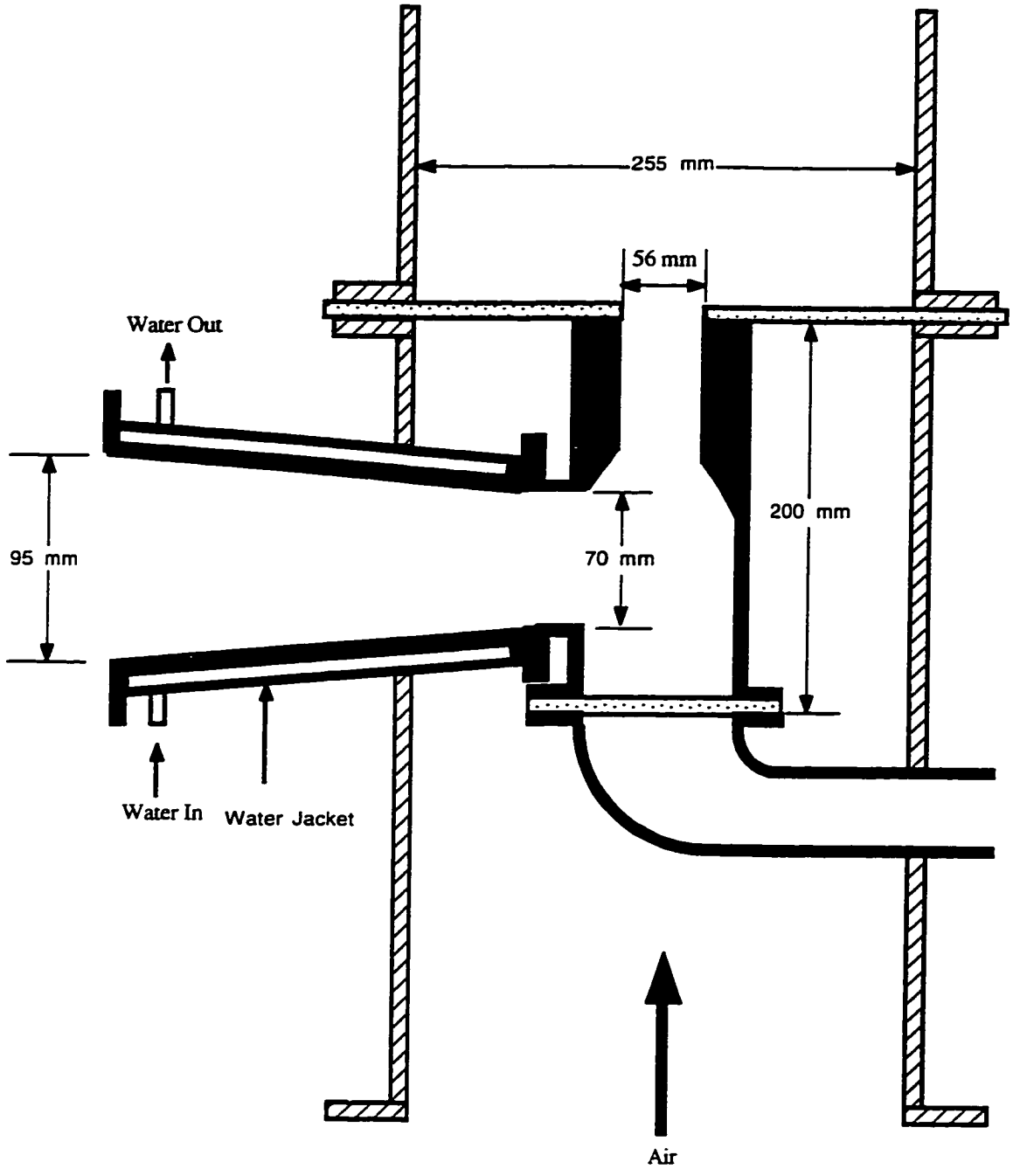

Figure 6.9 Cross-Sectional View of the Dual-Distributor Type Feeding System.

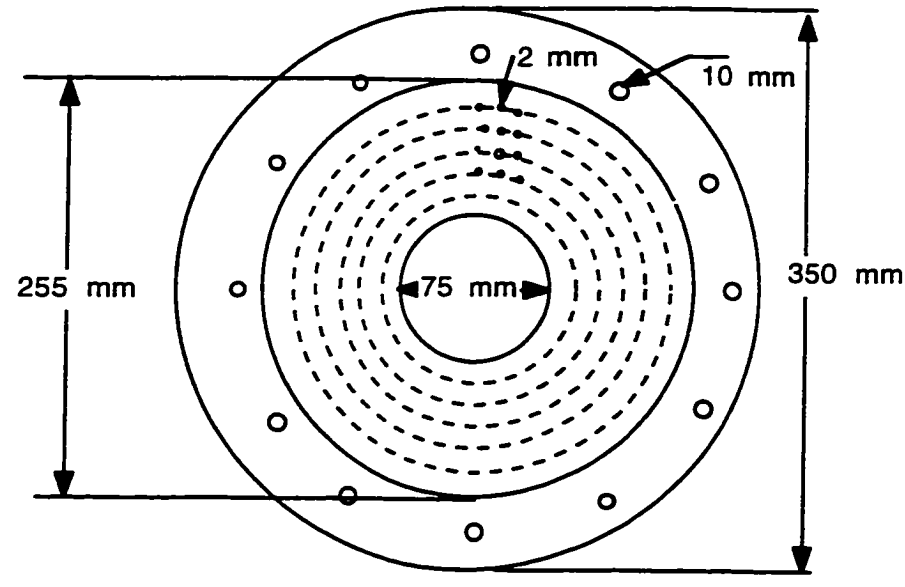

(a) Main

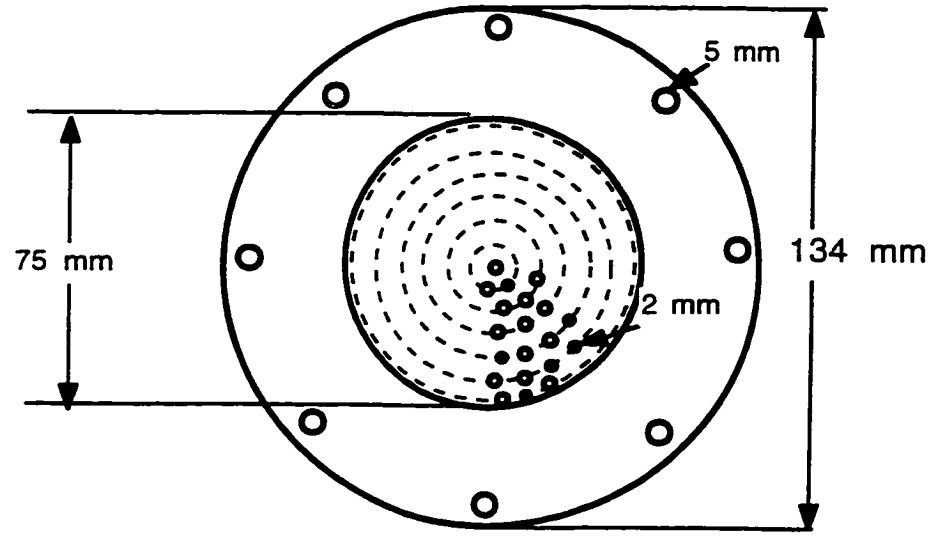

(b) Secondary

Figure 6.10 Main and Secondary Distributor Plates.

Fused Quartz Company, New Mexico, Missouri) were located 35 mm and 220 mm above the main distributor plate, for visual observation of the fluidization in the dense bed. The secondary fluidizing column also had a view window (40 mm x 100 mm) on the inner section and a second window (75 mm x 150 mm) on the outer section. These windows can stand temperatures up to 1200°C and were mounted on the steel columns by using a flange-gasket assembly. The bed material in the fluidizing column can be removed when required through a 40 mm port provided near the bottom of the bed.

A flexible blanket insulation material (Inswool-HP Blanket, A.P. Green Industries Inc., New Mexico, Missouri) was used to insulate the entire bed to reduce heat loss to the surrounding and to have enough energy for self-sustaining the reactions even at low equivalence ratios. This material has a low iron content, a high resistance to oxidation, reduction and corrosion, and can stand temperatures up to 1230°C.

6.2.5 Disengagement Section

A conically shaped enlarged section, having a bottom diameter of 255 mm, a top diameter of 355 mm and a height of 395 mm with an angle of inclination of 30° from the vertical, was mounted above the main fluidizing column. This enlarged disengagement section was made of 4 mm thick hot rolled steel. A view window (75 mm x 150 mm) was placed 80 mm from the top of the enlarged section. The top cover of this section was made of 8 mm thick stainless steel plate, and was connected to the outlet duct. This cover had two 75 mm x 75 mm view windows and a 40 mm diameter port for visual observations and for introducing the inert bed material, respectively. A pipe (6 mm thick, 310 stainless steel with recangular cross section of 40 mm x 80 mm) connected to the top of the enlarged section served as the gas outlet. This pipe served as a gas inlet into the cyclone.

A de-entrainment device consisting of 16 triangular blades (310 stainless steel) (Figure 6.11) was placed in the disengagement section. The blades were inclined at 30° to the

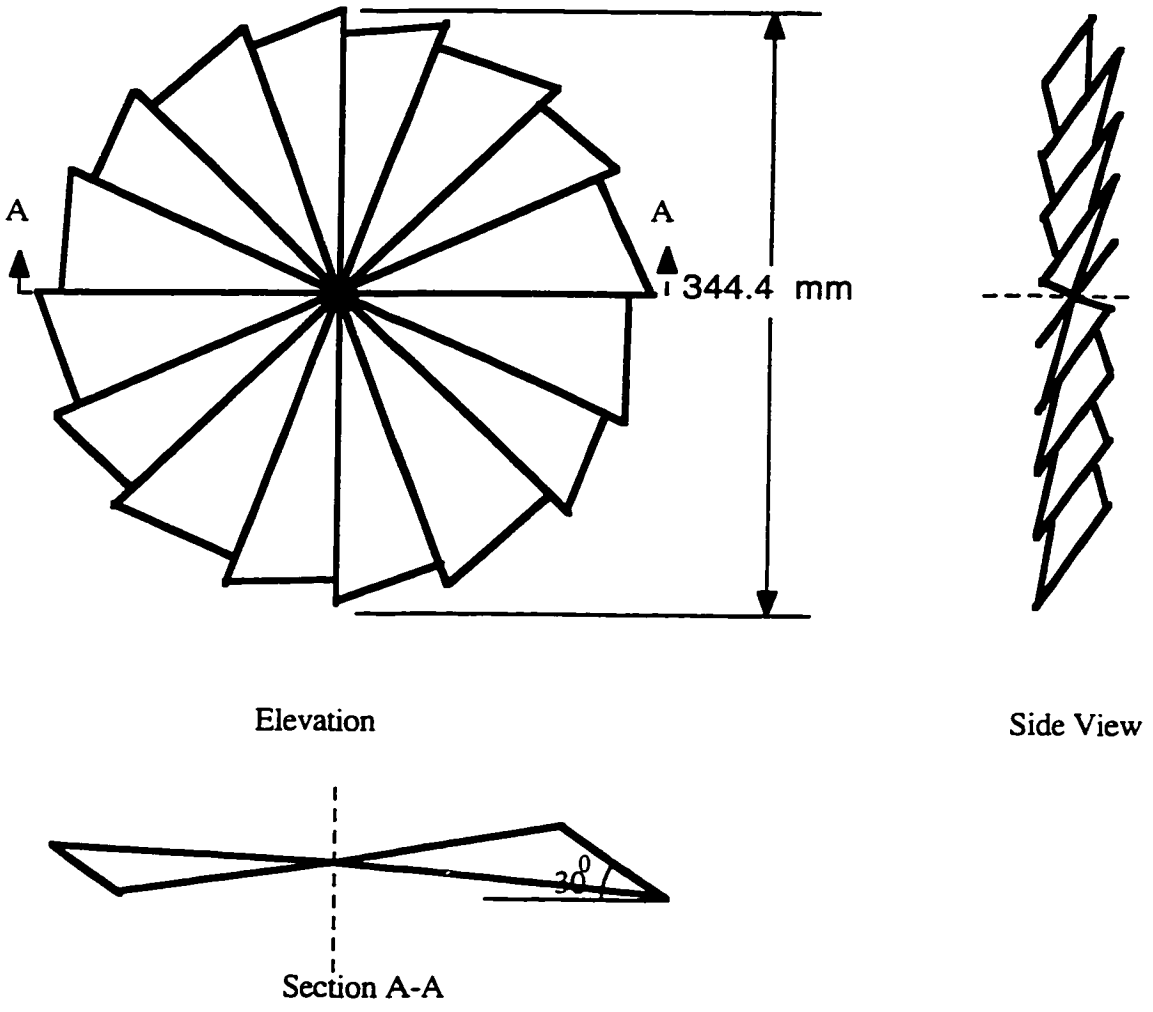

Figure 6.11 De-entrainment Device (Sadaka, 1994).

horizontal to reduce the elutriation rate from the fluidized bed. The distance from the top of one blade to the tip of the overlapping one was 61 mm. The de-entrainment device had a diameter of 344.4 mm, giving a clearance of 5.6 mm between the device and the wall of the disengagement section. The total open area of this device on the horizontal plane was 714 cm^2 (about 72% of the cross sectional area of the enlarged section and 141% of that of the fluidizing column).

6.2.6 Cyclone

The cyclone was connected to the exit of the disengagement section to capture the solid particles (dust, ash and char) escaping from the fluidized bed reactor. The cyclone (Figure 6.12) was made of 2 mm thick 310 stainless steel metal sheet capable of withstanding temperatures up to 1300°C. It consisted of a cylindrical section joined to a conical section. The cylindrical section had a 150 mm diameter and 300 mm height. The conical section had a height of 300 mm and was inclined at 10° to the vertical. The gas outlet was through a pipe of 75 mm diameter which extended 90 mm axially into the cyclone through the top. This pipe was further extended 150 mm axially into the after burner. The inlet gas was brought tangentially into the cylindrical section and a strong vortex was thus created inside the cyclone body. The fine dust and ash particles in the flow were subjected to centrifugal forces which move them radially outward, towards the inside cyclone surface on which the solids separate. The cyclone was, also, insulated using a flexible blanket insulation.

The solid particles (mainly ash), which escaped from the fluidized bed and separated from the gas stream by the cyclone, were collected in a cylindrical ash collector, of 0.470 m height and 0.275 m diameter, attached to the bottom of the cyclone. It was connected to the cyclone through a 1.0 m long vertical stainless steel pipe having an inner diameter of 75 mm. A view window (50 mm x 90 mm) was placed at the lower end of this pipe to view the ash movement. The lid of the ash collector was permanently welded to the end of the connecting

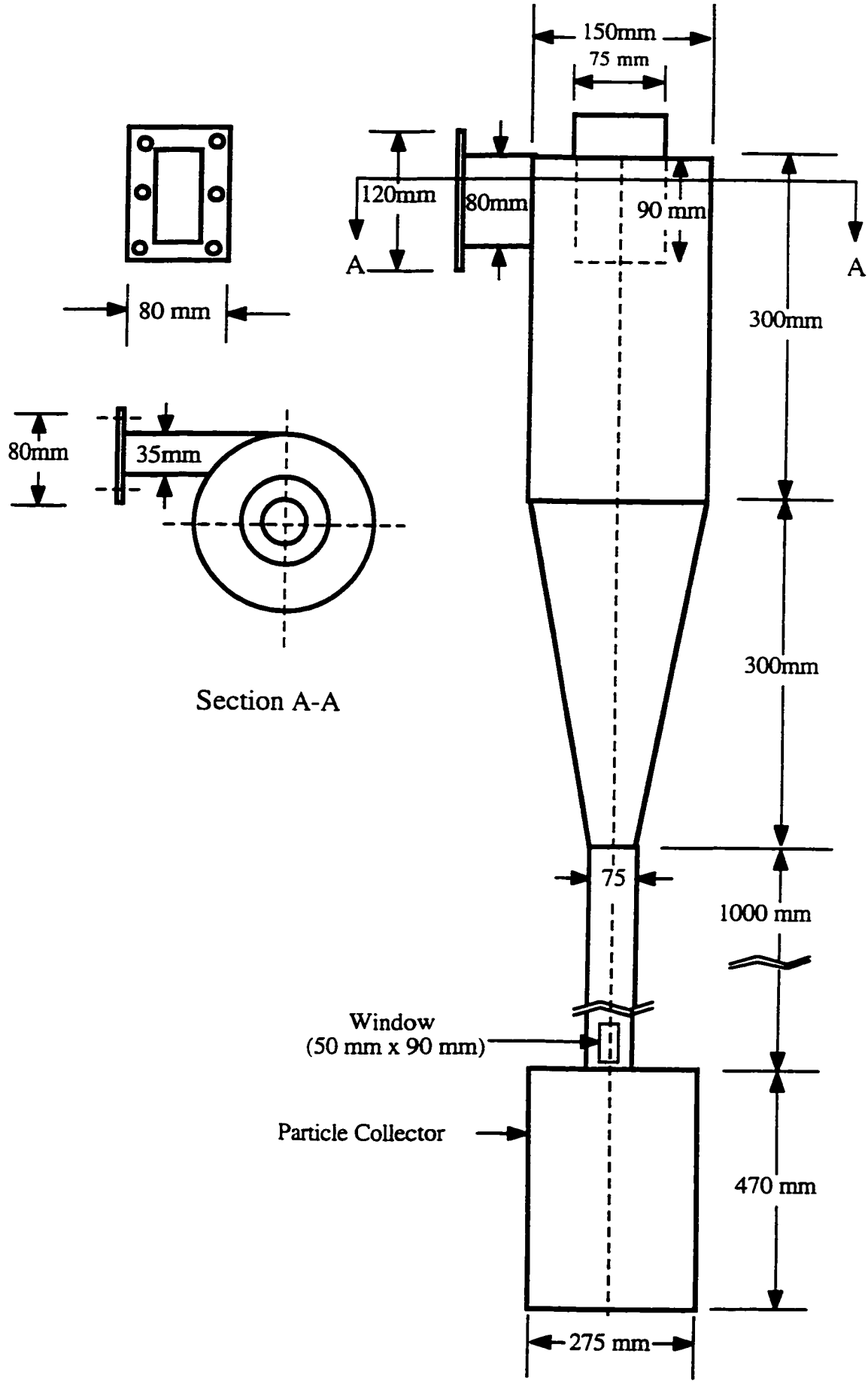

Figure 6.12 Cyclone.

pipe and the ash collector could easily be removed or attached to the lid by a simple clamp mechanism.

6.2.7 Afterburner

The afterburner is shown schematically in Figure 6.13. It consisted of two ignition electrodes, an air supply unit, a mixing chamber, a combustion chamber and an exhaust duct. The ignition chamber was constructed from 310 stainless steel and had an inside diameter and a height of 210 and 300 mm, respectively. The combustion chamber was, also, constructed from 310 stainless steel. It had an inside diameter and a height of 310 and 2000 mm, respectively. The exit gas from the cyclone entered the combustion chamber of the after burner from the bottom through a 150 mm inside diameter stainless steel pipe. Air was supplied to the combustion chamber through four pipes each having 60 mm inside diameter. The main air pipe had a damper for air flow regulation and an air flowmeter (Metal FLT-type, Cole Parmar Catalog No. N-03251-60, Chicago, Illinois). The air pipes had a horizontal angle of 15° and were welded tangentially to the wall of the mixing chamber to produce a swirling effect which created a complete air-gas mixing. Two ignition electrodes were welded to the end of the mixing chamber and connected to the ignition transformer. The electric arc electrode and the voltage ignition transformer assembled to the air supply unit start up the gas burning process. The exhaust duct was housed inside another pipe of 500 mm diameter for safety. Four brace cables supported the after burner from tilting.

6.3 Measurement and Data Acquisition Systems

6.3.1 Gas Sampling System

The gas sampling system consisted of gas sampling probe, vacuum pump, compressed air line, syringe and evacuated tubes. The stainless steel gas sampling probes with water cooling jackets (Figure 6.14) were 12.5 mm in diameter and 500 mm in length.

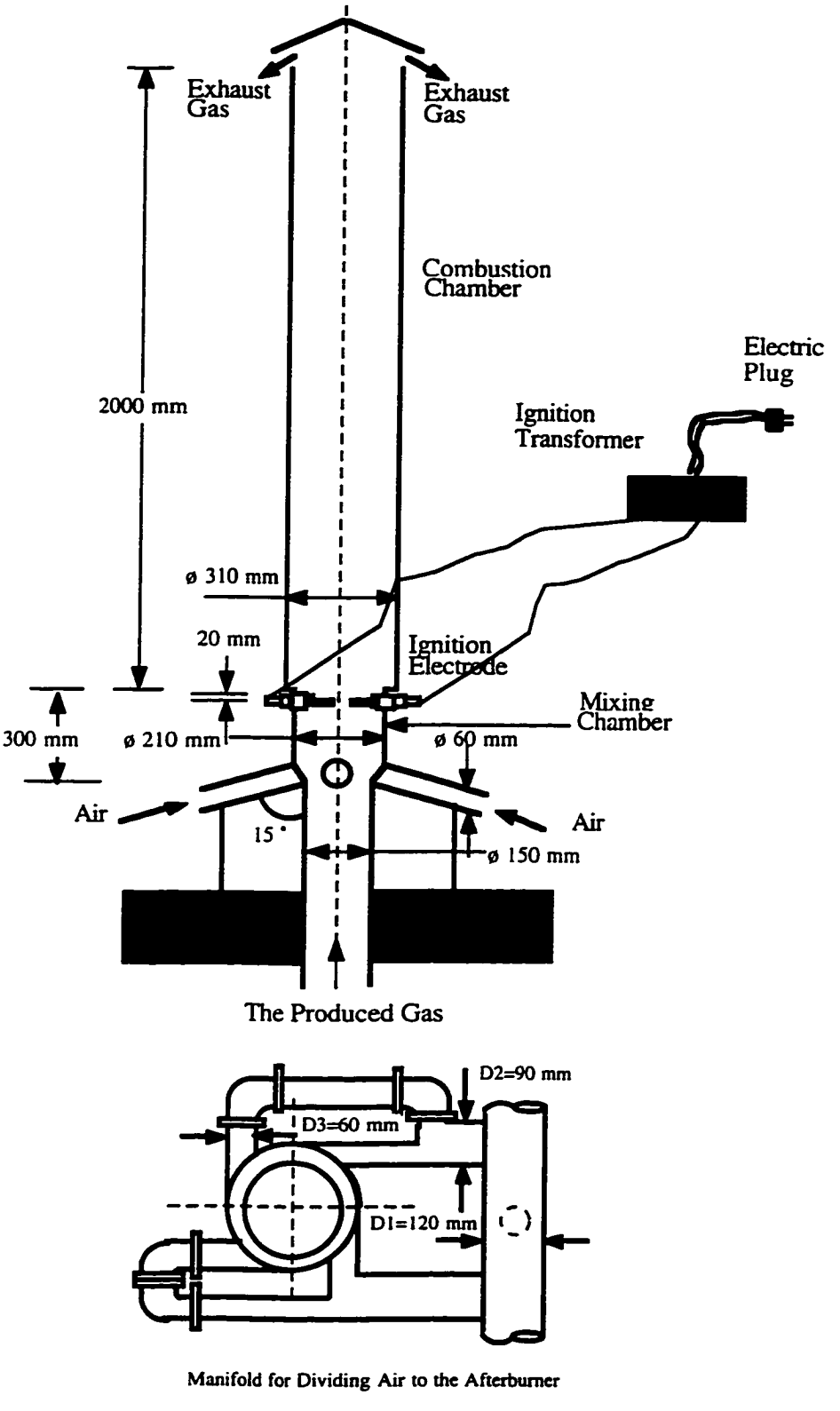

Figure 6.13. Afterburner (Sadaka, 1994).

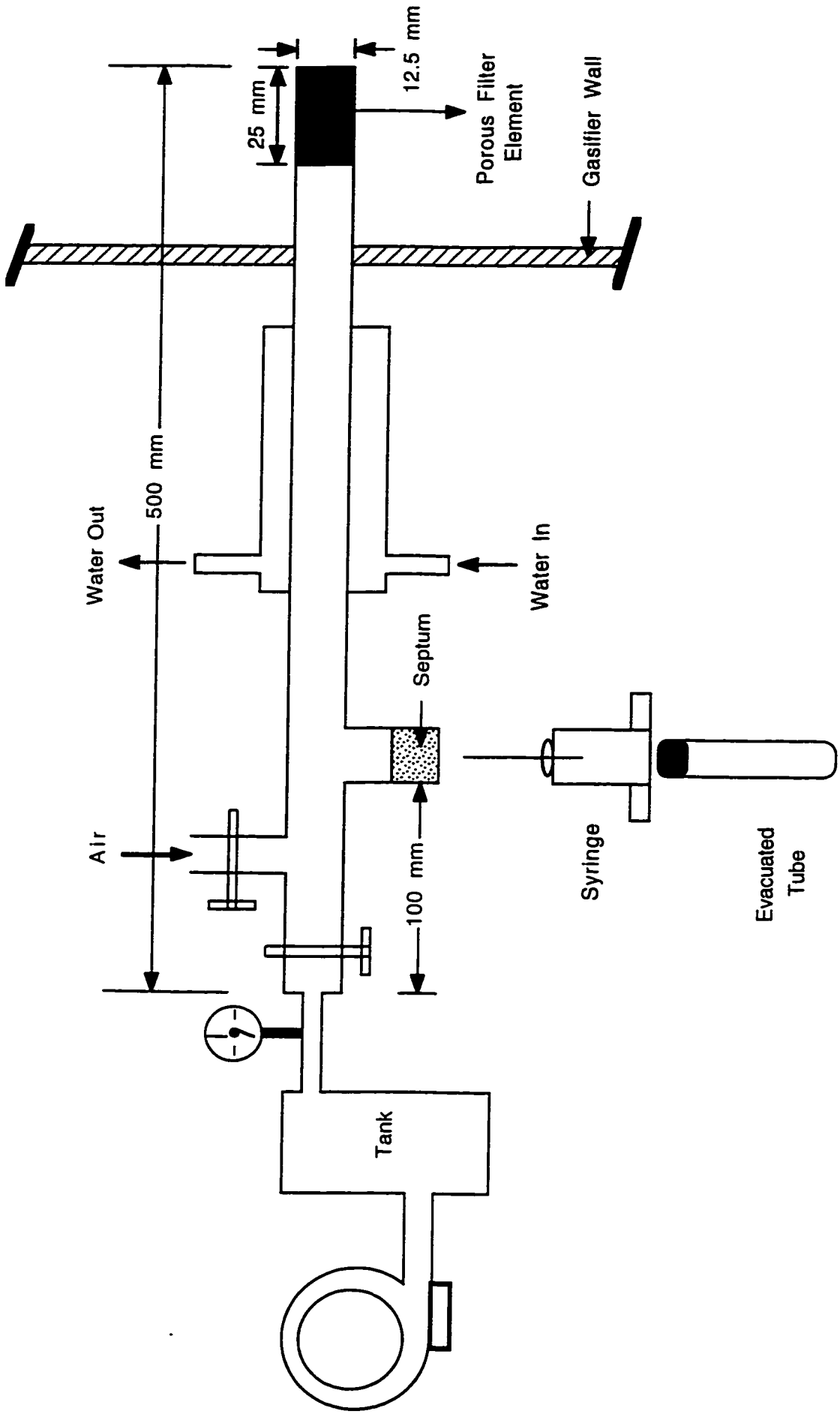

Figure 6.14 Gas Sampling System.

A 60 mesh size porous filter element (4F Series, Nupro Company, Willoughby, Ohio) was connected to the tip of the gas sampling probe to prevent fine particles from entering the gas sampling line. Compressed air was pumped through the probe before the comencement of sample collection to clean the gas line as well as the filter element. The air line was then closed and the vacuum pump opened to draw gas from the gasifier.

A syringe and evacuated tube assembly was used to collect the gas sample from the gas sampling probe. Vacutainer evacuated tubes (Model No. 6430, Becton Dickinson Vacutainer Systems, Rutherford, New Jersey) having a volume of 10 mL each were used to store the gas samples. These tubes were initially evacuated by the manufacturer up to 80% by volume. They were re-evacuated (up to 99% by volume) using a vacuum pump before being used. Figure 6.15 shows the gas sampling probe locations. Probes G_1, G_2 and G_3 were located in the dense bed of the fluidized bed reactor, probe G_4 was located in the freeboard region and probe G_5 was placed close to the bed exit at the middle of the enlarged section. Probe G_6 was placed at the exit of the cyclone.

6.3.2 Solids Sampling System

The solids sampling system consisted of particle sampling probes, vacuum pump, compressed air, water cooling jacket, storage vessel, and nitrogen line. Each probe (Figure 6.16) was used for the dynamic sampling of solids in the dense bed during the gasification process. It was made from a 427.5 mm long stainless steel tube of 8 mm inner diameter and 12.7 mm outer diameter. A stainless steel screen capsule was made to slide within an open-ended close tolerance pipe by means of pneumatic pistons. Compressed air was supplied throughout a run to prevent fine particles from entering the particle sampling line. The solid particles were sucked from the bed using a vacuum pump after stopping the air supply line. Another port connected to the sampling duct supplied inert cooling gas (nitrogen) to the sampling probe so that the sampled solid particles can be purged and cooled instantly. Figure 6.17 shows the solid particles sampling probe locations.

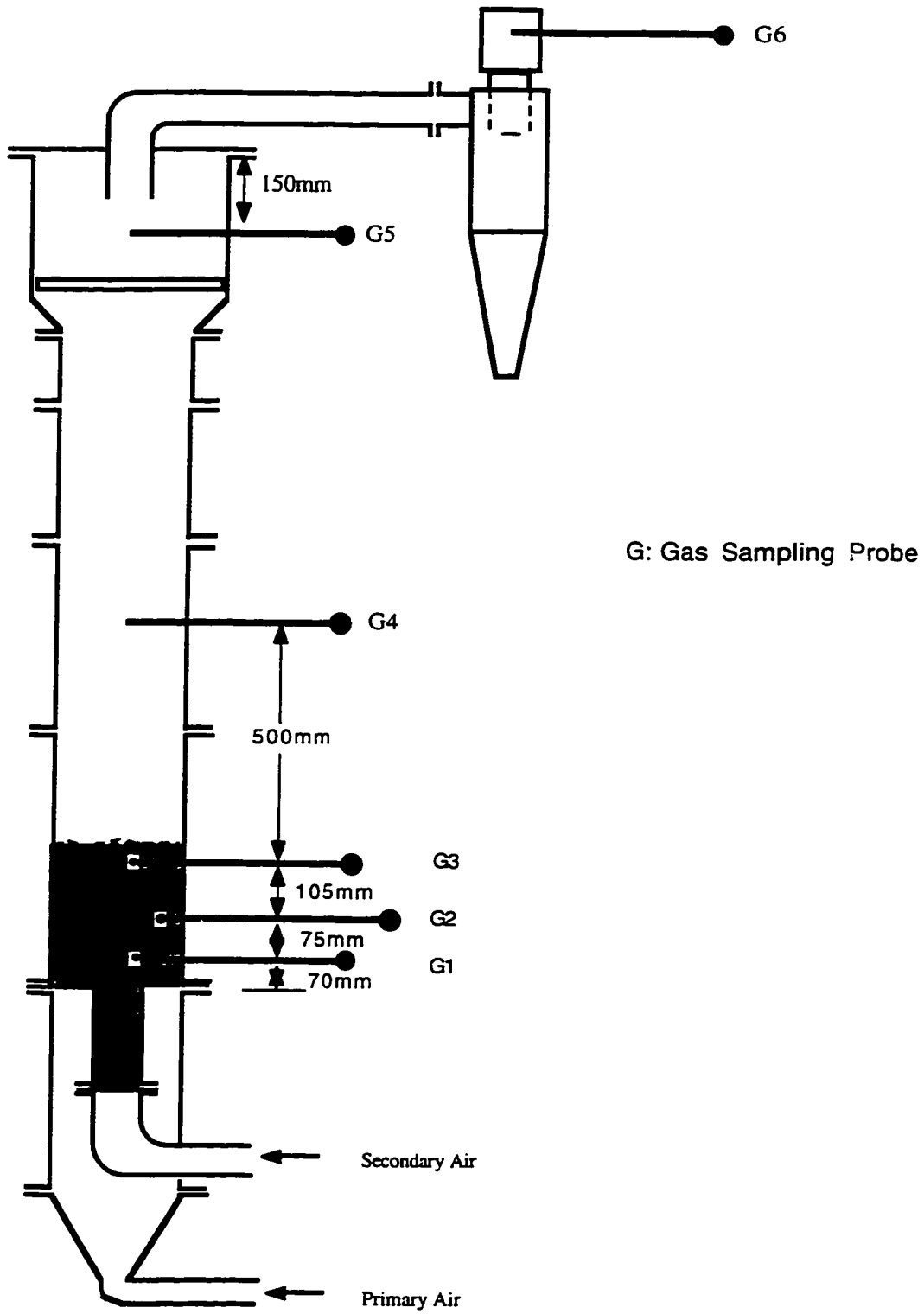

Figure 6.15 Location of Gas Sampling Probes.

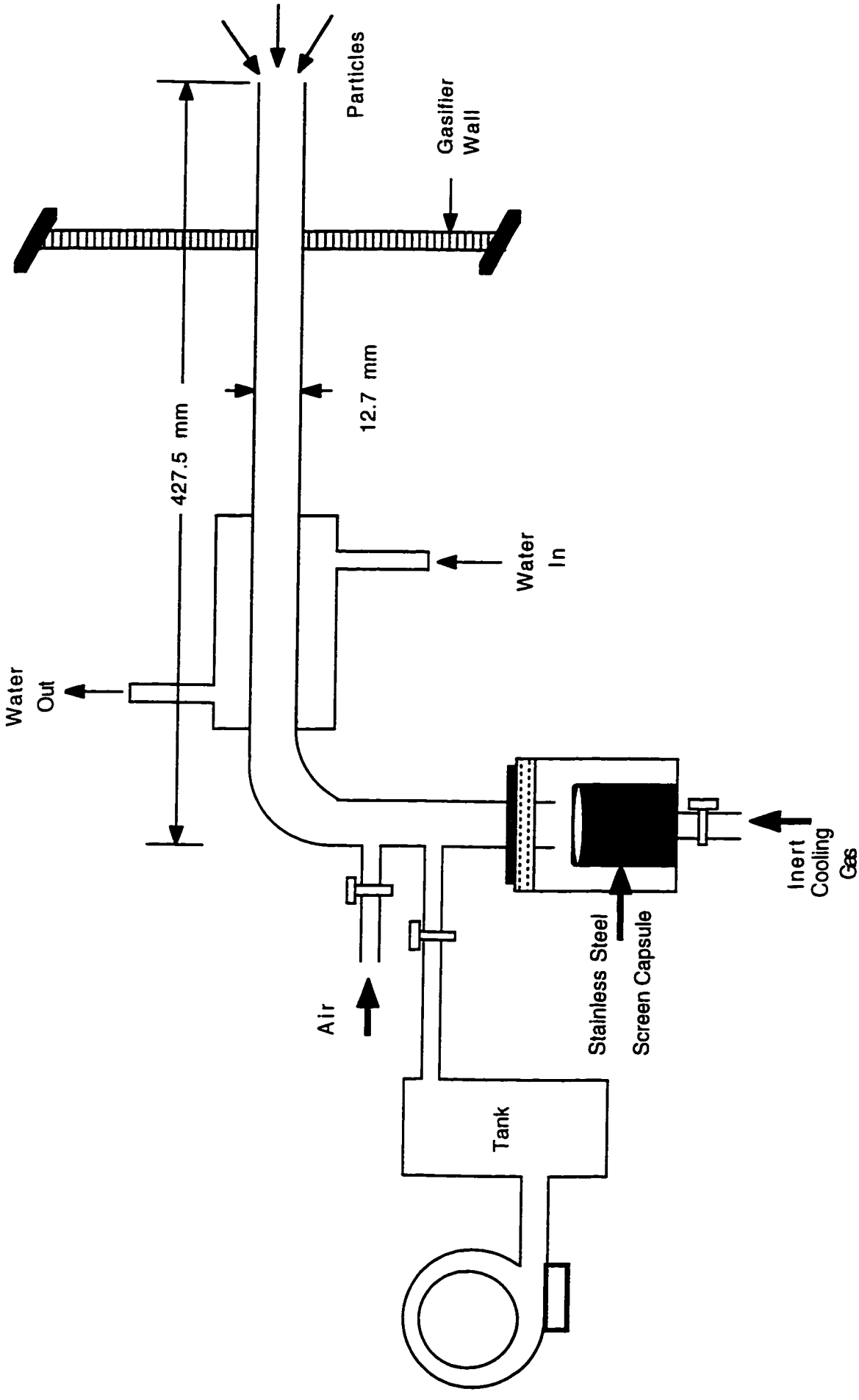

Figure 6.16 Solids Sampling System.

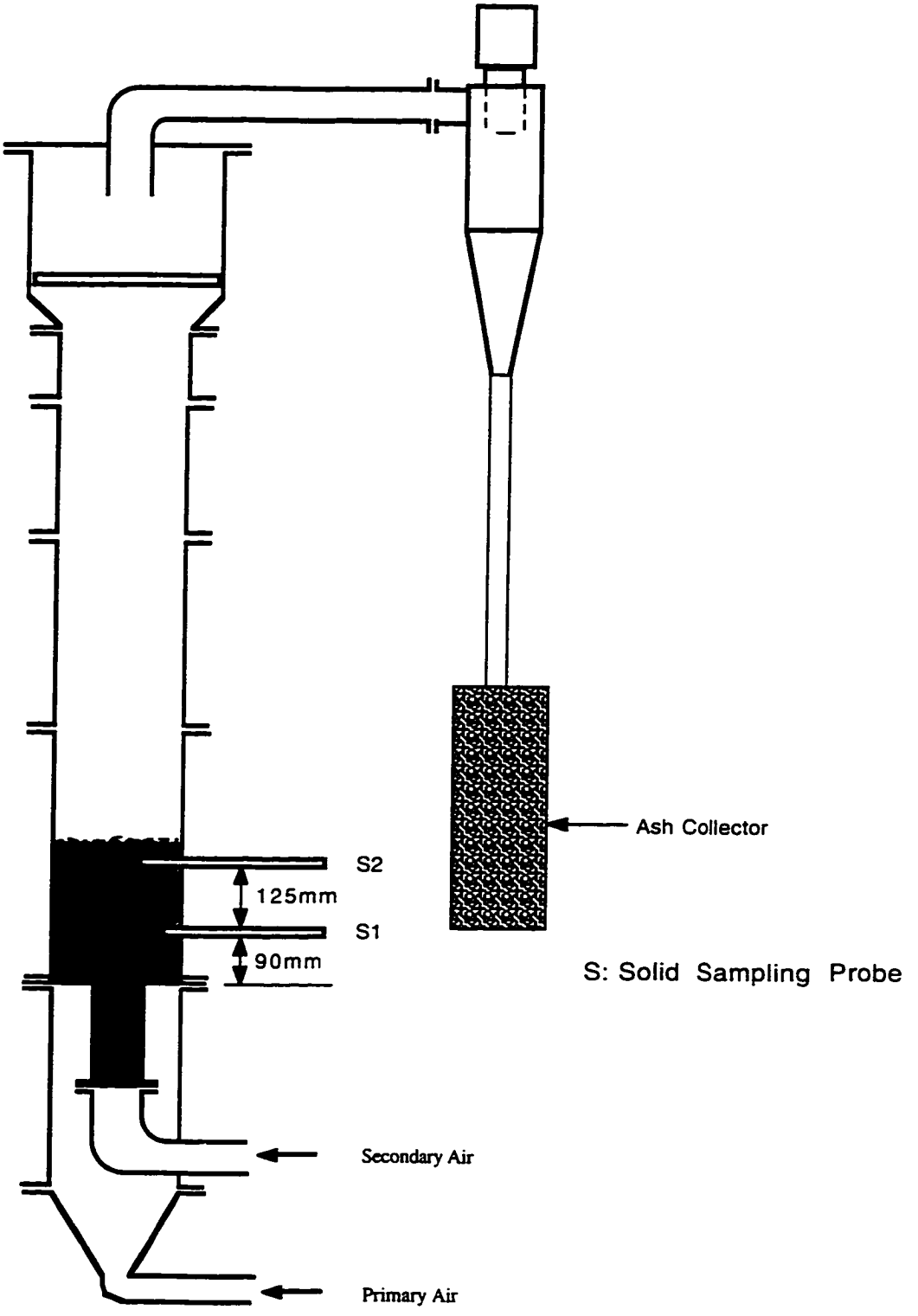

Figure 6.17 Location of Solids Sampling Probes.

6.3.3 Air Supply Rate Measurement System

The FLT-Type "Flow Cell Bypass Flowmeters" (Model No. 014344, Cole Parmer, Chicago, Illinois) were used to measure the air supply rates to the primary and secondary air supply lines. The flowmeters, ranging from 5 to 54 ft^3/m, were connected to horizontal pipelines. The length of the pipe section downstream from the flowmeter was kept greater than three times the pipe diameter, whereas the length upstream to the flowmeter was greater than eight times the pipe diameter as was recommended in the flowmeters operating manual. Each flowmeter can be used up to maximum temperature and pressure of 60°C and 1035 kPa, respectively, and accurate to 2.5 percent of its full scale.

6.3.4 Gas Flow Rate Measurement System

An upstream orifice plate (Figure 6.18) positioned on the duct between the cyclone and the stack was used to measure the gas production rate. The pressure drop across this plate was measured using a differential pressure transducer and the signals produced were conditioned and recorded on a computer. This pressure drop was then used to estimate the flow rate of the gases through the orifice plate.

6.3.5 Data Acquisition System

A data acquisition system was used for on-line recording and processing of the temperature and pressure drop in the fluidized bed gasifier. This system consisted of temperature probes, pressure tranducers, a d.c. power supply, a personal computer, and signal conditioning extentions for instrumentation (SCXI). The National Instruments SCXI is a multichannel signal conditioning and control system for use with personal computers. It comprised of a chassis that can house a variety of modules for any I/O needs. The SCXI system is programmed with LabVIEW (Laboratory Virtual Instrument Engineering Workbench), a National Instruments applications software package. The libraries of functions included in LabVIEW were used to develop a model for data acquisition, instrument control, data analysis, data presentation and data storage.

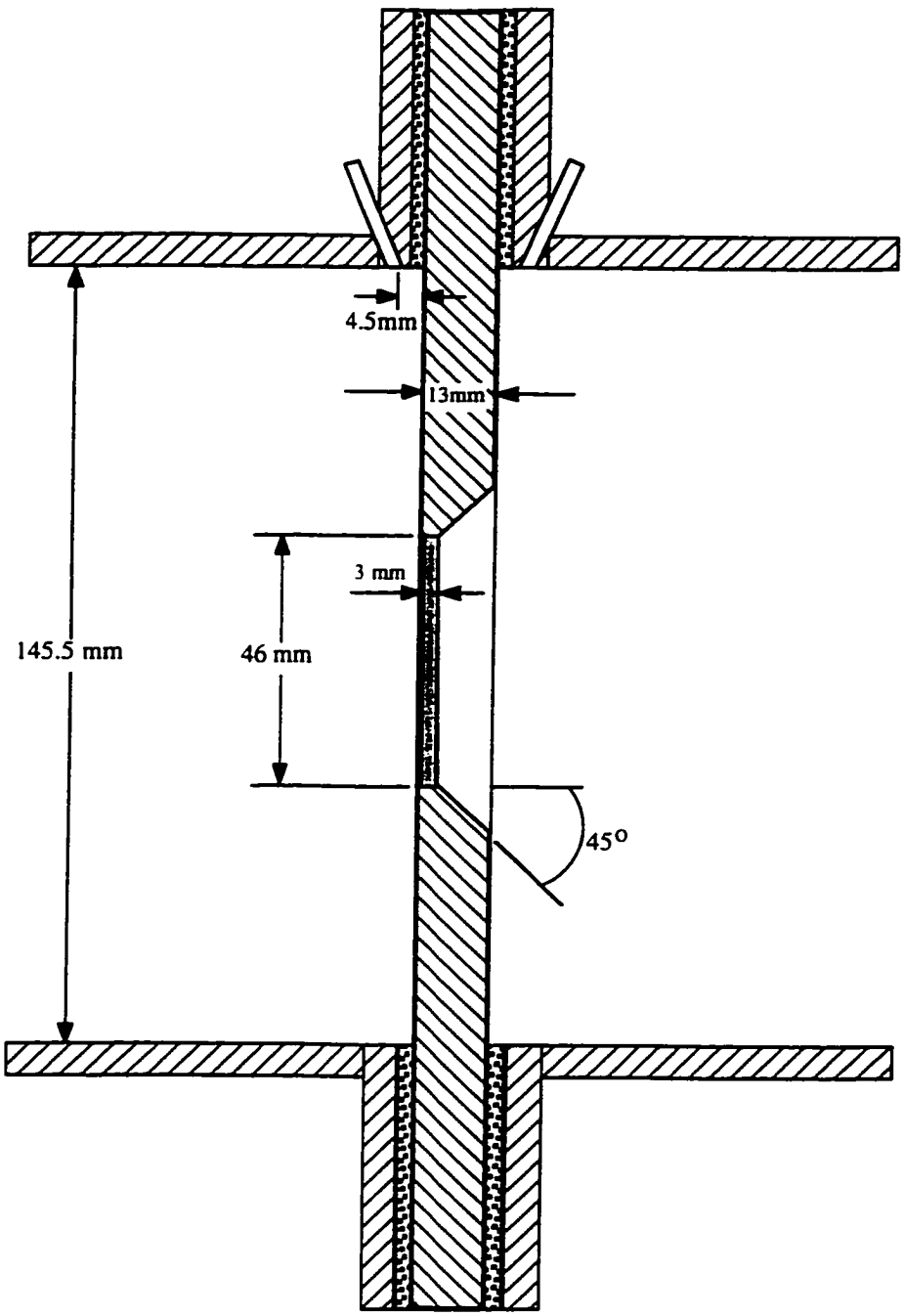

Figure 6.18 Orifice Plate.

The fluidized bed gasifier temperature variations were measured using Type-K special purpose thermocouple probes (Cole Parmer Cat. No. N-08516-70, Chicago, Illinois) with standard colour coded mini-connector plugs having a temperature range of 200-1372°C. The thermocouple probes were located such that the temperatures of the fluidizing gases before entry to the secondary column (T_1, T_2) and the main column (T_3) can be measured. The temperatures within the dense bed at different axial (T_4, T_5, T_6) and radial (T_7, T_8, T_9) positions were measured to monitor the temperature distribution in the dense bed. Thermocouple probes T_{10} and T_{11} were located in the freeboard to monitor the temperature variations in this region. Probes T_{12} and T_{13} were located at the inlet and outlet of the cyclone, respectively, and T_{14} was located in the afterburner. Figure 6.19 shows the temperature measurement system for the fluidized bed gasifier.

The pressure taps were installed vertically along the fluidized bed reactor at regular intervals, typically 100 to 200 mm, as shown in Figure 6.20. The outside opening of each tap was connected to a separate pressure transducer (OMEGA PX 185 - 015D5V, OMEGA Engineering Inc., Stamford, CT) using a piece of flexible plastic tubing. This transducer has two input channels and capable of producing an output voltage proportional to the pressure difference between the two input channels. The transducers have interchangeable diaphrams which provide a multirange working capacity. Twelve tranducers were used. The first measurement point (P_1) was located above the main distributor plate. The next four pressure taps (P_2, P_3, P_4, and P_5) were installed in the fluidizing column. The pressure drops in the freeboard just before the enlarged disengagement section were measured using taps P_6, and P_7. Taps P_8 and P_9 were installed in the de-entrainment device. Another measurement point in the freeboard (P_{10}) was positioned at the top of the enlarged section. Tap P_{11} was installed in the outlet duct connecting the bed exit to the cyclone inlet. A reference point (RS) was positioned below the secondary distributor plate and used to measure the pressure drop independently across this plate. The pressure transducers were rigidly mounted on a vero-board plugged to

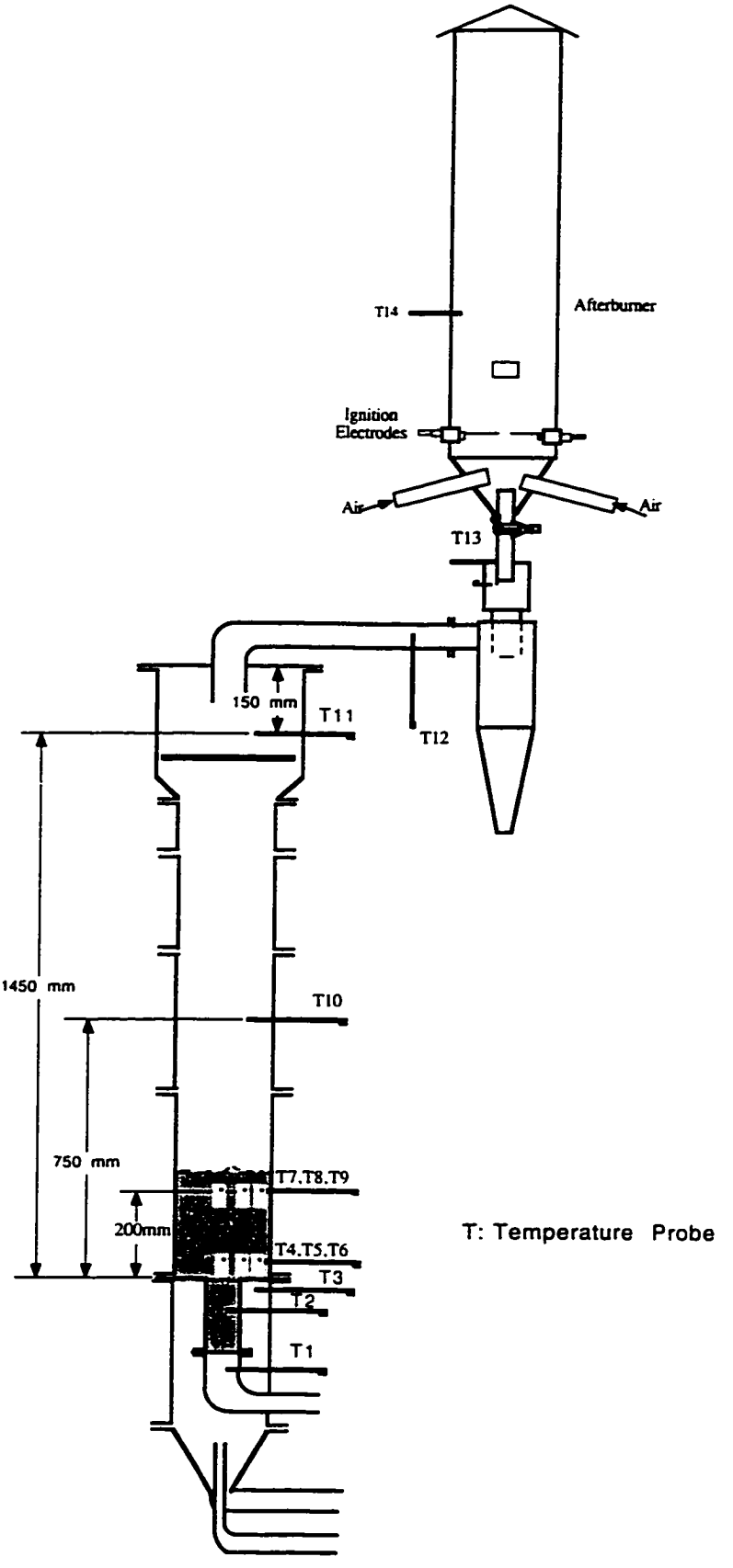

Figure 6.19. Location of Temperature Probes

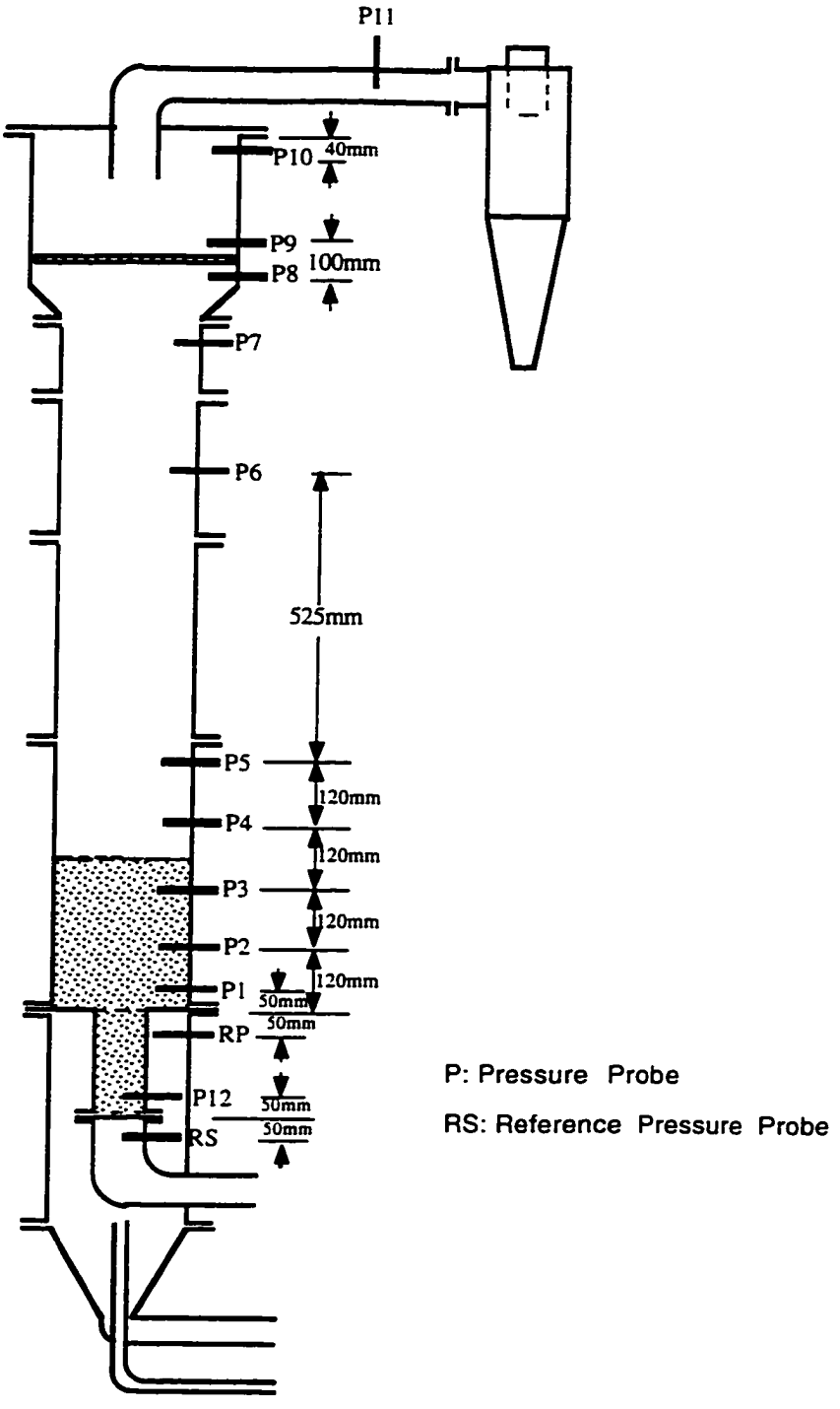

Figure 6.20 Location of Pressure Probes.

the side of an aluminium enclosure. This assembly was located on the wall in close proximity to the gasifier.

7. EXPERIMENTAL DESIGN

7.1 Preliminary Experiments

7.1.1 Physical and Chemical Properties of Rice Husks

Various thermochemical conversion systems such as combustors and gasifiers have been designed and tested for the recovery of energy from various biomass materials. However, comprehensive and reliable information on the rice husk properties pertaining to the design of such systems is lacking. Full understanding of the physical and chemical properties of rice husk is, therefore, essential for proper design of these systems.

The various aspects of physical and chemical properties of rice husks obtained from six varieties of rice (Lemont LG, ROK 14, ROK 16, ROK 32, CP 4 and Pa Potho) as related to thermochemical conversion processes were investigated. These included moisture content, bulk density, particle size, heating values, proximate analysis, ultimate analysis, ash composition and ash fusibility characteristics.

7.1.2 Agglomeration Characteristics of Inert Bed Materials

A major problem associated with the development of fluidized bed biomass gasifiers is the agglomeration of inert bed materials, in the presence of biomass ash, resulting in serious channeling and defluidization. The agglomeration characteristics of inert bed materials (silica and alumina sand particles) in the presence of lemont LG rice husk ash were, therefore, investigated to define conditions beyond which it is not safe to operate the gasifier.

The effects of five levels of temperature (750, 850, 900, 950 and 1000°C) and six levels of rice husk ash content (0.0, 5.0, 10.0, 15.0, 20.0 and 25.0%) (Table 7.1) on the

Table 7.1 Layout of Experimental Design for the Agglomeration Experiments.

Bed Material	Temperature (°C)	Ash Content (%)
Silica	750	0
		5
		10
		15
		20
		25
	850	0
		5
		10
		15
		20
		25
	900	0
		5
		10
		15
		20
		25
	950	0
		5
		10
		15
		20
		25
	1000	0
		5
		10
		15
		20
		25
Alumina	750	0
		5
		10
		15
		20
		25
	850	0
		5
		10
		15
		20
		25
	900	0
		5
		10
		15
		20
		25
	950	0
		5
		10
		15
		20
		25
	1000	0
		5
		10
		15
		20
		25

agglomeration characteristics of inert bed materials were studied using a high temperature muffle furnace (Isotemp Model No. 186A, Fischer Scientific, Toronto, Ontario).

7.1.3 Thermal Degradation and Kinetics of Rice Husks

Although the thermal degradation of some ligno-cellulose materials such as wood and their individual components has been extensively studied, the exact mechanism and kinetics of the reactions occurring are not yet completely clear. Data reported by several authors (Shafizadeh, 1968; Ramiah, 1970; Vantelon et al., 1990; and Tia et al., 1991) show large discrepancies, due mostly to the analytical methods used as well as the different ways of data treatment. However, reasonably accurate values of the kinetic parameters are necessary for the design and development of thermochemical conversion technologies. Therefore, in order to provide more reliable kinetic data it is necessary to conduct extensive thermogravimetric analysis on rice husks.

The thermogravimetric behaviour of rice husks was examined at 10, 20 and 50°C/minute heating rates in air (21% oxygen and 79% nitrogen), pure oxygen (99.5% oxygen, 50 ppm water, 40 ppm total hydrocarbons and 1 ppm solvents) and pure nitrogen (99.5% nitrogen and 0.5% oxygen) atmospheres between 25 and 700°C. The thermal degradation rates, the initial degradation temperature and the residual weight at 700°C were determined in the three atmospheres. The TGA curves were used to determine the kinetic parameters (energy of activation, preexponential factor and order of reaction).

7.2 Main Experiments

The effects of three levels of bed height (19.5, 25.5 and 31.5 cm), three levels of fluidization velocity (0.22, 0.28, and 0.33 m/s), based on the minimum fluidization velocity of

the inert bed material, and three levels of equivalence ratio (0.25, 0.30 and 0.35) on the performance (reactor temperature, bed pressure drop, product gas composition, product gas heating value, product gas yield, carbon conversion and energy recovery) of the fluidized bed rice husk gasifier were investigated. The experimental design layout is shown in Table 7.2.

The air-to-fuel ratio was the main variable and is described in this study by the equivalence ratio, which is defined as the air-to-fuel weight ratio divided by the air-to-fuel weight ratio of stoichiometric combustion. This ratio was computed by first determining the stoichiometric amount of air needed to combust the rice husks completely, to CO_2 and H_2O with only the minerals as residue. One kg of these rice husks requires 4.70 kg of air for stoichiometric combustion. The air supply rate to the secondary column was kept constant throughout the experiments whereas the primary air supply rate through the main distributor plate was varied to alter the fluidization velocity. The actual levels of operating variables for the fluidized bed rice husk gasification system are shown in Table 7.3.

Table 7.2 Layout of Experimental Design for the Main Experiment.

Bed Height (cm)	Fluidization Velocity (m/s)	Equivalence Ratio (-)
19.5	0.22	0.25
		0.30
		0.35
	0.28	0.25
		0.30
		0.35
	0.33	0.25
		0.30
		0.35
25.5	0.22	0.25
		0.30
		0.35
	0.28	0.25
		0.30
		0.35
	0.33	0.25
		0.30
		0.35
31.5	0.22	0.25
		0.30
		0.35
	0.28	0.25
		0.30
		0.35
	0.33	0.25
		0.30
		0.35

Table 7.3 Actual Rice Husk Feed Rates and Air Supply Rates.

Bed Height (cm)	Fluidization Velocity (m/s)	Equivalence Ratio (-)	Rice Husk Feed Rate (kg/min)	Primary Air Supply (m^3/min)	Secondary Air Supply (m^3/min)	Total Air Supply (m^3/min)
19.5	0.22	0.25	0.67	0.27	0.57	0.84
		0.30	0.56			
		0.35	0.48			
	0.28	0.25	0.86	0.45	0.57	1.02
		0.30	0.72			
		0.35	0.61			
	0.33	0.25	1.02	0.64	0.57	1.21
		0.30	0.85			
		0.35	0.73			
25.5	0.22	0.25	0.67	0.27	0.57	0.84
		0.30	0.56			
		0.35	0.48			
	0.28	0.25	0.86	0.45	0.57	1.02
		0.30	0.72			
		0.35	0.61			
	0.33	0.25	1.02	0.64	0.57	1.21
		0.30	0.85			
		0.35	0.73			
31.5	0.22	0.25	0.67	0.27	0.57	0.84
		0.30	0.56			
		0.35	0.48			
	0.28	0.25	0.86	0.45	0.57	1.02
		0.30	0.72			
		0.35	0.61			
	0.33	0.25	1.02	0.64	0.57	1.21
		0.30	0.85			
		0.35	0.73			

8. EXPERIMENTAL PROCEDURE

8.1 Preliminary Experiments

8.1.1 Physical and Chemical Properties of Rice Husks

8.1.1.1 Rice husk collection. Rice husk samples from six varieties of rice (Lemont LG, ROK 14, ROK 16, ROK 32, CP 4 and Pa Potho) were collected for the study. Lemont (long grain) was obtained from Broussard Rice Mills, Louisiana, USA and the remaining five samples (ROK 14, ROK 16, ROK 32, CP 4 and Pa Potho) were obtained from the West African Rice Research Station, Rokupr, Sierra Leone. Lemont and Pa Potho rice varieties were processed in rubber roller mills, ROK 14 was processed in small steel cylinder mills and ROK 16, ROK 32 and CP 4 were processed in large disc-sheller mills. ROK 14, CP 4 and Pa Potho were parboiled before milling. Parboiling consists basically of saturating the paddy with water and raising the temperature to that required to gelatinize the starchy endosperm.

Samples of approximately 5 kg of rice husks each were collected from each rice mill, placed in polyethylene bags and transported to the Thermal Analysis Laboratory at DalTech, Dalhousie University in Halifax, Nova Scotia, Canada. The rice husk samples were dried in forced air oven (Isotemp Oven Model No. 655F, Fisher Scientific, Toronto, Ontario) at 105°C for 24 hours to avoid deterioration due to moisture content. The dried samples were stored in polyethylene bags for future processing.

8.1.1.2 Rice husk sample preparation. Dried rice husk samples were coarse ground through a 20-mesh sieve on a medium size Wiley Mill (Model No. X876249, Brook Crompton Parkinson Limited, Toronto, Ontario). Approximately 1.0 kg of material from each sample was ground so that a sufficient quantity of material would be available for ash analysis. Portions

of the coarse ground samples were reground through a 40-mesh sieve on the Wiley Mill in order to narrow the range of the particle size and, thus, obtain homogeneous samples. Fine-ground samples were used for proximate, ultimate and heat value analyses.

8.1.1.3 Ash sample preparation. The ash samples were obtained by ashing the coarse ground rice husk in porcelain crucibles using a muffle furnace (Isotemp Muffle Furnace Model No. 186A, Fisher Scientific, Chicago, Illinois) at 600°C for one hour. The ash samples were allowed to cool down in a desiccator and then weighed. The process was repeated until constant weight was obtained. The samples were collected and stored in airtight containers until needed for the ash analyses.

8.1.1.4 Measurement of physical properties. The three most important physical properties related to thermochemical conversion are: moisture content, bulk density and particle size distribution.

8.1.1.4.1 Moisture content: Moisture content tests were performed on the as-received rice husk samples by oven drying method, ASTM D 3173-73 (Anon., 1983). Rice husk samples weighing approximately 0.5 kg each were placed in large aluminum dishes. The dishes containing the rice husks were placed in an air forced drying oven (Isotemp Oven Model No. 655F, Fisher Scientific, Toronto, Ontario) at 105°C and kept until a constant weight was achieved. Typical drying time was 24 hours. The moisture content of the various rice husk varieties was then calculated on wet basis as follows:

$$M.C._{wet} = \frac{(WW - DW)}{WW} X100 \qquad (8.1)$$

where:

WW is the wet weight of the rice husk sample (kg)

DW is the dry weight of the rice husk sample (kg)

The purpose of air-drying is to reduce the moisture in the samples to approximate equilibrium with the air of the laboratory, thereby minimize changes in moisture content when the sample is handled during analysis.

8.1.1.4.2 Bulk density: Bulk densities of the different rice husk varieties were determined according to ASTM Standard Method for the Bulk Density of Particulate Biomass Fuels, E 873-82 (Anon., 1983). A cylindrical container (6 cm in diameter and 6.2 cm high, inside dimensions) was used. The empty container was weighed using a Mettler Balance (Model No. PM 4600, Mettler Instrumente AG, Greifensee, Zurich). The container was filled by pouring loose rice husk from the top edge of the container. The container and sample were then weighed and the net mass of the material was divided by the volume of the container to obtain the bulk density as follows:

$$\rho_b = \frac{(F - E)}{V} \tag{8.2}$$

where:

ρ_b is the bulk density of the rice husk sample (kg/m^3)

F is the weight of container and rice husk sample (kg)

E is the weight of container (kg)

V is the volume of container (m^3)

8.1.1.4.3 Particle Size Distribution: Samples of rice husk from the six varieties were selected randomly for sieve analysis to determine the size distribution of rice husk particles. The size distribution was determined using eight standard sieves (Canadian Standard Sieve Series, W. S. Tyler Company of Canada Limited, St. Catharines, Ontario) and a bottom pan, the latter

collects everything that passes through the eighth sieve. The sieves were mounted in an electrical sieve shaker (Model Rx-86, Hoskin Scientific Limited., Gastonia, NC) driven by a 0.25-hp electric motor running at 1,725 rpm. The shaker was running at a speed of 350 rpm. About 1.0 kg of a rice husk sample was put into sieve no. 1, which was then covered with the sieve lid. The shaker was operated for 30 minutes. The rice husk particles collected in each sieve were analyzed for weight, width and length distribution. In order to obtain a complete description of the rice husk particle size distribution, length and width measurements were performed using a ruler marked off in millimeters as shown in Figure 8.1.

8.1.1.5 Measurement of chemical properties. The chemical properties of rice husk measured in this study are: heating value, proximate analysis, ultimate analysis, ash composition and ash fusibility.

8.1.1.5.1 Heating values: A bomb calorimeter (Parr Model 1241 Automatic Adiabatic Calorimeter, Parr Instrument Co., Moline, Illinois) was used to determine the higher heating value of the rice husk samples. The procedure used closely followed the Standard Test Method for Gross Calorific Values of Coal and Coke by the Adiabatic Bomb Calorimeter (D-2015-85) given in the American Society for Testing and Materials (ASTM, 1986). The bomb calorimeter measures the heat released by combustion of fuel with oxygen. This is referred to as the constant volume higher heating value (Ebeling and Jenkins, 1985). Difficulties were experienced in burning samples of rice husk in the bomb calorimeter. The sudden release of volatiles expelled the rice husk particles from the combustion crucibles, resulting in incomplete combustion. To avoid this problem, the fine-ground samples were moistened to 10 to 15% moisture content (wet basis) and formed into 0.5 to 1.0g pellets. The pellets were then oven dried prior to testing in the bomb calorimeter. The lower heating value was calculated from the higher heating value using Equation (4.4).

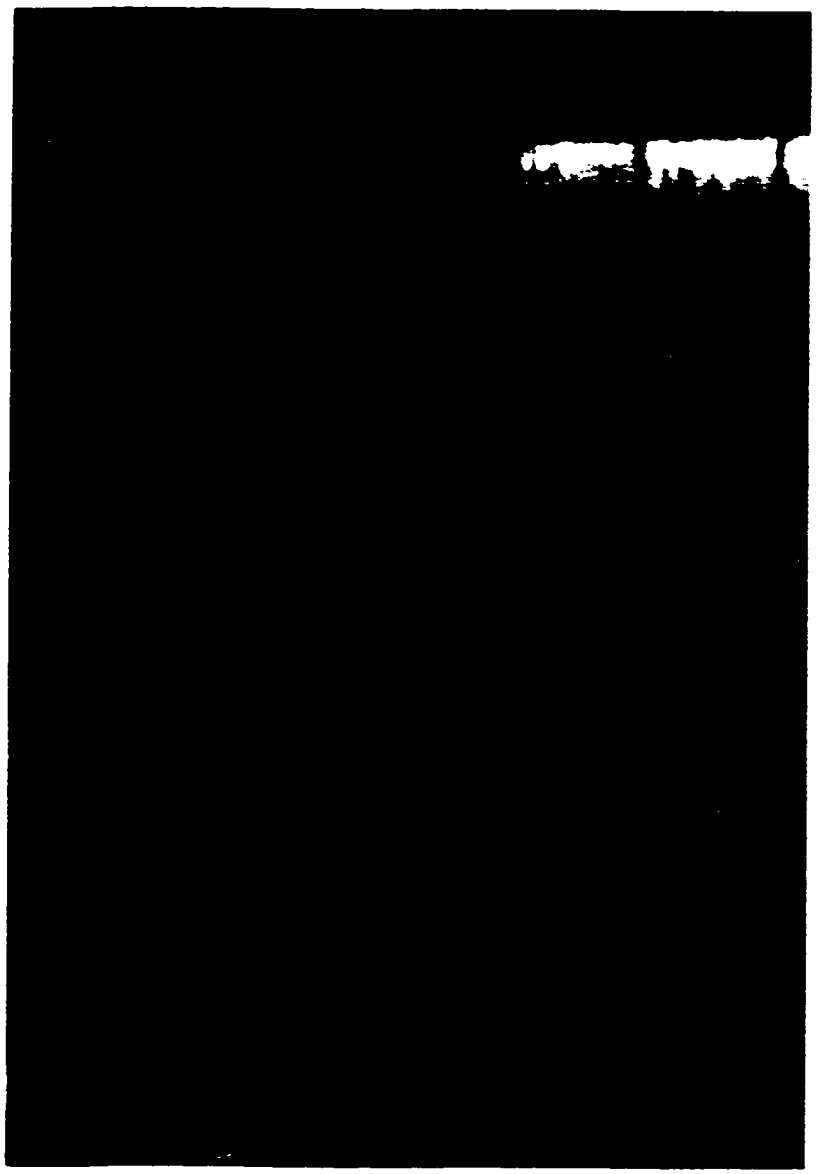

Figure 8.1 Sample size of rice husks.

8.1.1.5.2 Proximate analysis: The proximate analysis was performed on the fine-ground, oven-dried rice husk samples to determine the weight fractions of volatiles, ash and fixed carbon in the rice husk. The ASTM Standard Method for Proximate Analysis of Coal and Coke (D-3172-73 through D-3174-82 and D-3175- 82) was used (ASTM, 1986). Because rice husks are a highly volatile fuel, the modified version for sparkling fuels was used. Thus, the values of volatiles and ash were determined on dry matter basis. The fixed carbon was then obtained by subtracting from 100 the sum of volatile matter and ash contents.

8.1.1.5.3 Ultimate analysis: Ultimate analysis was performed on the fine-ground, oven-dried rice husk samples to determine the elemental composition. The weight fractions of carbon, hydrogen, nitrogen, sulphur, chlorine, and ash were determined, and the weight fraction of oxygen in the rice husk samples was calculated by the difference. Carbon, hydrogen, and nitrogen weight fractions were determined using a Perkin-Elmer LECO CHN Elemental Analyzer (Model No. 240, International Equipment Company, Needham Hts., MA). Sulphur was determined using the LECO induction furnace (LECO S-Analyzer, International Equipment Company, Needham Hts., MA). Chlorine was determined by following the Mercuric Nitrate Method given in Standard Methods for the examination of Water and Wastewater (APHA, 1985). The ASTM Standard Test Method for Ash in Wood (D-1102-84) was followed to determine the ash percentage in the rice husk sample (ASTM, 1986). Because of the lack of a simple, direct method for determining oxygen in biomass fuels, it is usually estimated by subtracting the sum of carbon, hydrogen, nitrogen, sulphur, chlorine and ash from 100.

8.1.1.5.4 Ash composition analysis: Ash composition analysis was performed on the ash samples obtained from rice husks. The weight fractions of silicon, potassium, calcium, phosphorus, magnesium, sulphur, chlorine, sodium, aluminium, iron, zinc and titanium and their oxides were determined. Silicon, phosphorus, and their oxides were determined using the method given by Shapiro (1975) for rapid analysis of silicate, carbonate and phosphate rocks.

Aluminium, calcium, magnesium, sodium, potassium, iron, zinc, titanium, and their oxides were determined by atomic absorption according to the procedure given by Abbey et al. (1974). Sulphur and sulphur dioxide were determined in a LECO induction furnace (Model No. 521-000, LECO Equipment Corporation, St. Joseph, Michigan).

8.1.1.5.5 Ash fusibility: Ash fusibility tests were performed on the ash samples from rice husk. The ASTM Standard test Method for Fusibility of Coal and Coke Ash (D-1857-68) was used (ASTM, 1986). The initial deformation temperature, softening temperature, hemispherical temperature, and fusion temperature in both an oxidizing (air) atmosphere and a reducing (60% CO, 40% CO_2) atmosphere were determined.

8.1.2 Agglomeration Characteristics of Inert Bed Materials

8.1.2.1 Inert bed materials. The silica sand used in this study was obtained from Nova Scotia Sand and Gravel Ltd (Shubenacadie, Nova Scotia, Canada). It was sieved manually to remove the fines and dust. The alumina sand was obtained from Diamonite Products Ltd., Shreve, Ohio, USA. The sand was very spherical in shape and was kiln fired at 1500°C. The main characteristics and chemical composition of the silica and alumina sand are given in Tables 8.1 and 8.2, respectively.

8.1.2.2 Rice husk. The rice husks (Lemont LG) were obtained from Broussard Rice Mill in Mermentau, Louisiana, USA. It was sieved to free it from dirt and foreign materials. The rice husk was used in its high-ash (pure ash) and low-ash (original rice husk) forms in this study. The pure ash was prepared by burning some of the rice husk in a muffle furnace at 600°C for several hours until there was no weight change in the sample.

8.1.2.3 Muffle furnace experiments. The sample size of sand (silica or alumina) used was 10g. Two sets of experiments were carried out in this study at five temperature

Table 8.1 Main Characteristics of the Silica Sand.

Characteristic	Value
Density (kg/m^3)	
Particle density	2660
Bulk density	1650
Particle size (μm)	
Maximum particle size	850
Mean particle size	410
Minimum particle size	120
Chemical composition (%)	
SiO_2	98-99
TiO_2	0.40
Fe_2O_3	0.35
Li_2O	0.30
Al_2O_3	0.15
CaO	0.10
MgO	0.04

Table 8.2 Main Characteristics of the Alumina Sand.

Characteristic	Value
Density (kg/m^3)	
Particle density	3450
Bulk density	2000
Particle size (μm)	
Maximum particle size	500
Mean particle size	380
Minimum particle size	250
Chemical composition (%)	
Al_2O_3	85.00-90.00
SiO_2	8.00-10.00
CaO	0.50-2.00
MgO	0.50-1.50
Na_2O	0.10-0.40
Fe_2O_3	0.10-0.30
TiO_2	0.05-0.15
K_2O	0.01-0.05

levels (750, 850, 900, 950 and 1000°C) and six levels of ash content (0.0, 5.0, 10.0, 15.0, 20.0 and 25.0%) using a muffle furnace (Isotemp Muffle Furnace Model No. 186A, Fischer Scientific, Toronto, Ontario). The first set was conducted with 0.0, 2.5, 5.0, 7.5, 10.0 and 12.5g of Lemont LG rice husk in its original particle size and the second set was conducted with 0.0, 0.5, 1.0, 1.5, 2.0 and 2.5g of pure ash of the same rice husk variety.

Thirty ceramic dishes were used in the first set of experiments. They were divided into five groups, having six dishes each. Each dish received 10g of sand. Each group (six dishes) received one of the six levels of ash content (0.0, 5.0, 10.0, 15.0, 20.0 or 25.0%) from the rice husk. The muffle furnace was brought to the desired temperature (750, 850, 900, 950 or 1000°C) and each group was placed into the muffle furnace at the desired temperature until constant weights were obtained. The dishes were then removed from the muffle furnace and placed in a desiccator to cool. The second set of experiments was carried out with the rice husk ash following the same procedure. The colour, structure and texture of the residual products were observed visually. A light microscope (Wild Leitz Aristophot, UNITRON Inc., Bohemia, New York) was used to investigate the structure of the sand-ash mixtures after heat treatment in the furnace. This microscope is a photomicrography device incorporating interchangeable lenses, extendable bellows and a 35 mm camera body, along with a transmitted light source mounted beneath the glass stage. The samples were exposed to the light source for some minutes and the pictures were then taken.

8.1.2.4 Scanning electron microscopy and energy dispersive x-ray analysis.

The images of the untreated (zero conversion) and muffle furnace treated rice husk, rice husk ash and pure sand samples were observed under an environmental scanning electron microscope (ElectroScan E3, AMRAY INC., Bedford, MA) at the Geological Survey Laboratory of the Atlantic Canada, Bedford Institute of Oceanography, Dartmouth, Nova Scotia. A digital energy dispersive x-ray analyser (Noran "Voyager", AMRAY INC.,

Bedford, MA), in combination with the environmental scanning electron microscope, was used to determine the elemental make-up of each sample. The energy dispersive x-ray analyser is controlled by a SUN workstation computer (AMRAY, INC., Bedford, MA) which is also an image analyser that can digitise, store, and process the environmental scanning electron microscope images. Colloidal graphite (a water based adhesive) was used to attach the samples to a holding disc according to the procedure used at the Geological Survey Laboratory of the Atlantic Canada, Nova Scotia (Moran, 1996).

The operation of the sample chamber of the environmental scanning electron microscope under partial pressure of water vapour, rather than a high vacuum as in older instruments, eliminated the need to coat the samples. The samples were placed in the environmental scanning electron microscope and their images and x-ray spectra were analysed at beam accelerating voltages from 10 kV to 25 kV while the instrument magnification remaining unchanged at 1000X. The contrast was increased until a bright image was observed at the center of the screen. The contrast and brightness were adjusted to obtain a well defined image occupying roughly the whole surface of the video signal monitor. The image was then focused and the environmental scanning electron microscopy photomicrograph was taken. The x-ray spectra of the samples were obtained by retracting the detector of the energy dispersive x-ray analyser in the environmental scanning electron microscope and centering the beam onto the surface of the sample. The x-ray spectra were accumulated for a few minutes until the spectral peaks and peak lists were generated.

8.1.3 Thermal Degradation and Kinetics of Rice Husks

8.1.3.1 Sample preparation. Dried rice husk samples (Lemont long grain variety from Broussard Rice Mills, Louisiana, USA and ROK 14, CP 4 and Pa Potho from the West African Rice Research Station, Rokupr, Sierra Leone) were coarse ground through a 20-mesh sieve (850 μm) on a medium size Wiley Mill (Model No. X876249, Brook Crompton

Parkinson Limited, Toronto, Ontario). Approximately 1.0 kg of rice husk from each sample was ground so that a sufficient quantity of material would be available for the analysis. Portions of the coarse ground samples were reground through a 40-mesh sieve (425 μm) on the Wiley Mill in order to narrow the range of the particle size and, thus, obtain homogenous samples. These were stored in air tight plastic containers until they were needed for the thermogravimetric analysis. This procedure ensured reproducible thermogravimetric results.

8.1.3.2 Thermal analysis. Rice husk samples were subjected to thermogravimetric analysis in dry air (21% oxygen and 79% nitrogen), in pure oxygen (99.5% oxygen, 50 ppm water, 40 ppm total hydrocarbons and 1 ppm solvents) and in pure nitrogen (99.5% nitrogen and 0.5% oxygen) atmospheres at three heating rates (10, 20 and 50°C/min.). In order to ensure the uniformity of the sample temperature, a small sample size is recommended. However, if the sample material is nonhomogeneous, a large sample size becomes necessary. In this study, several sample sizes were analysed in order to obtain information on temperature uniformity. A good reproducibility was achieved with sample sizes in the range of 10-20 mg. Therefore, samples weighing approximately 15 mg were used throughout the study. The samples were heated from ambient temperature to 700°C in a METTLER Thermal Analyzer (Mettler Instrumente AG, Model No. TG 50, Greifensee, Zurich).

The TG 50 Thermobalance consisted of a microbalance, which has a precision of ± 0.1 μg. The base with the furnace was controlled by a TA Processor. The furnace temperature in the TG 50 Thermobalance was controlled in such a way that the sample temperature followed the desired profile. For this purpose, the temperature equilibration function between the furnace and the sample was provided by the manufacturer (Mettler Instrumente AG). Besides the shape and colour of the sample, the heat transfer rate is principally dependent on the furnace temperature and the heat capacity of the sample. However, the coefficients of the temperature equilibration function, which are specific to the sample, have been proven to be constant for

small samples and equal to the standard values given by the manufacturer of the instrument. The precision of the temperature measurement for TG 50 Thermobalance is ± 2°C.

The continuous records of weight loss and temperature were obtained and analyzed using a METTLER Thermal Analysis Software (Mettler Instrumente AG, Model No. TA 72, Greifensee, Zurich) system to determine the following thermogravimetric analysis indices: thermal degradation rates, initial degradation temperature and residual weight at 700°C. The kinetic parameters (energy of activation, pre-exponential factor and order of reaction) were then determined from the TGA data.

8.2 Main Experiments

8.2.1 Rice Husk Collection

Rice husks (Lemont LG) used for the 27 gasification runs were obtained from Brousand Ricemills, Louisiana, United States of America. Rice husks are generated in large quantities from these rice mills and have no commercial value. The rice husks were properly stored to avoid any contamination during storage period. Rice husk is a relatively uniform material and it does not require any treatment before use.

8.2.2 Bed Material

Alumina sand used in the main experiments was obtained from Diamonite Products Polybron Division, U.S.A. The alumina sand was kiln fired at 1500°C and very spherical in shape. Sieve analysis was carried out on the sand to obtain the mean diameter and particle size distribution. The main characteristics and chemical composition of the alumina sand are given in Table 8.2.

8.2.3 Operating Procedure

Each run was started with the filling of the bed of alumina sand up to the required height. The auger water-cooling system was turned on and the minimum primary air supply rate required to fluidize the bed particles in the main fluidizing column of the reactor was supplied through the master propane start-up burner. The master propane shut-off valve was then opened and the main switch of the start-up burner turned on. The start-up period is necessary to preheat the bed up to the required temperature before commencement of fuel feeding.

When the bed temperature reaches a certain level (about 600°C), the start-up unit was shut down and the primary air supply kept on to cool the bottom section (wind-box) of the gasifier. The secondary air supply was turned on and adjusted to the minimum rate required to carry the bed particles from the secondary column into the main column. The rice husk was augered into the lower part of the fluidized bed, just above the secondary distributor plate and the rice husk feed rate was adjusted to allow 20% excess air in order to achieve complete combustion of the rice husks. The air and rice husk flow rates were varied to give the desired equivalence ratio. The bed was fluidized at this condition for half an hour to ensure that steady state condition was reached.

The pressure drops and temperatures were monitored and registered every two minutes on a central computer based data acquisition system and software. After the bed temperature stabilized, gas samples from six locations along the reactor and char samples from two locations in the dense bed were taken for analysis. When all sampling and data recording is complete, the rice husk flowrate was stopped and both the secondary and primary air flowrates were left on to burn the char still in the reactor. Simultaneously, the ash collector downstream the cyclone was removed and weighed. Samples of the ash were kept for analysis.

8.2.4 Sampling Procedure

8.2.4.1 Gas sampling. Gas sampling was carried out at the end of each run during the steady state. This procedure was started by purging the gas sampling probe with compressed air (550 kPa) to clean the gas sampling line from tar and particulates. The valve connecting the vacuum pump to the sampling probe was kept open for about two minutes to flush the sampling line with fresh gas from the gasifier. The valve was closed and samples collected using a syringe and an evacuated tube. The evacuated tube was kept in position for about one minute to allow it to be completely filled with the gas from the sampling line. Three samples were collected from each sampling position. The same procedure was repeated for the five other sampling probes.

8.2.4.2 Char sampling. Three different char samples were obtained for each run. One was obtained from the cyclone collector and the others obtained from the dense bed using the particle sampling probes. At the end of each run, the ash collector was removed from the bottom of the cyclone, covered with a lid and left to cool down. The solid particles sampling probes were supplied with air throughout the runs to prevent solid particles from entering the probe. During sampling, the air supply was closed and samples sucked from the bed into a storage vessel using a vacuum pump connected to the sampling probe. Another port connected to the sampling duct supplies inert cooling gas (nitrogen) to the sampling probe so that the sampled solid particles can be purged and cooled instantly. The samples were placed in aluminium dishes and sealed with airtight plastic covers until needed for analysis.

8.2.5 Analyses

8.2.5.1 Gas analysis. The quality of the gas samples was analyzed in terms of their composition using a gas chromatography (Hewlett Packed Model 5890 Series II, Atlanta, Georgia). The gas chromatography was calibrated using standard gases. Helium was used as

carrier gas at a flow rate of 30 mL/min. The column temperature was 45°C and the detector temperature was 250°C. From the average chromatograph analysis, the higher heating value (HHV) and the volumetric flow rate of the produced gas (Appendix A) were calculated. Other calculations that were performed include the volumetric gas yield, carbon conversion and energy recovery.

8.2.5.2 Char analysis. Bulk density tests were performed on all char samples from the cyclone collector to determine the fraction of sand in the char-sand mixtures. The char samples from the three locations were screened to separate the sand from the char using 200 mesh (75μm) sieve. Physical and chemical properties of the char samples were obtained by analysing their particle size distribution, carbon content, volatile matter content, ash content and heating value. These analyses were conducted in the Mining Engineering Department of DalTech, Dalhousie University, Halifax, Nova Scotia. The particle size distribution of the char collected by the cyclone was determined on a Master Particle Sizer (Model 2600, Malvern Instruments, Malvern, Worcestershire) and that collected from the dense bed was determined using sieves mounted in an electrical sieve shaker (Model Rx-86, Hoskin Scientific Limited, Gastonia, NC). The carbon content in the collected char samples were determined by drying a preweighed sample at 105°C for 24 hours and then burning combustibles from the char in an oven for one hour at 550°C. Ash and volatile matter contents in the samples were determined according to ASTM D 3714-73 and ASTM D 3175-77, respectively (ASTM, 1986). Heating value analyses were done on a bomb calorimeter (Parr Model 1261 Automatic Adiabatic Calorimeter, Parr Instrument Co., Moline, Illinois).

9. RESULTS

9.1 Preliminary Experiments

9.1.1 Physical and Chemical Properties of Rice Husks

9.1.1.1 Physical properties. The three critical physical parameters of biomass that affect its use in several ways are moisture content, bulk density and particle size distribution.

9.1.1.1.1 Moisture content: Table 9.1 shows the moisture content results of the various as-received rice husk varieties. The values ranged from 8.68% (ROK 14) to 10.44% (ROK 16).

9.1.1.1.2 Bulk density: Table 9.2 shows the bulk density results of the as-received rice husk samples. The bulk density ranged from a low of 86 kg/m^3 for ROK 16 rice husk to a high of 114 kg/m^3 for CP 4 rice husk. The varieties Lemont LG, ROK 14, ROK 32 and Pa Potho had a bulk density of 92, 106, 105 and 110 kg/m^3, respectively.

9.1.1.1.3 Particle size distribution: The results of the weight, length, and width distribution of randomly selected samples (from the six rice husk varieties) are given in Table 9.3. The measurements were based on a selection of 100 single rice husk particles that had both husk parts. About 55% of the particles ranged in length from 6.2 to 10.0 mm and in width from 1.7 to 2.4 mm. The results of these measurements and the sieve analysis were consistent.

9.1.1.2 Chemical properties. The critical thermochemical parameters of biomass that relate to its thermochemical conversion are heating value, proximate analysis, ultimate analysis, ash composition and ash fusibility.

Table 9.1 Moisture Content of As-received Rice Husks.

Rice Husk	Moisture Content* (%)
Lemont (LG)	9.08
ROK 14	8.68
ROK 16	10.44
ROK 32	10.20
CP 4	9.00
Pa Potho	10.16

* Average of three replicates.

Table 9.2 Bulk Density of As-received Rice Husks.

Rice Husk	Bulk Density* (kg/m^3)
Lemont (LG)	92
ROK 14	106
ROK 16	86
ROK 32	105
CP 4	114
Pa Potho	110

* Average of three replicates.

Table 9.3 Weight, Length, and Width Distribution of Lemont Rice Husks*.

Sieve Number	Mesh		Weight (%)**	Length (mm)		Width (mm)	
	Number	Size (mm)		Range	Average	Range	Average
1	7	2.80	2.06	11.6-12.4	2.0	2.8-4.0	3.4
2	8	2.36	14.22	10.2-11.4	10.8	2.4-2.8	2.6
3	10	2.00	23.60	8.8-10.0	9.4	2.0-2.4	2.2
4	12	1.70	31.34	6.2-8.0	7.1	1.7-2.0	1.9
5	14	1.40	18.72	4.0-6.0	5.0	1.4-1.7	1.6
6	18	1.00	7.37	3.2-4.0	3.6	1.0-1.4	1.2
7	20	0.85	1.17	1.5-2.4	2.0	0.8-1.0	0.9
8	25	0.71	0.67	0.8-1.2	1.0	0.7-0.9	0.8
pan	-	0.00	0.85	dust	dust	dust	dust

* Average of 100 measurements.
** Percent of total weight.

9.1.1.2.1 Heating value: The higher and lower heating values for the six rice husk samples are presented in Table 9.4. The average lower heating value for the rice husk varieties ranged from a low of 13.24 MJ/kg (ROK 14) to a high of 16.20 MJ/kg (ROK 16).

9.1.1.2.2 Proximate analysis: Rice husk has a relatively high volatile matter content, high ash content and low fixed carbon as shown in Table 9.5. The average volatile matter, fixed carbon and ash contents of the six rice husk varieties ranged from 63.00% (CP 4) to 70.20% (ROK 16), 12.40% (CP 4) to 14.50% (ROK 16) and 15.30% (ROK 16) to 24.60% (CP 4), respectively.

9.1.1.2.3 Ultimate analysis: The results of the ultimate analysis conducted on the rice husk samples are presented in Table 9.6. The weight fraction of carbon varied from 37.60% (Lemont LG) to 44.50% (ROK 16), oxygen varied from 31.37% (CP 4) to 36.56% (Lemont LG) and hydrogen varied from 4.70% (CP 4) to 5.51% (ROK 16). The nitrogen content of the rice husk samples was very low (0.38 to 0.51%) compared to coal (1.0 to 1.5%). The sulphur content of the rice husk samples was, also, relatively low (0.01 to 0.03%) compared to coal (0.5 to 10%). The chlorine content varied from 0.01 to 0.13%.

9.1.1.2.4 Ash composition: The composition of ash from rice husk samples is presented in two forms: (a) percentage by weight of mineral elements (Table 9.7) and (b) percentage by weight of mineral oxides (Table 9.8). The major mineral elements found in the rice husk ash samples were silicon, potassium, calcium, phosphorus and magnesium. Small amounts of aluminium, iron, sodium, sulphur, titanium and zinc were also detected. The weight percentage of each mineral element was estimated as a percentage of its oxide. The sum total of weight percentage of all mineral elements in rice husk ashes was between 44.97 and 48.11%. The major mineral oxide of the rice husk ash samples was SiO_2, followed by K_2O. Small amounts of CaO, $P2O_5$, MgO, Al_2O_3, Fe_2O_3, Na_2O, and SO_3 were also present, as well

Table 9.4 Heating Value of Rice Husks.

Rice Husk	Higher Heating Value (MJ/kg)	Lower Heating Value (MJ/kg)
Lemont (LG)	15.90	14.22
ROK 14	14.72	13.24
ROK 16	18.31	16.20
ROK 32	16.50	14.60
CP 4	14.92	13.40
Pa Potho	15.98	14.12

Table 9.5 Proximate Analysis of Rice Husks (Dry Basis).

Rice Husk	Volatile Matter (%)	Fixed Carbon (%)	Ash (%)
Lemont (LG)	66.40	13.60	20.00
ROK 14	67.30	13.90	18.80
ROK 16	70.20	14.50	15.30
ROK 32	67.30	14.00	18.70
CP 4	63.00	12.40	24.60
Pa Potho	67.60	14.20	18.20

Table 9.6 Ultimate Analysis of Rice Husks (Weight % Dry Basis).

Rice Husk	C	H	O	N	S	Cl	Ash
Lemont (LG)	37.60	5.42	36.56	0.38	0.03	0.01	20.00
ROK 14	42.10	4.98	33.66	0.40	0.02	0.04	18.80
ROK 16	44.50	5.51	34.18	0.46	0.02	0.03	15.30
ROK 32	42.30	4.95	33.49	0.46	0.01	0.09	18.70
CP 4	38.70	4.70	31.37	0.50	0.01	0.12	24.60
Pa Potho	42.60	5.10	33.44	0.51	0.02	0.13	18.20

Table 9.7 Mineral Element Composition of Rice Husk Ash*.

Mineral Element	Weight Percent of Rice Husk Ash (%)					
	Lemont (LG)	ROK 14	ROK 16	ROK 32	CP 4	Pa Potho
Si	45.00	44.00	43.00	42.00	42.00	46.00
K	1.80	1.90	2.90	2.30	1.70	1.40
Ca	0.38	0.42	1.40	0.32	0.24	0.20
P	0.37	0.25	0.58	0.39	0.26	0.02
Mg	0.34	0.25	0.87	0.27	0.18	0.18
Al	0.02	0.06	0.13	0.07	0.05	0.07
Fe	0.05	0.07	0.19	0.09	0.06	0.11
Na	0.06	0.17	0.07	0.17	0.02	0.06
S	0.05	0.38	0.55	0.51	0.40	0.05
Ti	0.01	0.02	0.02	0.03	0.05	0.01
Zn	0.005	0.01	0.02	0.01	0.005	0.005
O_2 + Others	51.91	52.47	50.27	53.84	55.03	51.89

* Estimated as percentages of their oxides.

Table 9.8 Mineral Oxides Composition of Rice Husk Ash (Wt. %)

Mineral Oxides	Rice Husk Ash					
	Lemont (LG)	ROK 14	ROK 16	ROK 32	CP 4	Pa Potho
SiO_2	96.00	94.00	92.00	90.00	90.00	97.00
K_2O	2.10	2.30	3.50	2.80	2.00	1.80
CaO	0.48	0.59	2.00	0.45	0.34	0.33
P_2O_5	0.59	0.57	1.20	0.89	0.60	0.03
MgO	0.44	0.41	1.40	0.45	0.30	0.30
Al_2O_3	0.05	0.11	0.25	0.13	0.09	0.13
Fe_2O_3	0.09	0.10	0.27	0.13	0.09	0.16
Na_2O	0.08	0.23	0.09	0.23	0.03	0.08
SO_3	0.10	0.88	1.08	1.10	1.12	0.11
TiO_2	0.035	0.04	0.04	0.05	0.06	0.02
ZnO	0.009	0.01	0.02	0.01	0.006	0.008
Others	0.026	0.76	0.15	3.76	5.364	3.032

as traces of TiO_2 and ZnO. The sum total of all mineral oxides present in rice husk ashes ranged from 94.44 to 99.97% on 100 basis.

9.1.1.2.5 Ash fusibility: The results of the ash fusibility tests conducted on the six rice husk samples are presented in Table 9.9 and shown in Figure 9.1. The tests determine the initial deformation temperature, softening temperature, hemispherical temperature and fluid temperature. The results obtained from the tests on ash fusibility in the oxidizing atmosphere revealed that the initial deformation temperature varied from 1349°C (Pa Potho) to 1486°C (ROK 32), the softening temperature varied from 1471°C (Pa Potho) to 1564°C (ROK32), the hemispherical temperature varied from 1580°C (Lemont LG) to 1627 °C (ROK 32), and the fluid temperature varied from 1650°C (Lemont LG) to 1678°C (ROK 32). The results obtained from the tests on ash fusibility in the reducing atmosphere indicated that the initial deformation temperatures for the six rice husk ash samples varied from 1330°C (Pa Potho) to 1460°C (ROK 14), the softening temperature varied from 1435°C (Lemont LG) to 1538°C (ROK 32), the hemispherical temperature varied from 1540°C (Pa Potho) to 1599°C (ROK 32) and the fluid temperature varied from 1600°C (Lemont LG) to 1649°C (ROK 32).

9.1.2 Agglomeration Characteristics of Inert Bed Materials

9.1.2.1 Agglomeration characteristics of silica sand. The results of the high temperature muffle furnace experiments conducted on the silica sand-rice husk and silica sand-rice husk ash mixtures are given in Tables 9.10 and 9.11, respectively. The rice husk Lemont LG variety, the feedstock in the main gasification experiments, was used in this experiment to investigate the agglomeration characteristics of silica sand. In either case, no melting of silica sand was observed at the temperature range and ash contents investigated. In all cases, the three-dimensional structure of the untreated rice husk was preserved and no changes in the structure of the sand were observed at all temperatures. However, there was a uniform change in the colour of the residual solids as both the temperature and ash content increased. Samples

Table 9.9 Deformation Temperature of Rice Husk Ash in Oxidizing and Reducing Atmospheres.

Rice Husk Ash	Temperature (°C)							
	Initial Deformation		Softening		Hemispherical		Fluid	
	O	R	O	R	O	R	O	R
Lemont (LG)	1440	1395	1498	1435	1580	1545	1650	1600
ROK 14	1480	1460	1540	1469	1618	1580	1669	1625
ROK 16	1394	1373	1536	1458	1600	1550	1655	1610
ROK 32	1486	1434	1564	1538	1627	1599	1678	1649
CP 4	1417	1410	1539	1506	1618	1585	1673	1636
Pa Potho	1349	1330	1471	1445	1582	1540	1652	1604

Note: O = oxidizing atmosphere, R = reducing atmosphere.

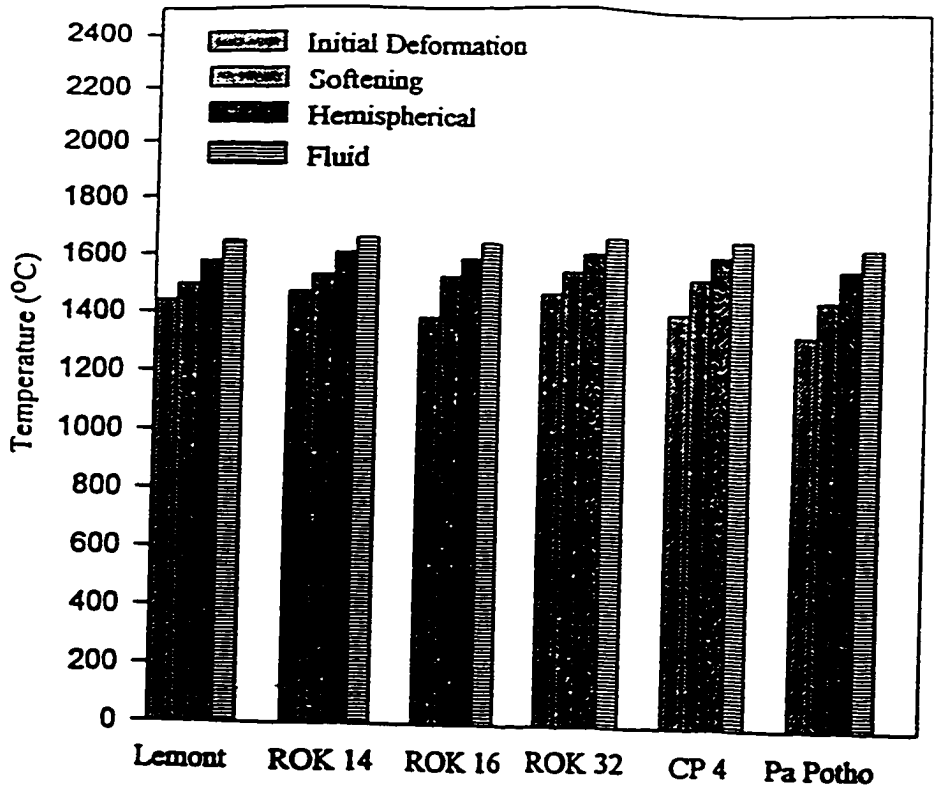

(a) Oxidizing atmosphere

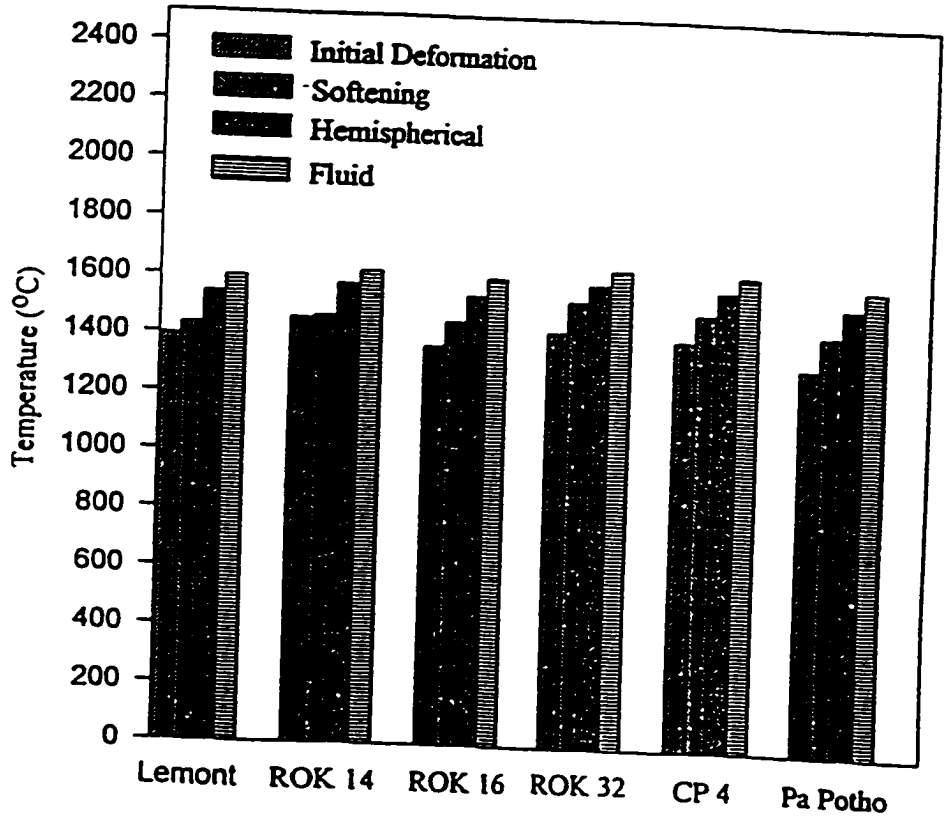

(b) Reducing atmosphere

Figure 9.1 Deformation temperature of rice husk ash in oxidizing and reducing atmospheres.

Table 9.10 Results of the high temperature furnace tests for silica sand-rice husk mixtures.

Temperature (°C)	Ash Content** (%)	Observations	
		Colour*	Structure
750	0	White-orange	No significant change
	5	Black-grey	No bonding of particles
	10	Black-grey	No bonding of particles
	15	Black-grey	Loose bonding of particles
	20	Black-grey	Loose bonding of particles
	25	Black-grey	Loose bonding of particles
850	0	White-orange	No significant change
	5	Whiter sand and black-grey ash	Slight bonding of sand particles round rice husk residue
	10	Black-grey	Slight bonding of sand particles around rice husk residue
	15	Black-grey	More sand particles bound around the rice husk residue forming a soft/easily breakable structure
	20	Black-grey	Soft and easily breakable structure
	25	Black-grey	Soft and easily breakable structure
900	0	White-orange	No significant change
	5	Greyish-black	Pronounced bonding; light, soft and easily breakable structure
	10	Grey-black-white	Light, soft and easily breakable structure
	15	Greyish black	Light, soft and easily breakable structure
	20	Greyish black	Light, soft and easily breakable structure
	25	Greyish black	Light, soft and easily breakable structure
950	0	White-orange	No significant change
	5	Greyish black	More pronounced bonding; light, soft and easily breakable structure
	10	Greyish black	Light, soft and easily breakable structure
	15	Greyish black	Light, soft and easily breakable structure
	20	Greyish black	Light, soft and easily breakable structure
	25	Greyish black	Light, soft and easily breakable structure
1000	0	White-orange	No significant change
	5	Greyish black	More pronounced bonding; light, soft and easily breakable structure
	10	Greyish black	Light, soft and easily breakable structure
	15	Greyish black	Light, soft and easily breakable structure
	20	Greyish black	Light, soft and easily breakable structure
	25	Greyish black	Light, soft and easily breakable structure

* The original colour of the sand was white.

** From Lemont LG rice husk.

Table 9.11 Results of the high temperature furnace tests for Silica sand-rice husk ash mixtures.

Temperature (°C)	Ash Content** (%)	Observations	
		Colour*	Structure
750	0	White-orange	No significant change
	5	Grey ash residue	Loose bonding of particles
	10	Grey ash residue	Loose bonding of particles
	15	Grey ash residue	Loose bonding of particles
	20	Grey ash residue	Loose bonding of particles
	25	Grey ash residue	Loose bonding of particles
850	0	White-orange	No significant change
	5	Whiter sand and grey ash	Some sand particles bound around ash residue
	10	White-greyish residue	More sand particles bound around ash residue
	15	White-greyish residue	Most of the sand particles bound around ash residue; soft and fragile structure
	20	White-greyish residue	Soft and fragile structure
	25	White-greyish residue	Soft and fragile structure
900	0	White-orange	No significant change
	5	Snow-white residue	Pronounced bonding; soft and fragile structure
	10	Snow-white residue	Soft and fragile structure
	15	Snow-white residue	Soft and fragile structure
	20	Snow-white residue	Soft and fragile structure
	25	Snow-white residue	Soft and fragile structure
950	0	White-orange	No significant change
	5	Snow-white residue	More pronounced bonding; soft and fragile structure
	10	Snow-white residue	Soft and fragile structure
	15	Snow-white residue	Soft and fragile structure
	20	Snow-white residue	Soft and fragile structure
	25	Snow-white residue	Soft and fragile structure
1000	0	White-orange	No significant change
	5	Snow-white residue	More pronounced bonding; soft and fragile structure
	10	Snow-white residue	Soft and fragile structure
	15	Snow-white residue	Soft and fragile structure
	20	Snow-white residue	Soft and fragile structure
	25	Snow-white residue	Soft and fragile structure

* The original colour of the sand was white.

** From Lemont LG rice husk.

with no ash showed white-orange colour at all temperatures. The colour of the silica sand-rice husk mixtures changed from black-grey to greyish black whereas the colour of the silica sand-rice husk ash mixtures changed from grey to snow-white.

The results of silica sand-rice husk mixtures treated at 750°C showed no signs of bonding at the lower ash contents (5.0 and 10.0%) but a very loose bonding of particles was observed in the samples that had high ash contents (15.0, 20.0 and 25.0%). When the samples were treated at higher temperatures (850, 900, 950 and 1000°C), there was a clear evidence of bonding in all samples. However, more pronounced bonding was observed at the temperature of 1000°C compared to those of 850, 900 and 950°C. All the bonds formed were light, soft and fragile.

In the case of the silica sand-rice husk ash mixtures, loosely bonded particles were observed in the samples treated at 750°C and at all levels of ash content. The results obtained with samples treated at higher temperatures (850, 900, 950 and 1000°C) were similar to the results obtained with the silica sand-rice husk mixtures treated at these temperatures, except that more sand particles bound around the ash particles in the case of the silica sand-rice husk ash mixtures. The structures formed in both cases were highly friable and would disintegrate easily.

Figures 9.2 to 9.7 show the photomicrographs of the environmental scanning electron microscopy and x-ray electron dispersive spectrometer analyses of the rice husk at room temperature, rice husk ash at room temperature, rice husk treated at 1000°C, rice husk ash treated at 1000°C, pure silica sand at room temperature and pure silica sand treated at 1000°C.

The ESEM of the original rice husk (zero conversion) at room temperature (Figure 9.2) revealed an array of sharp, peak-like structure with protuberances on the outer surface. The x-ray analysis indicated that the rice husk consisted predominantly of silica with only minor

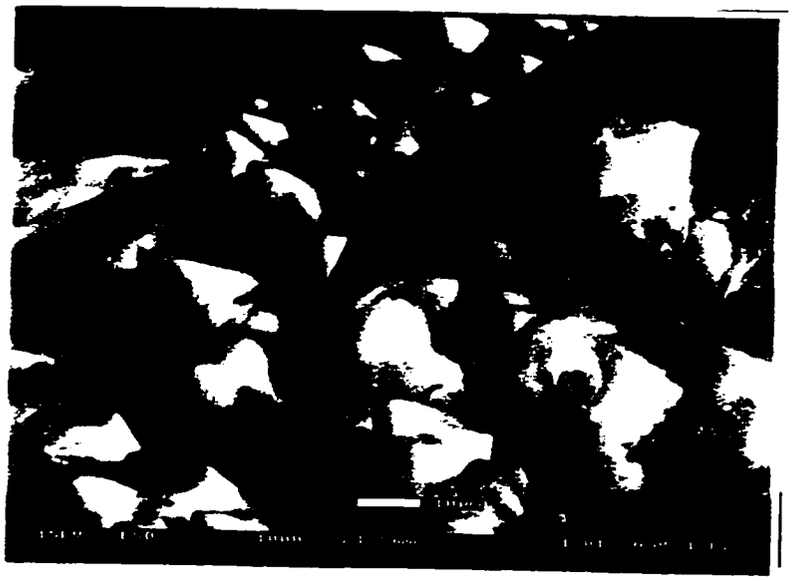

(a)

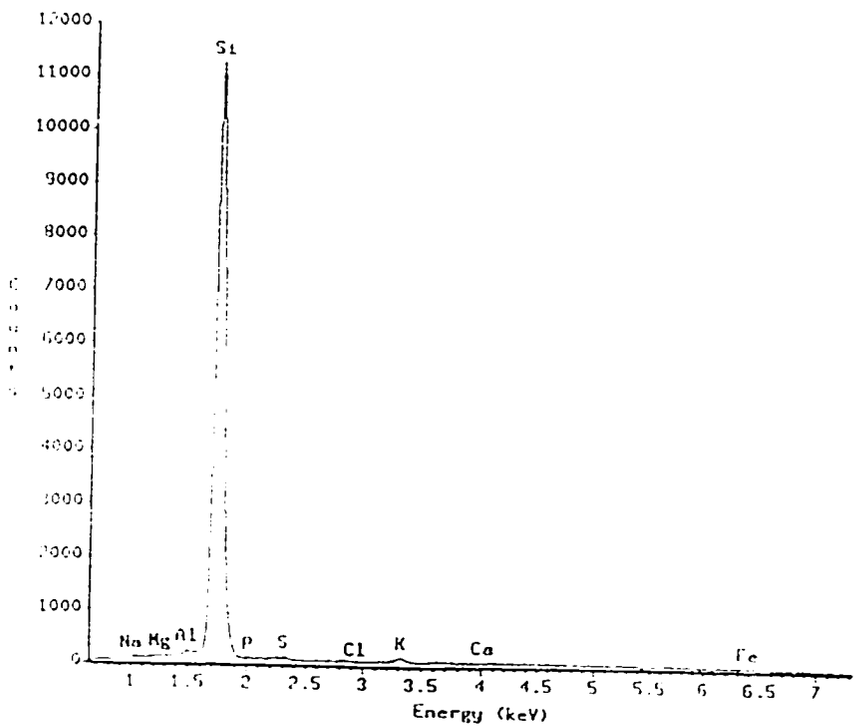

(b)

Figure 9.2 (a) ESEM photomicrograph, and (b) X-ray spectra of rice husk (Lemont LG) at room temperature.

(a)

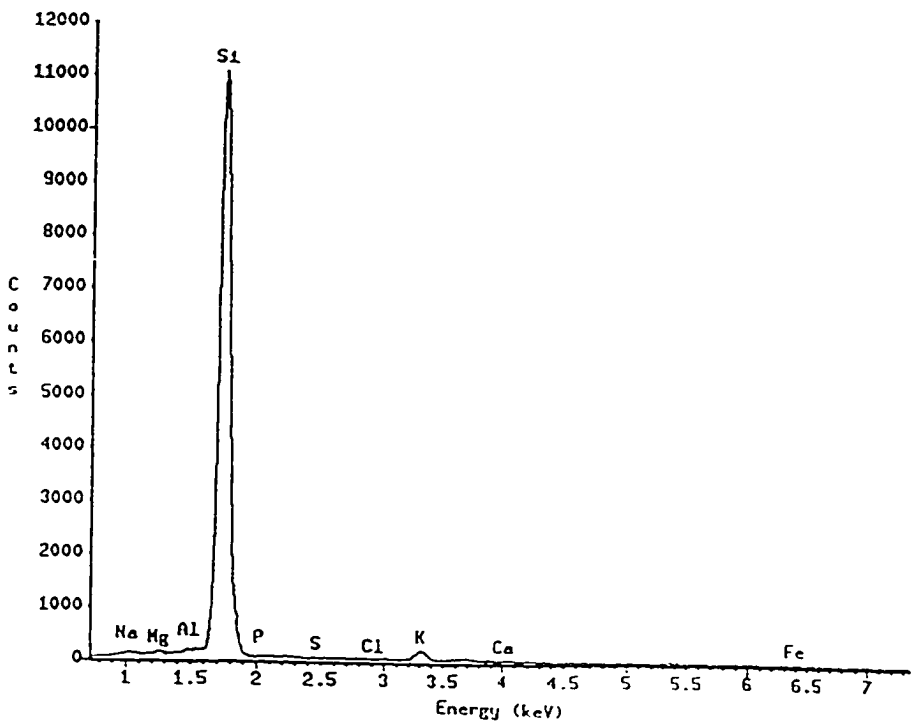

(b)

Figure 9.3 (a) ESEM photomicrograph, and (b) X-ray spectra of rice husk (Lemont LG) ash at room temperature.

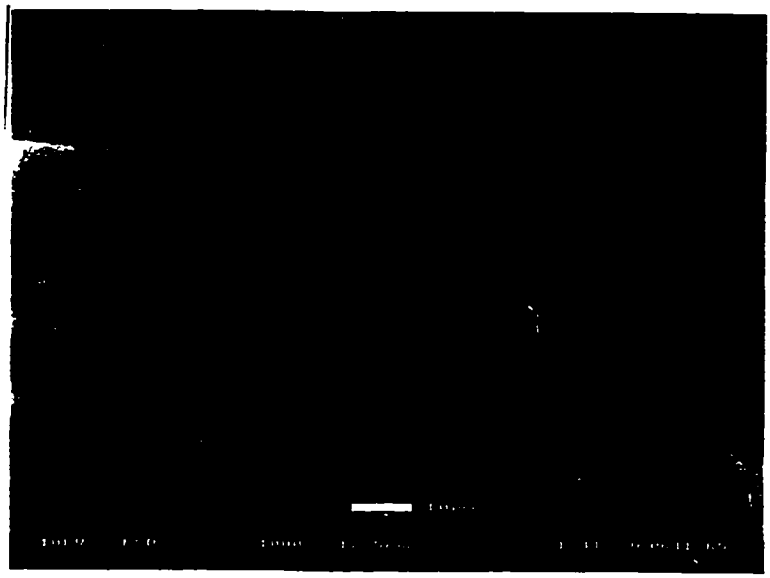

(a)

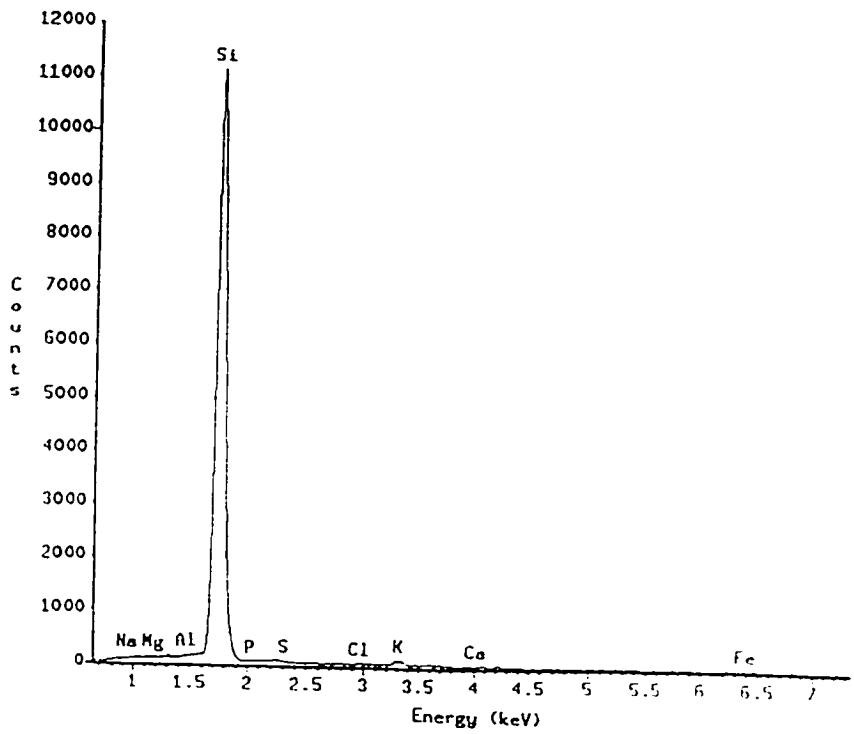

(b)

Figure 9.4 (a) ESEM photomicrograph, and (b) X-ray spectra of rice husk (Lemont LG) treated at 1000°C.

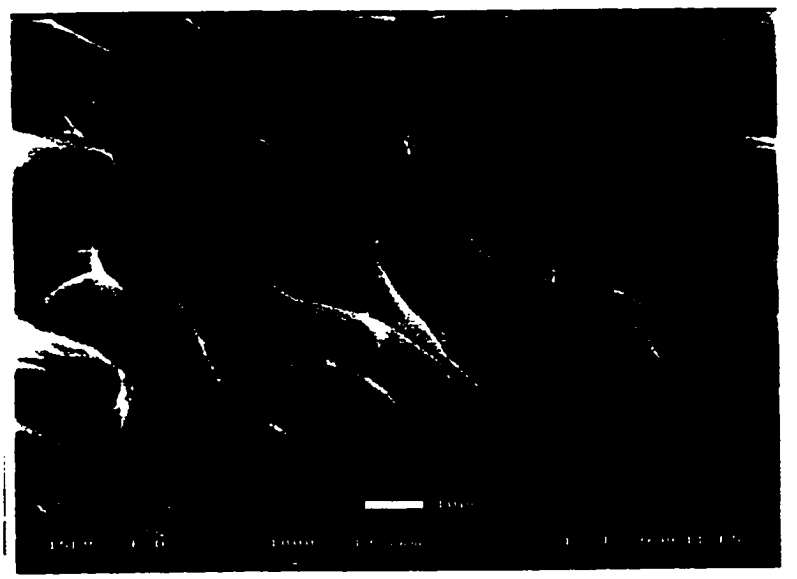

(a)

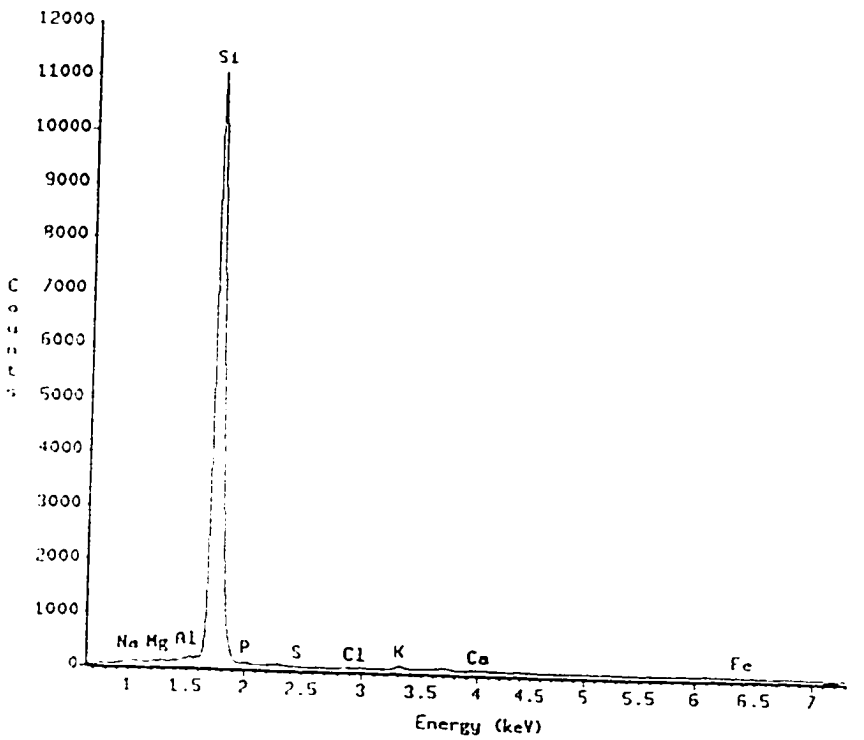

(b)

Figure 9.5 (a) ESEM photomicrograph, and (b) X-ray spectra of rice husk (Lemont LG) ash treated at 1000°C.

(a)

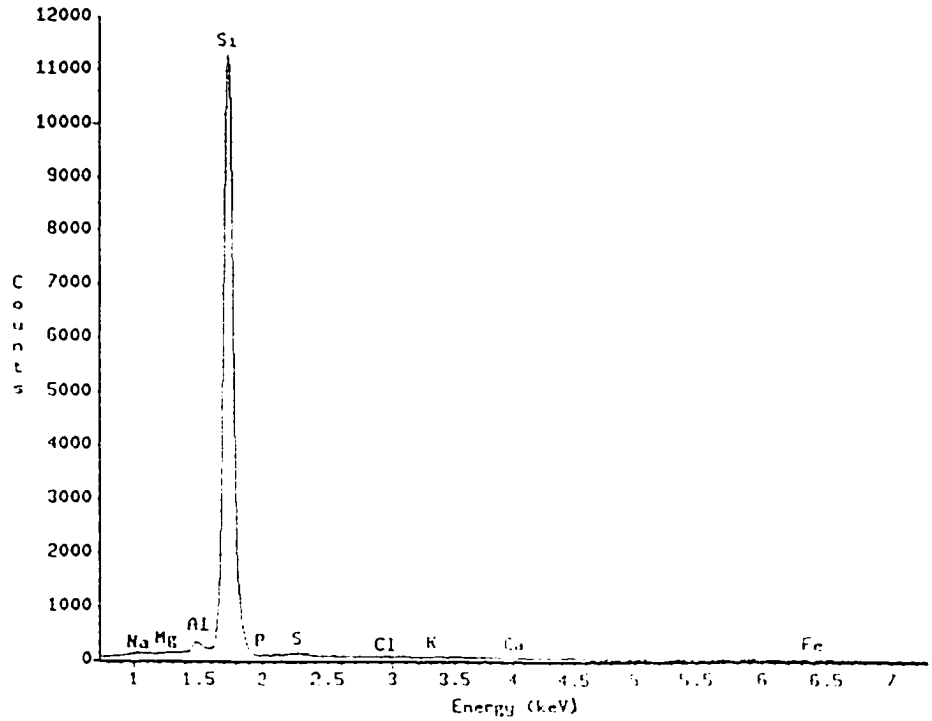

(b)

Figure 9.6 (a) ESEM photomicrograph, and (b) X-ray spectra of silica sand at room temperature.

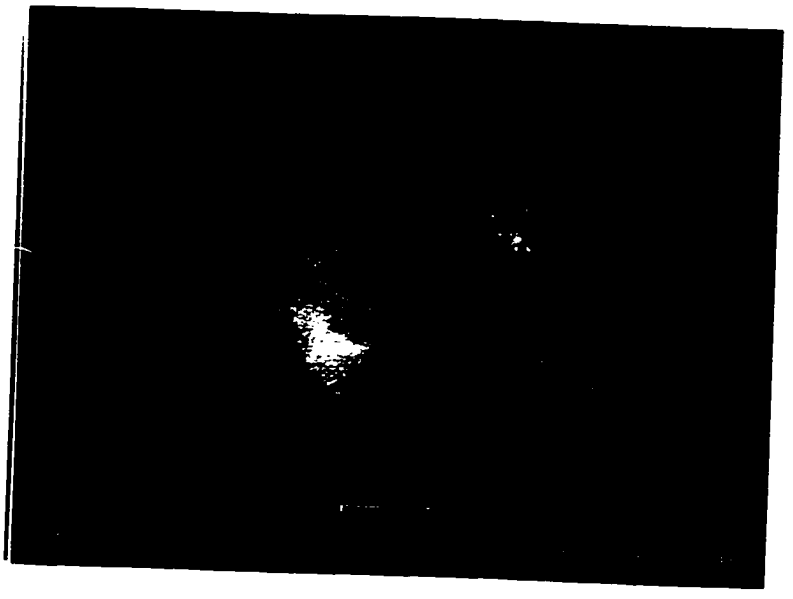

(a)

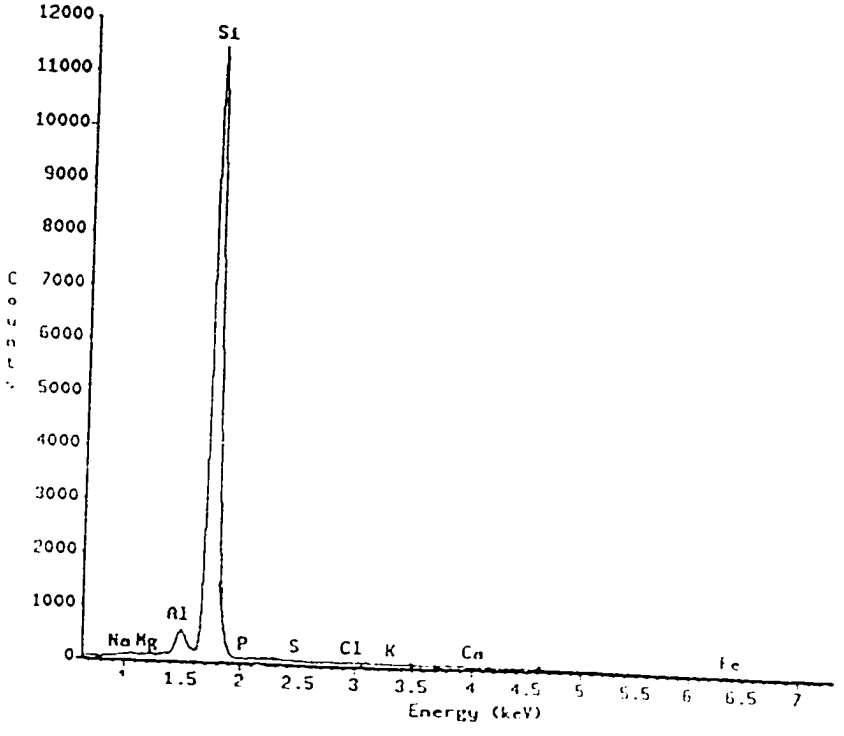

(b)

Figure 9.7 (a) ESEM photomicrograph, and (b) X-ray spectra of silica sand treated at 1000°C.

amounts of other mineral elements such as K, Al, Mg, P, Na, Ca, Cl and S. The rice husk ash (zero conversion) at room temperature (Figure 9.3) also had a similar sharp, peak-like structure to that of the original rice husk but with less pronounced protuberances on the outer surface. The x-ray spectra showed that the bulk of the rice husk ash consisted of Si followed by minor peaks of K, Al, Mg, P, Na and S. Slight peaks of Ca and Cl were also detected in the rice husk ash sample.

Treating the rice husk at 1000°C resulted in the formation of more pronounced peak-like projections with an insignificant particle size reduction (Figure 9.4). Similar results were obtained with the rice husk ash (Figure 9.5). The x-ray spectra of rice husk ash duplicated that of the rice husk. The major mineral component of both samples was Si, but K, Al, Mg, Na, P, Ca, Cl and S were detected as minor peaks with a significant reduction in the K peak compared to the samples that were treated at room temperature.

The ESEM photomicrograph of the pure silica particles at room temperature (Figure 9.6) were very similar to those treated at 1000°C (Figure 9.7). No signs of melting were observed when the silica sand was treated at 1000°C. The x-ray spectra of both samples showed that the major component of the sand was Si. Small peaks of Al were detected in untreated and heat treated samples. Much smaller peaks of Mg, Na, P, S, Cl, K and Ca were also detected.

The attempt to investigate the structure of the treated silica sand-rice husk and silica sand-rice husk ash mixtures under the ESEM was unsuccessful. As a consequence, a light microscope was employed. The microscopy picture of the silica sand-rice husk (Figure 9.8) and silica sand-rice husk ash mixtures (Figure 9.9) showed a weak bonding between the sand and the rice husk ash (rice husk and pure rice husk ash) particles. More sand particles bound to the rice husk ash particles as compared to the rice husk particles. There was no apparent indication of melting observed in the microscopy analyses of the silica sand and ash particles at all

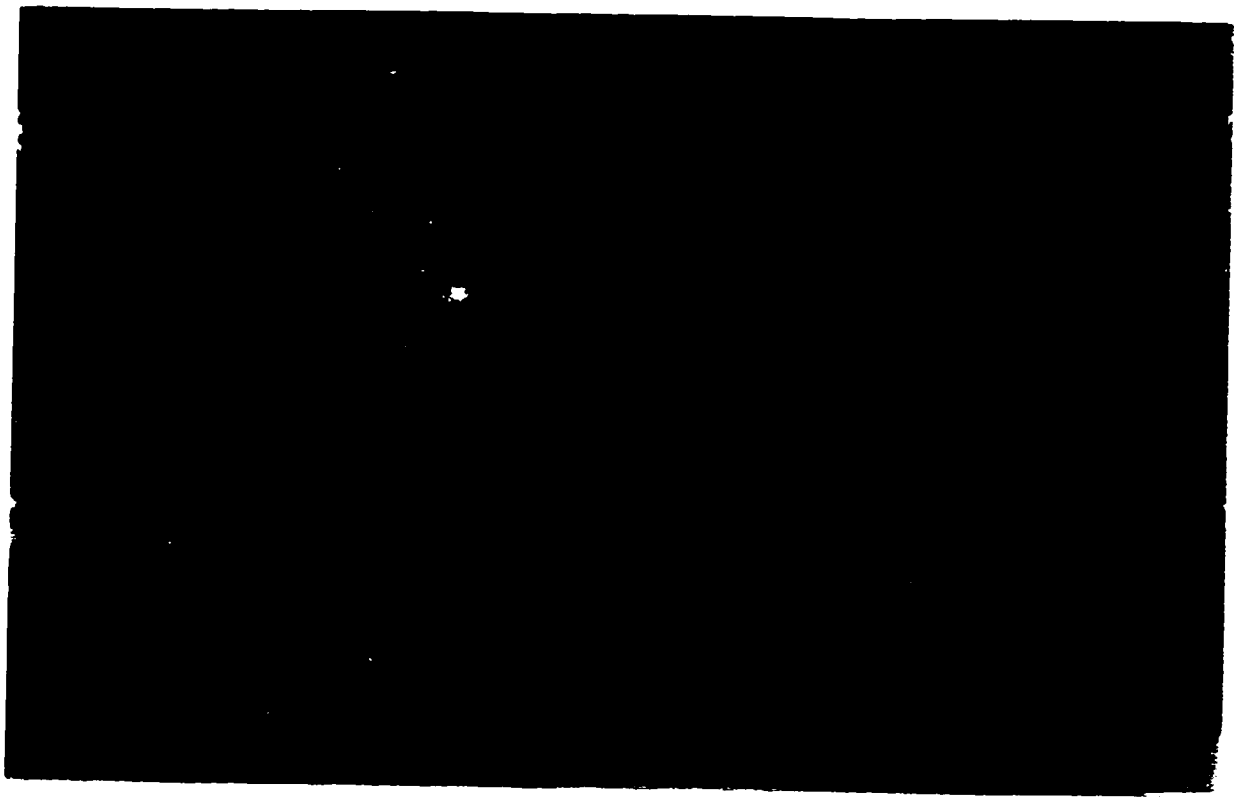

Figure 9.8 Light microscopy picture of silica sand-rice husk (Lemont LG) mixture treated at 1000°C.

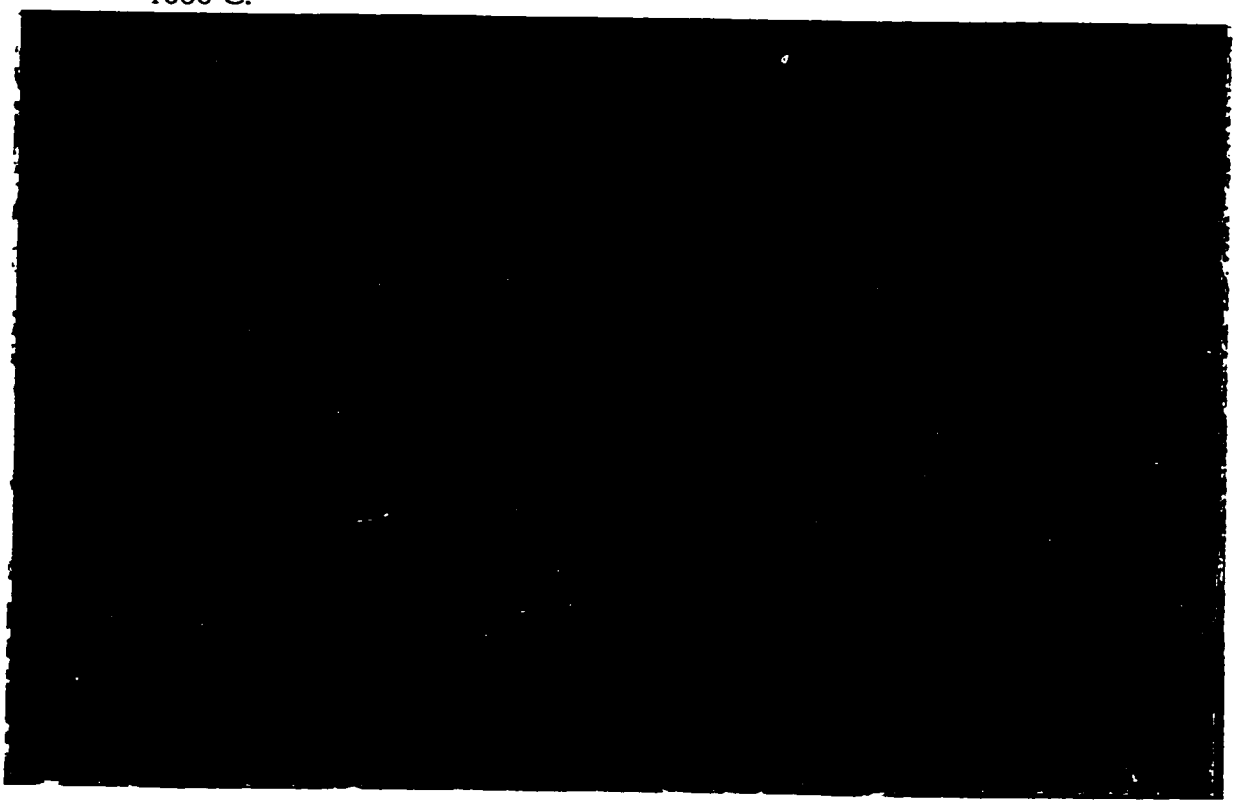

Figure 9.9 Light microscopy picture of silica sand-rice husk (Lemont LG) ash mixture treated at 1000°C.

temperatures investigated. However, most of the sand particles appeared to be in glassy form but many showed the presence of crystalline material condensed on or adhering to their surfaces.

9.1.2.2 Agglomeration characteristics of alumina sand. The rice husk Lemont LG variety, the feedstock in the main gasification experiments, was used in this experiment to investigate the agglomeration characteristics of alumina sand. Tables 9.12 and 9.13 give the visual results of the high temperature muffle furnace experiments conducted on the alumina sand-rice husk and alumina sand-rice husk ash mixtures, respectively. No melting of alumina sand was observed at the temperature range and ash contents investigated. In all cases, the three-dimensional structure of the original rice husk was preserved and no changes in the structure of the alumina sand were observed at all temperatures. Nevertheless, there was a uniform change in the colour of the residual solids as both the temperature and ash content increased. The colours ranged from white to cream in the case of pure alumina sand (zero ash content), black-grey to greyish black in the case of the rice husk and dark grey to greyish white in the case of the pure ash.

The results of alumina sand-rice husk mixtures treated at 750 and 850°C showed no signs of bonding at the five levels of ash content (5.0, 10.0, 15.0, 20.0 and 25.0%). However, when the samples were treated at 900°C, a very loose bonding of rice husk particles was observed at low ash contents (5.0 and 10.0%), and a more pronounced bonding of rice husk particles was observed at high ash contents (15.0, 20.0 and 25.0%), forming a fluffy structure that could easily break. At temperatures of 950 and 1000°C, and all levels of ash content, sand particles bound around the rice husk ash residue forming friable structures.

In the case of the alumina sand-rice husk ash mixtures, there was no bonding of particles in the samples treated at 750°C. At 850°C, a loose bonding of ash particles was observed at higher ash contents (15, 20 and 25%). On treating the samples at 900°C, the

Table 9.12 Results of the high temperature furnace tests for Alumina sand-rice husk mixtures.

Temperature (°C)	Ash Content** (%)	Observations	
		Colour*	Structure
750	0	Slightly changed from white to cream	No change in structure
	5	Black-grey	No bonding of particles
	10	Black-grey	No bonding of particles
	15	Black-grey	No bonding of particles
	20	Black-grey	No bonding of particles
	25	Black-grey	No bonding of particles
850	0	Slightly changed from white to cream	No change in structure
	5	Black-grey	No bonding of particles
	10	Black-grey	No bonding of particles
	15	Black-grey	No bonding of particles
	20	Black-grey-white	No bonding of particles
	25	Black-grey-white	No bonding of particles
900	0	Slightly changed from white to cream	No change in structure
	5	Grey-black-white	Loose bonding of rice husk particles
	10	Grey-black-white	Loose bonding of rice husk particles
	15	Greyish black	Rice husk particles bound together; fluffy and easily breakable structure
	20	Greyish black	Fluffy and easily breakable rice husk structure
	25	Greyish black	Fluffy and easily breakable rice husk structure
950	0	Slightly changed from white to cream	No change in structure
	5	Greyish black	Slight bonding of sand particles around the fluffy rice husk residue; soft structure which could break easily
	10	Greyish black	Soft and easily breakable structure
	15	Greyish black	Soft and easily breakable structure
	20	Greyish black	Soft and easily breakable structure
	25	Greyish black	Soft and easily breakable structure
1000	0	Slightly changed from white to cream	No change in structure
	5	Greyish black	Slight bonding of sand particles around the rice husk residue; soft and fragile structure
	10	Greyish black	Light, soft and fragile structure
	15	Greyish black	Light, soft and fragile structure
	20	Greyish black	Light, soft and fragile structure
	25	Greyish black	Light, soft and fragile structure

* The original colour of the sand was white.
** From Lemont LG rice husk.

Table 9.13 Results of the high temperature furnace tests for Alumina sand-rice husk ash mixtures.

Temperature (°C)	Ash Content** (%)	Observations	
		Colour*	Structure
750	0	Slightly changed from white to cream	No change in structure
	5	Dark grey	No bonding of particles
	10	Dark grey	No bonding of particles
	15	Dark grey	No bonding of particles
	20	Grey	No bonding of particles
	25	Grey	No bonding of particles
850	0	Slightly changed from white to cream	No change in structure
	5	Grey	No bonding of particles
	10	Light grey	No bonding of particles
	15	Light grey	Loose bonding of ash particles
	20	Light grey	Loose bonding of ash particles
	25	Light grey	Loose bonding of ash particles
900	0	Slightly changed from white to cream	No change in structure
	5	Light grey	Bonding of ash particles
	10	Light grey	Bonding of ash particles
	15	Whitish grey	Loose bonding of sand/ash particles
	20	Whitish grey	Loose bonding of sand/ash particles
	25	Whitish grey	Loose bonding of sand/ash particles
950	0	Slightly changed from white to cream	No change in structure
	5	Light grey	Bonding of sand particles around the soft ash residue; soft and easily breakable structure
	10	Light grey	Soft and easily breakable structure
	15	Whitish grey	Soft and easily breakable structure
	20	Whitish grey	Soft and easily breakable structure
	25	Whitish grey	Soft and easily breakable structure
1000	0	Slightly changed from white to cream	No change in structure
	5	Light grey	More sand particles bound around the ash residue; soft and fragile structure
	10	Light grey	Soft and fragile structure
	15	Whitish-grey	Soft and fragile structure
	20	Whitish-grey	Soft and fragile structure
	25	Whitish-grey	Soft and fragile structure

* The original colour of the sand was white.

** From Lemont LG rice husk.

ash particles bound together forming a soft, light and easily breakable structure at all ash contents. Loose bonding of alumina sand-ash particles was also observed at this temperature. The results obtained with samples treated at 950 and 1000°C were similar to the results obtained with the alumina sand-rice husk mixtures treated at these temperatures, except that more sand particles bound around the ash particles in the case of the alumina sand-rice husk ash mixtures.

Figures 9.10 and 9.11 show the photomicrographs of the environmental scanning electron microscopy and x-ray electron dispersive spectrometer analyses of the pure alumina sand at room temperature and pure alumina sand treated at 1000°C.

The ESEM photomicrograph of the pure alumina particles at room temperature (Figure 9.10) were very similar to those treated at 1000°C (Figure 9.11). No signs of melting were observed when the alumina sand was treated at 1000°C. The x-ray spectra of both samples showed that the major component of the sand was Al. Very small peaks of Si were detected in untreated and heat treated samples. Also, Na, Ca Mg and P appeared as minor peaks.

The problem encountered in attempting to investigate the structure of the treated silica sand-rice husk and silica sand-rice husk ash mixtures under the ESEM was, also, faced with the alumina sand-rice husk and alumina sand-rice husk ash mixtures. Inevitably, a light microscope was employed. The microscopy picture of the alumina sand-rice husk (Figure 9.12) and alumina sand-rice husk ash mixtures (Figure 9.13) showed a weak bonding between the sand and the (rice husk and pure rice husk ash) particles. More sand particles bound to the rice husk ash particles as compared to the rice husk particles. There was no apparent indication of melting observed in the microscopy analyses of the alumina sand and ash particles at all temperatures investigated.

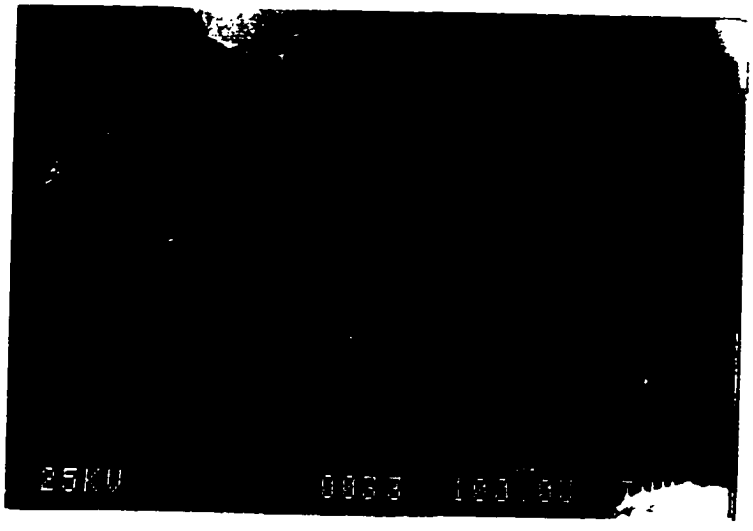

(a)

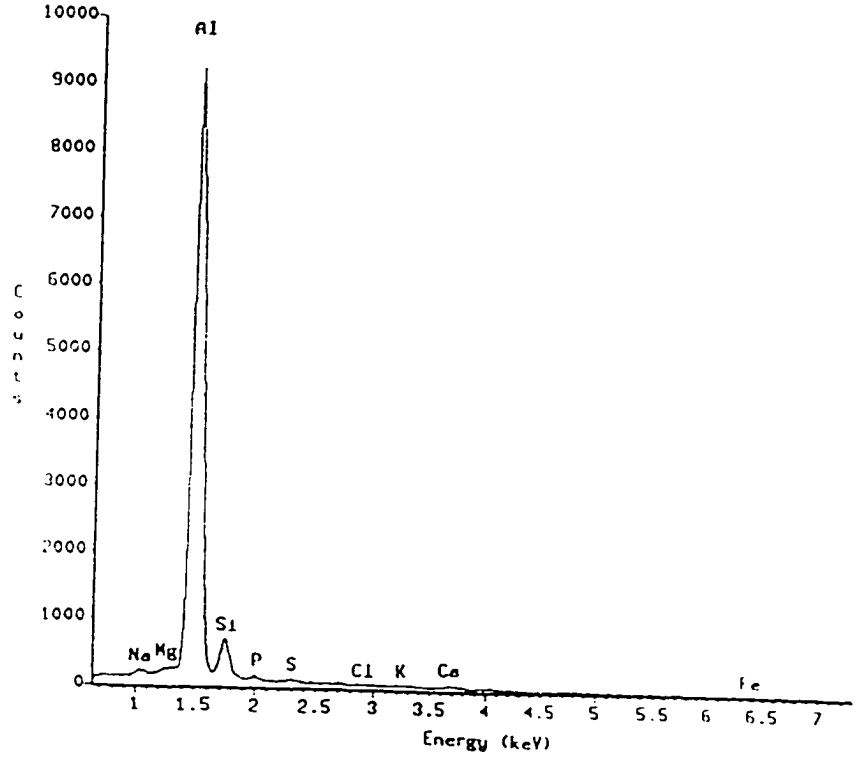

(b)

Figure 9.10 (a) ESEM photomicrograph, and (b) X-ray spectra of alumina sand at room temperature.

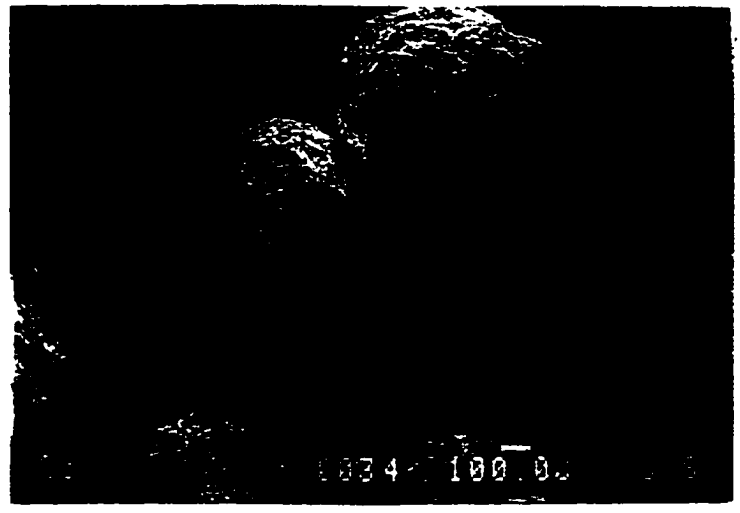

(a)

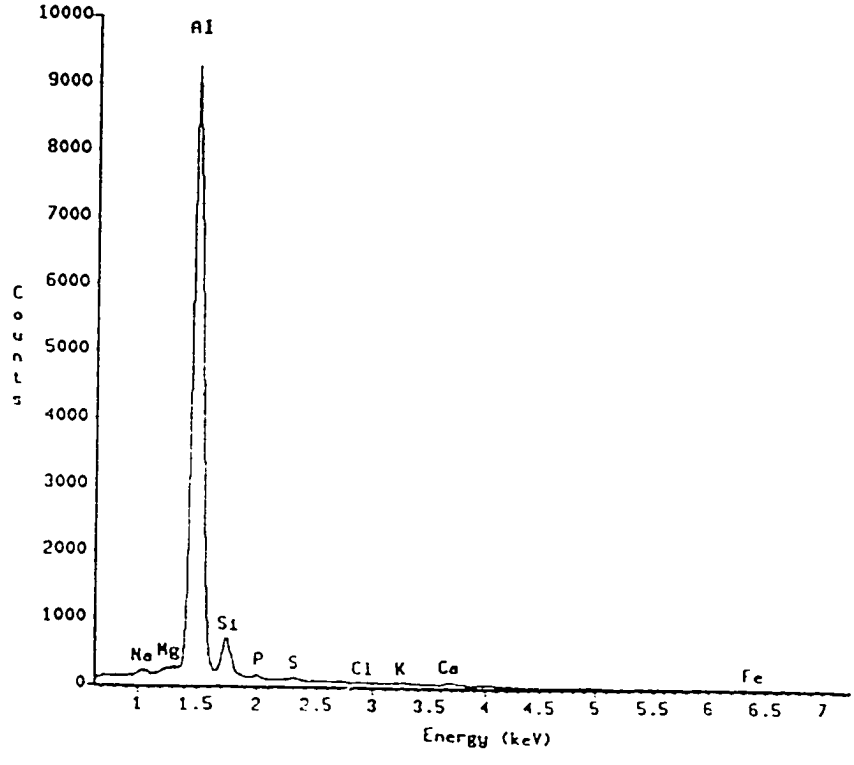

(b)

Figure 9.11 (a) ESEM photomicrograph, and (b) X-ray spectra of alumina sand treated at 1000°C.

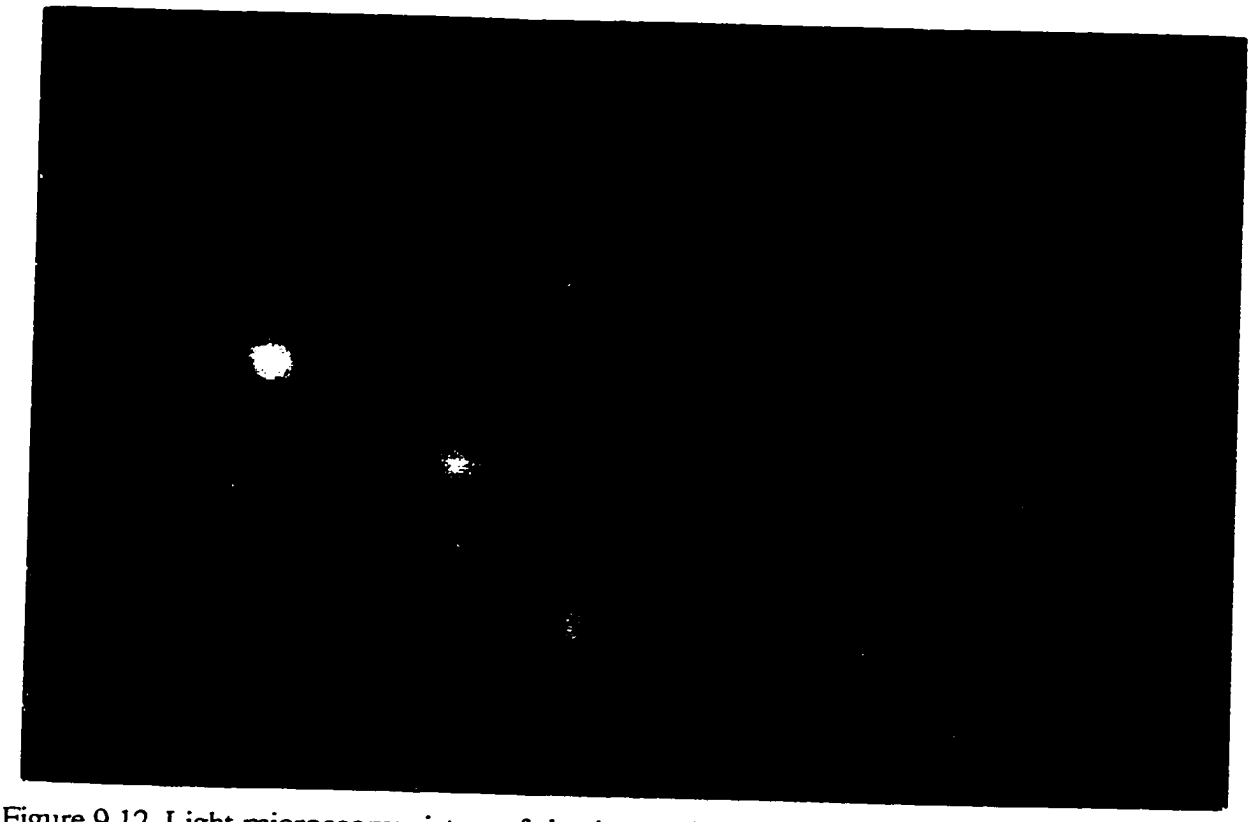

Figure 9.12 Light microscopy picture of alumina sand-rice husk (Lemont LG) mixture treated at 1000°C.

Figure 9.13 Light microscopy picture of alumina sand-rice husk (Lemont LG) ash mixture treated at 1000°C.

9.1.3 Thermal Degradation and Kinetics of Rice Husks

Of the six varieties of rice husk (Lemont LG, ROK 14, ROK 16, ROK 32, CP 4 and Pa Potho) used to determine the properties of rice husks (section 9.1.1), only four varieties (Lemont LG, ROK 14, CP 4 and Pa Potho) are considered in this analysis. ROK 14, ROK 16 and ROK 32 exhibited very similar properties (section 9.1.1) and are, therefore, expected to behave in essentially the same way in a thermogravimetric analyzer. One of the ROK rice husk varieties (ROK 14) was, therefore, used in addition to the other three rice husk varieties (Lemont LG, CP 4 and Pa Potho).

9.1.3.1 Thermal degradation. The thermogravimetric behaviour of the four varieties of rice husk (Lemont LG, ROK 14, CP 4 and Pa Potho) at different heating rates (10, 20 and 50°C/minute) in air, oxygen and nitrogen atmospheres is shown as thermograms on Figures 9.14-9.17. The results of thermogravimetric analysis (TGA) are presented in Table 9.14. Because the fine ground rice husk samples were powder-like, homogenous material, the results of the thermogravimetric analysis were reproducible within ± 0.01% by weight. It is evident from the TGA curves that two distinct overlapping reactions took place between 172 and 540°C under all atmospheres.

9.1.3.1.1 Thermal degradation rate: The TGA curves showed a slight weight loss occurring from ambient temperature to about 100°C. This was followed by a very slight loss of weight up to a temperature of 172-240°C, depending on the rice husk variety, heating rate and atmosphere used. There was then a major loss of weight when the temperature increased from 172-240°C to 291-369°C (the region in which the main degradation occurred, i. e., a weight loss of 37-44% for nitrogen, 36-42% for air and 66-71% for oxygen, respectively), depending on the rice husk variety and heating rate. This rapid degradation zone (172-369°C) is referred to as the active zone. A major change in the slope of all TGA curves was observed at the end of the active zone (at around 291-369°C), indicating the initiation of a second reaction zone. This zone terminated at around 540°C, except for oxygen, in which case it was apparent much

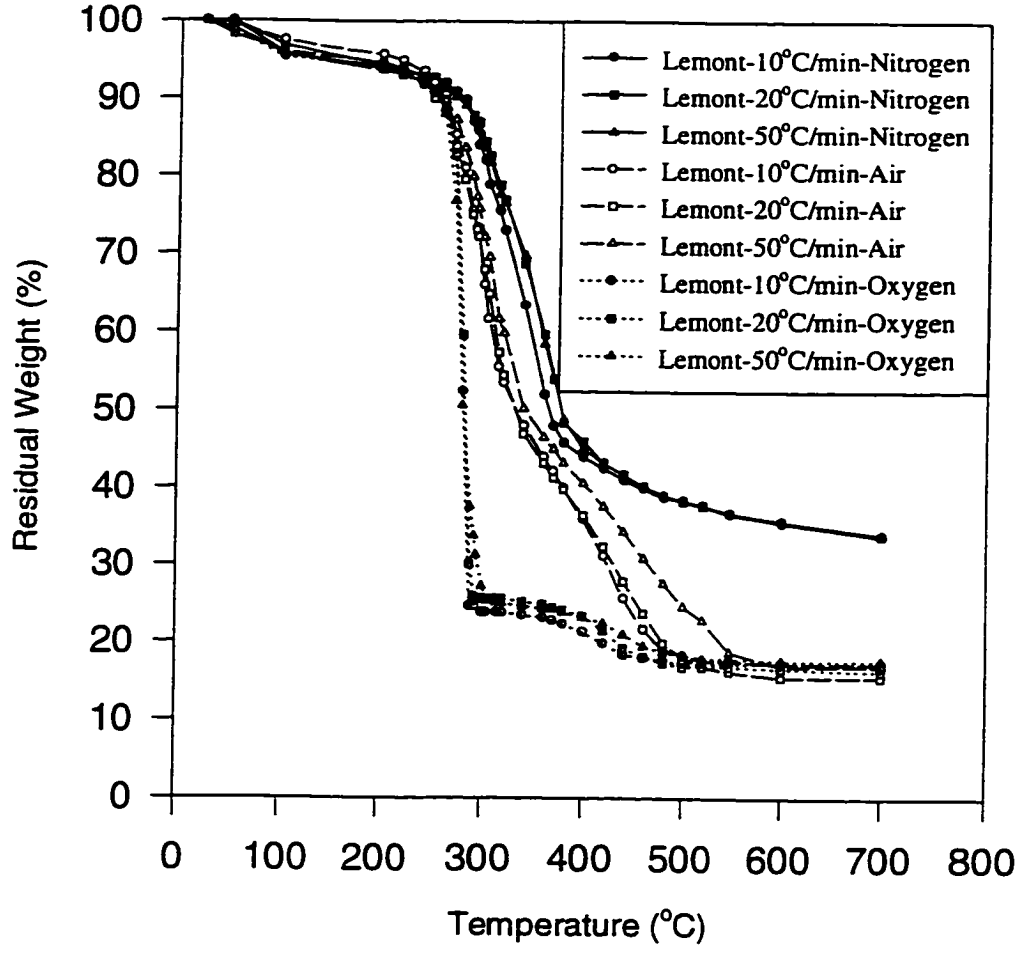

Figure 9.14 Thermograms of Lemont (LG) rice husk heated in nitrogen, air and oxygen atmospheres at different heating rates.

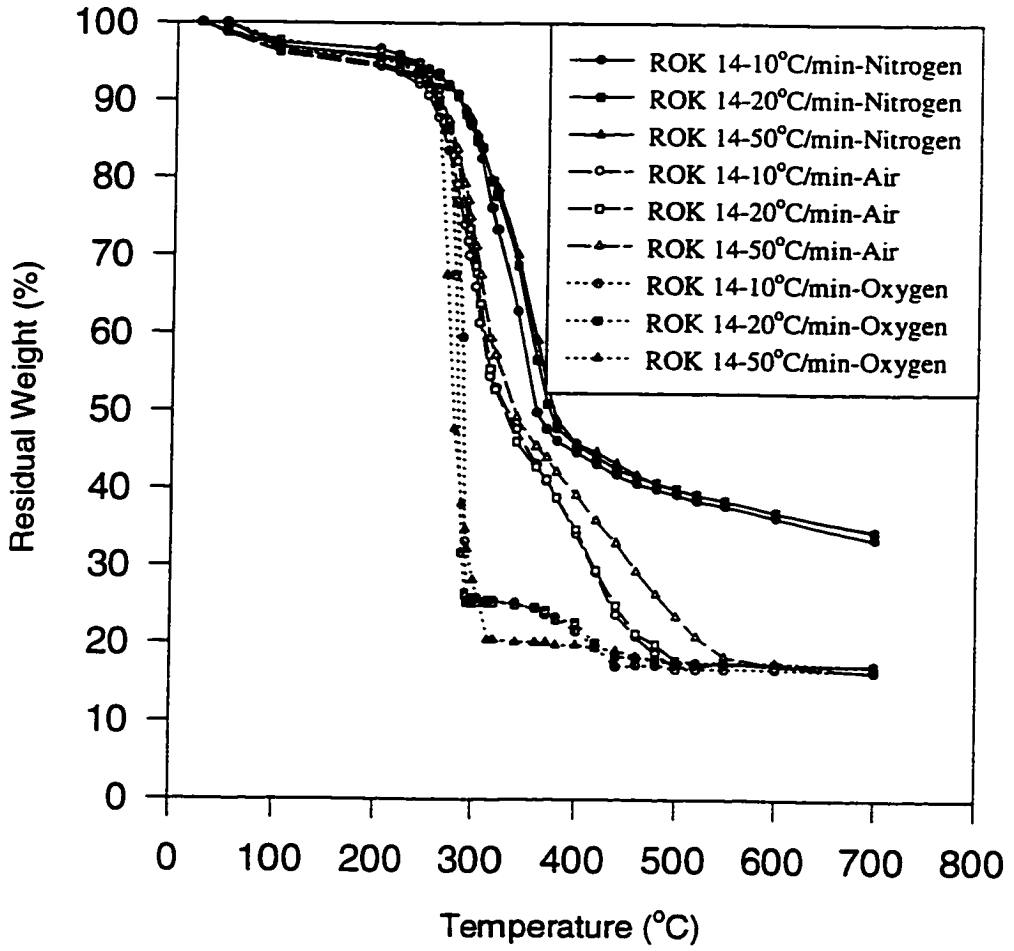

Figure 9.15 Thermograms of ROK 14 rice husk heated in nitrogen, air and oxygen atmospheres at different heating rates.

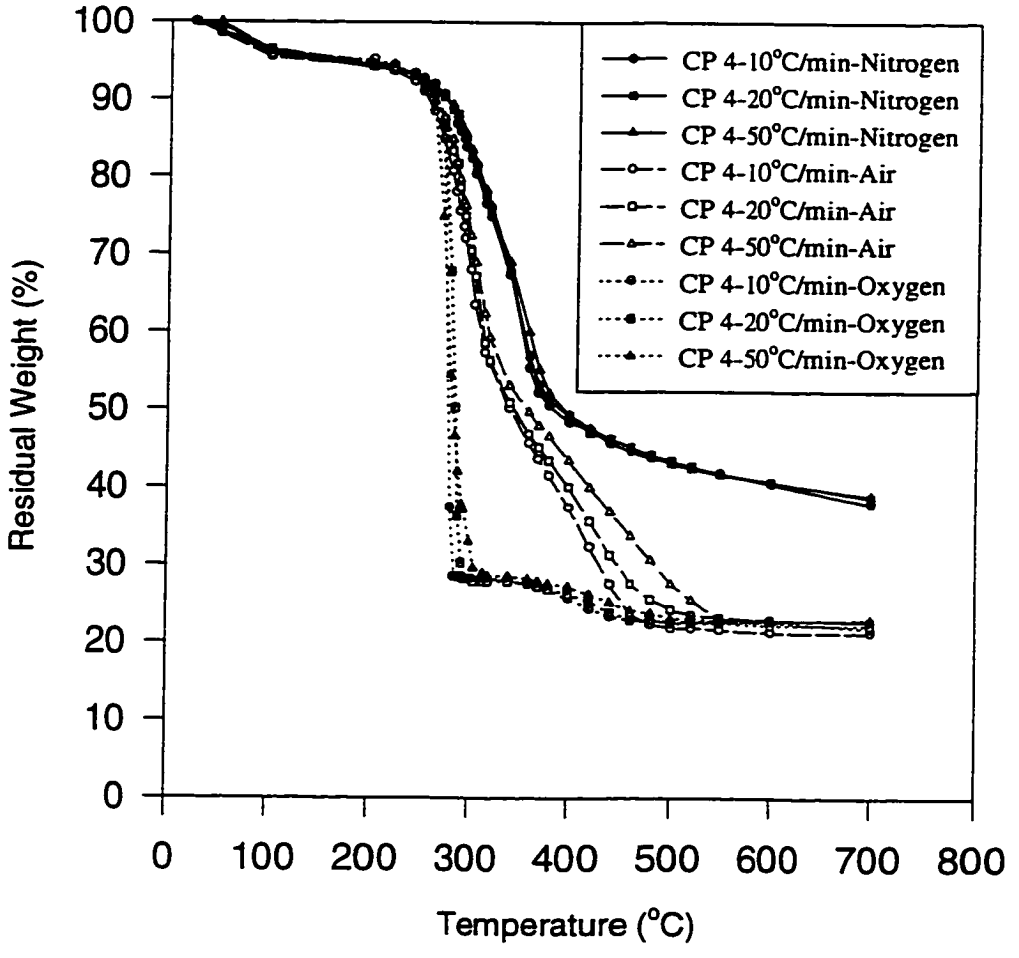

Figure 9.16 Thermograms of CP 4 rice husk heated in nitrogen, air and oxygen atmospheres at different heating rates.

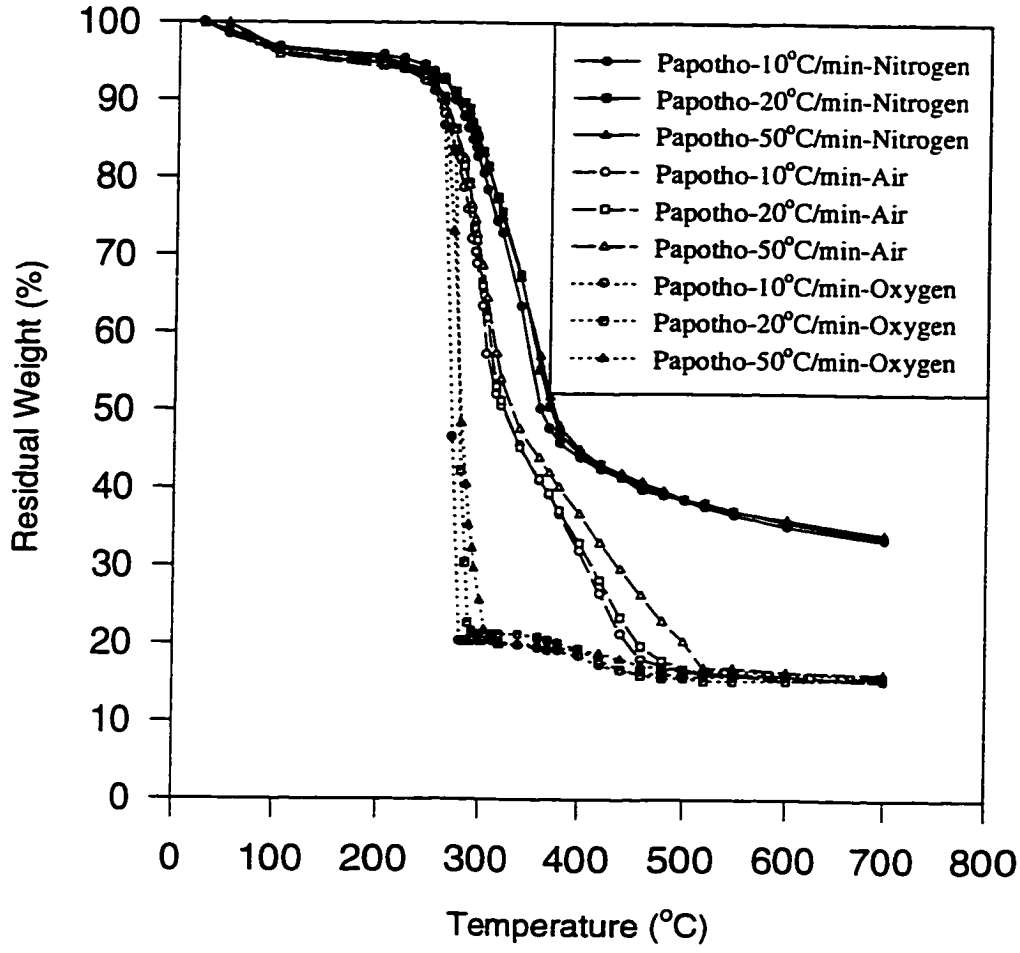

Figure 9.17 Thermograms of Papotho rice husk heated in nitrogen, air and oxygen atmospheres at different heating rates.

Table 9.14 Thermogravimetric Analysis of Rice Husks.

Rice Husk	Atmosphere	Heating Rate (°C/min)	Thermal Degradation Rate (%/min)		Initial Degradation Temperature (°C)	Residual Weight at 700°C (%)
			Active Zone	Passive Zone		
Lemont	Air	10	11.10	1.40	202	17.24
		20	13.80	1.70	191	16.48
		50	43.50	2.20	170	16.88
	Oxygen	10	24.20	1.50	217	16.88
		20	38.00	1.70	203	16.25
		50	55.00	2.40	172	17.62
	Nitrogen	10	7.30	0.50	230	33.77
		20	14.80	0.80	220	33.88
		50	34.00	1.50	184	34.00
ROK 14	Air	10	11.40	1.10	216	16.31
		20	18.80	1.50	210	17.11
		50	50.50	2.70	178	17.16
	Oxygen	10	28.00	2.00	227	16.43
		20	37.60	2.20	215	17.06
		50	68.50	0.50	182	17.11
	Nitrogen	10	8.30	0.30	240	33.47
		20	17.40	0.60	232	34.52
		50	36.98	2.00	195	34.58
CP 4	Air	10	8.50	1.00	212	21.26
		20	13.00	1.90	206	22.72
		50	42.00	1.90	175	22.86
	Oxygen	10	20.30	1.10	222	21.84
		20	33.00	1.30	211	22.20
		50	52.00	1.50	178	23.00
	Nitrogen	10	5.70	0.30	229	37.95
		20	13.20	0.80	223	38.73
		50	33.00	1.50	188	38.95
Pa Potho	Air	10	11.80	1.40	217	15.32
		20	24.80	2.90	212	15.86
		50	50.00	3.10	180	16.18
	Oxygen	10	28.50	1.20	224	15.32
		20	39.40	1.60	218	15.50
		50	60.00	2.00	186	15.82
	Nitrogen	10	8.30	0.50	240	33.46
		20	17.80	0.60	240	33.78
		50	40.00	1.50	197	34.13

Values are the average of 3 measurements with a coefficient of variation in the range of 0.01 to 0.8%.

earlier. The thermal degradation rates were lower in this zone compared to the active zone. Thus, the second reaction zone was referred to as the passive zone. During this zone, a weight loss of 10-13% for nitrogen, 32-37% for air and 6-7% for oxygen were achieved, respectively. Between the temperatures of 291-540°C and 700°C, there was essentially no further loss of weight.

Thermal degradation rate was largest at all heating rates for Pa Potho rice husk, except at 50°C/minute heating rate where ROK 14 rice husk exhibited the largest thermal degradation rate in oxygen atmosphere, followed by that in air atmosphere, whereas Pa Potho rice husk exhibited the largest thermal degradation rate in nitrogen atmosphere. The thermal degradation rate, both in the active and passive zones, increased with increases in heating rate for all rice husk samples in air, oxygen and nitrogen atmospheres, as shown in Figures 9.18 and 9.19. The proportional increase of thermal degradation rate with increases in heating rate was more in the active zone than in the passive zone for all samples. The thermal degradation rate in the active zone was higher in oxygen atmosphere for all the samples at all heating rates, followed by that in air and then nitrogen atmosphere. In the passive zone, it was observed to be higher in air atmosphere at most heating rates.

9.1.3.1.2 Initial Degradation Temperature: The temperature at which the overall degradation starts is termed initial degradation temperature. Figure 9.20 shows the initial degradation temperature for the rice husk varieties in air, nitrogen and oxygen atmospheres and at different heating rates. The initial degradation temperature for Pa Potho rice husk, which apparently had the highest thermal degradation rate at most heating rates, was the highest among the different rice husk samples in all atmospheres studied, with the exception of ROK 14 rice husk at 10°C/minute in oxygen (in that case ROK 14 rice husk has the highest initial degradation temperature). Pa Potho and ROK 14 rice husk samples behaved similarly at 10°C/minute in nitrogen atmosphere. With increases in heating rate, the initial degradation temperature decreased for all rice husk samples. Lemont LG rice husk started degrading in

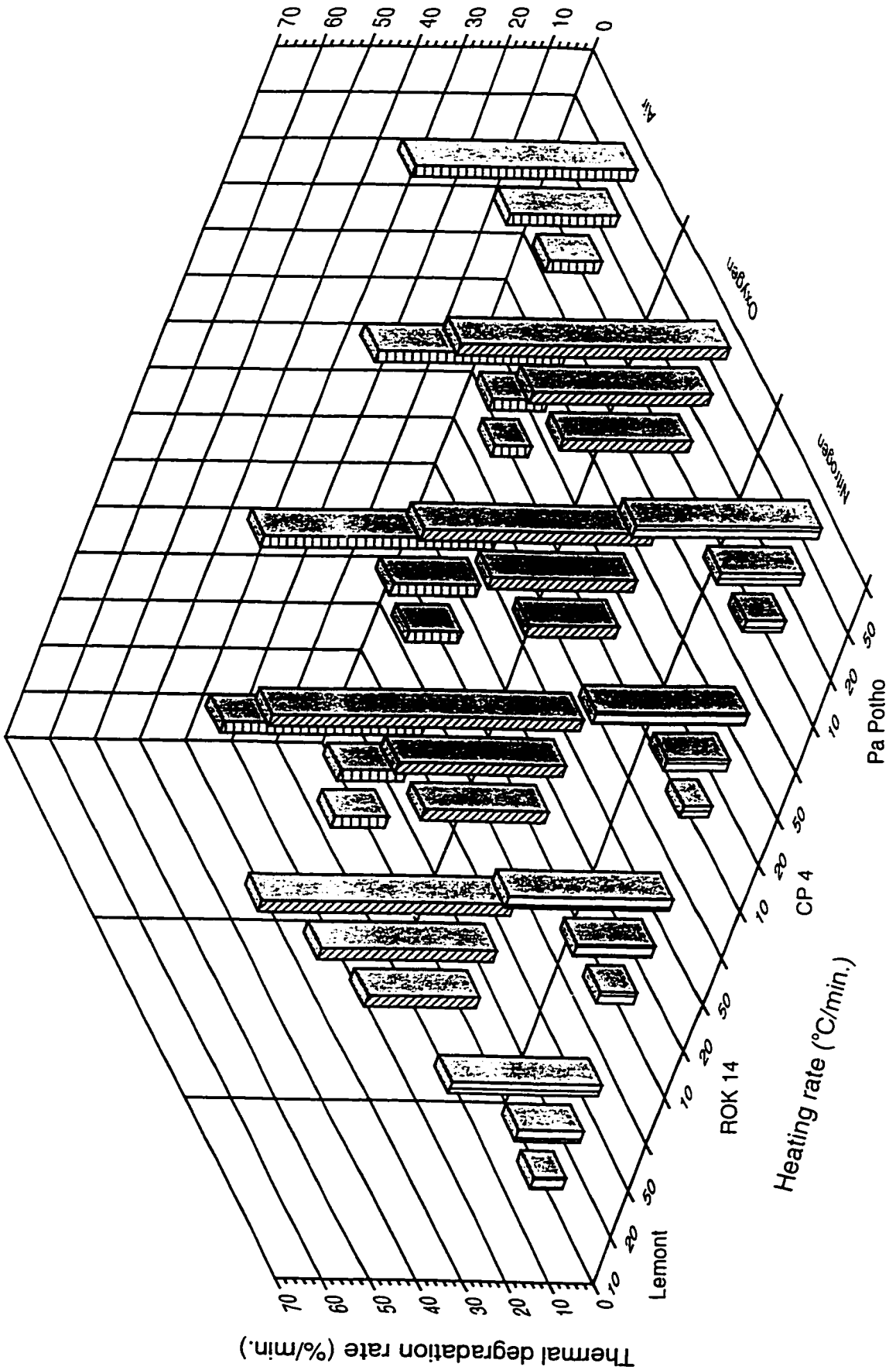

Figure 9.18 Thermal degradation rate in active zone.

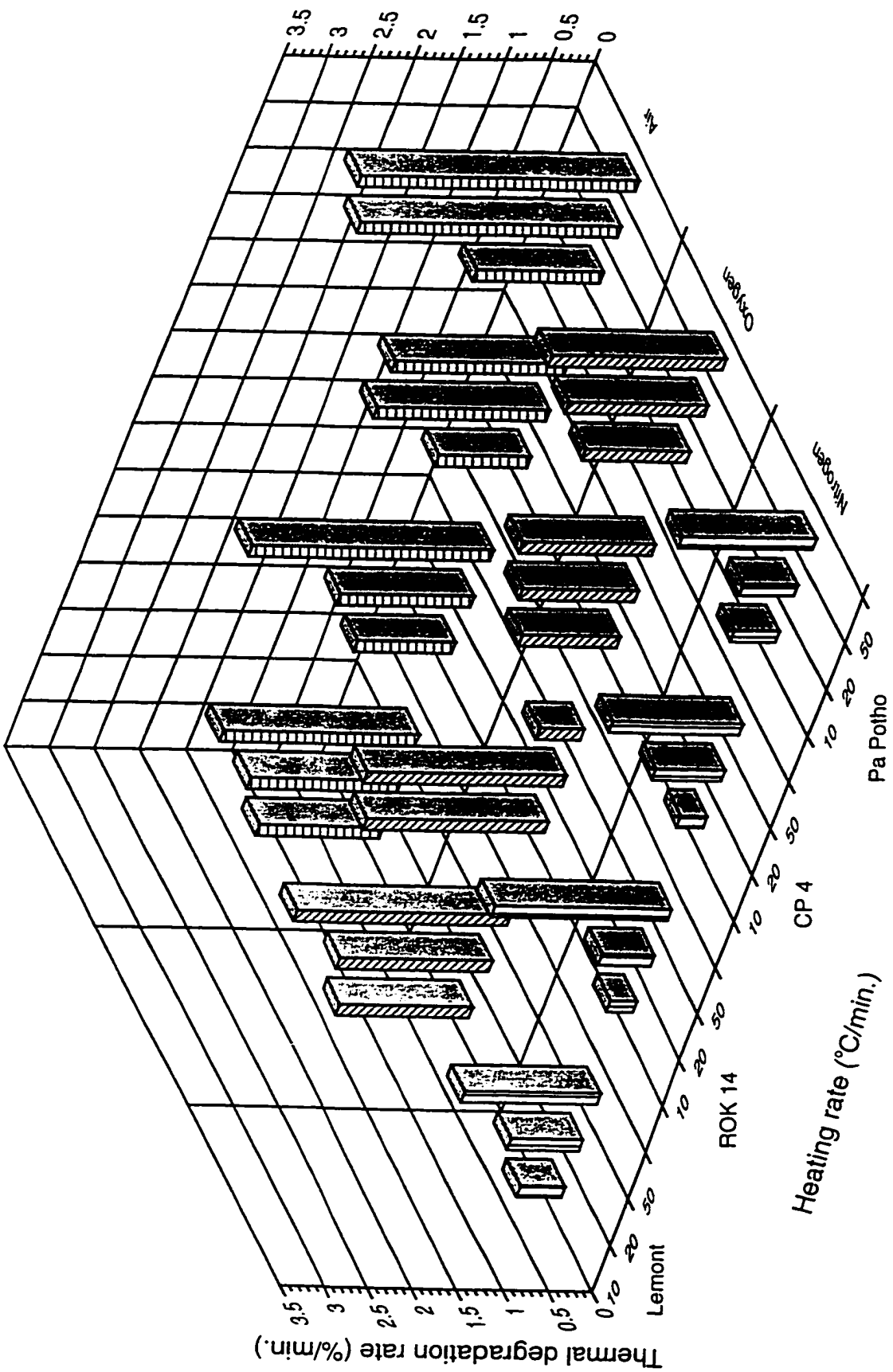

Figure 9.19 Thermal degradation rate in passive zone.

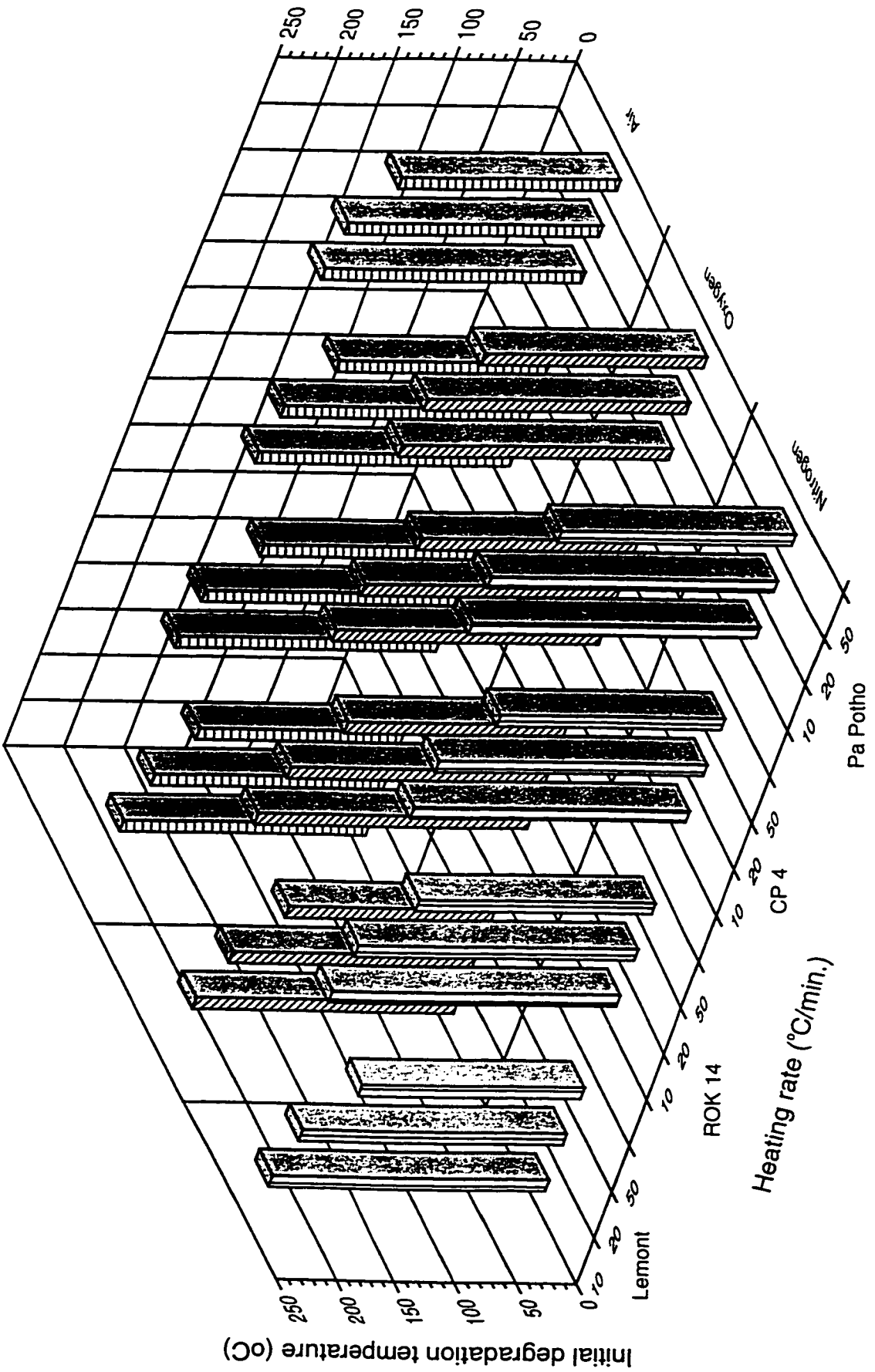

Figure 9.20 Initial degradation temperature.

oxygen at 172°C when heated at 50°C/minute, whereas at a heating rate of 10°C/minute, its initial degradation temperature was 217°C. Pa Potho started degrading at 224°C, 218°C, and 186°C when heated at 10, 20 and 50°C/minute, respectively. The initial degradation temperature was higher for all rice husk samples in nitrogen atmosphere than in both air and oxygen atmospheres at all heating rates.

9.1.3.1.3 Residual Weight at 700°C: The industrial processes for biomass gasification and liquefaction are usually designed for temperatures above 600°C. The higher temperatures are required to convert the char, at appreciable conversion rates, through heterogeneous reactions to gaseous components. Thus, a temperature level higher than 600°C (i.e. 700°C) was selected to compare the residual weights of different rice husk samples in this study. CP 4 rice husk exhibited the largest residual weight at 700°C in all atmospheres, in comparison to the other three rice husk samples as shown in Figure 9.21.

The residual weights at 700°C in the oxidative atmospheres of air (15.32-22.8%) and oxygen (15.32-23.00%) were lower in comparison with those obtained under nitrogen (about 33-39%). The residues obtained from TGA in the oxidative atmospheres were completely white in contrast to those obtained in the inert atmosphere which were completely black. It was also observed that the residual weights of the rice husk samples at 700°C in air and oxygen atmospheres were lower than their initial ash contents with percentages of ash lost ranging from about 2.95 to 13.10% in the case of air and 4.2 to 17.1% in the case of oxygen (Table 9.15), depending on the rice husk variety and the heating rate used.

9.1.3.2 Kinetic parameters. The kinetics of thermal decomposition reactions of carbonaceous materials is complicated in that the decomposition of carbonaceous materials involves a large number of reactions in parallel and series. Although TGA provides general information on the overall reaction kinetics, rather than individual reactions, it could be used as a tool for providing comparison kinetic data of various reaction parameters such as

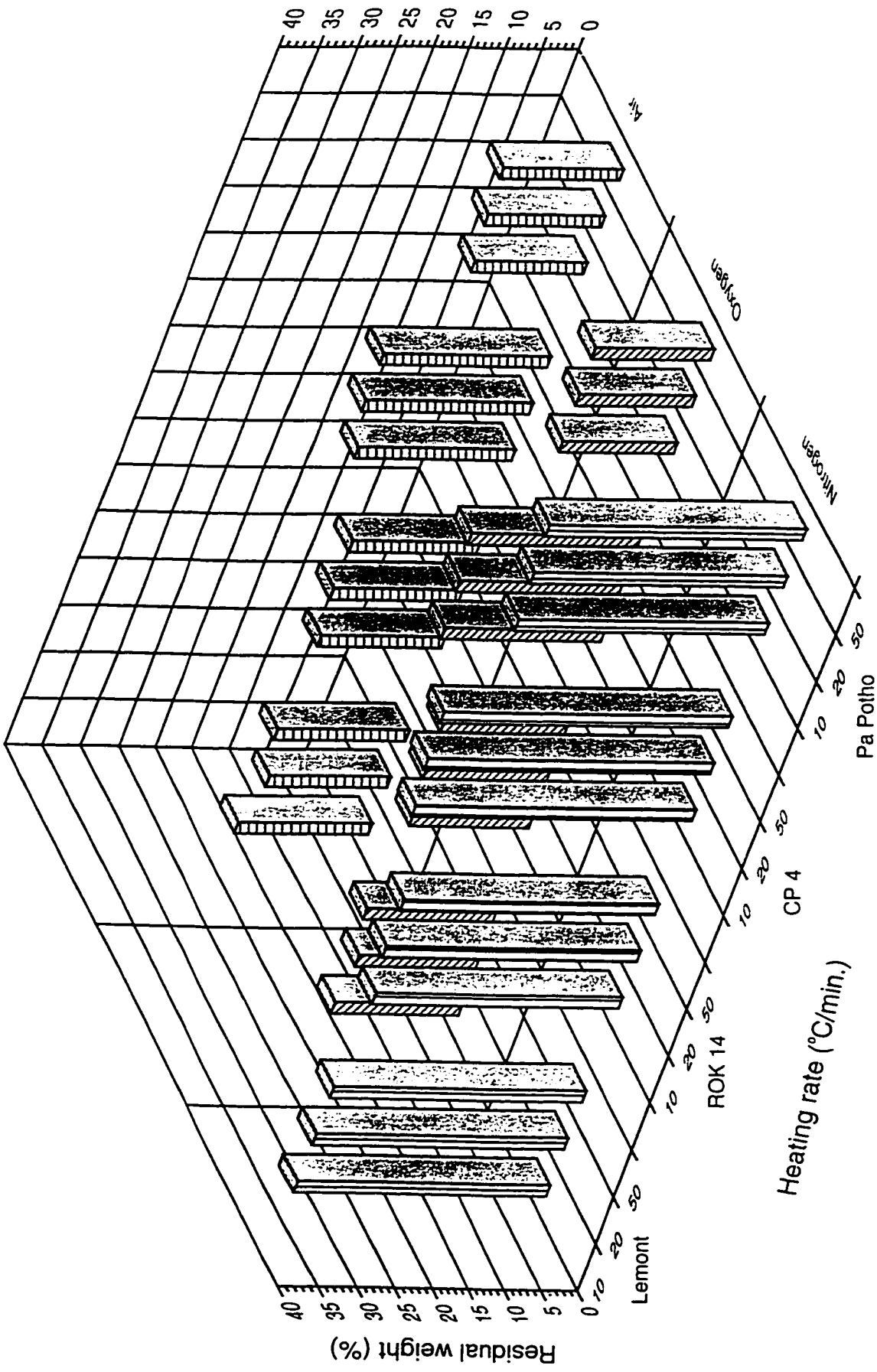

Figure 9.21 Residual weight at 700 C.

Table 9.15 Ash Lost in Air and Oxygen Atmospheres.

Rice Husk	Atmosphere	Heating Rate (°C/min)	Residual Weight at 700°C (%)[a]	Ash Content (% wb)[a]	Ash Lost (%)[b]
Lemont	Air	10	17.24	18.98	9.17
		20	16.48	18.96	13.10
		50	16.88	18.96	10.97
	Oxygen	10	16.88	19.64	14.05
		20	16.25	19.59	17.05
		50	17.62	19.41	9.22
ROK 14	Air	10	16.31	18.12	9.99
		20	17.11	18.07	5.31
		50	17.16	18.03	4.83
	Oxygen	10	16.43	18.43	10.85
		20	17.06	18.55	8.03
		50	17.11	18.38	6.91
CP 4	Air	10	21.26	23.50	9.53
		20	22.72	23.70	4.13
		50	22.86	23.70	2.95
	Oxygen	10	21.84	24.14	9.53
		20	22.20	24.19	8.23
		50	23.00	24.00	4.20
Pa Potho	Air	10	15.32	17.45	12.21
		20	15.86	17.53	9.53
		50	16.18	17.44	7.22
	Oxygen	10	15.32	17.94	14.60
		20	15.50	17.89	13.36
		50	15.82	17.75	10.87

[a] Percent of the original sample.
[b] Percent of the original ash.

temperature and heating rate. Other advantages of determining kinetic parameters from TGA are that only a single sample and considerably fewer data are required for calculating the kinetics over an entire temperature range in a continuous manner. Determination of the kinetic parameters from TGA data was based on the following rate expression (Wendlandt, 1974):

$$\frac{dX}{dt} = - A e^{\frac{E}{RT}} X^n \qquad (9.1)$$

where:

X	is the weight of sample undergoing reaction (kg)
t	is the time (min)
A	is the pre-exponential or frequency factor (1/min)
E	is the activation energy of the decomposition reaction (kJ/mol)
R	is the universal gas constant (kJ/mol.K)
T	is the absolute temperature (K)
n	is the order of reaction (-)

A technique based on the Arrhenius equation of the form presented by Goldfarb et al. (1968) and proposed by Duvvuri et al. (1975) was used to determine the kinetic parameters from typical curves of TG data over an entire temperature range in a continuous manner. The linearized form of the Arrhenius equation was used to determine A, E and n by applying least squares (multiple linear regression) technique. The simplified form of the linearized rate equation is the following:

$$y = B + Cx + Dz \qquad (9.2)$$

The parameters y, x, z, B, C and D in equation (9.2) are defined as follows:

$$y = \ln \{[-1/(w_o - w_f)][dw/dt]\}$$

$$x = 1/(RT)$$

$$z = \ln[(w - w_f)/(w_o - w_f)$$

$$B = \ln A$$

$$C = - E$$

$$D = n$$

where:

w_o is the initial weight of sample (kg)

w_f is the weight of residue at the end of the reaction (kg)

w is the weight of sample at time t (min)

It was evident from the TGA curves (Figures 9.14-9.17) that two prominent reaction zones existed during the thermal degradation of rice husk in air, oxygen or nitrogen atmosphere. Because of the two-step nature of decomposition, it was not possible to use the same kinetic parameters to describe the thermal degradation over the entire temperature range accurately. Therefore, the kinetic parameters were determined for each reaction zone separately. The coefficients B, C and D in Equation 9.2 (which correspond to the logarithm of pre-exponential factor (ln A), the energy of activation (E) and the order of reaction (n), respectively) were determined for each type of rice husk under air, oxygen and nitrogen atmospheres by the multiple linear regression analysis method using the thermogravimetric data.

Several researchers (Font et al., 1989; Tia et al., 1991; Ergudenler and Ghaly, 1992b; Varhegyi et al., 1994; and Williams and Besler, 1994) have suggested that to evaluate kinetic parameters from thermogravimetric data, the heating rate should be as slow as possible to avoid the effect of mass transfer. Tia et al. (1991) and Ergudenler and Ghaly (1992b) obtained good correlations when fitting TGA data by a single straight line at heating rates in the

neighbourhood of 20°C/minute. For heating rates above 20°C/minute, Tia et al. (1991) obtained poor correlation. Williams and Besler (1994), using TGA to study the pyrolysis of biomass materials, reported maximum activation energies at 20°C/minute for the low temperature regime and showed that activation energies for both high and low temperature regimes above 20°C/minute heating rate decreased with increasing heating rate to 80°C/minute. A heating rate of 20°C/minute was, therefore, used to determine the kinetic parameters in this study. The kinetic parameters obtained for the two prominent groups of reaction in air, oxygen and nitrogen atmospheres are given in Table 9.16.

In the first reaction zone, ten data points on each TGA curve were used to determine the kinetic parameters (ln A, E and n). The results of multiple linear regression analyses showed that kinetic parameters of the first reaction zone had 97.8-99.9% confidence. In nitrogen atmosphere, the activation energies ranged from 29.0 kJ/mol for Lemont LG rice husk to 35.4 kJ/mol for Pa Potho rice husk. The activation energies for rice husks in air atmosphere were of similar magnitude to those in nitrogen atmosphere, although generally higher at 37.0 kJ/mol for CP 4 rice husk to 54.7 kJ/mol for ROK 14 rice husk. In oxygen atmosphere, the activation energies were substantially higher at 142.7 kJ/mol for CP 4 rice husk to 188.5 kJ/mol for ROK 14 rice husk.

The results of multiple linear regression analyses (which were based on eight data points) showed that kinetic parameters of the second reaction zone had 86.4-94.5% confidence. Relatively lower activation energies were obtained in the second reaction zone. The highest activation energy in the second reaction zone was obtained in air atmosphere (21.0 kJ/mol) for ROK 14 rice husk, followed by that obtained in nitrogen atmosphere (17.7 kJ/mol) for Pa Potho rice husk and in oxygen atmosphere (16.6 kJ/mol) for ROK 14 rice husk.

The pre-exponential factors under air and nitrogen atmospheres in the first reaction zone were in the range of 10^3 to 10^6 min^{-1}. Under oxygen atmosphere, the pre-exponential

Table 9.16 Kinetic Parameters.

		First Reaction Zone				Second Reaction Zone			
Rice Husk	Atmosphere	TR (°C)	A (min^{-1})	E ($kJmol^{-1}$)	n (-)	TR (°C)	A (min^{-1})	E ($kJmol^{-1}$)	n (-)
Lemont (LG)	Air	191-321	3.77×10^{6}	53.4	1.41	321-510	1.41×10^{3}	20.8	0.47
	Oxygen	203-292	1.18×10^{14}	142.7	0.70	292-458	0.13×10^{2}	14.3	0.20
	Nitrogen	220-377	4.67×10^{3}	29.0	1.06	377-523	1.13×10^{2}	15.1	0.35
ROK 14	Air	210-312	6.38×10^{6}	54.7	1.57	312-504	1.53×10^{3}	21.0	0.49
	Oxygen	215-295	1.22×10^{17}	188.5	0.83	295-448	0.56×10^{2}	16.6	0.28
	Nitrogen	232-368	2.87×10^{4}	33.4	1.08	368-536	1.27×10^{2}	15.4	0.36
CP 4	Air	206-320	4.27×10^{4}	37.0	1.21	320-505	4.52×10^{2}	18.0	0.40
	Oxygen	211-295	9.12×10^{14}	143.0	0.70	295-456	0.28×10^{1}	15.9	0.29
	Nitrogen	223-367	7.25×10^{3}	30.0	0.91	367-540	5.14×10^{2}	16.3	0.30
Pa Potho	Air	212-317	9.18×10^{4}	40.0	1.64	317-495	7.66×10^{2}	19.3	0.55
	Oxygen	218-291	1.69×10^{15}	148.0	0.77	291-456	0.21×10^{2}	11.0	0.26
	Nitrogen	240-369	6.43×10^{4}	35.4	0.90	369-503	1.01×10^{2}	17.7	0.30

Note: TR= temperature range; A= pre-exponential factor; E = activation energy; n = order of reaction.

factor in the first reaction zone ranged as high as 10^{17} min^{-1}. The order of reactions determined in this study were in the range of 0.7 to 1.6 for the first reaction zone and 0.2 to 0.5 for the second reaction zone.

In addition to yielding kinetic data, TGA measurements were also used to yield data equivalent to a proximate analysis; namely moisture, volatile matter, char, and ash contents as shown for Pa Potho rice husk sample heated at 10°C/minute in nitrogen atmosphere (Figure 9.22). The results are presented in Table 9.17. The rice husk samples were ashed in air at 700°C. The weight of char ranged from 14.73% for CP 4 rice husk sample heated at 10°C/minute to 16.48% for Pa Potho rice husk sample heated at 50°C/minute. The fraction of volatile matter ranged from 56.46% for CP 4 rice husk sample heated at 10°C/minute to 63.17% for Pa Potho rice husk sample heated at 20°C/minute.

9.2 Main Experiments

Lemont LG Rice husk obtained from Brousand Ricemills, United States of America was used in these experiments because of its similarity in properties to some of the rice husk samples obtained from Sierra Leone, one of the countries for which this rice husk gasification technology is being developed. Another reason for using Lemont LG is the close proximity of the ricemills in the U. S. A. to the gasification laboratory in the Agricultural Engineering Department of DalTech, Dalhousie University, Halifax, Nova Scotia, Canada, compared to bringing rice husks from other possible sources like Sierra Leone, West Africa. It is important to note at this point that rice is not grown in Canada. Twenty seven experiments were conducted using three levels of bed height (19.5, 25.5 and 31.5 cm), three levels of fluidization velocity (0.22, 0.28 and 0.33 m/s) and three levels of equivalence ratio (0.25, 0.30 and 0.35).

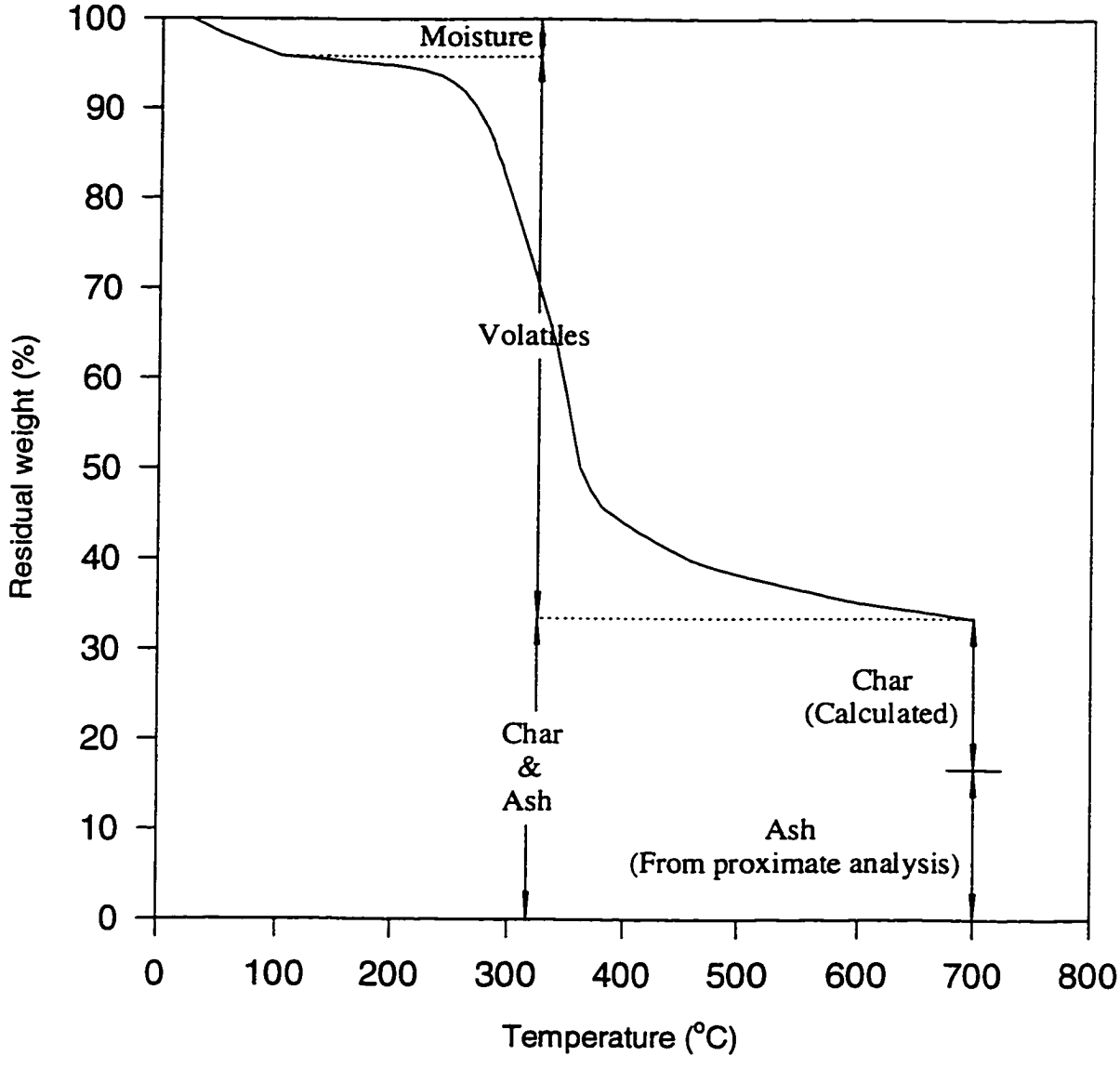

Figure 9.22 Thermogram of pa potho rice husk heated at 10°C/min showing moisture, volatile matter, char, and ash contents.

Table 9.17 Proximate Analysis of Rice Husk From TGA Measurements Under Nitrogen Atmosphere (% wet basis).

Rice Husk	Heating Rate (°C/min.)	Initial Moisture Content (%)	Volatile Matter (%)	Residual Weight at 700°C	
				Char (%)	Ash (%)
Lemont (LG)	10	5.08	61.15	14.79	18.98
	20	4.35	61.77	14.75	19.13
	50	4.15	61.85	14.83	19.17
ROK 14	10	4.23	62.30	15.47	18.00
	20	3.06	62.42	16.30	18.22
	50	3.01	62.42	16.34	18.23
CP 4	10	5.59	56.46	14.73	23.22
	20	4.18	57.09	15.16	23.57
	50	4.11	56.94	15.36	23.59
Pa Potho	10	4.15	62.39	16.02	17.44
	20	3.05	63.17	16.14	17.64
	50	3.01	62.86	16.48	17.65

9.2.1 Gasifier Temperature

The isothermal operation of fluidized bed reactors is essential for efficient operation. Temperature profiles can provide information regarding possible clinker formation at hot spots within the bed. The average temperatures recorded at the inlet below the secondary distributor plate (T_1), in the secondary column (T_2), wind box (T_3), dense bed (T_4-T_9), freeboard (T_{10} and T_{11}), cyclone (T_{12} and T_{13}) and the afterburner (T_{14}) are given in Tables 9.18 to 9.20. Figures 9.23 to 9.31 show the variations of bed temperature with time at different bed heights, fluidization velocities and equivalence ratios. Figure 9.32 shows the gasifier temperature profiles at different bed heights, fluidization velocities and equivalence ratios.

The lowest temperature readings were recorded below the secondary distributor plate (T_1) and ranged from 127 to 218°C. The temperatures recorded in the secondary column (T_2) and within the wind-box below the main distributor plate ranged from 400 to 644°C and 330 to 476°C, respectively. The variation of bed temperature with time shows that the dense bed (sand-fuel) temperatures (T_4-T_9) reached the operating temperature within about 16-20 minutes. The temperature profiles show that the dense bed was essentially isothermal while the temperatures recorded in the freeboard and gasifier exit dropped.

Higher temperature readings were recorded at the lowest bed height (19.5 cm). The temperature readings increase with higher values of fluidization velocity and/or higher values of equivalence ratio. The maximun temperatures of the dense bed (880°C), freeboard (856°C) and cyclone exit (805°C) were observed at the bed height of 19.5 cm, the fluidization velocity of 0.33 m/s and the equivalence ratio of 0.35 whereas the minimum temperatures of the dense bed (665°C), freeboard (607°C) and cyclone exit (500°C) were observed at the bed height of 31.5 cm, the fluidization velocity of 0.22 m/s and the equivalence ratio of 0.25.

Table 9.18 Temperature Measurements at the Inlet of the Fluidized Bed.

Bed Height (cm)	Fluidization Velocity (m/s)	Equivalence Ratio (-)	Temperature* (°C)		
			T_1	T_2	T_3
19.5	0.22	0.25	135	430	359
		0.30	138	551	384
		0.35	191	598	420
	0.28	0.25	140	466	376
		0.30	147	576	390
		0.35	215	633	456
	0.33	0.25	144	471	395
		0.30	149	588	404
		0.35	218	644	476
25.5	0.22	0.25	128	424	352
		0.30	131	530	361
		0.35	160	496	419
	0.28	0.25	133	432	369
		0.30	134	552	384
		0.35	163	610	432
	0.33	0.25	139	457	380
		0.30	145	578	390
		0.35	209	616	448
31.5	0.22	0.25	127	400	330
		0.30	130	478	334
		0.35	167	570	393
	0.28	0.25	130	415	346
		0.30	132	491	362
		0.35	170	571	400
	0.33	0.25	141	440	364
		0.30	145	524	371
		0.35	189	576	408

* Average of 10 measurements.

T_1 is the temperature below the secondary distributor plate.

T_2 is the temperature in the secondary column.

T_3 is the temperature in the wind box.

Table 9.19 Temperature Measurements in the Dense Bed.

Bed Height (cm)	Fluidization Velocity (m/s)	Equivalence Ratio (-)	Temperature* (°C) T_4	T_5	T_6	T_7	T_8	T_9	Mean (°C)	STD (°C)	CV (%)
19.5	0.22	0.25	704	707	702	700	705	704	704	2.42	0.32
		0.30	799	802	802	792	798	798	799	3.67	0.46
		0.35	850	854	856	840	847	848	849	5.67	0.67
	0.28	0.25	726	728	728	719	724	723	725	3.44	0.47
		0.30	820	825	824	812	818	819	820	4.71	0.57
		0.35	876	881	880	865	872	874	875	5.85	0.67
	0.33	0.25	744	747	746	740	745	743	744	2.48	0.33
		0.30	834	838	836	826	833	832	833	4.12	0.49
		0.35	880	885	885	872	878	879	880	4.88	0.55
25.5	0.22	0.25	693	696	695	688	693	691	693	2.88	0.42
		0.30	778	783	778	770	777	775	777	4.26	0.55
		0.35	841	843	844	832	839	839	840	4.27	0.51
	0.28	0.25	719	721	718	713	718	717	718	2.66	0.37
		0.30	803	806	804	797	802	801	802	3.06	0.38
		0.35	854	854	852	846	852	851	852	3.00	0.35
	0.33	0.25	725	725	721	718	723	721	723	2.59	0.36
		0.30	823	826	820	814	821	819	821	4.04	0.49
		0.35	855	858	854	846	854	852	853	4.02	0.47
31.5	0.22	0.25	663	669	667	661	666	665	665	2.86	0.43
		0.30	745	747	745	738	744	743	744	3.08	0.41
		0.35	813	817	812	804	811	811	811	4.23	0.52
	0.28	0.25	672	672	669	667	669	670	670	2.00	0.30
		0.30	750	753	751	744	749	754	750	3.54	0.47
		0.35	823	826	820	815	822	823	822	3.73	0.45
	0.33	0.25	701	704	699	695	701	700	700	2.97	0.42
		0.30	767	770	765	760	768	768	766	3.50	0.45
		0.35	830	832	829	821	828	830	828	3.83	0.46

* Average of 10 measurements.
STD is the standard Deviation.
CV is the coefficient of variance.

Table 9.20 Temperature Measurements at the Freeboard, Cyclone Inlet, Cyclone Exit and Afterburner.

Bed Height (cm)	Fluidization Velocity (m/s)	Equivalence Ratio (-)	Temperature* (°C)				
			Freeboard		Cyclone		After Burner
			T_{10}	T_{11}	T_{12}	T_{13}	T_{14}
19.5	0.22	0.25	664	623	564	534	700
		0.30	758	710	667	632	677
		0.35	814	793	747	694	643
	0.28	0.25	712	683	649	619	737
		0.30	805	779	748	721	706
		0.35	867	846	801	774	676
	0.33	0.25	734	713	673	652	732
		0.30	818	795	765	741	731
		0.35	877	856	828	805	735
25.5	0.22	0.25	662	616	553	518	691
		0.30	750	709	655	623	702
		0.35	817	775	728	694	653
	0.28	0.25	709	681	623	596	740
		0.30	789	765	706	683	724
		0.35	836	810	765	730	711
	0.33	0.25	719	696	637	616	746
		0.30	811	786	730	705	733
		0.35	839	815	784	762	716
31.5	0.22	0.25	647	607	531	500	680
		0.30	726	692	629	599	684
		0.35	787	748	697	663	662
	0.28	0.25	666	641	570	546	730
		0.30	741	714	662	637	707
		0.35	808	782	742	714	682
	0.33	0.25	696	675	612	591	741
		0.30	757	734	701	678	743
		0.35	819	797	765	740	721

* Average of 10 measurements.

T_{10}, T_{11} are the inlet and exit freeboard temperatures.

T_{12}, T_{13} are the inlet and exit cyclone temperatures.

T_{14} is the temperature in the afterburner.

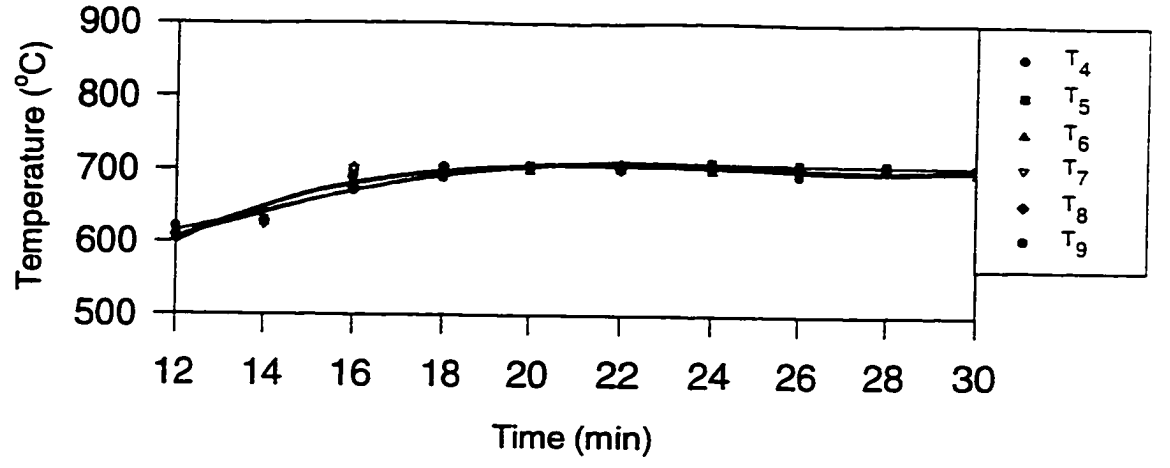

(a) Bed Height = 19.5 cm

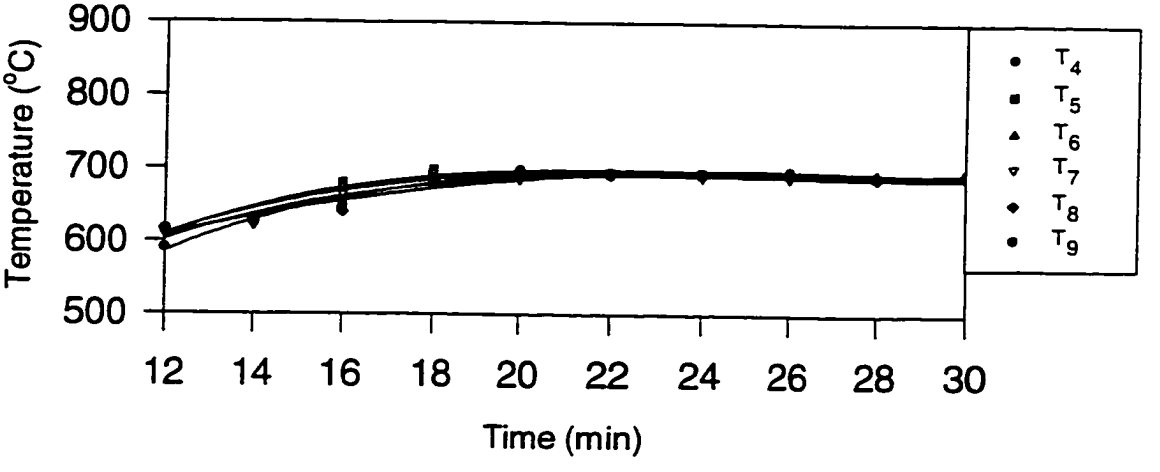

(b) Bed Height = 25.5 cm

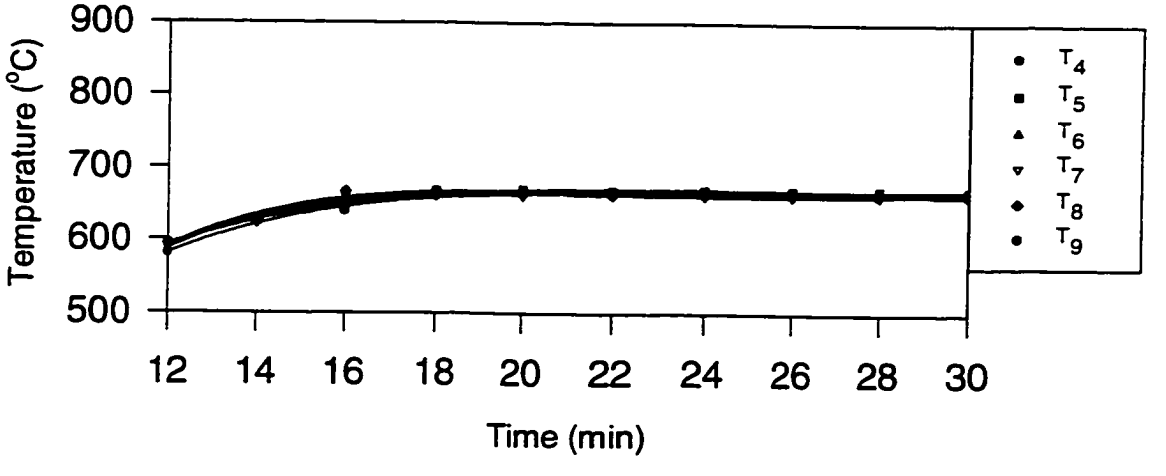

(c) Bed Height = 31.5 cm

Figure 9.23 Temperature distribution in the dense bed at the fluidization velocity of 0.22 m/s and the equivalence ratio of 0.25.

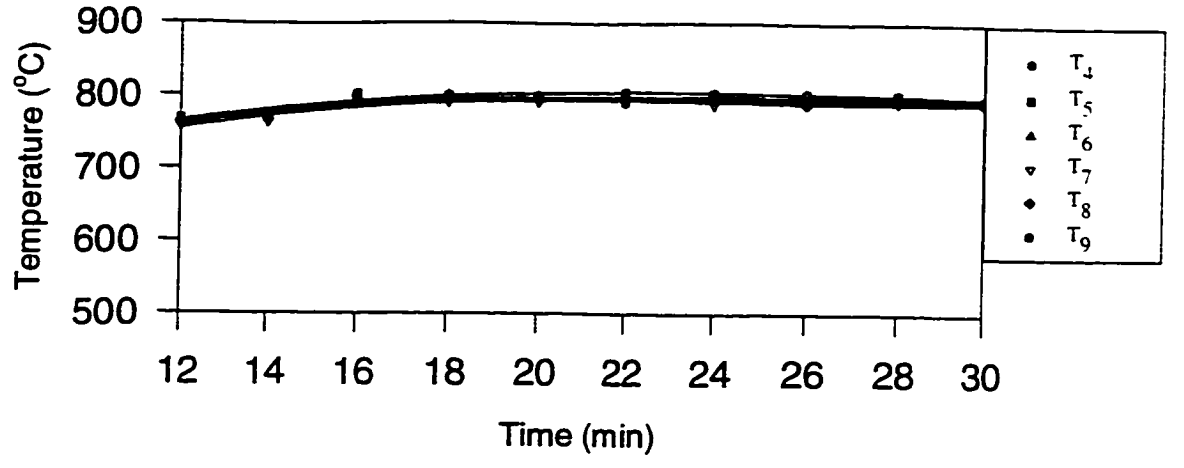

(a) Bed Height = 19.5 cm

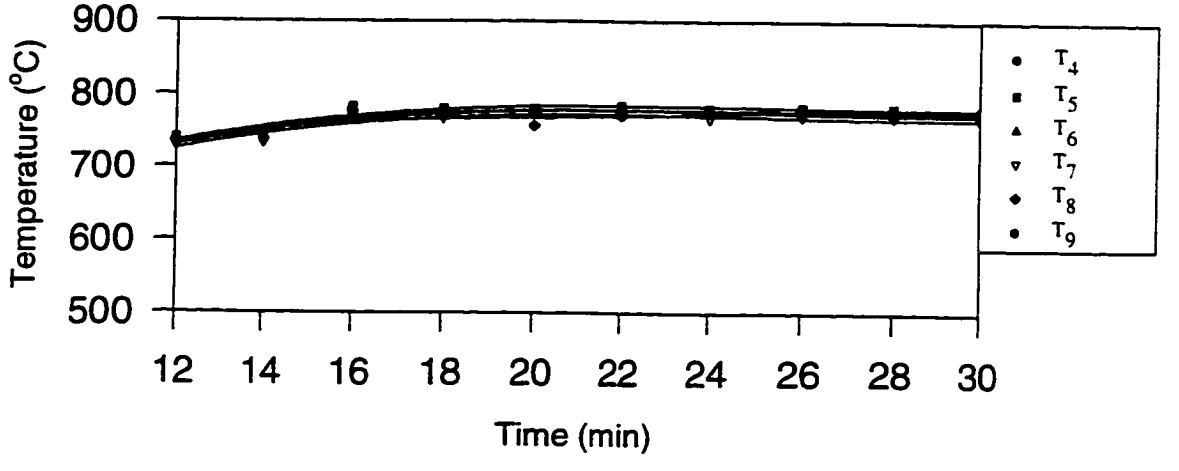

(b) Bed Height = 25.5

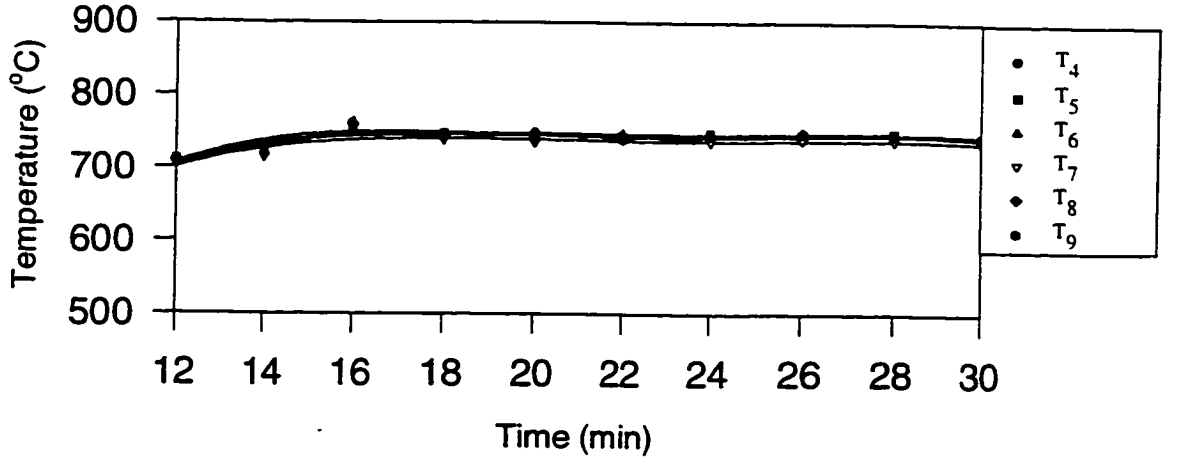

(c) Bed Height = 31.5 cm

Figure 9.24 Temperature distribution in the dense bed at the fluidization velocity of 0.22 m/s and the equivalence ratio of 0.30.

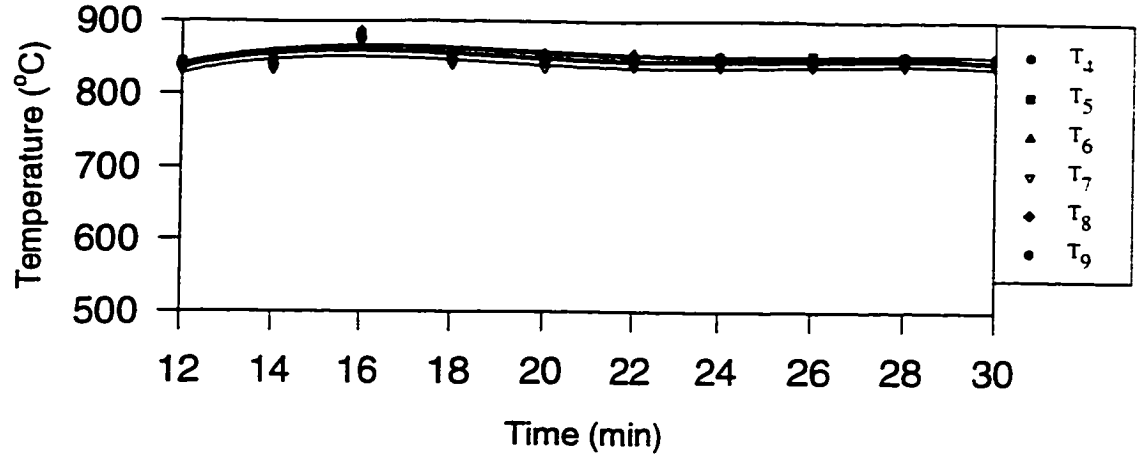

(a) Bed Height = 19.5

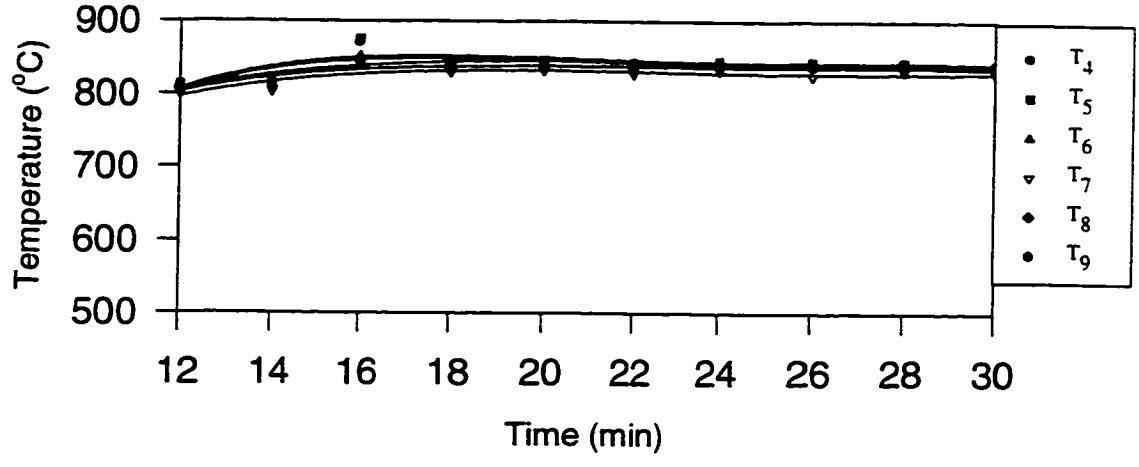

(b) Bed Height = 25.5 cm

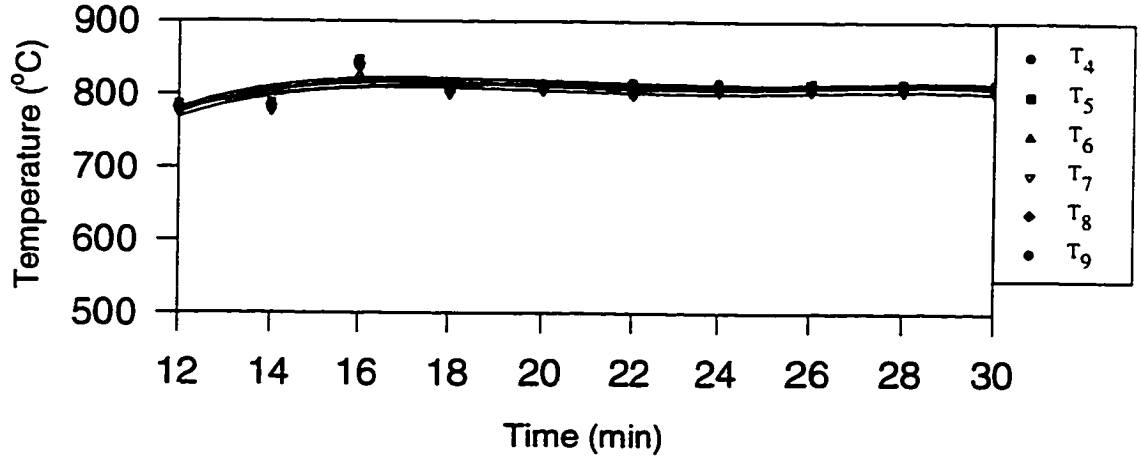

(c) Bed Height = 31.5 cm

Figure 9.25 Temperature distribution in the dense bed at the fluidization velocity of 0.22 m/s and the equivalence ratio of 0.35.

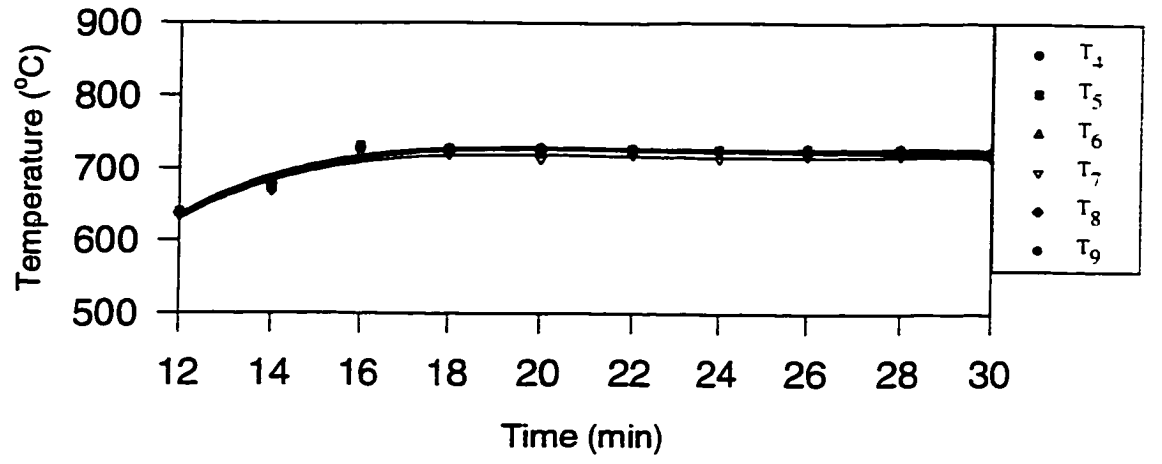

(a) Bed Height = 19.5 cm

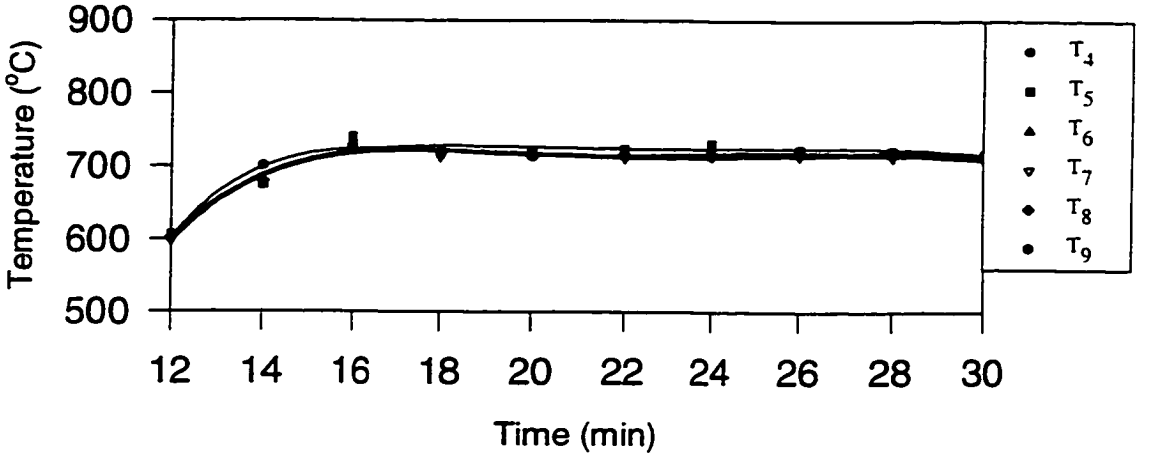

(b) Bed Height = 25.5 cm

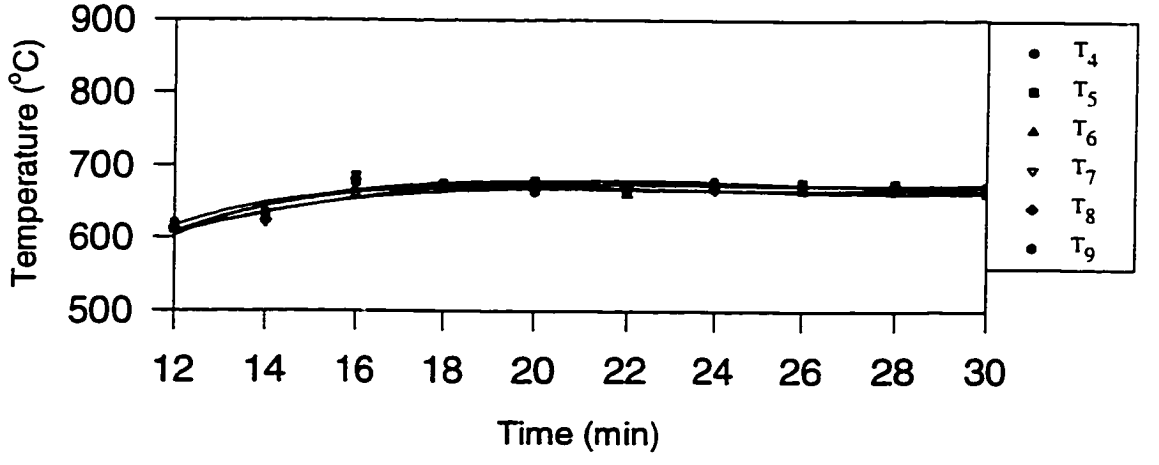

(c) Bed Height = 31.5 cm

Figure 9.26 Temperature distribution in the dense bed at the fluidization velocity of 0.28 m/s and the equivalence ratio of 0.25.

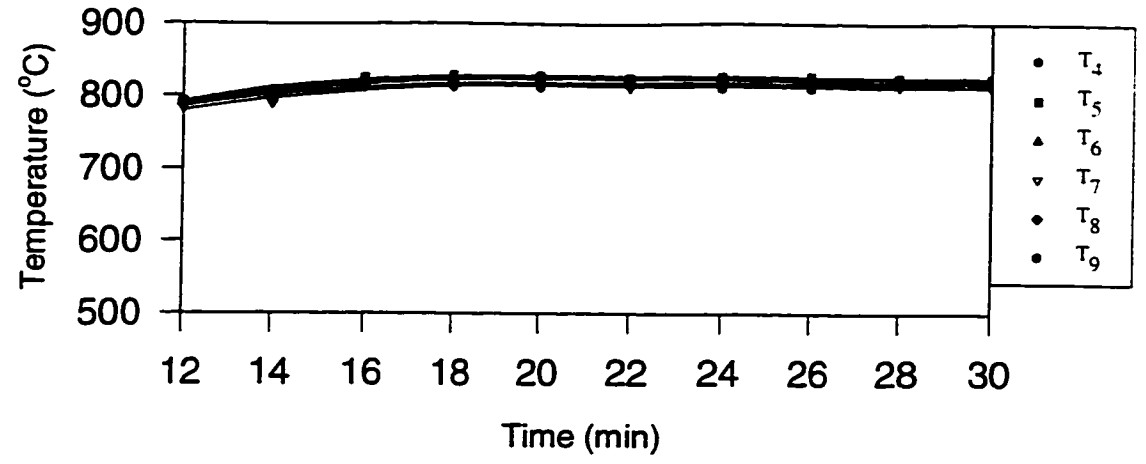

(a) Bed Height = 19.5 cm

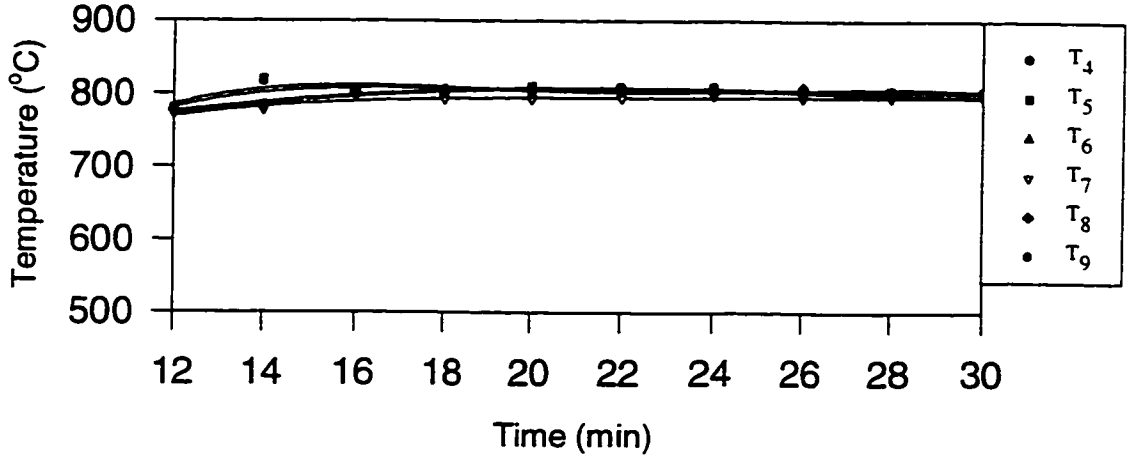

(b) Bed Height = 25.5 cm

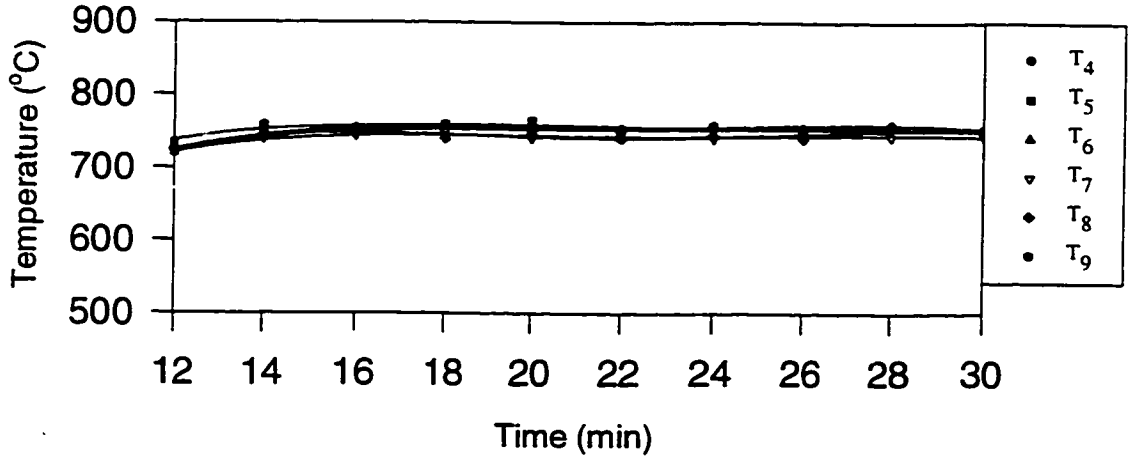

(c) Bed Height = 31.5 cm

Figure 9.27 Temperature distribution in the dense bed at the fluidization velocity of 0.28 m/s and the equivalence ratio of 0.30.

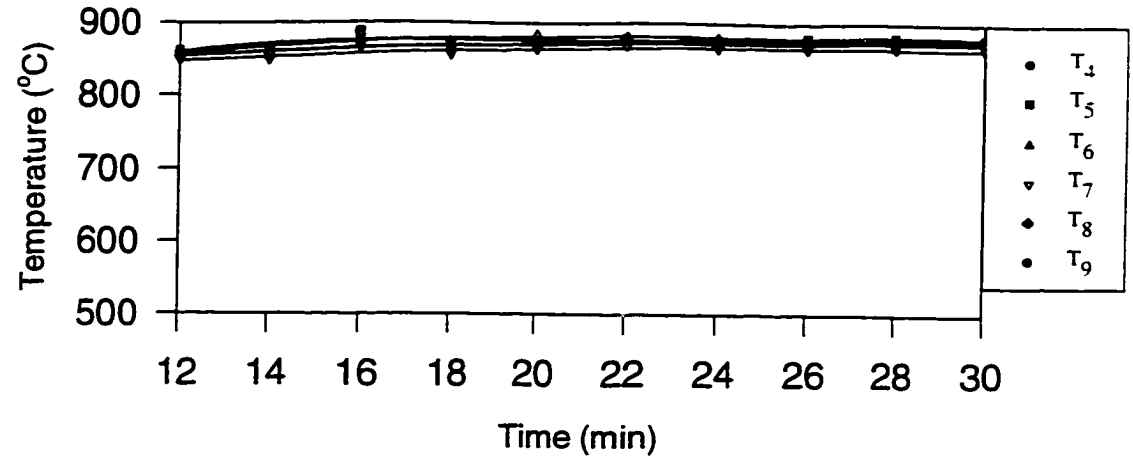

(a) Bed Height = 19.5 cm

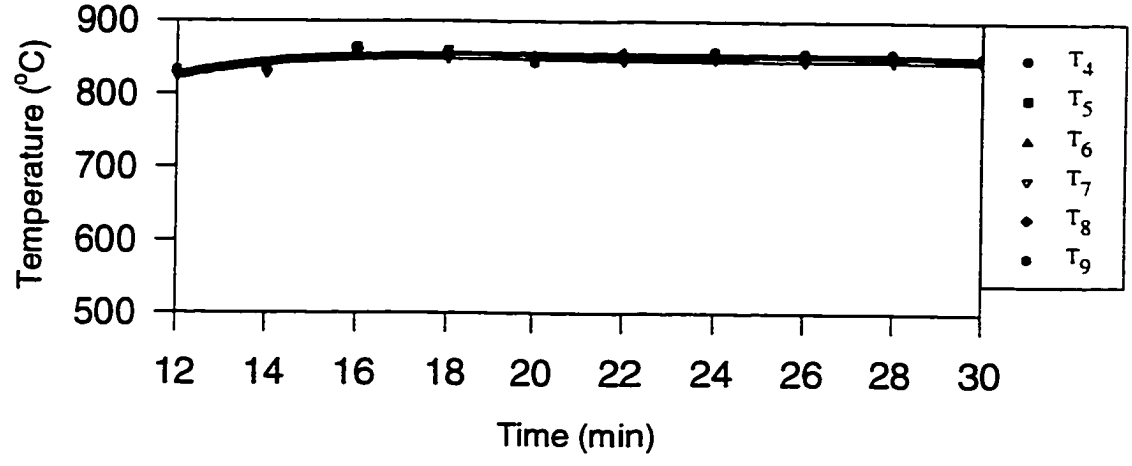

(b) Bed Height = 25.5 cm

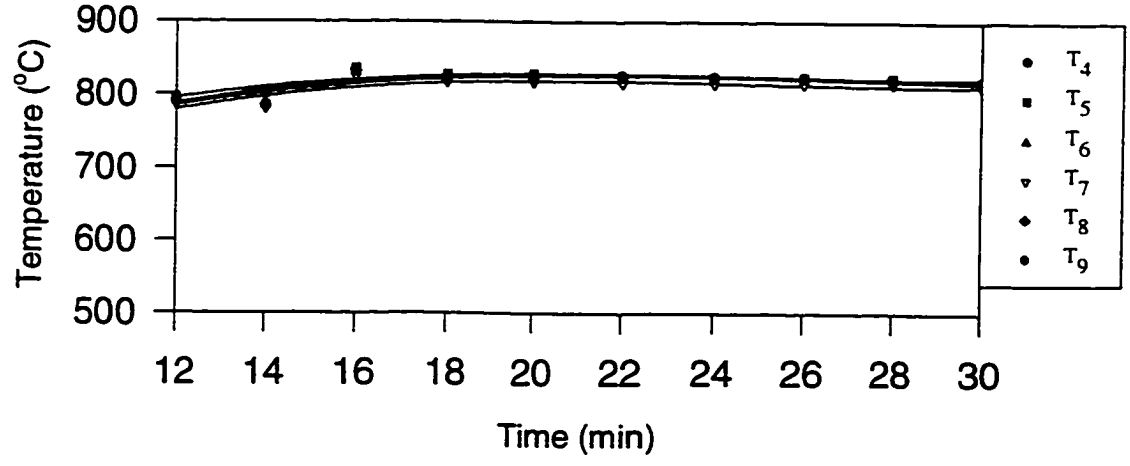

(c) Bed Height = 31.5 cm

Figure 9.28 Temperature distribution in the dense bed at the fluidization velocity of 0.28 m/s and the equivalence ratio of 0.35.

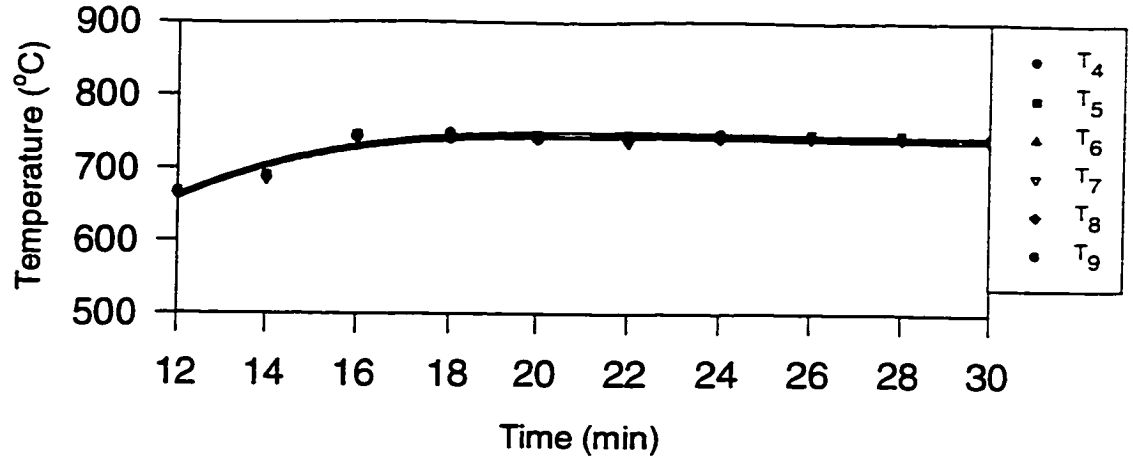

(a) Bed Height = 19.5 cm

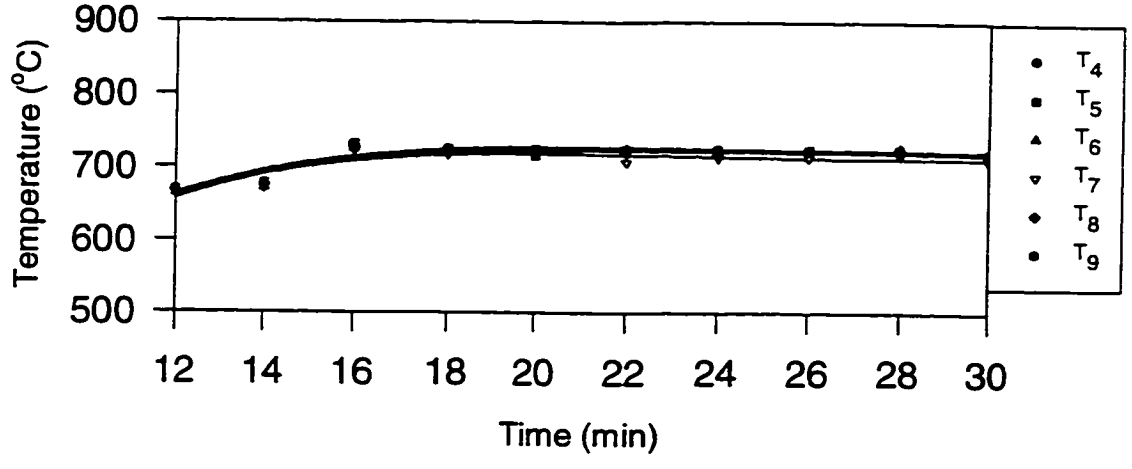

(b) Bed Height = 25.5 cm

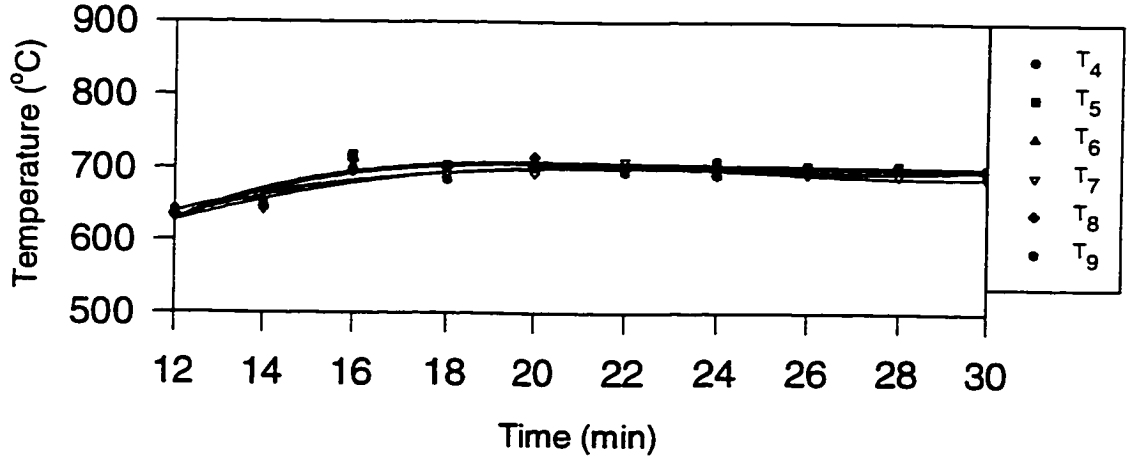

(c) Bed Height = 31.5 cm

Figure 9.29 Temperature distribution in the dense bed at the fluidization velocity of 0.33 m/s and the equivalence ratio of 0.25.

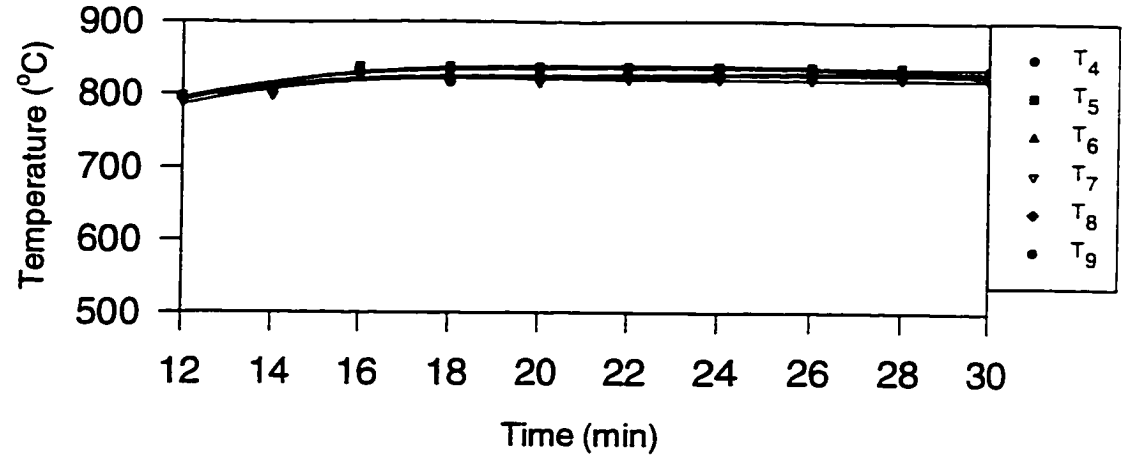

(a) Bed Height = 19.5 cm

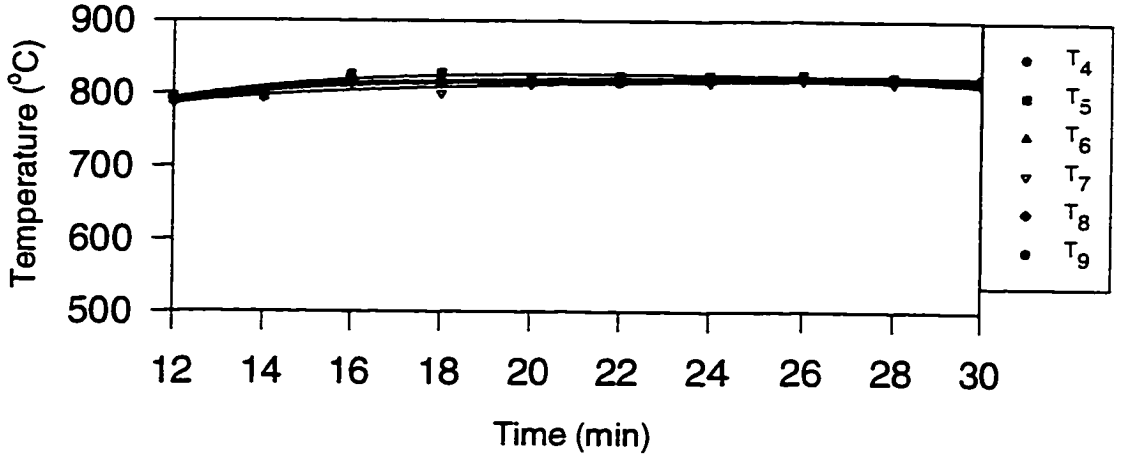

(b) Bed Height = 25.5 cm

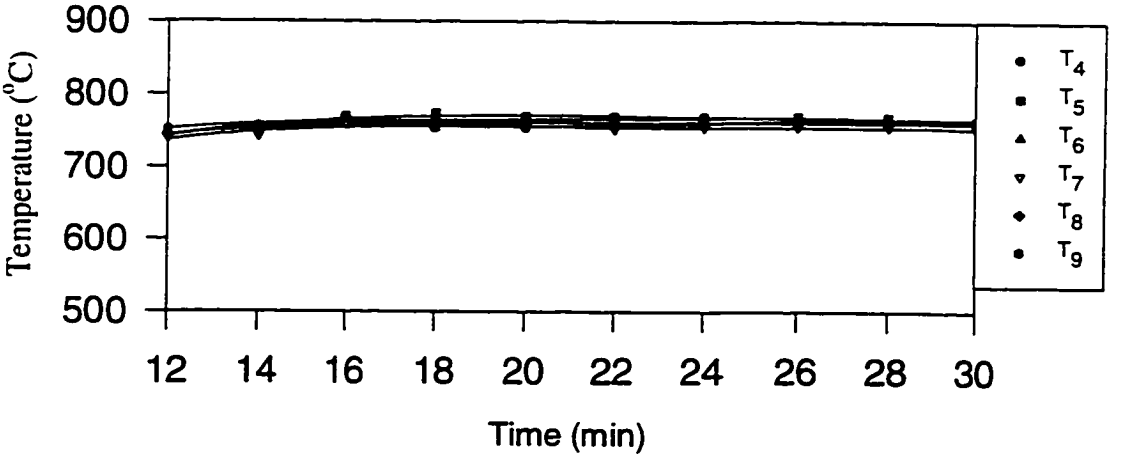

(c) Bed Height = 31.5 cm

Figure 9.30 Temperature distribution in the dense bed at the fluidization velocity of 0.33 m/s and the equivalence ratio of 0.30.

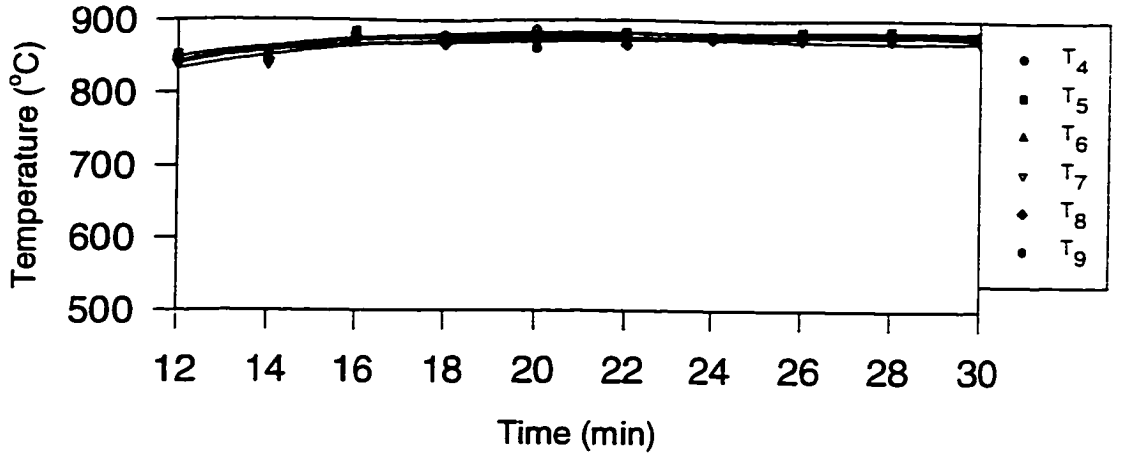

(a) Bed Height = 19.5 cm

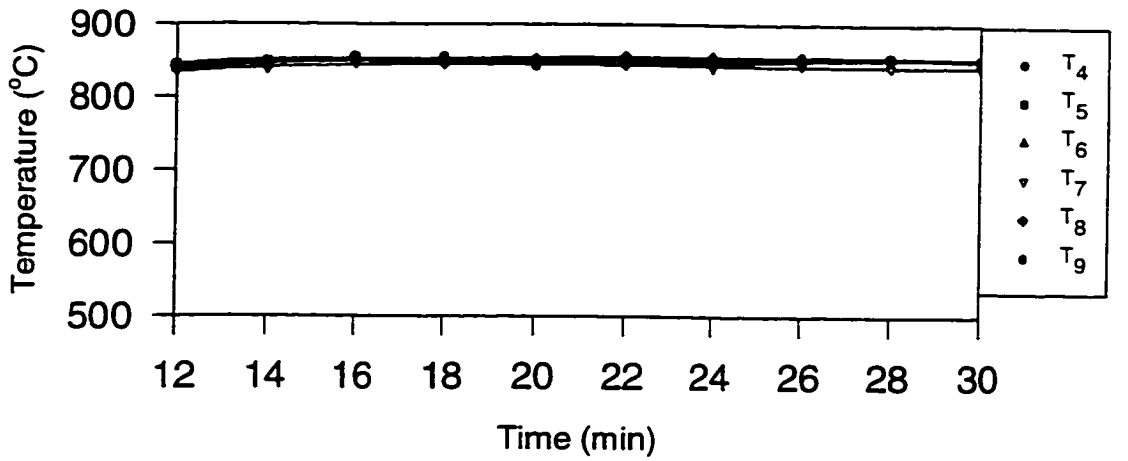

(b) Bed Height = 25.5 cm

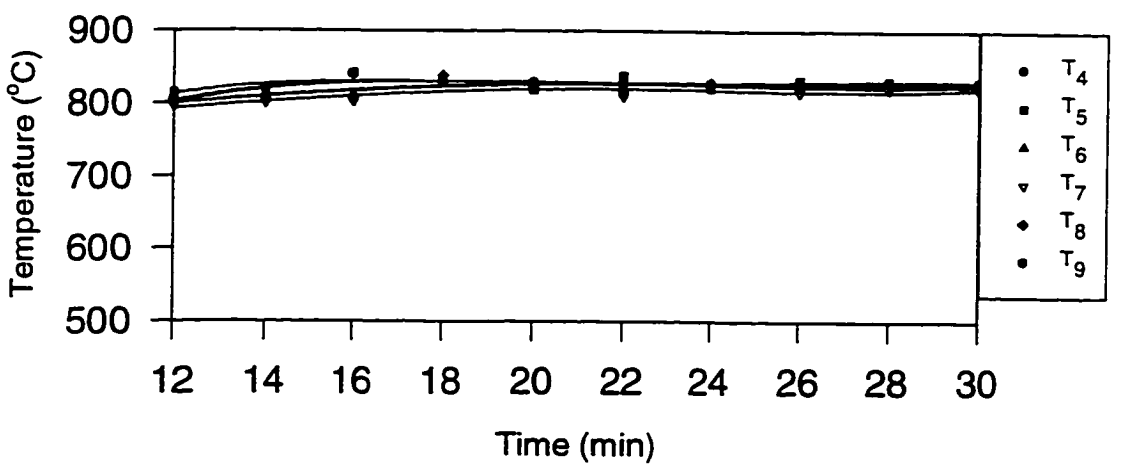

(c) Bed Height = 31.5 cm

Figure 9.31 Temperature distribution in the dense bed at the fluidization velocity of 0.33 m/s and the equivalence ratio of 0.35.

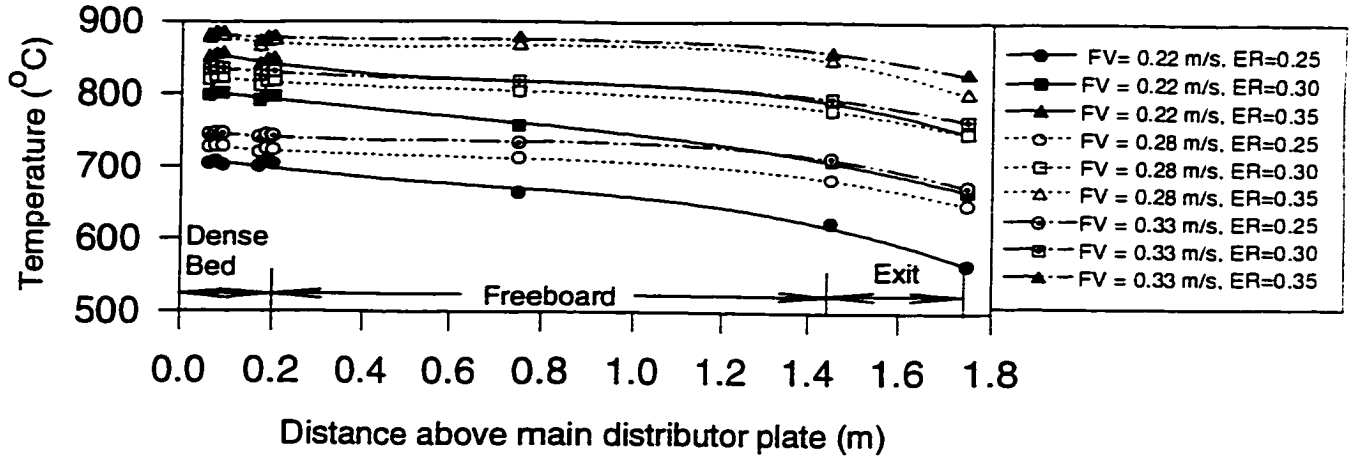

(a) Bed Height = 19.5 cm

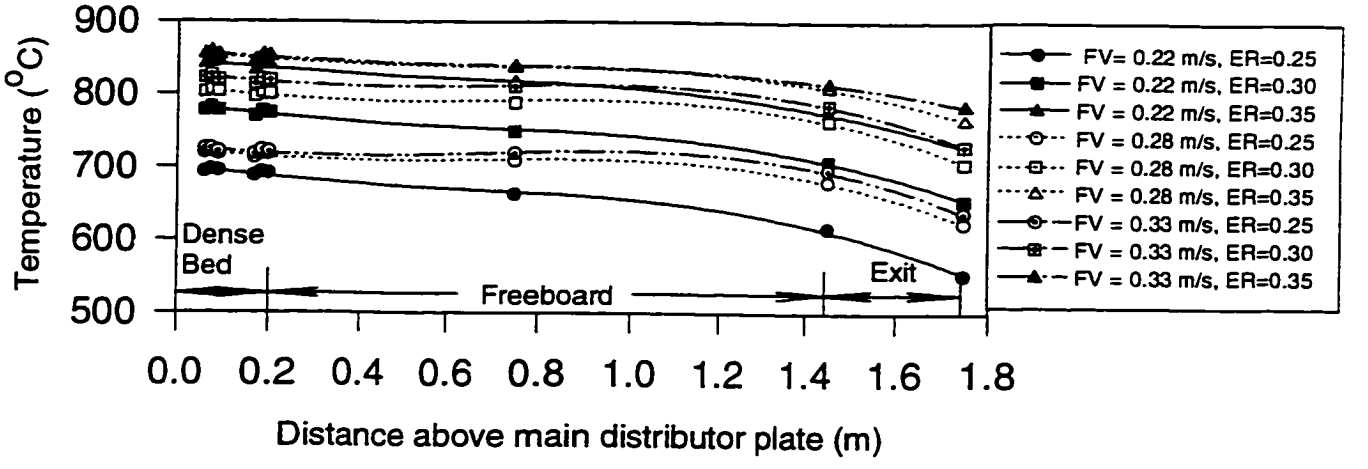

(b) Bed Height = 25.5 cm

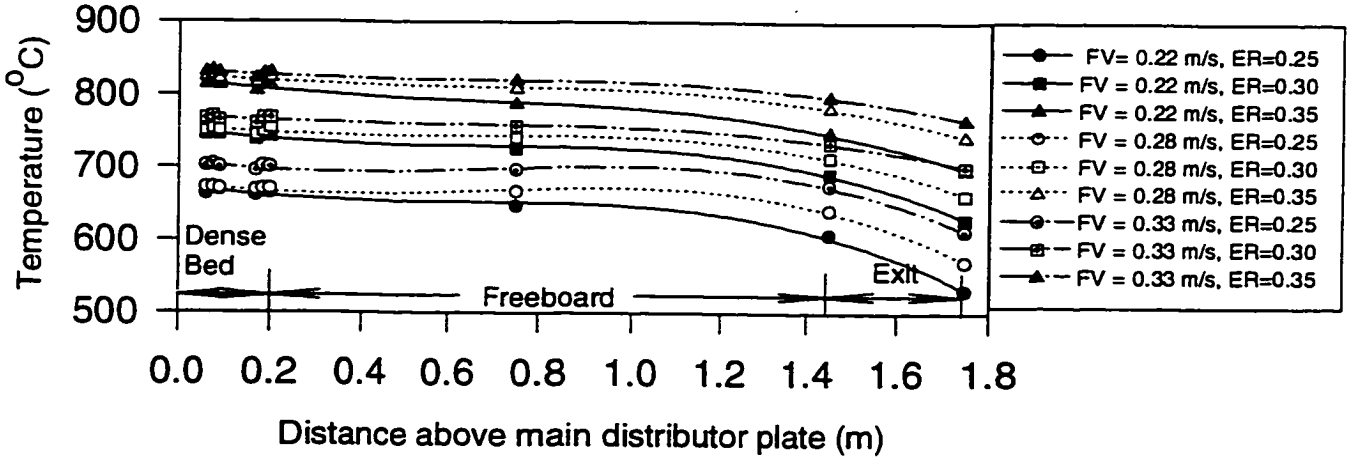

(c) Bed Height = 31.5 cm

Figure 9.32 Temperature profiles in the gasifier.

9.2.2 Gasifier Pressure Drop

Pressure drop across the fluidized bed indicates the general resistance to flow of the gases inside the gasifier. As reported by Jenkins (1980), low resistance is desired so as not to limit the velocity of the chemical reactions. The pressure drop distribution in the fluidized bed gasifier at various bed heights, fluidization velocities and equivalence ratios are summarized in Tables 9.21 and 9.22. Figure 9.33 shows the pressure drop profiles as a function of the distance from the main distributor plate at various bed heights, fluidization velocities and equivalence ratios.

Increasing the equivalence ratio resulted in lower pressure drops in the dense bed region, the freeboard region and the enlarged section of the fluidized bed gasifier at all bed heights and fluidization velocities. Increasing the fluidization velocity increased the pressure drop in the dense bed region, the freeboard region and the enlarged section of the fluidized bed gasifier. The pressure drop decreased in the dense bed from bottom to top while it remained essentially constant in both the freeboard region and the enlarged section.

The maximum pressure drop in the dense bed (6.1 kPa) was observed at the bed height of 31.5 cm, fluidization velocity of 0.33 m/s and the equivalence ratio of 0.25 and the minimum pressure drop in the dense bed (1.5 kPa) was observed at the bed height of 19.5 cm, fluidization velocity of 0.22 m/s and the equivalence ratio of 0.35. The pressure drop across the secondary distributor plate ranged between 0.8 and 1.6 kPa.

9.2.3 Gas Composition

The various components of the gas produced at various bed heights, fluidization velocities and equivalence ratios are summarized in Tables 9.23 to 9.25. The first, second and third gas sampling probes were located at 0.75, 1.45 and 2.00 m above the main distributor plate, respectively. An attempt to measure gas concentration profiles at different locations in

Table 9.21 Pressure Drop Distribution in the Dense Bed.

Bed Height (cm)	Fluidization Velocity (m/s)	Equivalence Ratio (-)	Pressure Drop (kPa)			
			P_1	P_2	P_3	P_4
19.5	0.22	0.25	3.3	2.3	1.9	1.9
		0.30	3.0	2.0	1.7	1.7
		0.35	2.6	1.8	1.6	1.5
	0.28	0.25	3.8	3.4	2.3	2.1
		0.30	3.4	2.7	2.1	2.0
		0.35	3.0	2.4	1.8	1.8
	0.33	0.25	4.3	3.4	2.8	2.5
		0.30	4.0	3.2	2.5	2.3
		0.35	3.7	3.0	2.3	2.2
25.5	0.22	0.25	4.3	3.1	2.5	2.2
		0.30	3.8	2.7	2.0	1.8
		0.35	3.0	2.0	1.8	1.6
	0.28	0.25	5.0	3.6	2.7	2.4
		0.30	4.4	3.1	2.2	2.0
		0.35	3.8	2.6	1.9	1.9
	0.33	0.25	5.3	4.1	3.0	2.7
		0.30	4.8	3.6	2.8	2.3
		0.35	4.2	3.1	2.3	2.1
31.5	0.22	0.25	4.8	3.4	2.4	2.3
		0.30	4.5	3.0	2.1	1.9
		0.35	4.2	2.8	1.8	1.7
	0.28	0.25	5.5	4.0	3.0	2.5
		0.30	5.1	3.8	2.7	2.1
		0.35	4.9	3.5	2.5	2.0
	0.33	0.25	6.1	4.5	3.5	3.1
		0.30	5.7	4.2	3.3	2.7
		0.35	5.3	3.9	3.0	2.4

Table 9.22 Pressure Drop Distribution in the Freeboard, Enlarged Section and Across the Secondary Distributor Plate.

Bed Height (cm)	Fluidization Velocity (m/s)	Equivalence Ratio (-)	Pressure Drop (kPa)						
			Freeboard			Enlarged Section			Across Secondary Distributor Plate
			P_5	P_6	P_7	P_8	P_9	P_{10}	P_s
19.5	0.22	0.25	1.9	1.9	1.9	1.9	1.9	1.9	0.8
		0.30	1.7	1.7	1.7	1.7	1.7	1.7	0.8
		0.35	1.5	1.5	1.5	1.5	1.5	1.5	0.8
	0.28	0.25	2.1	2.1	2.1	2.1	2.1	2.1	1.0
		0.30	2.0	2.0	2.0	2.0	2.0	2.0	1.0
		0.35	1.8	1.8	1.8	1.8	1.8	1.8	1.0
	0.33	0.25	2.4	2.4	2.4	2.4	2.4	2.4	1.2
		0.30	2.3	2.3	2.3	2.3	2.3	2.3	1.2
		0.35	2.2	2.2	2.2	2.2	2.2	2.2	1.2
25.5	0.22	0.25	2.2	2.2	2.2	2.2	2.2	2.2	1.1
		0.30	1.8	1.8	1.8	1.8	1.8	1.8	1.1
		0.35	1.6	1.6	1.6	1.6	1.6	1.6	1.1
	0.28	0.25	2.4	2.4	2.4	2.4	2.4	2.4	1.3
		0.30	2.2	2.2	2.2	2.2	2.2	2.2	1.3
		0.35	1.9	1.9	1.9	1.9	1.9	1.9	1.3
	0.33	0.25	2.6	2.6	2.6	2.6	2.6	2.6	1.4
		0.30	2.3	2.3	2.3	2.3	2.3	2.3	1.4
		0.35	2.1	2.1	2.1	2.1	2.1	2.1	1.4
31.5	0.22	0.25	2.3	2.3	2.3	2.3	2.3	2.3	1.2
		0.30	1.9	1.9	1.9	1.9	1.9	1.9	1.2
		0.35	1.7	1.7	1.7	1.7	1.7	1.7	1.2
	0.28	0.25	2.5	2.5	2.5	2.5	2.5	2.5	1.4
		0.30	2.1	2.1	2.1	2.1	2.1	2.1	1.4
		0.35	2.0	2.0	2.0	2.0	2.0	2.0	1.4
	0.33	0.25	3.1	3.1	3.1	3.1	3.1	3.1	1.6
		0.30	2.7	2.7	2.7	2.7	2.7	2.7	1.6
		0.35	2.4	2.4	2.4	2.4	2.4	2.4	1.6

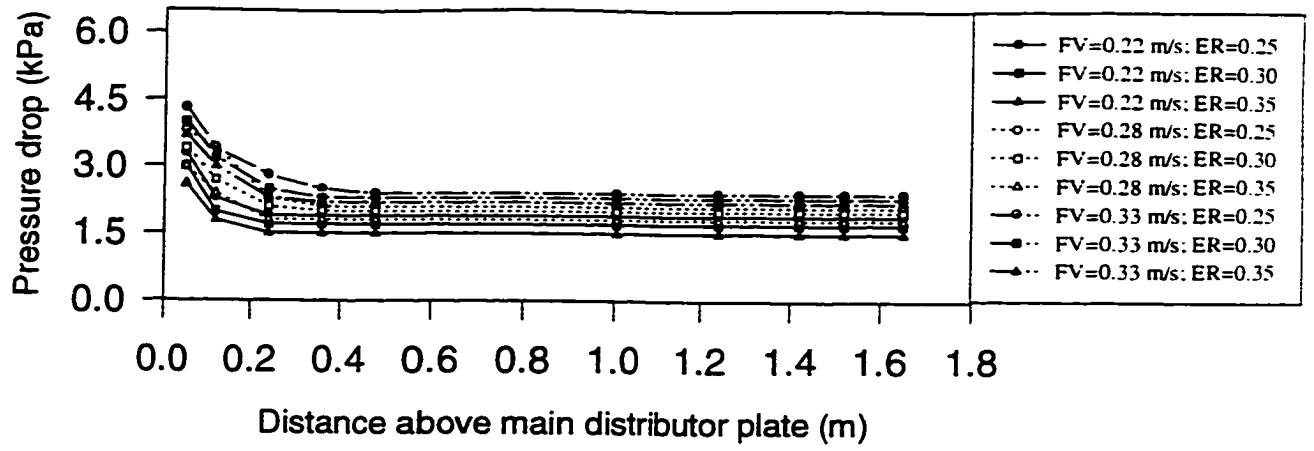

(a) Bed Height = 19.5 cm

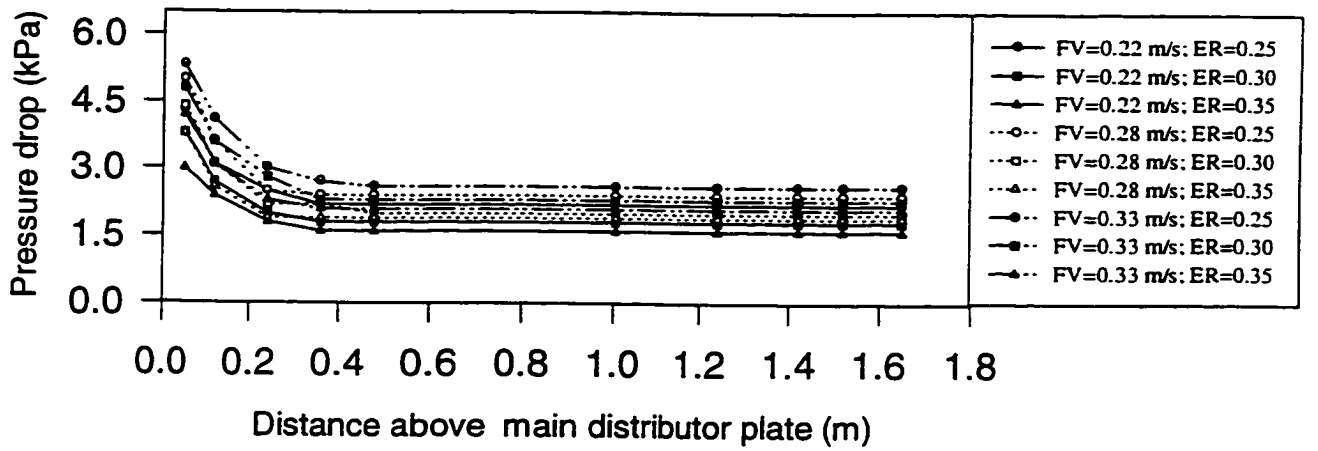

(b) Bed Height = 25.5 cm

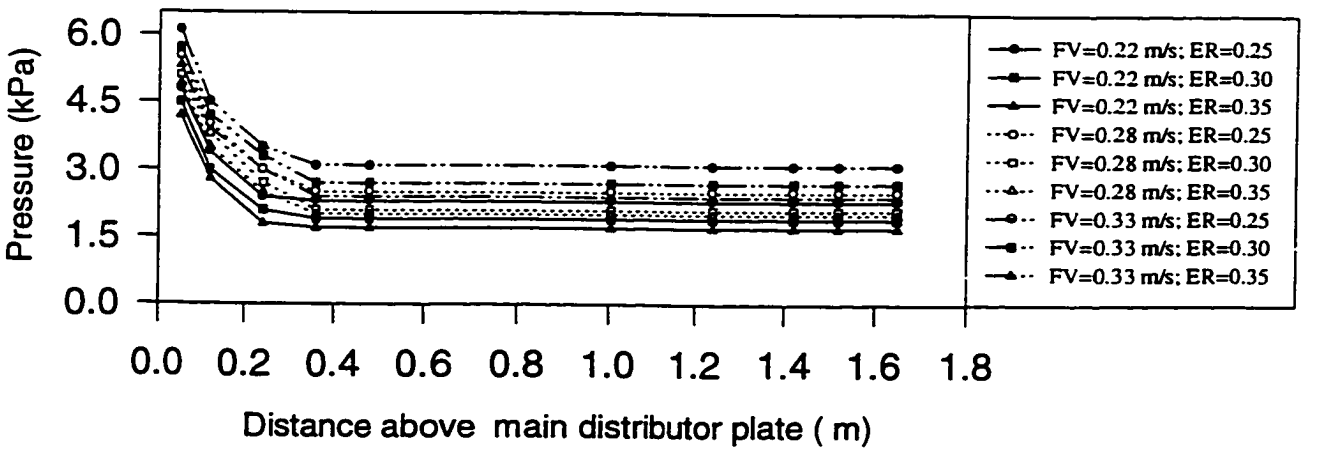

(c) Bed Height = 31.5 cm

Figure 9.33 Variation of pressure drop with fluidization velocity and equivalence ratio at various bed heights.

Table 9.23 Gas Composition Obtained at 0.75 m above the Main Distributor Plate.

Bed Height (cm)	Fluidization Velocity (m/s)	Equivalence Ratio (-)	Gas Composition (% Dry Basis)							
			CO_2	C_2H_m	C_2H_6	H_2	O_2	N_2	CH_4	CO
19.5	0.22	0.25	12.50	1.44	0.18	3.34	0.49	61.19	2.26	18.60
		0.30	13.96	1.12	0.03	3.04	0.50	64.28	2.05	15.02
		0.35	15.20	1.01	0.00	2.90	0.60	65.95	1.76	12.58
	0.28	0.25	12.88	1.34	0.10	2.99	0.18	62.36	2.11	18.04
		0.30	14.32	0.99	0.00	2.64	0.60	65.67	1.81	13.97
		0.35	15.62	0.76	0.00	2.24	0.63	66.77	1.63	12.35
	0.33	0.25	13.00	1.22	0.06	2.94	1.11	64.80	1.92	14.95
		0.30	14.64	0.81	0.00	2.56	0.96	66.61	1.84	12.58
		0.35	17.02	0.62	0.00	2.02	1.21	66.94	1.20	10.50
25.5	0.22	0.25	13.25	1.24	0.12	3.11	0.50	61.28	2.20	18.30
		0.30	14.38	1.01	0.06	2.96	0.35	65.24	1.90	14.50
		0.35	15.46	0.94	0.00	2.85	0.42	66.03	1.74	12.56
	0.28	0.25	13.55	1.21	0.08	2.87	0.40	62.46	2.08	17.35
		0.30	14.74	0.87	0.05	2.59	1.00	66.01	1.78	12.96
		0.35	15.76	0.74	0.01	2.18	0.70	66.86	1.62	12.13
	0.33	0.25	13.81	1.10	0.06	2.79	0.60	65.43	1.89	14.32
		0.30	14.91	0.79	0.01	2.37	0.70	66.83	1.65	12.74
		0.35	16.29	0.68	0.00	2.11	0.45	67.14	1.58	11.75
31.5	0.22	0.25	13.66	1.60	0.11	3.09	0.50	60.23	2.45	18.36
		0.30	14.76	0.99	0.11	2.89	0.45	65.05	1.77	13.98
		0.35	16.12	0.89	0.00	2.51	0.49	66.28	1.48	12.23
	0.28	0.25	13.97	1.12	0.08	2.86	0.39	62.84	2.00	16.74
		0.30	15.48	0.86	0.03	2.50	0.46	66.14	1.89	12.64
		0.35	16.40	0.65	0.00	2.13	0.38	66.99	1.42	12.03
	0.33	0.25	14.08	1.05	0.05	2.65	0.45	65.91	1.65	14.16
		0.30	15.94	0.74	0.01	2.29	0.54	66.93	1.50	12.05
		0.35	16.76	0.63	0.00	2.04	0.52	67.22	1.36	11.47

$C_2H_m = C_2H_2 + C_2H_4$

Table 9.24 Gas Composition Obtained at 1.45 m above the Main Distributor Plate.

Bed Height (cm)	Fluidization Velocity (m/s)	Equivalence Ratio (-)	Gas Composition (% Dry Basis)							
			CO_2	C_2H_m	C_2H_6	H_2	O_2	N_2	CH_4	CO
19.5	0.22	0.25	13.25	1.48	0.20	3.74	0.18	58.91	2.33	19.91
		0.30	14.70	1.15	0.04	3.64	0.40	61.47	2.30	16.30
		0.35	15.93	1.04	0.00	3.23	0.46	63.80	1.86	13.68
	0.28	0.25	13.50	1.45	0.14	3.58	0.16	59.47	2.26	19.44
		0.30	15.00	1.10	0.00	3.24	0.51	62.94	1.96	15.25
		0.35	16.15	0.97	0.00	3.11	0.43	63.99	1.83	13.52
	0.33	0.25	13.63	1.42	0.10	3.34	0.81	62.99	2.01	15.70
		0.30	15.10	0.99	0.00	3.31	0.15	64.39	1.91	14.15
		0.35	17.14	0.65	0.00	2.62	0.90	65.40	1.30	11.99
25.5	0.22	0.25	13.48	1.44	0.15	3.71	0.30	58.92	2.30	19.70
		0.30	15.00	1.09	0.11	3.54	0.30	61.88	2.20	15.88
		0.35	16.01	1.03	0.00	3.15	0.32	63.90	1.84	13.75
	0.28	0.25	13.75	1.40	0.11	3.47	0.20	59.52	2.26	19.29
		0.30	15.34	1.05	0.08	3.24	0.38	63.11	1.90	14.90
		0.35	16.51	0.95	0.05	3.10	0.20	64.12	1.72	13.35
	0.33	0.25	14.29	1.30	0.09	3.16	0.40	63.74	2.00	15.02
		0.30	15.40	0.96	0.01	3.04	0.70	64.58	1.86	13.45
		0.35	16.62	0.88	0.00	2.96	0.40	65.03	1.69	12.42
31.5	0.22	0.25	13.78	1.74	0.13	3.72	0.20	58.49	2.81	19.76
		0.30	15.65	1.07	0.11	3.50	0.26	63.13	2.10	14.18
		0.35	16.67	0.99	0.01	3.11	0.19	64.78	1.70	12.55
	0.28	0.25	14.07	1.32	0.11	3.40	0.18	60.74	2.20	17.98
		0.30	16.02	1.04	0.08	3.01	0.35	63.72	1.81	13.97
		0.35	16.80	0.94	0.00	2.93	0.08	65.37	1.68	12.20
	0.33	0.25	14.39	1.26	0.06	3.13	0.06	64.44	1.82	14.84
		0.30	16.34	0.92	0.02	3.02	0.14	65.10	1.72	12.74
		0.35	17.00	0.80	0.00	2.90	0.22	65.41	1.65	12.02

$C_2H_m = C_2H_2 + C_2H_4$

Table 9.25 Gas Composition Obtained at 2.00 m above the Main Distributor Plate.

Bed Height (cm)	Fluidization Velocity (m/s)	Equivalence Ratio (-)	Gas Composition (% Dry Basis)							
			CO_2	C_2H_m	C_2H_6	H_2	O_2	N_2	CH_4	CO
19.5	0.22	0.25	13.69	1.59	0.27	4.04	0.00	57.77	2.52	20.12
		0.30	15.18	1.24	0.14	3.96	0.07	60.31	2.46	16.64
		0.35	16.40	1.13	0.00	3.53	0.00	62.91	2.01	14.02
	0.28	0.25	13.95	1.57	0.23	3.98	0.13	58.02	2.46	19.66
		0.30	15.31	1.20	0.00	3.58	0.00	62.38	2.06	15.47
		0.35	16.60	1.07	0.00	3.51	0.00	62.94	2.02	13.85
	0.33	0.25	14.09	1.49	0.18	3.64	0.00	62.56	2.12	15.92
		0.30	15.52	1.09	0.00	3.60	0.00	63.37	2.07	14.35
		0.35	17.60	0.99	0.00	2.94	0.01	64.85	1.41	12.20
25.5	0.22	0.25	13.85	1.58	0.26	4.00	0.09	57.86	2.50	19.86
		0.30	15.64	1.18	0.11	3.84	0.04	60.74	2.43	16.02
		0.35	16.48	1.13	0.00	3.45	0.00	62.95	2.04	13.95
	0.28	0.25	14.18	1.54	0.23	3.86	0.04	58.20	2.45	19.50
		0.30	15.73	1.15	0.09	3.46	0.02	62.42	2.05	15.08
		0.35	16.94	1.04	0.06	3.31	0.00	63.17	1.90	13.58
	0.33	0.25	14.78	1.37	0.16	3.51	0.05	62.85	2.10	15.18
		0.30	15.92	1.06	0.03	3.43	0.00	63.92	2.02	13.62
		0.35	17.11	0.98	0.00	3.30	0.00	64.14	1.89	12.58
31.5	0.22	0.25	14.45	1.92	0.22	4.00	0.04	56.57	2.90	19.90
		0.30	16.23	1.17	0.12	3.78	0.08	61.30	2.37	14.95
		0.35	17.14	1.09	0.04	3.39	0.02	63.59	1.98	12.75
	0.28	0.25	14.50	1.41	0.21	3.77	0.00	59.46	2.36	18.29
		0.30	16.46	1.13	0.08	3.40	0.08	62.42	2.00	14.43
		0.35	17.23	1.05	0.00	3.26	0.00	64.11	1.85	12.50
	0.33	0.25	14.82	1.35	0.16	3.41	0.00	63.13	2.00	15.13
		0.30	16.62	1.01	0.08	3.32	0.08	63.98	1.91	13.00
		0.35	17.42	0.98	0.00	3.25	0.01	64.21	1.84	12.29

$C_2H_m = C_2H_2 + C_2H_4$

the dense bed proper was made as well, but turned out to be unsuccessful. The results revealed that oxygen and nitrogen concentrations decreased and the concentrations of CO_2, CO, H_2 CH_4, $C_2H_2 + C_2H_4$ and C_2H_6 increased with distance from the main distributor plate. The gas components obtained from the three sampling locations revealed that nitrogen was in the highest concentration (57.0-69.0 vol %). The concentration of CO_2 varied in the range 12.0-17.6 vol %. From the fuel gases which are of major interest, CO had the highest concentration (8.5-20.1 vol %), followed by H_2 (2.0-4.0 vol %), and then CH_4 (1.0-3.0 vol %). The other components ($C_2H_2 + C_2H_4$ and C_2H_6) were produced with lower concentrations.

Figures 9.34 to 9.41 show the profiles of the gas components. Generally, as the equivalence ratio was increased, the concentrations of CO_2 and N_2 increased while the concentration of the fuel gases (CO, H_2 CH_4, $C_2H_2 + C_2H_4$ and C_2H_6) decreased. For instance, the maximum amount of CO_2 (17.6 vol %) was obtained at the highest equivalence ratio (0.35) and the maximum amount of CO (20.1 vol %) was obtained at the lowest equivalence ratio (0.25). However, very close concentrations of the gas components were observed at the equivalence ratios of 0.25 and 0.30 for most runs. Increasing the fluidization velocity slightly increased the concentrations of CO_2 and N_2 and decreased the concentrations of CO, H_2, CH_4, $C_2H_2 + C_2H_4$ and C_2H_6. The gas composition was relatively insensitive to the bed height. No distinct trend between the concentration of O_2 in the product gas and all the parameters investigated was apparent. Its concentration varied from 0.0 to 1.2 vol %.

9.2.4 Gas Higher Heating Value

The higher heating value of the product gas was calculated based on the measured gas composition and the heating value of individual gas components as follows (Raissi and Trezek, 1987):

$$HHV_g = 0.3985X_{CH_4} + 0.1264X_{CO} + 0.1277X_{H_2} \qquad (9.3)$$

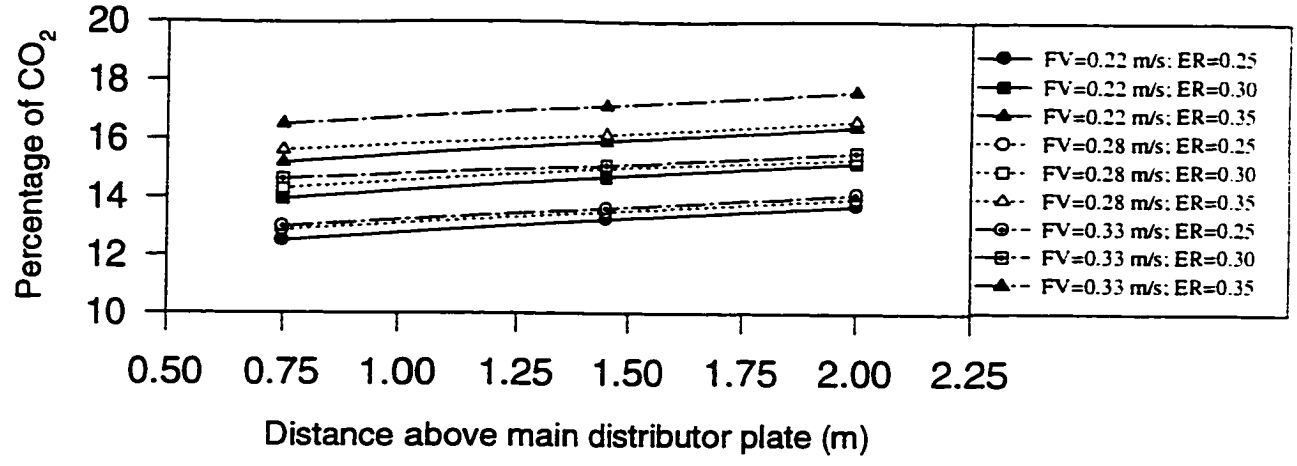

(a) Bed Height = 19.5 cm

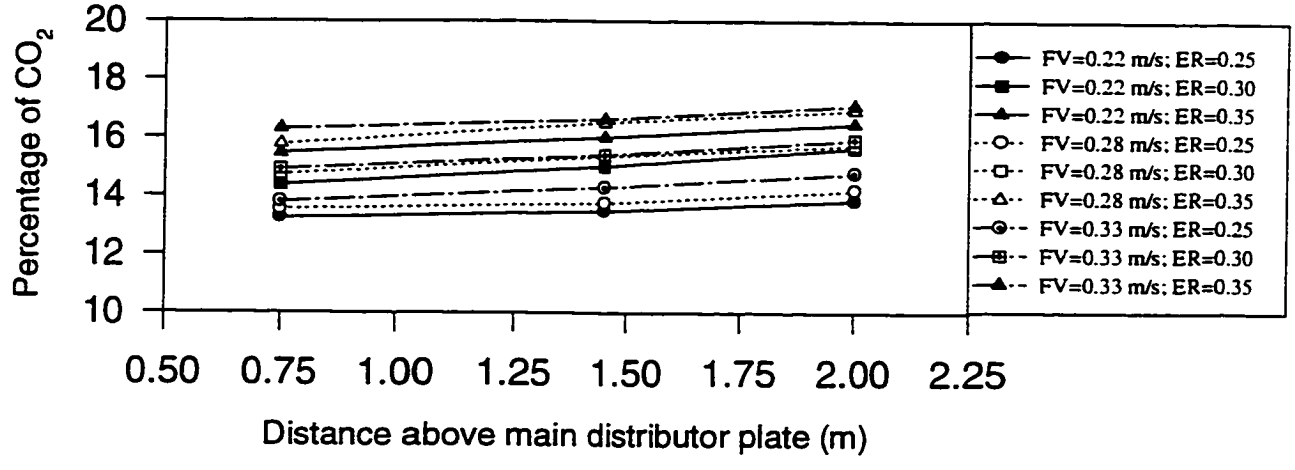

(b) Bed Height = 25.5 cm

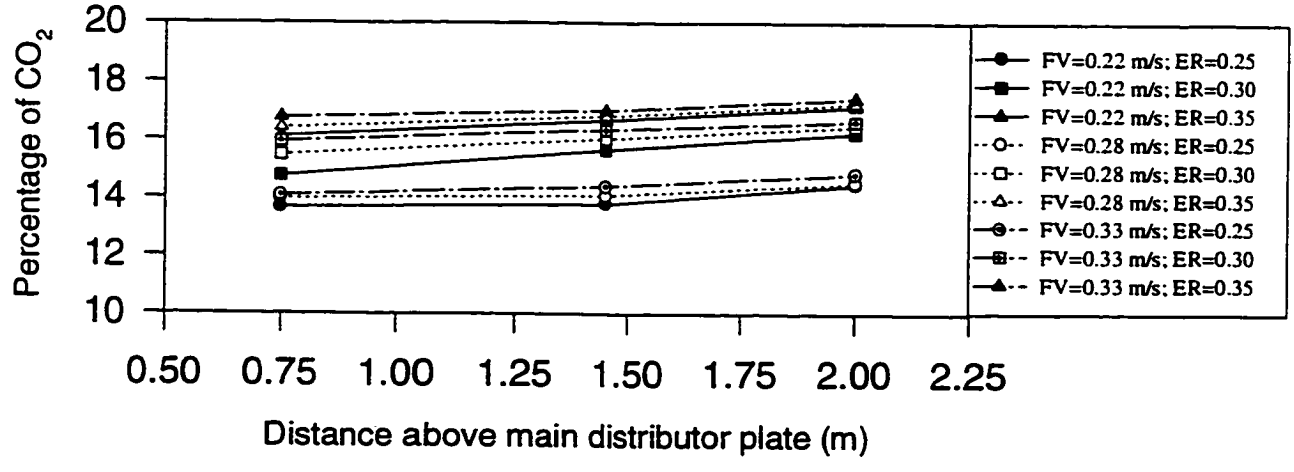

(c) Bed Height = 31.5 cm

Figure 9.34 Carbon dioxide (CO_2) content in the raw gas at various equivalence ratios, fluidization velocities and bed heights.

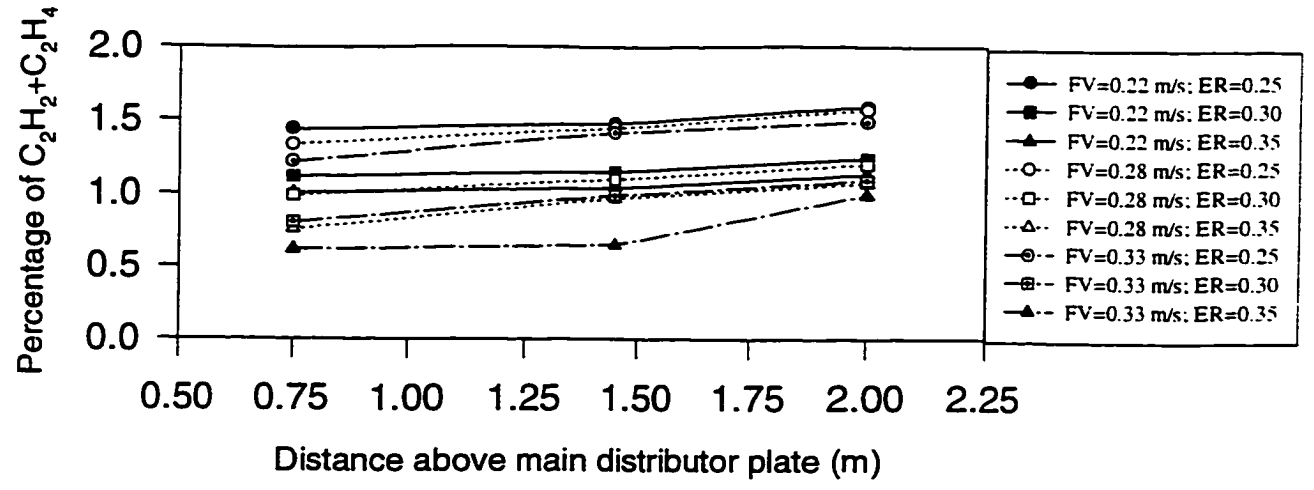

(a) Bed Height = 19.5 cm

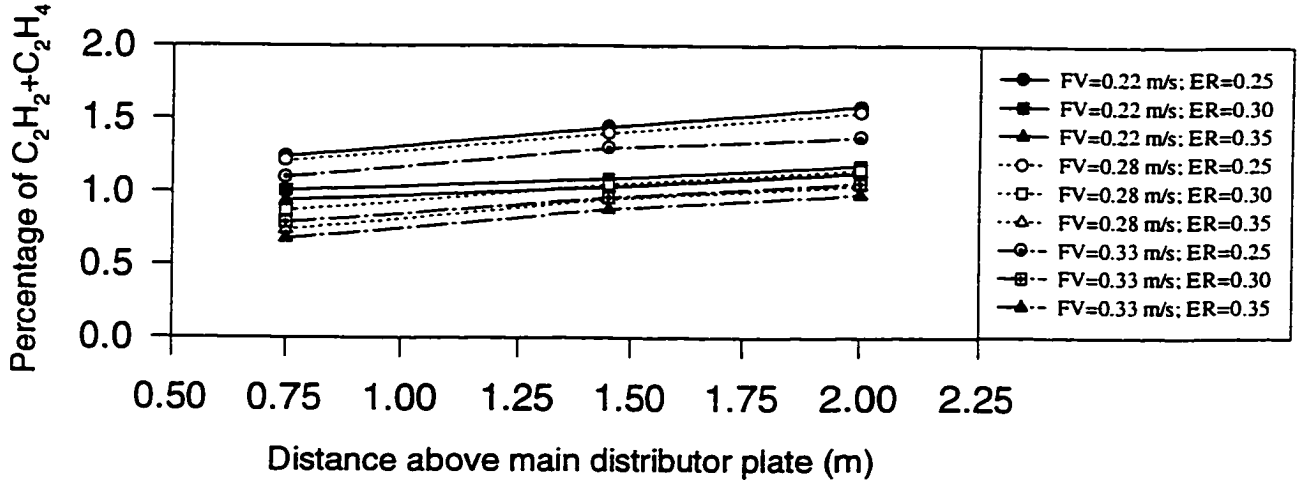

(b) Bed Height = 25.5 cm

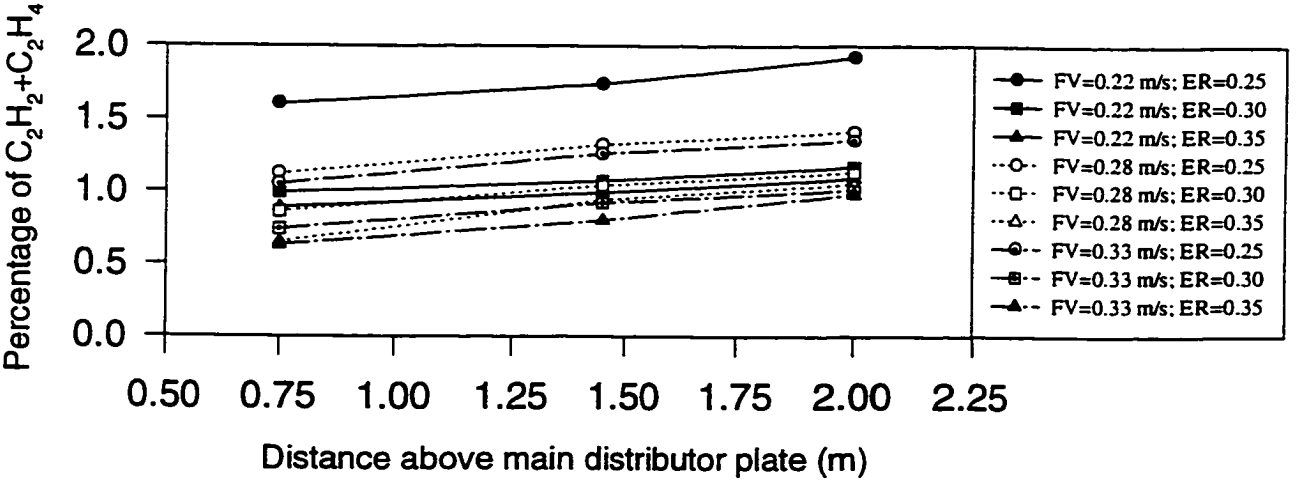

(c) Bed Height = 31.5 cm

Figure 9.35 Ethylene (C_2H_2) plus acetylene (C_2H_4) content in the raw gas at various equivalence ratios, fluidization velocities and bed heights.

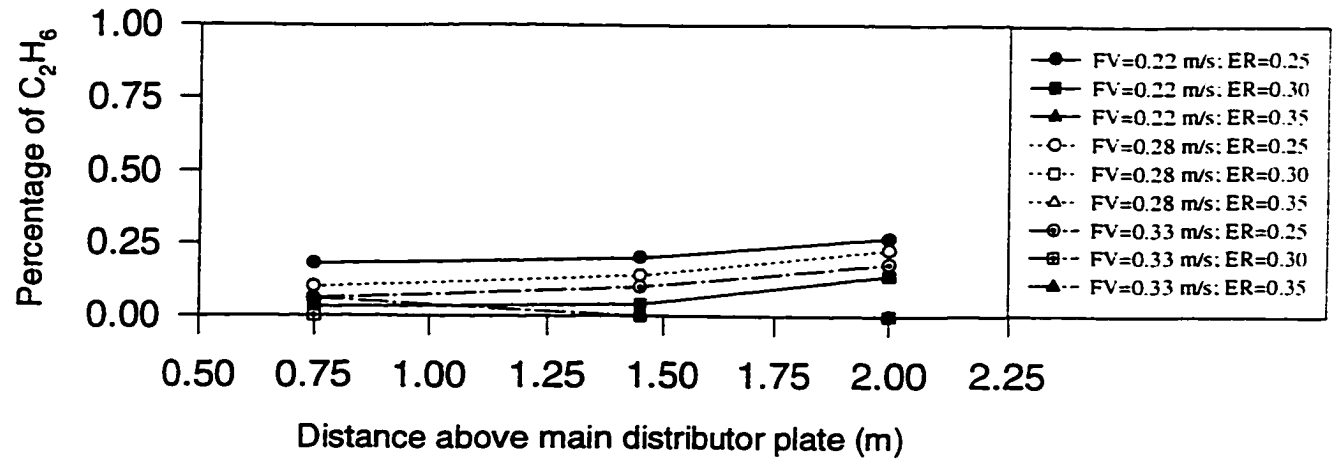

(a) Bed Height = 19.5 cm

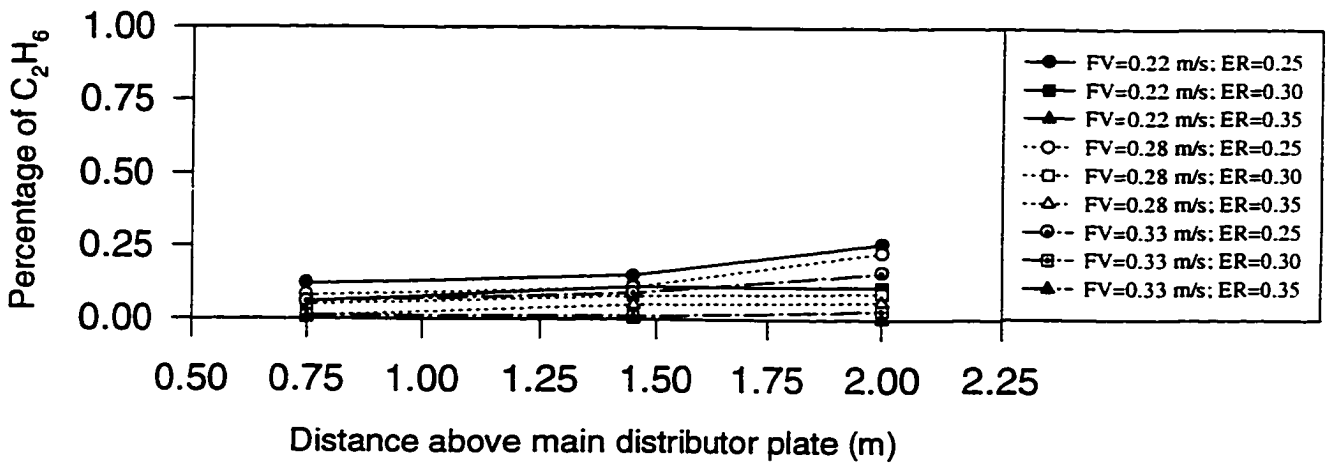

(b) Bed Height = 25.5 cm

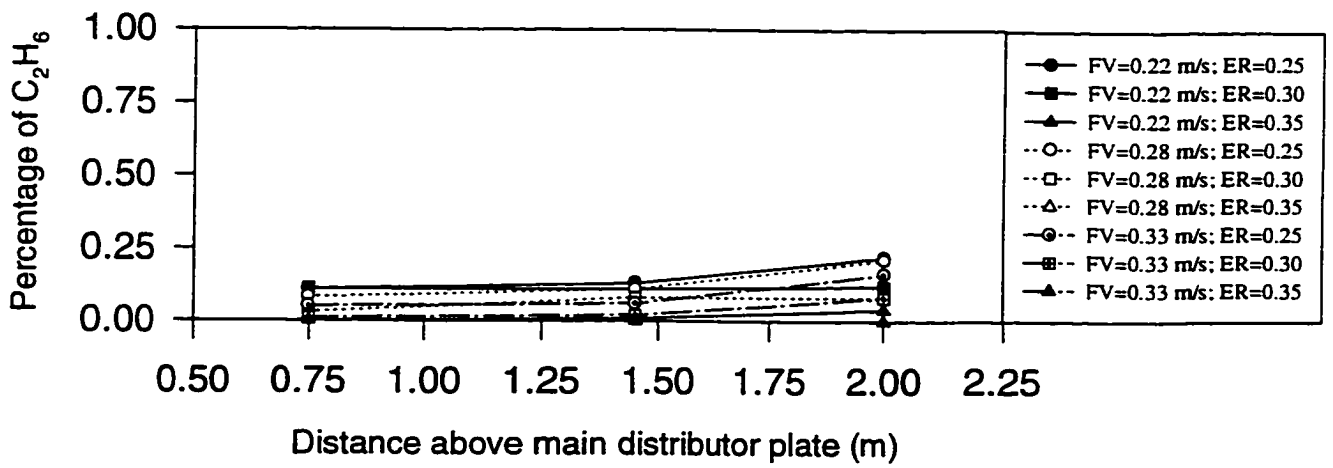

(c) Bed Height = 31.5 cm

Figure 9.36 Ethane (C_2H_6) content in the raw gas at various equivalence ratios, fluidization velocities and bed heights.

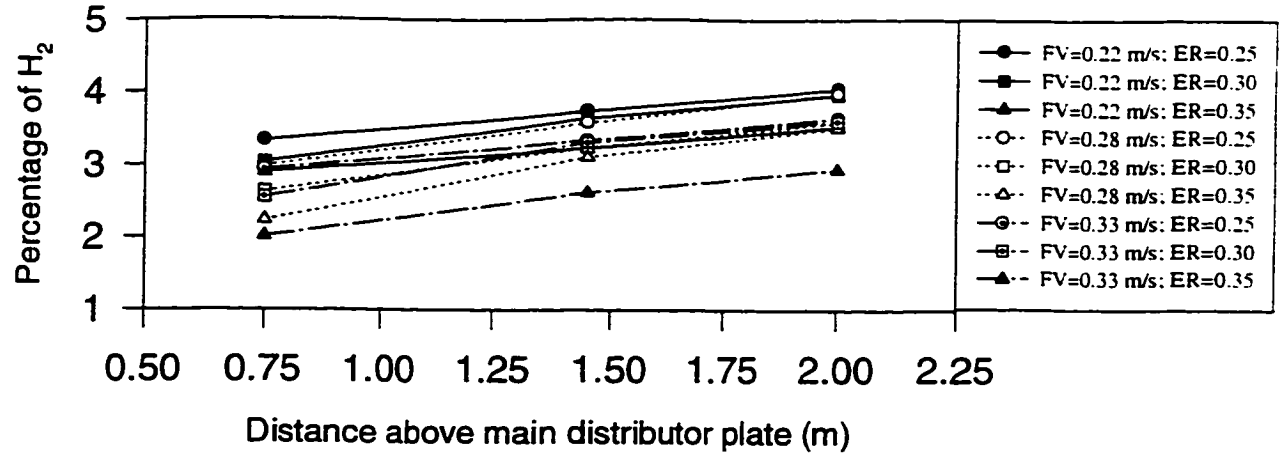

(a) Bed Height = 19.5 cm

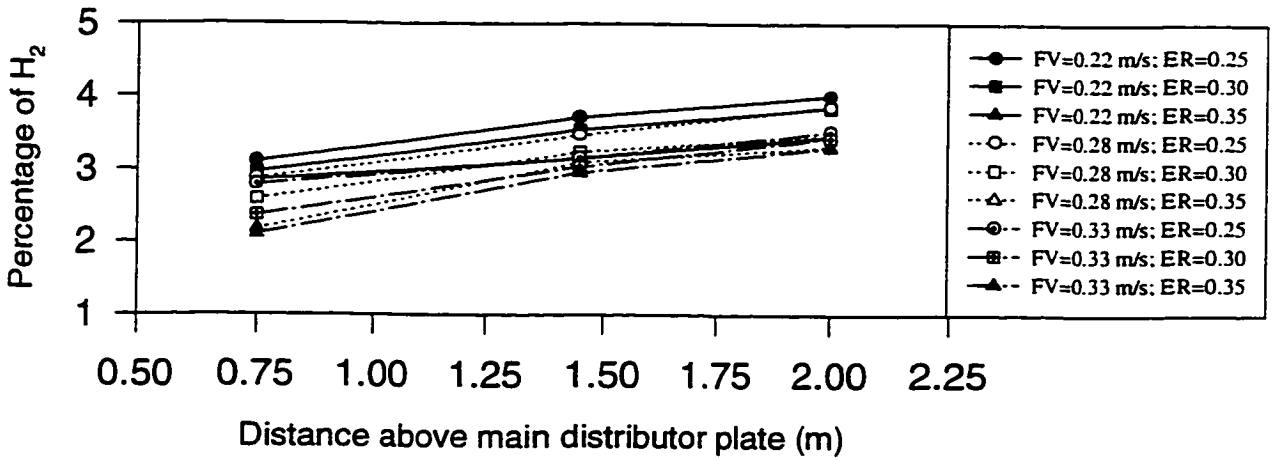

(b) Bed Height = 25.5 cm

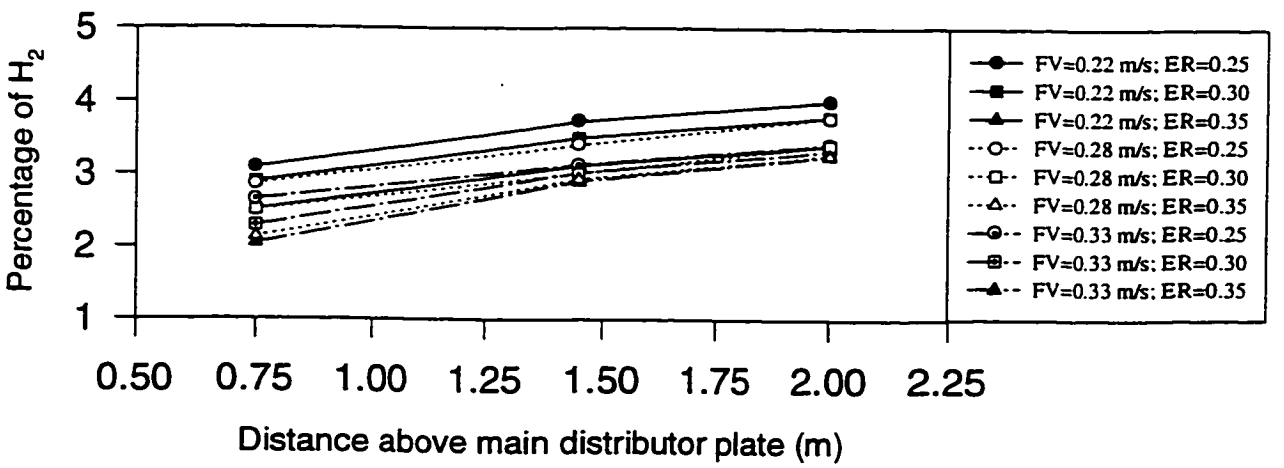

(c) Bed Height = 31.5 cm

Figure 9.37 Hydrogen (H_2) content in the raw gas at various equivalence ratios, fluidization velocities and bed heights.

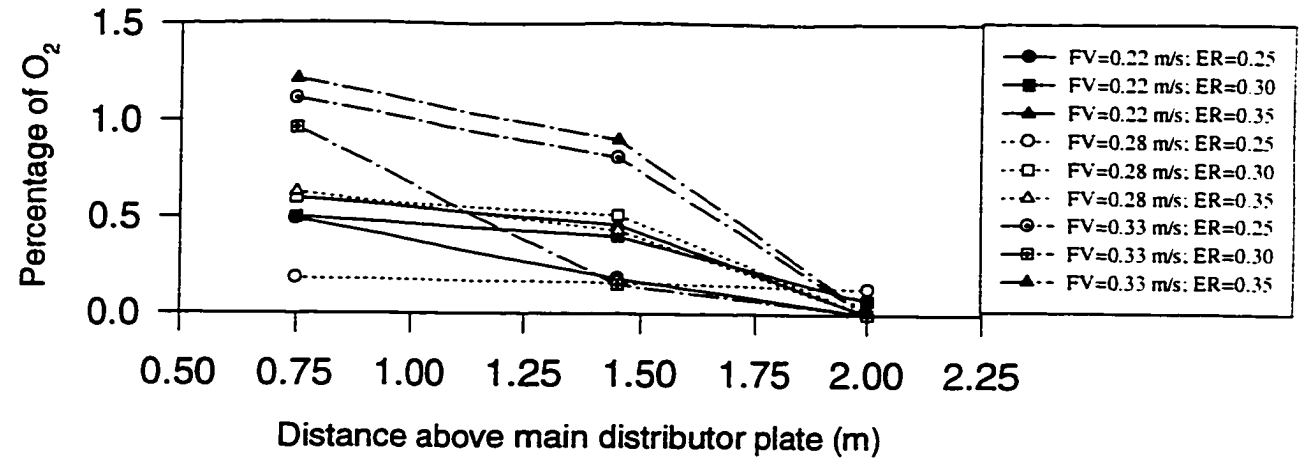

(a) Bed Height = 19.5 cm

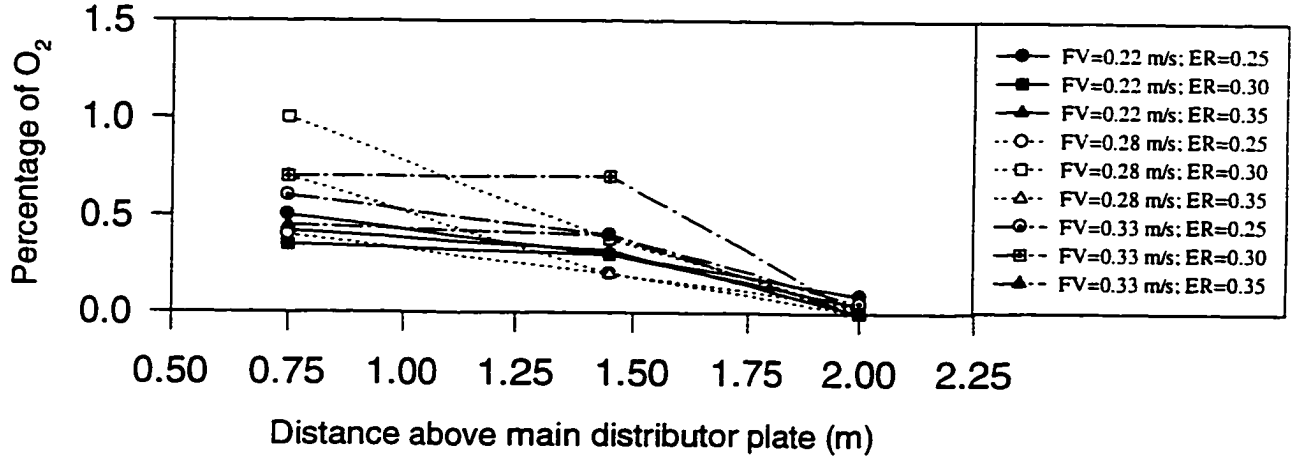

(b) Bed Height = 25.5 cm

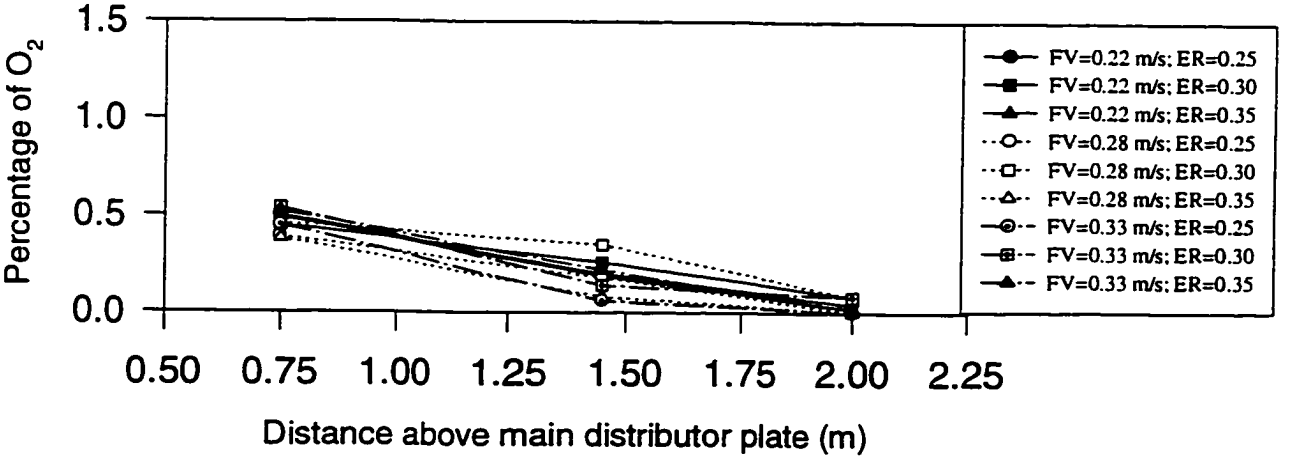

(c) Bed Height = 31.5 cm

Figure 9.38 Oxygen (O_2) content in the raw gas at various equivalence ratios, fluidization velocities and bed heights.

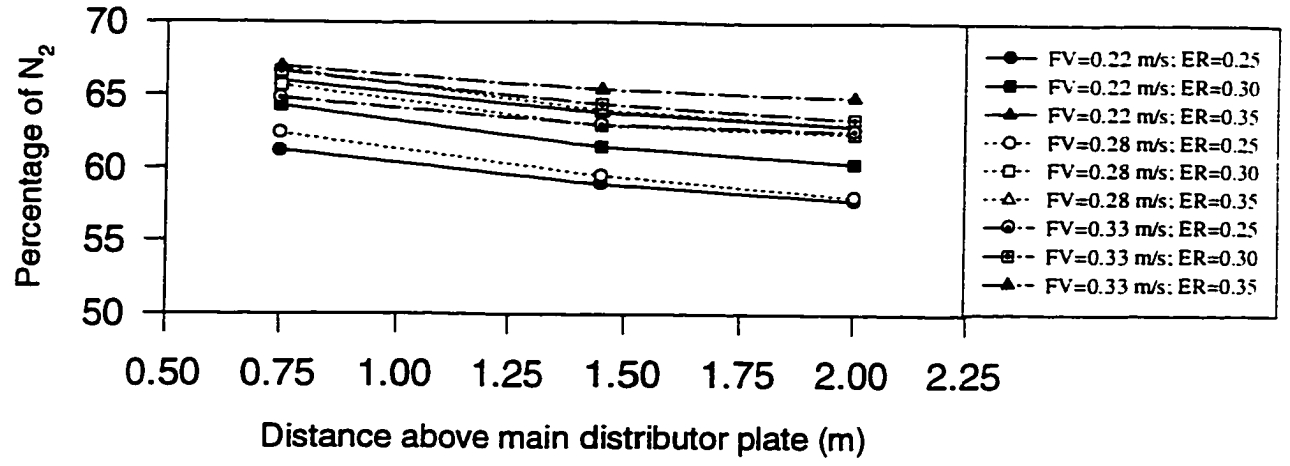

(a) Bed Height = 19.5 cm

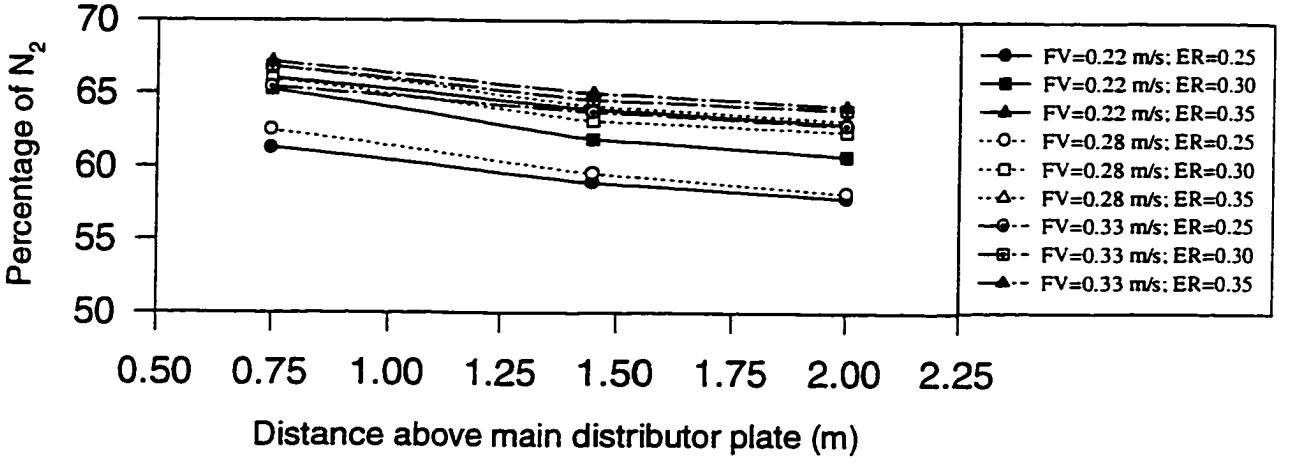

(b) Bed Height = 25.5 cm

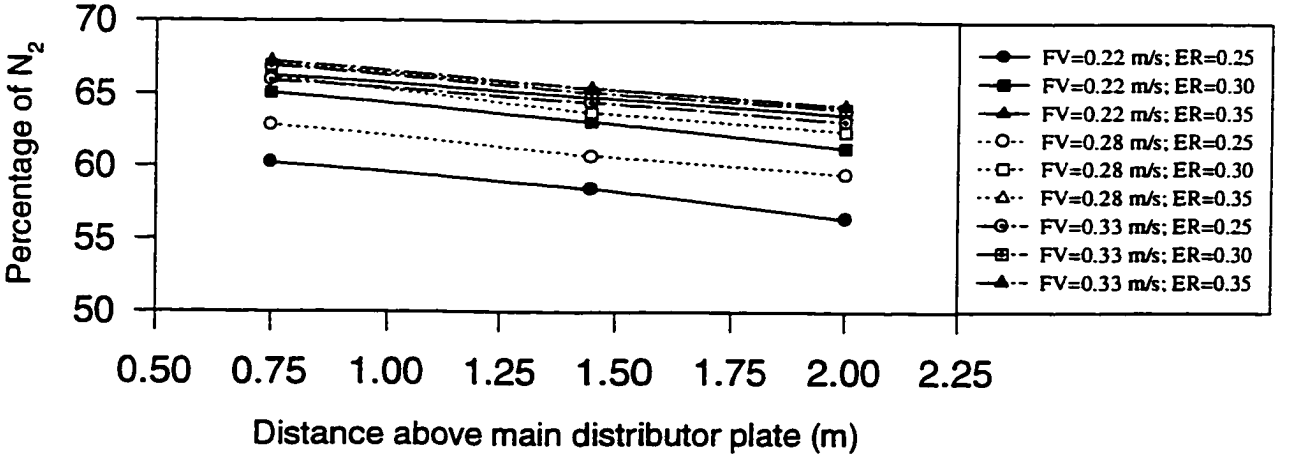

(c) Bed Height = 31.5 cm

Figure 9.39 Nitrogen (N_2) content in the raw gas at various equivalence ratios, fluidization velocities and bed heights.

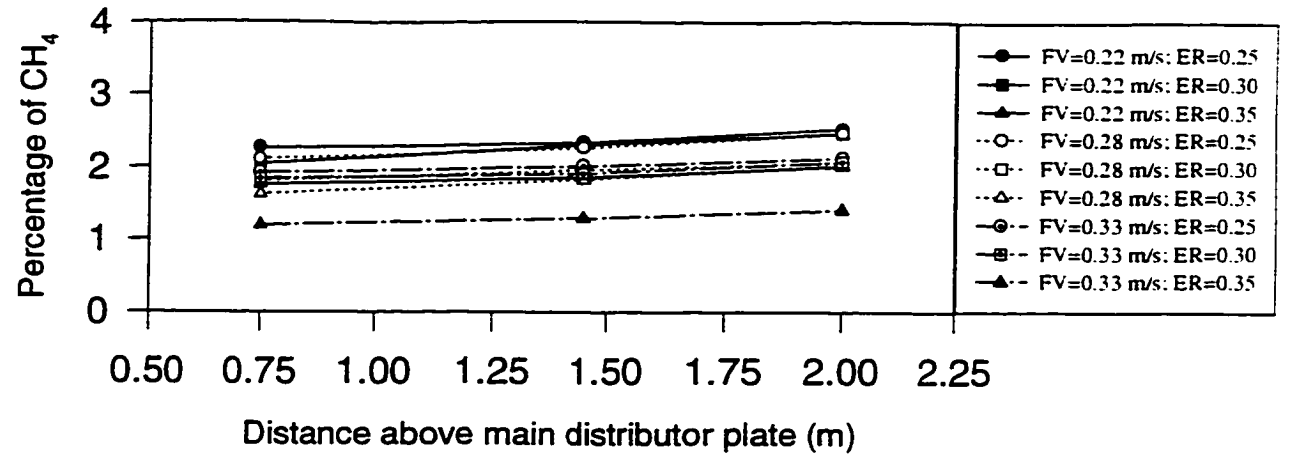

(a) Bed Height = 19.5 cm

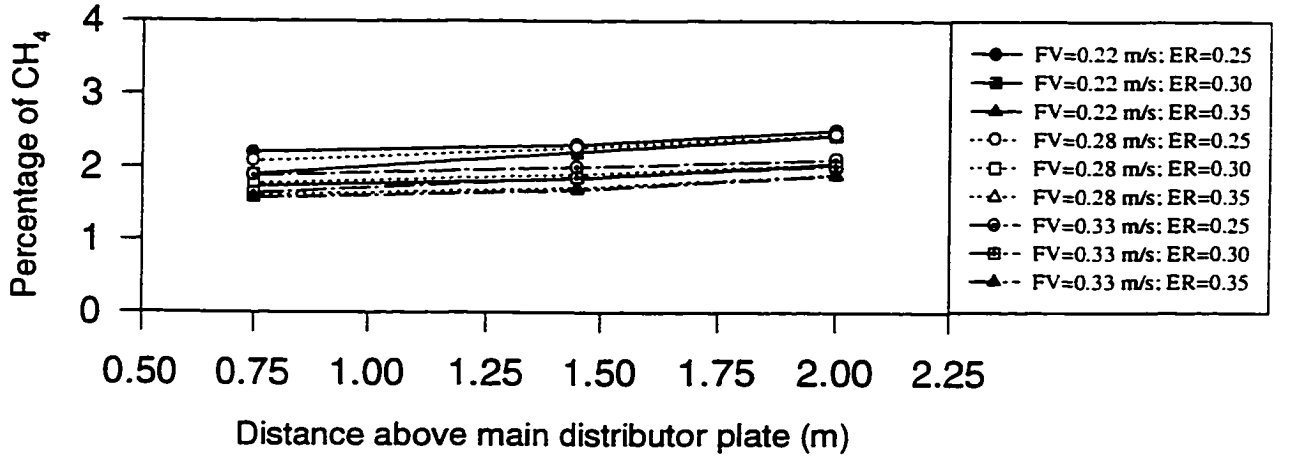

(b) Bed Height = 25.5 cm

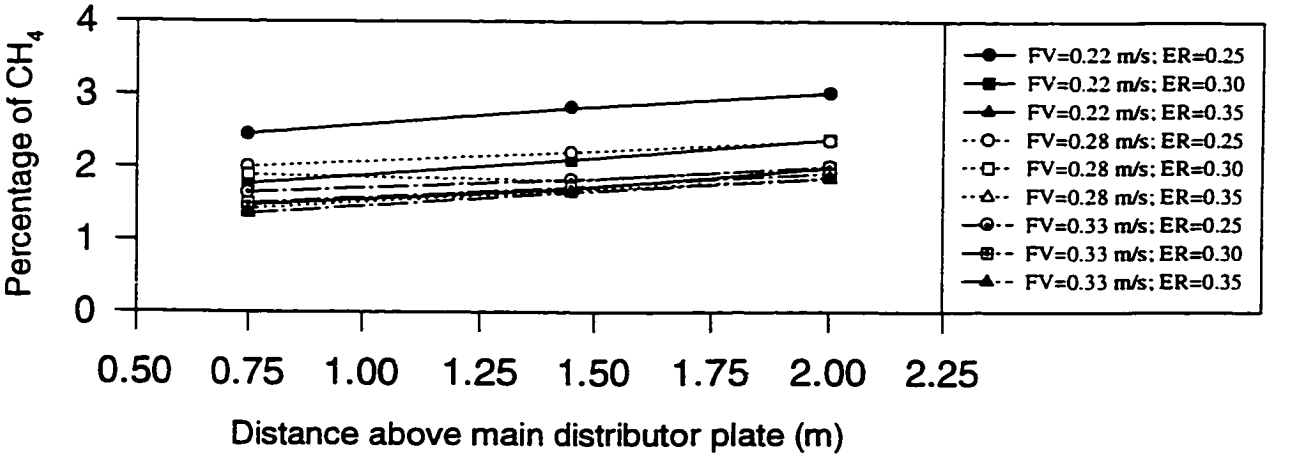

(c) Bed Height = 31.5 cm

Figure 9.40 Methane (CH_4) content in the raw gas at various equivalence ratios, fluidization velocities and bed heights.

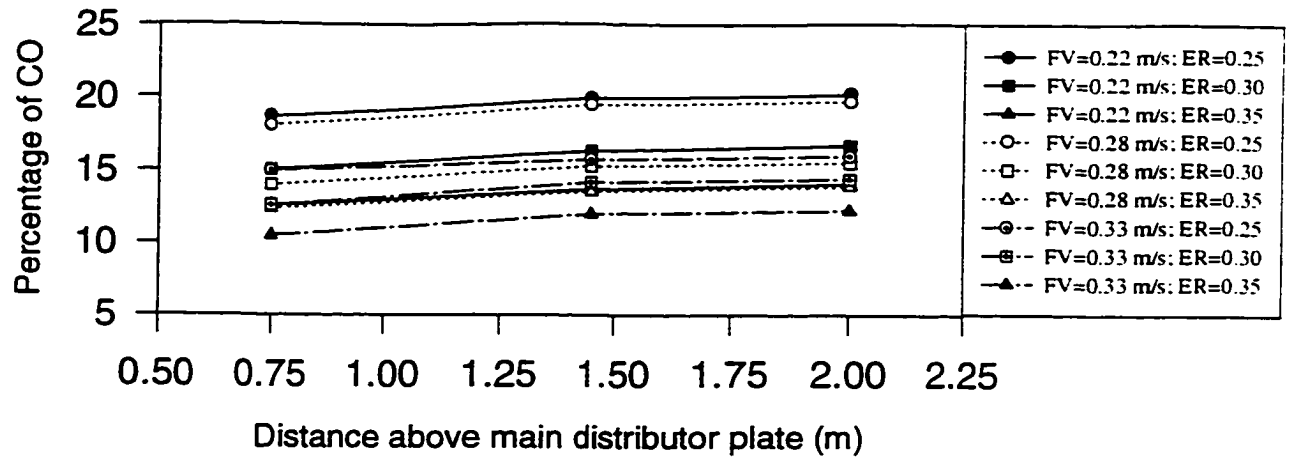

(a) Bed Height = 19.5 cm

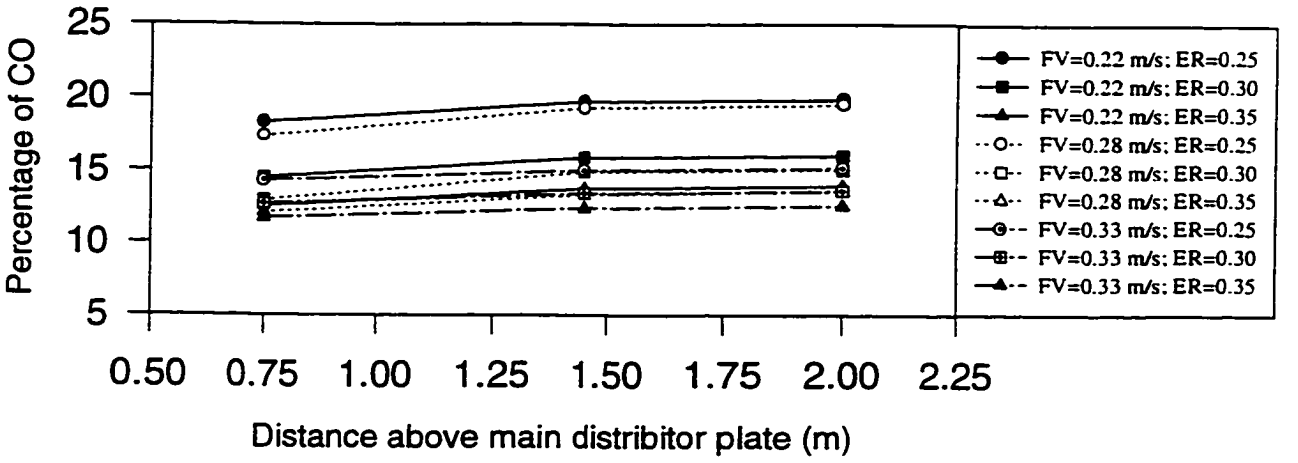

(b) Bed Height = 25.5 cm

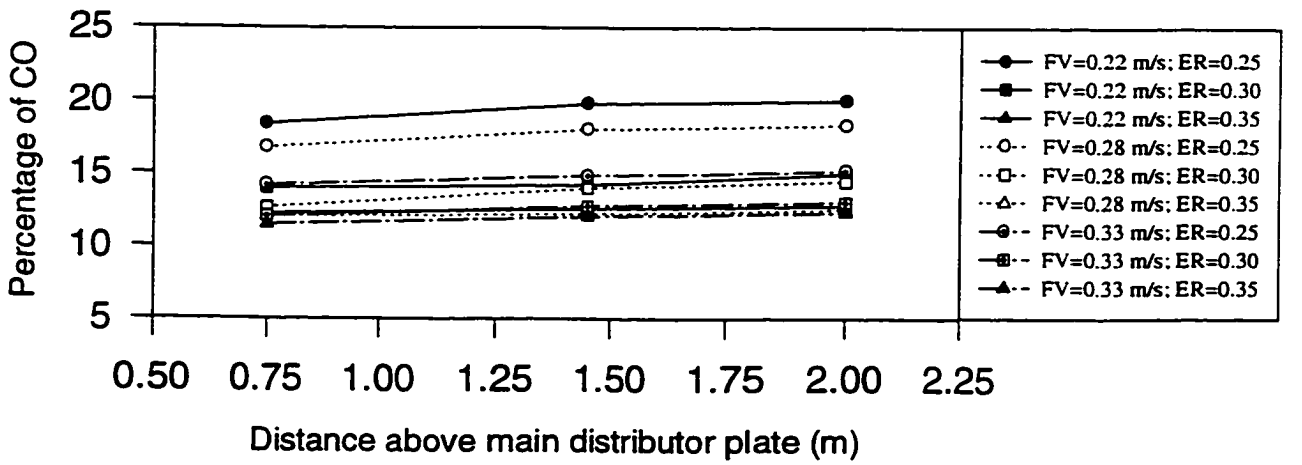

(c) Bed Height = 31.5 cm

Figure 9.41 Carbon monoxide (CO) content in the raw gas at various equivalence ratios, fluidization velocities and bed heights.

where:

HHV_g is the higher heating value of the dry product gas (MJ/Nm^3)

X_i is the volume percentage of gas species i in the dry gas

The measured hydrocarbons (C_2H_2, C_2H_4, C_2H_6 and CH_4) were considered as CH_4. Although this consideration is expected to underestimate the HHV of the product gas because the heating values of C_2H_2, C_2H_4 and C_2H_6 are higher than that of CH_4, the difference will be small due to the low concentrations of C_2H_2, C_2H_4 and C_2H_6. The effect of equivalence ratio, fluidization velocity and bed height on the gas higher heating value is presented in Table 9.26 and Figure 9.42.

The higher heating value of the product gas obtained from the first, second and third gas samplers ranged between 2.1-4.4, 2.4-4.8 and 2.8-5.0 MJ/Nm^3, respectively. It is clearly seen that the gas obtained from the third gas sampler located at the gasifier exit (2.00 m from the main distributor plate) had a better quality than the gases sampled at the other two positions. Therefore, all subsequent analyses and discussions were based on the gas sampled at the exit of the gasifier.

The higher heating value of the gas was mostly affected by the equivalence ratio and fluidization velocity. At the bed height of 31.5 cm and fluidization velocity of 0.22 m/s, increasing the equivalence ratio from 0.25 to 0.35 decreased the higher heating value of the gas by 40.0 % (from 5.03 to 3.03 MJ/Nm^3). Increasing the fluidization velocity from 0.22 to 0.33 m/s, while maintaining the bed height at 31.5 cm and the equivalence ratio at 0.25, decreased the higher heating value of the gas by 25.4 % (from 5.03 to 3.75 MJ/Nm^3). The maximum higher heating value of the gas (5.03 MJ/Nm^3) was obtained at the bed height of 31.5 cm, fluidization velocity of 0.22 m/s and the equivalence ratio of 0.25, while the minimum higher heating value of the gas (2.87 MJ/Nm^3) was obtained at the bed height of 19.5 cm, fluidization velocity of 0.33 m/s and the equivalence ratio of 0.35.

Table 9.26 Produced Gas Higher Heating Value.

Bed Height (cm)	Fluidization Velocity (m/s)	Equivalence Ratio (-)	Higher Heating Value (MJ/Nm^3)		
			G_4	G_5	G_6
19.5	0.22	0.25	4.32	4.59	4.80
		0.30	3.69	3.92	4.13
		0.35	3.06	3.30	3.47
	0.28	0.25	4.08	4.45	4.65
		0.30	3.22	3.56	3.71
		0.35	2.80	3.22	3.43
	0.33	0.25	3.54	3.82	3.96
		0.30	2.97	3.37	3.53
		0.35	2.39	2.63	2.87
25.5	0.22	0.25	4.13	4.51	4.75
		0.30	3.39	3.81	4.00
		0.35	3.02	3.28	3.47
	0.28	0.25	3.90	4.38	4.64
		0.30	3.04	3.50	3.66
		0.35	2.76	3.17	3.34
	0.33	0.25	3.38	3.65	3.80
		0.30	2.89	3.22	3.40
		0.35	2.66	2.97	3.16
31.5	0.22	0.25	4.40	4.84	5.03
		0.30	3.28	3.55	3.83
		0.35	2.81	3.06	3.28
	0.28	0.25	3.76	4.15	4.38
		0.30	3.02	3.32	3.54
		0.35	2.62	2.96	3.15
	0.33	0.25	3.22	3.53	3.75
		0.30	2.71	3.06	3.26
		0.35	2.50	2.87	3.09

G_4 Gas sampling probe at 0.75 m above the main distributor plate
G_5 Gas sampling probe at 1.45 m above the main distributor plate
G_6 Gas sampling probe at 2.00 m above the main distributor plate

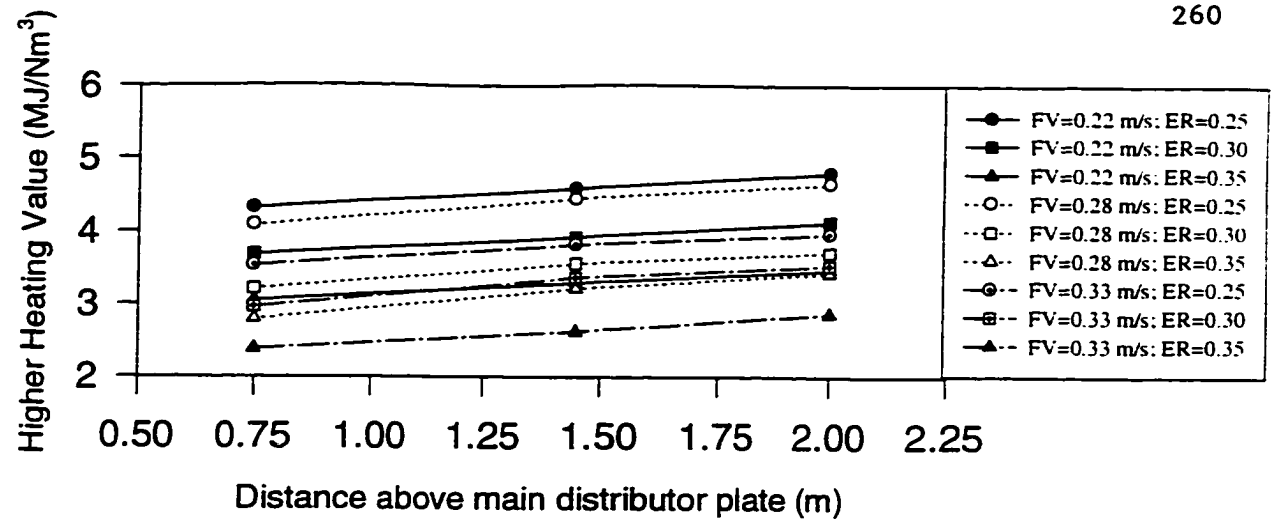

(a) Bed Height = 19.5 cm

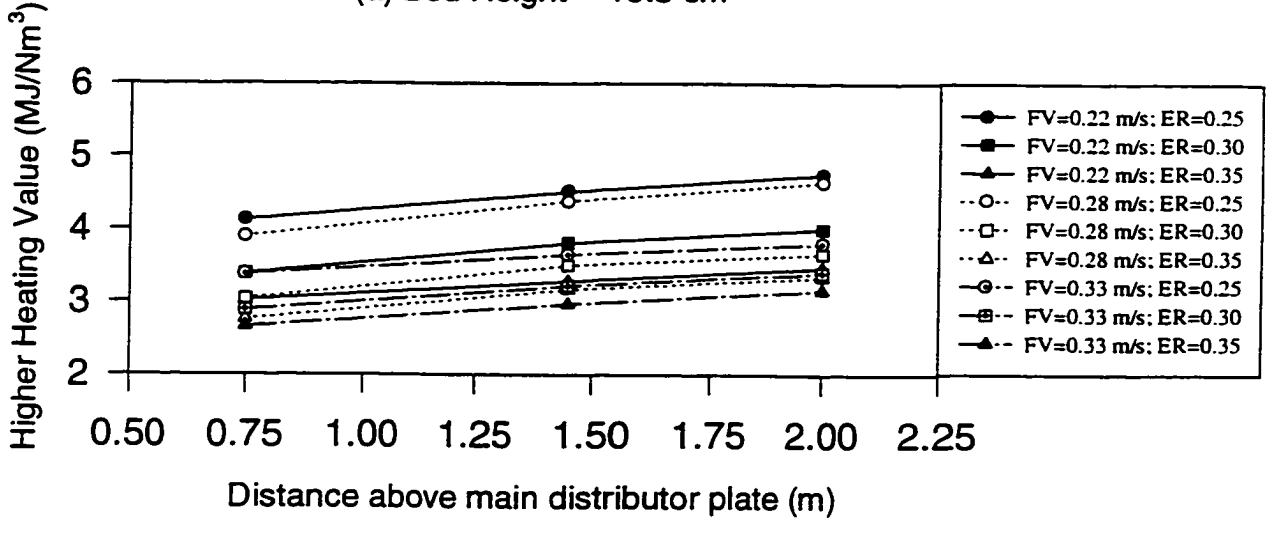

(b) Bed Height = 25.5 cm

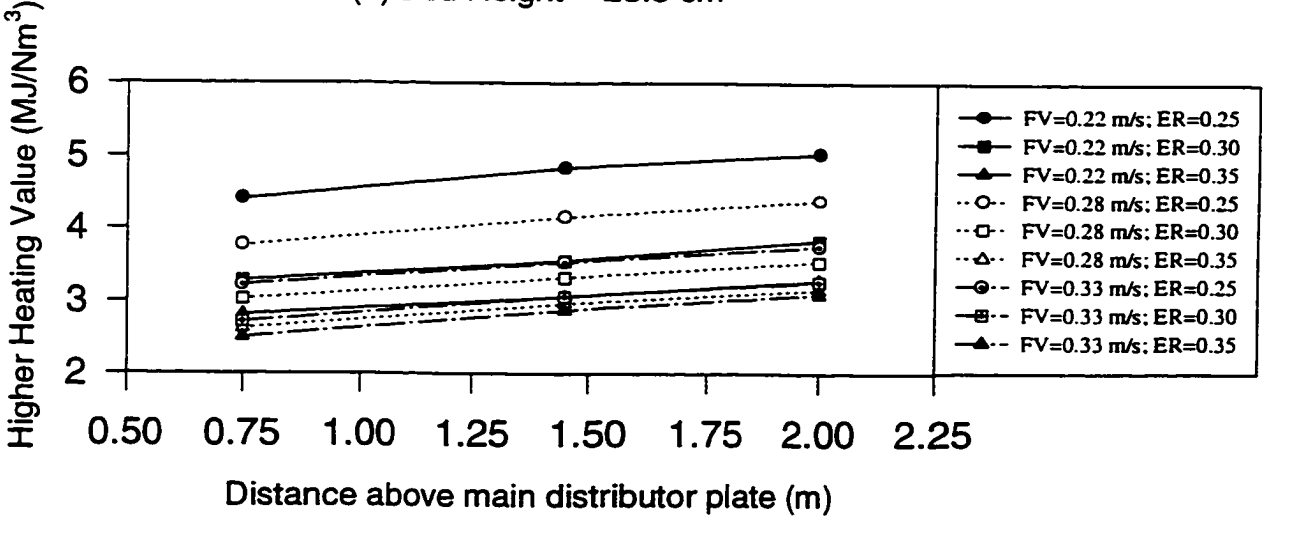

(c) Bed Height = 31.5 cm

Figure 9.42 Gas higher heating value at various distances from the main distributor plate, equivalence ratios, fluidization velocities and bed heights.

9.2.5 Gas Yield.

For better data interpretation and comparison, the gas production rates (measured at the exit of the gasifier using an orifice plate) were normalized at the standard temperature (25°C) and pressure (101.3 kPa). The gas production rate, normalized gas production rate and gas yield (amount of gas produced per unit weight of fuel) are summarized in Table 9.27. The gas yield at various equivalence ratios, fluidization velocities and bed heights is presented in Figure 9.43.

Increases in the equivalence ratio generally led to increased gas yield. For instance, at the bed height of 19.5 cm and fluidization velocity of 0.22 m/s, increasing the equivalence ratio from 0.25 to 0.35 resulted in the gas yield increasing from 1.49 to 2.02 Nm^3/kg. Similar trends were observed with other bed heights and fluidization velocities. The gas yield was slightly affected by changes in the fluidization velocity. Increasing the fluidization velocity from 0.22 to 0.33 m/s, the gas yield remained approximately constant up to the fluidization velocity of 0.28 m/s and then decreased slightly with further increase in fluidization velocity. The gas yield, however, did not change appreciably with changes in the bed height.

9.2.6 Tar Yield

No experimental data on tar could be collected because the amount of tar emitted from the fluidized bed gasifier (from visual observation) was relatively low.

9.2.7 Char

The composition of the char-sand mixture collected from the cyclone collector is given in Table 9.28. The char elemental (carbon and ash) and proximate analyses are presented in Tables 9.29 and 9.30, respectively. Results of the particle size distribution of the char collected from the cyclone collector and dense bed under two extreme experimental conditions are presented in Tables 9.31 and 9.32, respectively. They are only presented for two specific experiments since the distributions did not vary considerably with bed height, fluidization

Table 9.27 Gas Production Rate, Normalized Gas Production Rate and Gas Yield.

Bed Height (cm)	Fluidization Velocity (m/s)	Equivalence Ratio (-)	ΔP (kPa)	Gas Production Rate (m^3/min)	Normalized Gas Production Rate (Nm^3/min)	Gas Yield (Nm^3/kg)
19.5	0.22	0.25	0.45	2.71	1.00	1.49
		0.30	0.50	2.98	0.98	1.75
		0.35	0.55	3.15	0.97	2.02
	0.28	0.25	0.79	3.80	1.27	1.48
		0.30	0.89	4.17	1.25	1.74
		0.35	0.92	4.29	1.22	2.00
	0.33	0.25	0.99	4.31	1.39	1.36
		0.30	1.07	4.42	1.30	1.52
		0.35	1.20	4.66	1.29	1.77
25.5	0.22	0.25	0.45	2.68	1.00	1.49
		0.30	0.50	2.95	0.98	1.75
		0.35	0.52	3.11	0.96	2.00
	0.28	0.25	0.79	3.74	1.28	1.48
		0.30	0.85	4.02	1.25	1.74
		0.35	0.89	4.07	1.22	2.00
	0.33	0.25	0.87	4.12	1.38	1.40
		0.30	0.97	4.16	1.27	1.50
		0.35	0.99	4.30	1.24	1.70
31.5	0.22	0.25	0.45	2.62	1.01	1.50
		0.30	0.47	2.84	0.97	1.73
		0.35	0.50	2.98	0.95	1.98
	0.28	0.25	0.75	3.51	1.28	1.49
		0.30	0.78	3.76	1.23	1.71
		0.35	0.85	4.00	1.20	1.97
	0.33	0.25	0.85	3.83	1.32	1.30
		0.30	0.92	4.02	1.26	1.50
		0.35	0.99	4.18	1.23	1.70

ΔP is the pressure drop across the the orificemeter

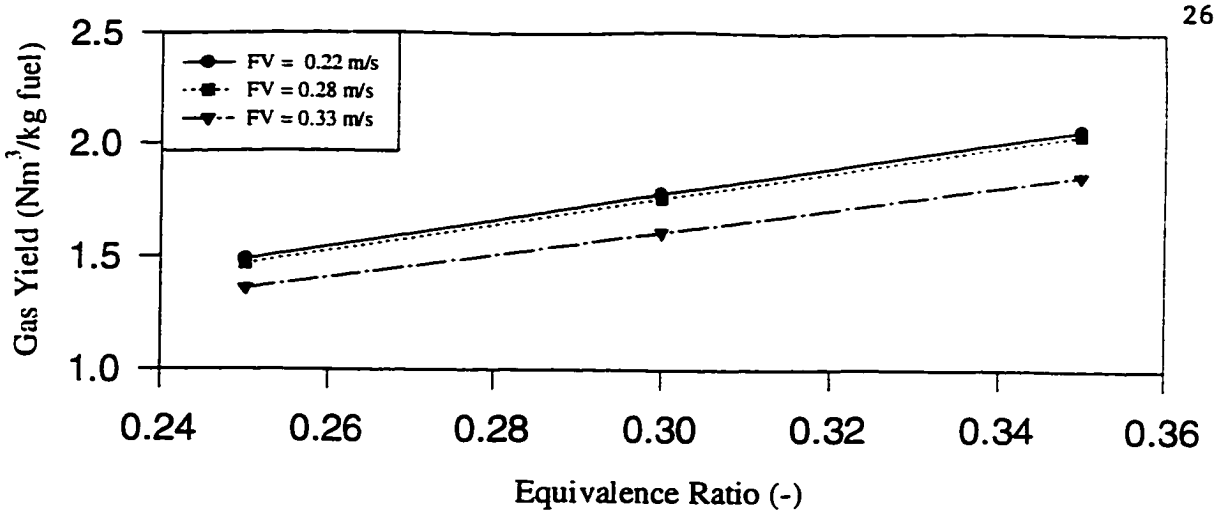

(a) Bed Height = 19.5 cm

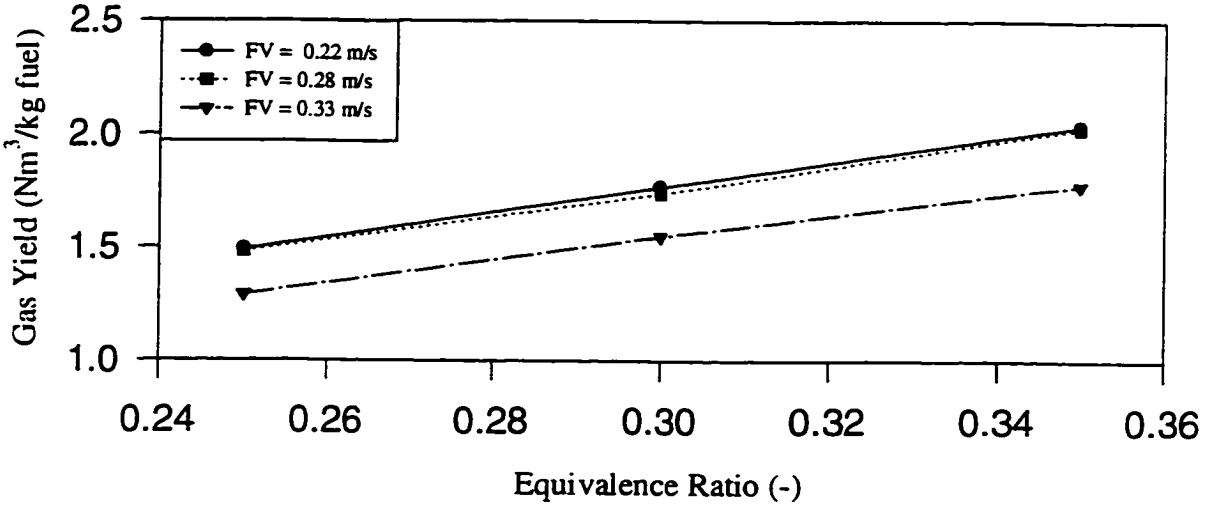

(b) Bed Height = 25.5 cm

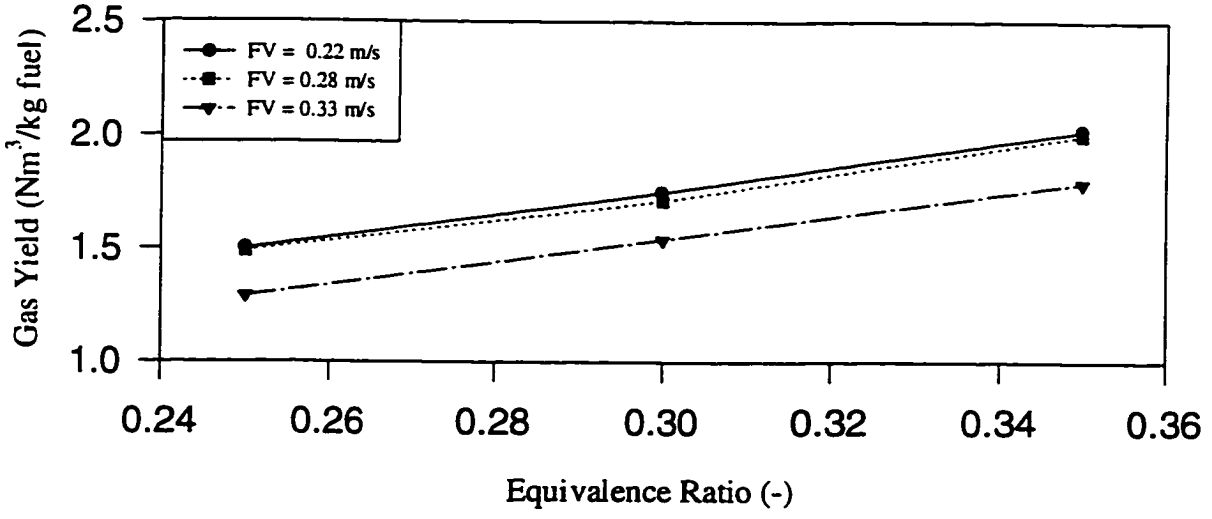

(c) Bed Height = 31.5 cm

Figure 9.43 Gas yield at various equivalence ratios, fluidization velocities and bed heights.

Table 9.28 Char-Sand Mixture Collected from the Cyclone Collector.

Bed Height (cm)	Fluidization Velocity (m/s)	Equivalence Ratio (-)	Total (kg)	Char		Sand	
				(kg)	(%)	(kg)	(%)
19.5	0.22	0.25	3.56	3.17	89.16	0.39	10.84
		0.30	3.31	2.92	88.19	0.39	11.81
		0.35	2.04	1.70	83.14	0.34	16.86
	0.28	0.25	4.58	3.93	85.85	0.65	14.15
		0.30	3.93	3.31	84.15	0.62	15.85
		0.35	2.96	2.37	80.22	0.59	19.78
	0.33	0.25	6.25	5.31	84.88	0.94	15.12
		0.30	4.96	4.11	82.94	0.85	17.06
		0.35	3.86	3.10	79.64	0.76	20.36
25.5	0.22	0.25	4.10	3.59	87.60	0.51	12.40
		0.30	3.47	2.94	84.81	0.53	15.19
		0.35	2.44	1.95	79.75	0.49	20.25
	0.28	0.25	5.33	4.44	83.25	0.89	16.75
		0.30	4.66	3.81	81.85	0.85	18.15
		0.35	3.34	2.62	78.32	0.72	21.68
	0.33	0.25	6.44	5.36	83.17	1.08	16.83
		0.30	5.33	4.35	81.68	0.98	18.32
		0.35	4.41	3.44	77.98	0.97	22.02
31.5	0.22	0.25	4.17	3.65	87.60	0.52	12.40
		0.30	3.80	3.09	81.32	0.71	18.68
		0.35	2.50	1.89	75.60	0.61	24.40
	0.28	0.25	5.82	4.91	84.33	0.91	15.67
		0.30	5.20	4.15	79.81	1.05	20.19
		0.35	3.89	2.93	75.35	0.96	24.65
	0.33	0.25	6.67	5.22	78.31	1.45	21.69
		0.30	5.58	4.17	74.77	1.41	25.23
		0.35	4.51	3.14	69.60	1.37	30.40

Table 9.29 Elemental Analysis and Higher Heating Value of Char from Cyclone Collector.

Bed Height (cm)	Fluidization Velocity (m/s)	Equivalence Ratio (-)	Carbon (%)	Ash (%)	Higher Heating Value (MJ/kg)
19.5	0.22	0.25	18.03	76.93	8.8
		0.30	14.01	83.24	6.6
		0.35	9.24	90.62	4.0
	0.28	0.25	17.18	80.13	7.7
		0.30	13.06	84.80	6.0
		0.35	7.17	91.44	3.7
	0.33	0.25	15.79	84.44	6.1
		0.30	12.78	86.32	5.4
		0.35	7.13	91.58	3.6
25.5	0.22	0.25	15.59	82.05	7.0
		0.30	11.09	87.60	5.0
		0.35	7.60	92.12	3.4
	0.28	0.25	14.81	82.89	6.7
		0.30	11.01	87.97	5.0
		0.35	5.93	92.98	3.1
	0.33	0.25	13.04	85.39	5.8
		0.30	8.53	89.30	4.4
		0.35	5.02	93.54	3.0
31.5	0.22	0.25	13.48	83.73	6.7
		0.30	11.07	88.01	5.5
		0.35	7.21	92.29	3.4
	0.28	0.25	13.03	82.72	6.0
		0.30	9.22	90.18	4.1
		0.35	5.89	93.48	2.9
	0.33	0.25	9.93	89.08	4.5
		0.30	7.25	92.26	3.4
		0.35	3.54	95.89	2.1

Table 9.30 Proximate Analysis of the Char from the Cyclone Collector (Dry basis).

Bed Height (cm)	Fluidization Velocity (m/s)	Equivalence Ratio (-)	Volatile Matter (%)	Fixed Carbon (%)	Ash (%)
19.5	0.22	0.25	5.99	17.08	76.93
		0.30	5.13	11.63	83.24
		0.35	3.58	5.80	90.62
	0.28	0.25	5.56	14.31	80.13
		0.30	5.24	9.96	84.80
		0.35	3.33	5.23	91.44
	0.33	0.25	5.22	10.34	84.44
		0.30	3.68	10.00	86.32
		0.35	3.51	4.91	91.58
25.5	0.22	0.25	5.75	12.20	82.05
		0.30	5.00	7.40	87.60
		0.35	3.46	4.42	92.12
	0.28	0.25	5.32	11.79	82.89
		0.30	4.98	7.05	87.97
		0.35	3.31	3.71	92.98
	0.33	0.25	4.96	9.65	85.39
		0.30	3.77	6.93	89.30
		0.35	3.20	3.26	93.54
31.5	0.22	0.25	5.45	11.82	82.73
		0.30	4.85	7.14	88.01
		0.35	3.34	4.37	92.29
	0.28	0.25	5.04	10.24	84.72
		0.30	4.52	5.30	90.18
		0.35	3.29	3.23	93.48
	0.33	0.25	4.68	6.24	89.08
		0.30	3.85	3.89	92.26
		0.35	2.86	1.25	95.89

Table 9.31 Particle Size Distribution of Char Sampled From Various Locations Under Run 1 Conditions.

Sieve Aperture (mm)	Average Diameter (mm)	Weight Percent Retained on Sieve		
		Cyclone Rejects	Dense Bed	
		Ash Bin	S 1	S 2
-2.800 + 2.000	2.400	-	0.49	0.36
-2.000 + 1.000	1.500	-	4.34	6.58
-1.000 + 0.500	0.750	-	40.36	45.83
-0.500 + 0.250	0.375	1.40	48.50	43.83
-0.250 + 0.150	0.200	3.80	5.24	2.78
-0.150 + 0.075	0.113	14.80	0.77	0.40
-0.075 + 0.063	0.069	28.50	0.30	0.22
-0.063 + 0.053	0.058	26.70	-	-
-0.053 + 0.045	0.049	19.20	-	-
-0.045 + 0.038	0.042	5.60	-	-

S_1 Solids sampling probe at 6.5 cm from the center of the dense bed.

S_2 Solids sampling probe at the center of the dense bed.

Run 1 Conditions: Bed Height = 19.5 cm
Fluidization Velocity = 0.22 m/s
Equivalence Ratio = 0.25

Table 9.32 Particle Size Distribution of Char Sampled From Various Locations Under Run 27 Conditions.

Sieve Aperture (mm)	Average Diameter (mm)	Weight Percent Retained on Sieve		
		Cyclone Rejects	Dense Bed	
		Ash Bin	S_1	S_2
-2.800 + 2.000	2.400	-	1.84	-
-2.000 + 1.000	1.500	-	7.01	5.70
-1.000 + 0.500	0.750	-	44.74	44.52
-0.500 + 0.250	0.375	0.40	43.23	45.43
-0.250 + 0.150	0.200	1.40	2.86	3.60
-0.150 + 0.075	0.113	13.20	0.28	0.59
-0.075 + 0.063	0.069	24.50	0.04	0.16
-0.063 + 0.053	0.058	28.10	-	-
-0.053 + 0.045	0.049	23.20	-	-
-0.045 + 0.038	0.042	9.20	-	-

S_1 Solids sampling probe at 6.5 cm from the center of the dense bed.
S_2 Solids sampling probe at the center of the dense bed.

Run 27 Conditions: Bed Height = 31.5 cm
Fluidization Velocity = 0.33 m/s
Equivalence Ratio = 0.35

velocity or equivalence ratio. A comparison of the elemental (carbon and ash) analysis of the char collected from the cyclone collector and dense bed are presented in Table 9.33 for selected runs. The contents of the other elements (hydrogen, nitrogen and sulphur) were negligible and, therefore, not presented.

The elutriated char from the fluidized bed reactor that was collected in the cyclone collector increased with increasing fluidization velocity and/or bed height. The maximum amount of char was produced at the bed height of 31.5 cm, the fluidization velocity of 0.33 m/s and the equivalence ratio of 0.22. Increasing the equivalence ratio increased the ash content in the char. On the other hand, increasing the equivalence ratio decreased the carbon content, the volatile matter content and the higher heating value of the char.

Table 9.31 shows that about 98% of the char particles collected from the cyclone collector ranged in diameter from 0.042 to 0.200 mm. It is also indicated that the diameters of about 98% and 99% of the char particles withdrawn from positions 1 and 2 in the dense bed, respectively, were larger than 0.250 mm. The particle size distribution of the char particles withdrawn from the dense bed at positions 1 (6.5 cm from the center of the dense bed) and 2 (center of the dense bed) are seen to be similar to each other and much coarser than those captured by the cyclone collector. A comparison of the few representative results of the elemental (carbon and ash) analysis of char sampled from the cyclone collector and dense bed showed that the cyclone rejects consisted of higher carbon and lower ash components. Also, variations in elemental composition between positions 1 to 2 in the dense bed were relatively small, consistent with indications from particle size distributions in Tables 9.31 and 9.32.

9.2.8 Carbon Conversion

Carbon conversion is an important parameter in any biomass conversion process. Achieving a high carbon conversion is important for overall plant efficiency and consequently for economical operation. The carbon conversion, defined as the degree to which the carbon in

Table 9.33 Carbon and Ash Contents of Char from Cyclone Collector and Dense Bed.

Bed Height (cm)	Fluidization Velocity (m/s)	Equivalence Ratio (-)	Cyclone Collector		S 1		S 2	
			C	Ash	C	Ash	C	Ash
19.5	0.22	0.25	18.03	76.93	12.84	82.28	12.23	82.85
	0.28	0.25	17.18	80.13	12.29	83.94	12.83	84.02
	0.33	0.25	15.79	84.44	10.57	87.22	9.63	88.93
25.5	0.22	0.25	15.59	82.05	11.79	82.56	10.81	83.75
	0.28	0.25	14.81	82.89	11.53	85.71	11.23	84.60
	0.33	0.25	13.04	85.39	8.87	88.82	8.47	90.71
31.5	0.22	0.25	13.48	82.73	11.31	85.08	11.47	84.15
	0.28	0.25	13.03	84.72	9.83	87.23	10.32	84.77
	0.33	0.25	9.93	89.08	5.79	90.12	5.68	92.37

S_1 Solids sampling probe at 6.5 cm from the center of the dense bed.
S_2 Solids sampling probe at the center of the dense bed.

the fuel has been converted into gaseous products, is sumarrized in Table 9.34 and presented in Figure 9.44 at various equivalence ratios, fluidization velocities and bed heights.

The carbon conversion was affected by both the equivalence ratio and fluidization velocity. The effect of changes in bed height on the carbon conversion was insignificant. At the bed height of 19.5 cm and fluidization velocity of 0.22 m/s, increasing the equivalence ratio from 0.25 to 0.35 resulted in the carbon conversion increasing from 74 to 84%. At the same bed height and the equivalence ratio of 0.22, increasing the fluidization velocity from 0.22 to 0.33 m/s decreased the carbon conversion from 74 to 59%. The carbon conversion spanned from 55.0 to 84.0% under all conditions investigated.

9.2.9 Material and Energy Balances

Because of the number of repetitive calculations that have to be made to calculate the material and energy balances, a computer code was developed. A listing of the computer code is included in Appendix B.

9.2.9.1 Material Balance. Material balance based on the inflow rates of the rice husk and air and outflow rates of the gas and char is given as follows:

$$G_{rh} + G_{air} = G_g + G_{ch} \tag{9.4}$$

where:

G_{rh} is the rice husk flow rate (kg/min)

G_{air} is the air flow rate (kg/min)

G_g is the gas flow rate (kg/min)

G_{ch} is the char flow rate (kg/min)

Table 9.34 Carbon Conversion.

Bed Height (cm)	Fluidization Velocity (m/s)	Equivalence Ratio (-)	Carbon Conversion (%)
19.5	0.22	0.25	74.3
		0.30	79.3
		0.35	84.1
	0.28	0.25	72.6
		0.30	74.1
		0.35	83.0
	0.33	0.25	59.1
		0.30	62.8
		0.35	68.6
25.5	0.22	0.25	73.8
		0.30	78.3
		0.35	84.0
	0.28	0.25	73.2
		0.30	74.2
		0.35	77.7
	0.33	0.25	58.0
		0.30	60.5
		0.35	67.7
31.5	0.22	0.25	78.3
		0.30	76.0
		0.35	81.0
	0.28	0.25	70.4
		0.30	72.6
		0.35	78.6
	0.33	0.25	55.0
		0.30	60.0
		0.35	67.0

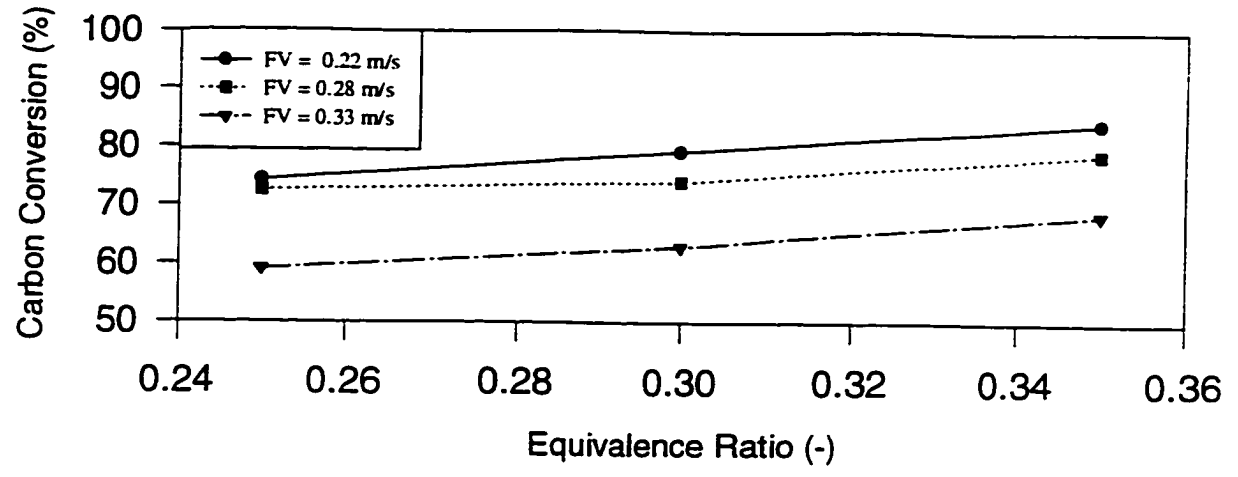

(a) Bed Height = 19.5 cm

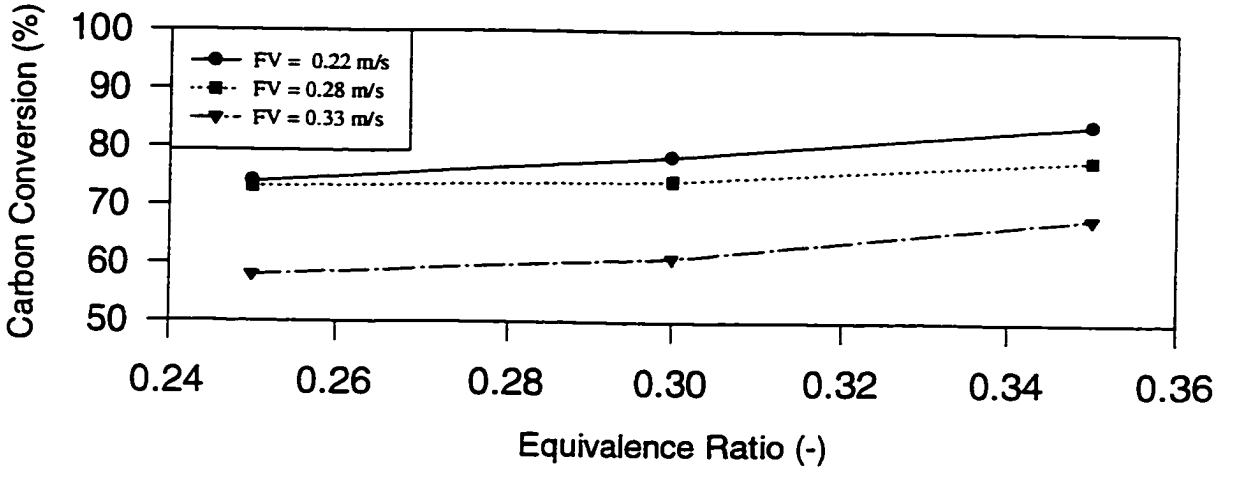

(b) Bed Height = 25.5 cm

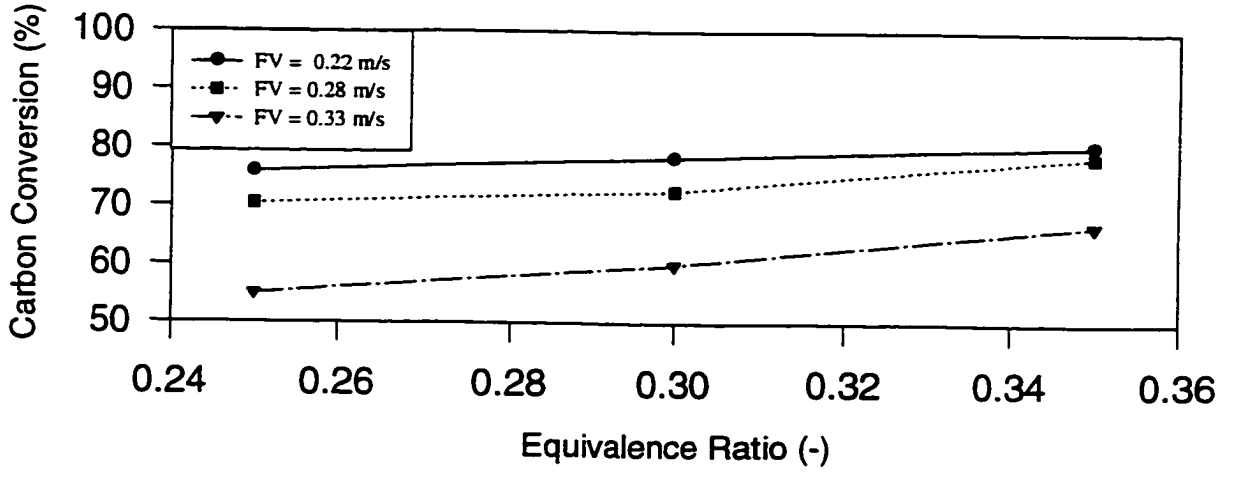

(c) Bed Height = 31.5 cm

Figure 9.44 Carbon conversion at various equivalence ratios, fluidization velecities and bed heights.

Air is assumed to consist of 79% by volume N_2 and 21% by volume O_2. Air actually contains 0.9% Argon, but Argon and N_2 are assumed inert and the Argon simply included with N_2.

For the carbon balance, it is assumed that the only carbon entering the gasifier is that in the rice husk, and that carbon leaves the gasifier in the gas and char. Thus, the material balance for carbon is given as follows:

$$x_{C_{rh}} G_{rh} = G_{ch} \sum x_{C_{ch}} + G_g \sum x_{C_g} \qquad (9.5)$$

where:

x_i is the amount of carbon in the rice husk ($i = C_{rh}$), the gas ($i = C_g$) and the char ($i = C_{ch}$).

Table 9.35 shows the material balance for carbon. The carbon flow rate decreased with the increase in equivalence ratio. There was an increase in carbon flow rate when the fluidization velocity was increased. The highest value of carbon outflow (0.328 kg/min.) was observed at the equivalence ratio of 0.25 and fluidization velocity of 0.33 m/s. Generally, higher closures (ratio of carbon outflow to carbon inflow) were observed at the equivalence ratio of 0.25.

9.2.9.2 Energy Balance. An overall energy balance was considered for the gasifier considering the different energy inflows and outflows as follows:

$$G_{rh} \times HHV_{rh} = G_{ch} \times (\Delta h_{sen} + \Delta h_{chem}) + G_g \times (\Delta h_{sen} + \Delta h_{chem}) + Q_{loss} \qquad (9.6)$$

where:

HHV_{rh} is the higher heating value of rice husk

Q_{loss} is the heat loss through the gasifier walls (MJ/kg)

Table 9.35 Material Balance for Carbon.

Bed Height (cm)	Fluidization Velocity (m/s)	Equivalence Ratio (-)	Input (kg/min)	Output (kg/min)	Ratio (-)
19.5	0.22	0.25	0.252	0.275	1.09
		0.30	0.211	0.222	1.05
		0.35	0.180	0.180	1.00
	0.28	0.25	0.323	0.332	1.03
		0.30	0.271	0.257	0.95
		0.35	0.229	0.215	0.94
	0.33	0.25	0.384	0.353	0.92
		0.30	0.320	0.294	0.92
		0.35	0.274	0.238	0.87
25.5	0.22	0.25	0.252	0.262	1.04
		0.30	0.211	0.208	0.99
		0.35	0.180	0.174	0.97
	0.28	0.25	0.323	0.318	0.99
		0.30	0.271	0.248	0.92
		0.35	0.229	0.210	0.91
	0.33	0.25	0.384	0.328	0.85
		0.30	0.320	0.258	0.81
		0.35	0.274	0.219	0.80
31.5	0.22	0.25	0.252	0.261	1.04
		0.30	0.211	0.203	0.96
		0.35	0.180	0.169	0.93
	0.28	0.25	0.323	0.299	0.93
		0.30	0.271	0.237	0.88
		0.35	0.229	0.202	0.88
	0.33	0.25	0.384	0.298	0.78
		0.30	0.320	0.245	0.77
		0.35	0.274	0.207	0.75

$\Delta h_{ch_{sen}}$ is the sensible heat out with the char (MJ/kg)

$\Delta h_{ch_{chem}}$ is the chemical energy out with the char (MJ/kg)

$\Delta h_{g_{sen}}$ is the sensible heat out with the gas (MJ/kg)

$\Delta h_{g_{chem}}$ is the chemical energy out with the gas (MJ/kg)

In calculating the efficiency of the gasifier, the critical values are energy into the gasifier in the rice husk and the energy out in the gas, since the gas is the desired output from the gasifier. This efficiency is referred to as the cold gas thermal efficiency. The energy balances are presented in Table 9.36. Figure 9.45 gives the cold gas thermal efficiency at various bed heights, fluidization velocities and equivalence ratios.

Both the energy recovered in the form of gas and the sensible energy of the gas decreased with increases in the equivalence ratio. The sensible energy observed was much less than 1.0% of the energy in the rice husk.

To account for the heat losses through all measuring ports and openings, the manufacturer of the insulating material recommended that the calculated heat losses through the reactor walls be increased by a factor of 2. Also to account for the heat losses through the non-insulated conical wall at the bottom of the reactor, Jenkins (1980) recommended to further increase the heat losses by a factor of 2. Increasing the equivalence ratio increased the heat losses through the gasifier walls and decreased the unaccounted losses. The heat losses were less than 1.0% of the energy in the rice husk and the unaccounted losses (in the form of tar, unburned carbon, water vapour, etc.), which ranged from 0.94 to 9.75 MJ/kg, correspond to 5.8 to 60.1% of the energy in the rice husk.

Table 9.36 Thermal Efficiency.

Bed Height	Fluidization Velocity	Equivalence Ratio	Energy In (MJ/kg)	Energy Out (MJ/kg)				Cold Gas Thermal Efficiency
(cm)	(m/s)	(-)	Rice Husk	Energy in Gas	Sensible Energy in Gas	Heat Losses	Others*	(%)
19.5	0.22	0.25	10.65	8.29	0.0054	0.0035	2.3511	77.84
		0.30	8.90	7.64	0.0040	0.0048	1.2512	85.84
		0.35	7.63	6.68	0.0028	0.0060	0.9412	87.55
	0.28	0.25	13.67	10.37	0.0193	0.0029	3.2778	75.86
		0.30	11.45	8.85	0.0154	0.0039	2.5807	77.29
		0.35	9.70	8.34	0.0147	0.0050	1.3403	85.98
	0.33	0.25	16.22	10.14	0.0209	0.0025	6.0566	62.52
		0.30	13.52	9.06	0.0153	0.0034	4.4413	67.01
		0.35	11.61	7.43	0.0152	0.0042	4.1606	64.00
25.5	0.22	0.25	10.65	8.22	0.0125	0.0034	2.4141	77.18
		0.30	8.90	7.44	0.0109	0.0045	1.4446	83.60
		0.35	7.63	6.53	0.0107	0.0059	1.0834	85.58
	0.28	0.25	13.67	10.25	0.0183	0.0028	3.3989	74.98
		0.30	11.45	8.63	0.0150	0.0038	2.8012	75.37
		0.35	9.70	7.97	0.0142	0.0048	1.7110	82.16
	0.33	0.25	16.22	9.73	0.0179	0.0024	9.7503	59.99
		0.30	13.52	8.50	0.0139	0.0033	5.0028	62.87
		0.35	11.61	7.94	0.0135	0.0041	3.6524	68.40
31.5	0.22	0.25	10.65	8.65	0.0140	0.0033	1.9827	81.22
		0.30	8.90	7.20	0.0103	0.0045	1.6852	80.90
		0.35	7.63	6.28	0.0101	0.0059	1.3340	82.31
	0.28	0.25	13.67	9.89	0.0151	0.0026	3.7623	72.35
		0.30	11.45	8.33	0.0133	0.0037	3.1030	72.75
		0.35	9.70	7.64	0.0130	0.0046	2.0424	78.76
	0.33	0.25	16.22	9.09	0.0161	0.0023	7.1116	56.04
		0.30	13.52	8.16	0.0132	0.0031	6.3437	60.36
		0.35	11.61	7.76	0.0129	0.0039	3.8332	66.84

* Unaccounted losses in the form of tar, unburned carbon in char and water vapour.

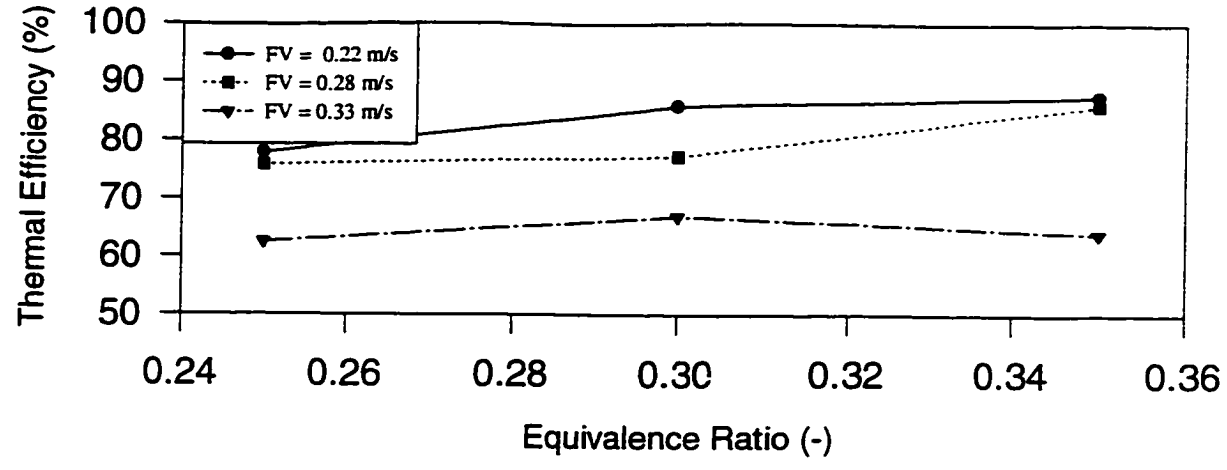

(a) Bed Height = 19.5 cm

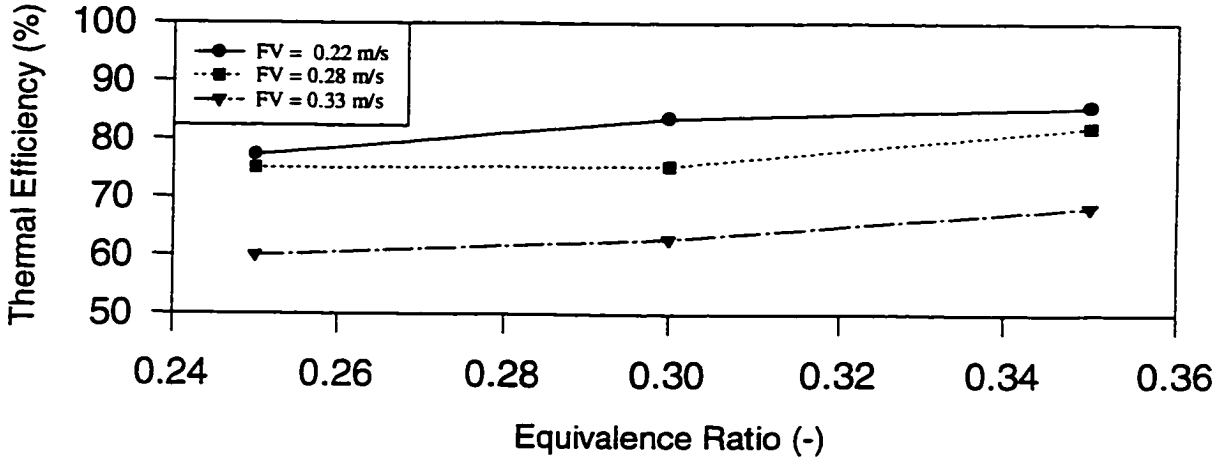

(b) Bed Height = 25.5 cm

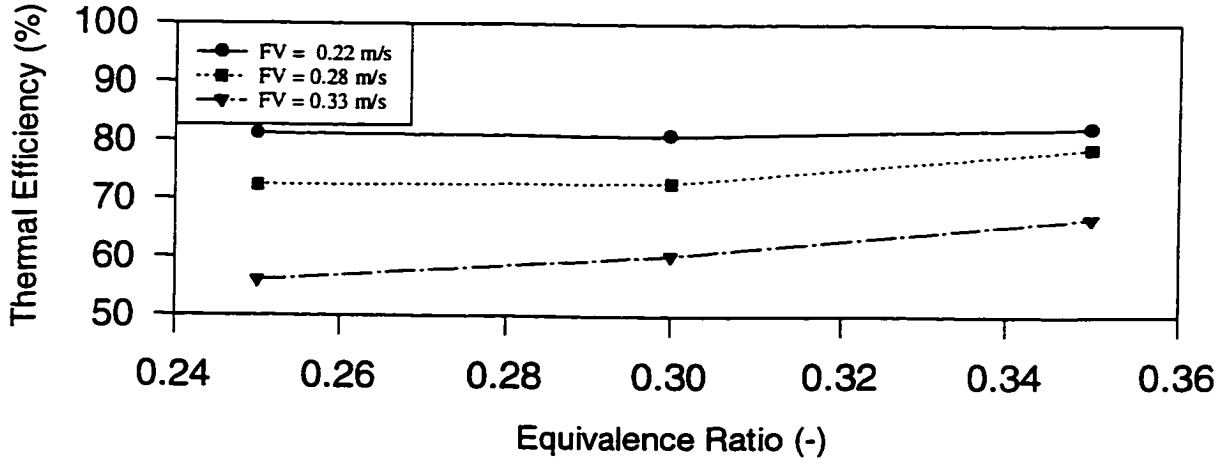

(c) Bed Height = 31.5 cm

Figure 9.45 Thermal efficiency at various equivalence ratios, fluidization velecities and bed heights.

The cold gas thermal efficiency increased with increasing equivalence ratio and decreased with increasing fluidization velocity. The maximum cold gas thermal efficiency (87.6%) was obtained at the highest equivalence ratio and lowest fluidization velocity and bed height whereas the minimum cold gas thermal efficiency (56.0%) was obtained at the lowest equivalence ratio and highest fluidization velocity and bed height.

9.2.10 Reproducibility

Fluidized bed gasifiers are envisaged to operate under steady state conditions. In order to check the reliability of the fluidized bed gasifier under such steady state operation three sets of gas samples were collected from the gasifier exit at 5 minute intervals after steady state was attained. The results of the selected extreme runs, 1 (bed height 19.5 cm, fluidization velocity 0.33 m/s and equivalence ratio 0.35) and 27 (bed height 31.5 cm, fluidization velocity 0.33 m/s and equivalence ratio 0.35) are summarized in Tables 9.37 and 9.38, respectively.

The produced gas not sampled burned in the after burner with a clearly visible flame. The flame had a red-orange colour caused by the combustion of carbon carried away with the gas. When the rice husk flowrate was stopped (i.e. at the end of a run), it was observed that the flame burned out in less than a minute. The flame burn out time was, however, not investigated due to limitations on equipment availability and analysis time.

9.3 MODEL RESULTS

Two models were used to predict the performance of the dual distributor fluidized bed gasifier. The first (the one-compartment model) is very simple and neglects the complex hydrodynamic conditions prevalent in the gasifier whereas those are taken

Table 9.37 Comparison of Results of Run 1.

Component	Sample 1	Sample 2	Sample 3	% Variation
Duration of Run (min)	20	25	30	-
Average Bed Temperature (°C)	695	702	704	± 7.72
Gas Composition (Volume %):				
CO_2	13.85	13.64	13.69	± 0.18
C_2H_m	1.37	1.48	1.59	± 0.18
C_2H_6	0.21	0.20	0.27	± 0.06
H_2	3.61	4.13	4.04	± 0.23
O_2	0.06	0.03	0.00	± 0.05
N_2	58.11	57.53	57.77	± 0.48
CH_4	1.72	2.61	2.52	± 0.80
CO	21.07	20.38	20.12	± 0.80
Higher Heating Value (MJ/Nm^3)	4.44	4.81	4.80	± 0.34
Gas Yield (Nm^3/kg fuel)	1.48	1.51	1.49	± 0.03
Carbon Conversion (%)	74.21	73.02	74.30	± 1.17
Thermal Efficiency (%)	70.04	78.85	77.84	± 7.87

Bed Height (cm)	19.50
Fluidization Velocity (m/s)	0.22
Equivalence Ratio (-)	0.25
Air Flow Rate (m^3/min)	0.84
Rice Husk Feed Rate (kg/min)	0.67

Table 9.38 Comparison of Results of Run 27.

Component	Sample 1	Sample 2	Sample 3	% Variation
Duration of Run (min)	20	25	30	-
Average Bed Temperature (°C)	822	823	828	± 5.20
Gas Composition (Volume %):				
CO_2	17.33	17.06	17.42	± 0.31
C_2H_m	1.04	1.04	0.98	± 0.05
C_2H_6	0.00	0.00	0.00	± 0.00
H_2	3.37	3.44	3.25	± 0.16
O_2	0.01	0.16	0.01	± 0.14
N_2	63.62	64.01	64.21	± 0.49
CH_4	1.88	1.77	1.84	± 0.09
CO	12.75	12.52	12.29	± 0.38
Higher Heating Value (MJ/Nm^3)	3.21	3.14	3.09	± 0.10
Gas Yield (Nm^3/kg fuel)	1.80	1.80	1.79	± 0.01
Carbon Conversion (%)	68.06	66.58	67.00	± 1.26
Thermal Efficiency (%)	69.20	69.24	66.84	± 2.24

Bed Height (cm)	31.50
Fluidization Velocity (m/s)	0.33
Equivalence Ratio (-)	0.35
Air Flow Rate (m^3/min)	1.21
Rice Husk Feed Rate (kg/min)	0.73

into consideration in the second (the two-compartment model). The first model has a single parameter (overall carbon conversion) that can be used to improve the fit between predicted and experimental gas compositions. On the other hand, the second model has two parameters (carbon conversion in the core and annular regions) that can be independently adjusted to account for the effect of various operating and design conditions on the composition of the gasification products.

9.3.1 Comparative Analysis

The one-compartment and two-compartment models were used to predict the composition of the gases produced by the dual distributor fluidized bed gasifier when using rice husk as a feedstock. Equation 5.22 was used to provide a quantitative indication of how well the predicted and experimental results fit each other. The results are shown in Appendix D (Figures D-1 to D-27). A typical example showing the effect of assumed carbon conversion on the mean error in product gas composition at various carbon conversion ratios (for the two-compartment model) and the bed height of 19.5 cm, fluidization velocity of 0.22 m/s and equivalence ratio of 0.25) is represented in Figure 9.46. Tables 9.39 and 9.40 show the carbon conversion and the mean error at various bed heights, fluidization velocities and equivalence ratios.

The overall carbon conversion estimated by the one-compartment model ranged from 70.0% (at the bed height of 19.5 cm, fluidization velocity velocity of 0.33 m/s and equivalence ratio of 0.25) to 88.6% (at the bed height of 31.5 cm, fluidization velocity of 0.22 m/s and equivalence ratio of 0.35) whereas that estimated by the two-compartment model ranged from 88.6% (at the bed height of 19.5 cm, fluidization velocity of 0.33 m/s and equivalence ratio of 0.25) to 98.9% (at the bed height of 31.5 cm, fluidization velocity of 0.22 m/s and equivalence ratio of 0.35). These results show the large improvement obtained by adding the hydrodynamic complexity of the gasifier to the two-compartment

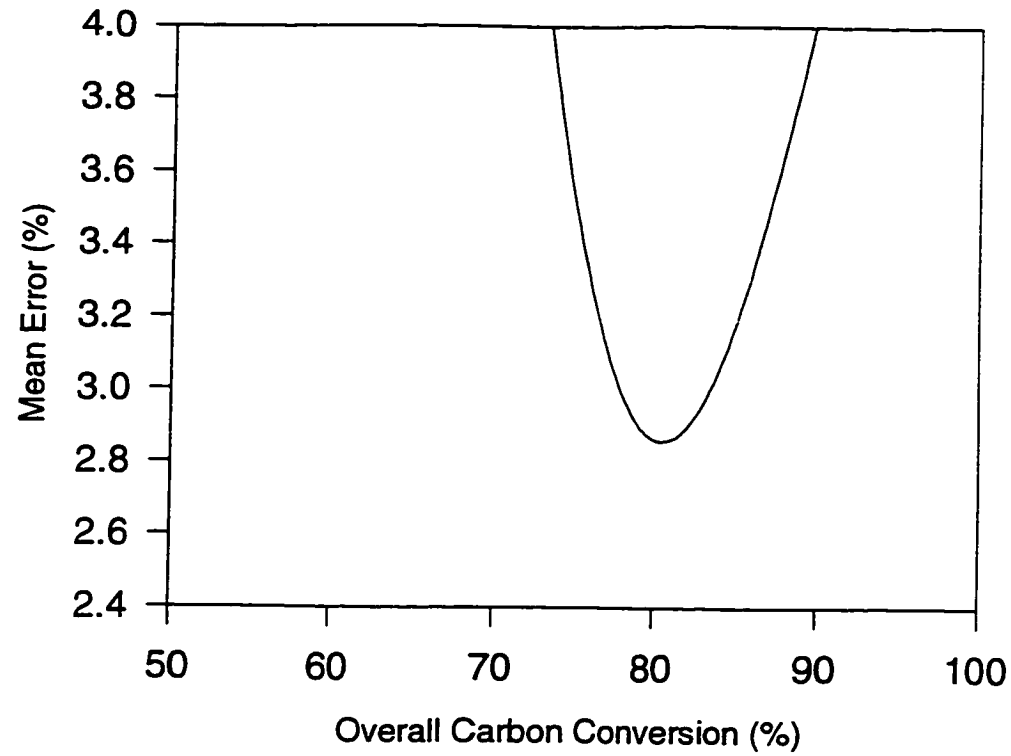

(a) One-Compartment Model

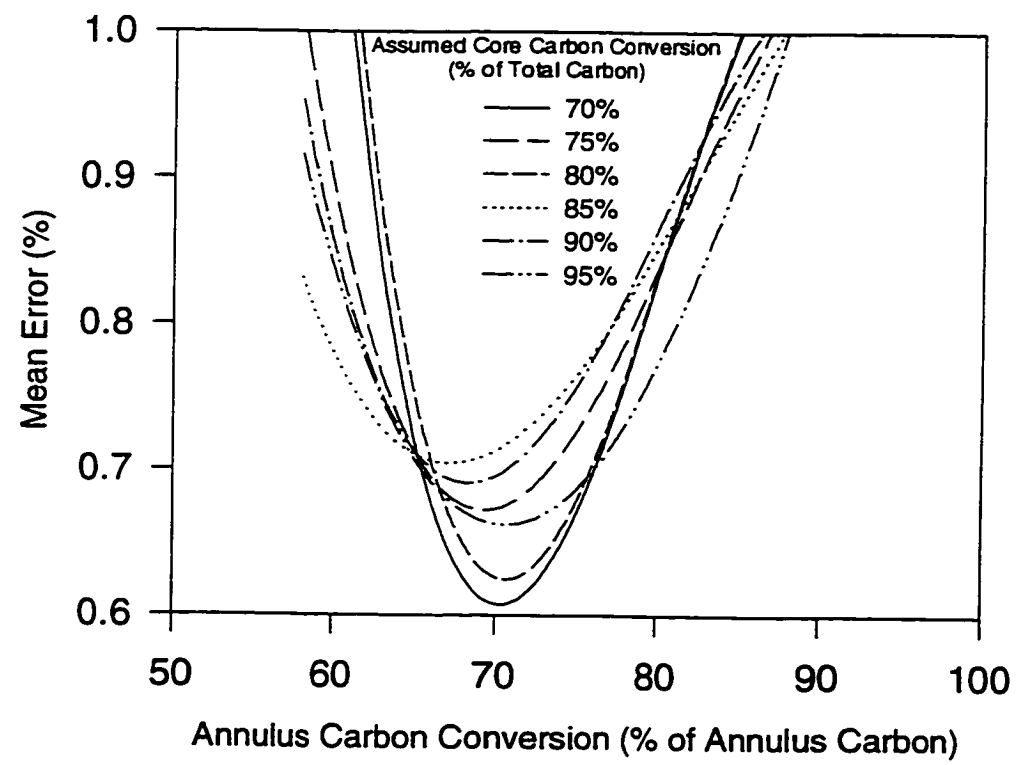

(b) Two-Compartment Model

Figure 9.46 Mean error in product gas composition at various carbon conversion ratios and the bed height of 19.5 cm, fluidization velocity of 0.22 m/s and equivalence ratio of 0.25.

Table 9.39 Carbon Conversion at Various Bed Heights, Fluidization Velocities and Equivalence Ratios.

Bed Height (cm)	Fluidization Velocity (m/s)	Equivalence Ratio (-)	Carbon Conversion (%)			
			One-Compartment Model	Two-Compartment Model		
			Overall	Core*	Annulus**	Overall
19.5	0.22	0.25	80.6	70.0	70.0	91.0
				75.0	70.5	92.6
				80.0	67.0	93.4
				85.0	69.5	95.4
				90.0	68.0	96.4
				95.0	68.0	98.4
		0.30	84.8	70.0	74.0	92.2
				75.0	74.0	93.5
				80.0	74.0	94.8
				85.0	74.0	96.1
				90.0	74.0	97.2
				95.0	73.5	98.6
		0.35	86.4	70.0	76.0	92.8
				75.0	75.0	93.8
				80.0	76.0	95.2
				85.0	76.0	96.4
				90.0	74.0	97.4
				95.0	74.0	98.7
	0.28	0.25	76.4	70.0	69.0	90.7
				75.0	68.0	92.0
				80.0	66.5	93.3
				85.0	68.5	95.3
				90.0	67.0	96.7
				95.0	67.0	98.4
		0.30	82.4	70.0	71.0	91.3
				75.0	70.0	92.5
				80.0	70.0	94.0
				85.0	70.0	95.5
				90.0	70.0	97.0
				95.0	70.0	98.5
		0.35	85.5	70.0	74.5	92.8
				75.0	76.0	93.8
				80.0	75.0	95.2
				85.0	72.0	96.4
				90.0	75.0	97.4
				95.0	75.0	98.8

* Percent of total carbon.

** Percent of carbon in annulus.

Table 9.39 Continued.

Bed Height (cm)	Fluidization Velocity (m/s)	Equivalence Ratio (-)	Carbon Conversion (%)			
			One-Compartment Model	Two-Compartment Model		
			Overall	Core*	Annulus**	Overall
	0.33	0.25	70.0	70.0	66.0	88.6
				75.0	65.0	89.5
				80.0	66.0	92.4
				85.0	65.0	94.7
				90.0	64.0	96.4
				95.0	64.0	98.2
		0.30	75.5	70.0	68.0	89.5
				75.0	70.0	92.5
				80.0	70.0	94.0
				85.0	70.0	95.5
				90.0	67.0	96.7
				95.0	67.0	98.4
		0.35	78.3	70.0	70.3	92.8
				75.0	70.0	93.8
				80.0	69.0	95.2
				85.0	69.0	96.4
				90.0	70.0	97.4
				95.0	70.0	98.5
25.5	0.22	0.25	80.6	70.0	70.5	91.2
				75.0	70.0	92.5
				80.0	70.5	94.1
				85.0	68.0	95.2
				90.0	68.0	96.8
				95.0	70.0	98.5
		0.30	85.5	70.0	74.0	92.2
				75.0	74.0	93.5
				80.0	72.0	94.4
				85.0	71.0	95.7
				90.0	76.0	97.6
				95.0	72.5	98.6
		0.35	87.5	70.0	78.0	93.4
				75.0	78.0	94.5
				80.0	79.0	95.8
				85.0	79.0	96.9
				90.0	78.0	97.8
				95.0	77.5	98.9

* Percent of total carbon.

** Percent of carbon in annulus.

Table 9.39 Continued.

Bed Height (cm)	Fluidization Velocity (m/s)	Equivalence Ratio (-)	Carbon Conversion (%)			
			One-Compartment Model	Two-Compartment Model		
			Overall	Core*	Annulus**	Overall
	0.28	0.25	76.8	70.0	69.0	90.7
				75.0	68.0	92.0
				80.0	69.0	93.8
				85.0	68.0	95.2
				90.0	67.0	96.7
				95.0	68.0	98.4
		0.30	83.0	70.0	70.5	91.2
				75.0	70.0	92.5
				80.0	70.0	94.0
				85.0	69.0	95.4
				90.0	70.0	97.0
				95.0	70.0	98.5
		0.35	86.8	70.0	74.0	92.2
				75.0	74.0	93.5
				80.0	73.5	94.7
				85.0	73.5	96.0
				90.0	74.0	97.4
				95.0	74.0	98.6
	0.33	0.25	72.1	70.0	65.0	89.5
				75.0	65.5	91.4
				80.0	67.5	93.5
				85.0	65.0	94.8
				90.0	65.0	96.5
				95.0	65.5	98.3
		0.30	76.8	70.0	68.0	90.4
				75.0	70.0	92.5
				80.0	70.0	94.0
				85.0	67.5	95.1
				90.0	67.5	96.8
				95.0	67.5	98.4
		0.35	78.6	70.0	70.0	91.0
				75.0	70.5	92.6
				80.0	70.0	94.0
				85.0	70.0	95.5
				90.0	70.0	97.0
				95.0	70.0	98.5

* Percent of total carbon.

** Percent of carbon in annulus.

Table 9.39 Continued.

Bed Height (cm)	Fluidization Velocity (m/s)	Equivalence Ratio (-)	Carbon Conversion (%)			
			One-Compartment Model	Two-Compartment Model		
			Overall	Core*	Annulus**	Overall
31.5	0.22	0.25	81.2	70.0	73.0	91.9
				75.0	73.0	93.3
				80.0	72.5	94.5
				85.0	73.5	96.0
				90.0	71.5	97.2
				95.0	72.5	98.6
		0.30	85.8	70.0	74.0	92.2
				75.0	74.0	93.5
				80.0	72.5	94.5
				85.0	72.0	95.8
				90.0	74.2	97.4
				95.0	75.0	98.7
		0.35	88.6	70.0	79.0	93.7
				75.0	80.0	95.0
				80.0	78.0	95.6
				85.0	80.0	97.0
				90.0	77.5	97.8
				95.0	77.5	98.9
	0.28	0.25	78.0	70.0	71.5	91.5
				75.0	70.0	92.5
				80.0	70.0	94.0
				85.0	71.0	95.7
				90.0	69.0	96.9
				95.0	70.0	98.5
		0.30	85.6	70.0	73.5	92.1
				75.0	73.5	93.4
				80.0	73.5	94.7
				85.0	73.0	96.0
				90.0	73.0	97.3
				95.0	72.0	98.6
		0.35	87.5	70.0	74.5	92.4
				75.0	75.0	93.7
				80.0	74.0	94.8
				85.0	73.0	96.0
				90.0	74.0	97.4
				95.0	74.0	98.7

* Percent of total carbon.

** Percent of carbon in annulus.

Table 9.39 Continued.

Bed Height (cm)	Fluidization Velocity (m/s)	Equivalence Ratio (-)	Carbon Conversion (%)			
			One-Compartment Model	Two-Compartment Model		
			Overall	Core*	Annulus**	Overall
	0.33	0.25	72.8	70.0	68.0	90.4
				75.0	69.5	92.4
				80.0	70.5	94.1
				85.0	70.0	95.5
				90.0	68.0	96.4
				95.0	68.0	98.4
		0.30	78.0	70.0	70.5	91.2
				75.0	72.0	93.0
				80.0	71.5	94.3
				85.0	71.0	95.7
				90.0	70.0	97.0
				95.0	70.0	98.5
		0.35	80.0	70.0	75.0	92.5
				75.0	75.0	93.7
				80.0	75.0	95.0
				85.0	75.0	96.3
				90.0	75.0	97.5
				95.0	75.0	98.7

* Percent of total carbon.

** Percent of carbon in annulus.

Table 9.40 Mean Error in Product Gas Composition at Various Bed Heights, Fluidization Velocities and Equivalence Ratios.

Bed Height (cm)	Fluidization Velocity (m/s)	Equivalence Ratio (-)	Mean Error (%)	
			One-Compartment Model	Two-Compartment Model
19.5	0.22	0.25	2.85	0.61
				0.67
				0.62
				0.70
				0.69
				0.65
		0.30	2.75	0.62
				0.66
				0.67
				0.63
				0.68
				0.64
		0.35	2.69	0.61
				0.65
				0.69
				0.68
				0.63
				0.62
	0.28	0.25	2.82	0.67
				0.75
				0.71
				0.75
				0.73
				0.72
		0.30	2.74	0.64
				0.70
				0.72
				0.64
				0.68
				0.66
		0.35	2.67	0.63
				0.69
				0.71
				0.68
				0.66
				0.64

Table 9.40 Continued.

Bed Height (cm)	Fluidization Velocity (m/s)	Equivalence Ratio (-)	Mean Error (%) One-Compartment Model	Mean Error (%) Two-Compartment Model
	0.33	0.25	3.05	0.62
				0.64
				0.75
				0.75
				0.70
				0.64
		0.30	2.88	0.62
				0.70
				0.63
				0.70
				0.67
				0.65
		0.35	2.55	0.62
				0.71
				0.65
				0.62
				0.69
				0.65
25.5	0.22	0.25	2.95	0.60
				0.66
				0.62
				0.70
				0.69
				0.64
		0.30	2.74	0.63
				0.67
				0.69
				0.70
				0.64
				0.65
		0.35	2.80	0.64
				0.63
				0.68
				0.69
				0.65
				0.62

Table 9.40 Continued.

Bed Height (cm)	Fluidization Velocity (m/s)	Equivalence Ratio (-)	Mean Error (%) One-Compartment Model	Mean Error (%) Two-Compartment Model
	0.28	0.25	2.80	0.66
				0.74
				0.68
				0.74
				0.73
				0.71
		0.30	2.74	0.63
				0.71
				0.69
				0.72
				0.64
				0.65
		0.35	2.65	0.63
				0.66
				0.69
				0.68
				0.64
				0.62
	0.33	0.25	2.97	0.62
				0.63
				0.71
				0.70
				0.67
				0.64
		0.30	2.89	0.61
				0.70
				0.63
				0.69
				0.68
				0.64
		0.35	2.55	0.61
				0.71
				0.69
				0.67
				0.61
				0.65

Table 9.40 Continued.

Bed Height (cm)	Fluidization Velocity (m/s)	Equivalence Ratio (-)	Mean Error (%)	
			One-Compartment Model	Two-Compartment Model
31.5	0.22	0.25	2.71	0.66
				0.68
				0.63
				0.69
				0.65
				0.62
		0.30	2.64	0.60
				0.66
				0.67
				0.66
				0.64
				0.61
		0.35	2.45	0.60
				0.64
				0.67
				0.62
				0.68
				0.62
	0.28	0.25	2.70	0.64
				0.73
				0.70
				0.66
				0.76
				0.68
		0.30	2.68	0.62
				0.67
				0.69
				0.67
				0.64
				0.62
		0.35	2.68	0.63
				0.61
				0.67
				0.69
				0.65
				0.62

Table 9.40 Continued.

Bed Height (cm)	Fluidization Velocity (m/s)	Equivalence Ratio (-)	Mean Error (%)	
			One-Compartment Model	Two-Compartment Model
	0.33	0.25	2.90	0.62
				0.63
				0.71
				0.70
				0.67
				0.65
		0.30	2.79	0.62
				0.67
				0.64
				0.62
				0.69
				0.65
		0.35	2.55	0.62
				0.66
				0.68
				0.70
				0.60
				0.63

model. The overall carbon conversion estimated by the two-compartment model increased with increasing amount of carbon converted in the core region.

The one-compartment model developed in this study is similar to those used by many investigators (Double and Bridgwater, 1985; Maniatis, 1986; Double et al., 1989; Gururajan et al., 1992; Ongiro et al., 1997; and Ergudenler et al., 1997) and provides reasonably good estimate of the product gas composition. The mean error between the predicted and measured product gas composition varied between 2.45% (at the bed height of 31.5 cm, fluidization velocity velocity of 0.22 m/s and equivalence ratio of 0.35) and 3.05% (at the bed height of 19.5 cm, fluidization velocity velocity of 0.33 m/s and equivalence ratio of 0.25).

The use of the two-compartment model resulted in 4-fold reduction in the mean errors (0.61-0.76%) and can, therefore, be considered as a statistically significant improved modeling approach. This improvement results mainly from the ability of the two-compartment model to account for the complex hydrodynamics present in the dual distributor fluidized bed gasifier. It was, therefore, used in all subsequent parametric studies.

9.3.2 Regression Analysis

The effects of equivalence ratio, fluidization velocity and bed height on the predicted best fit carbon conversion (by the two-compartment model) in the core and annular regions are presented in Figures 9.47 and 9.48. The predicted carbon conversions in the core and annular regions were most strongly affected by changes in the equivalence ratio and fluidization velocity but were practically insensitive to the variations in the bed height. Increasing the equivalence ratio increased the carbon conversion in the core region (percent of total carbon). However, the carbon conversion in the core region (percent of total carbon) remained approximately constant with increasing fluidization velocity up to a

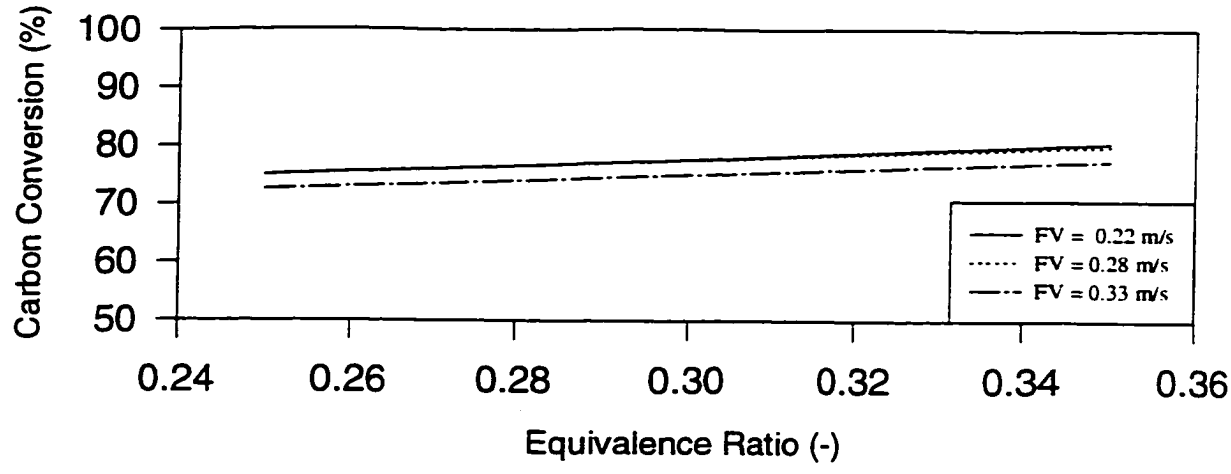

(a) Bed Height = 19.5 cm

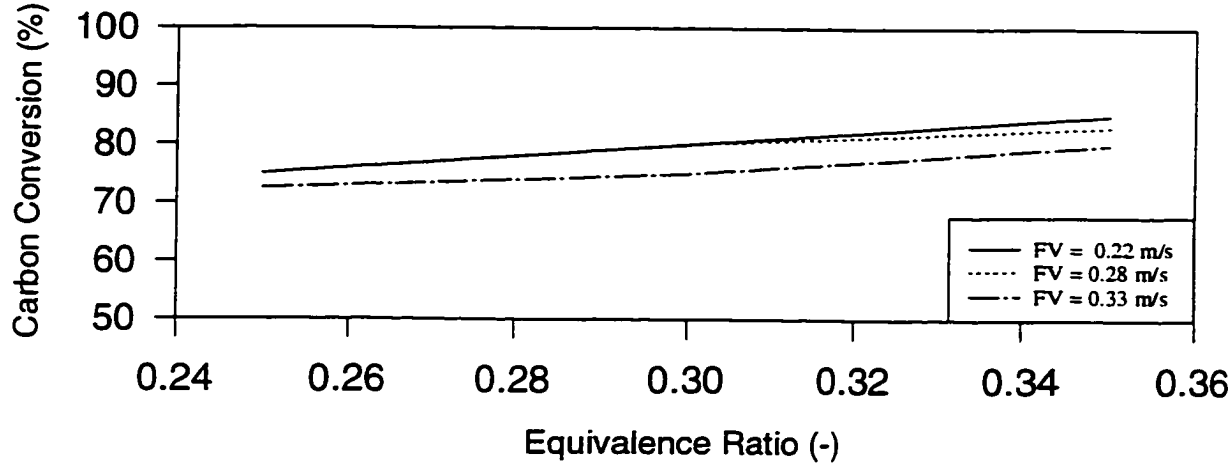

(b) Bed Height = 25.5 cm

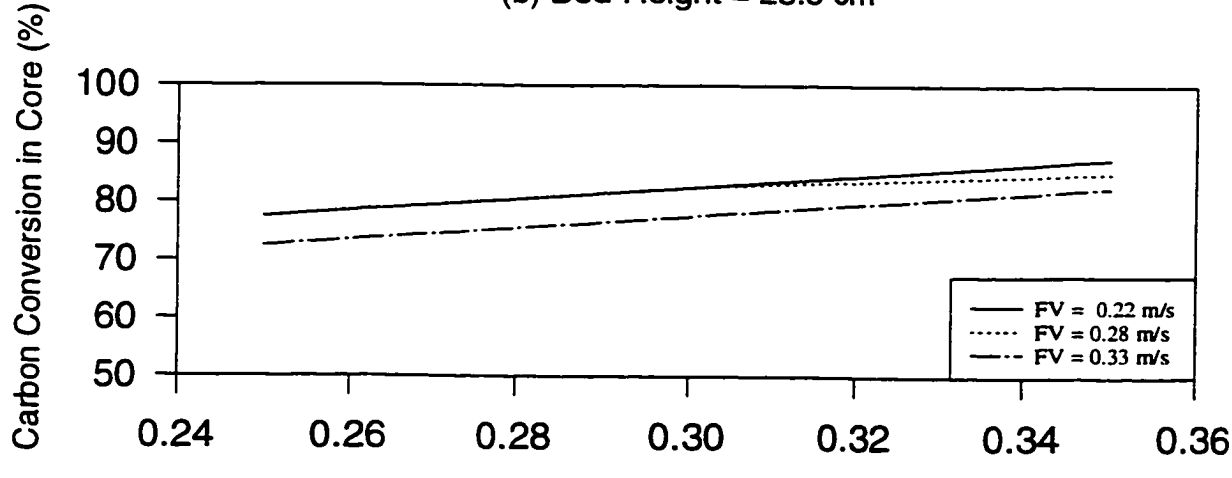

(c) Bed Height = 31.5 cm

Figure 9.47 Predicted carbon conversion (percent of total carbon) in the core region at various bed heights, fluidization velocities and equivalence ratios.

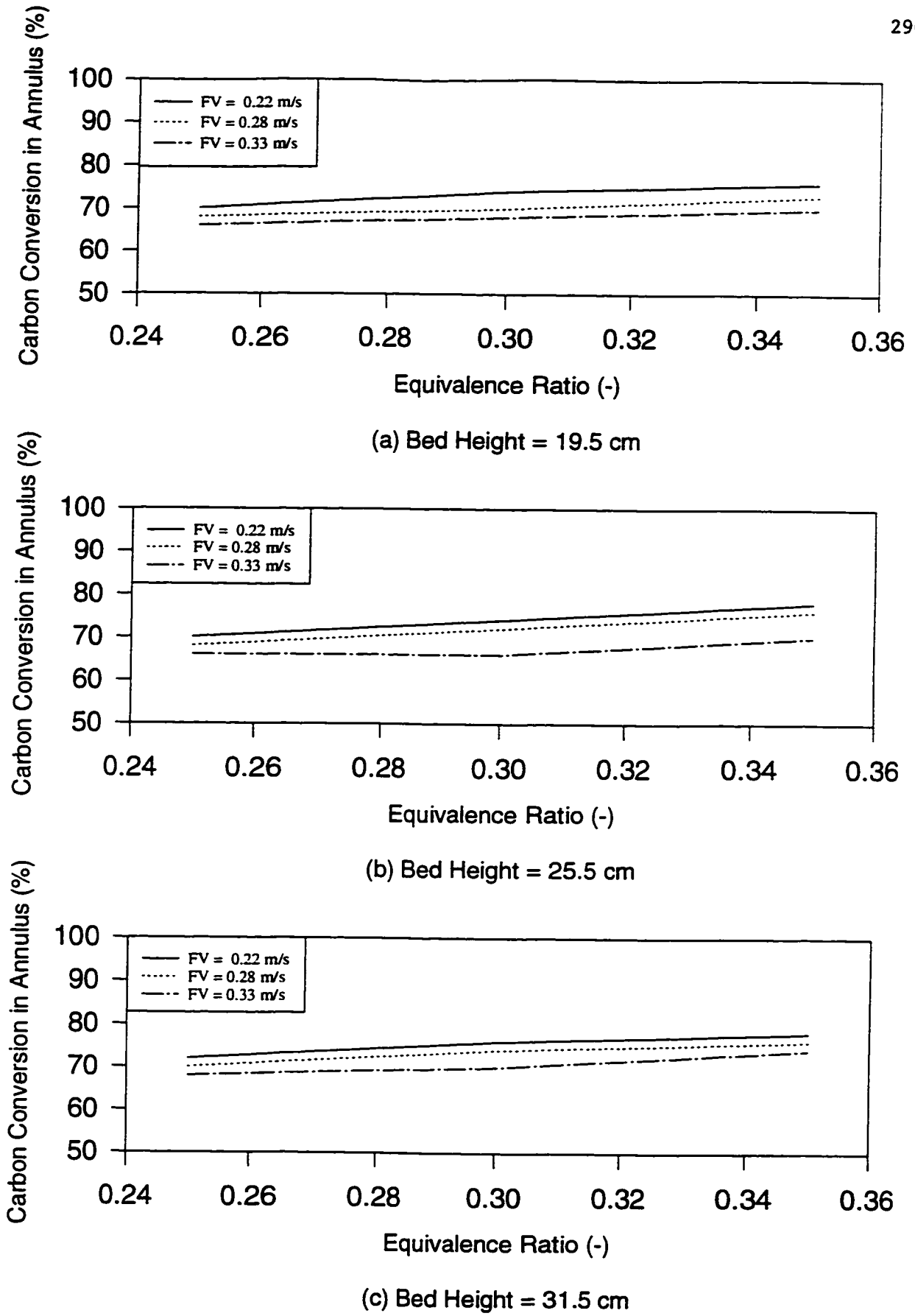

Figure 9.48 Predicted carbon conversion (percent of carbon in annulus) in the annular region at various bed heights, fluidization velocities and equivalence ratios.

point and then decreased with further increases in fluidization velocity. The carbon conversion in the annular region (percent of carbon in annulus) slightly increased when the equivalence ratio was increased and decreased when the fluidization velocity was increased. The decreasing trend of the carbon conversion in both the core and annular regions with increasing fluidization velocity is most probably due to the reduced residence time in both regions and to the greater tendency towards the formation of large bubbles which reduces intermixing between the gaseous and solid components involved in the various gasification reactions.

Regression analyses were performed on the predicted carbon conversions in the core and annular regions (under best fit conditions). The regression equation for the core carbon conversion as a function of bed height, fluidization velocity and equivalence ratio is as follows ($R^2 = 0.93$):

$$CC_{Core} = 10^{1.920} \times BH^{0.055} \times FV^{-0.192} \times ER^{0.424} \tag{9.9}$$

and the regression equation for the annulus carbon conversion as a function of bed height, fluidization velocity and equivalence ratio is as follows ($R^2 = 0.89$):

$$CC_{Annulus} = 10^{1.770} \times BH^{0.090} \times FV^{-0.213} \times ER^{0.323} \tag{9.10}$$

where:

CC_{Core} is the carbon conversion in core region (%)

$CC_{Annulus}$ is the carbon conversion in annular region (%)

BH is the bed height (cm)

FV is the fluidization velocity (m/s)

ER is the equivalence ratio (-)

The correlations clearly show the important role of the equivalence ratio (exponent varying between 0.323 and 0.424) followed by the fluidization velocity (exponent varying between -0.192 and -0.213). The bed height appeared to have insignificant effect on the carbon conversion (exponent varying between 0.055 and 0.090). A comparison between correlated and model-predicted carbon conversions is shown in Figures 9.49 and 9.50 for the core and annular regions, respectively. It clearly shows that a very good fit was obtained.

9.3.3 Sensitivity Analysis

The two-compartment model was used, in conjunction with the carbon conversion correlations (Equations 9.9 and 9.10), to conduct a sensitivity analysis. The effects of bed height, fluidization velocity, equivalence ratio, oxygen concentration in fluidizing gas and rice husk moisture content on the gasifier temperature, mole fraction of the combustible gas components, higher heating value of the gas and overall carbon conversion were investigated. The base value and the range through which each variable was changed are listed in Table 9.41.

9.3.3.1 Effect of bed height. Figures 9.51-9.54 show the effect of bed height on the core, annulus and exit temperatures, mole fractions of the combustible gas components, higher heating value of the gas and overall carbon conversion.

Generally, the core, annulus and exit temperatures show a decreasing trend with increasing bed height (as shown in Figure 9.51). Increasing the bed height from 12.5 to 37.5 cm decreased the temperature in the core from 814 to 752°C, the temperature in the annulus from 799 to 675°C and the temperature at the gasifier exit from 809 to 730°C. The decline in reactor temperature with increasing bed height occurs more gradually in the core region and exit than in the annular region. This could be attributed to the fact that particle circulation slows down with higher bed heights.

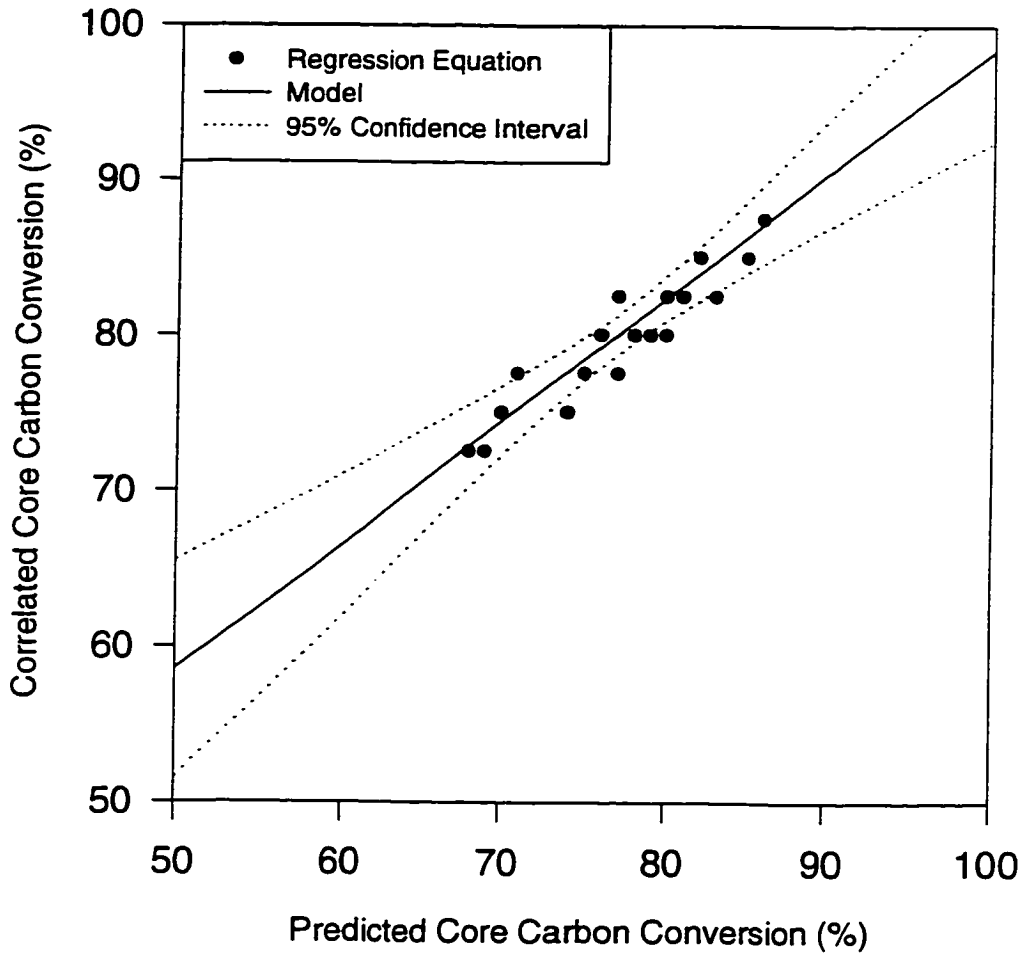

Figure 9.49 Comparison of correlated and predicted core carbon conversions at various bed heights, fluidization velocities and equivalence ratios.

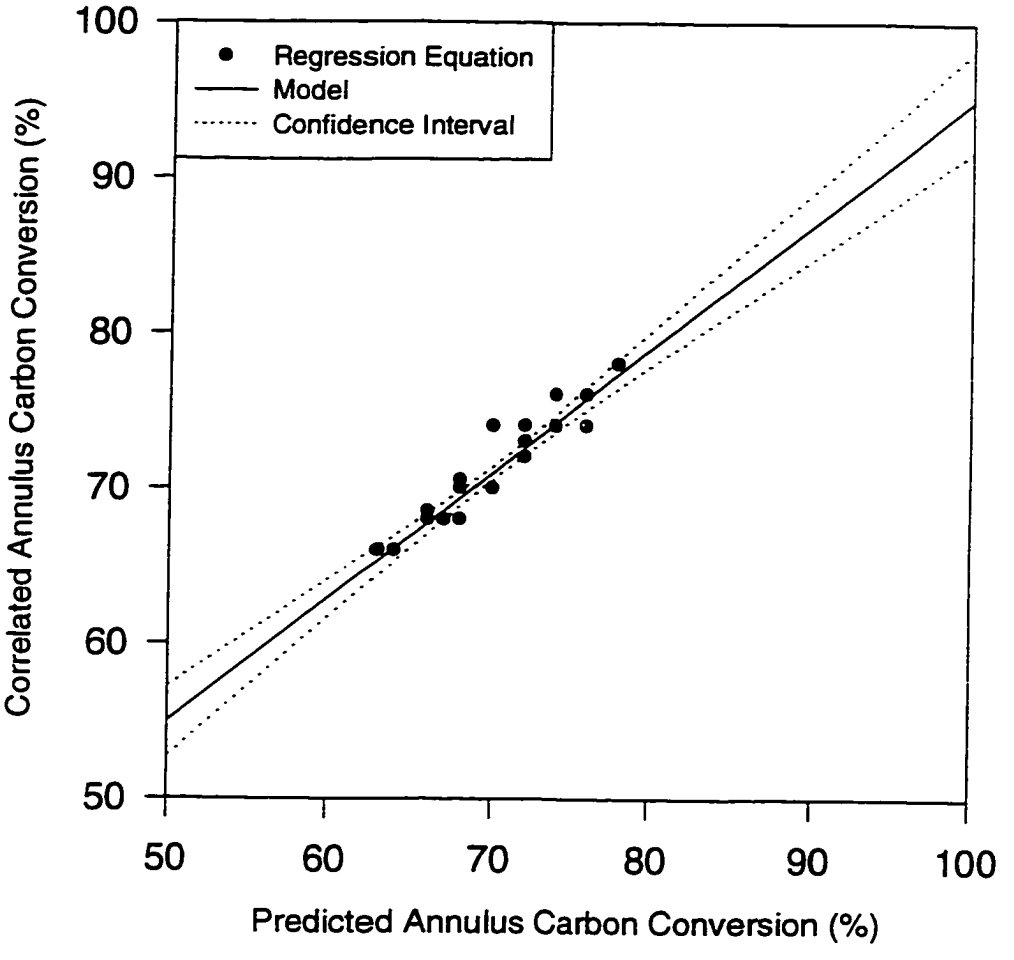

Figure 9.50 Comparison of correlated and predicted annulus carbon conversions at various bed heights, fluidization velocities and equivalence ratio.

Table 9.41 Base Values and Range of Variables Used in the Sensitivity Analysis.

Variable	Unit	Base	Range
Bed Height	(cm)	25.0	12.50 18.75 **25.00** 31.25 37.50
Fluidization Velocity	(m/s)	0.30	0.150 0.225 **0.300** 0.375 0.450
Equivalence Ratio	(-)	0.28	0.140 0.210 **0.280** 0.350 0.420
Oxygen Concentration	(%)	20.0	10.00 15.00 **20.00** 25.00 30.00
Moisture in Rice Husk	(%)	20.0	10.00 15.00 **20.00** 25.00 30.00

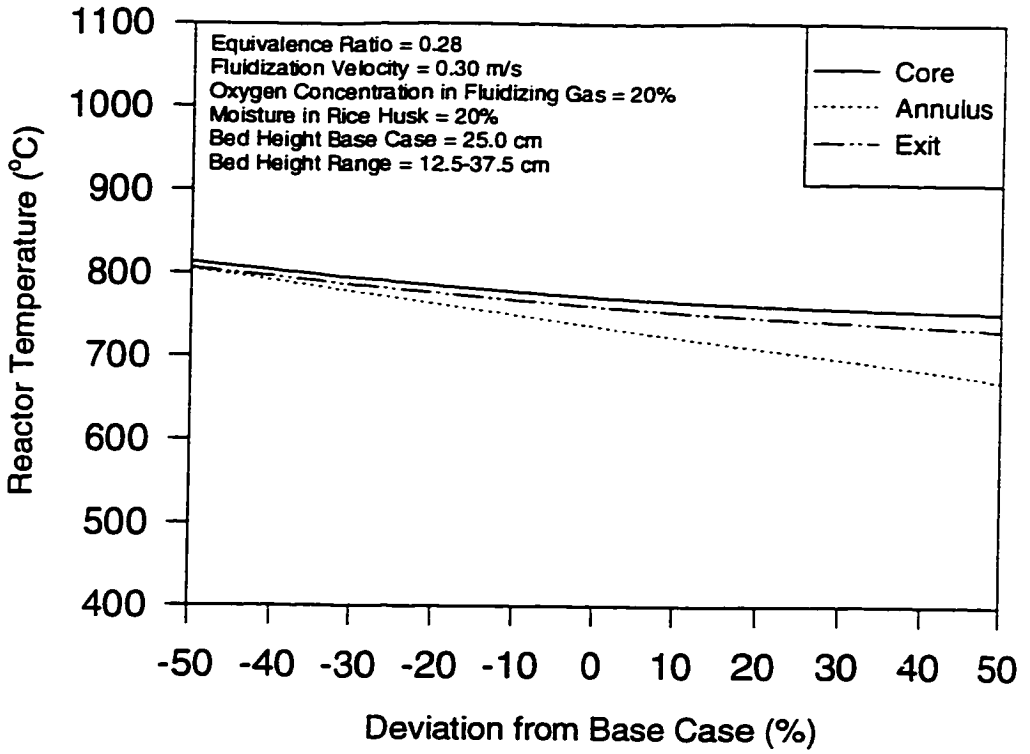

Figure 9.51 Effect of bed height on the predicted reactor temperatures.

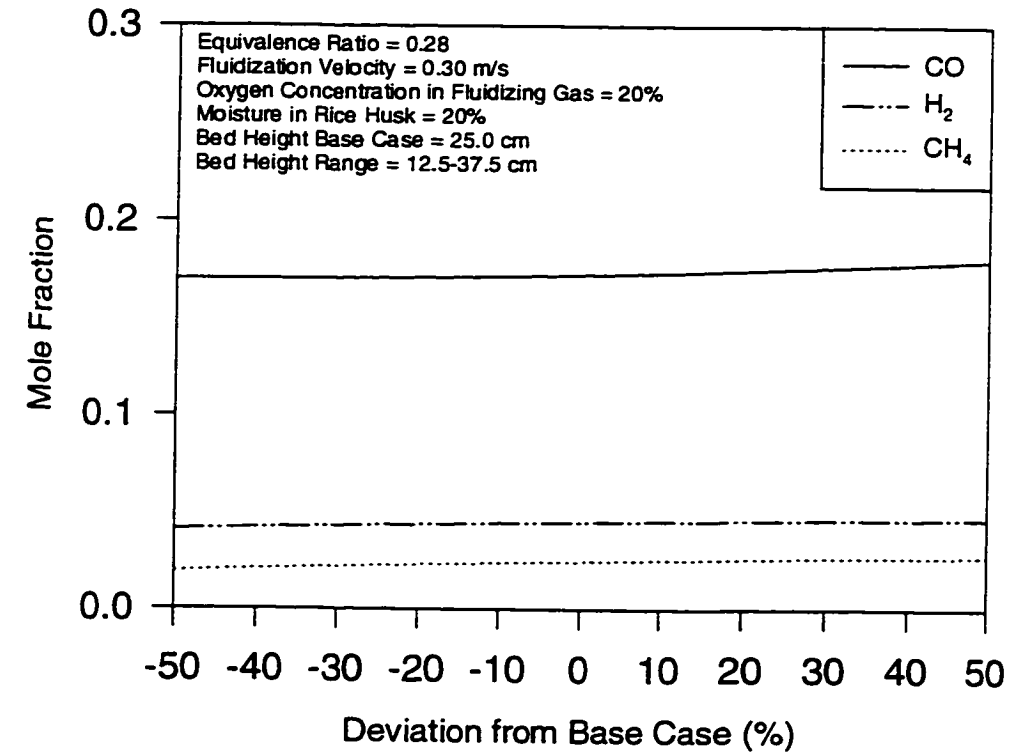

Figure 9.52 Effect of bed height on the predicted mole fractions of the fuel gas components.

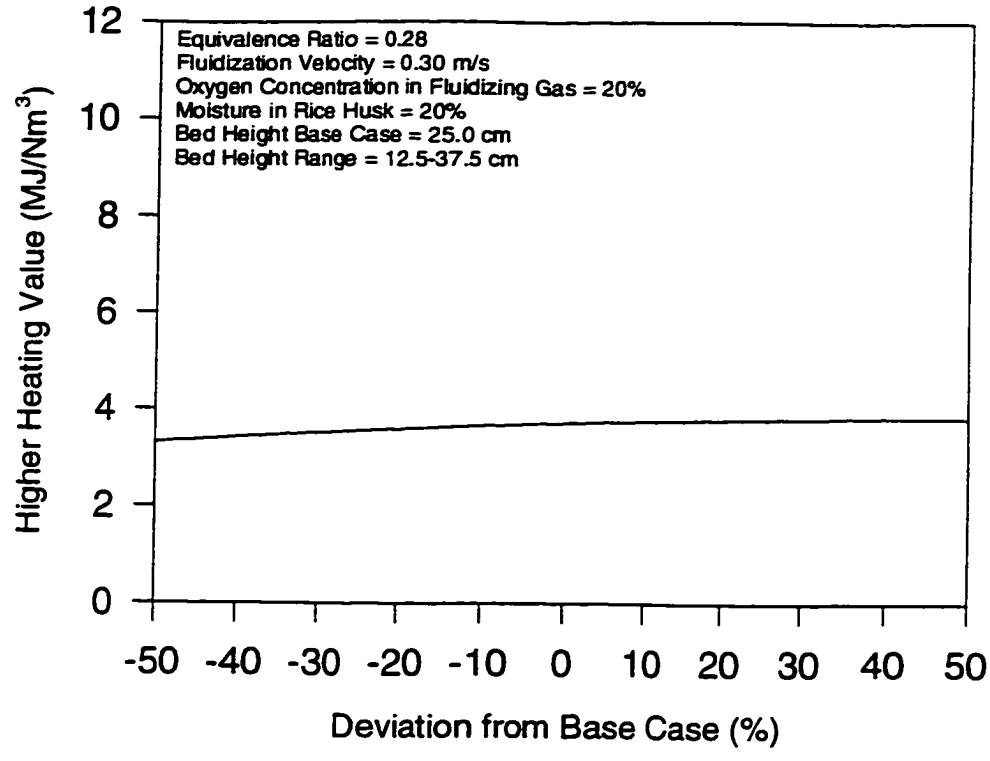

Figure 9.53 Effect of bed height on the predicted gas higher heating value.

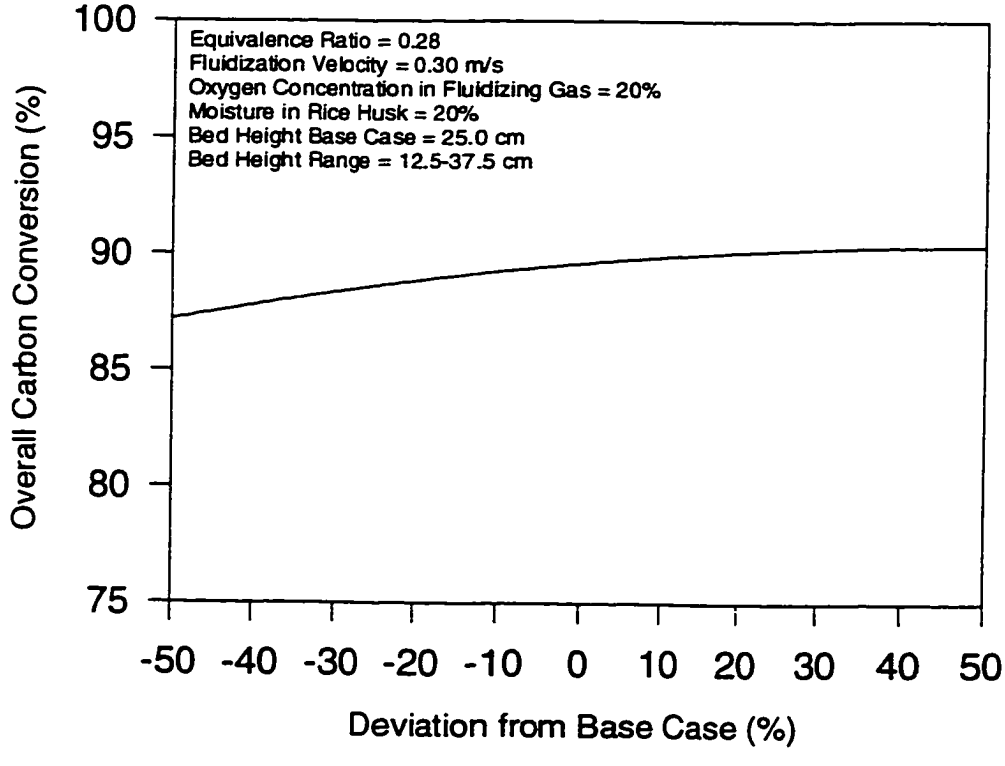

Figure 9.54 Effect of bed height on the predicted overall carbon conversion.

The mole fractions of the combustible components (CO, H_2 and CH_4) and the higher heating value of the gas are relatively insensitive to variations of ± 50% of the bed height from the base case as shown in Figures 9.52 and 9.53, respectively. This ability of the fluidized bed gasifier to produce a gas with a relatively constant heating value regardless of the bed height is an indication of the good mixing and fluidization achieved in the reactor and could be an important feature in some applications where a constant heating value may be desirable.

Changes in the bed height only had a moderate effect on the overall carbon conversion. Although the bed height was varied from 12.5 to 37.5 cm (200% increase in bed height) in this sensitivity analysis, the overall carbon conversion increased from 87.0 to 90.5% (only 4.0%). This could be due to the nature of the two compartment model which accurately describe the phenomena taking place in the reactor.

9.3.3.2 Effect of fluidization velocity. Figures 9.55-9.58 show the effect of fluidization velocity on the core, annulus and exit temperatures, mole fractions of the combustible gas components, higher heating value of the gas and overall carbon conversion.

Figure 9.55 shows increase in the core, annulus and exit temperatures with increases in the fluidization velocity. Increasing the fluidization velocity from 0.15 to 0.45 m/s increased the temperature from 524 to 872°C in the core, from 499 to 847°C in the annulus and from 513 to 863°C at the gasifier exit. The sensitivity of the reactor temperature to the fluidization velocity could be attributed to the fact that increasing the fluidization velocity increased the core gas velocity and circulation rate within the annular region with the consequent enhanced char particle entrainment into the annulus, a situation which tends to increase the reactor temperature.

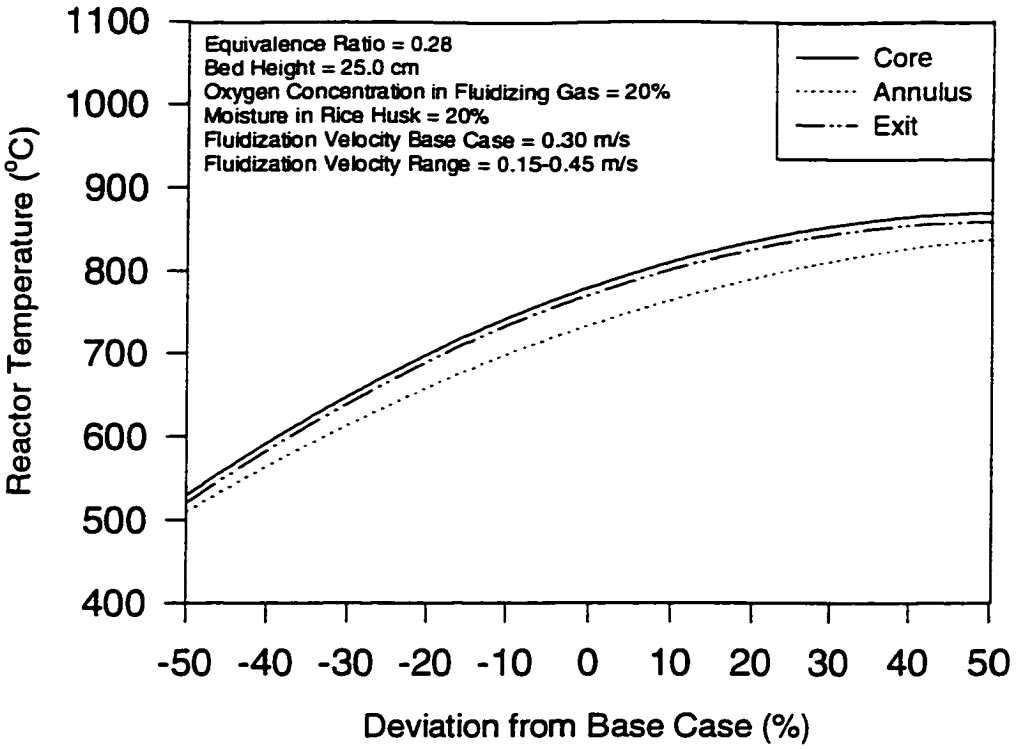

Figure 9.55 Effect of fluidization velocity on the predicted reactor temperatures.

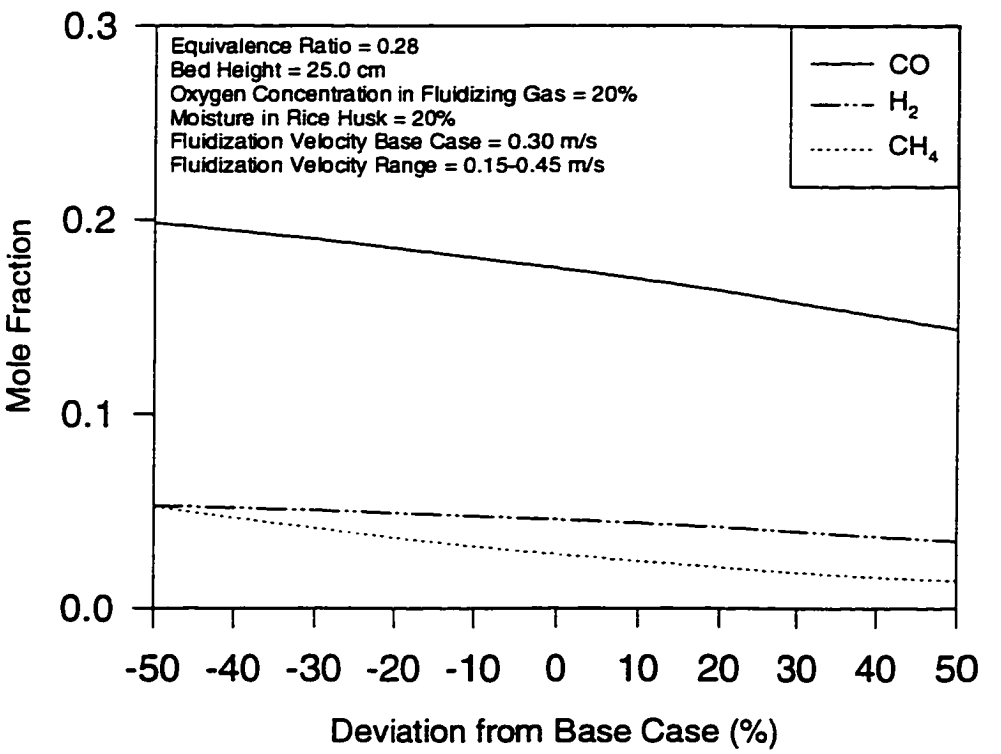

Figure 9.56 Effect of fluidization velocition on the predicted mole fractions of the fuel gas components.

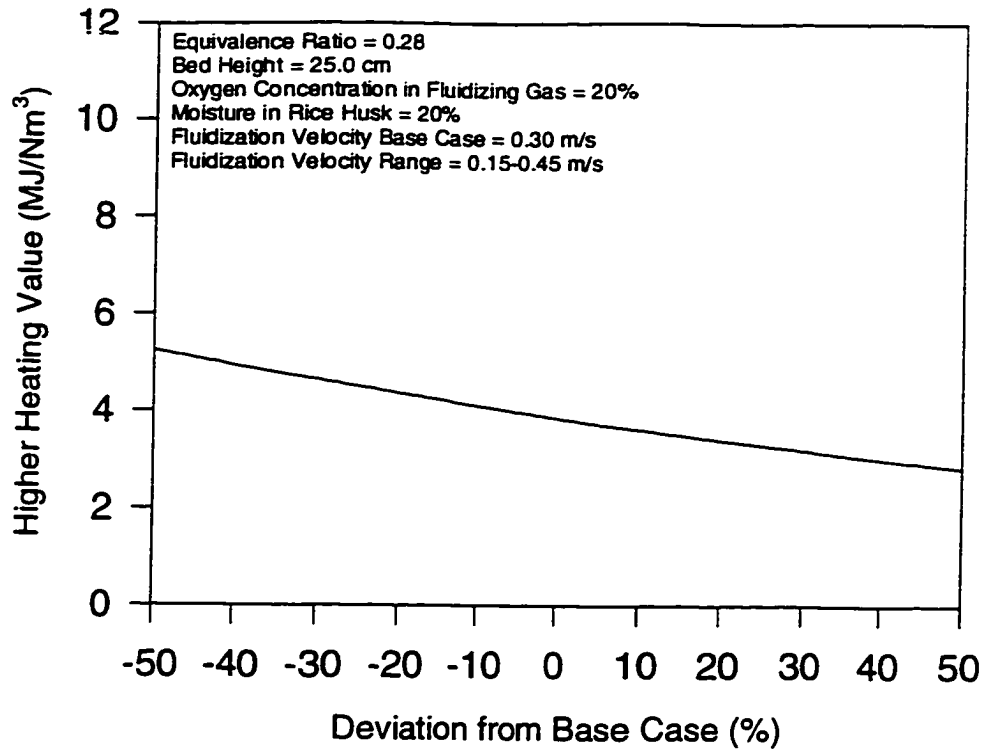

Figure 9.57 Effect of fluidization velocity on the predicted gas higher heating value.

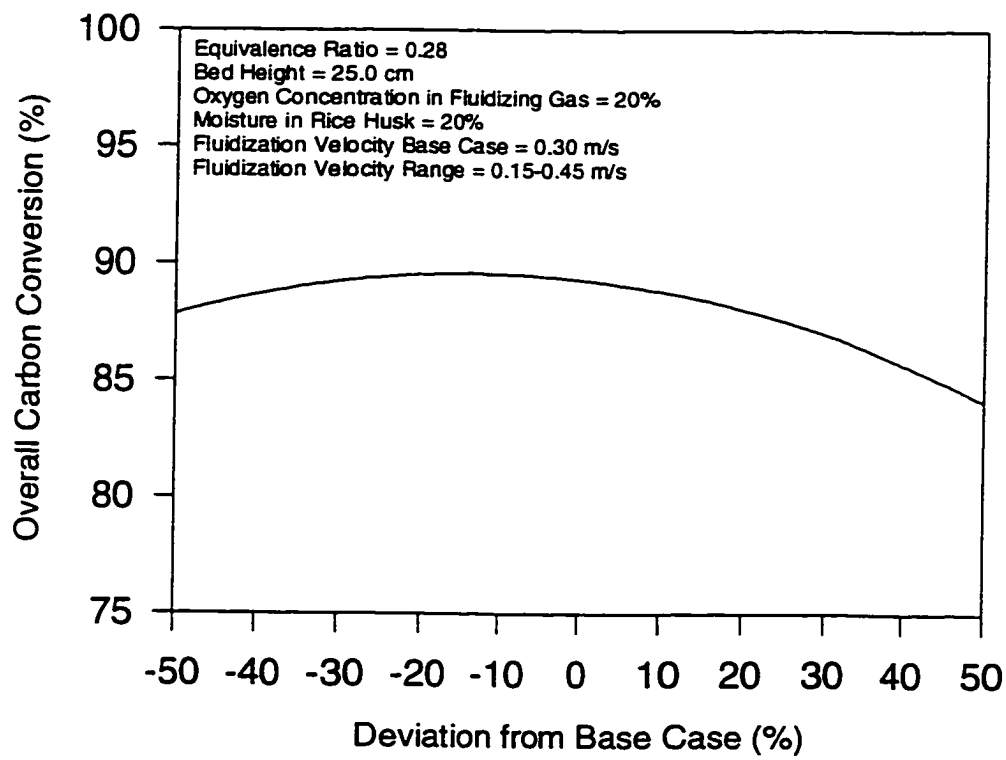

Figure 9.58 Effect of fluidization velocity on the predicted overall carbon conversion.

In Figure 9.56, the mole fractions of the combustible gas components CO, H_2 and CH_4 are seen to decrease as the fluidization velocity increases. When the fluidization velocity was increased from 0.15 to 0.45 m/s, the predicted mole fractions of CO, H_2 and CH_4 decreased from 19.6 to 14.5%, 5.2 to 3.5% and 5.0 to 1.6%, respectively. The higher heating value of the gas showed a similar decrease (from 5.1 to 3.0 MJ/Nm^3) with increasing fluidization velocity as shown in Figure 9.57. Increasing the fluidization velocity would reduce the amount of chemical energy in the system thereby boosting the temperature of the system by converting the energy of the product gas to sensible heat.

The overall carbon conversion slightly increased with fluidization velocity until a point is reached and then decreased with further increase in fluidization velocity as illustrated in Figure 9.58. At this point, it is possible that higher linear velocities were attained in the reactor resulting in reducing the retention time of gases and enhancing the carry over of fine char particles from the reactor and, hence, lower conversion to gases. This effect shows clearly the importance of considering particle elutriation in the solids population balance of a fluidized bed.

9.3.3.3 Effect of equivalence ratio. Figures 9.59-9.62 show the effect of equivalence ratio on the core, annulus and exit temperatures, mole fractions of the combustible gas components, higher heating value of the gas and overall carbon conversion.

Figure 9.59 shows that increasing the equivalence ratio from 0.14 to 0.42 resulted in proportional increases in the gasifier core, annulus and exit temperatures of from 624 to 950°C, from 588 to 932°C and from 606 to 939°C, respectively. This observation facilitates control of the operating temperature through simple adjustment of the air/fuel ratio.

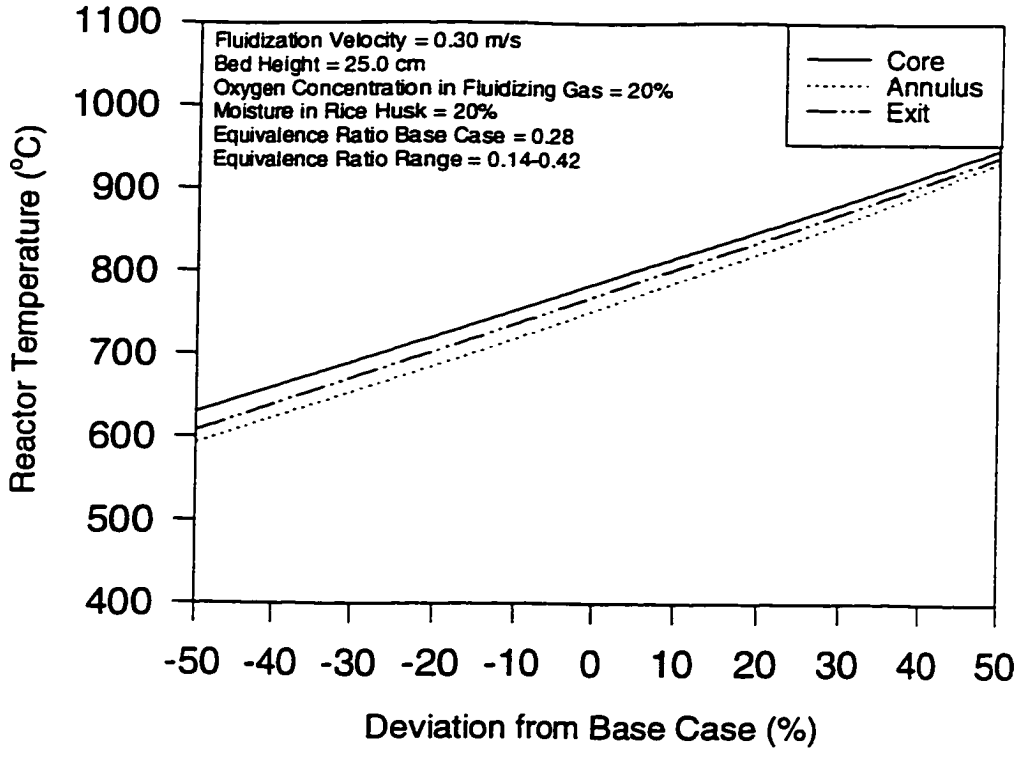

Figure 9.59 Effect of equivalence ratio on the predicted reactor temperatures.

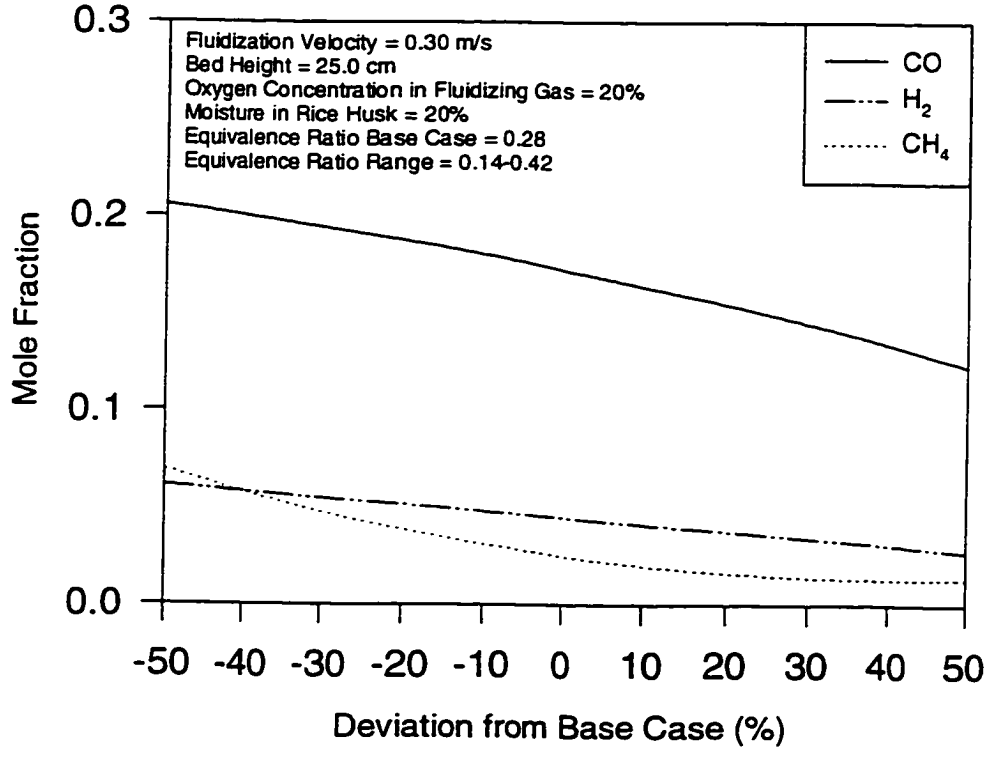

Figure 9.60 Effect of equivalence ratio on the predicted mole fractions of the fuel gas components.

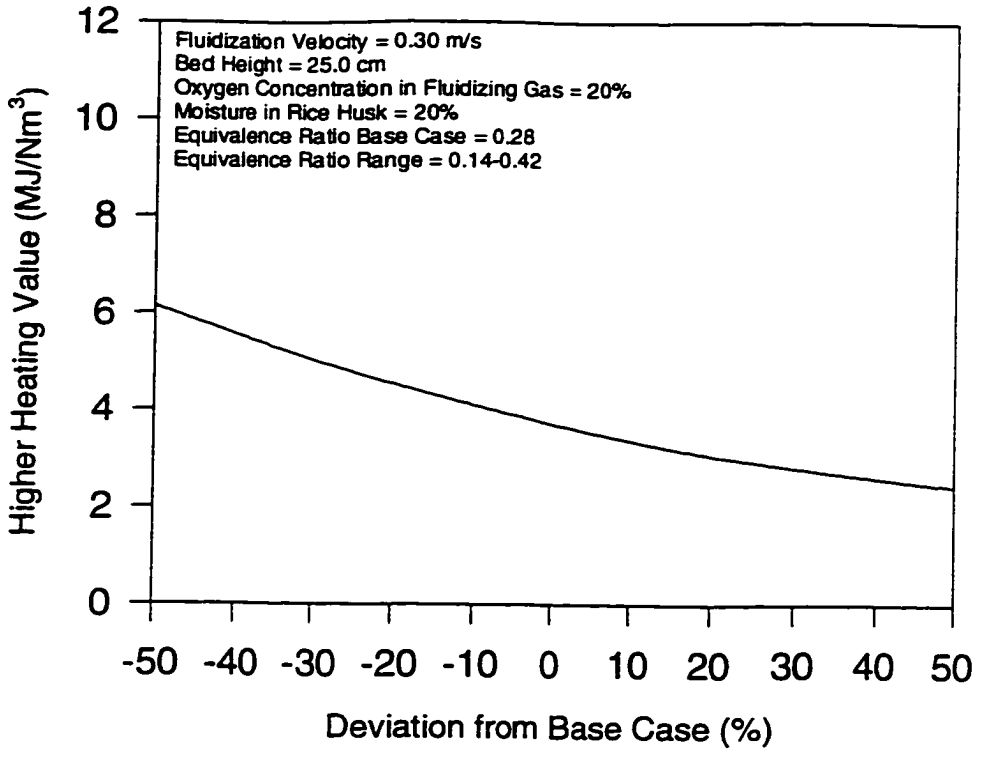

Figure 9.61 Effect of equivalence ratio on the predicted gas higher heating value.

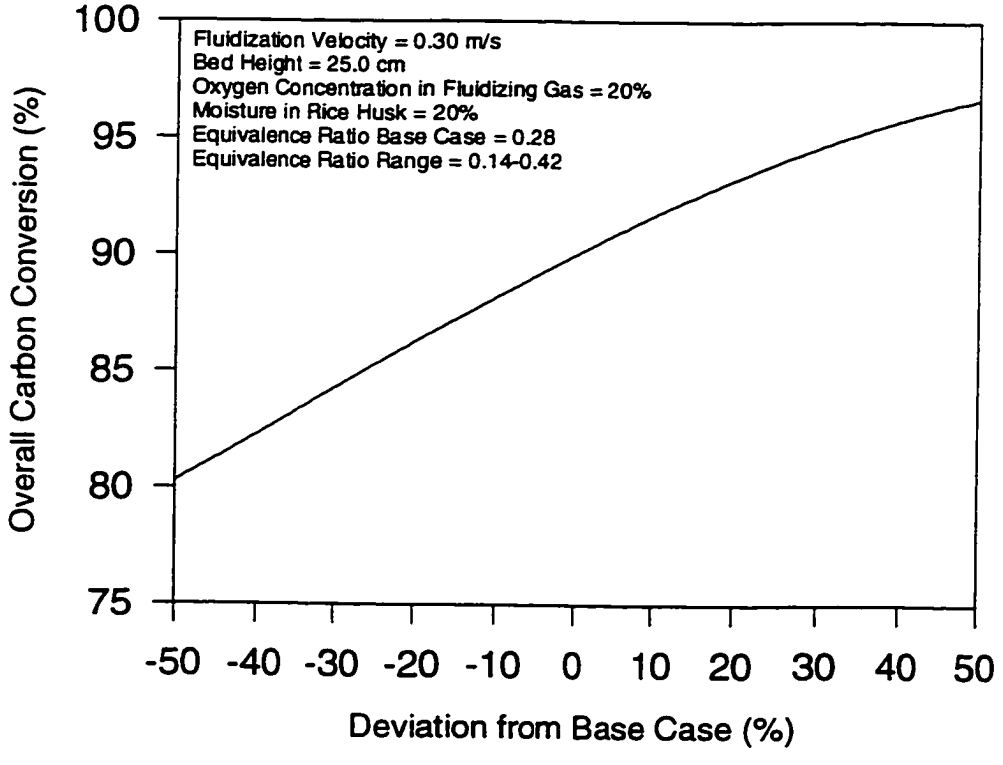

Figure 9.62 Effect of equivalence ratio on the predicted overall carbon conversion.

The equivalence ratio also appears to have a pronounced effect on mole fractions of the combustible gas components CO, H_2 and CH_4 and the higher heating value of the gas. Increasing the equivalence ratio from 0.14 to 0.42 decreased the mole fraction of CO from 20.6 to 12.3%, the mole fraction of H_2 from 6.1 to 2.7%, the mole fraction of CH_4 from 6.9 to 1.3% (Figure 9.60) and the higher heating value of the gas from 6.2 to 2.4 MJ/Nm^3 (Figure 9.61). The counterpart of the increase in reactor temperature (energy production) with an increasing equivalence ratio is that the output gas is gradually poorer in combustible gases as the equivalence ratio is increased, resulting in lower gas higher heating value. Thus, one has to compromise between a low operating temperature leading to higher percentage of combustible gases accompanied by higher percentages of char and tar, and a high temperature producing less char and tar as well as low combustible gases.

On increasing the equivalence ratio from 0.14 to 0.42, the overall carbon conversion increased from 80.2 to 96.6% as shown in Figure 9.62. The higher degree of combustion with the consequent increase in operating temperature with equivalence ratio spurs all reaction rates and thus increases carbon conversion.

9.3.3.4 Effect of oxygen concentration. Figures 9.63-9.66 show the effect of oxygen concentration in the fluidizing gas on the core, annulus and exit temperatures, mole fraction of the combustible gas components, higher heating value of the gas and overall carbon conversion.

It is apparent from Figure 9.63 that reactor temperature increases with the relative amount of oxygen available in the fluidizing gas. Increasing the concentration of oxygen in the fluidizing gas from 10 to 30% increased the gasifier core, annulus and exit temperatures from 520 to 887°C, from 475 to 871°C and from 494 to 884°C, respectively. The availability of more oxygen favours the exothermic combustion reactions and, hence, an increased reactor temperature.

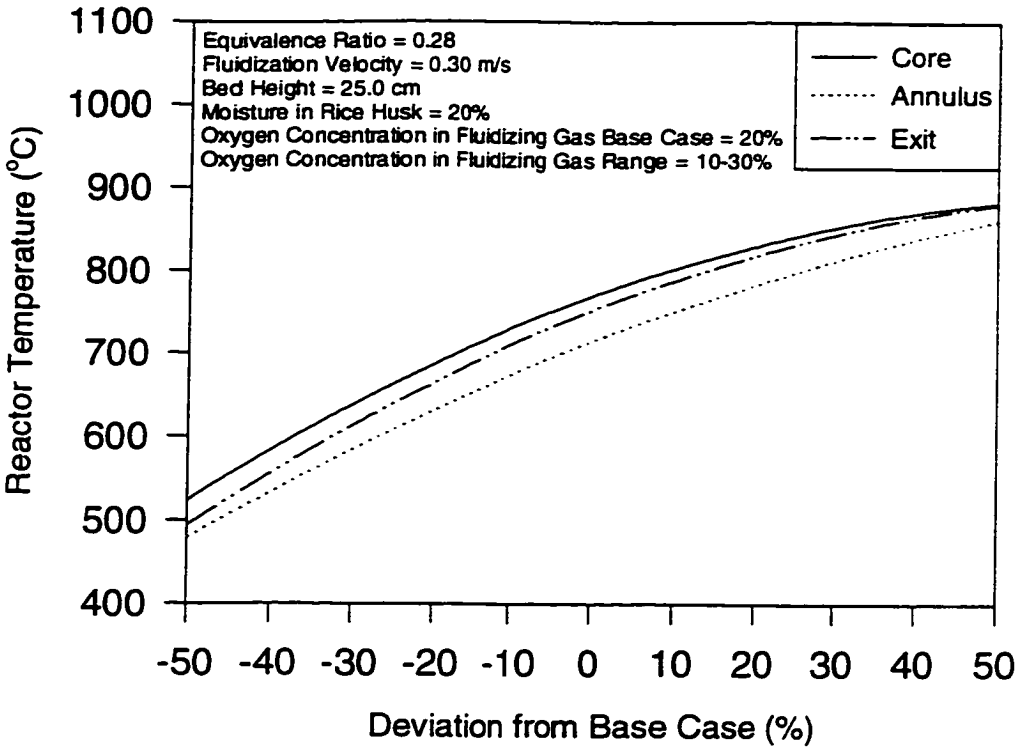

Figure 9.63 Effect of oxygen concentration in fluidizing gas on the predicted reactor temperatures.

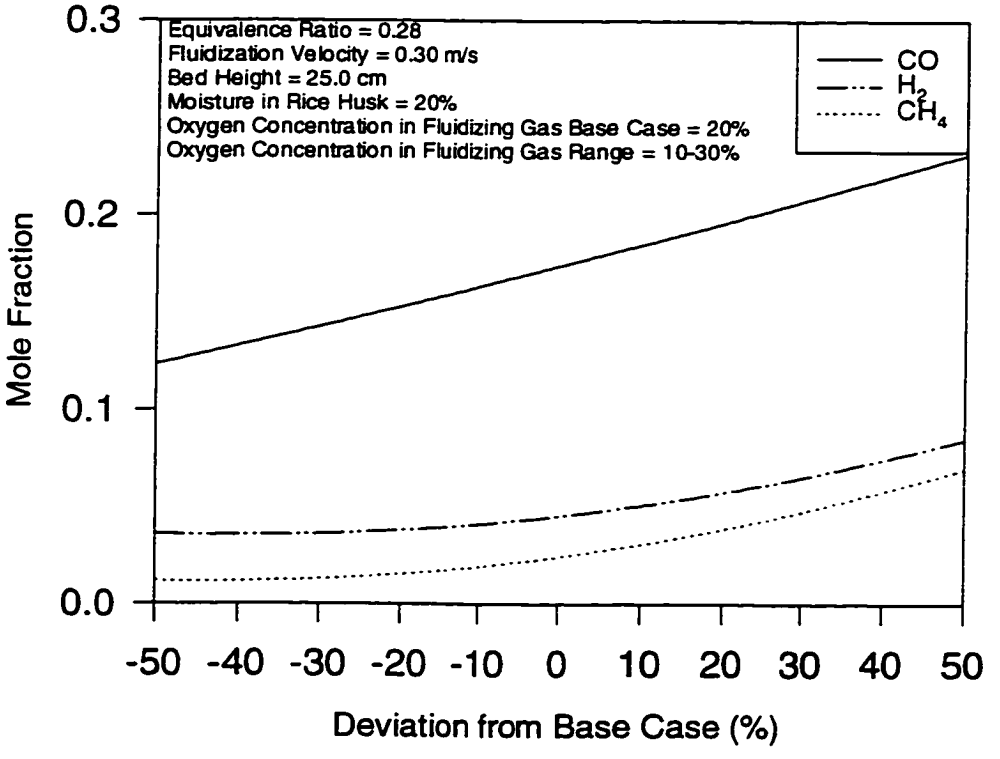

Figure 9.64 Effect of oxygen concentration in fluidizing gas on the predicted mole fractions of the fuel gas components.

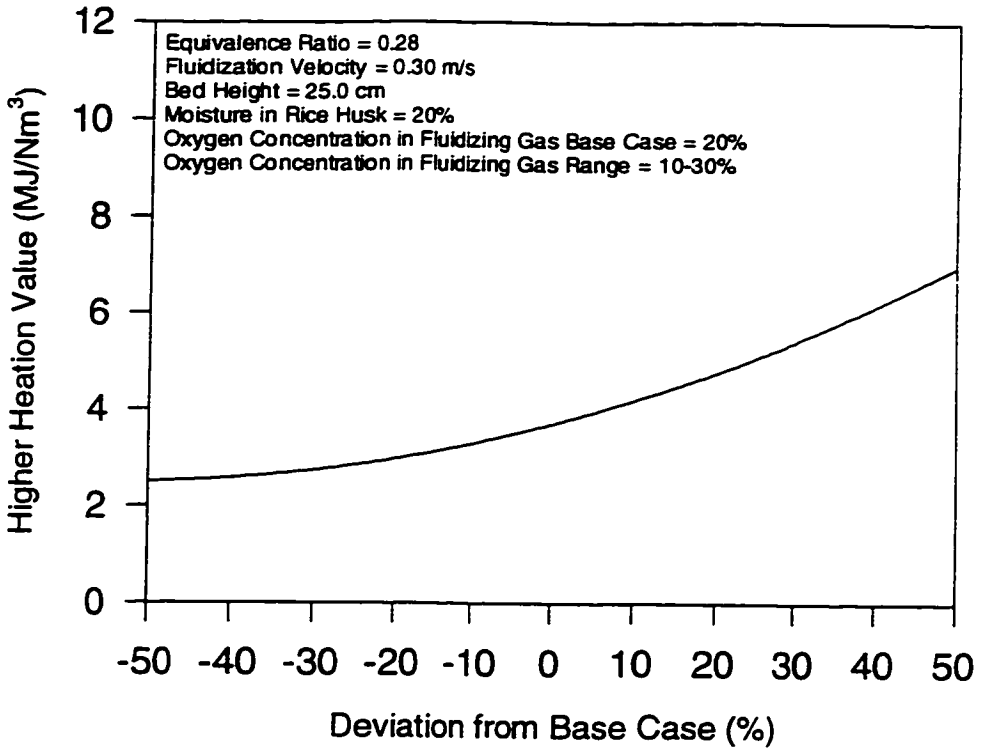

Figure 9.65 Effect of oxygen concentration in fluidizing gas on the predicted gas higher heating value.

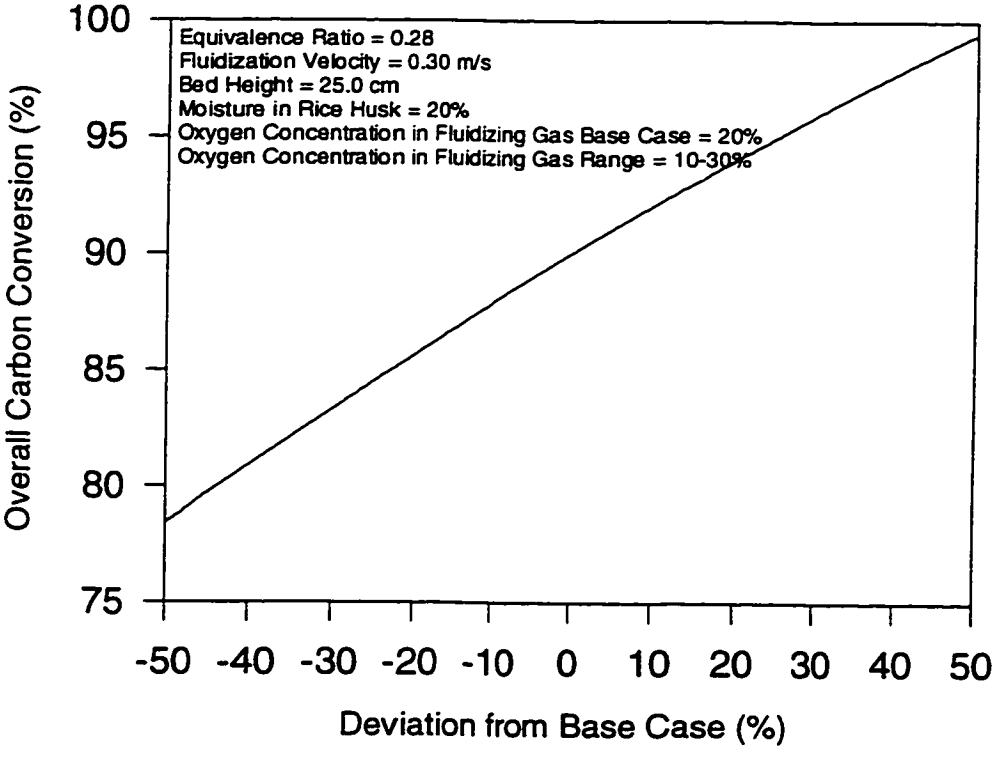

Figure 9.66 Effect of oxygen concentration in fluidizing gas on the predicted overall carbon conversion.

Generally, increases in the mole fractions of CO, H_2 and CH_4 were observed when the oxygen concentration in the fluidizing gas was increased from 10 to 30% (Figure 9.64). However, the increase in the mole fraction of CO was substantial, owing to the increase of the displacement of the shift reaction in the sense of increased production of CO at the expense of H_2. There was, also, a significant increase (from 2.5 to 7.0 MJ/Nm^3) in the predicted higher heating value of the gas when the oxygen concentration in the fluidizing gas was increased from 10 to 30% as shown in Figure 9.65. The increase in higher heating value is the direct result of increased concentration of the combustible components of the gas (CO, H_2 and CH_4) and of decreased concentrations of N_2 in the inlet gas.

An increase in the concentration of oxygen in the fluidizing gas from 10 to 30% significantly increased the overall carbon conversion from 79.1 to 98.6% as shown in Figure 9.66. Increases in the concentration of oxygen in the fluidizing gas are critical, since more heat is provided through increased combustion reactions which enhances endothermic gasification reactions, thereby resulting in higher overall carbon conversion.

9.3.3.5 Effect of rice husk moisture content. Figures 9.67-9.70 show the effect of moisture content in rice husk on the predicted core, annulus and exit temperatures, mole fractions of the combustible gas components, higher heating value of the gas and overall carbon conversion. This parameter was investigated because of its variability (according to rice variety and weather conditions) in typical feedstocks.

As shown in Figure 9.67, increased moisture in the rice husk was found to moderate the reactor core, annulus and exit temperatures. When the moisture content is increased from 10 to 30%, the reactor core, annulus and exit temperatures decreased from 800 to 571°C, from 768 to 504°C and from 791 to 545°C, respectively. Although too much water makes the gasification temperature more difficult to sustain as reported by

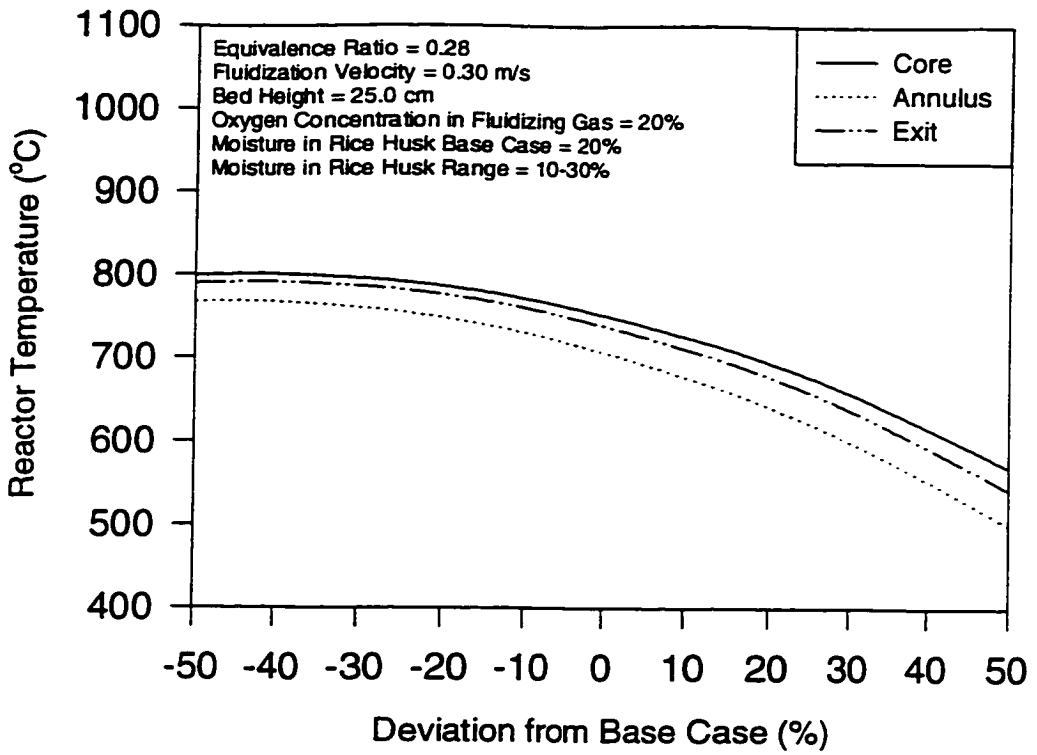

Figure 9.67 Effect of rice husk moisture content on the predicted reactor temperatures.

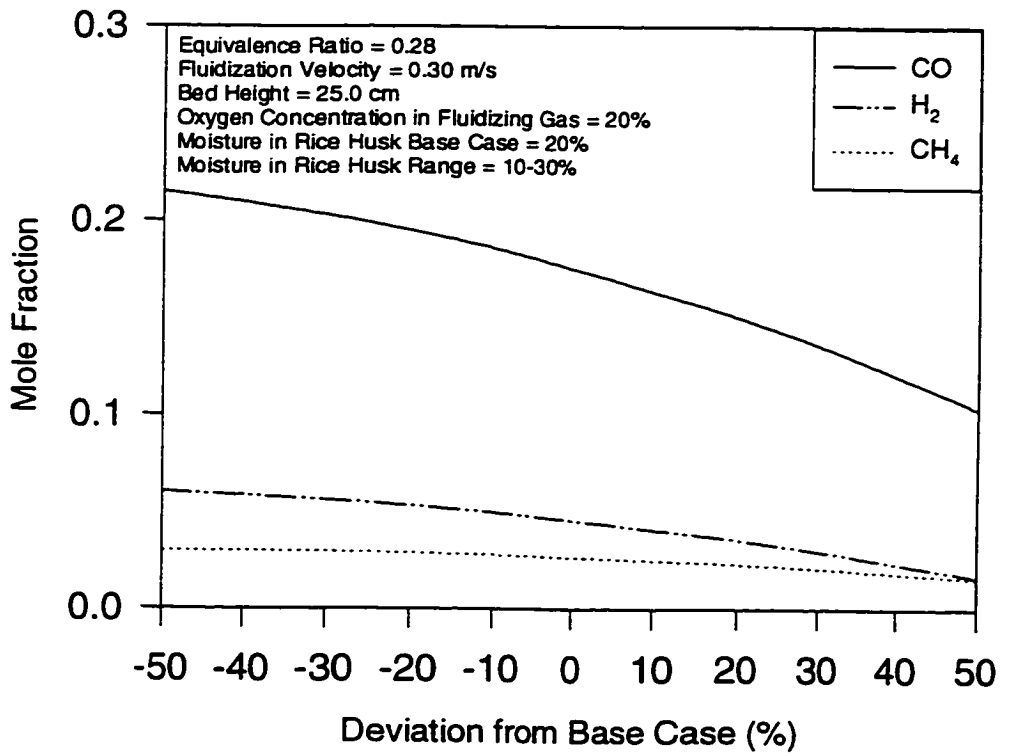

Figure 9.68 Effect of moisture in rice husk on the predicted mole fractions of the fuel gas components.

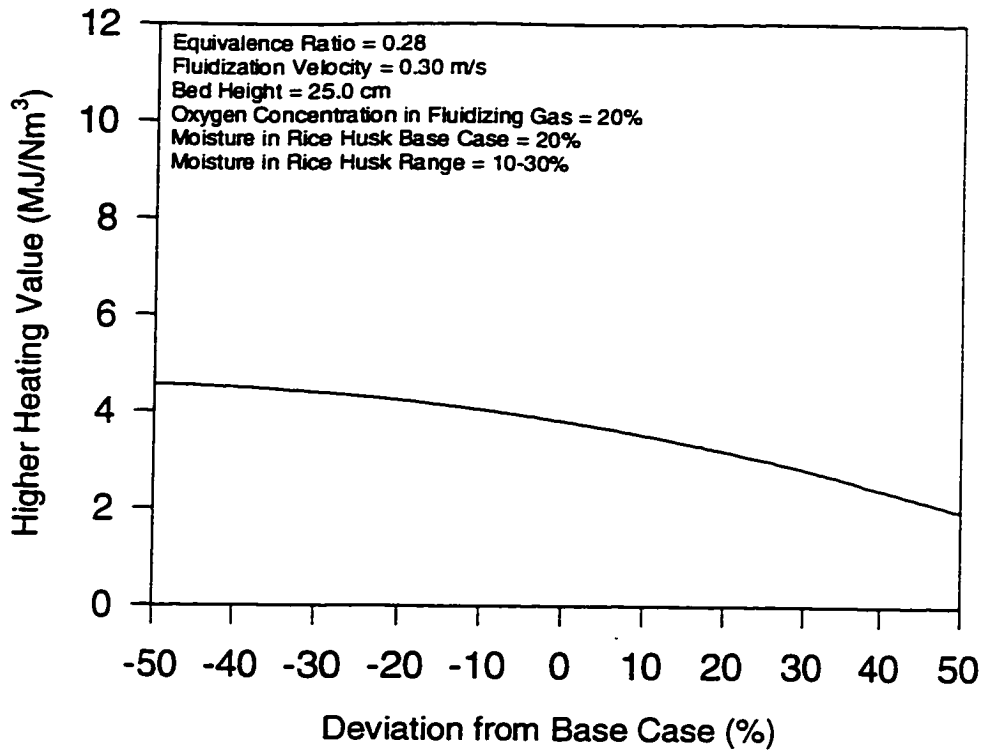

Figure 9.69 Effect of rice husk moisture content on the predicted gas higher heating value.

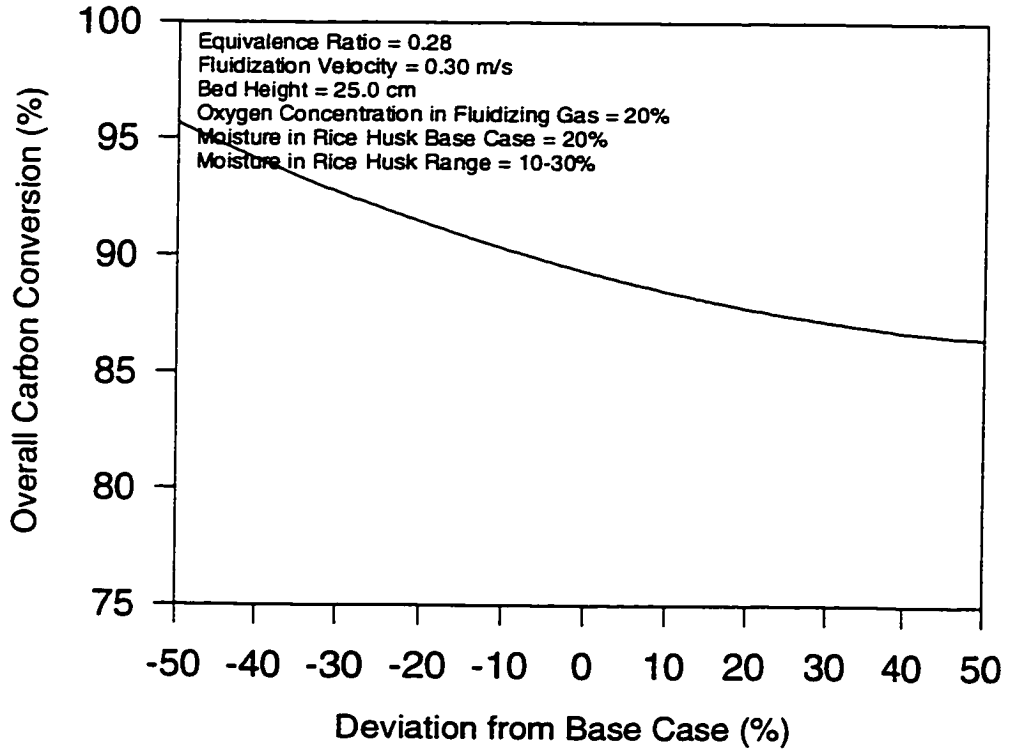

Figure 9.70 Effect of rice husk moisture content on the predicted overall carbon conversion.

Black et al. (1980) and Bacon et al. (1985), the reduced reactor temperature is advantageous for slagging fuels because the endothermal steam generation exposes the mineral matter of the fuel to lower temperatures and reduces slag formation. This, however, should be balanced against vapourization of water and poor ignition of wet fuel.

Figure 9.68 shows that the mole fractions of CO and H_2 decreased with increasing moisture in rice husk whereas that of CH_4 remained approximately constant. This behaviour could be related to the change in temperature. A decrease in temperature results in a decrease of the rate of reaction between water vapour and carbon, resulting in a decrease in the production of the mole fractions of CO and H_2. Also, increased moisture in rice husk severely reduces the higher heating value of the gas (from 4.5 to 2.0 MJ/Nm^3) as shown in Figure 9.69. A high moisture content of the feedstock increases the amount of water in the product gas and, thus, its sensible heat at the cost of the chemically bonded energy. Apparently, increased loss in gas higher heating value occurs when the moisture content was increased from 20 to 30%. Therefore, to obtain a gas of significant heating value, the moisture content of rice husk should not exceed 20%.

The carbon conversion decreases from 96.0 to 86.2% when the moisture content in rice husk was increased from 10 to 30% (Figure 9.70). This is due to the latent heat of the evaporation of water which absorbs a large amount in the energy generated in the gasification process and lowers the reaction temperature.

10. DISCUSSION

10.1 Preliminary Experiments

10.1.1 Physical and Chemical Properties of Rice Husks

10.1.1.1 Physical properties. The three physical properties of rice husk studied were: moisture content, bulk density and particle size distribution.

10.1.1.1.1 Moisture content: The moisture content of rice husk substantially affects its quality as a fuel source. An increase in moisture content of the rice husk decreases its heating value, which in turn reduces the conversion efficiency and performance of the system because a large amount of energy would be used for vapourization of the fuel moisture during conversion. Thus, a dry fuel material is preferred for combustion, whereas a certain amount of moisture in the fuel is beneficial for gasification (Desrosiers, 1981; and Ghaly et al., 1989a). The rice husks, as-received, were fairly dry; the moisture contents measured ranged from 8.68 to 10.44%. Hence, drying rice husk before feeding into combustion and/or gasification systems was not necessary. The measured values are very much within the range reported in the literature of 5 to 16% (Beagle, 1978; and Kaupp and Goss, 1981). The moisture contents of the rice husk samples that originated from Sierra Leone (ROK 16, ROK 14, ROK 32, CP 4 and Pa Potho) were similar to the sample obtained from the U. S. A. (Lemont LG).

10.1.1.1.2 Bulk density: The low bulk density of rice husks (86-114 kg/m^3) may reduce its residence time in the reactor, resulting in a lower conversion efficiency. It may, also, give rise to poor mixing characteristics and a non-uniform temperature distribution, both of which can create unfavourable operating conditions of thermochemical conversion systems (Bilbao et al., 1988). Densification of rice husk by briquetting or pelletizing can increase its

density to a range of 550-700 kg/m^3 (Kaupp, 1984). Some of the major advantages of these techniques include high volumetric density and energy, lower transportation and storage costs and lower emissions during combustion (Kaupp, 1984; and Carre et al., 1988). However, the high investment and energy input required for briquetting and pelletization as well as the poor ignitability are the major constraints of rice husk densification which make such processes unattractive. The measured values of bulk density are within the ranges reported in the literature of 83-125 kg/m^3 (Kaupp, 1984; BTG, 1990; and Fan et al., 1992).

10.1.1.1.3 Particle size distribution: For efficient thermochemical conversion processes, it is generally preferable to use a uniform feedstock with respect to particle size and distribution. For example, a particle size too large may cause secondary reactions to occur within the particles that may lead to the formation of undesired products such as char and tars. On the other hand, if the particle size is too small, the feedstock may not be retained in the reaction zone long enough for complete conversion, thereby resulting in low conversion efficiencies. However, feeding small particles such as rice husk directly into the bed (Ghaly et al., 1989b) has the advantage of diminishing the carry-over of fine particles. Particle size and size distribution also affect fuel flow in the reactor; incorrect dimensions may cause incomplete conversion (Miles, 1982). The measured size distribution of the as-received rice husk varieties (6.2-10.0 mm long and 1.7-2.4 mm wide) was considered suitable for fluidized bed gasification and was handled very easily by an auger feeding system.

10.1.1.2 Thermochemical properties. The thermochemical properties of rice husk studied were: heating value (higher and lower), proximate analysis, ultimate analysis, ash composition and ash fusibility.

10.1.1.2.1 Heating value: The heating value is an important thermal property for the modeling of thermochemical conversion systems (Jenkins and Summer, 1986). It is usually expressed as higher heating value (HHV) and lower heating value (LHV). The higher heating

value is the amount of sensible heat which can be released from the combustion of fuel if water, both in the fuel and generated during combustion, exit at a steady flow in a condensed state. The lower heating value is the amount of sensible heat which is extracted from the combustion of fuel if water, both in the fuel and generated during combustion, exit at a steady flow in a gaseous state (Chandra and Payne, 1986). Since it is very difficult to recover the heat of vapourization in actual gasification processes, the higher heating value provides high estimates of the heating value of the fuel. It is, therefore, realistic to present the heating value of a fuel for gasification as lower heating value, which excludes the heat of vapourization of the water produced, on an ash inclusive basis and with reference to the moisture content of the fuel.

The lower heating values of the six rice husk varieties were very similar (13.24-16.20 MJ/kg). ROK 16 rice husk, however, had a higher energy content (16.20 MJ/kg). The reasonably good energy content of ROK 16 rice husk could be attributed to its lower ash content (15.30%) compared to those of Lemont LG, ROK 14, ROK 32, CP 4 and Pa Potho rice husk samples (18.20-24.60%). This further confirmed the fact that decreases in ash content result in higher energy content of the fuel. Weight for weight, rice husk has an energy value about half that of coal (≈ 32.00 MJ/kg) and is, therefore, an important potential energy source.

10.1.1.2.2 Proximate analysis: The results showed that rice husk has a relatively high volatile matter content (63.00-70.20%), high ash content (15.30-24.60%) and low fixed carbon content (12.40-14.50%). The volatile matter content of fuels is important because it characterizes the expected contamination of the product gas with condensible vapours in any thermochemical conversion system. The volatiles burn as gaseous products in the flame, whereas the fixed carbon burns slowly and without flame. Therefore, the volatile matter content of fuel has a great influence on the combustion process and on the design of the combustion chamber (Strehler, 1985). Rice husk, as other biomass fuels, has relatively high volatile matter content (60 to 70%) compared to lignite and bituminous coals (25 to 40%). Because of the high volatile matter content, rice husk is more readily devolatilized than lignite

and bituminous coals, thus, yielding considerably less fixed carbon residue (Graboski and Bain, 1981). This makes rice husk a potentially useful fuel for pyrolysis and gasification; less heat is required for reactions due to the high volatile matter content which makes it possible to gasify at lower temperatures (Schiefelbein, 1989).

The ash content of rice husk is startlingly high (15.30-24.60%) compared to that of wood of 1-2% (BTG, 1990) and wheat straw of 3-5% (Ghaly and Al-Taweel, 1990). Continuous ash removal during gasification is, therefore, essential when rice husk is used as a fuel.

Beagle (1978) reported the contents of volatile matter, fixed carbon and ash in rice husk to range from 56.40 to 69.30%, 12.70 to 17.40% and 15.80 to 23.00%, respectively. The ranges compiled and reported by Ebeling and Jenkins (1985) for rice husk volatile matter, fixed carbon and ash contents were 60.2 to 62.1%, 20.7 to 21.8% and 16.9 to 17.2%, respectively. It has been noted that the presence of even minute amounts of water can greatly influence these tests (Kaupp, 1984). This could be the reason for the existence of a wide range of proximate analysis data for a given fuel. Crop harvesting and processing techniques that introduce foreign materials could also be a contributing factor.

10.1.1.2.3 Ultimate analysis: Ultimate analysis is particularly important in evaluating the fuel feedstock in terms of its pollution potential and, also, to determine the theoretical air-fuel ratio. The results showed that the major elemental constituents of rice husk are carbon, oxygen and hydrogen. The measured values of these three components are in the ranges reported by Ebeling and Jenkins (1985). Low concentrations of nitrogen, sulphur and chlorine can also be found.

The major elements (C, O and H) are important in assessing the heat value and the suitability of the material as a fuel (Ghaly and Al-Taweel, 1990). The other elements (N, S and

Cl) provide information on production of undesirable products (such as nitrous and sulphurous oxides) during the thermochemical conversion process with regard to environmental pollution problems. The low fractions of nitrogen, sulphur and chlorine offer environmentally more desirable fuel properties.

10.1.1.2.4 Ash composition: Ash composition is an important consideration in thermochemical conversion systems when biomass is used as a fuel. It indicates the potential for the formation of undesirable bonded deposits on combustor surfaces and possible disposal problems of the ash. Fused ash or slag is formed when the temperature rises above the melting temperature of the eutectic mixtures in the ash. Slagging and clinker formation can seriously reduce, or completely block, the flows of gas, air and biomass fuels in combustors and gasifiers. Non-slagging reactors are usually controlled to operate below the ash softening temperature by varying the fuel and air inputs.

The sum total of all mineral elements present in rice husk ashes on 100 basis confirmed the notion that the constituents of rice husk ashes do exist in forms other than elements. Since the mineral elements were estimated as percentages of their oxides, oxygen could have contributed significantly to the high percentage of the mineral elements not accounted for. The measured values of rice husk ash composition are very much within the ranges reported in the literature. The reported SiO_2 content of rice husk ash ranged from 95% to 97% (Kaupp, 1984). The ash composition of various rice husk varieties compiled by Beagle (1978) were: SiO_2 (90.27-96.97%), K_2O (0.58-3.15%), CaO (0.25-2.70%), P_2O_5 (0.24-0.57%), MgO (0.015-0.67%), Al_2O_3 (traces-0.08%), Fe_2O_3 (traces-1.01%), Na_2O (0.34-0.78%), and SO_3 (0.27-2.70%).

The combined weight fraction of SiO_2, Al_2O_3 and Fe_2O_3 in rice husk ash samples used in this study ranged from 90.18% (CP 4) to 97.29% (Pa Potho). This satisfies the ASTM C618-78 requirement for chemical constitution which stipulates a minimum of 70%. The MgO

content of the ash ranged from a low of 0.30% (CP 4, Pa Potho) to a high of 0.45% (ROK 32) and that of Na_2O ranged from a low of 0.03% (CP 4) to a high of 0.23% (ROK 14, ROK 16). These also satisfy the ASTM requirements which are put at a maximum of 5% and 1.5% for MgO and Na_2O, respectively (ASTM, 1978). No ASTM requirement for other mineral element compositions could be found in the open literature.

10.1.1.2.5 Ash fusibility: The behaviour of rice husk ash at high temperatures was determined by conducting ash fusibility analysis. The inorganic compounds of most high ash containing biomass fuels melt at high temperatures and, on cooling, form slag and clinker which may result in serious operational problems. Because rice husk has a high ash content (15.30 to 24.60%), the slagging behaviour is highly dependent on the ash melting temperature, which is influenced by the presence of trace elements giving rise to the formation of low melting temperature eutectic mixtures. For gasification purposes, therefore, the melting behaviour of the fuel ash should be determined in both oxidizing and reducing modes.

The ash fusibility temperatures (1349-1678°C) obtained in the oxidizing atmosphere indicated that the temperatures in rice husk thermochemical conversion systems must be kept below 1349°C to avoid slagging problems. The ash fusibility temperatures for all ash samples were lower in the reducing atmosphere (1330-1649°C) than those in the oxidizing atmosphere. During gasification, the reducing atmosphere is predominant. This indicates that fluidized bed rice husk gasifiers can be operated with no slagging problems since these gasifiers normally operate at temperatures between about 600 and 900°C.

Osman (1982) reported an initial deformation temperature of 1439°C and a fluid temperature of over 1650°C for rice husk ash in a nitrogen atmosphere. CTC (1983) have measured the initial deformation and fluid temperatures of rice husk ash in oxidizing and reducing atmospheres. This group reported an initial deformation temperature of 1440°C and a fluid temperature of 1650°C in the oxidizing atmosphere, and an initial deformation

temperature of 1400°C and a fluid temperature of 1600°C in the reducing atmosphere. The variation in the ash fusibility temperatures in this study could be attributed to the variations in the composition of the ashes. Kaupp (1984) reported that the softening and melting temperatures of biomass materials are significantly reduced in the presence of large amounts of low melting temperature mineral oxides such as K_2O and Na_2O in the ash. Sondreal and Ellman (1975) studied the effects of individual oxides of mineral elements on fusion temperatures of ash. According to their study, increased percentages of oxides of silicon, potassium, iron, sodium, and sulphur in the ash decreased its fusion temperature. The fusion temperature of ash increased with increases in oxides of calcium, magnesium, and aluminum. The percentage of phosphorus oxide was found to have no effect on fusion temperature.

10.1.2 Agglomeration Characteristics of Inert Bed Materials

10.1.2.1 Agglomeration characteristics of silica sand. The visual observation of the heat treated silica sand-rice husk and rice husk ash mixtures indicated that the loose bonding of silica particles around the ash residue at 750°C was most likely physical in nature; there was no apparent chemical interaction between the silica sand and the rice husk ash. However, when the samples were treated at the higher temperatures (850, 900, 950 and 1000°C), some chemical interaction appeared to have taken place.

The analyses of the environmental scanning electron microscopy and light microscopy showed no structural changes in the pure silica sand (which has a melting temperature >1600°C) and no meltdown of rice husk ash at even the highest temperature (1000°C) studied. However, the silica sand-rice husk ash mixtures loosely agglomerated, forming friable structures that can break up easily, when treated at the higher temperatures (850, 900, 950 and 1000°C). Although these temperatures were well below the melting temperatures of rice husk ash and silica sand, some chemical interaction appeared to have taken place. Huffman et al.

(1981) and Ergudenler and Ghaly (1993a) found that significant partial melting of ashes occurred at temperatures as low as 200-400°C below the initial deformation temperature.

The rice husk ash used in this study contained a very high concentration of SiO_2 (96.00%). Other mineral oxides present are: K_2O (2.10%), P_2O_5 (0.59%), CaO (0.48%), MgO (0.44%), Na_2O (0.08%), Fe_2O_3 (0.09%), Al_2O_3 (0.05%), TiO_2 (0.03) and ZnO (0.01%). The relative compositions of these oxides in the silica sand-rice husk ash mixtures will determine the type and condition of the agglomerates formed. As shown in Table 10.1, K_2O and P_2O_5 are the only two major mineral oxides which have low melting temperatures. Significant decrease in the melting temperature of biomass ashes in the presence of large amounts of low melting mineral oxides such as K_2O and Na_2O was reported by several authors (Kaupp, 1984; Perkins et al., 1984; Ergudenler and Ghaly, 1993a). The agglomeration process was linked to sodium by Perkins et al. (1984) and to potassium by Ergudenler and Ghaly (1993). The phase diagrams for the SiO_2-$K_2O.SiO_2$ (Figure 10.1) and the SiO_2-$Na_2O.SiO_2$ (Figure 10.2) systems show that if the amount of K_2O in the SiO_2-$K_2O.SiO_2$ system is higher than 25% and that of Na_2O in the SiO_2-$Na_2O.SiO_2$ system is higher than 30%, the silicates would melt at temperatures around 800°C. The phase diagram of the ternary system SiO_2-$K_2O.SiO_2$-$Na_2O.SiO_2$ (Figure 10.3) may be thought of in terms of three subsidiary ternary systems: $K_2O.SiO_2$-$Na_2O.SiO_2$-$K_2O.2SiO_2$, $K_2O.2SiO_2$-$Na_2O.SiO_2$-$Na_2O.2SiO_2$ and $K_2O.2SiO_2$-$Na_2O.2SiO_2$-SiO_2. The subsidiary system $K_2O.SiO_2$-$Na_2O.SiO_2$-$K_2O.2SiO_2$ shows that at concentrations of 40.1% K_2O, 11.7% Na_2O and 48.2% SiO_2, a eutectic would form at 645°C. The second subsidiary system $K_2O.2SiO_2$-$Na_2O.SiO_2$-$Na_2O.2SiO_2$ reveals that a eutectic would occur at concentrations of 25.4% K_2O, 17.2% Na_2O and 57.4% SiO_2 and a temperature of 665°C. In the $K_2O.2SiO_2$-$Na_2O.2SiO_2$-SiO_2 system, a eutectic would occur at concentrations of 22.9% K_2O, 7.6% Na_2O and 69.5% SiO_2 and at a temperature of 540°C. Comparison of the qualitative results on the elemental composition obtained by energy dispersive x-ray analysis with the phase diagrams in Figures 10.1, 10.2 and 10.3, it can be concluded that the potassium and sodium contents in the rice

Table 10.1 Melting temperature of selected mineral oxides*.

Mineral oxides	Melting Temperature (°C)
SiO_2	1610
K_2O	350
P_2O_5	580
Na_2O	1275
CaO	2614
MgO	2852
Fe_2O_3	1560

* Data taken from the Handbook of Chemistry and Physics, CRC Press, 69th Edition (Weast, 1989).

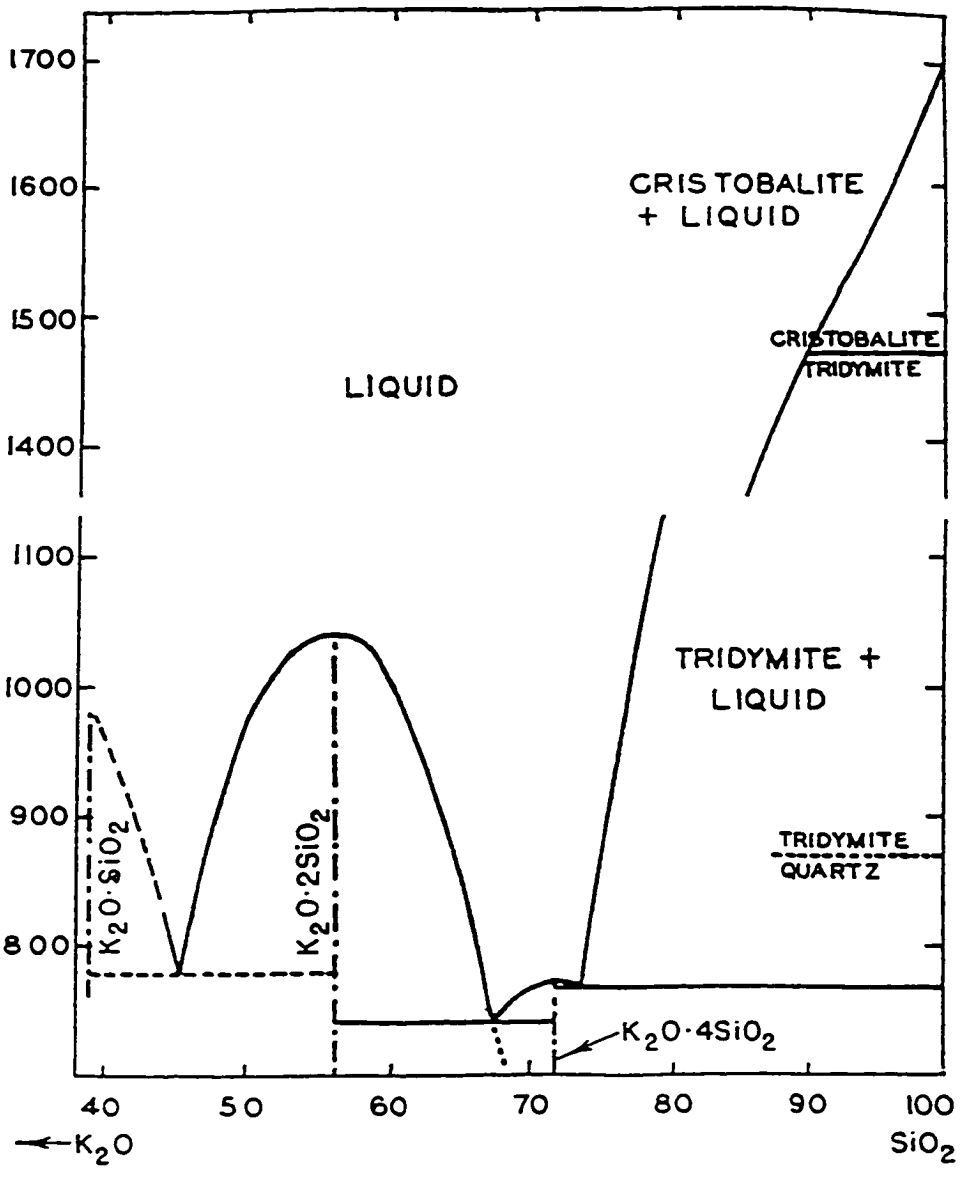

Figure 10.1 Phase diagram for SiO_2-$K_2O.SiO_2$ system (Levin et al., 1956).

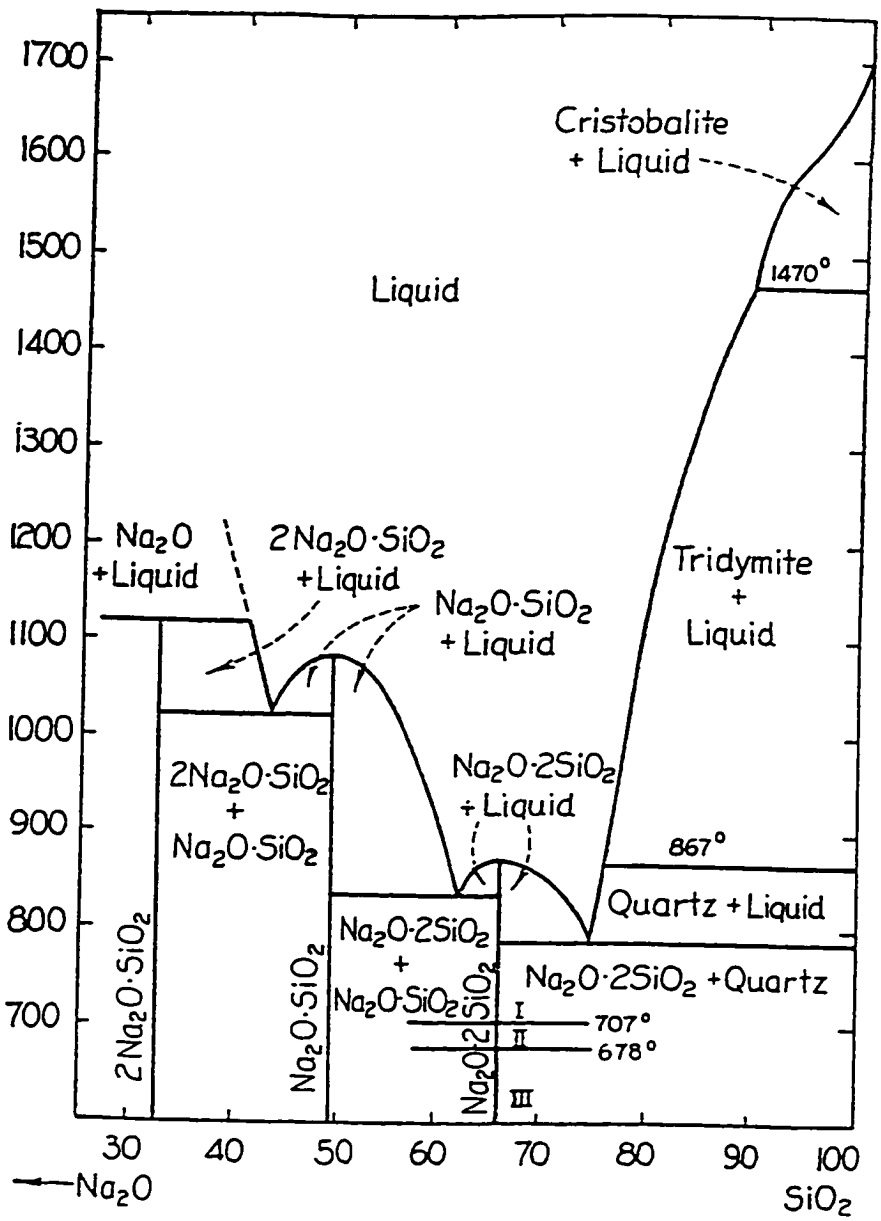

Figure 10.2 Phase diagram for SiO_2-$Na_2O.SiO_2$ system (Levin et al., 1956)

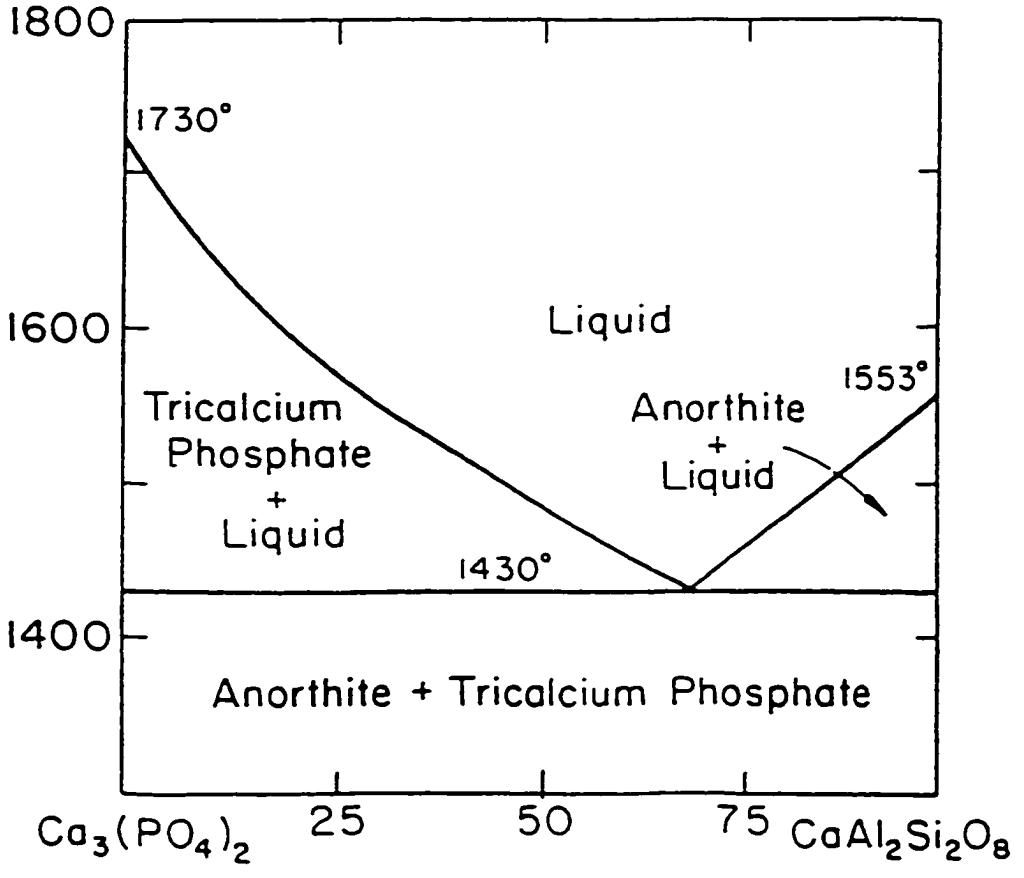

Figure 10.3 Phase diagram for SiO_2-$K_2O.SiO_2$-$Na_2O.SiO_2$ system (Levin et al., 1956).

husk ash were unsuitable for decreasing the melting temperature of the sand-ash mixture below 1470°C. The phase diagram for $Ca_3(PO_4)_2$-$CaAl_2Si_2O_8$ system (Figure 10.4) showed that in the presence of CaO, Al_2O_3, and SiO_2, P_2O_5 does not reduce the temperature of formation below 1430°C. These observations confirm the result of this study that the loose agglomerates formed do not involve a liquid phase.

It has been reported that the ash obtained from rice husk by slow combustion at low temperatures contains amorphous silica, whereas rice husk ash formed at higher temperatures contains mostly crystalline silica (Hanafi and Abo-El-Enein, 1980). Bartha and Huppertz (1974) and Hanafi and Abo-El-Enein (1980) reported that the crystalline silica in rice husk ash comprises mostly tridymite and cristobalite and very small proportions of quartz. It is known that silica undergoes transformation from β-quartz to ∝-tridymite at a temperature of 870°C (Sosman, 1927). During this transformation foreign inclusions could possibly enter the structure as an interstitial solid solution (Eitel, 1948). These inclusions involve the valence-compensating elements and require an open structure transform of silica. Since tridymite is of an open structure, it can easily accommodate additional elements. Thus, it can be inferred that the silica in rice husk ash undergoes a similar structural change at temperatures in the region of 870°C. With the presence of mineral oxides intermixed with silica in rice husk ash, these oxides, especially the low melting temperature mineral oxides (K_2O, Na_2O and P_2O_5) may have interacted with the silica during this transformation of silica sand and rice husk ash, resulting in the agglomeration of ash on silica sand. These agglomerates were very weak and friable due to very low concentrations of the aforementioned low melting temperature mineral oxides in rice husk ash.

The crystalline nature of silica at high temperatures was further confirmed by examining the samples under a light microscope. The glassy appearance of silica particles and the presence of some crystalline material adhering to their surfaces, as observed under the light microscope, could be attributed to the condensation of the low melting temperature mineral

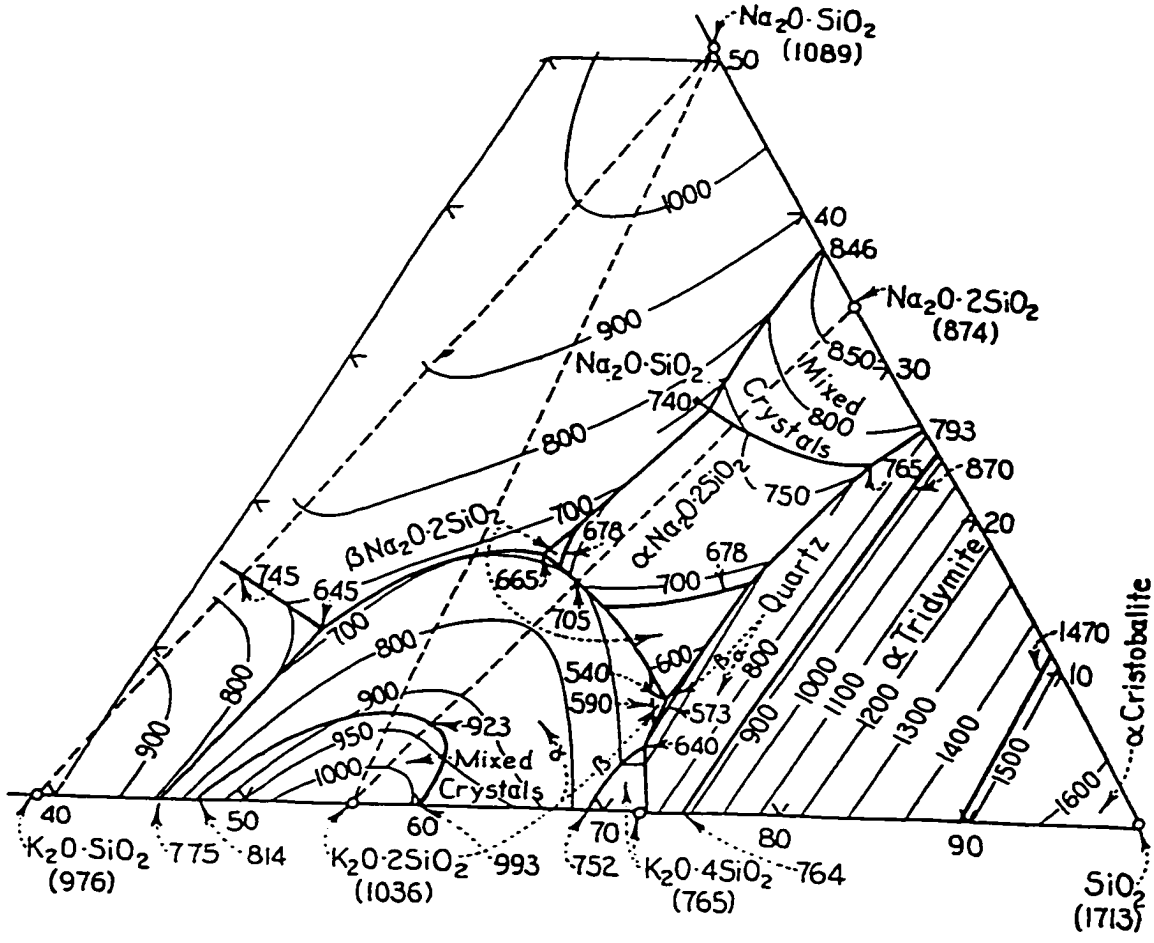

Figure 10.4. Phase diagram for $Ca_3(PO_4)_2$-$CaAl_2Si_2O_8$ system (Levin et al., 1956).

oxides on the silica particles. This may have provided an initial sticky surface to which ash particles adhered. The very low concentrations of K_2O, Na_2O and P_2O_5 in the rice husk ash were insufficient for the formation of strong and stable agglomerates.

10.1.2.2 Agglomeration characteristics of alumina sand. The visual observation of the heat treated alumina sand-rice husk and rice husk ash mixtures indicated that the loose bonding of alumina particles around the ash residue at 900°C was most likely physical in nature; there was no apparent chemical interaction between the alumina sand and the rice husk ash. However, the weak bonding of particles which resulted in the formation of friable structures at the temperatures of 950 and 1000°C suggested that some interaction appeared to have taken place between the alumina sand and rice husk ash particles. Since particle deformation was absent in these samples, even in the region of the bonds, it is, therefore, most likely that the friable structures were formed solely by surface bonding of particles. The x-ray energy dispersive spectrometer results in this study have shown that the bulk of the rice husk ash consisted of silica. Since silica is inert, its presence at the surface of rice husk ash will favour a film diffusion controlled reaction (Boateng et al., 1991).

As already discussed, the rice husk ash used in this study contained a very high concentration of SiO_2 (96.00%) with very small amounts of K_2O (2.10%), P_2O_5 (0.59%), CaO (0.48%), MgO (0.44%), Na_2O (0.08%), Fe_2O_3 (0.09%), Al_2O_3 (0.05%), TiO_2 (0.03) and ZnO (0.01%). It has been reported that the ash obtained from rice husk after chemical treatment or by slow combustion at low temperatures contains amorphous silica, whereas rice husk ash formed at higher temperatures contains mostly crystalline silica (Hanafi and Abo-El-Enein, 1980). Further, it is known that crystalline or metallic materials form bond zones by diffusion of the material and this does not alter the shape of the original particles (Siegell, 1984). Since the alumina sand and rice husk ash particles retained their original structures at the temperature of 1000°C, the mechanism for bonding at this temperature was diffusion.

The analyses of the ESEM photomicrographs showed no structural changes in the pure alumina sand (which has a melting temperature >2000°C) and no meltdown of rice husk ash at the temperature of 1000°C. It is, therefore, reasonable to assume that no chemical interaction took place between the alumina sand and the rice husk ash. Hence, the weak bonding that took place between the alumina sand and rice husk ash mixtures at the temperature of 1000°C cannot be attributed to the formation of low melting temperature eutectics. This is a view opposing to the postulation of Groeneveld and Hos (1983) and Jenkins (1989), that rice husk ash is highly prone to slagging at temperatures as low as 900°C due to its high silica content (90-97%) and alleged low mineral melting temperature (800-1000°C).

Evidence for the significant observation that the mechanism of bonding does not appear to involve a liquid phase lies in the relative compositions of the mineral oxides in the alumina sand-rice husk ash mixtures. Bartha and Huppertz (1974) and Hanafi and Abo-El-Enein (1980) reported that the crystalline silica in rice husk ash comprises mostly tridymite and cristobalite and very small proportions of quartz. The melting temperatures of quartz, tridymite and cristobalite (Figure 10.5) are 1470°C, 1670°C and 1710°C, respectively, (Sosman, 1927). This indicates that rice husk ash cannot form eutectic mixtures at temperatures below 1470°C.

The melting temperature of the system Al_2O_3-SiO_2 increases with increasing alumina content (Hall and Insley, 1947). These authors showed that at concentrations less than 5.5% Al_2O_3, a eutectic cannot occur below 1545°C. They also showed that increases in the amounts of K_2O and/or Na_2O lowers the melting temperature of the system K_2O-Na_2O-Al_2O_3-SiO_2. But the mole percent of K_2O should be higher than 65% in the system K_2O-Al_2O_3-$4SiO_2$-SiO_2 and that for Na_2O should vary from 30% to 60% in the system Na_2O-Al_2O_3-$6SiO_2$-SiO_2 at temperatures above 1470°C so as to form eutectic mixtures (Levin et al., 1956). Thus, the presence of K_2O and Na_2O in notably low concentrations in rice husk ash will not result in the formation of eutectic mixtures at the temperatures studied.

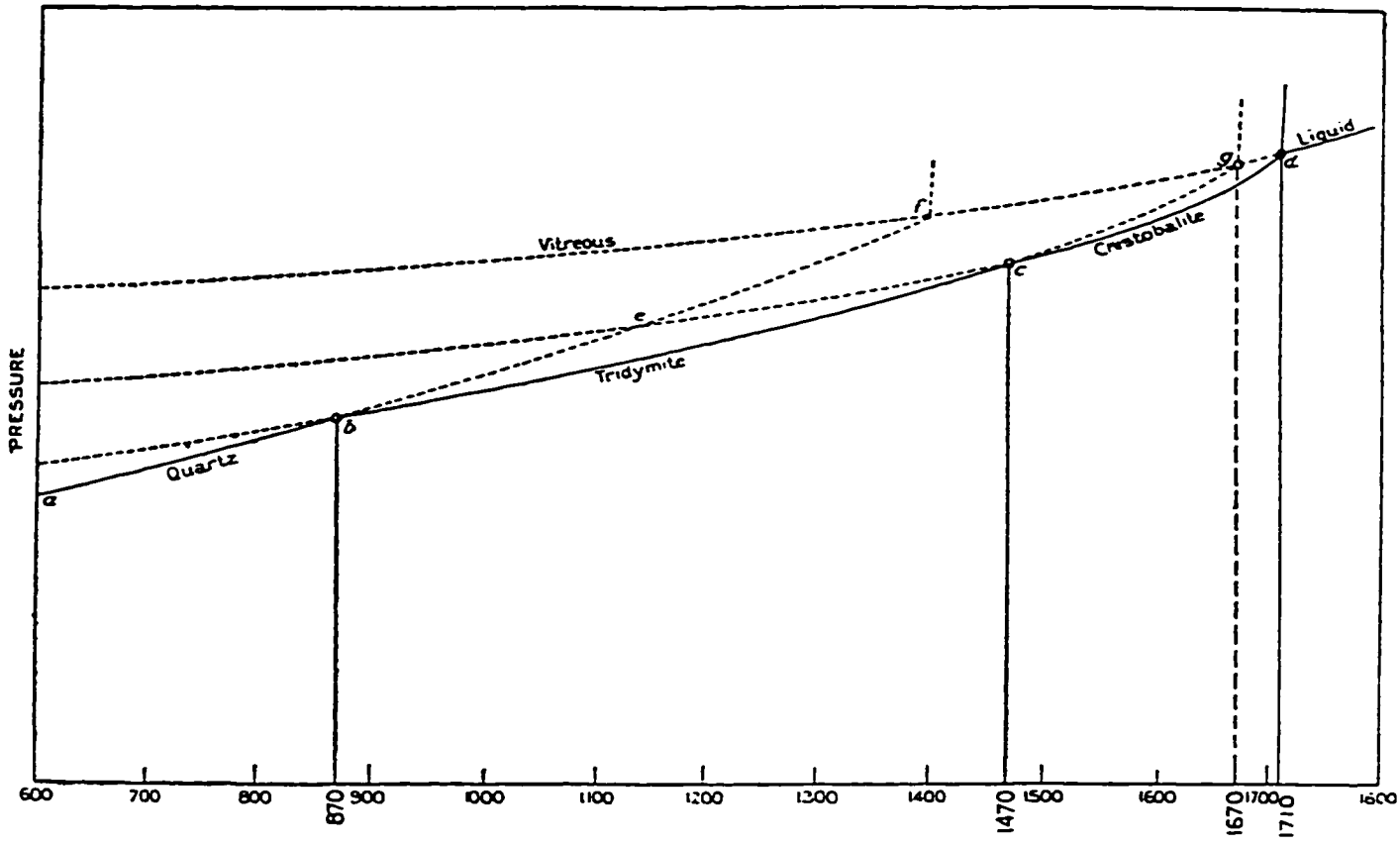

Figure 10.5 Imaginary vapour-pressure curves of the principal forms of silica. Ab, upper part of the stability range of quartz; bc, stability range of tridymite; cd, stability range of cristobalite; e, metastable inversion point of quartz and cristobalite; c, melting temperature of quartz; g, metastable melting temperature of tridymite; d, melting temperature of cristobalite (Sosman, 1927).

Increases in the percentage of alkaline earth metals such as MgO and CaO increase the melting temperature of the system $CaO-MgO-Al_2O_3-SiO_2$ (Jones, 1953; and Ergudenler and Ghaly 1993b). Jones (1953) also reported that rice husk ash has no tendency to melt at temperatures below 1667°C when mixed with less than 15% CaO concentrations. It has been shown by Sondreal and Ellman (1975) that the percentage of P_2O_5 have no effect on the melting temperature of ash. On the other hand, Fe_2O_3 and SO_3 have been reported to have dominating effects on the slagging characteristics of biomass ash; they significantly lower melting temperatures (Osman, 1982). These effects may be negligible with rice husk ash containing very small amounts of Fe_2O_3 and SO_3 (0.09% and 0.10%, respectively).

From the overall evaluation of the results, it is inferred that the concentration of the mineral oxides, especially the low melting temperature mineral oxides such as K_2O, Na_2O and P_2O_5, in the rice husk ash were unsuitable for the formation of eutectic mixtures below 1470°C. Furthermore, the severe slagging problems that have been reported to occur in rice husk gasifiers are not directly related to the high ash content of rice husk or its silica content.

10.1.3 Thermal Degradation and Kinetics of Rice Husks

10.1.3.1 Thermal degradation. As already mentioned, only four rice husk varieties (Lemont LG, ROK 14, CP 4 and Pa Potho) of the six varieties (Lemont LG, ROK 14, ROK 16, ROK 32, CP 4 and Pa Potho) used to determine the properties of rice husks (section 9.1.1), were considered in this analysis. ROK 14, ROK 16 and ROK 32 exhibited very similar properties (section 9.1.1) and are, therefore, expected to behave in essentially the same way in a thermogravimetric analyzer. One of the ROK rice husk varieties (ROK 14) was, therefore, used in addition to the other three rice husk varieties (Lemont LG, CP 4 and Pa Potho).

10.1.3.1.1 Thermal degradation rate: Generally, four stages of weight loss were identified. The first stage, starting from ambient temperature to about 100°C, represented loss of water present in the material and superficial or external water bounded by surface tension. The second stage, showing a slight weight loss that appeared to be relatively constant, could be due to loss of light vilatiles. The next stage of weight loss, referred to as the active or first reaction zone, represented the evolution of the volatile compounds generated during conversion of primary hemicellulose and cellulose (Shafizadeh, 1968; and Ramiah, 1970; Koufopanos et al., 1989; Bining and Jenkins, 1992; Williams and Besler, 1994; and Varhegyi, 1994). The weight changes in the passive or second reaction zone are attributed to lignin conversion (Shafizadeh, 1968; Ramiah, 1970; Koufopanos et al., 1989; Bining and Jenkins, 1992; Williams and Besler, 1994; and Varhegyi et al., 1994).

The thermal degradability is affected by the chemical composition of rice husk (cellulose, hemicellulose and lignin) because different components of lignocellulosic materials have different thermal behaviours. Earlier studies (Ramiah, 1970; and Shafizadeh and DeGroot, 1976) on the thermal decomposition of the individual components of lignocellulosic materials (cellulose, hemicellulose and lignin) indicated that decomposition of hemicellulose starts first (150-350°C), followed by the cellulose (275-350°C) and finally by the lignin (250-500°C). Accordingly, the higher thermal degradation rate of Pa Potho rice husk at most heating rates and all atmospheres investigated is due to larger percentages of cellulose and hemicellulose components in comparison to those of Lemont LG, ROK 14, and CP 4 as shown in Table 10.2. Antal et al. (1980) reported a similar finding with various biomass materials, including cellulose, paper, wood and manure. They suggested that the higher the cellulose content of the material, the greater the extent of devolatilization. Larger percentages of volatile matter and lower ash contents of Pa Potho as compared to those of CP 4 might have also contributed to their higher thermal degradability. These results are in close agreement with those reported by Lipska-Quinn et al. (1985) and Ghaly and Ergudenler (1991) for rice straw and wheat straw, respectively. However, the results also showed that at 50°C/minute heating rate, the thermal

Table 10.2 Chemical Composition of Rice Husks (Dry extractive free basis).

Rice Husk	Cellulose (%)	Hemicellulose (%)	Lignin (%)	Ash (%)
Lemont	29.20	20.10	30.70	20.00
ROK 14	33.47	21.03	26.70	18.80
CP 4	25.89	18.10	31.41	24.60
Pa Potho	35.50	21.35	24.95	18.20

Values are the average of 3 measurements with a coefficient of variation in the range of 0.5 to 1.8%.

degradation rate of ROK 14 rice husk is largest in oxygen, followed by that in air, whereas Pa Potho rice husk is the largest in nitrogen atmosphere. This indicates that ROK 14 rice husk is more easily thermochemically degradable in an oxidizing atmosphere, whereas Pa Potho rice husk is more easily thermochemically degradable in an inert atmosphere.

Researchers have generally found that oxygen has a profound effect on the thermal decomposition of various materials. Shafizadeh and DeGroot (1976) reported a higher rate of thermal decomposition by oxidation of cellulose in the presence of air (or oxygen) than in the absence of air (or oxygen). Smith et al. (1991) studied the burning profiles of two bituminous coals and their chars in a mixture of oxygen-nitrogen atmosphere using TGA. The results of their study revealed that increasing oxygen concentration decreased the maximum temperature of weight loss and increased the maximum devolatilization rate. Vantelon et al. (1990) used TGA to study the thermal degradation of oil shales in various oxygen-nitrogen atmospheres. Their results indicated that atmospheres containing increasing amounts of oxygen significantly enhanced the degradation process. They assumed that in the presence of oxygen, two processes develop simultaneously: a simple thermal degradation process, and a thermochemical process combining temperature and oxygen effects. The present study identifies the critical role oxygen plays in the decomposition of rice husks. In the presence of oxygen, decomposition is catalyzed, thus, resulting in higher thermal decomposition rates relative to the data obtained in the nitrogen environment. This feature relates to increased susceptibility of organic species to oxygen. Apparently, the thermal degradation in oxygen is caused primarily by oxidation reactions. These reactions provide a type of oxy-cellulose, which, on further heating, decomposes with evolution of carbon dioxide, carbon monoxide and water.

The result that the thermal degradation rate increased with increases in heating rate for all rice husk samples is consistent with findings reported in the literature. Lipska-Quinn et al. (1985) investigated the thermal degradation of rice straw and its components in both air and nitrogen atmospheres at different heating rates using TGA with heating rates of 5-40°C/minute.

Their results revealed that heating rates above 20°C/minute markedly increased the rate of degradation in the active zone. Raman et al. (1981) used TGA to study the devolatilization of biomass with heating rates of 40 and 160°C/minute. Their results indicated that the temperature at which the maximum rate of devolatilization occurred was mainly affected by the heating rate. Tia et al. (1991) used TGA to determine the pyrolysis kinetics of Thai lignite at heating rates of 5-50°C/minute. Under the conditions studied, the heating rate showed little effect on the TG curves and ultimate yield of volatiles, but significantly affected the volatile evolution rate.

10.1.3.1.2 Initial degradation temperature: The results showed that the initial degradation temperature was higher for all rice husk samples in nitrogen atmosphere than in the oxidative atmospheres of air and oxygen at all heating rates. This is due to the fact that in an oxidative atmosphere, decomposition is catalyzed, thus, resulting in a low oxidation onset temperature relative to the data obtained in an inert atmosphere.

The result that the initial degradation temperature decreased with increases in heating rate for all rice husk samples and in all atmospheres investigated is consistent with findings reported in the literature. Lipska-Quinn et al. (1985) observed marked decrease in initial degradation temperature for rice straw and its components in both air and nitrogen atmospheres while increasing heating rate. As observed by Shafizadeh and McGinnis (1970), the rate of thermal degradation of hemicellulose and lignin components of lignocellulosic materials is lower than that of cellulose. Thus, the higher percentage of cellulose in Pa Potho rice husk compared with that in Lemont LG rice husk, might have caused the higher initial degradation temperature for Pa Potho rice husk compared to those of Lemont LG, ROK 14, and CP 4 rice husk samples.

10.1.3.1.3 Residual weight at 700°C: The higher residual weight exhibited by CP 4 rice husk at 700°C in all atmospheres might be related to the larger ash content of CP 4 rice husk as compared with that of other rice husk samples. The increase in residual weight with

increases in heating rate for all samples is consistent with the observations of Lipska-Quinn et al. (1985) and Ghaly and Ergudenler (1991) on the thermal degradation of rice straw and wheat straw, respectively. In their studies, the authors stated that sufficient time was not available for the consecutive reactions (fragmentation, formation of combustible volatiles, dehydration and the formation of carbonaceous char) to occur at higher heating rates.

The lower residual weights at 700°C obtained in the oxidative atmospheres of air and oxygen in comparison with that obtained under nitrogen indicates the profound effect an oxidative environment has in enhancing the deterioration and the thermal degradation of cellulosic materials. The catalytic effect of the alkali metal oxides, especially potash, present in the rice husk ash on the carbon-oxygen reaction has been investigated by Khan and Esztergar (1990). This is a highly exothermic, very fast reaction and, therefore, very effective in the removal of carbon from char. The authors concluded that surface oxide complexes on the char surface may serve a key role in char reactivity. Their results further revealed that preoxidized chars lose weight faster and at slightly lower temperature during nonisothermal (TG) treatment compared to fresh chars.

The high residual weight obtained in nitrogen atmosphere implies not only that the carbon in the rice husk is not fully utilized but the residues also contain a substantial amount of volatiles. This is substantiated by the completely black residue obtained in the nitrogen atmosphere. The lower residual weights of the rice husk samples at 700°C obtained in air and oxygen atmospheres compared to their initial ash contents with percentages of ash lost ranging from about 2.95 to 13.10% and 4.2 to 17.1% in air and oxygen atmospheres, respectively, indicates that not only the oxidative atmospheres caused total burnout of the fixed carbon in the char but also the oxidation and volatilization of some minerals in the ash. Table 10.3 shows that the bulk of the mineral oxides in the rice husk ash samples has a very high melting temperature and, therefore, an even higher boiling temperature. However, K_2O and P_2O_5 fractions, which have low melting and boiling temperatures, are indeed boiled off within the

Table 10.3 Composition, Melting and Boiling Temperatures of Selected Mineral Oxides in Rice Husk Ashes.

Mineral Oxide	Weight Fraction (%)	*Melting Temperature (°C)	*Boiling Temperature (°C)
SiO_2	90.0-97.0	1610	2230
K_2O	1.8-2.8	350	-
P_2O_5	0.6-1.2	250	300
CaO	0.3-0.6	2614	2850
MgO	0.3-0.4	2852	3600
Fe_2O_3	0.1-0.2	1565	-
Na_2O	0.0-0.2	1275	-
Al_2O_3	0.0-0.1	2072	2980

* Data taken from the Handbook of Chemistry and Physics, CRC Press, 69th Edition (Weast, 1989).

temperature range considered in this study. The boiling-off of these mineral oxides (K_2O and P_2O_5), which account for 2.40-6.00% of the total mineral oxide composition of the ash, may have contributed to some of the losses in ash. The remaining 1.25-3.95% (for air) and 1.80-11.05% (for oxygen) losses of the ash could not be accounted for as this was beyond the scope of this study. It is possible, however, that oxides of alkali metals such as Na_2O or K_2O may have formed low melting temperature eutectics with the silica found in the ash (Ergudenler and Ghaly, 1993a), and some of these eutectics boiled off within the temperature range used in this study. Similar observations were found in the results reported by Aho and Huotari (1985) and Khan and Esztergar (1990), although reasons for ash losses were not discussed in their study.

10.1.3.2 Kinetic parameters. The kinetic parameters (activation energy, pre-exponential factor and order of reaction) of the four varieties of rice husk (Lemont LG, ROK 14, CP 4 and Pa Potho) used for the thermogravimetric analyses were determined at the heating rate of 20°C/minute in three different atmospheres (nitrogen, air and oxygen) for the two principal reaction zones applying thermo-analytical techniques to the reaction kinetics.

The kinetic parameters were mainly influenced by the atmosphere imposed on the samples. The activation energies determined in the first reaction zone for the various rice husk varieties under nitrogen atmosphere (29.0-35.4 kJ/mol) were higher than the value of 20.0 kJ/mol found in the literature for the low temperature devolatilization of oil-palm solid waste in nitrogen atmosphere (Williams and Besler, 1994), but were somewhat lower than the values of 69.0-79.0 kJ/mol given for the pyrolysis of rice straw (Bining and Jenkins, 1992). This is probably due to the higher heating rates (50 and 100°C/minute) used by these authors. In air atmosphere, the activation energies obtained for the various rice husk varieties (37.0-54.7 kJ/mol) were much lower than those reported by Ergudenler and Ghaly (1992b) for wheat straw (69.3-81.3 kJ/mol), and those reported by Bining and Jenkins (1992) for rice straw (110.0-175.0 kJ/mol). The activation energies determined in this study under oxygen atmosphere (142.7-188.5 kJ/mol) were in the range reported by Bining and Jenkins (1992) for

the decomposition of rice straw (118.0-260.0 kJ/mol) between 170 and 300°C using TGA. The higher values of activation energy and pre-exponential factor obtained in oxygen atmosphere compared to those obtained in air and nitrogen atmospheres may be due to the very rapid rate of reaction.

The lower kinetic parameters obtained in the second reaction zone compared to those obtained in the first reaction zone may be due to the fact that lignin, which has lower decomposition rates than cellulose and hemicellulose components of rice husk, was condensed to char (Milne, 1981). Bining and Jenkins (1992) and Ergudenler and Ghaly (1992b) also reported lower kinetic parameters in this zone compared to the first reaction zone. Bining and Jenkins (1992) obtained typical values of activation energies on the order of 1 kJ/mol in nitrogen atmosphere, 10 kJ/mol in air atmosphere and 30 kJ/mol in oxygen atmosphere for rice straw.

The order of reactions determined in this study were in good agreement with those reported by Ergudenler and Ghaly (1992b) for wheat straw. Bining and Jenkins (1992) assumed first order reactions in their studies.

Data in the literature for the activation energy of biomass decomposition are clearly dependent on the biomass; this is inevitable since they have different compositions of cellulose, hemicellulose and lignin and contain different trace metals both of which have been shown to influence the decomposition reaction (Shafizadeh, 1968; and Hamad, 1981). The sample to sample variation observed in this study was most likely a result of probable compositional variations. Although these kinetic parameters are only global values resulting from a complex kinetic system with multiple simultaneous reactions, these values can be used for crude estimates and comparisons.

The results of the proximate analysis (moisture, volatile matter, char, and ash contents) of rice husk samples determined from TGA measurements showed that the lowest weight of char (fixed carbon) was obtained for CP 4 rice husk heated at 10°C/minute and the highest was obtained for Pa Potho rice husk heated at 50°C/minute. This implies that the rate of removal of char was faster in the case of Pa Potho rice husk than that in the CP 4 rice husk. The results also showed that the volatile matter content was lowest for CP 4 rice husk heated at 10°C/minute and highest for Pa Potho rice husk heated at 20°C/minute, indicating that the rate of removal of volatile matter was faster in the Pa Potho rice husk than that in the CP 4 rice husk. Compared with the values obtained from analytical proximate analysis (% wet basis), the ultimate yield from TGA is slightly lower due to the relatively slow heating rate used in TGA compared to that of the analytical proximate analysis of 600-900°C/minute (Howard, 1981).

10.2 Main Experiments

10.2.1 Gasifier Temperature

The experimental results revealed that the gasifier temperature is very sensitive to changes in bed height, fluidization velocity and equivalence ratio. The significant increase in the mean bed temperature with lower levels of bed height can be explained by the thermal fly-wheel effect of the bed material. This effect was reduced when the total amount of bed material was reduced due to the reduced bed height resulting in higher bed temperatures. The gasifier temperature increased with increases in fluidization velocity as a result of increased amount of air introduced to the system. Increasing the amount of air increased the rate of the exothermic reactions which released energy and, thus, raised the temperature. Increasing the fluidization velocity also caused high mixing which increased the reaction rates as reported by Ghaly et al. (1989d). The increase in gasifier temperatures with increasing equivalence ratio can be explained by the fact that at higher equivalence ratios more air (or oxygen) per unit weight of fuel is available, hence more fuel is burnt (exothermic carbon combustion) releasing heat.

It is shown that the temperature profile within the fluidized bed was very uniform as compared with a downdraft gasifier, in which the temperature can swing by as much as 300 to 400°C (Jenkins, 1980). This stability attested to good particle distribution within the bed. It is due to the large heat exchange generated by the rapidly moving solid particles and does away with the harmful hot spots occurring in downdraft or updraft gasifiers. The behaviour of the freeboard temperature, close to the bed surface (T_{10}), indicates freeboard char gasification as it is only about 3-40°C lower than the bed temperature. The lower temperatures of the freeboard, close to the exit (T_{11}), and the cyclone (T_{12} and T_{13}) could be attributed to heat losses through the gasifier walls. The temperatures measured at the wall region of the dense bed were lower than the mean bed temperature due to the low solid circulation in this region and the heat losses through the gasifier walls. The bed temperatures observed in this study (665-880°C) are very much within the range reported in the literature of 627-927°C (Bacon et al., 1985; Maniatis et al., 1988; Boateng et al., 1992; Ergudenler, 1993; Sadaka, 1994; and Narváez et al., 1996) for desirable operation of a fluidized bed gasifier.

10.2.2 Gasifier Pressure Drop

With increasing distance from the main distributor plate, the pressure drop in the dense bed dropped whereas the pressure drop in the freeboard region remained constant. However, the pressure drops in both the dense bed and the freeboard regions increased with increasing fluidization velocity and/or decreasing equivalence ratio. The increase in pressure drop in both the dense bed and the freeboard regions with increasing fluidization velocity was due to the increase in the gas flow rate resulting from increased air flow and rice husk feed rates (in order to maintain constant equivalence ratio). The increasing pressure drop in both the dense bed and the freeboard regions with decreasing equivalence ratio was, also, due to the increase in gas production rate owing to increased rice husk feed rate. The increase in air flow and rice husk feed rates due to increased fluidization velocity and/or decreased equivalence ratio resulted in a net increase in the total mass of the bed material and in considerably higher solid (especially char) concentrations in the freeboard. Low pressure drops at the start were observed for each

run because no gases were being produced. The bed pressure drop ranged from 1.5 to 6.1 kPa, indicating good fluidization quality and no agglomeration problems. Ergudenler (1993) reported substantiallly low pressure drop across the dense bed at channeling conditions due to agglomeration.

In order to provide good distribution, it is necessary to restrict the gas or gas and solids flow so that pressure drops across the distributor amount to from 0.5 to 20.0 kPa (Porter et al., 1984). These authors identified two schools of thought. One contends that the pressure drop across the distributor should be at least 30% of the average bed pressure drop, and another maintains the former is true but a maximum of 2.5 kPa is required. Agarwal et al. (1962) advocated that the distributor pressure drop should be about 10% of the average bed pressure drop. Whitehead (1971) reported that a pressure drop ratio within 0.02 to 0.50 is acceptable. Probably, the actual design of the distributor has a tremendous effect on the pressure drop required to achieve good gas distribution. In this study, the observed pressure drop across the secondary distributor plate ranged between 0.8 and 1.6 kPa and the pressure drop ratio was about 0.44, indicating good distribution of the gas was achieved.

10.2.3 Gas Composition

The gas analyses results showed that no important deleterious effect on gas composition was apparent with increasing bed height but the equivalence ratio and fluidization velocity affected the gas composition. Increasing the equivalence ratio and/or the fluidization velocity resulted in an increase in the non combustible fraction CO_2 as well as in N_2 and a corresponding decrease in the combustible fractions (CO, H_2, CH_4, C_2H_2, C_2H_4 and C_2H_6). This behaviour is due to the higher degree of combustion that takes place at higher values of equivalence ratio and/or fluidization velocity. At higher values of equivalence ratio and/or fluidization velocity, more air is supplied in the gasifier in relation to rice husk and hence more char can be burned to form CO_2 at the expense of combustible gases (CO, H_2, CH_4, C_2H_2, C_2H_4 and C_2H_6). The low combustible gas components at higher values of equivalence ratio

and/or the fluidization velocity can, also, be attributed to the high concentration of N_2 resulting from higher actual air to fuel ratio. High fluidization velocities could have also resulted in a shorter resisdence time for the char in the gasifier thereby losing some of the energy in char which would otherwise be in the form of combustible gases. The equivalence ratio of 0.25 and the fluidization velocity of 0.22 m/s appeared to be the optimum values with respect to the quality of the gas because the concentrations of the combustible components reached their maximum value at this equivalence ratio and fluidization velocity.

The insignificant effect of bed height on the gas composition is the result of the relatively small amount of char left for gasification once the pyrolysis process is completed. The relatively small amount of gas from the gasification reaction of char with steam and carbon dioxide is thus hardly affecting the product gas composition. However, this gasification reaction determines the maximum char quantity that can be converted per unit time at a given char hold-up in the fluidized bed gasifier. The char hold-up is dependent on the char reactivity, the char production rate (or fuel feed rate), the operating temperature and the bed height (van den Aarsen et al. (1982).

The results showed that the higher the position in the freeboard the better the gas quality. This result would be anticipated since the de-entrainment device in the enlarged section of the fluidized bed gasifier would reduce particle entrainment, thereby increasing the residence time of reacting substances which will lead to more complete conversions, higher reaction efficiencies and thus contributing to gas quality. The depletion of oxygen with increasing distance from the main distributor plate due to chemical reactions is clearly indicated in the results. This indicated that a large fraction of O_2 was converted in the lower section of the bed. This high conversion in the dense bed region is possibly due to the moderate gas velocities used in this study, since the small bubbles generated under these conditions assure good gas exchange between phases.

Examining the influence of the temperature on the gas composition from various biomass materials, it has been reported that there is a maximum in the concentration of CO, H_2 and CH_4 in the temperature range of 650-750°C while in the same range CO_2 passes through a minimum (Desrosiers, 1981; Maniatis et al., 1988; and Schoeters et al., 1989). Similar bed temperatures (665-744°C) were obtained in the present study when the gasifier was operated at the equivalence ratio of 0.25 which gave the maximum mole fraction of the combustible gas components.

The product gas composition in this study agree reasonably well with data presented in studies of biomass gasification from fluidized bed gasifiers of similar scale of operation, as shown in Table 10.4. Czernik et al. (1994) and Narváez et al. (1996) got higher H_2 contents because they injected secondary air into their freeboards and used catalysts (calcined dolomite) in their beds. Both factors could increase the H_2 content in the fuel gas.

10.2.4 Gas Higher Heating Value

The results revealed a pronounced effect of the equivalence ratio and fluidization velocity on the higher heating value of the gas. Increasing the equivalence ratio resulted in a decrease of the higher heating value of the gas due to decreases in the concentrations of methane and other light hydrocarbons which have relatively large heating values. Also, the higher concentration of nitrogen observed at higher equivalence ratios contributed to the low gas higher heating values. Nitrogen has a diluting effect on the product gas; it lowers its energy content. Desrosiers (1981) showed a shift from chemical energy to sensible heat with increasing equivalence ratio for the fluidized bed gasification of wood. The results also indicated that the effect of the fluidization velocity on the product gas higher heating value was dependent on the equivalence ratio. Lower values of the higher heating value of the gas were obtained at the highest fluidization velocity (0.33 m/s) due to the higher concentrations of combustion products caused by the increase of the air flow rate.

Table 10.4 Comparison of Product Gas Composition With Some Published Results.

Feedstock	Gas Composition (Dry vol. %)								Source
	CO_2	C_2H_m	C_2H_6	H_2	O_2	N_2	CH_4	CO	
Rice husk	14.5	1.9	0.2	4.0	0.04	56.6	2.9	19.9	Present Study
Coconut shell	17.9	2.1	0.1	6.7	0.53	51.5	4.7	16.5	Maniatis (1990)
Municipal solid waste	10.7	2.7	0.9	4.6	1.10	57.3	2.3	14.6	Czernik et al. (1994)
Palm oil shell	13.8	1.9	-	5.0	5.64	64.8	2.1	13.8	Maniatis (1990)
Pine sawdust	13.0	1.6	-	9.5	-	58.3	2.7	13.0	Narváez et al. (1996)
Wheat straw	13.8	2.8	-	6.8	0.20	47.8	4.9	23.4	Ergudenler and Ghaly (1992a)
Wood shavings	18.8	2.4	-	6.8	1.90	65.0	4.4	16.1	Schoeters (1989)
Wood wastes	16.4	1.5	0.2	9.0	0.90	54.0	3.5	13.7	Czernik et al. (1994)

Generally, the higher heating value of the gas was slightly higher at the bed height of 19.5 cm due to higher gasifier temperatures and lower temperature differences experienced at this bed height which were especially influencing the gaseous portion of the hydrocarbons and, therefore, the higher heating value of the gas.

The equivalence ratio at which the maximum higher heating value was obtained, 0.25, is close to the thermodynamic prediction of 0.28 for air gasification of dry wood (Desrosiers, 1981). In Table 10.5, the higher heating value of the product gas is compared to published results from gasifiers of similar scale of operation. Although Maniatis (1990) employed an external heat source by means of two electrical resistance elements and van den Aarsen et al. (1982) reintroduced coarse particles separated from the gas stream into the reactor bed, the results of this study compare well with published data especially for air gasification. Boateng et al. (1992) reported significantly higher values of product gas higher heating value for the steam gasification of rice hull, which is an expected result since the product gas is not diluted by nitrogen.

The energy output of the gasifier can be expressed as the heating value of the gas produced per kg of the feed material on a dry ash free basis from the product of the gas heating value and gas yield. The results indicated that for the optimum operating conditions (bed height of 31.5 cm, fluidization velocity of 0.22 m/s and equivalence ratio of 0.25), the energy output from the gasifier is 7.5 MJ/kg. Using a feed rate of 1.02 kg/minute would result in the production of enough gas (127.5 kW) to operate a 32 kW internal combustion engine operating at 25% efficiency.

10.2.5 Gas Yield

The gas yield increased linearly with increasing equivalence ratio but was not appreciably affected by the changes in the fluidization velocity and/or bed height. This increase

Table 10.5 Comparison of Higher Heating Value of the Gas With Some Published Results.

Feedstock	Gasifying Medium	HHV (MJ/Nm^3)	Source
Rice husk	Air	2.9-5.0	Present Study
Rice husk	Air	1.5-5.6	Maniatis (1990)
Coconut shell	Air	3.4-6.2	Maniatis (1990)
Palm oil shell	Air	3.5-6.2	Maniatis (1990)
Wheat straw	Air	5.0-7.3	Ergudenler and Ghaly (1992a)
Beach wood	Air	5.0-6.6	Van den Aarsen et al. (1982)
Wood waste	Air	5.2	Czernik et al. (1994)
Wood waste	Air + O_2	1.4-8.0	Black et al. (1979)
Rice hull	Steam	11.1-12.1	Boateng et al. (1992)
Municipal solid waste	Air	5.4	Czernik et al. (1994)

of the gas yield with equivalence ratio could be due to the greater production of gas in the initial rice husk devolatilization, which is more rapid at higher equivalence ratios (i.e., at higher temperatures) and to the endothermal reactions of gasification of char: on increasing the temperature the tar cracking and steam reforming reactions are favoured with the resulting decrease of the same and the gas yield increases. The high gas yield of rice husk obtained in this study can be explained by a possible catalytic effect of the ash: it is abundant in rice husk and its K_2O content favours the char-steam reaction. Several researchers (Walawender et al., 1986; Corella et al., 1989; Maniatis et al., 1989; Czernik et al., 1994; and Narváez et al. 1996) have reported increased gas yield with increases in the bed temperature. Narváez et al. (1996) reported the decomposition of tar by secondary reactions to be accompanied by a proportional increase in gas yields.

10.2.6 Tar Yield

When biomass is gasified, the resulting gas is expected to contain trace amounts of condensable materials, or "tars." In the fluidized bed system used in this study, the high heatup rates made possible with the circulating sand, along with short residence times in the gasification reactor, effectively reduce the tendency to form these tars. This is consistent with the findings of Overend (1982) that the amount of condensable tar produced by a fluidized bed gasifier is expected to be very low if a well behaved fluidization is maintained and if the bed temperature is adequate ($\approx 800^{\circ}C$).

10.2.7 Char

The results of the analyses performed on the char collected from the cyclone collector indicated that for a given equivalence ratio the amount solid particles that escaped from the gasifier increased with increasing fluidization velocity and/or bed height. The increase in solid particles entrainment with fluidization velocity is due to the shorter residence time of the particles in the reactor. The amounts of sand particles that escaped from the system are comparable to those reported by Sadaka (1994) but quite lower than those reported by

Ergudenlar (1993), which is the result of an improved separation efficiency of the de-entrainment device in the top of the reactor used by Sadaka (1994) and in this study.

The decrease in the carbon content and the increase in the ash content of the char with increases in the equivalence ratio were good indications of high carbon conversion (resulting from higher bed temperatures achieved at higher equivalence ratios). This, also, resulted in lower calorific values due to the reduced amount of unburned carbon in the char. The decrease in the volatile matter content of the char with increasing equivalence ratio indicated that the rice husk particles might be partially pyrolyzed or oxidized with some of the volatile matter content still remaining in the char.

The finer particles sampled in the cyclone collector had higher carbon contents because of shorter residence times inside the gasifier. The insignificant variations in particle size distribution and composition of the char samples obtained from different positions in the dense bed indicated that the well-mixed solids assumption is probably valid.

10.2.8 Carbon Conversion

The carbon conversion is based on the total carbon in rice husk and the carbon converted into dry gases. It was affected by changes in the equivalence ratio and fluidization velocity but was not affected by changes in the bed height. The carbon conversion increased due to decreased char formation as the equivalence ratio was increased. Increasing the fluidization velocity resulted in reducing the residence time of gases and enhancing the carry over of fine char particles from the bed. Since the escaped fines are not completely converted, this resulted in a decrease of carbon conversion.

Although the carbon conversion attained in this study (55.0 to 84.0%) was comparable to values in the range of 50-85% reported by several researchers (Maniatis et al., 1988; Corella et al., 1989; Maniatis et al., 1989; and Schiefelbein, 1989) for various biomass fuels and

somewhat higher than the value of 31-46% reported by Boateng et al. (1992) for the steam gasification of rice hull, it is too low for economic power production. Carbon conversion in full-scale plants will be improved to a certain extent by increasing the freeboard height and the residence time of the particles (Maniatis et al., 1989). However, conversions close to 100% can be achieved only by efficient recycling of all separated particulates (Maniatis et al., 1989; and Boateng et al. 1992).

10.2.9 Material and Energy Balances

10.2.9.1 Material Balance. The material balance was based on the inflow rates of the rice husk and air and outflow rates of the gas and char. Tar was considered negligible due to its extremely small production rate. The moisture in the produced gas which is comparable to that of hydrogen and oxygen was, also, neglected and could give very low closures for these components. The weight fractions of nitrogen in the rice husk and char are small enough to neglect their contributions. Therefore, the material balance analysis was carried out only on carbon.

The mass balance closure for carbon ranged from 75 to 109%. Mass balance closures in the range of 90-110% have been generally considered acceptable (Black et al., 1980; Raman et al., 1981; and Maniatis, 1990). On this principle, the results of the mass balances that show discrepancies over the range of ±10 should be rejected. Errors in the measurements of the rice husk feed rate, char flow rate, produced gas flow rate, ultimate and proximate analyses and unaccounted tar yield were the major sources of non-closure. However, reported mass balance closures for carbon of 82 to 102 (Chern et al. 1989) and of 70 to 117 (Egudenler, 1993) were comparable to that obtained in this study. Considering the various uncertainties explained above and the consistency of our results with those reported in the literature, the results of the mass balance were fairly good.

10.2.9.2 Energy Balance.

The higher values of energy in the form of gas observed at the highest equivalence ratio (0.35) may be due to higher gas yield resulting from higher gasifier temperatures. The sensible heat in gas was affected by the gasifier temperature as well as the rate of heat loss through the gasifier walls. The heat losses obtained in this study were very low (< 1%) due to the fact that the gasifier was well insulated. However, higher unaccounted losses were observed due mainly to the high unburned carbon and sensible heat in the char.

Cold gas thermal efficiency as high as 87.6% was obtained in this study because of the low heat losses from the gasifier. Schoeters et al. (1989) reported cold gas thermal efficiency of 50.0% for the gasification of wood shavings in a bench scale fluidized bed gasifier. They mentioned that in larger units the efficiency should be between 80.0 and 90.0%. Thermal efficiencies in the range of 26.1-87.3% have been attained by several researchers (Chern et al. 1989; Maniatis et al., 1989; Schiefelbein, 1989; Ergudenler, 1993; and Sadaka, 1994) under normal operating conditions of fluidized bed biomass gasifiers. A common conclusion is that the overall efficiency can be improved further if the sensible heat of the product gas could be recuperated in a heat exchanger. In this study, the sensible heat of the gas accounted for a very small percentage of the total energy of the rice husk and, thus, its contribution to the cold gas thermal efficiency was insignificant.

10.2.10 Reproducibility

The three gas samples collected from the gasifier exit at 5 minute intervals after steady state was attained showed good and acceptable agreement between these results, indicating that the fluidized bed gasifier will produce identical results under steady state conditions.

10.3 Model Validation

Mathematical models are powerful tools for gaining a fundamental understanding of engineering processes and the scaling-up, designing and optimization of these processes. However, before developed models can be utilized for these purposes, they have to be validated by testing their ability to simulate experimental results. Thus, to investigate the validity of the two-compartment model, the predicted core, annulus and exit temperatures, the mole fractions of the combustible components of the gas, higher heating value of the gas, and overall carbon conversion were compared with those experimentally obtained from the gasification of rice husk in a dual distributor type fluidized bed reactor at various bed heights (19.5, 25.5 and 31.5 cm), fluidization velocities (0.22, 0.28 and 0.33 m/s) and equivalence ratios (0.25, 0.30 and 0.35).

10.3.1 Gasification Temperature

A comparison of the temperatures (core, annulus and exit) predicted using the two-compartment model (Equations 9.9 and 9.10) with those experimentally measured are shown in Figures 10.6 to 10.8. The experimentally measured core temperature is taken as the average of the two temperatures measured at the center of the dense bed of the gasifier (T_4 and T_7). Similarly, the experimentally measured annulus temperature is taken as the average of the two temperatures measured at the walls of the dense bed of the gasifier (T_6 and T_9). The measured exit temperature is the temperature at which the exit gas compositions were sampled. Generally the model predictions of the core, annulus and exit temperatures were in reasonably close agreement with actual core, annulus and exit temperatures observed during the experiments. This reasonably good agreement between model predictions and experimental measurements could be attributed to the ability of the two-compartment model to take the complex bed hydrodynamics into consideration.

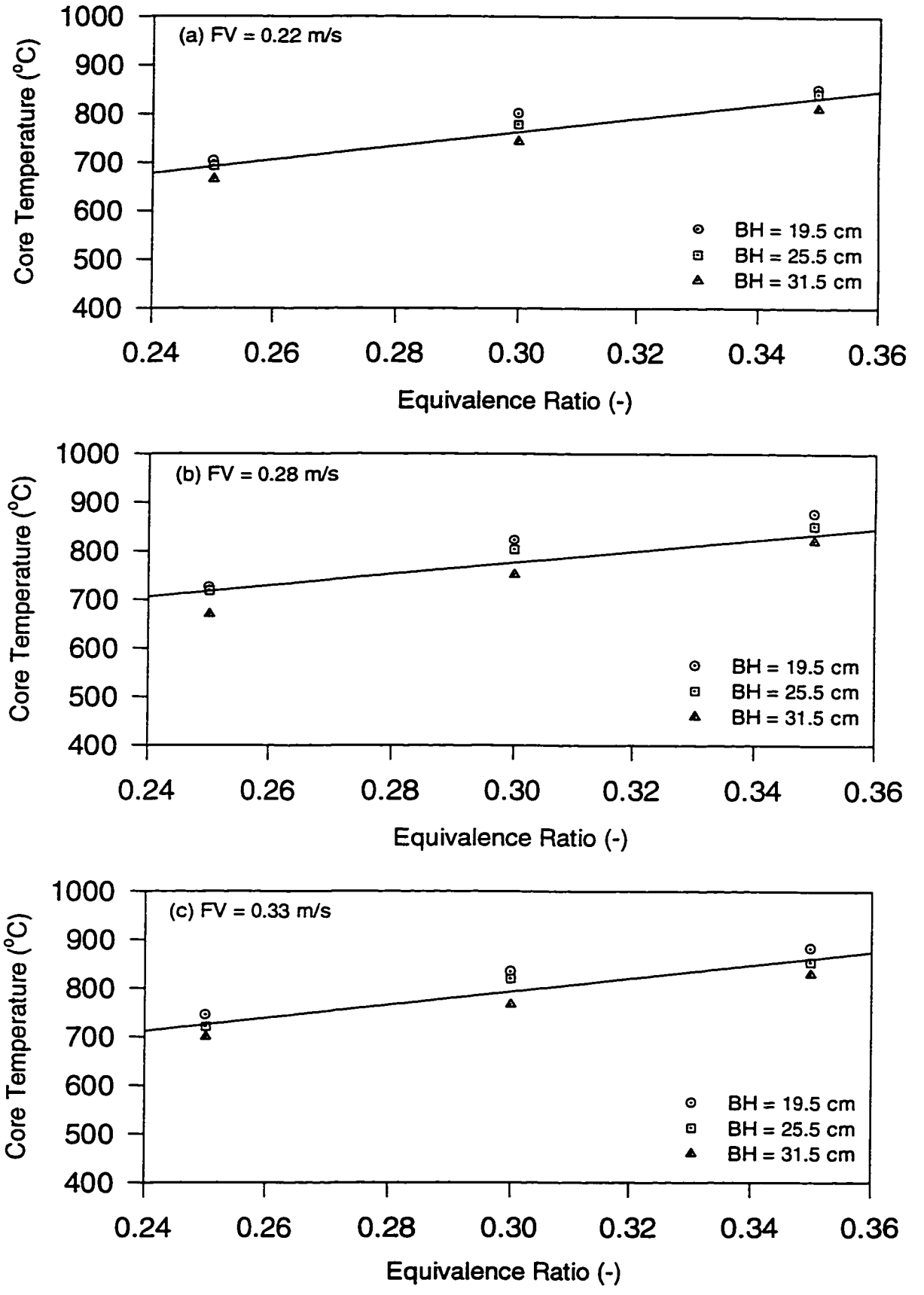

Figure 10.6 Comparison of predicted and measured core temperatures at various equivalence ratios, fluidization velocities and bed heights.

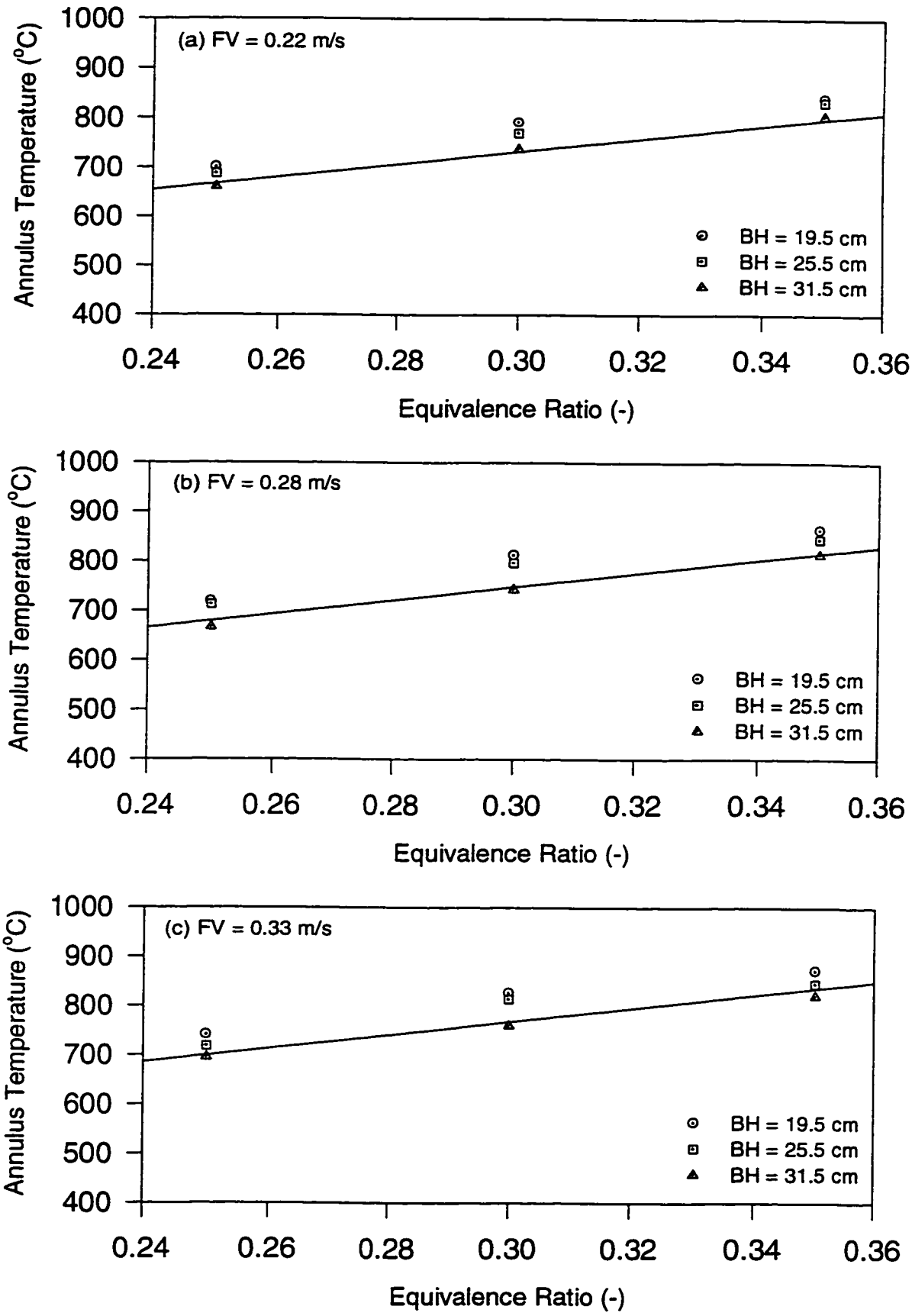

Figure 10.7 Comparison of predicted and measured annulus temperatures at various equivalence ratios, fluidization velocities and bed heights.

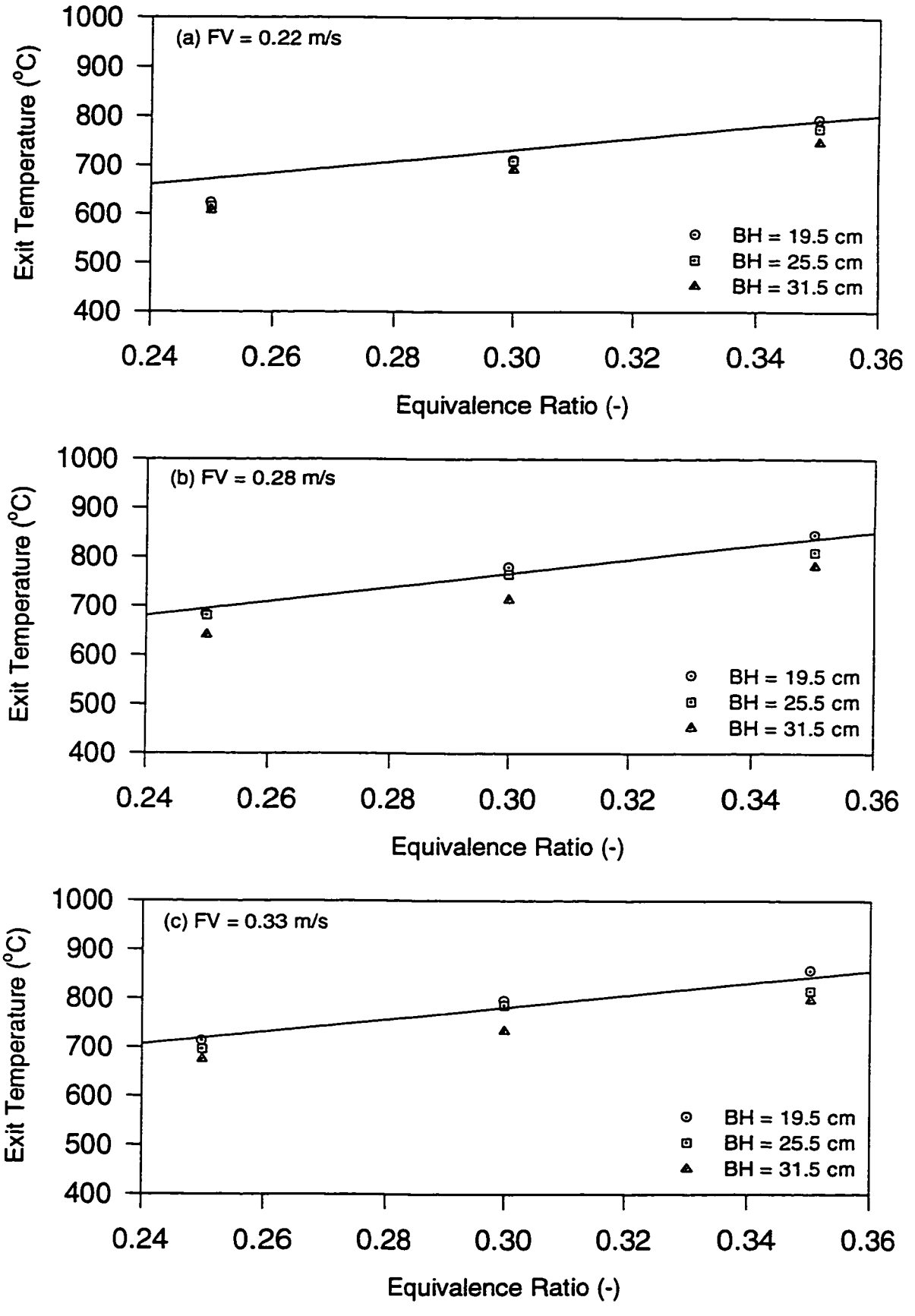

Figure 10.8 Comparison of predicted and measured exit temperatures at various equivalence ratios, fluidization velocities and bed heights.

However, the model appeared to slightly underpredict the annulus temperature and overpredict the exit temperature. The model predictions of the core temperature were slightly higher (~ 5.0%) than those of the annulus temperature. Since the solid particles in each region are assumed to be well mixed, the average temperature in different parts of these regions is expected to be substantially the same. The decline in temperature is best elucidated by considering the temperature history of a particle moving from the core to the annulus, assuming a solids heating process. While the time spent by a particle in the core is an insignificant fraction of that spent in the annulus, the former time is spent under the influence of a much higher heat transfer coefficient and a higher driving force since the fluidizing gas velocity is about one order of magnitude higher than in the annulus. Particles leaving the core would therefore be warmer than, and would discharge their heat on joining, the annular solids. This transfer would occur partly by conduction to the surrounding particles and partly by convection to the gas percolating through the annulus.

10.3.2 Gas Composition

The comparisons of the predicted and the measured mole fractions of CO, H_2 and CH_4 are presented in Figures 10.9 to 10.11. The predicted and experimental mole fractions of CO, H_2 and CH_4 were in very good agreement. However, the predicted mole fractions of H_2 appeared slightly higher than the experimental results under all treatment combinations whereas those of CH_4 appeared slightly higher only at the lower equivalence ratio (0.25).

10.3.3 Higher Heating Value

A comparison of the predicted and the experimental higher heating value of the gas is presented in Figure 10.12. A trend similar to that of CH_4 was observed. This was because CH_4 was the main contributor to the higher heating value of the gas. The predicted higher heating value of the gas agreed reasonably well with that obtained experimentally. This indicates that the model did a creditable job of correlating the product gas higher heating value.

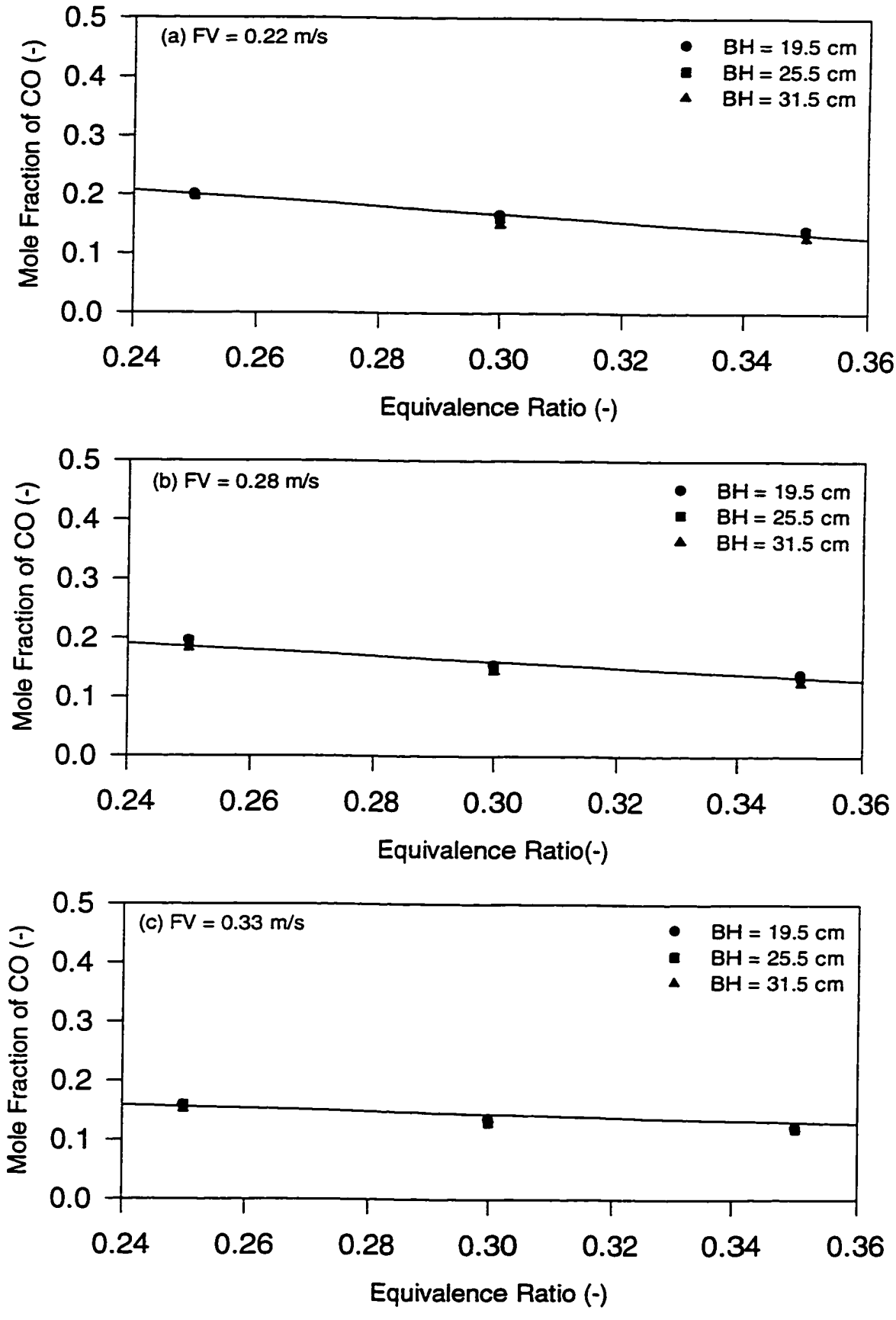

Figure 10.9 Comparison of predicted and measured mole fractions of CO at various equivalence ratios, fluidization velocities and bed heights.

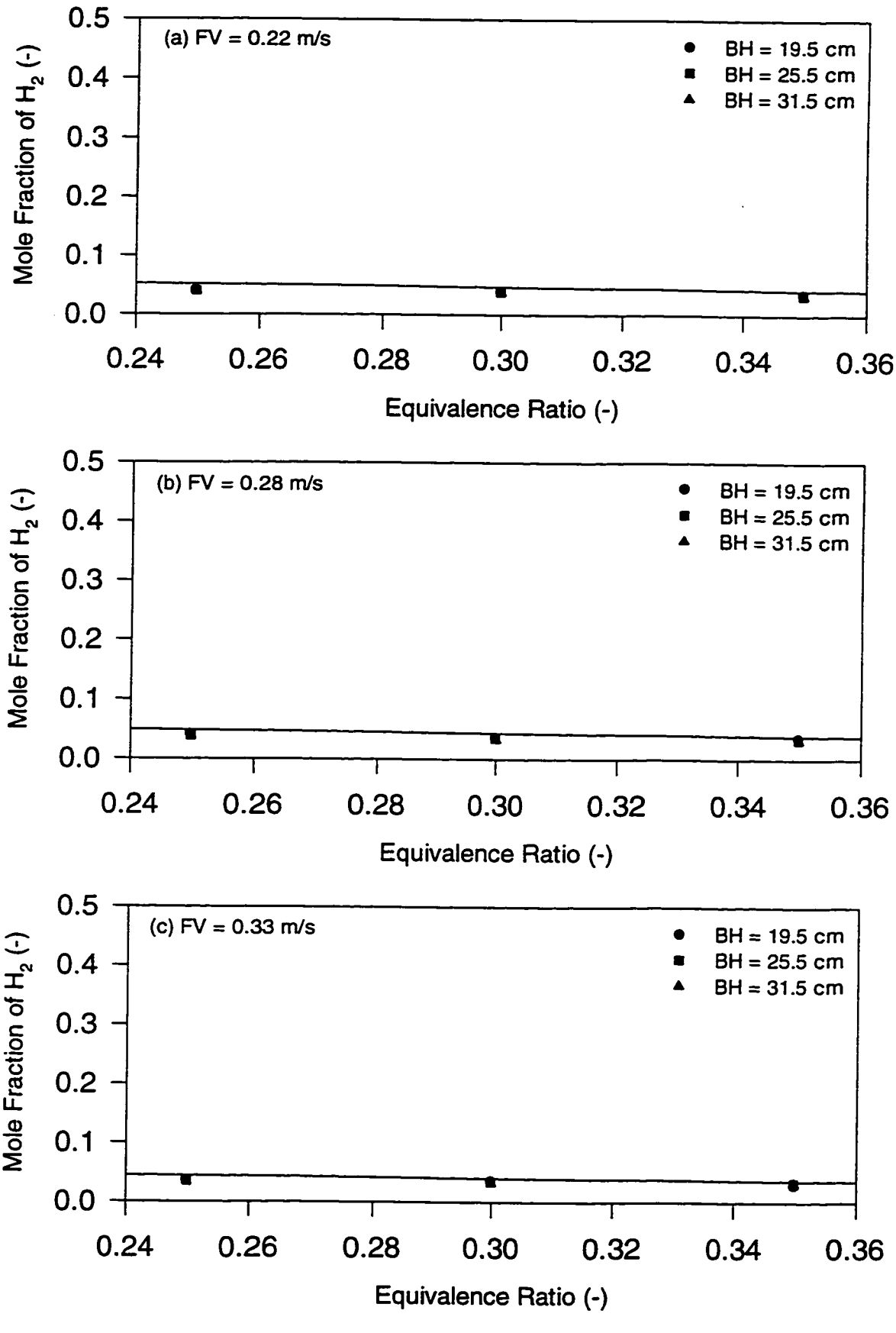

Figure 10.10 Comparison of predicted and measured mole fractions of H_2 at various equivalence ratios, fluidization velocities and bed heights.

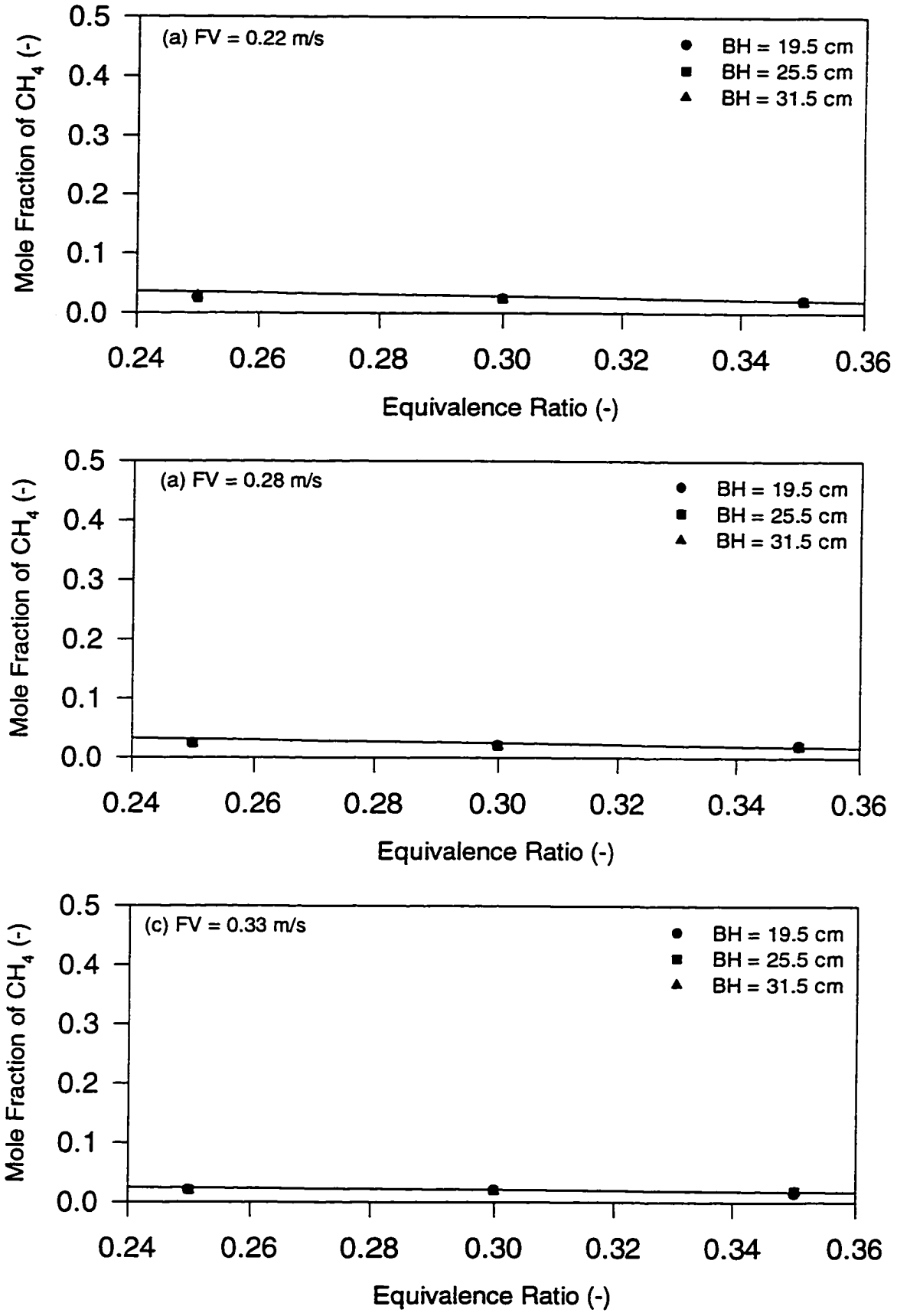

Figure 10.11 Comparison of predicted and measured mole fractions of CH_4 at various equivalence ratios, fluidization velocities and bed heights.

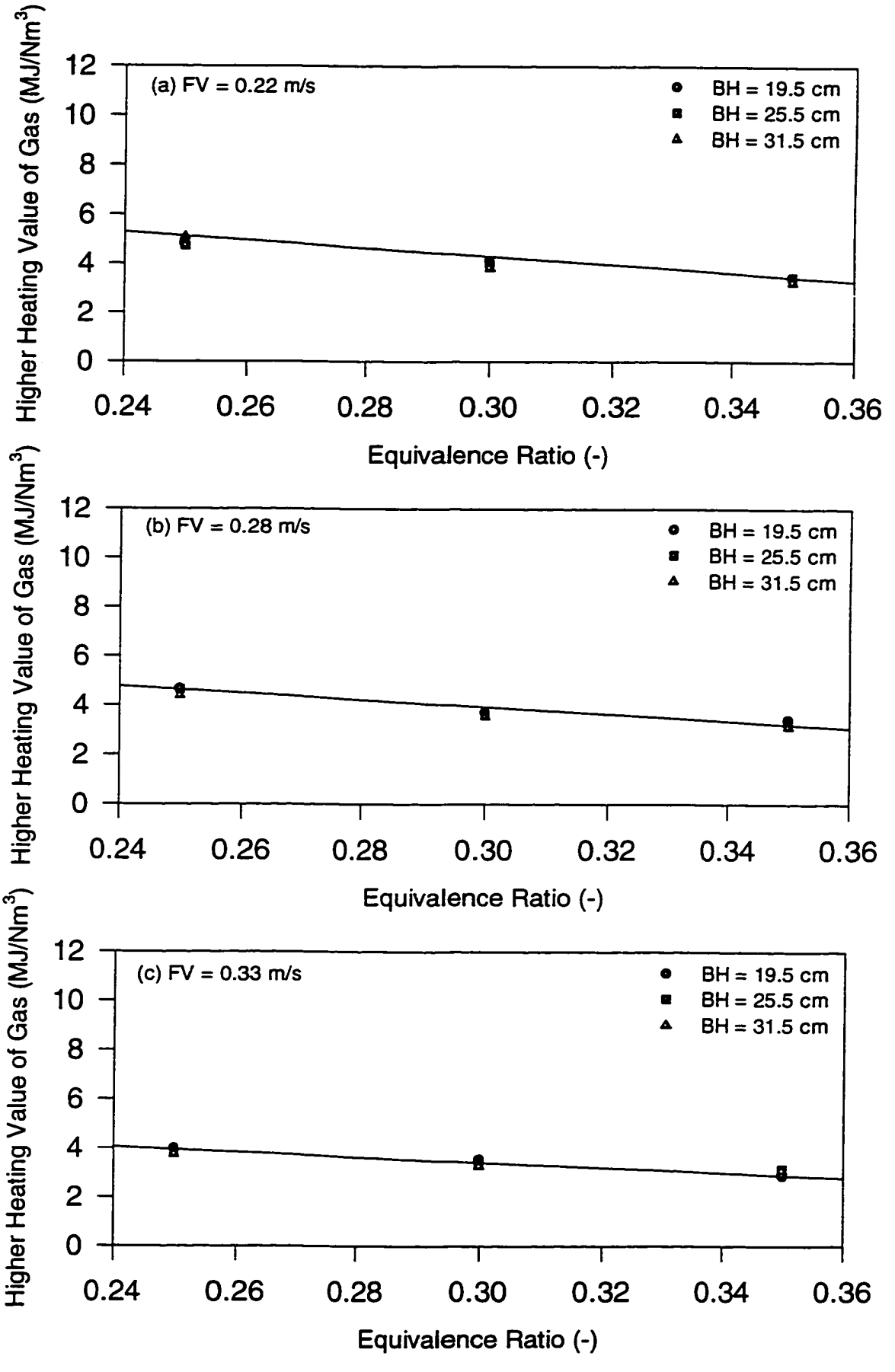

Figure 10.12 Comparison of predicted and measured gas higher heating value at various equivalence ratios, fluidization velocities and bed heights.

10.3.4 Carbon Conversion

Figure 10.13 shows a comparison between the predicted and measured overall carbon conversion. Apparently, the discrepancy between calculated and measured values of the overall carbon conversion was relatively large for a number of experiments. The much higher predicted overall carbon conversion than those calculated from the carbon content in the solids collected in the cyclone collector could be attributed to the fact that heavier ash tends to move to the bottom of the ash collector while the char concentrates at the top and thus the samples taken may not have been representative. This results in lower carbon conversion than what it would have been if the whole sample was analyzed. The very large amount of random error which is more obvious at lower equivalence ratios is probably due to the fact that there was more char in the cyclone collector under those conditions. Despite the fact that the discrepancy between calculated and measured values of the overall carbon conversion was very large, the order of magnitude was well predicted, which is important in relation to predicting the maximum rice husk conversion capacity per unit reactor-volume.

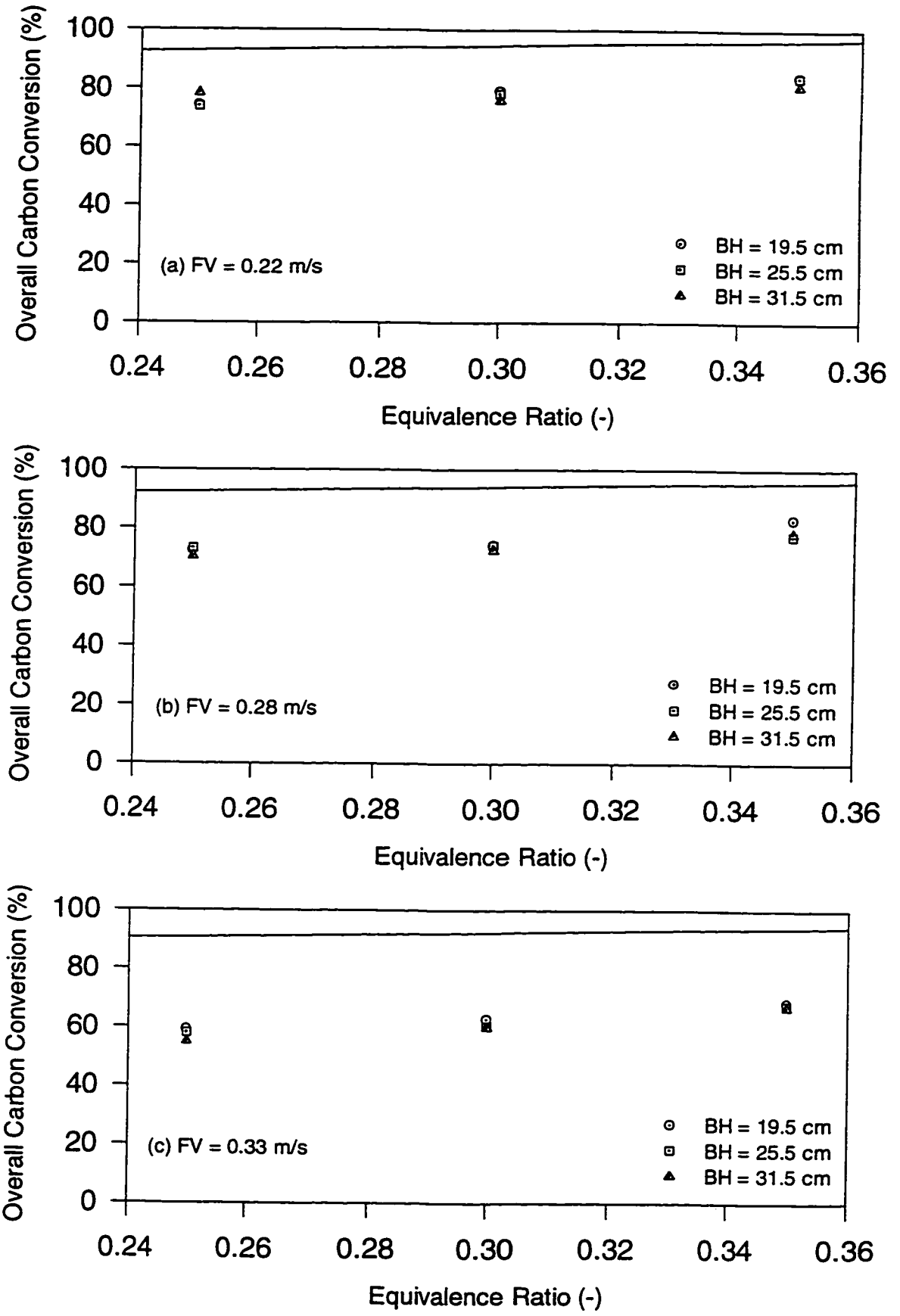

Figure 10.13 Comparison of predicted and measured overall carbon conversions at various equivalence ratios, fluidization velocities and bed heights.

11. CONCLUSIONS

11.1 Apparatus

The feeding system of the existing dual distributor fluidized bed gasifier was modified to handle rice husk. The data acquisition and measurement system, used for the continuous monitoring of the fuel feed rate, reactor temperatures, pressure drops, and air and gas flowrates, was upgraded. Gas and particles sampling probes were designed, fabricated and used to withdraw gas samples from six axial positions in the gasifier and solids from two axial positions in the dense bed of the gasifier, respectively.

1. The modified auger of the feeding system handled the rice husk efficiently. It provided a very good compaction of rice husk at the auger exit which was necessary to avoid hot gas backflow into the feeder.

2. The upgraded data acquisition and measurement system performed very well and was trouble free.

   (a) The gasifier temperatures at 14 different locations along the height of the reactor were monitored and recorded at various operating conditions with an accuracy of $\pm 0.1^{\circ}C$.

   (b) The pressure drop measurements across the fluidized bed provided useful information on the quality of fluidization.

3. The gas and solid sampling probes performed satisfactorily.

(a) The three gas sampling probes located in the freeboard and exit of the gasifier performed very well but the three gas sampling probes located in the dense bed clogged due to ash deposits at the tip of the probes and, therefore, required regular cleaning.

(b) No problems were encountered with the particles sampling probes.

11.2 Preliminary Experiments

Preliminary experiments were conducted to assess the suitability of rice husk as a gasification fuel, to determine the feasible range of operating conditions for fluidized bed gasification of rice husk and to obtain data for proper design of thermochemical conversion systems.

1. The various aspects of physical and chemical properties of rice husk samples obtained from six varieties of rice (Lemont LG, ROK 14, ROK 16, ROK 32, CP 4, and Pa Potho) pertaining to the design of thermochemical conversion systems were determined. These included moisture content, bulk density, particle size, heating values, proximate analysis, ultimate analysis, ash composition and ash fusibility characteristics.

   (a) Moisture content ranged from 8.68 to 10.44% (wet basis), and bulk density ranged from 86 to 114 kg/m^3.

   (b) The particle size distribution of majority of the particles (55%) ranged in length from 6.2 to 10.0 mm and in width from 1.7 to 2.4 mm.

(c) Rice husk is a unique biomass material having a high ash content of 15.30 to 24.60%. The ash in rice husk contained 90 to 97% silica.

(d) The very low concentrations of nitrogen (0.38 to 0.51%), sulphur (0.014 to 0.034%) and chlorine (0.01 to 0.13%) offer environmentally more desirable fuel properties.

(e) The lower heating value of all the rice husk samples were found to lie in a fairly narrow range (13.24 to 16.20 MJ/kg) when expressed on a dry, ash free basis. Volatile matter contents were in excess of 60% by weight (dry basis) for all samples.

(f) The initial deformation temperature of the rice husk ash in the oxidizing and the reducing atmospheres ranged from 1349 to 1486°C and 1330 to 1460°C, respectively.

2. The agglomeration characteristics of inert bed materials (silica and alumina sand particles) in the presence of rice husk ash were investigated at elevated temperatures to define conditions beyond which it is not safe to operate the gasifier.

(a) Rice husk ash particles treated at higher temperatures (850-1000°C) formed weak bonds at the surface of the silica and alumina sand particles resulting in soft and friable agglomerates.

(b) The mechanism of bonding is somewhat obscure, and does not appear to involve a liquid phase. A possible mechanism of formation considers that the condensation of low melting temperature mineral oxides (K_2O, Na_2O and

P_2O_5) present in rice husk ash, upon the Si or Al particles provides an initial sticky surface to which ash particles adhere. These low melting temperature mineral oxides represent minor constituents of rice husk ash and, therefore, not suitable for the formation of strong and stable agglomerates. Since the bonds formed did not alter the shape of the particles, diffusion of the materials is a possible mechanism responsible for the formation of such friable structures. There is also the possibility of physical entrapment of the Si or Al particles by the minute whiskers at the surface of the rice husk ash.

3. The thermogravimetric analysis (TGA) technique was used to study the thermochemical behaviour of four types of rice husk (Lemont, ROK 14, CP 4, and Pa Potho) at three heating rates (10, 20, and 50°C/min) in air, oxygen and nitrogen atmospheres. The thermograms showed two distinct reaction zones. The thermal degradation rate in active and passive zones, the initial degradation temperature, and the residual weight at 700°C were determined.

   (a) The initial degradation temperature decreased while both the thermal degradation rate and the residual weight at 700°C increased when the heating rate was increased.

   (b) The higher the cellulosic content of the rice husk, the higher the thermal degradation rate and the initial degradation temperature. Also, higher ash content in the rice husk resulted in a higher residual weight at 700°C.

   (c) The thermal degradation rate in active zone was higher in the presence of oxygen than in the presence of air and nitrogen.

(d) More residual weight was recorded in the nitrogen atmosphere compared to the oxidative atmospheres of air and oxygen. The residual weights of the rice husk samples at 700°C in air and oxygen atmospheres were lower than their initial ash contents with percentages of ash lost ranging from about 2.95 to 13.10% in the case of air and 4.20 to 17.05% in the case of oxygen.

4. The kinetic parameters (activation energy, pre-exponential factor and order of reaction) of four varieties of rice husk, which can be used in the design of thermochemical conversion systems) were determined for the two distinct reaction zones. The thermal degradation indices obtained at the heating rate of 20°C/min under air, nitrogen and oxygen atmospheres were employed. The kinetic parameters were influenced principally by the gas phase atmosphere imposed on the samples. Sample to sample variation was also apparent.

(a) In the first reaction zone, the activation energies obtained under nitrogen ranged from 29.0 kJ/mol for Lemont LG rice husk to 35.4 kJ/mol for Pa Potho rice husk. The activation energies for rice husk in air atmosphere were of similar magnitude to those in nitrogen atmosphere, although generally higher at 37.0 kJ/mol for CP 4 rice husk to 54.7 kJ/mol for ROK 14 rice husk. In oxygen atmosphere, the activation energies were substantially higher at 142.7 kJ/mol for CP 4 rice husk to 188.5 kJ/mol for ROK 14 rice husk.

(b) The highest activation energy in the second reaction zone was obtained in air atmosphere (21.0 kJ/mol) for ROK 14 rice husk, followed by that obtained in nitrogen atmosphere (17.7 kJ/mol) for Pa Potho rice husk and in oxygen atmosphere (16.6 kJ/mol) for ROK 14 rice husk.

(c) The pre-exponential factors under air and nitrogen atmospheres in the first reaction zone were in the range of 10^3 to 10^6 min^{-1}. Under oxygen atmosphere, the pre-exponential factor in the first reaction zone ranged as high as 10^{17} min^{-1}.

(d) The order of reactions determined in this study were in the range of 0.7 to 1.6 for the first reaction zone and 0.2 to 0.5 for the second reaction zone.

11.3 Main Experiments

Gasification experiments were designed to investigate the effects of bed height (19.3, 25.5 and 31.5 cm), fluidization velocity (0.22, 0.28 and 0.33 m/s) and equivalence ratio (0.25, 0.30 and 0.35) on the performance of the fluidized bed rice husk gasifier.

1. Steady operating conditions, a uniform temperature distribution in the dense bed, a consistent pressure drop, good mixing of solids and gases were observed in the fluidized bed rice husk gasifier.

2. The reactor temperature was affected by the bed height, fluidization velocity and equivalence ratio.

   (a) The gasifier temperature showed an increasing trend with increasing equivalence ratio and fluidization velocity and a decreasing trend with increasing bed height.

   (b) The minimum and maximum temperatures of the dense bed were 665°C (at the bed height of 31.5 cm, the fluidization velocity of 0.22 m/s and the equivalence

ratio of 0.25) and 880°C (at the bed height of 19.5 cm, the fluidization velocity of 0.33 m/s and the equivalence ratio of 0.35), respectively.

(b) The dense bed temperatures practically reached the steady state condition within about 16-20 minutes. The temperature profiles showed that the dense bed was essentially isothermal while the temperatures recorded in the freeboard and gasifier exit dropped.

3. The pressure drop in the reactor was affected by the bed height, fluidization velocity and equivalence ratio.

(a) Increasing the fluidization velocity and/or decreasing the equivalence ratio resulted in higher pressure drops in the dense bed, freeboard region and enlarged section whereas increasing the bed height increased the pressure drop only in the dense bed.

(b) The minimum and maximum pressure drops observed in the reactor were 1.5 kPa and 6.1 kPa, respectively.

(c) The pressure drop across the secondary distributor plate ranged between 0.8 kPa and 1.6 kPa.

4. The gas composition was affected by the equivalence ratio and fluidization velocity but was relatively insensitive to changes in the bed height.

(a) Generally, increasing the equivalence ratio and/or increasing the fluidization velocity increased the concentrations of CO_2 and N_2 and decreased the concentrations of CO, H_2 CH_4, $C_2H_2 + C_2H_4$ and C_2H_6. The concentrations of

the combustible components of the gas reached their maximum value at the equivalence ratio of 0.25.

(b) No distinct trend between the concentration of O_2 in the product gas and all the parameters investigated was apparent.

(c) The concentrations of the noncombustible components of the gas decreased while the concentrations of the combustible components of the gas increased with distance from the main distributor plate.

(d) The concentrations of the gas components revealed that nitrogen was in the highest concentration (57.0-69.0 vol. %). The concentration of CO_2 varied in the range 12.0-17.6 vol. %. From the fuel gases which are of major interest, CO had the highest concentration (8.5-20.1 vol. %), followed by H_2 (2.0-4.0 vol. %), and then CH_4 (1.0-3.0 vol. %). The other components (C_2H_2 + C_2H_4 and C_2H_6) were produced with lower concentrations.

5. The higher heating value of the gas was affected by the equivalence ratio and fluidization velocity but was relatively insensitive to changes in the bed height. Increasing the equivalence ratio and/or the fluidization velocity decreased the higher heating value of the gas. The maximum higher heating value of the gas (5.03 MJ/Nm^3) was obtained at the bed height of 31.5 cm, fluidization velocity of 0.22 m/s and the equivalence ratio of 0.25.

6. Increases in the equivalence ratio generally led to increased gas yield. The gas yield remained approximately constant up to the fluidization velocity of 0.28 m/s and then decreased slightly with further increase in fluidization velocity. The gas yield, however, did not change appreciably with changes in the bed height. The gas yield ranged from

1.30 Nm^3/kg fuel (at the bed height of 31.5 cm, fluidization velocity of 0.33 m/s and equivalence ratio of 0.25) to 2.02 Nm^3/kg (at the bed height of 19.5 cm, fluidization velocity of 0.22 m/s and equivalence ratio of 0.35).

7. The fact that the gas was free of tar is beneficial for the further use of the gas. Tar-free gas indicates a high environmental acceptability of the fluidized bed gasification process.

8. The elutriated char from the reactor increased with increasing fluidization velocity and/or bed height but decreased with increasing equivalence ratio. The particle size distributions of the char samples withdrawn from different locations in the dense bed were similar to each other and much coarser than those captured by the cyclone collector. Also, variations in elemental composition between char samples withdrawn from the dense bed were relatively small, indicating that the solids were well mixed and distributed.

9. The carbon conversion, which spanned from 55.0 to 84.0% under all conditions investigated, increased with the increase in equivalence ratio and/or the decrease in fluidization velocity but was not significantly affected by changes in the bed height.

10. The cold gas thermal efficiency increased with increasing equivalence ratio and decreased with increasing fluidization velocity but was practically insensitive to changes in the bed height. The maximum cold gas thermal efficiency (87.6%) was obtained at the highest equivalence ratio and lowest fluidization velocity and bed height.

11.4 Modeling

Two mathematical models based on thermodynamic approach were developed using the ASPEN PLUS process simulator and used to simulate the performance of the dual distributor fluidized bed gasifier. The first (the single-compartment model) neglects the complex hydrodynamic conditions prevalent in the gasifier whereas those are taken into consideration in the second (the two-compartment model). The first model has a single parameter (overall carbon conversion) that can be used to improve the fit between predicted and experimental gas compositions whereas the second model has two parameters (carbon conversion in the core and annular regions) that can be independently adjusted to account for the effect of various operating and design conditions on the composition of the gasification products.

1. The one-compartment model provides reasonably good estimate of the product gas composition. The mean error between the predicted and measured product gas composition varied between 2.45% (at the bed height of 31.5 cm, fluidization velocity of 0.22 m/s and equivalence ratio of 0.35) and 3.05% (at the bed height of 19.5 cm, fluidization velocity of 0.33 m/s and equivalence ratio of 0.25).

2. The use of the two-compartment model resulted in 4-fold reduction in the mean errors (0.61-0.76%) and can, therefore, be considered as a statistically significant improved modeling approach. This improvement results mainly from the ability of the two-compartment model to account for the complex hydrodynamics present in the dual distributor fluidized bed gasifier.

3. A sensitivity analysis was performed on the two-compartment model at a wide range of operating/design conditions (bed height, fluidization velocity, equivalence ratio, oxygen concentration in fluidizing gas and moisture content in rice husk).

(a) The bed height was shown to have a significant positive effect on the core, annulus and exit temperatures, but only a small effect on the gas composition, higher heating value and carbon conversion. This implies that the gasifier can be operated at any bed height near the targeted operating conditions without significantly affecting the gasifier output.

(b) An increase in the fluidization velocity increases the core, annulus and exit temperatures but decreases the mole fractions of the combustible gas components (CO, H_2 and CH_4) and the higher heating value of the gas. The overall carbon conversion slightly increased with fluidization velocity until a point is reached and then decreased with further increase in fluidization velocity.

(c) Increasing the equivalence ratio resulted in proportional increases in the gasifier core, annulus and exit temperatures as well as in the overall carbon conversion and decreases in the mole fractions of the combustible gas components CO, H_2 and CH_4 and the higher heating value of the gas.

(d) Increasing the concentration of oxygen in the fluidizing gas increased the gasifier core, annulus and exit temperatures, and the mole fractions of CO, H_2 and CH_4. There was, also, a significant increase in the higher heating value of the gas and the overall carbon conversion.

(e) Increasing moisture in the rice husk was found to moderate the reactor core, annulus and exit temperatures. The mole fractions of CO and H_2 decreased with increasing moisture in rice husk but that of CH_4 remained approximately constant. Also, increased moisture in rice husk severely reduces the higher heating value of the gas. Apparently, increased loss in gas higher heating value

occurs when the moisture content was increased from 20 to 30%. Therefore, to obtain a gas of significant heating value, the moisture content of rice husk should not exceed 20%. The overall carbon conversion decreases when the moisture content in rice husk was increased.

4. The predictions of the two-compartment model were compared with those experimentally obtained from the gasification of rice husk in the dual distributor fluidized bed reactor at various bed heights (19.5, 25.5 and 31.5 cm), fluidization velocities (0.22, 0.28 and 0.33 m/s) and equivalence ratios (0.25, 0.30 and 0.35). Predictions of the core, annulus and exit temperatures as well as the mole fractions of the combustible gas components and product gas higher heating value agreed reasonably well with experimental data.

12. RECOMMENDATIONS

This study has brought about a number of considerations which may be of potential interest for future work in the area of biomass gasification.

1. On-line gas analysis would provide better understanding of the dynamic behaviour of the fluidized bed gasifier.

2. Long-run tests (of several days) should be undertaken to observe any possible char or tar build up, agglomeration or any other operational problems.

3. Addition of a particle sampling probe at the gas duct after the cyclone to permit capture and analysis of fines which are entrained with the exit gas will give an idea of the dirtiness of the gas at the gasifier exit and, thus, the level of gas cleaning required or reinjection of solids captured by the cyclone to increase residence times and gasification efficiencies.

4. A gas clean-up system should be adapted to the gasifier to generate gas of engine quality.

5. Attempts should be made to run a diesel engine completely or partially on the gas produced by the dual distributor type fluidized gasifier. The response time of the gasifier to a variation of the load should be compared to the response time of the engine, in order to obtain the same flexibility as with diesel oil.

6. The developed dual distributor fluidized bed gasifier models should be tested with different types of biomass materials.

7. A complete and detailed economic evaluation of the fluidized bed gasification process should be undertaken.

13. REFERENCES

Abbey, S., N. J. Lee and J. L. Bouvier. 1974. Analysis of rocks and minerals using an atomic absorption spectrophotometer. Paper No. 74-19, Part 5. Department of Energy, Mines and Resources, Ottawa, Ontario.

Abrahmasen, A. R. and D. Geldart. 1980. Behaviour of gas-fluidized beds of fine powders. Part I. Homogenous expansion. Powder Technology 26(1): 35-42.

Addis E. J., W. Bagshaw, B. A. Napier, E. A. Rogers, S. Rafailidis and R. Clift. 1991. Proceedings of the Eleventh International Conference on Fluidized Bed Combustion. E. J. Anthony (ed.), ASME, New York, pp. 763-770.

Agarwal, J. C., W. L. Davis and D. T. King. 1962. Fluidized bed coal dryer. Chemical Engineering Progress 58(1): 85-95.

Aho, M. And J. Huotari. 1985. The effects of atmosphere on pyrolysis of solid fuels produced in Finland. In: Fundamentals of Thermochemical Biomass Conversion. R. P. Overend, T. A. Milne, and L. K. Mudge (eds.), Elsevier Applied Science Publishers, New York, pp. 429-435.

Anderson, B. A. and B. Leckner. 1989. Particle mass flux in the freeboard of a fluidized bed boiler. Powder Technology 58(1): 25-37.

Annamalia, K. A., J. M. Sweeten and S. C. Ranalingan. 1987. Estimation of gross heating value of biomass fuels. Transactions of the American Society of Agricultural Engineers 30(4): 1205-1208.

Anon. 1978. Annual Book of ASTM Standards. American Society for Testing and Materials, Philadelphia, PA. 19103.

Anon., 1983. Annual Book of ASTM Standards. American Society for Testing and Materials, Philadelphia, PA. 19103.

Antal, M. J., H. L. Friedman and F. E. Rogers. 1980. Kinetics of cellulose pyrolysis in nitrogen and steam. Combustion Science and Technology 21(2): 141-149.

APHA. 1985. Standard Methods for the Examination of Water and Wastewaters. American Public Health Association, Washington, DC.

Arastoopour, H., M. H. Hariri and A. Rehmat. 1989. Agglomeration in a fluidized bed with a central jet. In: Fluidization VI. J. R. Grace J. R., L. W. Shemite and M. A Bergougnou (eds.), Engineering Foundation, New York, pp. 563-570.

ASPEN PLUS, 1994. "ASPEN PLUS Users Guide", Aspen Technology Inc., Cambridge, Massachusetts.

ASTM. 1978. American Society for Testing and Materials, Specifications for Pozzolanas, ASTM C618-78, Philadelphia.

ASTM. 1986. Annual Book of ASTM Standards. American Society for Testing and Materials, Philadelphia, PA.

Bacon, D.W., Downie, J. C. Hsu and J. Peters. 1985. Modelling of fluidized bed wood gasifiers. In: Fundamentals of Thermochemical Biomass Conversion. R. P. Overend, T.

A. Milne and K. L. Mudge (eds.). Elsevier Applied Science Publishers, London, UK, pp. 717-732.

Baeyens, J. and D. Geldart. 1986. Solids Mixing. In: Gas Fluidization Technology. John Wiley & Sons. New York.

Baeyens, J., D. Geldart and S. Y. Wu. 1992. Elutriation of fines from gas fluidized beds of Geldart A-type powders - Effect of adding superfines. Powder Technology 71(1): 71-80.

Bai, D. R. 1992. Axial distribution of the cross-sectional averaged voidage in fast fluidized beds. Powder Technology 71(1): 51-58.

Baldyga, J., R. Bourne and B. Zimmermann. 1994. Investigation of mixing in jet reactors using fast, competitive-consecutive reactions. Chemical Engineering Science 49(12): 1937-1964.

Barnard, G. and L. Kristoferson. 1985. Agricultural Residues as Fuel in the Third World. Earthscan Technical Report No. 4, London, UK.

Bartha, P., and A. Huppertz. 1974. The structure of silica in rice husks and their crystallization. Presented at the Rice By-Product Utilization International Conference, Valencia, Spain.

Beagle, E. 1978. Rice Husk Conversion to Energy. Agricultural Services Bulletin 31, Food and Agricultural Organization, Rome, Italy.

Beeckmans, J. M. and Z. Yu. 1992. Continuous separation of solids in a mechanical fluidized bed. Powder Technology 70(1): 77-81.

Beenackers, A. A. and A. V. Bridgewater. 1989. Gasifiaction and pyrolysis of biomass in Europe. In: Pyrolysis and Gasification. Ferrero, G. L., K. Maniatis, A. V. Bridgewater (eds.), Elsevier Applied Science, London, UK, pp. 129-157.

Bento, J. 1989. Reactor for continuous conversion of agro-forestral residual biomasses into combustible gas and charcoal. University of Twente, The Netherlands.

Bernard, G. W. 1984. Small scale gasification in practice in developing countries. In: Bioenergy 84. H. Engeus and A. Ellegard (eds.). Elsevier Applied Science Publishers, London, UK, pp. 218-235.

Bilbao, R., J. L. Lezaun, M. Menendez and J. C. Abanades. 1988. Model of mixing/segregation for sand-straw mixtures in fluidized beds. Powder Technology 56(1): 149-155.

Bilodeau, J. D., N. Therien, P. Proulx, S. Czernik and E. Chornet. 1993. A mathematical model of fluidized bed biomass gasification. Canadian Journal of Chemical Engineering 71(2): 549-557.

Bining, A. S. and B. M. Jenkins. 1992. Thermochemical reaction kinetics for rice straw from an approximate integral technique. American Society of Agricultural Engineers, Paper No. 92-6029, St. Joseph, MI.

Black, J. W., K. G. Bircher and K. A. Chisholm. 1980. Fluidized bed gasification of solid wastes and biomass: the CIL Program. In: Thermal Conversion of Solid Wastes and Biomass. American Chemical Society Symposium Series 130, Washington, D. C., pp. 351-361.

Boateng, A. A. 1989. The Potentials of Rice Husk Ash Cement in Guyana. Paper presented at the 5th EEC Conference on Biomass for Energy and Industry, Lisbon, Portugal, Oct. 9-13.

Boateng, A. A., L. T. Fan, W. P. Walawender and C. S Chee. 1991. Morphological development of rice-hull-derived charcoal in a fluidized bed reactor. Fuel 70(5): 995-1000.

Boateng, A. A., W. P. Walawender, L. T. Fan and C. S. Chee. 1992. Fluidized bed steam gasification of rice hull. Bioresource Technology 40(2): 235-239.

Boie, W. 1952. Wissenschaftliche Zeitschnift der Technischen Hochschule Dresden 2(3): 687. Cited by Annamalia et al. (1987).

Bridgwater, A. V. 1989. Economic and market opportunities for biomass derived fuels. In: Pyrolysis and Gasification. G. L. Ferrero, K. Maniatis, A. Buekens and A. V. Bridgwater (eds.), Elsevier Applied Science, London, UK, pp. 111-128.

Bridgwater, A. V. 1995. The technical and economic feasibility of biomass gasification for power generation. Fuel 74(3): 631-653.

Bridgwater, A. V. and G. D. Evans. 1993. An assessment of thermochemical conversion systems for processing biomass and refuse. ETSU Report B/T1/00207/REP, UK Department of Trade & Industry.

Brink, D. L. 1981. Gasification. In: Organic Chemicals from Biomass. I. S. Goldstein (ed.), CRC Press, Florida, pp. 45-54.

BTG. 1990. State of the art of rice husk gasification. A report prepared for the Dutch Ministry of Foreign Affairs. Biomass Technology Group, University of Twente, Enschede, The Netherlands.

Buekens, A. G. and J. G. Schoeters. 1985. Modeling of biomass gasification. In: Fundamentals of Thermochemical Biomass Conversion. R. P. Overend, T. A. Milne and K. L. Mudge (eds.), Elsevier Applied Science Publishers, London, UK, pp. 619-689.

Capart, R., A. Elamin, S. Ammar and M. Gelus. 1989. Survey of biomass liquefaction. In: Pyrolysis and Gasification. G. L. Ferrero, K. Maniatis, A. Buekens and A. V. Bridgwater (eds.), Elsevier Applied Science, London, UK, pp. 158-168.

Caram, H. and N. Amundson. 1979. Fluidized bed gasification reactor modelling I. Model description and numerical results for a single bed. Industrial and Engineering Chemistry Process Design and Development 18(1): 80-102.

Carre, J., L. Lacrosse and Y. Schenkel. 1988. Comparison between wood gasification and densified briquettes gasification. In: Research in Thermochemical Biomass Conversion. A. V. Bridgwater and J. L. Kluester (eds.), Elsevier Applied Science, London, pp. 655-666.

Chakraverty, A. and S. Kaleemullah. 1991. Conversion of rice husk into amorphous silica and combustible gas. Energy Conversion and Management 32(6): 565-570.

Chandra, P. K. and F. A. Payne. 1986. Turndown ratio of a gasifier - Combustor predicted by a simulation model. Transactions of the American Society of Agricultural Engineers 29(6): 1748-1753.

Chang, C.C., L.T. Fan and W. P. Walawender. 1980. Dynamic modelling of biomass gasification in a fluidized bed. Journal of the American Institute of Chemical Engineers 80 (214): 80-90.

Chatterjee P. K., A. B. Datta, and K. M. Kundu. 1995. Fluidized bed gasification of coal. Canadian Journal of Chemical Engineering 73(1): 204-210.

Chen, C. C. and M. H. Rei. 1980. Gasification of rice husk. Presented at Bio-Energy 80 World Congress and Exposition, Atlanta, GA, April 21.

Chen, N. H. and R. Aris. 1992. Determination of Arrhenius constants by linear and nonlinear fitting. Journal of the American Institute of Chemical Engineers 38(4): 626-628.

Chern, S. M. and W. P. Walawender. 1989. Analytical calculation of equilibrium gas composition in a C-H-O-inert system. Journal of the American Institute of Chemical Engineers 35(4): 673-675.

Chern, S. M., W. P. Walawender and L. T. Fan. 1989. Mass and energy balance analyses of a downdraft gasifier. Biomass 18(1): 127-151.

Chiba, S., T. Chiba, A. W. Nienow and H. Kobayashi. 1979. The minimum fluidization velocity, bed expansion and pressure-drop profiles for binary particle mixtures. Powder Technology 22(2): 255-269.

Cho, Y. S. and B. Joseph. 1981. Heterogeneous model for moving bed coal gasification reactors. Industrial and Engineering Chemistry Process Design and Development 20(2): 314-418.

Chornet, E., R. Arsenault, C. Roy and Grandios. 1980. Pyrolysis/gasification of agricultural residues as a source of fuel for Canadian farm operations. In: Proceedings of the Second Bioenergy R&D Seminar. Sponsored by Energy Project Office, National Research Council of Canada, Ottawa, Ontario, pp. 137-140.

Clift, R. 1986. Hydrodynamics of Gas Fluidized Beds. In: Gas Fluidization Technology. D. Geldart (ed.), John Wiley & Sons. New York.

Clift, R. and J.R. Grace. 1985. Continuous bubbling and slugging. In: Fluidization. J.F. Davidson, R. Clift and D. Harrison, (eds.), Academic Press, New York.

Clift, R., M. Ghadiri and A. C. Hoffman.1991. A critique of two models for cyclone performance. Journal of the American Institute of Chemical Engineers 37(2): 289-191.

Corella, J., J. Herguido and J. Gonzalez-Saiz. 1989. Steam gasification of biomass in fluidized bed-Effect of the type of feedstock. In: Pyrolysis and Gasification. G. L Ferrero, K. Maniatis, A. Beukens and A. V. Bridgwater (eds.), Elsevier Science Publishers, London, UK, pp. 619-623.

Cozzani, V., A. Lucchesi, G. Stoppato and G. Maschio. 1977. A new method to determine the composition of biomass by thermogravimetric analysis. Canadian Journal of Chemical Engineering 75(1): 127-133.

Cranfield, R. R. and D. Geldart. 1974. Large particle fluidization. Chemical Engineering Science 29(4): 935-947.

Cruz, I. E.1984. Rice Hull Energy Conversion Systems. Developments in the Philippines. FAO, Rome, Italy.

CTC. 1983. Report on chemical composition of rice hulls. Commercial Testing and Engineering Co., Denver, CO.

Czernik, S., P. G. Koeberle, P. Jollez, J. F. Bilodeau and E. Chornet. 1994. Gasification of residual biomass via the biosyn fluidized bed technology. In: Advances in Thermochemical Biomass Conversion. A. V. Bridgwater (ed.), Blackie Academic and Professional, Glasgow, U. K., pp. 423-437.

Davidson, J. F. and B. O. G. Schuler. 1960. Bubble formation at an orifice in an invicid liquid. Transactions of the Institution of Chemical Engineers 38(6): 335-341.

Davidson, J. F. and D. Harrison. 1963. Fluidized Particles. Cambridge University Press, Cambridge.

Deglise, X. and P. Magne. 1987. Pyrolysis and industrial charcoal. In: Biomass: Regenerable Energy. Hall, D. O. and R. P. Overend (eds.), pp. 221-235.

DeGrooth, J. H. 1967. Scaling up gas-fluidized bed reactors. Proceedings of the International Symposium on Fluidization. Eindhoven, Netherlands University Press, Amsterdam.

Demirbas, A. 1997. Calculation of higher heating values of biomass fuels. Fuel 76(5): 431-434.

Desrosiers, R. 1981. Thermodynamics of gas-char reactions. In: Biomass gasification - Principles and Technology. T. B Reed (ed.), New Jersey, Noyes Data Corporation, pp. 119-153.

Double, J. M. and A. V. Bridgwater. 1985. Sensitivity of theoretical gasifier performance to system parameters. In: Energy From Biomass. W. Palz, J. Coombs and D. O Hall (eds.), Elsevier Applied Science Publishers, London, UK, pp. 915-919.

Double, J. M., E. L Smith and A. V. Bridgwater. 1989. Computer modeling of fluidized bed gasification. In: Pyrolysis and Gasification. G. L Ferrero, K. Maniatis, A. Buekens and A. V Bridgwater (eds.), Elsevier Applied Science, London, UK, pp. 651-655.

Duvvuri, M. S., S. P. Muhlenkamp, K. Z. Iqbal and J. R. Welker. 1975. The pyrolysis of natural fuels. Journal of Fire and Flammability 6(2): 468-477.

Ebeling, J. M. and B. M. Jenkins. 1985. Physical and chemical properties of biomass fuels. Transactions of the American Society of Agricultural Engineers 28(3): 898-902.

Eitel, W. 1948. Silicate Melt Equilibra. Rutgers University Press, New Brunswick, NJ, USA.

Ergudenler, A. 1993. Gasification of Wheat Straw in a Dual-Distributor Type Fluidized Bed Reactor. Unpublished Ph.D. Thesis, Technical University of Nova Scotia, Halifax, Nova Scotia, Canada.

Ergudenler, A. and A. E Ghaly. 1993. Agglomeration of alumina sand in a fluidized bed straw gasifier at elevated temperatures. Bioresource Technology 43(2): 259-268.

Ergudenler, A. and A. E. Ghaly. 1992a. Quality of gas produced from wheat straw in a dual-distributor type fluidized bed gasifier. Biomass and Bioenergy 3(2): 419-430.

Ergudenler, A. and A. E. Ghaly. 1993a. Agglomeration of silica sand in a fluidized bed gasifier operating on wheat straw. Biomass and Bioenergy 4(2): 135-147.

Ergudenler, A. and A.E. Ghaly. 1991. Effect of bed temperature on agglomeration in a fluidized bed straw gasifier. Canadian Society of Agricultural Engineers Paper No. 91-305, Ottawa, Ontario.

Ergudenler, A. and Ghaly, A. E. 1992b. Determination of reaction kinetics of wheat straw using thermogravimetric analysis. Journal of Applied Biochemistry and Biotechnology, 34/35(1):75-91.

Ergudenler, A., A. E. Ghaly, F. Hamdullahpur, and A. M. Al-Taweel. 1997. Mathematical modeling of fluidized bed straw gasifier - I: Model development. Energy Sources 19(5):1065-1084.

Ergun, S. 1952. Fluid flow through packed columns. Chemical Engineering Progress 48(1): 89-94.

Fan, L. T., A. A. Boateng and W. P Walawender. 1992. Surface fractal dimension of rice hull-derived charcoal from a fluidized-bed reactor. Canadian Journal of Chemical Engineering 70(1): 387-390.

Fan, L. T., K. Tojo and C. C. Chang. 1979. Modeling of shallow fluidized bed combustion of coal particles. Industrial and Engineering Chemistry Process Design and Development 18(2): 333-337.

FAO, 1986. Wood Gas as Engine Fuel. FAO Forestry Paper No. 72, Rome, Italy.

FAO. 1996. Production Yearbook. Basic data unit statistics division, Food and Agricultural Organization of the United Nations, Rome, Italy.

Foley, G. and G. Barnard. 1985. Biomass Gasification in Developing Countries. Earthscan Technical Report No. 1, London, UK.

Font, R., A. Marcilla, E. Verdu and J. Devesa. 1989. Chemicals from almond shells by pyrolysis in fluidized bed. In: Pyrolysis and Gasification. G.L. Ferrero, K. Maniatis, A. Buekens and A.V. Bridgwater (eds). Elsevier Applied Science, London, UK, pp. 230-237.

Fournol, A. B., M. A. Bergougnou and C. G. J. Baker. 1973. Solids entrainment in a large fluidized bed. Canadian Journal of Chemical Engineering 51(2): 401-404.

Fung, A. S. and F. Hamdullahpur. 1993. Effect of bubble coalescence on entrainment in gas fluidized beds. Powder Technology 77(3): 251-265.

Gariboldi, F. 1974. Rice Milling Equipment, Operation and Maintenance. Food and Agriculture Organization of the united Nations, Agricultural Services Bulletin No. 22, Rome, Italy.

Gariboldi, F. 1984. Rice Parboiling. Food and Agriculture Organization of the United Nations, Agricultural Services Bulletin No. 56, Rome, Italy.

Geldart, D. 1986. Introduction. In: Gas Fluidization Technology. D. Geldart (ed.), John Wiley and Sons, New York, pp. 1-9.

Geldart, D. 1986b. Characterization of fluidized powders. In: Gas Fluidization Technology. D. Geldart (ed.), John Wiley and Sons, New York, pp. 33-51.

Geldart, D. 1986c. Particle entrainment and carryover. In: Gas Fluidization Technology. D. Geldart (ed.), John Wiley and Sons, New York, 123-153.

Geldert, D. and M. J. Rhodes. 1992. Survey of current world-wide research in gas fluidization. Powder Technology 71(1): 1-46.

Gera, D. and M. Guatam. 1994. Variation of throughflow velocity in a 2-D rising bubble. Powder Technology 79(2): 257-263.

Ghaly, A. E and A. M. Al-Taweel. 1990. Physical and thermochemical properties of cereal straws. Energy Sources 12(1): 131-145.

Ghaly, A. E, A. M. Al-Taweel and A. Ergudenler. 1989b. Development and evaluation of a straw feeding system for fluidized bed gasifiers. In: Proceedings of 7th Bioenergy R&D Seminar. E. N Hogan (ed.), Ottawa, Ontario, pp. 279-303.

Ghaly, A. E, A. M. Al-Taweel, F. Hamdullahpur and I. Ugwu. 1989a. Physical and Chemical properties of cereal straw as related to thermochemical conversion. In: Proceedings of 7th. Bioenergy R&D Seminar. E. N Hogan (ed.). Ottawa, Ontario, pp. 655-661.

Ghaly, A. E. and A. Ergudenler. 1991. Thermal degradation of cereal straws in air and nitrogen. Journal of Applied Biochemistry and Biotechnology 28/29(1): 111-126.

Ghaly, A. E., A. Ergudenler and I. Ugwu. 1990. Mixing patterns and residence time determination in a fluidized bed system. American Society of Agricultural Engineers Paper No. 89-6086, St. Joseph, Michigan.

Ghaly, A. E., A. M. Al-Taweel and A. Ergudenler. 1989d. Development and evaluation of a straw feeding system for fluidized bed gasifiers. In: Proceedings of 7th Bioenergy R&D Seminar. E. N. Hogan (ed.). Ottawa, Ontario, pp. 287-295.

Ghaly, A. E., A. M. Al-Taweel and G. D. M. Mackay. 1986. Development of an innovative energy efficient pilot scale gasification system for low density solid waste. Project proposal submitted for support to Renewable Energy Division, Energy Mines and Resources, Canada, Ottawa, Ontario.

Ghaly, A. E., A. M. Al-Taweel, F. Hamdullahpur and A. Ergudenler. 1989e. Thermogravimetric characteristics of straws. In: Proceedings of 7th Bioenergy R&D Seminar. E.N. Hogan (ed.), Ottawa, Ontario, pp. 647-654.

Gogolek, P. E. G. and H. A. Becker. 1992. Calculation of the expansion of a bubbling fluidized bed of coarse particles. Powder Technology 71(1):107-110.

Gogolek, P. E. G. and J. R. Grace 1995. Fundamental hydrodynamics related to pressurized fluidized bed combustion. Progress in Energy Combustion Science 21(2): 419-451.

Goldfarb, I. J., R. Guchan and A. C Meeks. 1968. Kinetic analysis of thermogravimetry. Part II. Programmed temperatures. Report No. ARML-TR-68-181. Air Force Laboratory, Wright-Patterson AFB, Ohio.

Goyal, A. 1980. Mathematical Modeling of Entrained-Flow Coal Gasification Reactors. Unpublished Ph.D. Thesis, Illinois Institute of Technology, Chicago, Illinois, USA.

Graboski, M. and R. Bain. 1981. Properties of biomass relevant to gasification. In: Biomass Gasification - Principles and Technology. T. B. Reed (ed.), Noyes Data Corporation, Park Ridge, New Jersey, pp. 41-69.

Grace, J. and H. I. deLasa. 1978. Reaction near the grid in fluidized beds. Journal of the American Institute of Chemical Engineers 24(2): 364-366.

Grace, J. R. 1986. Fluidized beds as chemical reactors. In: Gas Fluidization Technology. D. Geldart (ed.), John Wiley & Sons Inc., New York, New York.

Grace, J. R. and C. J. Lim. 1987. Permanent jet formation in beds of particulate solids. Canadian Journal of Chemical Engineering 65(1): 160-161.

Grace, J. R. and R. Clift. 1974. On the two phase theory of fluidization. Chemical Engineering Science 29(1): 327-334.

Grist, D. H. 1975. Rice. Longmans, Green and Co., London, England.

Groeneveld, M. J. and J. J. Hos. 1983. Gasification of various wastes in an annular cocurrent moving bed gasifier. In: Energy From Biomass. Elsevier Applied Science, London, pp. 406-409.

Gumz, W. 1950. Gas Producers and Blast Furnaces: Theory and Methods of Calculations. Wiley, New York, New York.

Gururajan, V. S., P. K. Agarwal and J. B. Agnew. 1992. Mathematical modelling of fluidized bed coal gasifiers. Transaction of the Institution of Chemical Engineers 70(1): 211-237.

Hall. F. P and H. Insley. 1947. Phase diagrams for ceramists. Journal of American Ceramic Society 30(11): 33-48.

Hamad, M. A. 1981. Thermal characteristics of rice hulls. Journal of Chemical Technology and Biotechnology 31(3): 624-626.

Hamdullahpur, F. and G. D. M. Mackay. 1986. Two-phase flow behaviour in the freeboard of a gas fluidized bed. Journal of the American Institute of Chemical Engineers 32(12): 2047-2055.

Hanafi, S. and S. A. Abo-El-Enein. 1980. Surface properties of silicas produced by thermal treatment of rice husk ash. Thermochimica 37(1): 137-143.

Horio, M., A. Taki, Y. S. Hsieh and I. Muchi. 1980. Elutriation and particle transport through the freeboard of a gas-solid fluidized bed. In: Fluidization. J. R. Grace and J. M. Matsen (eds.), Plenum Press, New York, pp. 217-224.

Hos, J. J. and M. J. Groeneveld. 1987. Biomass Gasification. In: Biomass: Regenerable Energy. Hall, D.O. and Overend, R.P. (eds.), John Wiley and Sons, pp. 237-255.

Howard, J. B. 1981. Fundamentals of coal pyrolysis and hydropyrolysis. In: Chemistry of coal utilization - second supplementary volume. M. A. Elliott (ed.), John Wiley and Sons, pp. 665-784.

Huffman, G. P., F. E. Huggins, and G. R. Dunmyre. 1981. Investigation of the high temperature behaviour of coal ash in reducing and oxidizing atmospheres. Fuel 60(2): 585-597.

Ismail, S. and J. C. Chen. 1984. Volume fraction of solids in the freeboard region of fluidized beds. American Institute of Chemical Engineers Symposium Series 80(234): 114-118.

Jaraiz, E., S. Kimura and O. Levenspiel. 1992. Vibrating beds of fine particles: Estimation of interparticle forces from expansion and pressure drop experiments. Powder Technology 72(1): 23-30.

Jenkins, B. M. 1980. Downdraft Gasification Characteristics of California Residue-Derived fuels. Unpublished Ph.D. Thesis, University of California, Davis.

Jenkins, B. M. 1989. Physical properties of biomass. In: Biomass Handbook. O. Kitani and C. W. Hall (eds.), Gordon and Breach Science Publishers, New York, NY, pp. 860-891.

Jenkins, B. M. 1997. A comment on the optimal sizing of a biomass utilization facility under constant and variable cost scaling. Biomass and Bioenergy 13(1): 1-9.

Jenkins, B. M. and H.R. Summer. 1986. Harvesting and handling agricultural residues for energy. Transactions of the American Society of Agricultural Engineers 29(3): 825-826.

Jenkins, B. M., J. F. Arthur, G. E. Miller and P.S. Parsons. 1984. Logistics and economics of biomass utilization. Transactions of the American Society of Agricultural Engineers 27(6): 1898-1904.

Jenkinson, D. S. 1981. The fate of plant and animal residues in soil. In: The Chemistry of Soil Processes. D. J. Greenland and M. H. B. Hayes (eds.), John Wiley, London, UK.

Johnson, J. L. 1974. Kinetics of bituminous coal char gasification with gases containing steam and hydrogen. Advances in Chemistry Series 131: 145-151.

Jones, J. D. 1953. New refractory from vegetable source. In: Canadian Metals. Westman Publications Limited, Toronto, pp. 22-24.

Kapur, T., T. C. Kandpal and H. P. Garg. 1997. Rice processing in India: A generalized framework for energy demand estimation. International Journal of Energy Research 21(1): 309-325.

Kaupp, A. 1984. Gasification of Rice Hulls: Theory and Praxis. Friedr. Vieweg & Sons Braunschweig/Wiesbaden, Germany.

Kaupp, A. and J. R. Goss. 1981. State-of-the-art for small scale (up to 50 kW) gas producer engine systems. Final report. Contract No. 53-319R-0-141, Bio-resources for energy, Timber Management Research, US Department of Agriculture, Forest Service, Washington, DC.

Khan, M. R. and E. P. Esztergar. 1990. Influence of oxygen preabsorption on nonisothermal char reactivity. Seventh Annual International Pittsburgh Conference. A. Flowers and M. J. Mayfield (eds.), Pittsburgh, PA, pp. 75-82.

Kimura, T., J. C. Bi, S. Uemiya and T. Kojima. 1993. Analysis of local reactions in a laboratory scale jetting fluidized bed coal gasifier. Fuel Processing Technology 36(1): 219-225.

Kohan, S. M. 1980. Preliminary economic overview of large-scale thermal conversion systems using wood feedstocks. American Chemical Society Symposium Series 130(3): 29-42.

Koufopanos, C. A., G. Maschio and A. Lucchesi. 1989. Kinetic modeling of the pyrolysis of biomass and biomass components. Canadian Journal of Chemical Engineering 67(1): 75-84.

Kraus, U. 1985. Test results from pilot plants for firing wood and straw in the Federal Republic of Germany. In: Energy from Biomass. W. Palz, J. Coombs and D. O. Hall (eds.), Elsevier Applied Science Publishers, London, UK, pp. 799-803.

Kunii, E. and O. Levenspiel. 1990. Fluidized bed reactor models. 1. For bubbling beds of fine, intermediate, and large particles. 2. For the lean phase: freeboard and fast fluidization. Industrial and Engineering Chemistry Research 29(6): 1226-1234.

Kunii, E. and O. Levenspiel. 1991. Effect of particles in bubbles on fluidized bed mass and heat transfer kinetics. Journal of Chemical Engineering Japan 24(2), 183-188.

La Nauze, R. D. 1986. A review of the fluidized bed combustion of biomass. Journal of the Institute of Energy, June: 66-76.

Langille, W. H. and A. E. Ghaly. 1991. Environmental impact of alternative utilization of cereal straw. American Society of Agricultural Engineers Paper No. 91-6008, St. Joseph, Michigan.

Lepori, W. A. 1982. Fluidized bed technology for biomass gasification. Paper presented at Solar and Biomass Workshop, Atlanta, GA.

Lepori, W. A., C. B. Parnell Jr., D. B. Carney, P. P. Ling, T. C. Pollock and R. G. Tobias. 1983. Small-Scale Power Generation from Biomass - Technical Potential, American Society of Agricultural Engineers Paper No. 83-3542, ASAE, St. Joseph, Michigan.

Levin, E. M., H. F. McMurdie and F. P. Hall. 1956. Phase Diagrams for Ceramists. Columbus, Ohio: The American Ceramic Society.

Lewis, W. K., E. R. Gilliland and P. M. Lang. 1962. Entrainment from fluidized beds. American Institute of Chemical Engineers Symposium Series 58(38): 65-78.

Liinanki, L., N. Lindman, S. O. Sjoberg and E. Strom. 1985. Methane yield from gasification at high temperature and pressure. In: Fundamentals of Thermochemical Biomass Conversion. R. P. Overend, T. A. Milne and K. L. Mudge (eds.), Elsevier Applied Science Publishers, London, UK, pp. 923-936.

Lin, K. H., H. C. van Ness and M. M. Abbott. 1984. Reaction kinetics, reactor design and thermodynamics. In: Chemical Engineers' Handbook. R. H. Perry and D. W. Green (eds.), McGraw-Hill Book Company, New York.

Liou, T. H., F. W. Chang and J. J. Lo. 1997. Pyrolysis kinetics of acid-leached rice husk. Industrial and Engineering Chemistry Research 36(3): 568-571.

Lipska-Quinn, A. E., S. H. Zeronian, and K. M. McGee. 1985. Thermal degradation of rice straw and its components. In: Fundamentals of Thermochemical Biomass Conversion. R. P. Overend, T. A. Milne and K. L. Mudge (eds.), Elsevier Applied Science Publishers, Essex, England, pp. 453-471.

Luan, T. C. and T. C. Chou. 1990. Recovery of silica from the gasification of rice husks/coal in the presence of a pilot flame in a modified fluidized bed. Industrial and Engineering Chemistry Research 29(9): 1922-1927.

Lucchesi, A. and G. Maschio. 1982. Study on the pyroslysis and gasification of agricultural wastes. In: Energy from Biomass. A. Strub, P. Chartier and G. Schleser (eds.), Applied Science Publishers, London, UK, pp. 1109-1111.

Mahin, D. B. 1990. Energy from rice residues (special issue), Bioenergy Systems Report, Office of Energy, USAID, Washington, DC.

Maniatis, K. 1986. Fluidized Bed Gasification of Biomass. Unpublished Ph. D. Thesis, Aston University, Aston, UK.

Maniatis, K. 1990. Fluidized bed gasification of agricultural residues. Paper Presented at the International Symposium on Application and Management of Energy in Agriculture - Role of Biomass Fuels. New Delhi, India, May 21-23.

Maniatis, K., A. V. Bridgwater and A. Buekens. 1989. Fluidized bed gasification of wood: Performance of a demonstration plant. In: Pyrolysis and Gasification. G. L. Ferrero, K. Maniatis, A. Buekens and A. V. Bridgwater (eds.), Elsevier Applied Science, London, UK, pp. 274-281.

Maniatis, K., A. V. Bridgwater, and A. Buekens. 1988. Fluidized bed gasification of wood. In: Research in Thermochemical Biomass Conversion. A. W. Bridgwater and J. L. Kluester (eds.), Elsevier Applied Science, London, pp. 1094-1105..

Mansaray, K. G. and A. E. Ghaly. 1997a. Physical and chemical properties of rice husks. Energy Sources 19(9): 989-1004.

Mansaray, K. G. and A. E. Ghaly. 1997b. Agglomeration characteristics of alumina sand-rice husk ash mixtures at elevated temperatures. Energy Sources 19(9): 1005-1025.

Manurung, R. and A. A. C. M. Beenackers. 1985. Gasification of rice husk in a small downdraft moving bed. In: Energy From Biomass. W. Palz, J. Coombs and D. O. Hall (eds.), Elsevier Applied Science Publishers, London, UK, pp. 900-904.

Markhevka, V. I., V. A. Basov, T. K. Melik-Akhnazarov and D. I. Orochko. 1971. The flow of a gas jet into a fluidized bed. Theoretical Foundations of Chemical Engineering 5(1): 80-85.

Massimilia, L. 1985. Gas Jet in Fluidized Beds. 2nd. Ed., Academic Press, New York.

Mathur, K.B. and N. Epstein. 1974. Spouted Beds. Academic Press, New York.

Matsen, J. M., S. Hovmand and J. F. Davidson. 1969. Expansion of fluidized beds in slug flow. Chemical Engineering Science 24(8): 1743-1754.

Matsui, I., D. Kunii and T. Furusawa. 1987. Study of char gasification by carbon dioxide. 1. Kinetic study by thermogavimetric analysis. Industrial and Engineering Chemistry Research 26(1): 91-95.

Mendis, M. S. 1989. Biomass gasification: Past experiences and future prospects in developing countries. In: Pyrolysis and Gasification. G. L. Ferrero, K. Maniatis, A. Buekens and A. V. Bridgwater (eds), Elsevier Applied Science, London, UK, pp. 111-128.

Merry, J. M. 1975. Penetration of vertical jets into fluidized beds. American Institute of Chemical Engineers 21(3): 507-510.

Miles, T. R. 1982. Preparation of biomass for gasification. In: Proceedings of the Biomass-to-Methanol Specialists Workshop. Durango, CO, U. S. Department of Energy, pp. 95-118.

Milne, T. 1981. Pyrolysis - The thermal behaviour of biomass below 600°C. In: Biomass Gasification - Principles and Technology, T. B. Reed (ed.), Noyes Data Corporation, Park Ridge, New Jersy, pp. 91-118.

Miwa, K., S. Mori T. Koto and I. Muchi. 1972. Behaviour of bubbles in gaseous fluidized bed. Institution of Chemical Engineers 12(1): 181-185.

Mleczko, L. and K. J. Marschall. 1997. Performance of an internally circulating fluidized bed reactor for the catalytic oxidative coupling of methane. Canadian Journal of Chemical Engineering 75(3): 610-618.

Moran, K. 1996. Geological Survey Laboratory of the Atlantic Canada, Bedford Institute of Oceanography, Dartmouth, Nova Scotia. Personal Communication.

Mori, S. and C. Y. Wen. 1975. Estimation of bubble diameter in gaseous fluidized beds. American Institute of Chemical Engineers 21 (1): 109-115.

Narváez, I., A. Orío, M. P. Aznar and J. Corella. 1996. Biomass gasification with air in an atmospheric bubbling fluidized bed. Effect of six operational variables on the quality of the produced gas. Industrial and Engineering Chemistry Research 35(10): 2110-2120.

Nienow, A. W., P. N. Rowe and L. Y. L. Cheung, 1978. A quantitative analysis of the mixing of two segregating powders of different density in a gas-fluidized bed. Powder Technology 20(1): 89-97.

Ongiro, A. 1997. Technoeconomic Modelling of Integrated Advanced Power Cycles. Unpublished Ph. D. Thesis, Technical University of Nova Scotia, Halifax, Nova Scotia.

Ongiro, A., V. I. Ugursal, A. M. Al-Taweel and G. La Jeunesse. 1996. Thermodynamic simulation of a steam CHP plant using ASPEN PLUS. Applied Thermal Engineering 16(3): 263-271.

Osman, E. A. 1982. A Study of the Effects of Ash Chemical Composition and Additives on Fusion Temperature in Relation to Slag Formation During Gasification of Biomass. Unpublished Ph.D. Thesis, University of California, Davis.

Overend, R. 1982. Wood gasification - A Review of Recent Canadian Experience. National Research Council of Canada, Ottawa, Ontario, Canada, NRCC No. 20094.

Payne, F. A. and J. G. Alphin. 1983. Exhaust gas recirculation for control of updraught gasifier grate temperature. American Society of Agricultural Engineers Paper No. 83-3072, St. Joseph, Michigan.

Peel, R. B. and F. J. Santos. 1980. Fluidized Bed Combustion of Vegetable Fuels: Applications. London, UK, pp. IIB-2-1 IIB 2-9.

Pereira, J., K. Chandrasekharan and P. H. Calderbank. 1981. A revised model for predicting the performance of a fluidized-bed catalytic reactor. Chemical Engineering Science 36(2): 239-242.

Perkins, D., D. W. Brekke, and F. R. Karner. 1984. Analysis of atmospheric fluidized bed combustion agglomerates. Report DOE/FC/10120-1608. U. S. Department of Energy, Washington, D. C.

Porter, F. P., G. A. Schurr, D. F. Wells and T. Semrau. 1984. Solids drying and gas-solid systems. In: Chemical Engineers' Handbook. R. H. Perry and D. W. Green (eds.), McGraw-Hill Book Company, New York.

Puchyr, D. M. J., A. K. Mehrotra and L. A. Behie. 1997. Modeling a circulating fluidized bed riser reactor with gas-solid downflow at the wall. Canadian Journal of Chemical Engineering 75(2): 317-326.

Purdy, M. J. 1983. Operation and Modeling of a Pilot-Scale Fluidized Bed Coal Gasifier. Unpublished Ph.D. Thesis, North Carolina State University, Raleigh, NC.

Purdy, M., R. M. Felder and J. K. Ferrell. 1981. Coal gasification in a pilot scale fluidized bed reactor I. Gasification of a devolatilized bituminous coal. Industrial and Engineering Chemistry Process Design and Development 20(2): 675-682.

Raissi, A. R. and G. J. Trezek. 1987. Parameters Governing Biomass Gasification. Industrial and Engineering Chemical Research 26(2): 221-228.

Raman, K. P., W. P. Walawender, L. T Fan and C. C. Chang. 1981. Mathematical model for fluid bed gasification of biomass material. Application to feedlot manure. Industrial and Engineering Chemistry Process Design and Development 20(2): 686-692.

Ramiah, M. V. 1970. Thermogravimetric and differential thermal analysis of cellulose, hemicellulose and lignin. Journal of Applied Polymer Science 14(6): 1323-1337.

Reed, T. B. 1981. Biomass Gasification - Principles and Technology. Energy Technology Review No. 67, Noyes Data Corporation, Park Ridge, New Jersey.

Rei, M. H., F. S. Lin and T. B Su. 1986. Catalytic gasification of rice hull. (II) The steam reforming reaction. Journal of Applied Catalysis 26(1): 27-37.

Roach, P. E. 1993. The penetration of jets into fluidized beds. Fluid Dynamics Research 11(1): 197-216.

Rossi, A. 1984. Fuel characteristics of wood and non-wood biomass fuels. In: Progress in Biomass Conversion V. Academic Press, Inc., New York, pp. 69-99.

Rowe, P. N. 1993. A model for chemical reaction in the entry region of a gas fluidized bed reactor. Chemical Engineering Science 48(12): 2519-2524.

Rowe, P. N. and A. W. Nienow. 1976. Particle mixing and segregation in gas fluidized beds - A Review. Powder Technology 15(1): 141-147.

Rowe, P. N. and B. A. Patridge. 1965. An X-ray study of bubbles in fluidized beds. Transactions of the Institution of Chemical Engineers 43: T157-T175.

Rowe, P. N. and H. Masson. 1980. Fluidized bed bubbles observed simultaneously by probe and X-rays. Chemical Engineering Science 35(7): 1443-1447.

Sadaka, S. 1994. Air-Steam Gasification of Wheat Straw in a Fluidized Bed Reactor. Unpublished Ph.D. Thesis, Alexandra University, Egypt.

Salour, D., B. M. Jenkins, M. Vafei, and M. Kayhanian. 1989. Combustion of rice straw and straw/wood fuel blends in a fluidized bed reactor. American Society of Agricultural Engineers Paper No. 89-6574, St. Joseph, MI.

Schiefelbein, G. F. 1989. Biomass thermal gasification research. Biomass 19(1): 145-159.

Schoeters, J., K. Maniatis, and A. Bueckens. 1989. The fluidized bed gasification of biomass: Experimental studies on bench scale reactor. Biomass 19(1):129-143.

Shafizadeh, F. 1968. Pyrolysis and combustion of cellulosic materials. Advances in Carbohydrate Chemistry 23(2): 419-474.

Shafizadeh, F. 1985. Pyrolytic reactions and products of biomass. In: Fundamentals of Thermochemical Biomass Conversion. R. P. Overend, T. A. Milne and K. L. Mudge (eds.), Elsevier Applied Science Publishers, London, UK, pp. 183-217.

Shafizadeh, F. and G. D. McGinnis. 1970. Chemical composition and thermal analysis of cottonwood. Carbohydrate Research 16: 273-282.

Shafizadeh, F. and W. F. DeGroot. 1976. Combustion Characteristics of Cellulosic Fuels. In: Thermal Uses and Properties of Carbohydrates and Lignins. Academic Press, New York, NY, pp. 1-18.

Shapiro, L. 1975. Rapid analysis of silicate, carbonate, and phosphate rocks. U. S. Geological Survey Bulletin No. 1401, US Government Printing Office, Washington, DC.

Siegell, J. H. 1984. High-temperature de-fluidization. Powder Technology 38(1): 13-22.

Smith, I. W., T. F. Wall, B. R. Stanmore, D. J. Harris, J. Y. Chen and D. K. Zhang. 1991. Coal combustion testing: optimum laboratory procedure. National Energy Research, Development and Demonstration Council, NERDDP/EG91/993, Canberra, ACT, Australia, 89 pp.

Sondreal, E. A. and R. C. Ellman. 1975. Fusibility of ash from lignite and its correlation with ash compositions. Technical Report, GFERC/R1-75-1, Bureau of Mines, Pittsburgh, PA.

Sosman, R. B. 1927. The properties of silica. In: Monograph Series 37. American Chemical Society, Washington, D. C., 50 pp.

Spencer, D. S. C. 1967. The operation of small rice mills in Sierra Leone. Proceedings of the Easter Conference. Njala University College, University of Sierra Leone, April.

Squires, A.M. 1973. Role of solid mixing in fluidized bed reaction kinetics. American Institute of Chemical Engineers Symposium Series 69(1): 8-17.

Staniforth, A. R. 1979. Cereal Straw. Clarendon Press, Oxford.

Staniforth, A. R. 1982. Straw for Fuel, Feed and Fertilizer. Farming Press Limited, Suffolk, UK.

Steenari, B. M. and O. Lindqvist. 1997. Stabilisation of biofuel ashes for recycling to forest soil. Biomass and Bioenergy 13(1): 39-50.

Strehler, D. 1985. Results from research work in heat generation from wood and straw. In: Energy From Biomass. W. Palz, J. Coombs and D. O Hall (eds.), Elsevier Applied Science Publishers, London, UK, pp. 788-792.

Stull, D. R. and H. Prophet. 1971. JANAF Thermochemical Table, Second Edition. Office of Standard Reference Data, National Bureau of Standards.

Sun, G. and J. R. Grace. 1992. Effect of particle size distribution in different fluidization regimes. American Institute of Chemical Engineers 38(5): 716-722.

Sundaresan, S. and N. Amundson. 1979a. Studies in char gasification - I: A lumped model. Chemical Engineering Science 34(2): 345-354.

Sundaresan, S. and N. Amundson. 1979b. Studies in char gasification - II: The Davidson-Harrison two phase model of fluidization. Chemical Engineering Science 34(2): 355-358.

Swan, E. A. 1993. Fluidization Characteristics of a Dual-Distributor Fluidized Bed Reactor. Unpublished M. A. Sc. Thesis, Technical University of Nova Scotia, Halifax, Nova Scotia.

Terdyothin, A. and P. Wilbulswas. 1989. Feasibility of co-generation using rice husk as fuel. International Conference on Energy Sources Management and Energy Saving Technology, Beijing, China, September.

Tia, S., S. C. Bhattacharya and P. Wibulswas. 1991. Thermogravimetric analysis of Thai lignite-II. Char combustion kinetics. Energy Conversion and Management 31 (3): 277-284.

Tillman, D. A. 1987. Biomass Combustion. Biomass: In: Regenerable Energy. Hall, D. O. and Overend, R. P. (eds.), John Wiley and Sons, pp. 203-219.

Toomey, R. D. and H. F. Johnstone. 1952. Gaseous fluidization of solid particles. Chemical Engineering Progress 48 (5): 220-226.

van den Aarsen, F. G. 1985. Operation and Modeling of a Fluidized Bed Gasifier. Unpublished Ph.D. Thesis, University of Twente, The Netherlands.

van den Aarsen, F. G., A. A. Beenackers and W. P. M. van Swaaij.1986. Modelling of a fluidized bed wood gasifier. In: Fluidization V. K. Ostergaard and A. Sorensen (eds.), Engineering Foundation, New York, NY, pp. 521-530.

van den Aarsen, F. G., A. A. C. M. Beenackers, and van W. P. M. Swaaij. 1982. Performance of rice husk fuelled fluidized bed pilot plant gasifier. International Producer Gas Conference. Colombo, Sri Lanka, pp. 381-392.

van Swaaij, W. P. M. 1981. Gasification - The process and the technology. In: Energy from Biomass. W. Palz, P. Chartier and D. O. Hall (eds.), Applied Science Publishers, London and New York, pp. 485-494.

Vantelon, J. P., C. Breillat, F. Gaboriaud and A. Alaoui-Sosse. 1990. Thermal degradation of Timahdit oil shales: Behaviour in inert and oxidizing environments. Fuel 69(1): 211-215.

Varhegyi, G., P. Szabo and M. J. Antal. 1994. Reaction kinetics of the thermal decomposition of hemicellulose and cellulose in biomass materials. In: Advances in Thermochemical Biomass Conversion. A. V. Bridgwater (ed.), Blackie Academic and Professional, London, UK, pp-760-770.

Volk, W., C. A. Johnson and H. H. Stotler, 1962. Effect of reactor internals on quality of fluidization. Chemical Engineering Progress 58(3): 44-47.

von Fredersdorff, C. G. and M. A. Elliott. 1963. Coal Gasification. In: Chemistry of Coal Utilization. H. H. Lowry (ed.), John Wiley and Sons, New York, pp. 892-1022.

Walawender, W. P., Chern, S. M. and Fan, L. T. 1985. Wood Chip Gasification in a Commercial Downdraught Gasifier. In: Fundamentals of Thermochemical Biomass Conversion. R. P. Overend, T. A. Milne and K. L. Mudge (eds.), Elsevier Applied Science Publishers, London, UK, pp. 911-921.

Walawender, W. P., D. A. Hoveland, D. Anfwidsson and L. T. Fan. 1982. Steam gasification of wheat straw in a fluidized bed. In: Proceedings of the Sixth International FPRS Industrial Wood Energy Forum. Vol. 2, pp. 263-272.

Walawender, W. P., S. M. Chern and L. T. Fan. 1986. Influence of operating parameters on the performance of a wood-fed downdraft gasifier. In: Energy From Biomass and Wastes. D. L. Klass (ed.). Elsevier Applied Science Publishers and Institute of Gas Technology, London, UK, pp. 607-627.

Wang, W. and C. M. Konishita. 1993. Kinetic model of biomass gasification. Solar Energy 51(1): 19-25.

Watkinson. A. P., J. P. Lucas and C. J. Lim. 1991. A prediction of the performance of commercial coal gasifiers. Fuel 70(2): 519-527.

Weast, R. C. 1989. Handbook of Chemistry and Physics. 69th Edition, CRC Press, Boca Raton, FL.

Weimer, A. W. and D. E. Clough. 1981. Modeling a low pressure steam-oxygen fluidized bed coal gasifying reactor. Chemical Engineering Science 36(1): 549-567.

Weimer, A. W. and G. J. Quarderer. 1983. On dense-phase voidage and bubble size in high-pressure fluidized beds of fine powders. Paper Presented at the 1983 American Institute of Chemical Engineers Journal Meeting, Washington DC, October 31, 1983.

Wen, C. Y. and L. H. Chen. 1982. Fluidized bed freeboard phenomena: Entrainment and Elutriation. American Institute of Chemical Engineers 28 (1): 117-128.

Wen, C. Y. and L. T. Fan. 1975. Heterogenous models. In: Models for Flow Systems and Chemicals Reactors. Chemical Processing and Engineering Vol. 3, Marcel Dekker Inc., New York, NY.

Wen, C. Y. and Y. H. Yu. 1966. Mechanics of fluidization. Chemical Engineering Progress Symposium Series 62 (2): 100-111.

Wendlandt, W. W. 1974. Thermal Methods of Analysis. Second Edition, John Wiley & Sons, New York.

Whitehead, A. B. 1971. Some problems in large-scale fluidized beds. In: Fluidization. J. F. Davidson and D. Harrison (eds.). Academic Press, London and New York.

Wilen, C. P., K. Sipila, P. Stahlbert and J. Ahokas. 1985. Pelletization of straw. In: Energy From Biomass. Palz, W., J. Coombs and D. O. Hall (eds.), Elsevier Applied Science Publishers, London, UK, pp. 778-782.

Williams, P. T. And S. Besler. 1994. Thermogravimetric analysis of the components of biomass. In: Advances in Thermochemical Biomass Conversion. A. V. Bridgwater (ed.), Blackie Academic and Professional, London, UK, pp-771-783.

World Bank. 1996. World Development Report, Washington, DC.

Yang, G., Z. Huang and L. Zhao. 1984. Radial gas dispersion in a fast fluidized bed. In: Fluidization. D. Kunii and R. Toei (eds.), Engineering Foundation, New York, NY, pp. 145-152.

Yang, W. C. 1981. Jet penetration in a pressurized fluidized bed. Industrial and Engineering Chemistry Fundamentals 20(3): 297-300.

Yates, J. G., D. J. Cheesman and Y. A. Sergeev. 1994. Experimental observations of voidage distribution around bubbles in a fluidized bed. Chemical Engineering Science 49(12): 1885-1895.

Zhao, G. Y., C. W. Zhu and V. Hlavacek. 1994. Fluidization of micro-size ceramic powders in a small-diameter fluidized bed. Powder Technology 79(2): 227-235.

APPENDICES

APPENDIX A

"Calculation of Volumetric Gas Flow Rate Through the Orifice Plate"

Calculation of Volumetric Gas Flow Rate Through the Orifice Plate

The volumetric gas flow rate through the orificemeter was determined using the following equation:

$$q = K_o A_o \sqrt{\frac{2\Delta P}{\rho_{mix}}} \qquad (A.1)$$

where:

- q is the volumetric gas flow rate (m^3/min)
- A_o is the cross-sectional area of the orifice (m^2)
- K_o is the orifice coefficient (-)
- ΔP is the pressure drop across the orifice plate (Pa)
- ρ_{mix} is the density of the gas (kg/m^3)

Orifice coefficient, K_o, of 0.6 was used (Grace, 1986). Pressure drop, ΔP, was measured using a pressure transducer. Density of the gas mixture was calculated using the following equation:

$$\rho_{mix} = \frac{\sum_{i=1}^{7} (n_i \rho_i)}{n_T} \qquad (A.2)$$

where:

- n_i is the number of moles of the specie (-)
- n_T is the total number of moles of the species (-)
- ρ_i is the density of the specie (kg/m^3)

The mole fractions of the species obtained from the gas analyses were used in the above equation as the number of moles. The density of each specie was calculated using the following ideal gas equation:

$$\rho_i = \frac{M_i P}{R_o T} \qquad \text{(A.3)}$$

where:

M_i is the molecular weight of the specie (kg/kmole)

R_o is the universal gas constant (kJ/kmole.K)

P is the absolute pressure (kPa)

T is the exit gas temperature (K)

APPENDIX B

"Mass and Energy Balance Program"

Mass and Energy Balance Program

```
IMPLICIT REAL *8 (A-H,O-Z)
     REAL *8 FEEDS(4),FEEDP(3),FEEDU(7),FEEDR191(3,2),FEEDR192(3,2),
    + FEEDR193(3,2),FEEDR211(3,2),FEEDR212(3,2),FEEDR213(3,2)
    + ,FEEDR311(3,2),FEEDR312(3,2),FEEDR313(3,2),
    + FEEDG191(3,8),FEEDG192(3,8),
    + FEEDG193(3,8),FEEDG211(3,8),FEEDG212(3,8),FEEDG213(3,8)
    + ,FEEDG311(3,8),FEEDG312(3,8),FEEDG313(3,8)
    + ,FEEDH191(3,3),FEEDH192(3,3),
    + FEEDH193(3,3),FEEDH211(3,3),FEEDH212(3,3),FEEDH213(3,3)
    + ,FEEDH311(3,3),FEEDH312(3,3),FEEDH313(3,3),
    + PRODG191(3,3),PRODG192(3,3),
    + PRODG193(3,3),PRODG211(3,3),PRODG212(3,3),PRODG213(3,3)
    + ,PRODG311(3,3),PRODG312(3,3),PRODG313(3,3),
    + CHARP191(3,5),CHARP192(3,5),
    + CHARP193(3,5),CHARP211(3,5),CHARP212(3,5),CHARP213(3,5)
    + ,CHARP311(3,5),CHARP312(3,5),CHARP313(3,5),
    + CHARC191(3,3),CHARC192(3,3),
    + CHARC193(3,3),CHARC211(3,3),CHARC212(3,3),CHARC213(3,3)
    + ,CHARC311(3,3),CHARC312(3,3),CHARC313(3,3),
    + CHARA191(3,3),CHARA192(3,3),
    + CHARA193(3,3),CHARA211(3,3),CHARA212(3,3),CHARA213(3,3)
    + ,CHARA311(3,3),CHARA312(3,3),CHARA313(3,3),
    +CARBONI1(3,3),CARBONI2(3,3),CARBONI3(3,3),CARBONI4(3,3),
    +CARBONI5(3,3),CARBONI6(3,3),CARBONI7(3,3),CARBONI8(3,3),
    +CARBONI9(3,3),
    +TMASS1(3,3),TMASS2(3,3),TMASS3(3,3),TMASS4(3,3),
    +TMASS5(3,3),TMASS6(3,3),TMASS7(3,3),TMASS8(3,3),
    +TMASS9(3,3), RHOP(8),CFRAC(8)

     OPEN (13, FILE='DATAIN.DAT', STATUS='OLD',BLANK='NULL')
     OPEN (14, FILE='DATAO.DAT',STATUS='UNKNOWN')

C    READ DESIGN CONDITIONS

     DO I=1,4
     READ (13,*) FEEDS(I)
     ENDDO
     DO I=1,3
     READ (13,*)FEEDP(I)
```

```
 ENDDO
 DO I=1,7
READ (13,*) FEEDU(I)
 ENDDO
 DO I=1,3
READ (13,*)(FEEDR191(I,J),J=1,2)
 ENDDO
 DO I=1,3
READ (13,*)(FEEDR192(I,J),J=1,2)
 ENDDO
 DO I=1,3
READ (13,*)(FEEDR193(I,J),J=1,2)
 ENDDO
 DO I=1,3
READ (13,*)(FEEDR211(I,J),J=1,2)
 ENDDO
 DO I=1,3
READ (13,*)(FEEDR212(I,J),J=1,2)
 ENDDO
 DO I=1,3
READ (13,*)(FEEDR213(I,J),j=1,2)
 ENDDO
 DO I=1,3
READ (13,*)(FEEDR311(I,J),j=1,2)
 ENDDO
 DO I=1,3
READ (13,*)(FEEDR312(I,J),j=1,2)
 ENDDO
 DO I=1,3
READ (13,*)(FEEDR313(I,J),j=1,2)
 ENDDO
 DO I=1,3
READ (13,*)(FEEDG191(I,J),j=1,8)
 ENDDO
 DO I=1,3
READ (13,*)(FEEDG192(I,J),j=1,8)
 ENDDO
 DO I=1,3
READ (13,*)(FEEDG193(I,J),j=1,8)
 ENDDO
 DO I=1,3
READ (13,*)(FEEDG211(I,J),j=1,8)
 ENDDO
```

```
 DO I=1,3
READ (13,*)(FEEDG212(I,J),j=1,8)
 ENDDO
 DO I=1,3
READ (13,*)(FEEDG213(I,J),j=1,8)
 ENDDO
 DO I=1,3
READ (13,*)(FEEDG311(I,J),j=1,8)
 ENDDO
 DO I=1,3
READ (13,*)(FEEDG312(I,J),j=1,8)
 ENDDO
 DO I=1,3
READ (13,*)(FEEDG313(I,J),j=1,8)
 ENDDO
 DO I=1,3
 READ (13,*)(FEEDH191(I,J),j=1,3)
 ENDDO
 DO I=1,3
 READ (13,*)(FEEDH192(I,J),j=1,3)
 ENDDO
 DO I=1,3
READ (13,*)(FEEDH193(I,J),j=1,3)
 ENDDO
 DO I=1,3
READ (13,*)(FEEDH211(I,J),j=1,3)
 ENDDO
 DO I=1,3
READ (13,*)(FEEDH212(I,J),j=1,3)
 ENDDO
 DO I=1,3
READ (13,*)(FEEDH213(I,J),j=1,3)
 ENDDO
 DO I=1,3
READ (13,*)(FEEDH311(I,J),j=1,3)
 ENDDO
 DO I=1,3
READ (13,*)(FEEDH312(I,J),j=1,3)
 ENDDO
 DO I=1,3
READ (13,*)(FEEDH313(I,J),j=1,3)
 ENDDO
 DO I=1,3
```

```
 READ (13,*)(PRODG191(I,J),j=1,3)
  ENDDO
  DO I=1,3
 READ (13,*)(PRODG192(I,J),j=1,3)
  ENDDO
  DO I=1,3
 READ (13,*)(PRODG193(I,J),j=1,3)
  ENDDO
  DO I=1,3
 READ (13,*)(PRODG211(I,J),j=1,3)
  ENDDO
  DO I=1,3
 READ (13,*)(PRODG212(I,J),j=1,3)
  ENDDO
  DO I=1,3
 READ (13,*)(PRODG213(I,J),j=1,3)
  ENDDO
  DO I=1,3
 READ (13,*)(PRODG311(I,J),j=1,3)
  ENDDO
  DO I=1,3
 READ (13,*)(PRODG312(I,J),j=1,3)
  ENDDO
  DO I=1,3
 READ (13,*)(PRODG313(I,J),j=1,3)
  ENDDO
  DO I=1,3
 READ (13,*)(CHARP191(I,J),j=1,5)
  ENDDO
  DO I=1,3
 READ (13,*)(CHARP192(I,J),j=1,5)
  ENDDO
  DO I=1,3
 READ (13,*)(CHARP193(I,J),j=1,5)
  ENDDO
  DO I=1,3
 READ (13,*)(CHARP211(I,J),j=1,5)
  ENDDO
  DO I=1,3
 READ (13,*)(CHARP212(I,J),j=1,5)
  ENDDO
  DO I=1,3
READ (13,*)(CHARP213(I,J),j=1,5)
```

```
  ENDDO
  DO I=1,3
 READ (13,*)(CHARP311(I,J),j=1,5)
  ENDDO
  DO I=1,3
 READ (13,*)(CHARP312(I,J),j=1,5)
  ENDDO
  DO I=1,3
 READ (13,*)(CHARP313(I,J),j=1,5)
  ENDDO
  DO I=1,3
 READ (13,*)(CHARC191(I,J),j=1,3)
  ENDDO
  DO I=1,3
 READ (13,*)(CHARC192(I,J),j=1,3)
  ENDDO
  DO I=1,3
 READ (13,*)(CHARC193(I,J),j=1,3)
  ENDDO
  DO I=1,3
 READ (13,*)(CHARC211(I,J),j=1,3)
  ENDDO
  DO I=1,3
 READ (13,*)(CHARC212(I,J),j=1,3)
  ENDDO
  DO I=1,3
 READ (13,*)(CHARC213(I,J),j=1,3)
  ENDDO
  DO I=1,3
 READ (13,*)(CHARC311(I,J),j=1,3)
  ENDDO
  DO I=1,3
 READ (13,*)(CHARC312(I,J),j=1,3)
  ENDDO
  DO I=1,3
 READ (13,*)(CHARC313(I,J),j=1,3)
  ENDDO
  DO I=1,3
 READ (13,*)(CHARA191(I,J),j=1,3)
  ENDDO
  DO I=1,3
 READ (13,*)(CHARA192(I,J),j=1,3)
  ENDDO
```

```
      DO I=1,3
     READ (13,*)(CHARA193(I,J),j=1,3)
      ENDDO
      DO I=1,3
     READ (13,*)(CHARA211(I,J),j=1,3)
      ENDDO
      DO I=1,3
     READ (13,*)(CHARA212(I,J),j=1,3)
      ENDDO
      DO I=1,3
     READ (13,*)(CHARA213(I,J),j=1,3)
      ENDDO
      DO I=1,3
     READ (13,*)(CHARA311(I,J),j=1,3)
      ENDDO
      DO I=1,3
     READ (13,*)(CHARA312(I,J),j=1,3)
      ENDDO
      DO I=1,3
     READ (13,*)(CHARA313(I,J),j=1,3)
      ENDDO
     CLOSE (13)

C    CALCULATE CARBON CONVESION

C    CARBON IN AND OUT

    DO I=1,3
     CARBONI1(I,1)=FEEDR191(I,1)*FEEDU(1)/100
     CARBONI2(I,1)=FEEDR192(I,1)*FEEDU(1)/100
     CARBONI3(I,1)=FEEDR193(I,1)*FEEDU(1)/100
     CARBONI4(I,1)=FEEDR211(I,1)*FEEDU(1)/100
     CARBONI5(I,1)=FEEDR212(I,1)*FEEDU(1)/100
     CARBONI6(I,1)=FEEDR213(I,1)*FEEDU(1)/100
     CARBONI7(I,1)=FEEDR311(I,1)*FEEDU(1)/100
     CARBONI8(I,1)=FEEDR312(I,1)*FEEDU(1)/100
     CARBONI9(I,1)=FEEDR313(I,1)*FEEDU(1)/100

C     TOTAL MASS FLOW RATE AND CHAR FLOW RATE
     RHO=1.01325D5/(287*298.15)

     TMASS1(I,1)=FEEDR191(I,1)+RHO*FEEDR191(I,2)
```

```
      TMASS2(I,1)=FEEDR192(I,1)+RHO*FEEDR192(I,2)
      TMASS3(I,1)=FEEDR193(I,1)+RHO*FEEDR193(I,2)
      TMASS4(I,1)=FEEDR211(I,1)+RHO*FEEDR211(I,2)
      TMASS5(I,1)=FEEDR212(I,1)+RHO*FEEDR212(I,2)
      TMASS6(I,1)=FEEDR213(I,1)+RHO*FEEDR213(I,2)
      TMASS7(I,1)=FEEDR311(I,1)+RHO*FEEDR311(I,2)
      TMASS8(I,1)=FEEDR312(I,1)+RHO*FEEDR312(I,2)
      TMASS9(I,1)=FEEDR313(I,1)+RHO*FEEDR313(I,2)
      ENDDO

C     DENSITY OF CONSTITUENT
      R0=8.314D3
      RHOP(8)=R0/28.0
      RH2O=R0/18.0
      RHOP(1)=R0/44.0
      RHOP(4)=R0/2.0
      RHOP(5)=R0/32.0
      RHOP(7)=R0/16.0
      RHOP(6)=R0/28.0
      RHOP(2)=0.5*R0/28+0.5*R0/26.0
      RHOP(3)=R0/30
      P0=1.01325D5
      T0=298.15
      DO I=1,8
      RHOP(I)=P0/(RHOP(I)*T0)
      ENDDO

      DO I=1,3
      TMASS1(I,2)=0.0
      TMASS2(I,2)=0.0
      TMASS3(I,2)=0.0
      TMASS4(I,2)=0.0
      TMASS5(I,2)=0.0
      TMASS6(I,2)=0.0
      TMASS7(I,2)=0.0
      TMASS8(I,2)=0.0
      TMASS9(I,2)=0.0
      ENDDO

C     PRODUCT GAS DENSITY

      DO I=1,3
      DO J=1,8
      TMASS1(I,2)=TMASS1(I,2)+FEEDG191(I,J)/100.0*RHOP(J)
```

```
 ENDDO
 ENDDO
 DO I=1,3
 DO J=1,8
 TMASS2(I,2)=TMASS2(I,2)+FEEDG192(I,J)/100.0*RHOP(J)
 ENDDO
 ENDDO
 DO I=1,3
 DO J=1,8

 TMASS3(I,2)=TMASS3(I,2)+FEEDG193(I,J)/100.0*RHOP(J)
 ENDDO
 ENDDO
 DO I=1,3
 DO J=1,8

 TMASS4(I,2)=TMASS4(I,2)+FEEDG211(I,J)/100.0*RHOP(J)
 ENDDO
 ENDDO
 DO I=1,3
 DO J=1,8

 TMASS5(I,2)=TMASS5(I,2)+FEEDG212(I,J)/100.0*RHOP(J)
 ENDDO
 ENDDO
 DO I=1,3
 DO J=1,8

 TMASS6(I,2)=TMASS6(I,2)+FEEDG213(I,J)/100.0*RHOP(J)
 ENDDO
 ENDDO
 DO I=1,3
 DO J=1,8

 TMASS7(I,2)=TMASS7(I,2)+FEEDG311(I,J)/100.0*RHOP(J)
 ENDDO
 ENDDO
 DO I=1,3
 DO J=1,8
 TMASS8(I,2)=TMASS8(I,2)+FEEDG312(I,J)/100.0*RHOP(J)
 ENDDO
 ENDDO
 DO I=1,3
```

```
      DO J=1,8
      TMASS9(I,2)=TMASS9(I,2)+FEEDG313(I,J)/100.0*RHOP(J)
      ENDDO
      ENDDO

      DO I=1,3
C      GAS MASS FLOW RATE
      TMASS1(I,3)=TMASS1(I,2)*PRODG191(I,2)
      TMASS2(I,3)=TMASS2(I,2)*PRODG192(I,2)
      TMASS3(I,3)=TMASS3(I,2)*PRODG193(I,2)
      TMASS4(I,3)=TMASS4(I,2)*PRODG211(I,2)
      TMASS5(I,3)=TMASS5(I,2)*PRODG212(I,2)
      TMASS6(I,3)=TMASS6(I,2)*PRODG213(I,2)
      TMASS7(I,3)=TMASS7(I,2)*PRODG311(I,2)
      TMASS8(I,3)=TMASS8(I,2)*PRODG312(I,2)
      TMASS9(I,3)=TMASS9(I,2)*PRODG313(I,2)

C      REFUSE MASS FLOW RATE
      TMASS1(I,2)=TMASS1(I,1)-TMASS1(I,3)
      TMASS2(I,2)=TMASS2(I,1)-TMASS2(I,3)
      TMASS3(I,2)=TMASS3(I,1)-TMASS3(I,3)
      TMASS4(I,2)=TMASS4(I,1)-TMASS4(I,3)
      TMASS5(I,2)=TMASS5(I,1)-TMASS5(I,3)
      TMASS6(I,2)=TMASS6(I,1)-TMASS6(I,3)
      TMASS7(I,2)=TMASS7(I,1)-TMASS7(I,3)
      TMASS8(I,2)=TMASS8(I,1)-TMASS8(I,3)
      TMASS9(I,2)=TMASS9(I,1)-TMASS9(I,3)

      ENDDO

      WRITE (14,*) 'MASS FLOW RATES'
      WRITE (14,50) 'TOT-I','RICE H','AIR','GAS','CHAR'
50    FORMAT(',1X,5(A10,2X))
45    FORMAT (',1X,5(F10.4,2X))
      DO I=1,3
      WRITE (14,45)TMASS1(I,1),FEEDR191(I,1),RHO*FEEDR191(I,2)
     +  ,TMASS1(I,3),TMASS1(I,2)
     ENDDO
     DO I=1,3
      WRITE (14,45)TMASS2(I,1),FEEDR192(I,1),RHO*FEEDR192(I,2)
     +  ,TMASS2(I,3),TMASS2(I,2)
      ENDDO
     DO I=1,3
```

```
      WRITE (14,45)TMASS3(I,1),FEEDR193(I,1),RHO*FEEDR193(I,2)
     + ,TMASS3(I,3),TMASS3(I,2)
       ENDDO
       DO I=1,3
       WRITE (14,45)TMASS4(I,1),FEEDR211(I,1),RHO*FEEDR211(I,2)
     + ,TMASS4(I,2),TMASS4(I,2)
       ENDDO
       DO I=1,3
       WRITE (14,45)TMASS5(I,1),FEEDR212(I,1),RHO*FEEDR212(I,2)
     + ,TMASS5(I,3),TMASS5(I,2)
       ENDDO
       DO I=1,3
       WRITE (14,45)TMASS6(I,1),FEEDR213(I,1),RHO*FEEDR213(I,2)
     + ,TMASS6(I,3),TMASS6(I,2)
       ENDDO
       DO I=1,3
       WRITE (14,45)TMASS7(I,1),FEEDR311(I,1),RHO*FEEDR311(I,2)
     + ,TMASS7(I,3),TMASS7(I,2)
       ENDDO
       DO I=1,3
       WRITE (14,45)TMASS8(I,1),FEEDR312(I,1),RHO*FEEDR312(I,2)
     + ,TMASS8(I,3),TMASS8(I,2)
       ENDDO
       DO I=1,3
       WRITE (14,45)TMASS9(I,1),FEEDR313(I,1),RHO*FEEDR313(I,2)
     + ,TMASS9(I,3),TMASS9(I,2)
       ENDDO
       WRITE (14,*)
       WRITE (14,*)  'REST OF RESULTS'
       WRITE (14,*)

C      CARBON IN REFUSE
       DO I=1,3
       CARBONI1(I,3)=TMASS1(I,2)*CHARC191(I,1)/100
       CARBONI2(I,3)=TMASS2(I,2)*CHARC192(I,1)/100
       CARBONI3(I,3)=TMASS3(I,2)*CHARC193(I,1)/100
       CARBONI4(I,3)=TMASS4(I,2)*CHARC211(I,1)/100
       CARBONI5(I,3)=TMASS5(I,2)*CHARC212(I,1)/100
       CARBONI6(I,3)=TMASS6(I,2)*CHARC213(I,1)/100
       CARBONI7(I,3)=TMASS7(I,2)*CHARC311(I,1)/100
       CARBONI8(I,3)=TMASS8(I,2)*CHARC312(I,1)/100
       CARBONI9(I,3)=TMASS9(I,2)*CHARC313(I,1)/100
       ENDDO
```

```
C     CARBON IN GAS
C     CARBON IN EACH GAS SPECIE CALCULATION
      CFRAC(8)=12.0/28
      CFRAC(1)=1.0*12/44
      CFRAC(4)=0.0
      CFRAC(5)=0.0
      CFRAC(7)=12.0/16.0
      CFRAC(6)=0.0
      CFRAC(2)=0.5*24.0/28.0+0.5*24.0/26.0
      CFRAC(3)=24.0/30.0
      DO I=1,3
      CARBONI1(I,2)=0.0
      CARBONI2(I,2)=0.0
      CARBONI3(I,2)=0.0
      CARBONI4(I,2)=0.0
      CARBONI5(I,2)=0.0
      CARBONI6(I,2)=0.0
      CARBONI7(I,2)=0.0
      CARBONI8(I,2)=0.0
      CARBONI9(I,2)=0.0

       ENDDO

     DO I=1,3
     DO J=1,8
    CARBONI1(I,2)=CARBONI1(I,2)+0.01*TMASS1(I,3)*FEEDG191(I,J)
   + *CFRAC(J)
    CARBONI2(I,2)=CARBONI2(I,2)+0.01*TMASS2(I,3)*FEEDG192(I,J)
   + *CFRAC(J)
    CARBONI3(I,2)=CARBONI3(I,2)+0.01*TMASS3(I,3)*FEEDG193(I,J)
   + *CFRAC(J)
    CARBONI4(I,2)=CARBONI4(I,2)+0.01*TMASS4(I,3)*FEEDG211(I,J)
   + *CFRAC(J)
    CARBONI5(I,2)=CARBONI5(I,2)+0.01*TMASS5(I,3)*FEEDG212(I,J)
   + *CFRAC(J)
    CARBONI6(I,2)=CARBONI6(I,2)+0.01*TMASS6(I,3)*FEEDG213(I,J)
   + *CFRAC(J)
    CARBONI7(I,2)=CARBONI7(I,2)+0.01*TMASS7(I,3)*FEEDG311(I,J)
   + *CFRAC(J)
    CARBONI8(I,2)=CARBONI8(I,2)+0.01*TMASS8(I,3)*FEEDG312(I,J)
   + *CFRAC(J)
    CARBONI9(I,2)=CARBONI9(I,2)+0.01*TMASS9(I,3)*FEEDG313(I,J)
   + *CFRAC(J)
```

```
      ENDDO
      ENDDO

C       CARBONI(I,1)= CARBON IN
C       CARBONI(I,2)=CARBON IN GAS
C       CARBON (I,3) =CARBON IN CHAR
C       PRINT OUT
      WRITE (14,35) 'CARBON IN','C IN GAS','C IN CHAR','C-OUT',
     + 'C-OUT:C-IN'
      WRITE (14,*)
 35   FORMAT (',1X,6(A12,2X))
      DO I=1,3
      WRITE (14,25) CARBONI1(I,1),CARBONI1(I,2),CARBONI1(I,3),
     + CARBONI1(I,2)+CARBONI1(I,3),(CARBONI1(I,2)+CARBONI1(I,3))/
     + CARBONI1(I,1)*100

      ENDDO
      WRITE (14,*)

 25   FORMAT (',1X,6(F10.5,4X))

      DO I=1,3
      WRITE (14,25) CARBONI2(I,1),CARBONI2(I,2),CARBONI2(I,3),
     + CARBONI2(I,2)+CARBONI2(I,3),(CARBONI2(I,2)+CARBONI2(I,3))/
     + CARBONI2(I,1)*100

      ENDDO
      WRITE (14,*)
      DO I=1,3
      WRITE (14,25) CARBONI3(I,1),CARBONI3(I,2),CARBONI3(I,3),
     + CARBONI3(I,2)+CARBONI3(I,3),(CARBONI3(I,2)+CARBONI3(I,3))/
     + CARBONI3(I,1)*100

      ENDDO
      WRITE (14,*)
      DO I=1,3
      WRITE (14,25) CARBONI4(I,1),CARBONI4(I,2),CARBONI4(I,3),
     + CARBONI4(I,2)+CARBONI4(I,3),(CARBONI4(I,2)+CARBONI4(I,3))/
     + CARBONI4(I,1)*100

      ENDDO
      WRITE (14,*)
      DO I=1,3
```

```
  WRITE (14,25) CARBONI5(I,1),CARBONI5(I,2),CARBONI5(I,3),
 + CARBONI5(I,2)+CARBONI5(I,3),(CARBONI5(I,2)+CARBONI5(I,3))/
 + CARBONI5(I,1)*100

  ENDDO
   WRITE (14,*)
  DO I=1,3
  WRITE (14,25) CARBONI6(I,1),CARBONI6(I,2),CARBONI6(I,3),
 + CARBONI6(I,2)+CARBONI6(I,3),(CARBONI6(I,2)+CARBONI6(I,3))/
 + CARBONI6(I,1)*100

  ENDDO
   WRITE (14,*)
  DO I=1,3
  WRITE (14,25) CARBONI7(I,1),CARBONI7(I,2),CARBONI7(I,3),
 + CARBONI7(I,2)+CARBONI7(I,3),(CARBONI7(I,2)+CARBONI7(I,3))/
 + CARBONI7(I,1)*100

  ENDDO
   WRITE (14,*)
  DO I=1,3
  WRITE (14,25) CARBONI8(I,1),CARBONI8(I,2),CARBONI8(I,3),
 + CARBONI8(I,2)+CARBONI8(I,3),(CARBONI8(I,2)+CARBONI8(I,3))/
 + CARBONI8(I,1)*100

  ENDDO
   WRITE (14,*)
  DO I=1,3
  WRITE (14,25) CARBONI9(I,1),CARBONI9(I,2),CARBONI9(I,3),
 + CARBONI9(I,2)+CARBONI9(I,3),(CARBONI9(I,2)+CARBONI9(I,3))/
 + CARBONI9(I,1)*100

  ENDDO

  END
```

APPENDIX C

"Aspen Simulation Input File"

Aspen Simulation Input File

The following computer listing is an ASPEN input file typical of the simulation models created for this study. The version of the ASPEN program used in this study was ASPEN Plus version 9.3. This is a commercial release of ASPEN supported by ASPEN Technology, Inc. of Cambridge, Massachusetts, U. S. A.

```
New
TITLE:  MODELING FLUIDIZED BED RICE HUSK GASIFICATION

IN-UNITS SI ENTHALPY-FLO=KW MOLE-HEAT-CA='KJ/KMOL-K' POWER=KW &
     PRESSURE=BAR TEMPERATURE=C DELTA-T=C &
     MOLE-ENTHALP='KJ/KMOL' MASS-ENTHALP='KJ/KG' &
     MOLE-ENTROPY='KJ/KMOL-K' MASS-ENTROPY='KJ/KG-K' &
     MASS-HEAT-CA='KJ/KG-K' WORK=KJ HEAT=KJ PDROP=BAR &
     VOL-HEAT-CAP='KJ/CUM-K'

DEF-STREAMS MCINCPSD ALL

DATABANKS SOLIDS / COMBUST / PURECOMP / INORGANIC / &
     NOASPENPCD

PROP-SOURCES SOLIDS / COMBUST / PURECOMP / INORGANIC

COMPONENTS
   H2O H2O H2O /
   N2 N2 N2 /
   O2 O2 O2 /
   RICE-H * RICE-H /
   NO2 NO2 NO2 /
   NO NO NO /
   S S S /
   SO2 O2S SO2 /
   SO3 O3S SO3 /
   H2 H2 H2 /
   CL2 CL2 CL2 /
   HCL HCL HCL /
   C C C /
```

```
    CO CO CO /
    CO2 CO2 CO2 /
    ASH * ASH /
    CH4 CH4 CH4 /
    C2H6 C2H6 C2H6 /
    C2H4 C2H4 C2H4 /
    C2H2 C2H2 C2H2

 FLOWSHEET
    BLOCK DECOMP IN=RICE-H OUT=INBURNER QDECOMP
    BLOCK BURN IN=INBURNER AIR-1 OUT=PRODUCTS
    BLOCK SEPARATE IN=PRD-1 OUT=SOLIDS GAS-1
    BLOCK CALORI-1 IN=GIN CAIR OUT=GASO
    BLOCK CALOR-11 IN=GASES OUT=GIN
    BLOCK CALOR-3 IN=GASO OUT=GCOOL QNET
    BLOCK WALL IN=SOLIDS AIR-2 OUT=PRODU-2
    BLOCK GAS-M IN=GAS-2 GAS-1 OUT=GASES
    BLOCK SEP-2 IN=SGAS OUT=REFUSE GAS-2
    BLOCK M1 IN=AIR OUT=AIR-1
    BLOCK M2 IN=AIR-P OUT=AIR-2
    BLOCK CLGAS IN=PRODUCTS OUT=PRD-1
    BLOCK SCG IN=PRODU-2 OUT=SGAS

PROPERTIES SYSOP0
    PROPERTIES IDEAL / RK-SOAVE

NC-COMPS RICE-H PROXANAL ULTANAL SULFANAL

NC-PROPS RICE-H ENTHALPY HCOALGEN 6 / DENSITY DCOALIGT

NC-COMPS ASH PROXANAL ULTANAL SULFANAL

NC-PROPS ASH ENTHALPY HCOALGEN / DENSITY DCOALIGT

PROP-DATA HEAT
    IN-UNITS ENG
    PROP-LIST HCOMB
    PVAL RICE-H 11700

PROP-DATA RKSKIJ-1
    IN-UNITS SI ENTHALPY-FLO=KW MOLE-HEAT-CA='KJ/KMOL-K' POWER=KW
&
      PRESSURE=BAR TEMPERATURE=C DELTA-T=C  &
```

```
   MOLE-ENTHALP='KJ/KMOL' MASS-ENTHALP='KJ/KG' &
   MOLE-ENTROPY='KJ/KMOL-K' MASS-ENTROPY='KJ/KG-K' &
   MASS-HEAT-CA='KJ/KG-K' WORK=KJ HEAT=KJ PDROP=BAR &
   VOL-HEAT-CAP='KJ/CUM-K'

PROP-LIST RKSKIJ
BPVAL H2O CO2 .0737000000
BPVAL N2 CO2 -.0315000000
BPVAL N2 O2 -7.8000000E-3
BPVAL N2 SO2 .0578000000
BPVAL N2 H2 .0978000000
BPVAL N2 CO .0374000000
BPVAL N2 CH4 .0278000000
BPVAL N2 C2H6 .0407000000
BPVAL N2 C2H4 .0798000000
BPVAL O2 N2 -7.8000000E-3
BPVAL SO2 CH4 .1279000000
BPVAL SO2 N2 .0578000000
BPVAL H2 CO2 -.3426000000
BPVAL H2 CO .0804000000
BPVAL H2 CH4 -.0222000000
BPVAL H2 C2H6 -.1667000000
BPVAL H2 C2H4 -.0681000000
BPVAL H2 N2 .0978000000
BPVAL CO H2 .0804000000
BPVAL CO CH4 .0322000000
BPVAL CO C2H6 -.0278000000
BPVAL CO N2 .0374000000
BPVAL CO2 H2 -.3426000000
BPVAL CO2 CH4 .0933000000
BPVAL CO2 C2H6 .1363000000
BPVAL CO2 C2H4 .0533000000
BPVAL CO2 N2 -.0315000000
BPVAL CO2 H2O .0737000000
BPVAL CH4 CO2 .0933000000
BPVAL CH4 SO2 .1279000000
BPVAL CH4 H2 -.0222000000
BPVAL CH4 CO .0322000000
BPVAL CH4 C2H6 -7.8000000E-3
BPVAL CH4 C2H4 .0189000000
BPVAL CH4 N2 .0278000000
BPVAL C2H6 CO2 .1363000000
BPVAL C2H6 H2 -.1667000000
```

```
    BPVAL C2H6 CO -.0278000000
    BPVAL C2H6 CH4 -7.8000000E-3
    BPVAL C2H6 C2H4 8.90000000E-3
    BPVAL C2H6 N2 .0407000000
    BPVAL C2H4 CO2 .0533000000
    BPVAL C2H4 H2 -.0681000000
    BPVAL C2H4 CH4 .0189000000
    BPVAL C2H4 C2H6 8.90000000E-3
    BPVAL C2H4 N2 .0798000000
    BPVAL C2H4 C2H2 .0596000000


 PROP-SET ALL-SUBS
    IN-UNITS ENG
    PROPNAME-LIS VOLFLMX MASSVFRA MASSSFRA RHOMX MASSFLOW TEMP
&
       PRES UNITS='LB/CUFT' SUBSTREAM=ALL


 STREAM AIR
    SUBSTREAM MIXED TEMP=25.00000 PRES=1.013529 MOLE-FLOW=1
    MOLE-FRAC N2 0.79 / O2 0.21


 STREAM AIR-P
    SUBSTREAM MIXED TEMP=25 PRES=1.01325 MOLE-FLOW=1
    MOLE-FRAC N2 .79 / O2 .21


 STREAM CAIR
    SUBSTREAM MIXED TEMP=25 PRES=1 <ATM> MASS-FLOW=1
    MASS-FRAC O2 1


 STREAM RICE-H
    SUBSTREAM NCPSD TEMP=25.00000 PRES=1.013529
    MASS-FLOW RICE-H .00949
    COMP-ATTR RICE-H PROXANAL ( 15.0 9.27 60.37 21.28 )
    COMP-ATTR RICE-H ULTANAL ( 23.35 37.6 5.43 0.38 0.01  &
      0.03 33.2 )
    COMP-ATTR RICE-H SULFANAL ( .01 0.01 0.01 )
    SUBS-ATTR PSD ( 0 0 0 0 0 0 0.1 0.2 0.3 0.4 )
 DEF-STREAMS HEAT QDECOMP
```

```
DEF-STREAMS HEAT QNET

BLOCK GAS-M MIXER

BLOCK CALOR-3 HEATER
  PARAM TEMP=25 PRES=1 <ATM>

BLOCK CALOR-11 HEATER
  PARAM TEMP=25 PRES=1 <ATM>

BLOCK CLGAS HEATER
  PARAM TEMP=600 PRES=0

BLOCK SCG HEATER
  PARAM TEMP=600 PRES=0

BLOCK DECOMP RYIELD
  IN-UNITS ENG
  PARAM TEMP=77.0 PRES=14.7
  MASS-YIELD MIXED H2O 0.2 / NCPSD ASH 0.2 / CIPSD C  &
    0.1 / MIXED H2 0.1 / N2 0.1 / CL2 0.1 / S 0.1 /  &
    O2 0.1
  COMP-ATTR NCPSD ASH PROXANAL ( 0 0 0 100 )
  COMP-ATTR NCPSD ASH ULTANAL ( 100 0 0 0 0 0 0 )
  COMP-ATTR NCPSD ASH SULFANAL ( 0 0 0 )
  SUBS-ATTR 1 CIPSD PSD ( 0 0 0 0 0 0 0 0.1 0.2 0.3  &
    0.4 )
  SUBS-ATTR 2 NCPSD PSD ( 0 0 0 0 0 0 0 0.1 0.2 0.3  &
    0.4 )

BLOCK CORE RGIBBS
  PARAM PRES=1.013529 DUTY=0
  PROD H2O / N2 / O2 / NO2 / NO / S / SO2 / SO3 /  &
    H2 / CL2 / HCL / C SS / CO / CO2 / CH4 / C2H6  &
    / C2H4 / C2H2
  PROD-FRAC C .3
  PROPERTIES RK-SOAVE

BLOCK CALORI-1 RGIBBS
  PARAM PRES=0 DUTY=0
  PROD H2O / N2 / O2 / NO2 / NO / SO2 / CO2 / CL2
BLOCK ANNULUS RGIBBS
  PARAM PRES=0 DUTY=0
```

```
    PROD O2 / N2 / SO2 / CO / C SS / CH4 / CO2 /  &
      C2H4 / CL2 / H2
    PROD-FRAC C .4

  BLOCK M1 MULT
    PARAM FACTOR=.999

  BLOCK M2 MULT
    PARAM FACTOR=.9999

  BLOCK SEP-2 SSPLIT
    FRAC MIXED REFUSE 0
    FRAC CIPSD REFUSE 1
    FRAC NCPSD REFUSE 1

  BLOCK SEPARATE SSPLIT
    IN-UNITS ENG
    FRAC MIXED SOLIDS 0
    FRAC CIPSD SOLIDS 1
    FRAC NCPSD SOLIDS 1

  DESIGN-SPEC AIR1
    DEFINE C MOLE-FLOW STREAM=INBURNER SUBSTREAM=CIPSD &
      COMPONENT=C
    DEFINE H2 MOLE-FLOW STREAM=INBURNER SUBSTREAM=MIXED &
      COMPONENT=H2O
    DEFINE O2 MOLE-FRAC STREAM=AIR SUBSTREAM=MIXED COMPONENT=O2
    DEFINE MULT BLOCK-VAR BLOCK=M1 VARIABLE=FACTOR &
      SENTENCE=PARAM
F     STOIC=C+0.5*H2
F     ER=0.25
F     IF (DABS(O2).LT.1.0D-8) O2=1.0
F       STOIC=ER*STOIC/O2
    SPEC "MULT" TO "STOIC"
    TOL-SPEC "1D-5"
    VARY BLOCK-VAR BLOCK=M1 VARIABLE=FACTOR SENTENCE=PARAM
    LIMITS "1.0D-5" "10"

  DESIGN-SPEC AIR2
    DEFINE C MOLE-FLOW STREAM=SOLIDS SUBSTREAM=CIPSD &
      COMPONENT=C
    DEFINE H2 MOLE-FLOW STREAM=INBURNER SUBSTREAM=MIXED &
      COMPONENT=H2O
```

```
    DEFINE O2 MOLE-FRAC STREAM=AIR SUBSTREAM=MIXED COMPONENT=O2
    DEFINE MULT BLOCK-VAR BLOCK=M2 VARIABLE=FACTOR &
      SENTENCE=PARAM
F     STOIC=C
F     ER=0.25
F     IF (DABS(O2).LT.1.0D-8) O2=1.0
F     STOIC=ER*STOIC/O2
    SPEC "MULT" TO "STOIC"
    TOL-SPEC "1D-5"
    VARY BLOCK-VAR BLOCK=M2 VARIABLE=FACTOR SENTENCE=PARAM
    LIMITS "1.0D-5" "10"

  DESIGN-SPEC DUTY
    DEFINE Q1 BLOCK-VAR BLOCK=CLGAS VARIABLE=QCALC &
      SENTENCE=PARAM
    DEFINE Q2 BLOCK-VAR BLOCK=DECOMP VARIABLE=QCALC &
      SENTENCE=PARAM
    DEFINE XC BLOCK-VAR BLOCK=BURN VARIABLE=FRAC &
      SENTENCE=PROD-FRAC ID1=C
    DEFINE H2 MOLE-FLOW STREAM=INBURNER SUBSTREAM=MIXED &
      COMPONENT=H2
    DEFINE C MOLE-FLOW STREAM=INBURNER SUBSTREAM=CIPSD &
      COMPONENT=C
    DEFINE C1 MOLE-FLOW STREAM=SOLIDS SUBSTREAM=CIPSD &
      COMPONENT=C
    DEFINE T1 STREAM-VAR STREAM=PRODUCTS SUBSTREAM=MIXED &
      VARIABLE=TEMP
    DEFINE T2 STREAM-VAR STREAM=PRODU-2 SUBSTREAM=MIXED &
      VARIABLE=TEMP
    DEFINE XM1 STREAM-VAR STREAM=PRODUCTS SUBSTREAM=MIXED &
      VARIABLE=MASS-FLOW
    DEFINE XM2 STREAM-VAR STREAM=PRODU-2 SUBSTREAM=MIXED &
      VARIABLE=MASS-FLOW
F       RAT=H2*68.3174+C*94.0518
F       RAT2=C1*94.0518
F        IF (DABS(RAT).LT.1.0D-8) RAT=1.0
F       R=RAT2/RAT
F       RATIO=1.0-R
F      IF (DABS(T1).LT.100) T1=100.0
F       RATIO=XM2*(T2-25.0)+XM1*(T1-25.0)
F       IF (DABS(RATIO).LT.1.0D-8) RATIO=1000
F       RATIO=XM1*(T1-25.0)/RATIO
    SPEC "DABS(Q1)" TO "DABS(Q2)*RATIO "
```

```
    TOL-SPEC "1"
    VARY BLOCK-VAR BLOCK=CLGAS VARIABLE=TEMP SENTENCE=PARAM
    LIMITS "400" "2000"

  DESIGN-SPEC DUTY1
    DEFINE Q1 BLOCK-VAR BLOCK=SCG VARIABLE=QCALC SENTENCE=PARAM
    DEFINE Q2 BLOCK-VAR BLOCK=DECOMP VARIABLE=QCALC &
      SENTENCE=PARAM
    DEFINE XC BLOCK-VAR BLOCK=BURN VARIABLE=FRAC &
      SENTENCE=PROD-FRAC ID1=C
    DEFINE C MOLE-FLOW STREAM=INBURNER SUBSTREAM=CIPSD &
      COMPONENT=C
    DEFINE H2 MOLE-FLOW STREAM=INBURNER SUBSTREAM=MIXED &
      COMPONENT=H2
    DEFINE C1 MOLE-FLOW STREAM=SOLIDS SUBSTREAM=CIPSD &
      COMPONENT=C
    DEFINE T1 STREAM-VAR STREAM=PRODUCTS SUBSTREAM=MIXED &
      VARIABLE=TEMP
    DEFINE T2 STREAM-VAR STREAM=PRODU-2 SUBSTREAM=MIXED &
      VARIABLE=TEMP
    DEFINE XM1 STREAM-VAR STREAM=PRODUCTS SUBSTREAM=MIXED &
      VARIABLE=MASS-FLOW
    DEFINE XM2 STREAM-VAR STREAM=PRODU-2 SUBSTREAM=MIXED &
      VARIABLE=MASS-FLOW
F       RAT=H2*68.3174+C*94.0518
F       RAT2=C1*94.0518
F       IF (DABS(RAT).LT.1.0D-8) RAT=1.0
F       RATIO=RAT2/RAT
F       RATIO=XM1*(T1-25.0)+XM2*(T2-25.0)
F       IF (DABS(RATIO).LT.1.0D-8) RATIO=1000
F       RATIO=XM2*(T2-25.0)/RATIO
    SPEC "DABS(Q1)" TO "DABS(Q2)*RATIO"
    TOL-SPEC "1"
    VARY BLOCK-VAR BLOCK=SCG VARIABLE=TEMP SENTENCE=PARAM
    LIMITS "100" "2000"

  FORTRAN COMBUST
    IN-UNITS ENG
    VECTOR-DEF ULT COMP-ATTR STREAM=RICE-H SUBSTREAM=NCPSD &
      COMPONENT=RICE-H ATTRIBUTE=ULTANAL
    DEFINE WATER COMP-ATTR-VAR STREAM=RICE-H SUBSTREAM=NCPSD &
      COMPONENT=RICE-H ATTRIBUTE=PROXANAL ELEMENT=1
    DEFINE H2O BLOCK-VAR BLOCK=DECOMP VARIABLE=YIELD &
```

```
      SENTENCE=MASS-YIELD ID1=MIXED ID2=H2O
    DEFINE ASH BLOCK-VAR BLOCK=DECOMP VARIABLE=YIELD &
      SENTENCE=MASS-YIELD ID1=NCPSD ID2=ASH
    DEFINE CARB BLOCK-VAR BLOCK=DECOMP VARIABLE=YIELD &
      SENTENCE=MASS-YIELD ID1=CIPSD ID2=C
    DEFINE H2 BLOCK-VAR BLOCK=DECOMP VARIABLE=YIELD &
      SENTENCE=MASS-YIELD ID1=MIXED ID2=H2
    DEFINE N2 BLOCK-VAR BLOCK=DECOMP VARIABLE=YIELD &
      SENTENCE=MASS-YIELD ID1=MIXED ID2=N2
    DEFINE CL2 BLOCK-VAR BLOCK=DECOMP VARIABLE=YIELD &
      SENTENCE=MASS-YIELD ID1=MIXED ID2=CL2
    DEFINE SULF BLOCK-VAR BLOCK=DECOMP VARIABLE=YIELD &
      SENTENCE=MASS-YIELD ID1=MIXED ID2=S
    DEFINE O2 BLOCK-VAR BLOCK=DECOMP VARIABLE=YIELD &
      SENTENCE=MASS-YIELD ID1=MIXED ID2=O2
C   FACT IS THE FACTOR TO CONVERT THE ULTIMATE ANALYSIS TO
C   A WET BASIS.
F   FACT = (100 - WATER) / 100
F   H2O  = WATER / 100
F   ASH  = ULT(1) / 100 * FACT
F   CARB = ULT(2) / 100 * FACT
F   H2   = ULT(3) / 100 * FACT
F   N2   = ULT(4) / 100 * FACT
F   CL2  = ULT(5) / 100 * FACT
F   SULF = ULT(6) / 100 * FACT
F   O2   = ULT(7) / 100 * FACT
  EXECUTE BEFORE BLOCK DECOMP

;ER = 0.25, FV = 0.22

SENSITIVITY GAS
  DEFINE H2O MOLE-FRAC STREAM=GASES SUBSTREAM=MIXED &
    COMPONENT=H2O
  DEFINE N2 MOLE-FRAC STREAM=GASES SUBSTREAM=MIXED &
    COMPONENT=N2
  DEFINE O2 MOLE-FRAC STREAM=GASES SUBSTREAM=MIXED &
    COMPONENT=O2
  DEFINE H2 MOLE-FRAC STREAM=GASES SUBSTREAM=MIXED &
    COMPONENT=H2
  DEFINE CO MOLE-FRAC STREAM=GASES SUBSTREAM=MIXED &
    COMPONENT=CO
  DEFINE CO2 MOLE-FRAC STREAM=GASES SUBSTREAM=MIXED &
    COMPONENT=CO2
```

```
    DEFINE CH4 MOLE-FRAC STREAM=GASES SUBSTREAM=MIXED &
      COMPONENT=CH4
    DEFINE C2H6 MOLE-FRAC STREAM=GASES SUBSTREAM=MIXED &
      COMPONENT=C2H6
    DEFINE C2H4 MOLE-FRAC STREAM=GASES SUBSTREAM=MIXED &
      COMPONENT=C2H4
    DEFINE C2H2 MOLE-FRAC STREAM=GASES SUBSTREAM=MIXED &
      COMPONENT=C2H2
    DEFINE COUT MASS-FLOW STREAM=SOLIDS SUBSTREAM=CIPSD &
      COMPONENT=C
    VECTOR-DEF ULT COMP-ATTR STREAM=RICE-H SUBSTREAM=NCPSD &
      COMPONENT=RICE-H ATTRIBUTE=ULTANAL
    DEFINE PROX COMP-ATTR-VAR STREAM=RICE-H SUBSTREAM=NCPSD &
      COMPONENT=RICE-H ATTRIBUTE=PROXANAL ELEMENT=1
    DEFINE M STREAM-VAR STREAM=RICE-H SUBSTREAM=NCPSD &
      VARIABLE=MASS-FLOW
    DEFINE MG STREAM-VAR STREAM=GASES SUBSTREAM=MIXED &
      VARIABLE=MASS-FLOW
    DEFINE MA STREAM-VAR STREAM=AIR SUBSTREAM=MIXED &
      VARIABLE=MASS-FLOW
    DEFINE VA STREAM-VAR STREAM=AIR SUBSTREAM=MIXED &
      VARIABLE=STDVOL-FLOW
    DEFINE T BLOCK-VAR BLOCK=BURN VARIABLE=TEMP SENTENCE=PARAM
    DEFINE QNET INFO-VAR INFO=HEAT VARIABLE=DUTY STREAM=QNET
    DEFINE CC2 BLOCK-VAR BLOCK=WALL VARIABLE=FRAC &
      SENTENCE=PROD-FRAC ID1=C
    DEFINE CC1 BLOCK-VAR BLOCK=BURN VARIABLE=FRAC &
      SENTENCE=PROD-FRAC ID1=C
F     FAC1=100/(100-H2O)
F     FAC2=(100-PROX)/100
F     CIN=FAC2*M*ULT(2)/100
F     IF (DABS(CIN).LT.1.0D-12) CIN=1.0
F     CC=(CIN-COUT)/CIN
F     N2=N2*FAC1
F     O2=O2*FAC1
F     H2=H2*FAC1
F     CO=CO*FAC1
F     CO2=CO2*FAC1
F     CH4=CH4*FAC1
F     CNHM=(C2H4+C2H2)*FAC1
F     C2H6=C2H6*FAC1
  TABULATE 1 "CO2*100" COL-LABEL="CO2"
  TABULATE 2 "CNHM*100" COL-LABEL="C2HM"
```

```
   TABULATE 3 "C2H6*100" COL-LABEL="C2H6"
   TABULATE 4 "H2*100" COL-LABEL="H2"
   TABULATE 5 "O2*100" COL-LABEL="O2"
   TABULATE 6 "N2*100" COL-LABEL="N2"
   TABULATE 7 "CH4*100" COL-LABEL="CH4"
   TABULATE 8 "CO*100" COL-LABEL="CO"
   TABULATE 9 "MG    " COL-LABEL="GAS " "FLOW" UNIT-LABEL="KG/S"
   TABULATE 10 "CC*100" COL-LABEL="CARBON" "CONVERS"
   TABULATE 11 "M*60" COL-LABEL="RICE-H" "FLOW" UNIT-LABEL= &
     "KG/MIN"
   TABULATE 12 "MA*60" COL-LABEL="AIR" "MASS" "FL" UNIT-LABEL= &
     "KG/MIN"
   TABULATE 13 "VA*60" COL-LABEL="AIR" "VOL" "FL" UNIT-LABEL= &
     "CUM/MIN"
   TABULATE 14 "T" COL-LABEL="GASF" "TEMP" UNIT-LABEL="DEG C"
   TABULATE 15 "QNET/MG" COL-LABEL="LHV" UNIT-LABEL="KJ/KG"
   TABULATE 16 "(1-CC2)*100" COL-LABEL="CARB CON" "IN REAC2"
   TABULATE 17 "(1-CC1)*100" COL-LABEL="CARB CON" "IN REAC1"
   VARY BLOCK-VAR BLOCK=BURN VARIABLE=FRAC SENTENCE=PROD-FRAC
&
     ID1=C
   RANGE LOWER="0.01" UPPER="0.3" NPOINT="26"

SENSITIVITY GAS-1
   DEFINE H2O MOLE-FRAC STREAM=GASES SUBSTREAM=MIXED &
     COMPONENT=H2O
   DEFINE N2 MOLE-FRAC STREAM=GASES SUBSTREAM=MIXED &
     COMPONENT=N2
   DEFINE O2 MOLE-FRAC STREAM=GASES SUBSTREAM=MIXED &
     COMPONENT=O2
   DEFINE H2 MOLE-FRAC STREAM=GASES SUBSTREAM=MIXED &
     COMPONENT=H2
   DEFINE CO MOLE-FRAC STREAM=GASES SUBSTREAM=MIXED &
     COMPONENT=CO
   DEFINE CO2 MOLE-FRAC STREAM=GASES SUBSTREAM=MIXED &
     COMPONENT=CO2
   DEFINE CH4 MOLE-FRAC STREAM=GASES SUBSTREAM=MIXED &
     COMPONENT=CH4
   DEFINE C2H6 MOLE-FRAC STREAM=GASES SUBSTREAM=MIXED &
     COMPONENT=C2H6
   DEFINE C2H4 MOLE-FRAC STREAM=GASES SUBSTREAM=MIXED &
     COMPONENT=C2H4
   DEFINE C2H2 MOLE-FRAC STREAM=GASES SUBSTREAM=MIXED &
```

```
      COMPONENT=C2H2
    DEFINE COUT MASS-FLOW STREAM=SOLIDS SUBSTREAM=CIPSD &
      COMPONENT=C
    VECTOR-DEF ULT COMP-ATTR STREAM=RICE-H SUBSTREAM=NCPSD &
      COMPONENT=RICE-H ATTRIBUTE=ULTANAL
    DEFINE PROX COMP-ATTR-VAR STREAM=RICE-H SUBSTREAM=NCPSD &
      COMPONENT=RICE-H ATTRIBUTE=PROXANAL ELEMENT=1
    DEFINE M STREAM-VAR STREAM=RICE-H SUBSTREAM=NCPSD &
      VARIABLE=MASS-FLOW
    DEFINE MG STREAM-VAR STREAM=GASES SUBSTREAM=MIXED &
      VARIABLE=MASS-FLOW
    DEFINE MA STREAM-VAR STREAM=AIR SUBSTREAM=MIXED &
      VARIABLE=MASS-FLOW
    DEFINE VA STREAM-VAR STREAM=AIR SUBSTREAM=MIXED &
      VARIABLE=STDVOL-FLOW
    DEFINE T BLOCK-VAR BLOCK=BURN VARIABLE=TEMP SENTENCE=PARAM
    DEFINE QNET INFO-VAR INFO=HEAT VARIABLE=DUTY STREAM=QNET
    DEFINE CC2 BLOCK-VAR BLOCK=WALL VARIABLE=FRAC &
      SENTENCE=PROD-FRAC ID1=C
    DEFINE CC1 BLOCK-VAR BLOCK=BURN VARIABLE=FRAC &
      SENTENCE=PROD-FRAC ID1=C
F     FAC1=100/(100-H2O)
F     FAC2=(100-PROX)/100
F     CIN=FAC2*M*ULT(2)/100
F     IF (DABS(CIN).LT.1.0D-12) CIN=1.0
F     CC=(CIN-COUT)/CIN
F     N2=N2*FAC1
F     O2=O2*FAC1
F     H2=H2*FAC1
F     CO=CO*FAC1
F     CO2=CO2*FAC1
F     CH4=CH4*FAC1
F     CNHM=(C2H4+C2H2)*FAC1
F     C2H6=C2H6*FAC1
  TABULATE 1 "CO2*100" COL-LABEL="CO2"
  TABULATE 2 "CNHM*100" COL-LABEL="C2HM"
  TABULATE 3 "C2H6*100" COL-LABEL="C2H6"
  TABULATE 4 "H2*100" COL-LABEL="H2"
  TABULATE 5 "O2*100" COL-LABEL="O2"
  TABULATE 6 "N2*100" COL-LABEL="N2"
  TABULATE 7 "CH4*100" COL-LABEL="CH4"
  TABULATE 8 "CO*100" COL-LABEL="CO"
  TABULATE 9 "MG    " COL-LABEL="GAS " "FLOW" UNIT-LABEL="KG/S"
```

```
   TABULATE 10 "CC*100" COL-LABEL="CARBON" "CONVERS"
   TABULATE 11 "M*60" COL-LABEL="RICE-H" "FLOW" UNIT-LABEL= &
     "KG/MIN"
   TABULATE 12 "MA*60" COL-LABEL="AIR" "MASS" "FL" UNIT-LABEL= &
     "KG/MIN"
   TABULATE 13 "VA*60" COL-LABEL="AIR" "VOL" "FL" UNIT-LABEL= &
     "CUM/MIN"
   TABULATE 14 "T" COL-LABEL="GASF" "TEMP" UNIT-LABEL="DEG C"
   TABULATE 15 "QNET/MG" COL-LABEL="LHV" UNIT-LABEL="KJ/KG"
   TABULATE 16 "(1-CC2)*100" COL-LABEL="CARB CON" "IN REAC2"
   TABULATE 17 "(1-CC1)*100" COL-LABEL="CARB CON" "IN REAC1"
   VARY BLOCK-VAR BLOCK=WALL VARIABLE=FRAC SENTENCE=PROD-FRAC
&
     ID1=C
   RANGE LOWER="0.01" UPPER="0.4" NPOINT="20"

;ER = 0.25, FV = 0.22


SENSITIVITY GAS-TEM
   DEFINE H2O MOLE-FRAC STREAM=GASES SUBSTREAM=MIXED &
     COMPONENT=H2O
   DEFINE N2 MOLE-FRAC STREAM=GASES SUBSTREAM=MIXED &
     COMPONENT=N2
   DEFINE O2 MOLE-FRAC STREAM=GASES SUBSTREAM=MIXED &
     COMPONENT=O2
   DEFINE H2 MOLE-FRAC STREAM=GASES SUBSTREAM=MIXED &
     COMPONENT=H2
   DEFINE CO MOLE-FRAC STREAM=GASES SUBSTREAM=MIXED &
     COMPONENT=CO
   DEFINE CO2 MOLE-FRAC STREAM=GASES SUBSTREAM=MIXED &
     COMPONENT=CO2
   DEFINE CH4 MOLE-FRAC STREAM=GASES SUBSTREAM=MIXED &
     COMPONENT=CH4
   DEFINE C2H6 MOLE-FRAC STREAM=GASES SUBSTREAM=MIXED &
     COMPONENT=C2H6
   DEFINE C2H4 MOLE-FRAC STREAM=GASES SUBSTREAM=MIXED &
     COMPONENT=C2H4
   DEFINE C2H2 MOLE-FRAC STREAM=GASES SUBSTREAM=MIXED &
     COMPONENT=C2H2
   DEFINE COUT MASS-FLOW STREAM=SOLIDS SUBSTREAM=CIPSD &
     COMPONENT=C
   VECTOR-DEF ULT COMP-ATTR STREAM=RICE-H SUBSTREAM=NCPSD &
```

```
      COMPONENT=RICE-H ATTRIBUTE=ULTANAL
    DEFINE PROX COMP-ATTR-VAR STREAM=RICE-H SUBSTREAM=NCPSD &
      COMPONENT=RICE-H ATTRIBUTE=PROXANAL ELEMENT=1
    DEFINE M STREAM-VAR STREAM=RICE-H SUBSTREAM=NCPSD &
      VARIABLE=MASS-FLOW
    DEFINE MG STREAM-VAR STREAM=GASES SUBSTREAM=MIXED &
      VARIABLE=MASS-FLOW
    DEFINE MA STREAM-VAR STREAM=AIR SUBSTREAM=MIXED &
      VARIABLE=MASS-FLOW
    DEFINE VA STREAM-VAR STREAM=AIR SUBSTREAM=MIXED &
      VARIABLE=STDVOL-FLOW
    DEFINE T STREAM-VAR STREAM=GAS-1 SUBSTREAM=MIXED &
      VARIABLE=TEMP
    DEFINE QNET INFO-VAR INFO=HEAT VARIABLE=DUTY STREAM=QNET
    DEFINE CC2 BLOCK-VAR BLOCK=WALL VARIABLE=FRAC &
      SENTENCE=PROD-FRAC ID1=C
    DEFINE CC1 BLOCK-VAR BLOCK=BURN VARIABLE=FRAC &
      SENTENCE=PROD-FRAC ID1=C
    DEFINE T2 STREAM-VAR STREAM=SGAS SUBSTREAM=MIXED &
      VARIABLE=TEMP
    DEFINE T3 STREAM-VAR STREAM=GASES SUBSTREAM=MIXED &
      VARIABLE=TEMP
F     FAC1=100/(100-H2O)
F     FAC2=(100-PROX)/100
F     CIN=FAC2*M*ULT(2)/100
F     IF (DABS(CIN).LT.1.0D-12) CIN=1.0
F      CC=(CIN-COUT)/CIN
F     N2=N2*FAC1
F     O2=O2*FAC1
F     H2=H2*FAC1
F     CO=CO*FAC1
F     CO2=CO2*FAC1
F     CH4=CH4*FAC1
F     CNHM=(C2H4+C2H2)*FAC1
F     C2H6=C2H6*FAC1
F     OVC=((1-CC1)+(CC1)*(1-CC2))*1.0D2
  TABULATE 1 "(1-CC2)*100" COL-LABEL="CARB CON" "IN REAC2" &
    UNIT-LABEL="PER"
  TABULATE 2 "(1-CC1)*100" COL-LABEL="CARB CON" "IN REAC1" &
    UNIT-LABEL="PER"
  TABULATE 3 "OVC          " COL-LABEL="OVERALL" "CONV" &
    UNIT-LABEL="PER"
  TABULATE 4 "QNET/MG" COL-LABEL="HHV" UNIT-LABEL="MJ/KG"
```

```
   TABULATE 5 "T" COL-LABEL=" CORE" "TEMP" UNIT-LABEL="DEG C"
   TABULATE 6 "T2" COL-LABEL="ANNULUS" "TEMP" UNIT-LABEL="DEG C"
   TABULATE 7 "T3" COL-LABEL="EXIT" "TEMP" UNIT-LABEL="DEG C"
   VARY BLOCK-VAR BLOCK=BURN VARIABLE=FRAC SENTENCE=PROD-FRAC
&
     ID1=C
   RANGE LOWER="0.01" UPPER="0.3" NPOINT="26"

;ER = 0.25, FV = 0.22

SENSITIVITY GAS-TEM1
  DEFINE H2O MOLE-FRAC STREAM=GASES SUBSTREAM=MIXED &
    COMPONENT=H2O
  DEFINE N2 MOLE-FRAC STREAM=GASES SUBSTREAM=MIXED &
    COMPONENT=N2
  DEFINE O2 MOLE-FRAC STREAM=GASES SUBSTREAM=MIXED &
    COMPONENT=O2
  DEFINE H2 MOLE-FRAC STREAM=GASES SUBSTREAM=MIXED &
    COMPONENT=H2
  DEFINE CO MOLE-FRAC STREAM=GASES SUBSTREAM=MIXED &
    COMPONENT=CO
  DEFINE CO2 MOLE-FRAC STREAM=GASES SUBSTREAM=MIXED &
    COMPONENT=CO2
  DEFINE CH4 MOLE-FRAC STREAM=GASES SUBSTREAM=MIXED &
    COMPONENT=CH4
  DEFINE C2H6 MOLE-FRAC STREAM=GASES SUBSTREAM=MIXED &
    COMPONENT=C2H6
  DEFINE C2H4 MOLE-FRAC STREAM=GASES SUBSTREAM=MIXED &
    COMPONENT=C2H4
  DEFINE C2H2 MOLE-FRAC STREAM=GASES SUBSTREAM=MIXED &
    COMPONENT=C2H2
  DEFINE COUT MASS-FLOW STREAM=SOLIDS SUBSTREAM=CIPSD &
    COMPONENT=C
  VECTOR-DEF ULT COMP-ATTR STREAM=RICE-H SUBSTREAM=NCPSD &
    COMPONENT=RICE-H ATTRIBUTE=ULTANAL
  DEFINE PROX COMP-ATTR-VAR STREAM=RICE-H SUBSTREAM=NCPSD &
    COMPONENT=RICE-H ATTRIBUTE=PROXANAL ELEMENT=1
  DEFINE M STREAM-VAR STREAM=RICE-H SUBSTREAM=NCPSD &
    VARIABLE=MASS-FLOW
  DEFINE MG STREAM-VAR STREAM=GASES SUBSTREAM=MIXED &
    VARIABLE=MASS-FLOW
  DEFINE MA STREAM-VAR STREAM=AIR SUBSTREAM=MIXED &
    VARIABLE=MASS-FLOW
```

```
    DEFINE VA STREAM-VAR STREAM=AIR SUBSTREAM=MIXED &
      VARIABLE=STDVOL-FLOW
    DEFINE T STREAM-VAR STREAM=GAS-1 SUBSTREAM=MIXED &
      VARIABLE=TEMP
    DEFINE QNET INFO-VAR INFO=HEAT VARIABLE=DUTY STREAM=QNET
    DEFINE CC2 BLOCK-VAR BLOCK=WALL VARIABLE=FRAC &
      SENTENCE=PROD-FRAC ID1=C
    DEFINE CC1 BLOCK-VAR BLOCK=BURN VARIABLE=FRAC &
      SENTENCE=PROD-FRAC ID1=C
    DEFINE T2 STREAM-VAR STREAM=SGAS SUBSTREAM=MIXED &
      VARIABLE=TEMP
    DEFINE T3 STREAM-VAR STREAM=GASES SUBSTREAM=MIXED &
      VARIABLE=TEMP
F     FAC1=100/(100-H2O)
F     FAC2=(100-PROX)/100
F     CIN=FAC2*M*ULT(2)/100
F     IF (DABS(CIN).LT.1.0D-12) CIN=1.0
F     CC=(CIN-COUT)/CIN
F     N2=N2*FAC1
F     O2=O2*FAC1
F     H2=H2*FAC1
F     CO=CO*FAC1
F     CO2=CO2*FAC1
F     CH4=CH4*FAC1
F     CNHM=(C2H4+C2H2)*FAC1
F     C2H6=C2H6*FAC1
F     OVC=((1-CC1)+(CC1)*(1-CC2))*1.0D2
  TABULATE 1 "(1-CC2)*100" COL-LABEL="CARB CON" "IN REAC2" &
    UNIT-LABEL="PER"
  TABULATE 2 "(1-CC1)*100" COL-LABEL="CARB CON" "IN REAC1" &
    UNIT-LABEL="PER"
  TABULATE 3 "OVC          " COL-LABEL="OVERALL" "CONV" &
    UNIT-LABEL="PER"
  TABULATE 4 "QNET/MG" COL-LABEL="HHV" UNIT-LABEL="MJ/KG"
  TABULATE 5 "T" COL-LABEL=" CORE" "TEMP" UNIT-LABEL="DEG C"
  TABULATE 6 "T2" COL-LABEL="ANNULUS" "TEMP" UNIT-LABEL="DEG C"
  TABULATE 7 "T3" COL-LABEL="EXIT" "TEMP" UNIT-LABEL="DEG C"
  VARY BLOCK-VAR BLOCK=BURN VARIABLE=FRAC SENTENCE=PROD-FRAC
&
    ID1=C
  RANGE LOWER="0.01" UPPER="0.3" NPOINT="26"
```

```
SENSITIVITY GAS3
  DEFINE H2O MOLE-FRAC STREAM=GASES SUBSTREAM=MIXED &
    COMPONENT=H2O
  DEFINE N2 MOLE-FRAC STREAM=GASES SUBSTREAM=MIXED &
    COMPONENT=N2
  DEFINE O2 MOLE-FRAC STREAM=GASES SUBSTREAM=MIXED &
    COMPONENT=O2
  DEFINE H2 MOLE-FRAC STREAM=GASES SUBSTREAM=MIXED &
    COMPONENT=H2
  DEFINE CO MOLE-FRAC STREAM=GASES SUBSTREAM=MIXED &
    COMPONENT=CO
  DEFINE CO2 MOLE-FRAC STREAM=GASES SUBSTREAM=MIXED &
    COMPONENT=CO2
  DEFINE CH4 MOLE-FRAC STREAM=GASES SUBSTREAM=MIXED &
    COMPONENT=CH4
  DEFINE C2H6 MOLE-FRAC STREAM=GASES SUBSTREAM=MIXED &
    COMPONENT=C2H6
  DEFINE C2H4 MOLE-FRAC STREAM=GASES SUBSTREAM=MIXED &
    COMPONENT=C2H4
  DEFINE C2H2 MOLE-FRAC STREAM=GASES SUBSTREAM=MIXED &
    COMPONENT=C2H2
  DEFINE COUT MASS-FLOW STREAM=SOLIDS SUBSTREAM=CIPSD &
    COMPONENT=C
  VECTOR-DEF ULT COMP-ATTR STREAM=RICE-H SUBSTREAM=NCPSD &
    COMPONENT=RICE-H ATTRIBUTE=ULTANAL
  DEFINE PROX COMP-ATTR-VAR STREAM=RICE-H SUBSTREAM=NCPSD &
    COMPONENT=RICE-H ATTRIBUTE=PROXANAL ELEMENT=1
  DEFINE M STREAM-VAR STREAM=RICE-H SUBSTREAM=NCPSD &
    VARIABLE=MASS-FLOW
  DEFINE MG STREAM-VAR STREAM=GASES SUBSTREAM=MIXED &
    VARIABLE=MASS-FLOW
  DEFINE MA STREAM-VAR STREAM=AIR SUBSTREAM=MIXED &
    VARIABLE=MASS-FLOW
  DEFINE VA STREAM-VAR STREAM=AIR SUBSTREAM=MIXED &
    VARIABLE=STDVOL-FLOW
  DEFINE T BLOCK-VAR BLOCK=BURN VARIABLE=TEMP SENTENCE=PARAM
  DEFINE QNET INFO-VAR INFO=HEAT VARIABLE=DUTY STREAM=QNET
  DEFINE CC2 BLOCK-VAR BLOCK=WALL VARIABLE=FRAC &
    SENTENCE=PROD-FRAC ID1=C
F   FAC1=100/(100-H2O)
F   FAC2=(100-PROX)/100
F   CIN=FAC2*M*ULT(2)/100
F   IF (DABS(CIN).LT.1.0D-12) CIN=1.0
```

```
 F       CC=(CIN-COUT)/CIN
 F       N2=N2*FAC1
 F       O2=O2*FAC1
 F       H2=H2*FAC1
 F       CO=CO*FAC1
 F       CO2=CO2*FAC1
 F       CH4=CH4*FAC1
 F       CNHM=(C2H4+C2H2)*FAC1
 F       C2H6=C2H6*FAC1
    TABULATE 1 "CO2*100" COL-LABEL="CO2"
    TABULATE 2 "CNHM*100" COL-LABEL="C2HM"
    TABULATE 3 "C2H6*100" COL-LABEL="C2H6"
    TABULATE 4 "H2*100" COL-LABEL="H2"
    TABULATE 5 "O2*100" COL-LABEL="O2"
    TABULATE 6 "N2*100" COL-LABEL="N2"
    TABULATE 7 "CH4*100" COL-LABEL="CH4"
    TABULATE 8 "CO*100" COL-LABEL="CO"
    TABULATE 9 "MG    " COL-LABEL="GAS " "FLOW" UNIT-LABEL="KG/S"
    TABULATE 10 "CC*100" COL-LABEL="CARBON" "CONVERS"
    TABULATE 11 "M*60" COL-LABEL="RICE-H" "FLOW" UNIT-LABEL= &
      "KG/MIN"
    TABULATE 12 "MA*60" COL-LABEL="AIR" "MASS" "FL" UNIT-LABEL= &
      "KG/MIN"
    TABULATE 13 "VA*60" COL-LABEL="AIR" "VOL" "FL" UNIT-LABEL= &
      "CUM/MIN"
    TABULATE 14 "T" COL-LABEL="GASF" "TEMP" UNIT-LABEL="DEG C"
    TABULATE 15 "QNET/MG" COL-LABEL="LHV" UNIT-LABEL="KJ/KG"
    TABULATE 16 "(1-CC2)*100" COL-LABEL="CARB CON" "IN REAC2"
    VARY BLOCK-VAR BLOCK=BURN VARIABLE=FRAC SENTENCE=PROD-FRAC
&
      ID1=C
    RANGE LOWER="0.01" UPPER="0.4" NPOINT="20"

STREAM-REPOR MOLEFLOW MASSFLOW MOLEFRAC MASSFRAC  &
      PROPERTIES=ALL-SUBS
```

APPENDIX D

"Mean Error in Product Gas Composition"

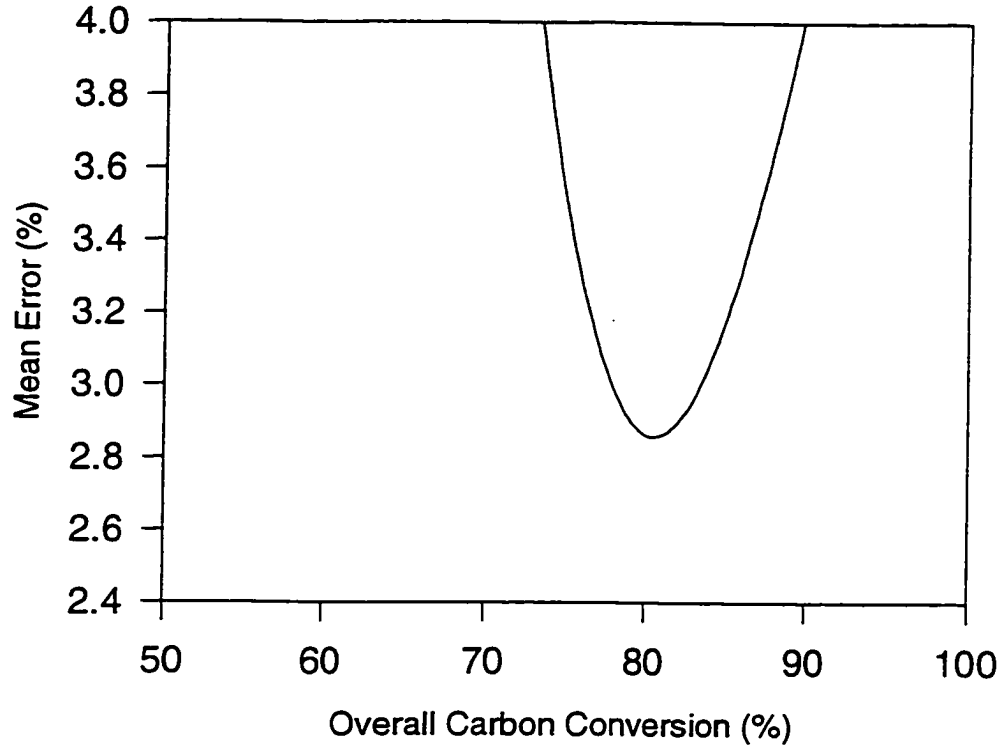

(a) One-Compartment Model

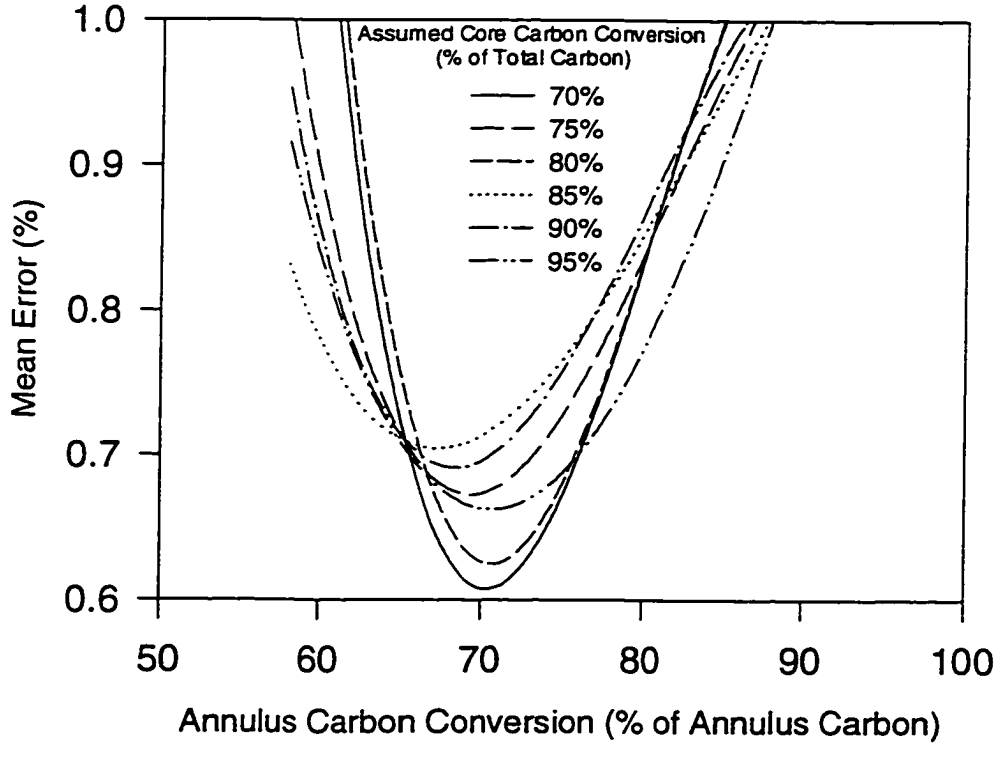

(b) Two-Compartment Model

Figure D-1 Mean error in product gas composition at various carbon conversion ratios and the bed height of 19.5 cm, fluidization velocity of 0.22 m/s and equivalence ratio of 0.25.

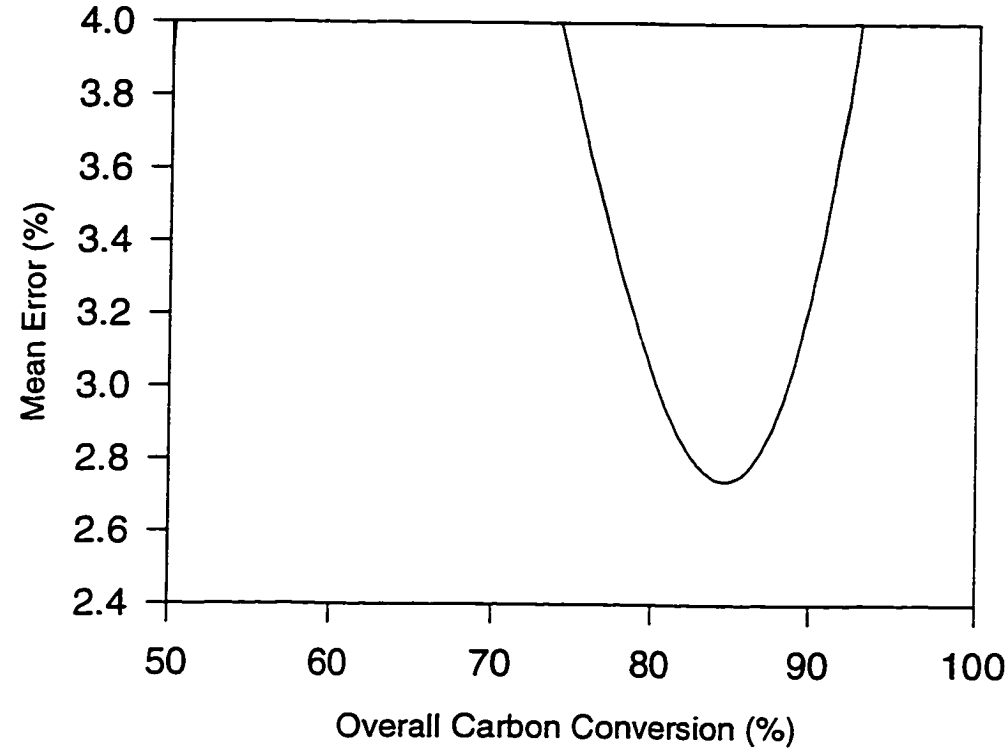

(a) One-Compartment Model

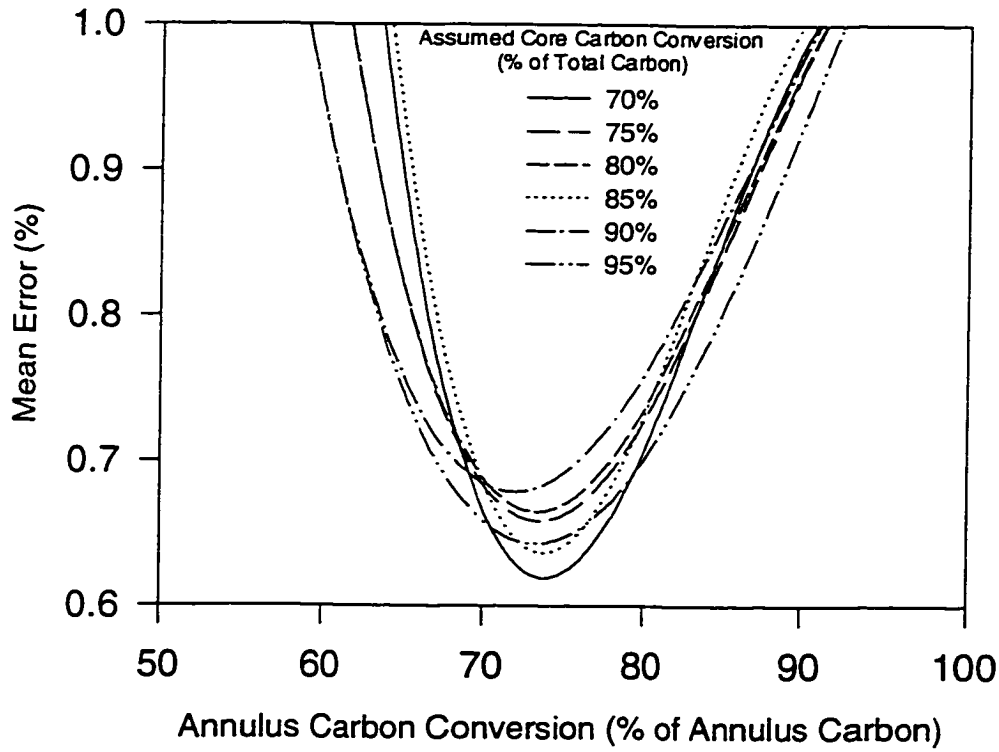

(b) Two-Compartment Model

Figure D-2 Mean error in product gas composition at various carbon conversion ratios and the bed height of 19.5 cm, fluidization velocity of 0.22 m/s and equivalence ratio of 0.30.

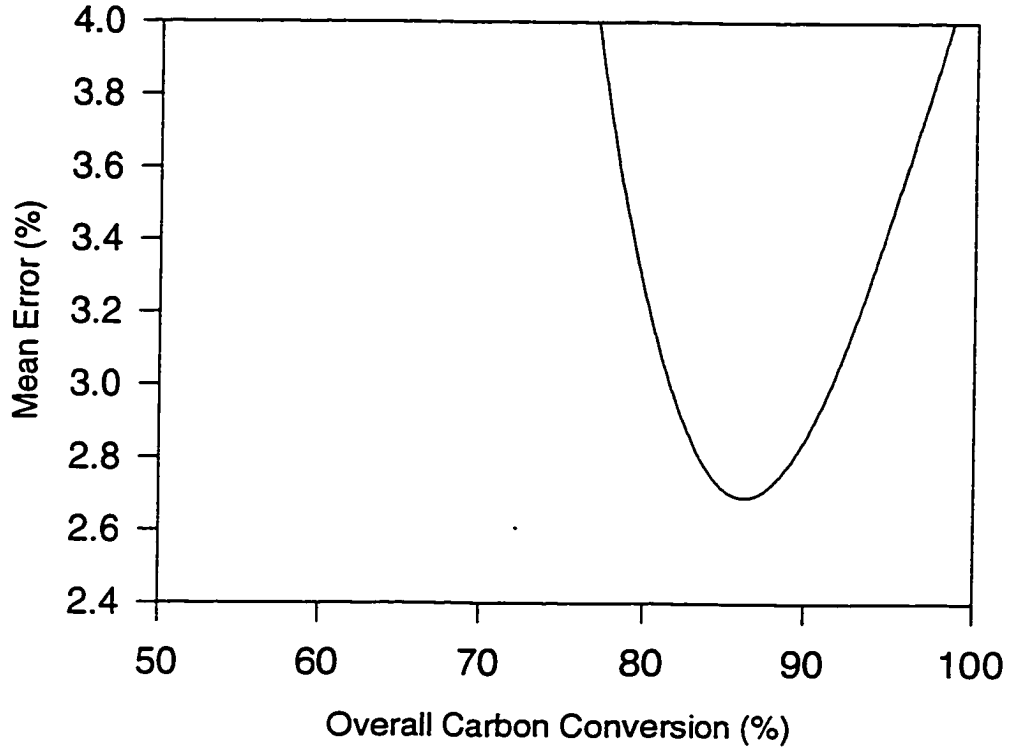

(a) One-Compartment Model

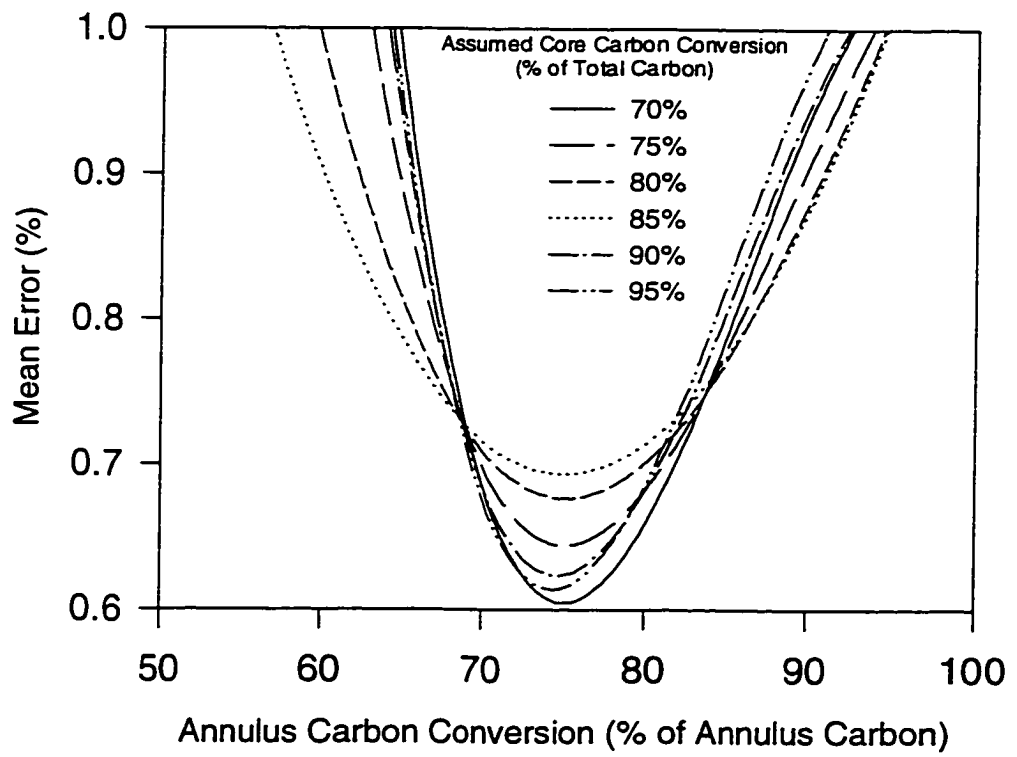

(b) Two-Compartment Model

Figure D-3 Mean error in product gas composition at various carbon conversion ratios and the bed height of 19.5 cm, fluidization velocity of 0.22 m/s and equivalence ratio of 0.35.

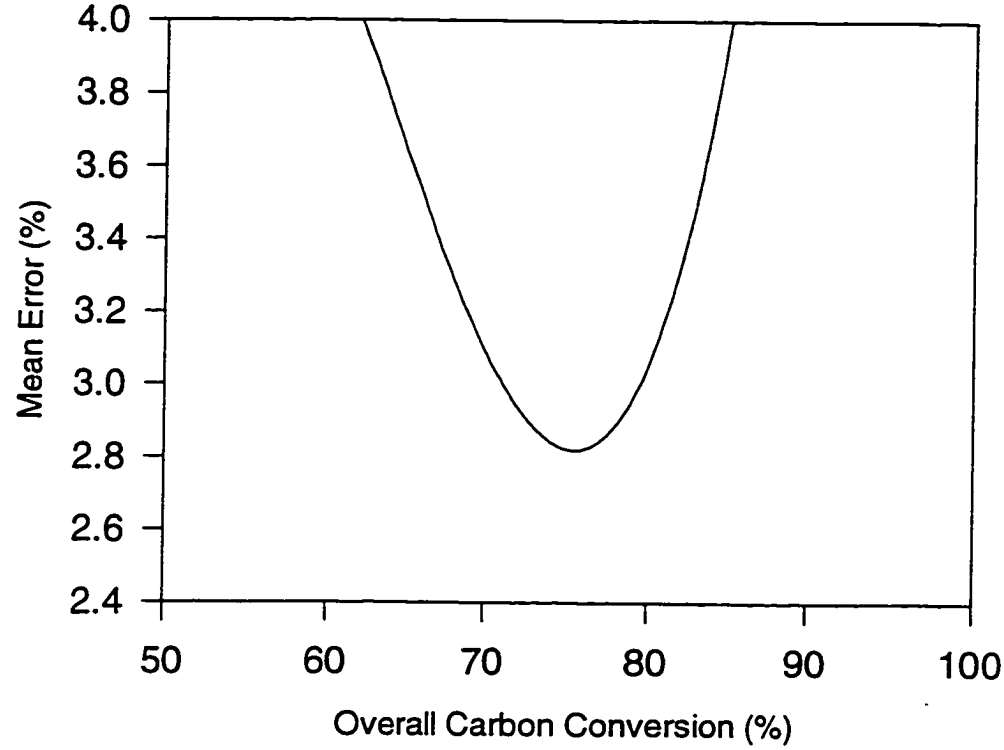

(a) One-Compartment Model

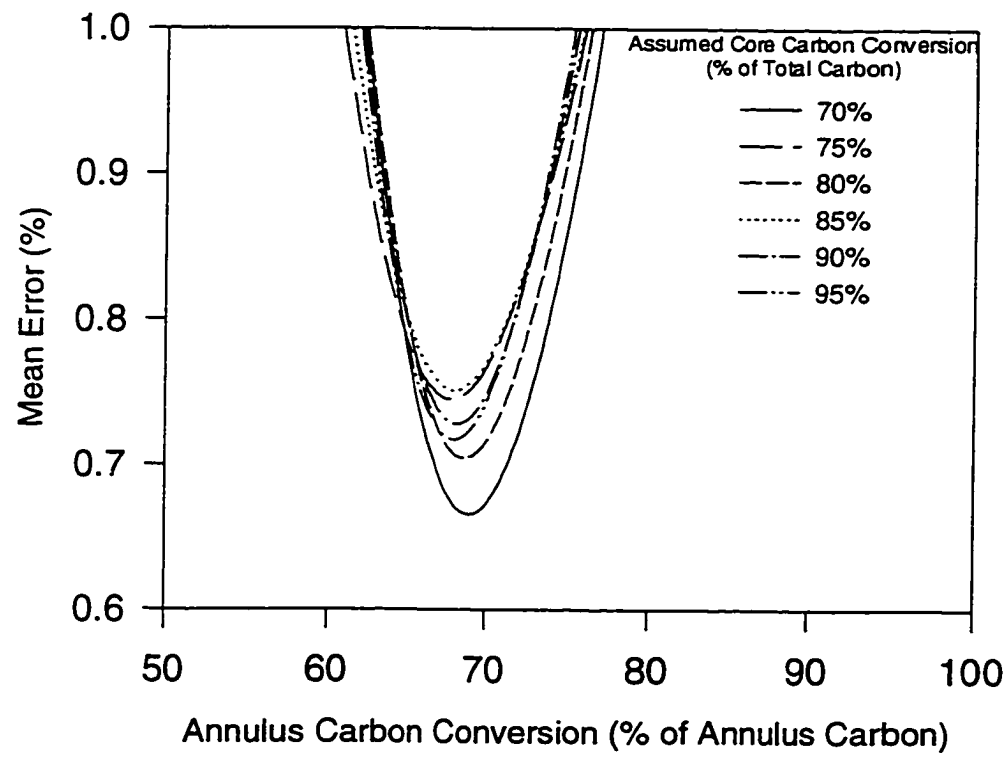

(b) Two-Compartment Model

Figure D-4 Mean error in product gas composition at various carbon conversion ratios and the bed height of 19.5 cm, fluidization velocity of 0.28 m/s and equivalence ratio of 0.25.

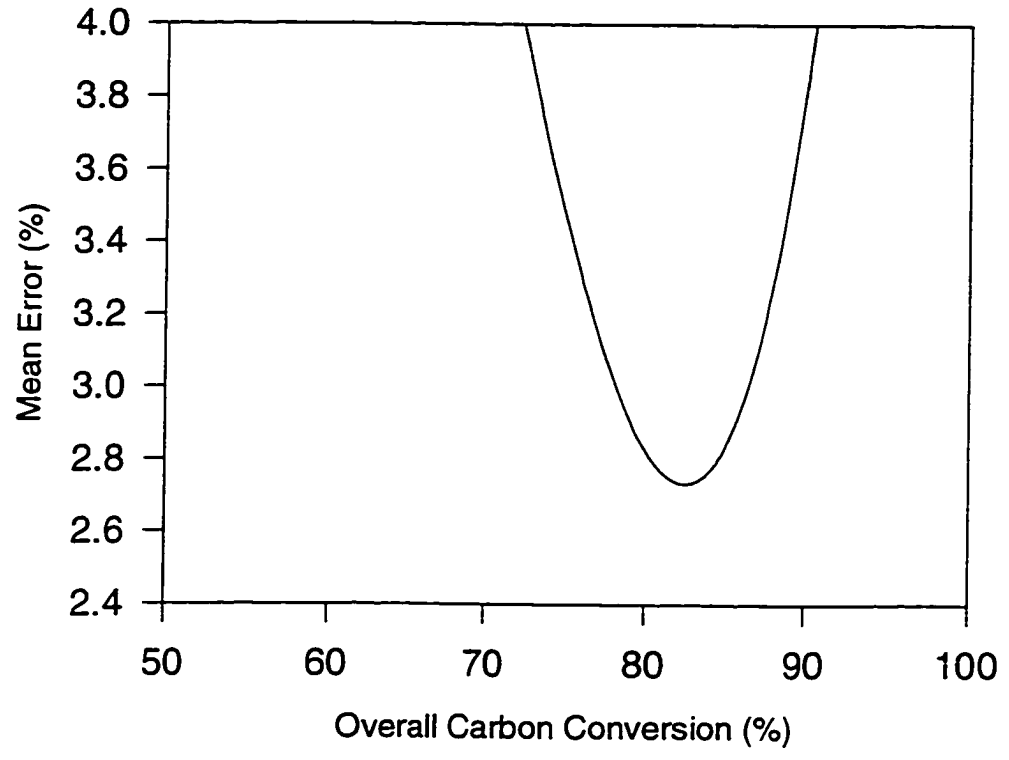

(a) One-Compartment Model

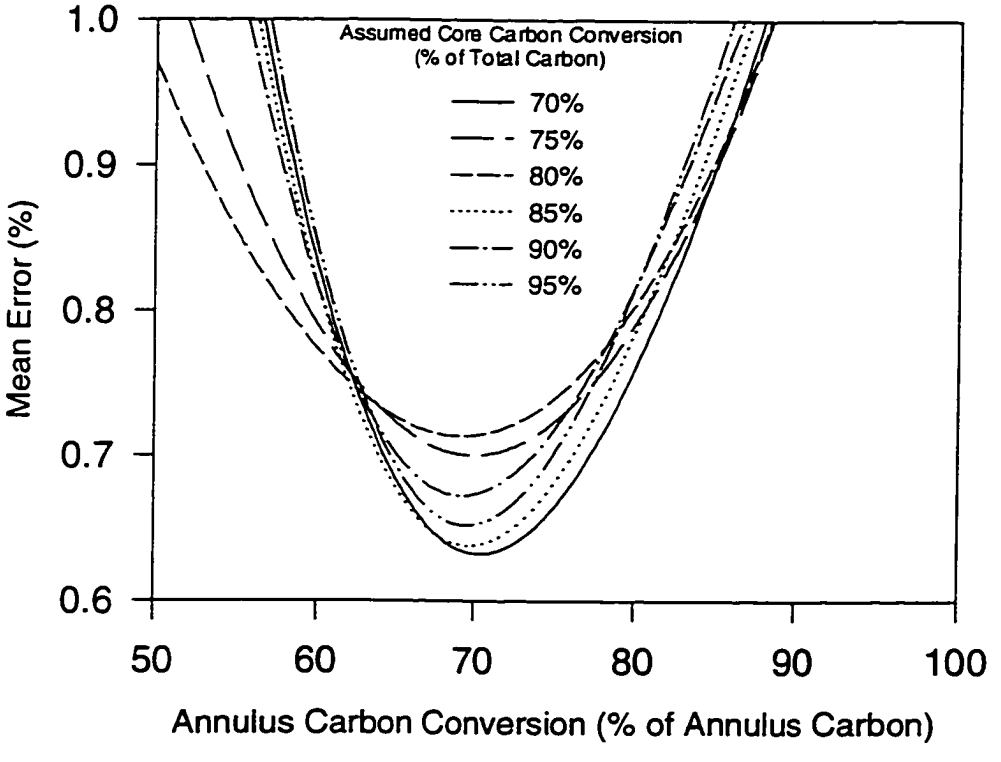

(b) Two-Compartment Model

Figure D-5 Mean error in product gas composition at various carbon conversion ratios and the bed height of 19.5 cm, fluidization velocity of 0.28 m/s and equivalence ratio of 0.30.

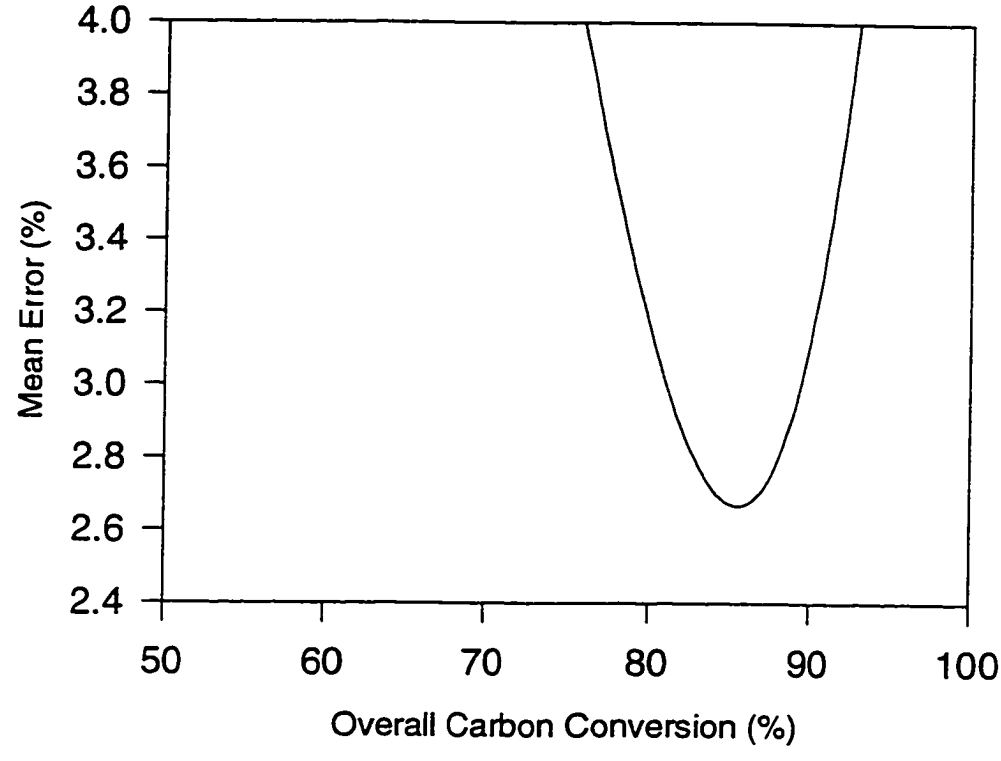

(a) One-Compartment Model

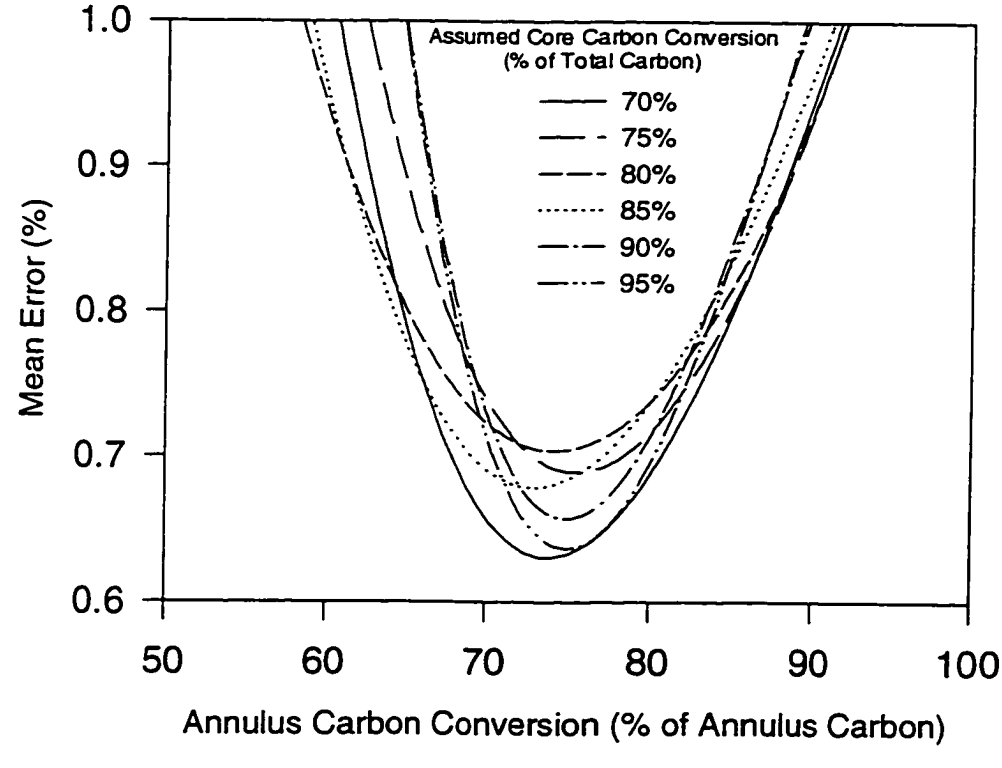

(b) Two-Compartment Model

Figure D-6 Mean error in product gas composition at various carbon conversion ratios and the bed height of 19.5 cm, fluidization velocity of 0.28 m/s and equivalence ratio of 0.35.

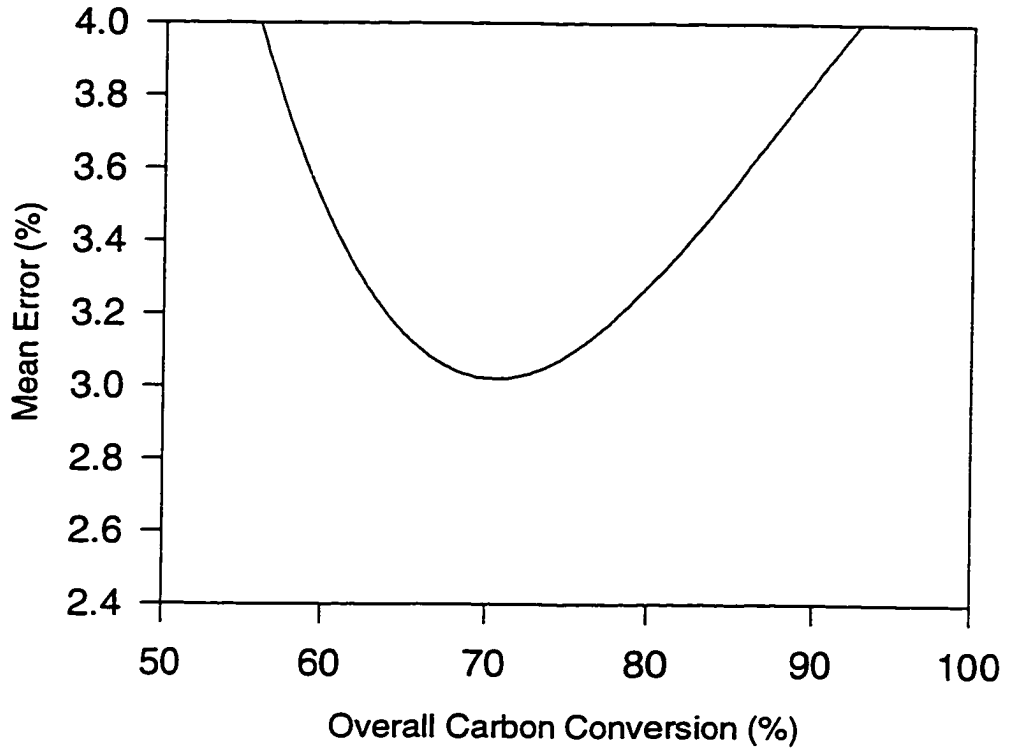

(a) One-Compartment Model

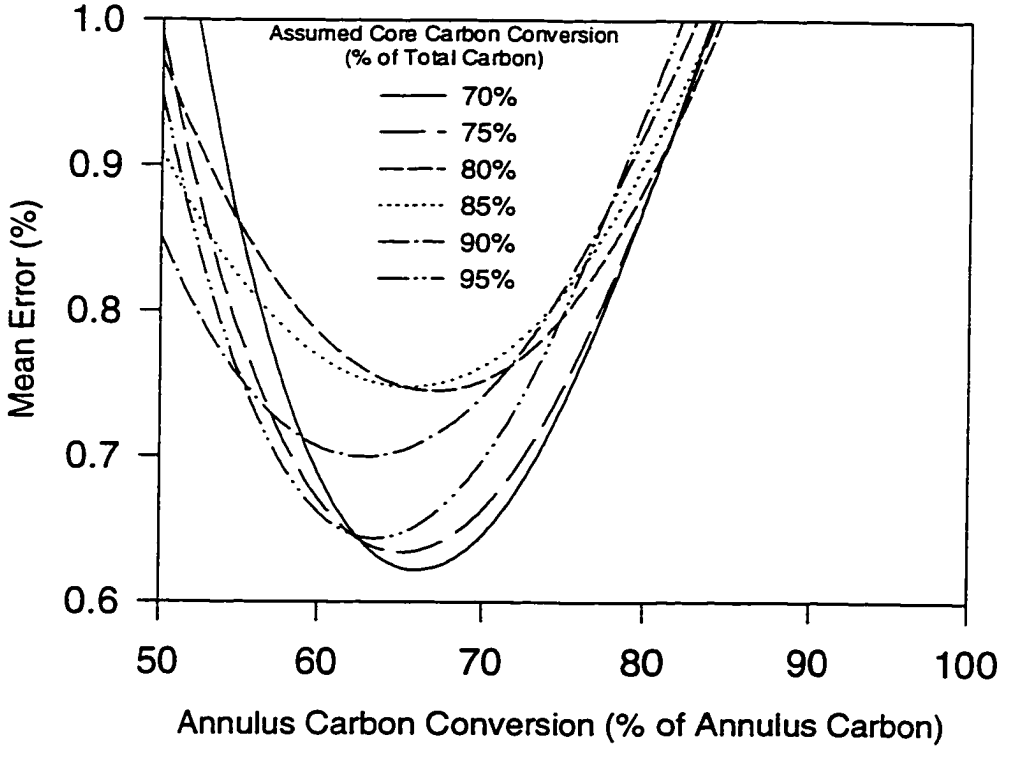

(b) Two-Compartment Model

Figure D-7 Mean error in product gas composition at various carbon conversion ratios and the bed height of 19.5 cm, fluidization velocity of 0.33 m/s and equivalence ratio of 0.25.

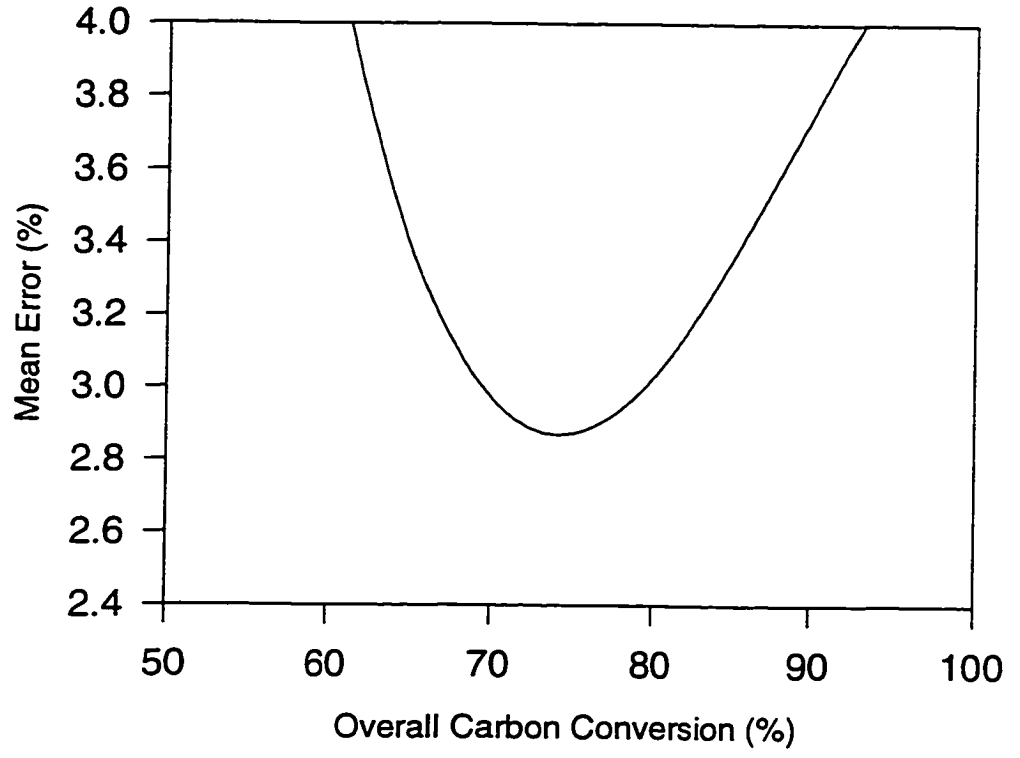

(a) One-Compartment Model

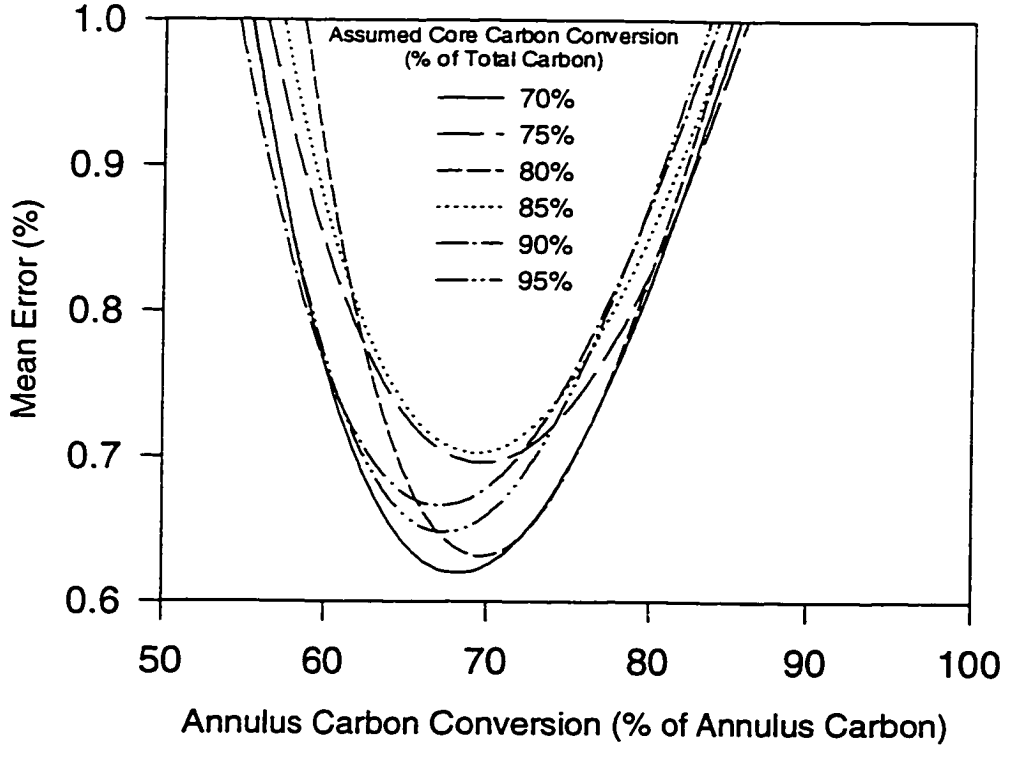

(b) Two-Compartment Model

Figure D-8 Mean error in product gas composition at various carbon conversion ratios and the bed height of 19.5 cm, fluidization velocity of 0.33 m/s and equivalence ratio of 0.30.

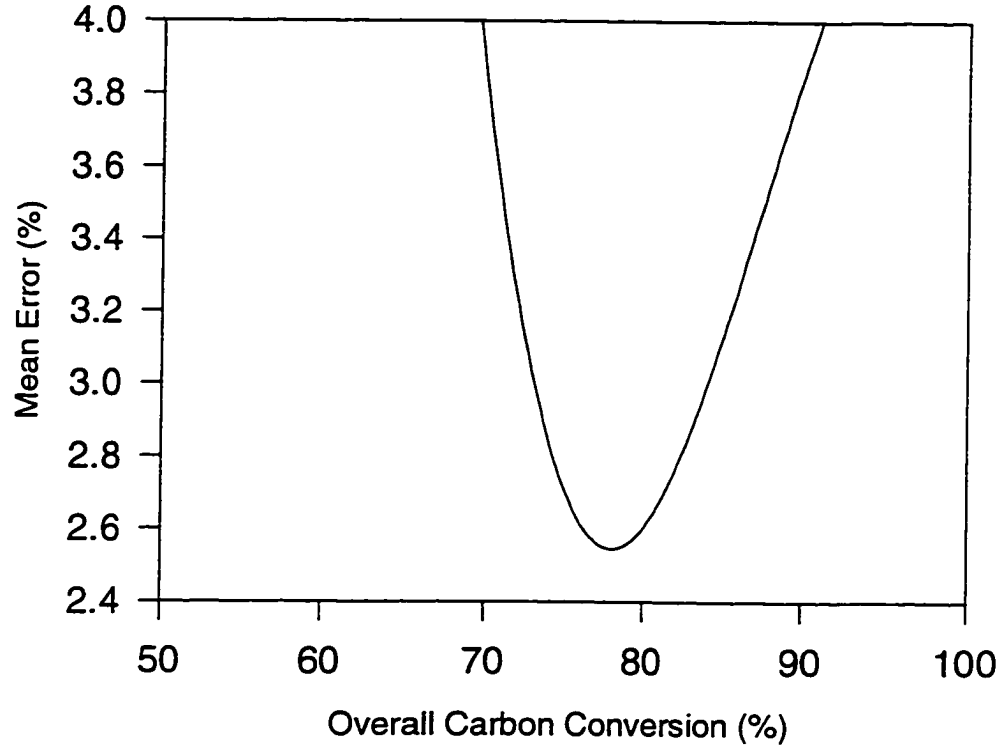

(a) One-Compartment Model

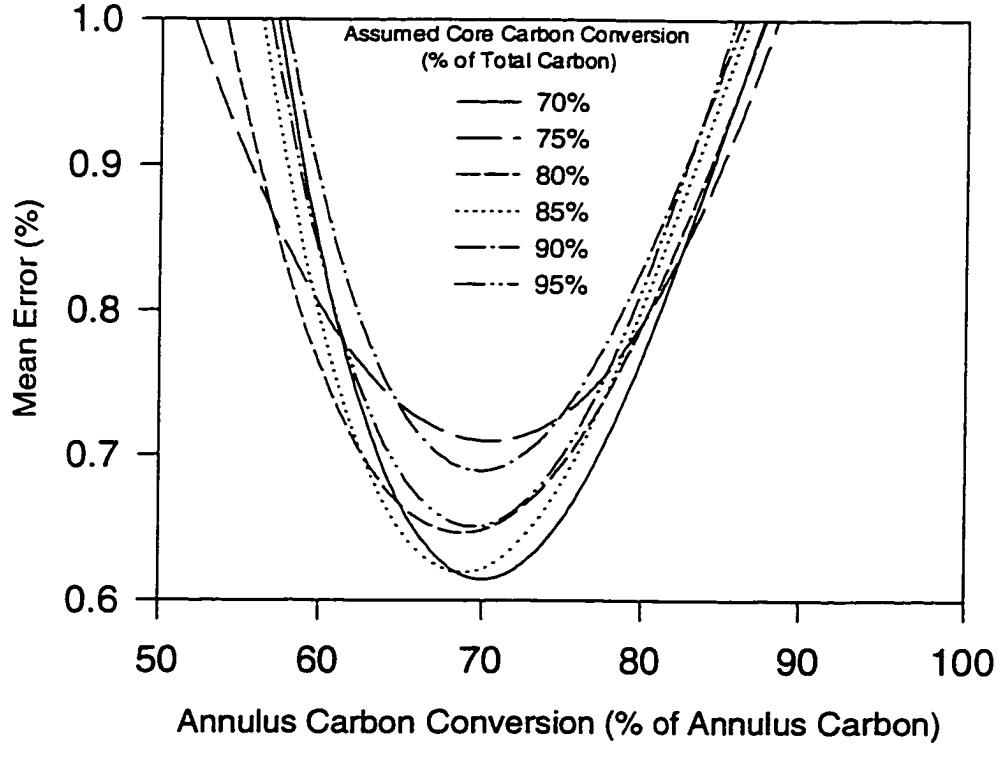

(b) Two-Compartment Model

Figure D-9 Mean error in product gas composition at various carbon conversion ratios and the bed height of 19.5 cm, fluidization velocity of 0.33 m/s and equivalence ratio of 0.35.

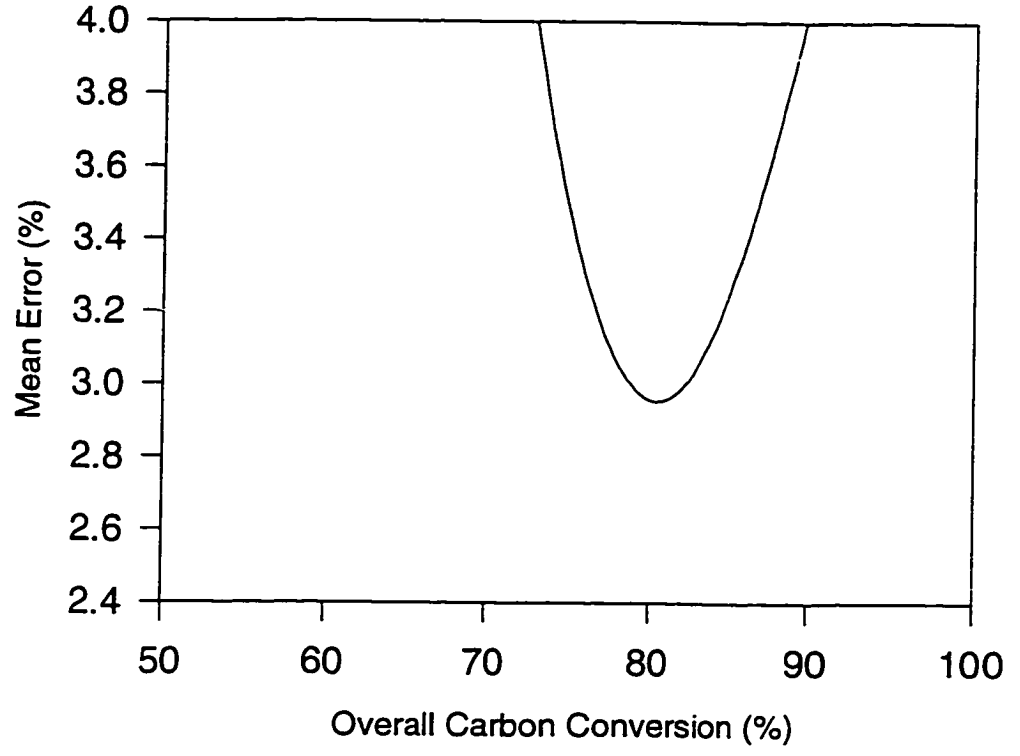

(a) One-Compartment Model

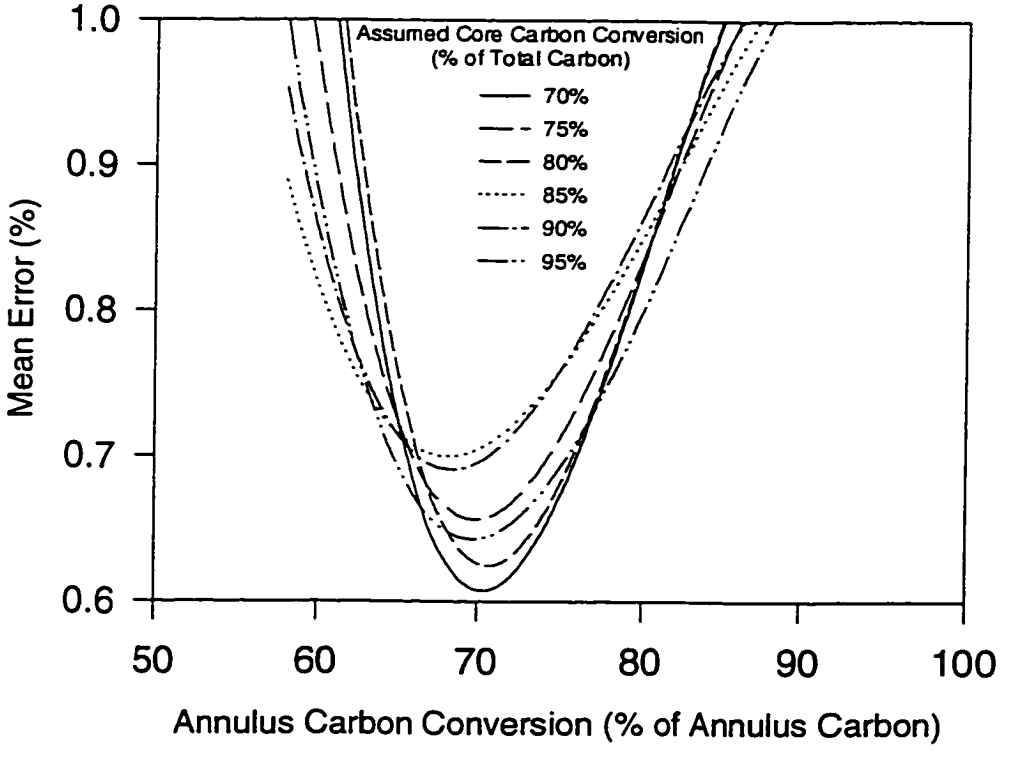

(b) Two-Compartment Model

Figure D-10 Mean error in product gas composition at various carbon conversion ratios and the bed height of 25.5 cm, fluidization velocity of 0.22 m/s and equivalence ratio of 0.25.

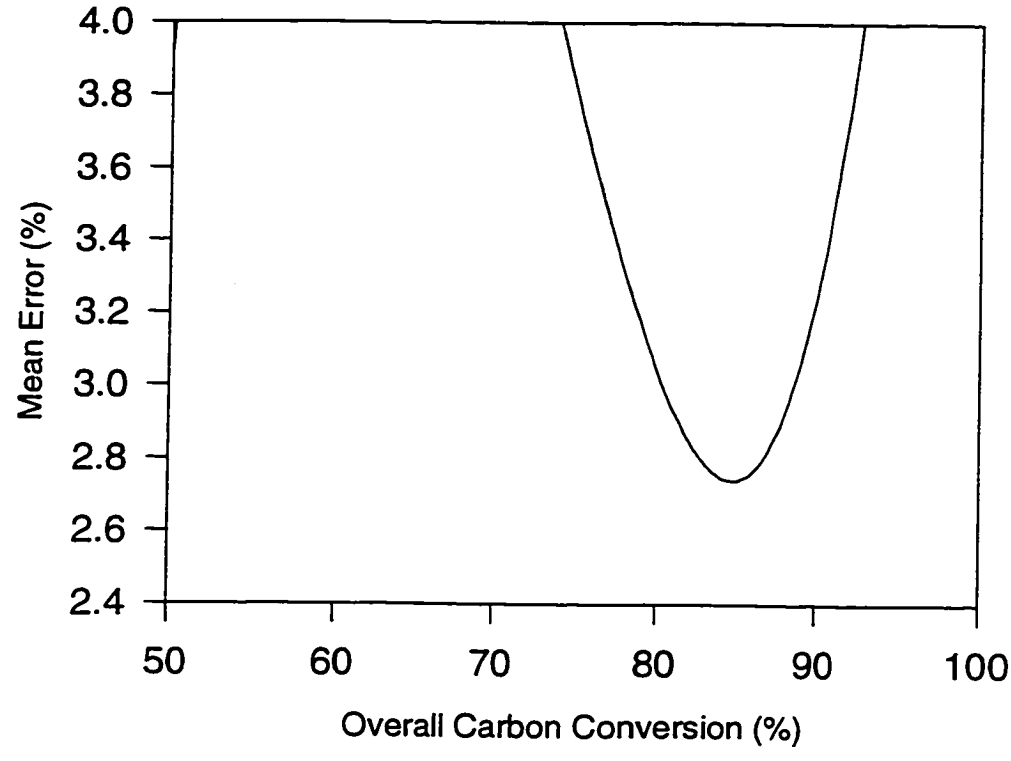

(a) One-Compartment Model

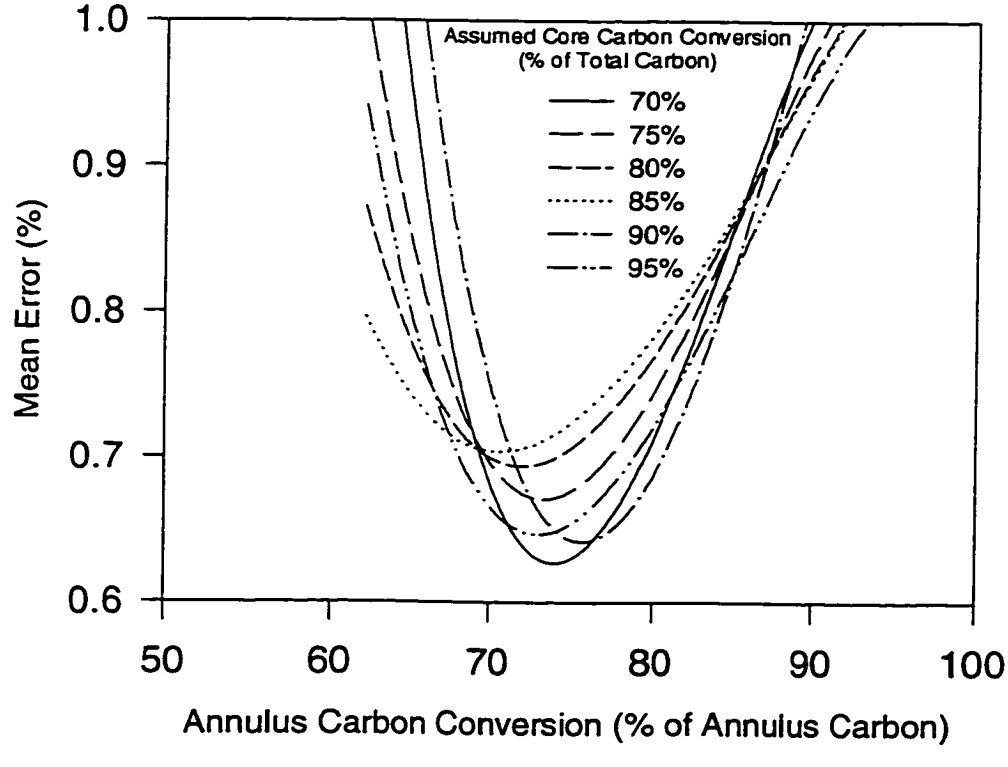

(b) Two-Compartment Model

Figure D-11 Mean error in product gas composition at various carbon conversion ratios and the bed height of 25.5 cm, fluidization velocity of 0.22 m/s and equivalence ratio of 0.30.

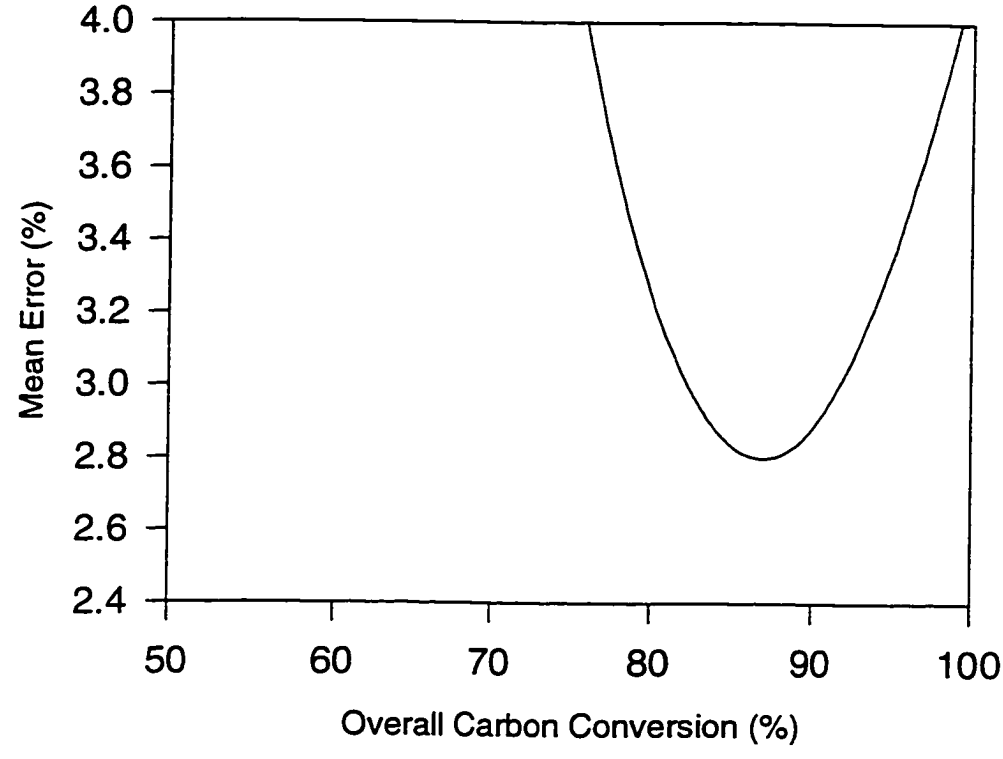

(a) One-Compartment Model

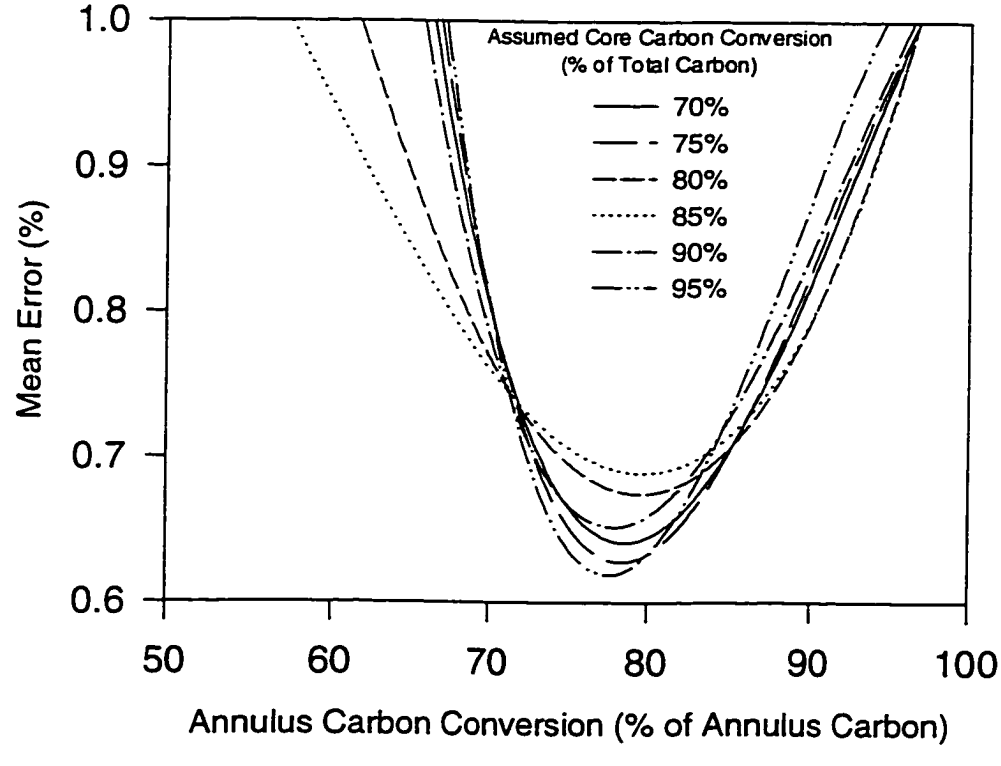

(b) Two-Compartment Model

Figure D-12 Mean error in product gas composition at various carbon conversion ratios and the bed height of 25.5 cm, fluidization velocity of 0.22 m/s and equivalence ratio of 0.35.

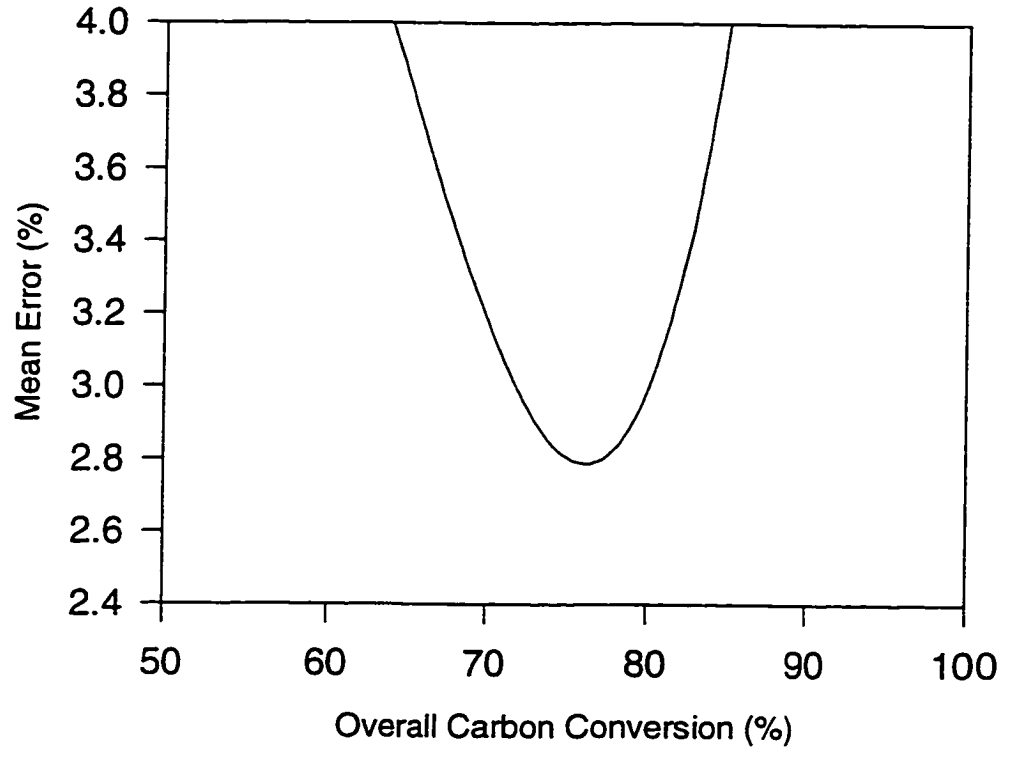

(a) One-Compartment Model

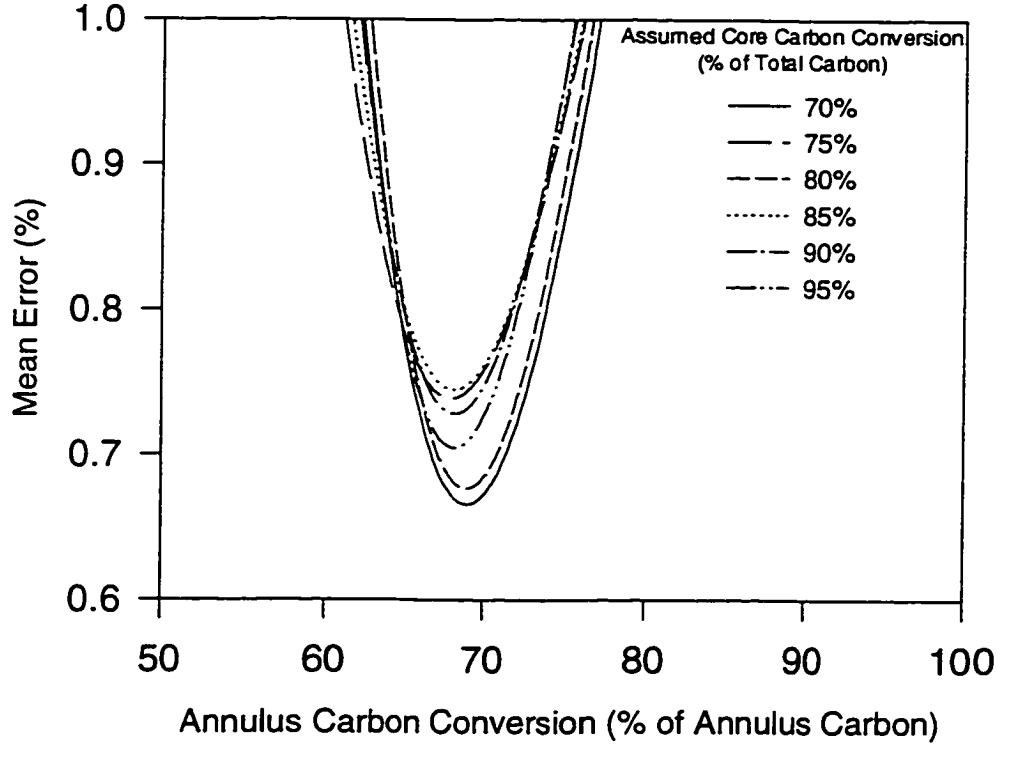

(b) Two-Compartment Model

Figure D-13 Mean error in product gas composition at various carbon conversion ratios and the bed height of 25.5 cm, fluidization velocity of 0.28 m/s and equivalence ratio of 0.25.

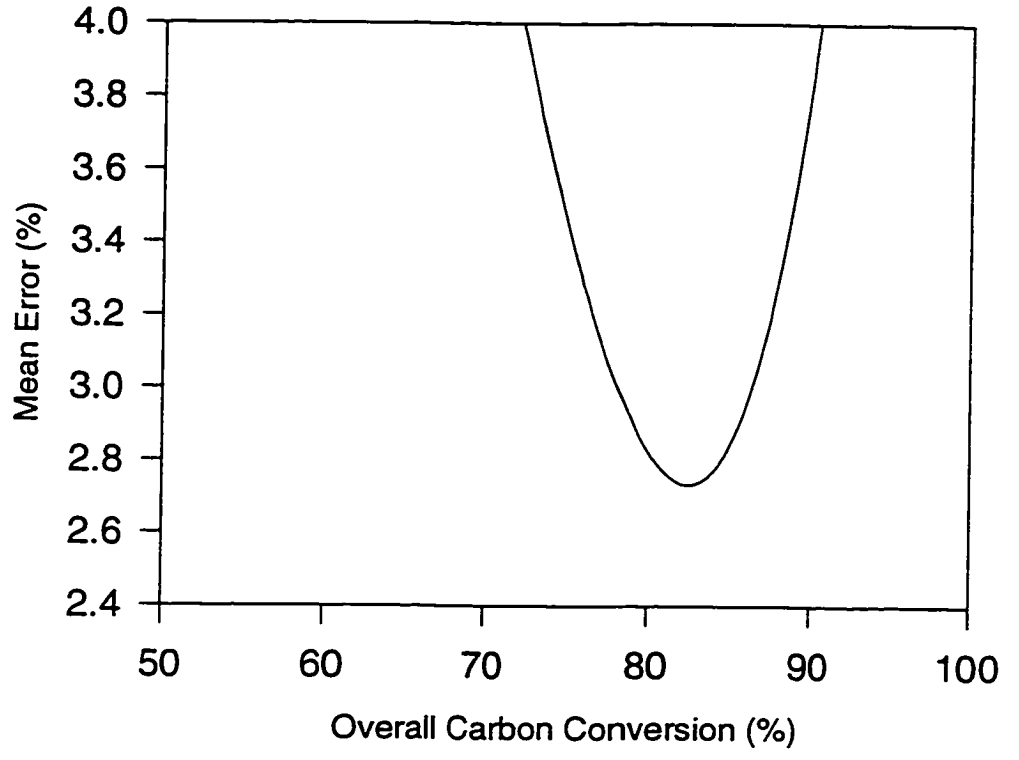

(a) One-Compartment Model

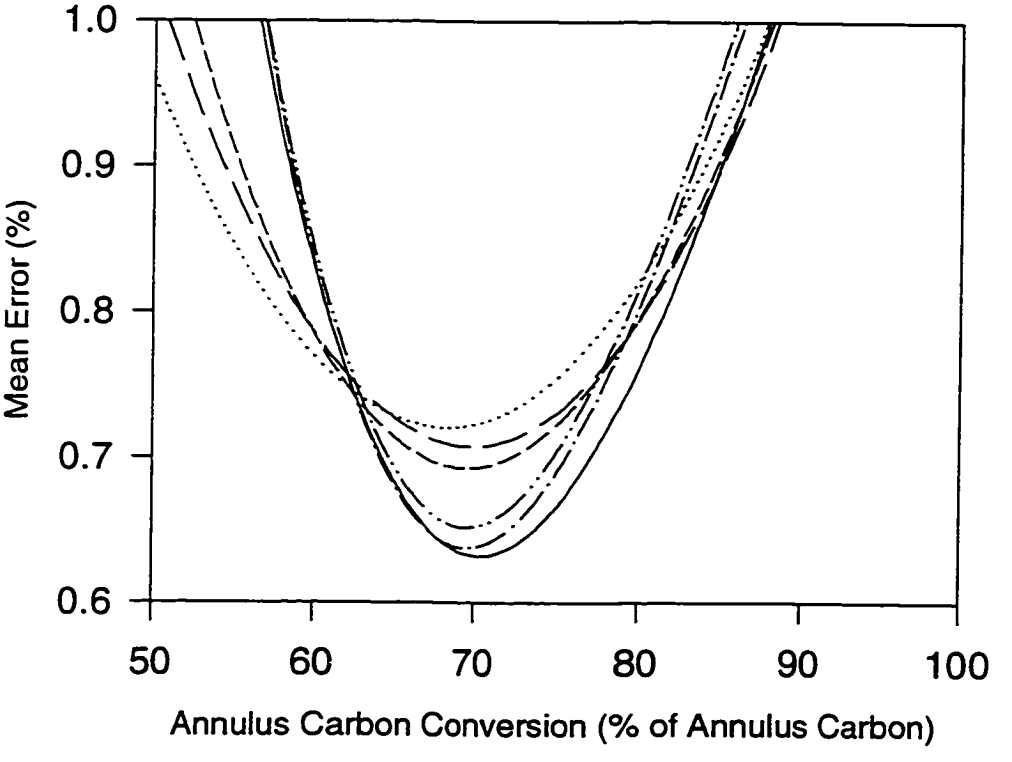

(b) Two-Compartment Model

Figure D-14 Mean error in product gas composition at various carbon conversion ratios and the bed height of 25.5 cm, fluidization velocity of 0.28 m/s and equivalence ratio of 0.30.

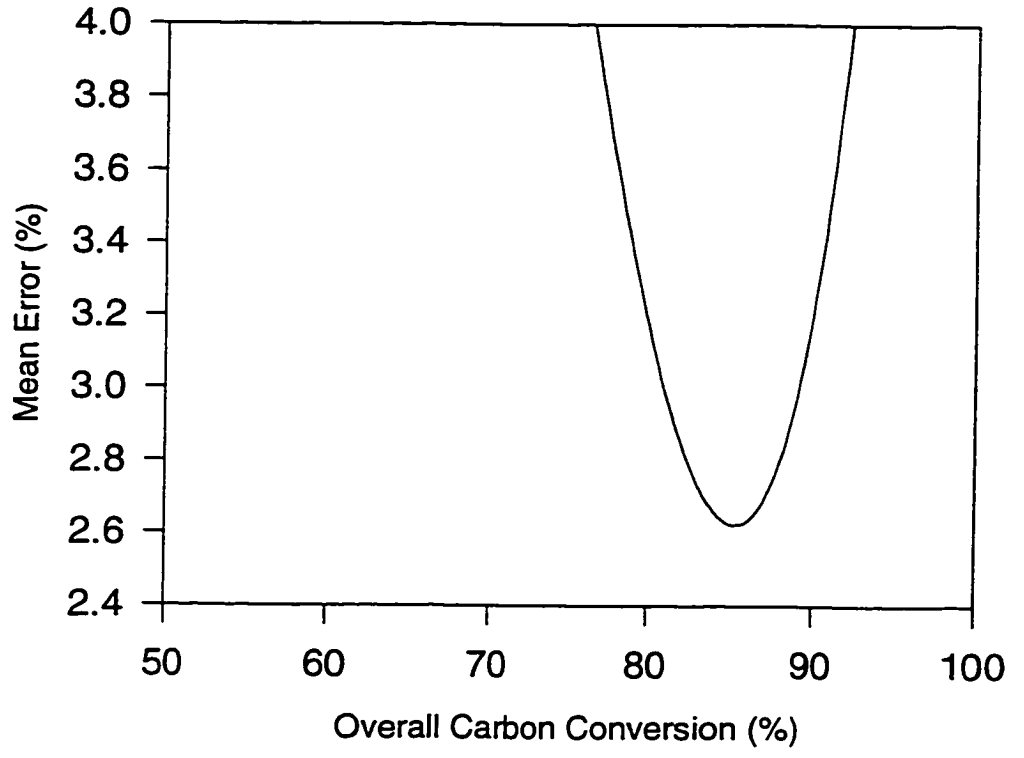

(a) One-Compartment Model

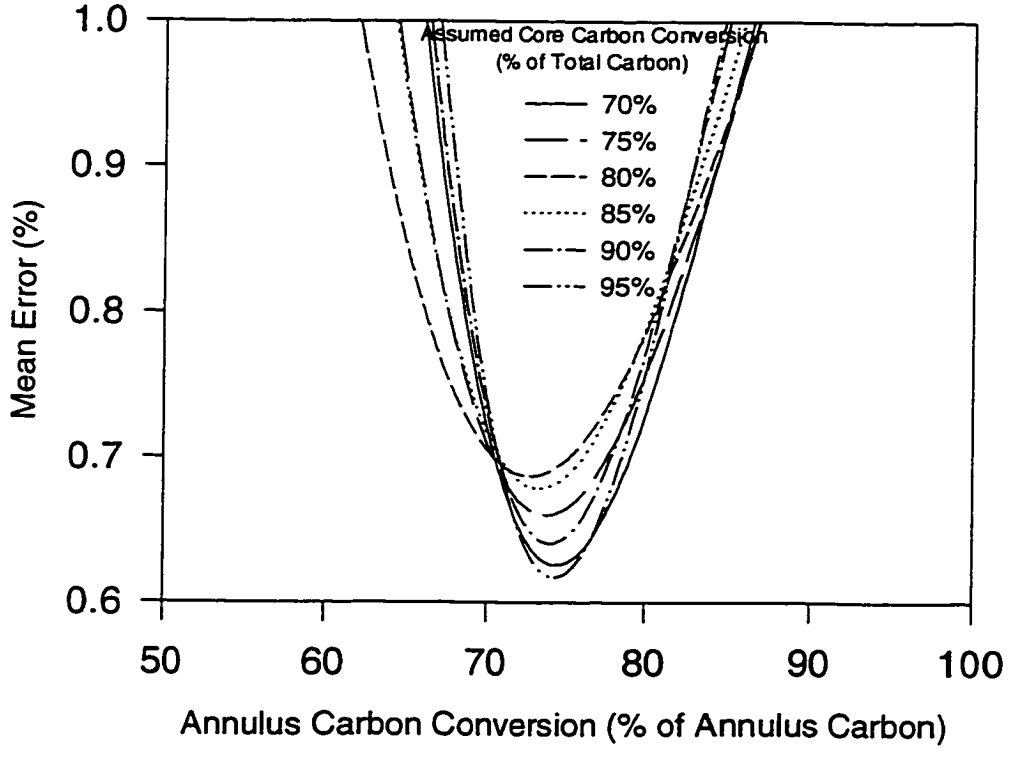

(b) Two-Compartment Model

Figure D-15 Mean error in product gas composition at various carbon conversion ratios and the bed height of 25.5 cm, fluidization velocity of 0.28 m/s and equivalence ratio of 0.35.

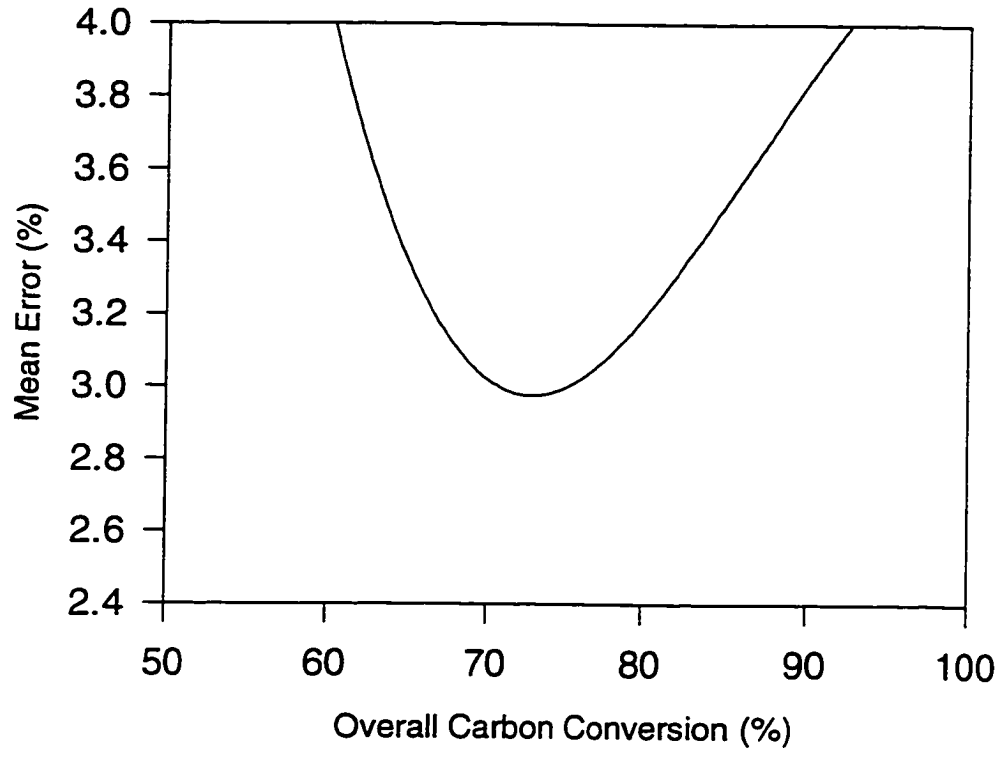

(a) One-Compartment Model

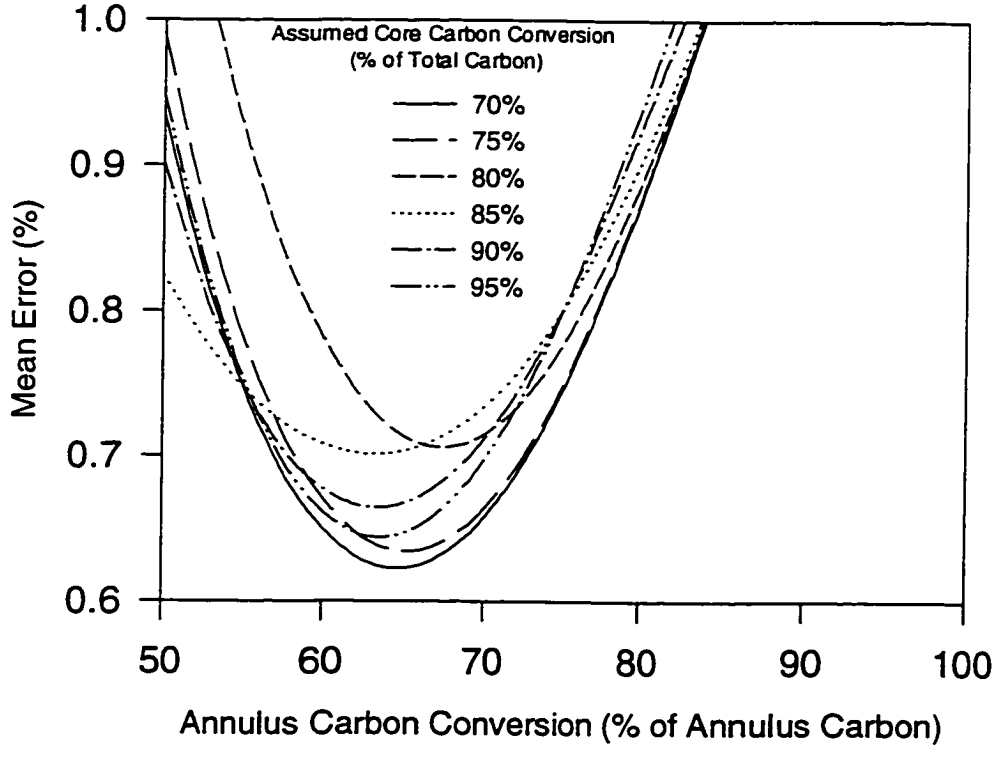

(b) Two-Compartment Model

Figure D-16 Mean error in product gas composition at various carbon conversion ratios and the bed height of 25.5 cm, fluidization velocity of 0.33 m/s and equivalence ratio of 0.25.

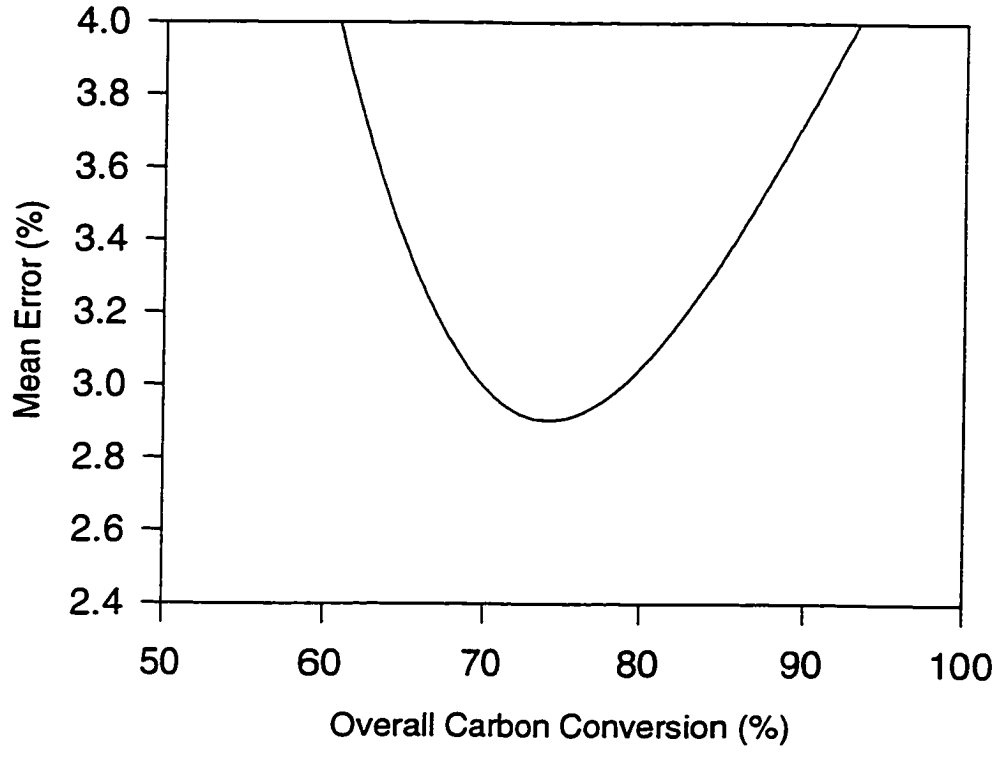

(a) One-Compartment Model

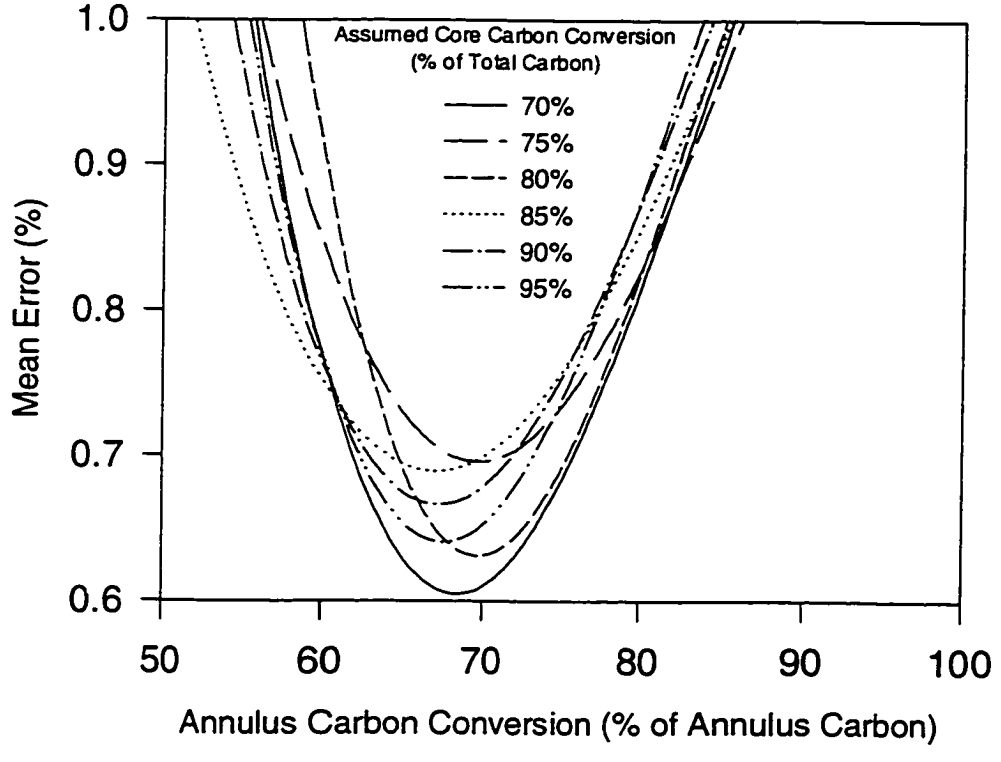

(b) Two-Compartment Model

Figure D-17 Mean error in product gas composition at various carbon conversion ratios and the bed height of 25.5 cm, fluidization velocity of 0.33 m/s and equivalence ratio of 0.30.

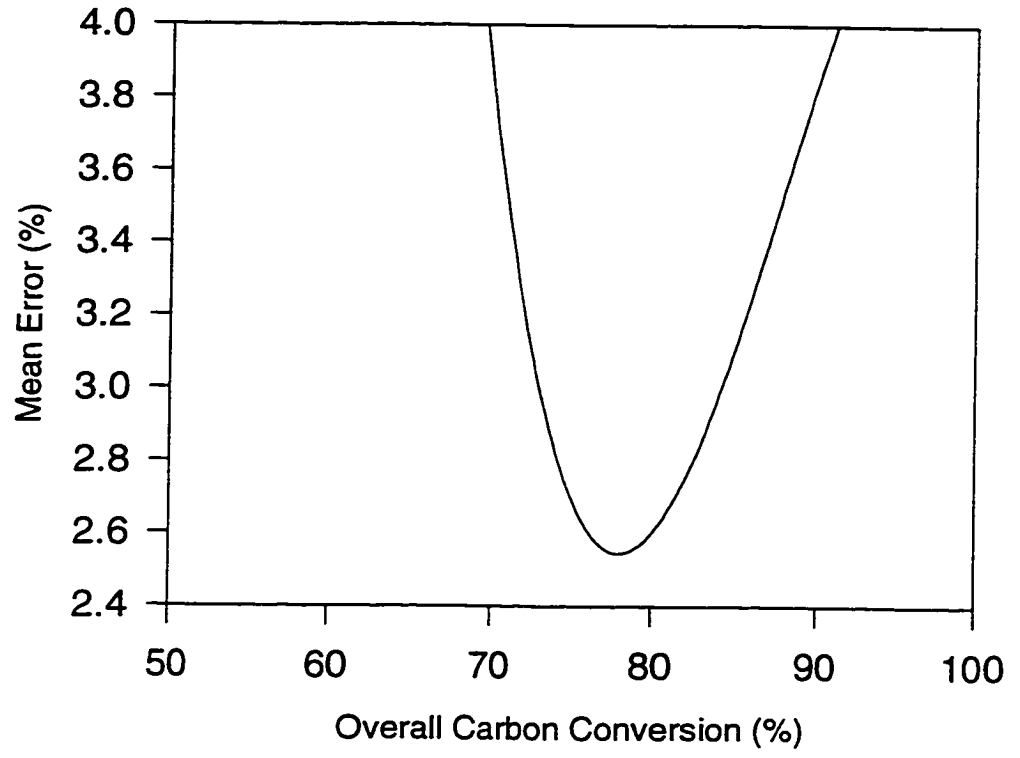

(a) One-Compartment Model

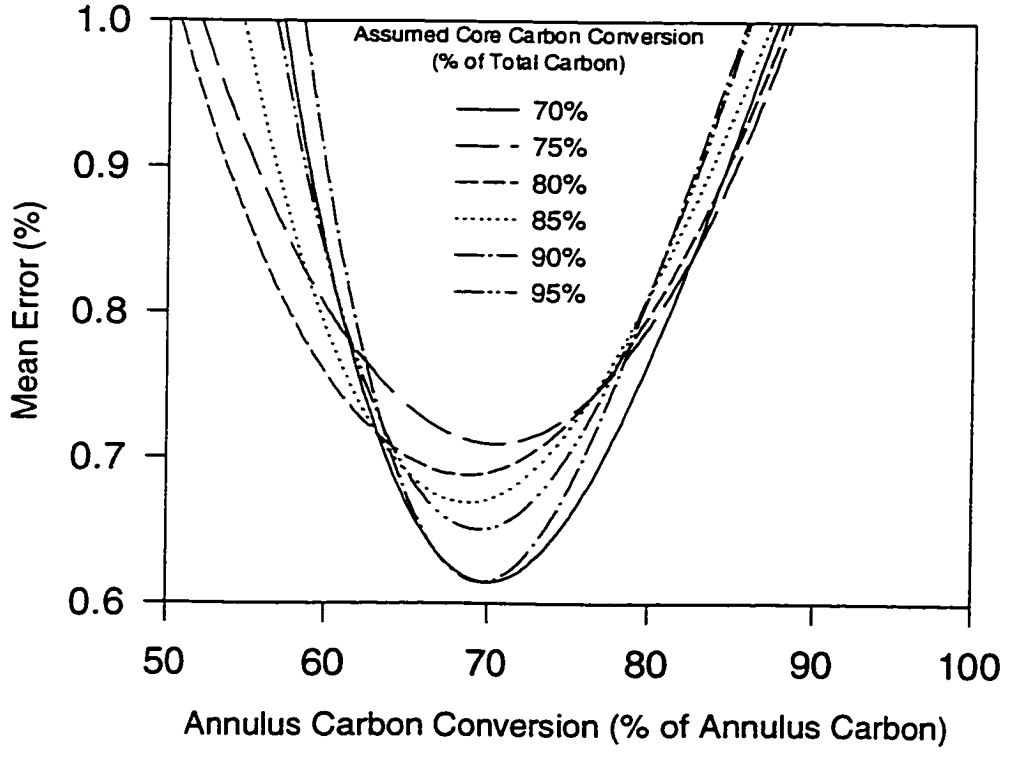

(b) Two-Compartment Model

Figure D-18 Mean error in product gas composition at various carbon conversion ratios and the bed height of 25.5 cm, fluidization velocity of 0.33 m/s and equivalence ratio of 0.35.

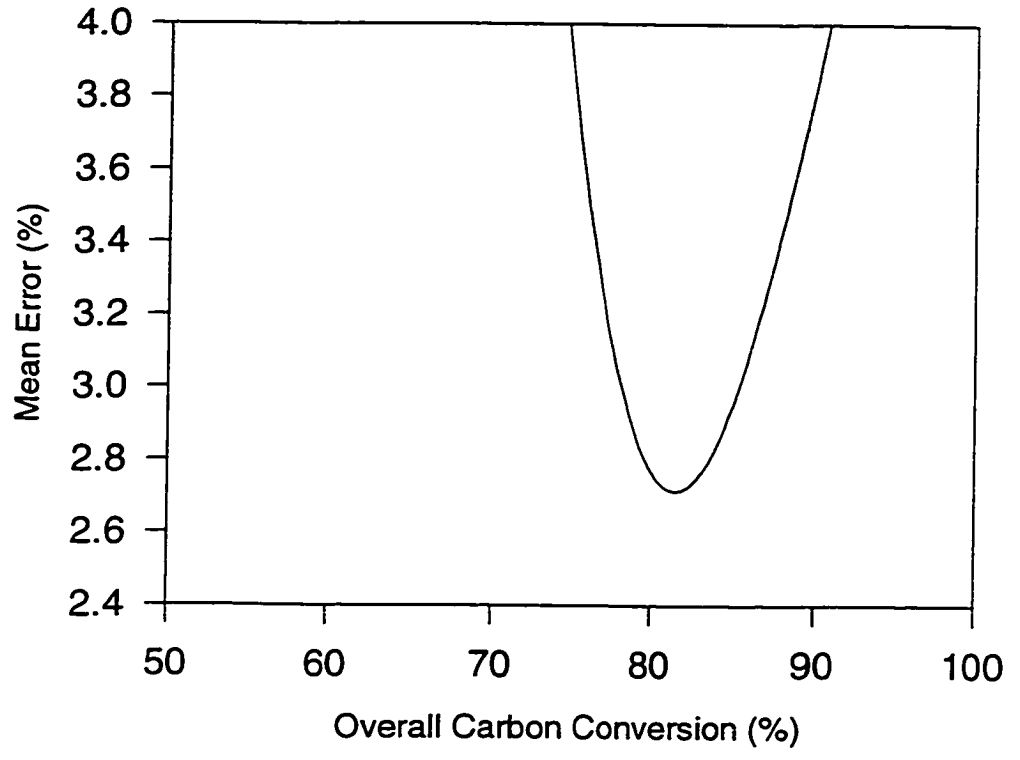

(a) One-Compartment Model

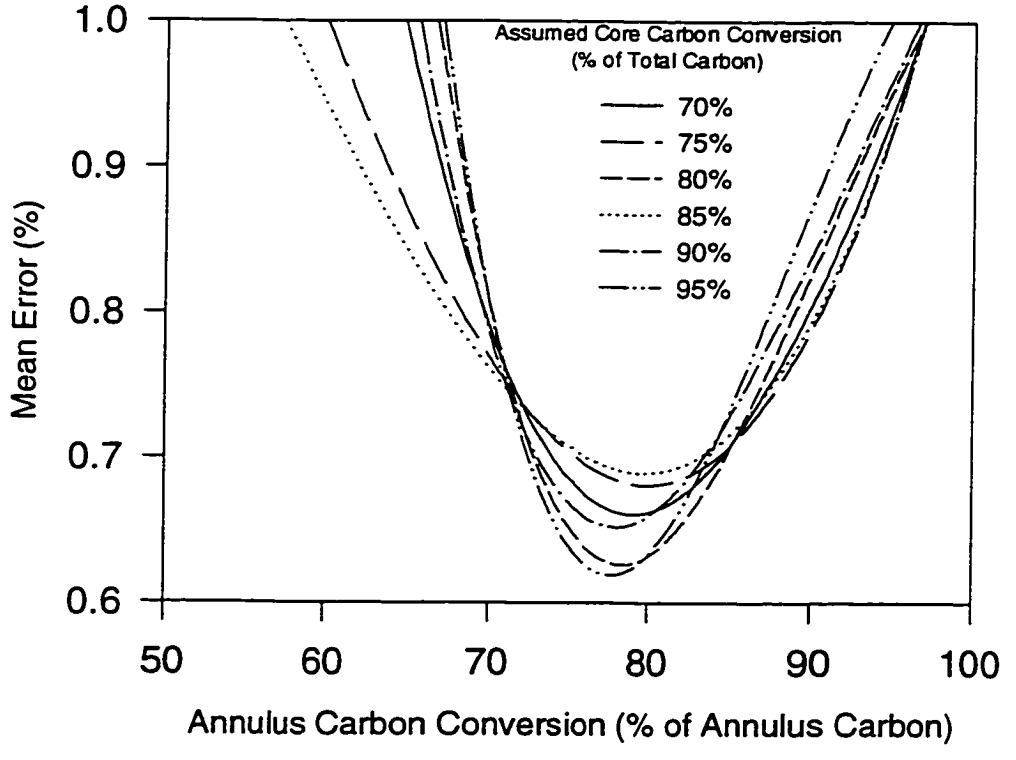

(b) Two-Compartment Model

Figure D-19 Mean error in product gas composition at various carbon conversion ratios and the bed height of 31.5 cm, fluidization velocity of 0.22 m/s and equivalence ratio of 0.25.

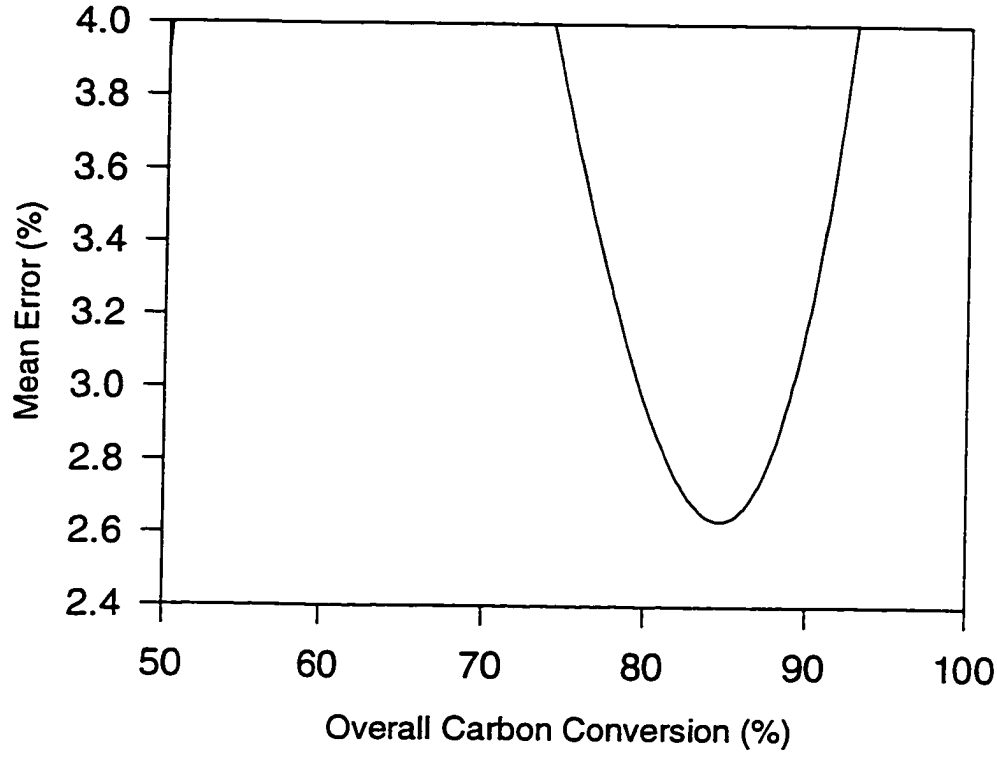

(a) One-Compartment Model

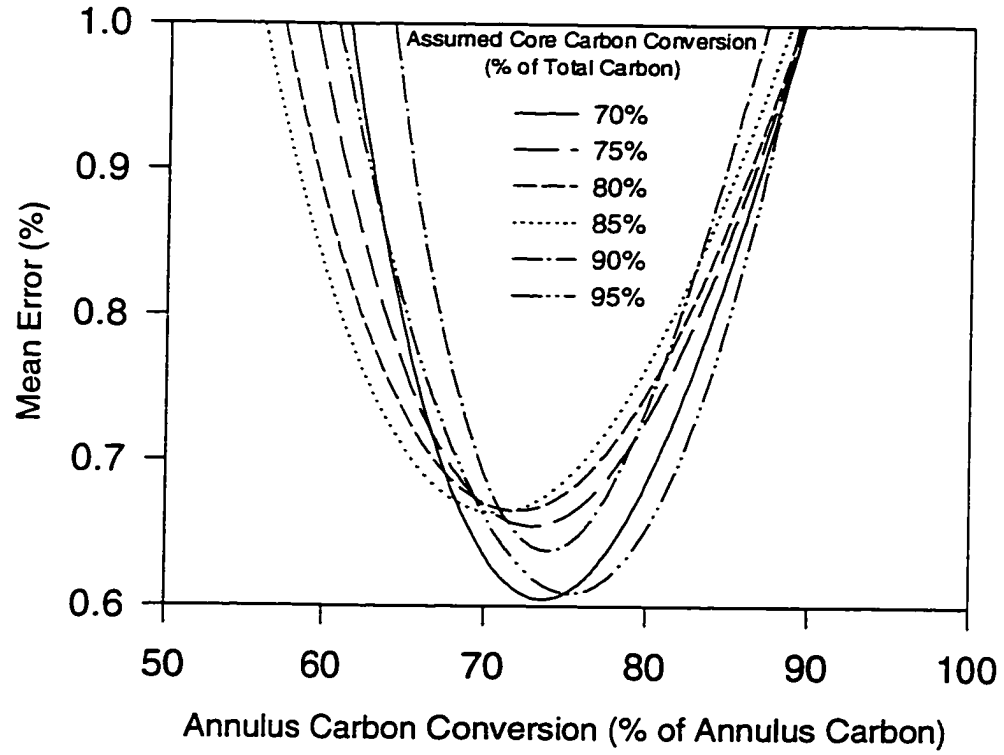

(b) Two-Compartment Model

Figure D-20 Mean error in product gas composition at various carbon conversion ratios and the bed height of 25.5 cm, fluidization velocity of 0.22 m/s and equivalence ratio of 0.30.

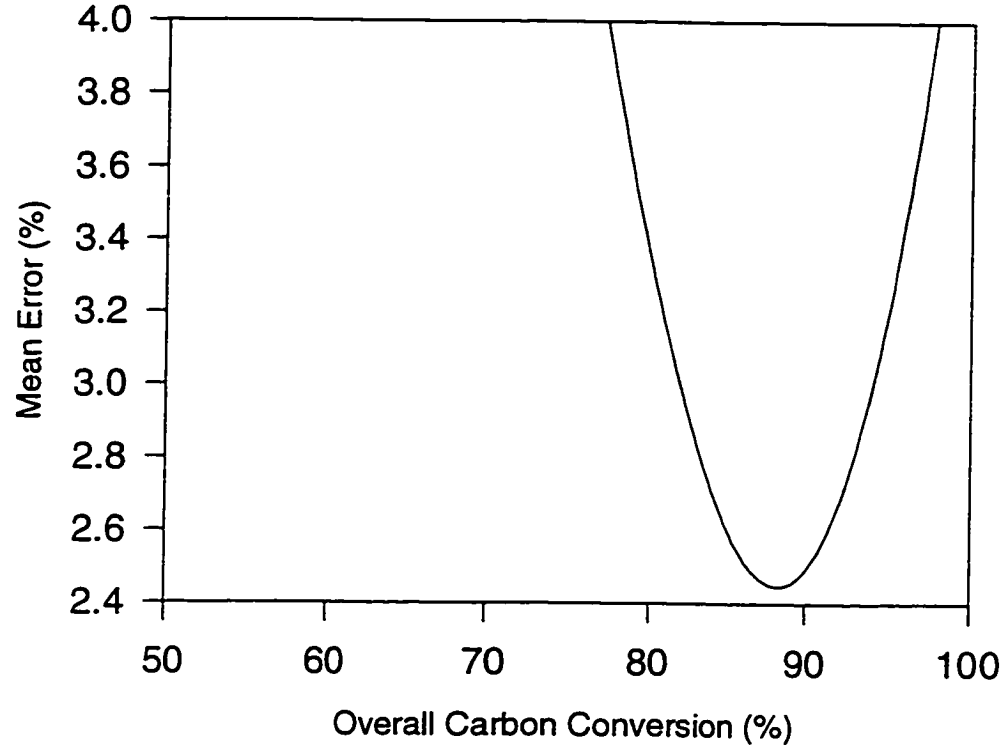

(a) One-Compartment Model

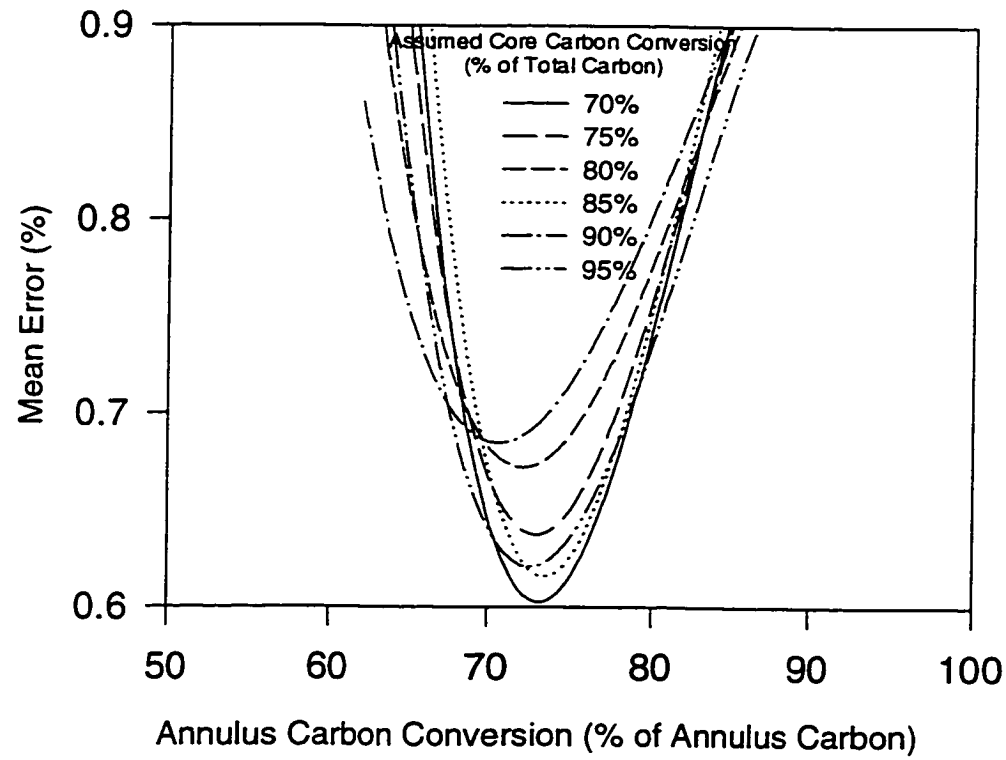

(b) Two-Compartment Model

Figure D-21 Mean error in product gas composition at various carbon conversion ratios and the bed height of 31.5 cm, fluidization velocity of 0.22 m/s and equivalence ratio of 0.35.

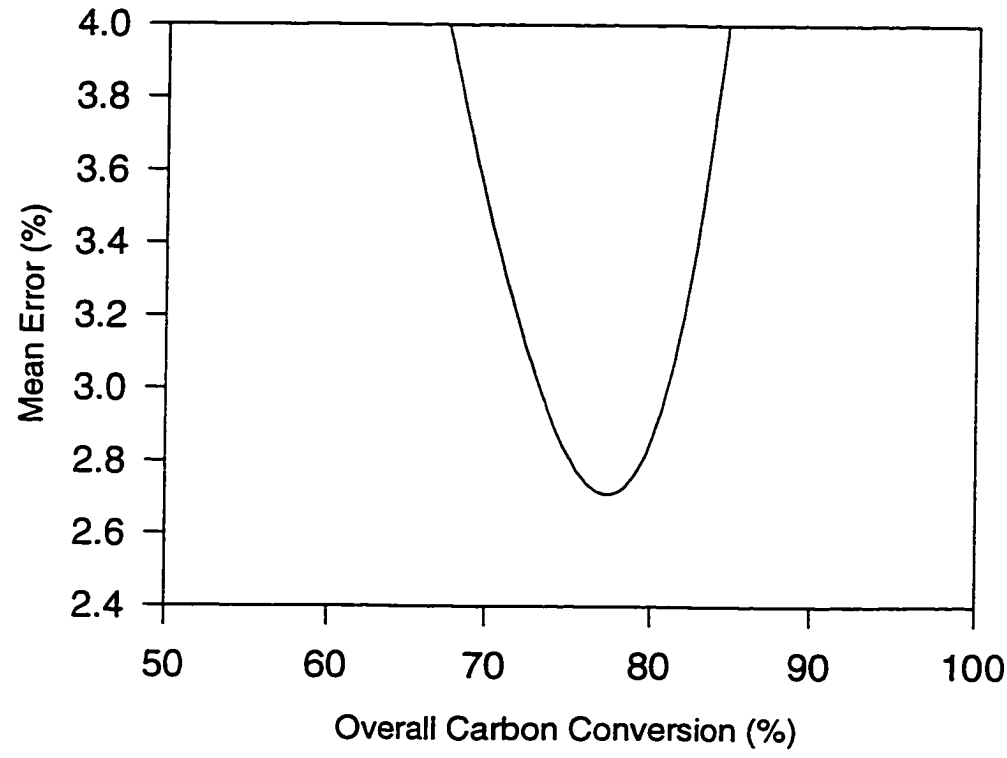

(a) One-Compartment Model

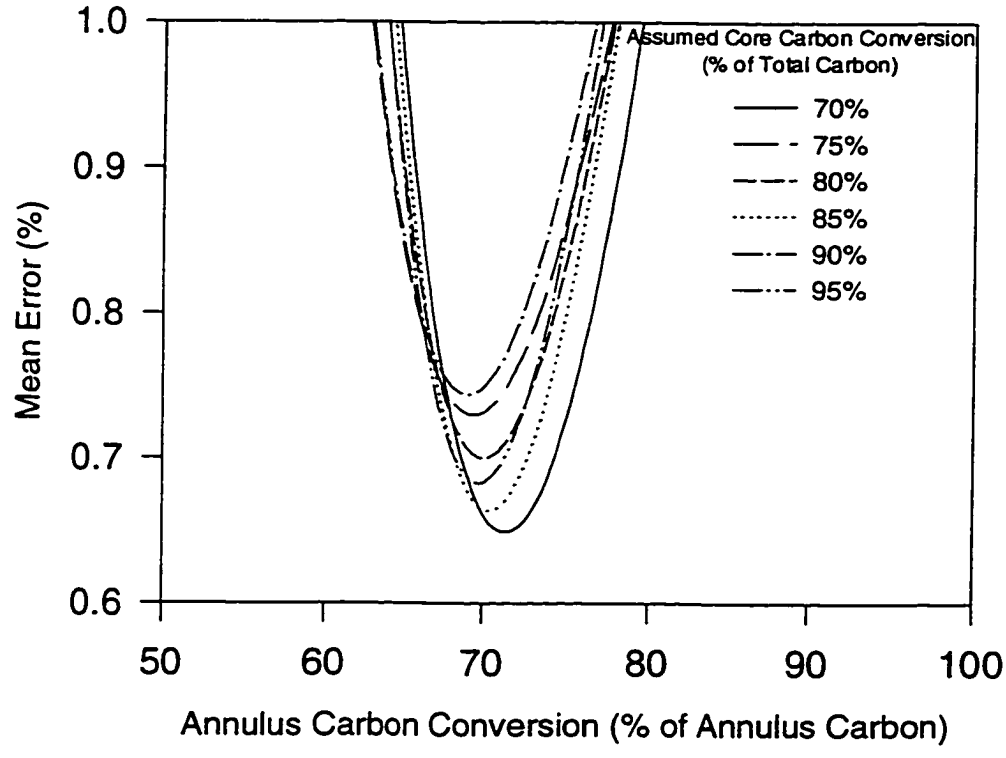

(b) Two-Compartment Model

D-22 Mean error in product gas composition at various carbon conversion ratios and the bed height of 31.5 cm, fluidization velocity of 0.28 m/s and equivalence ratio of 0.25.

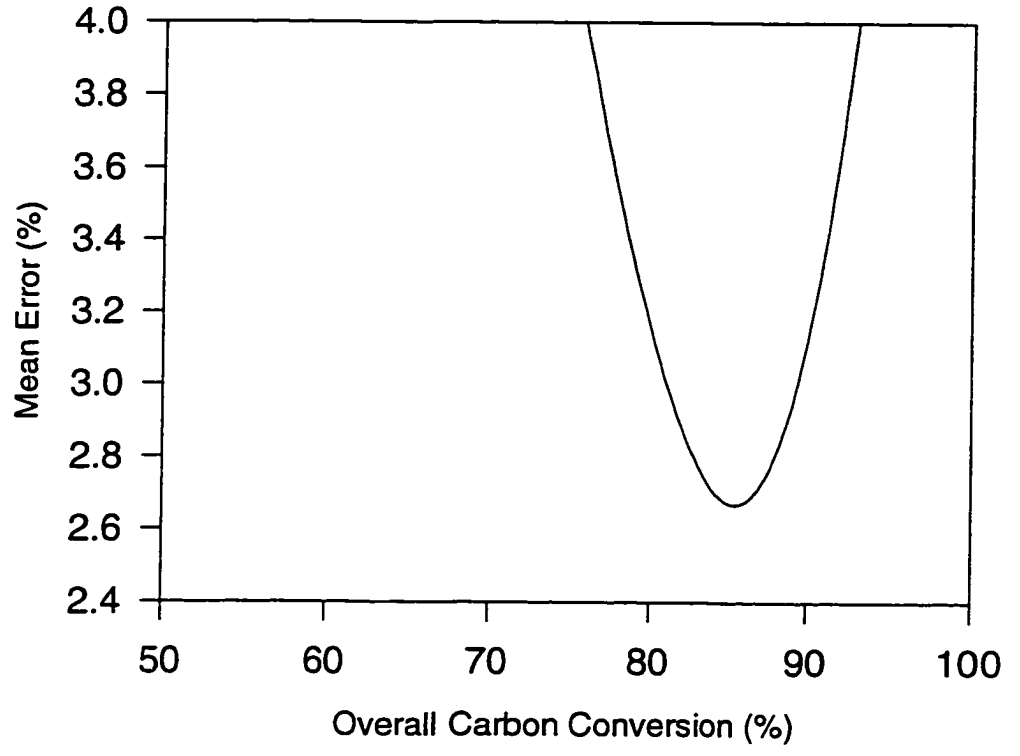

(a) One-Compartment Model

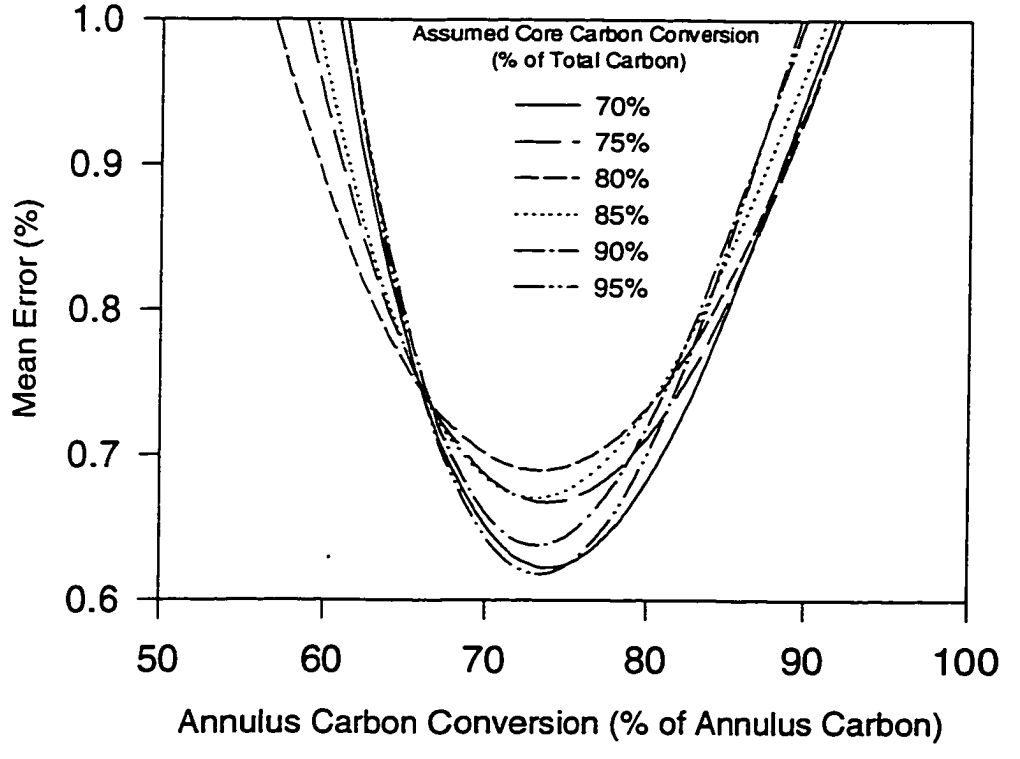

(b) Two-Compartment Model

Figure D-23 Mean error in product gas composition at various carbon conversion ratios and the bed height of 31.5 cm, fluidization velocity of 0.28 m/s and equivalence ratio of 0.30.

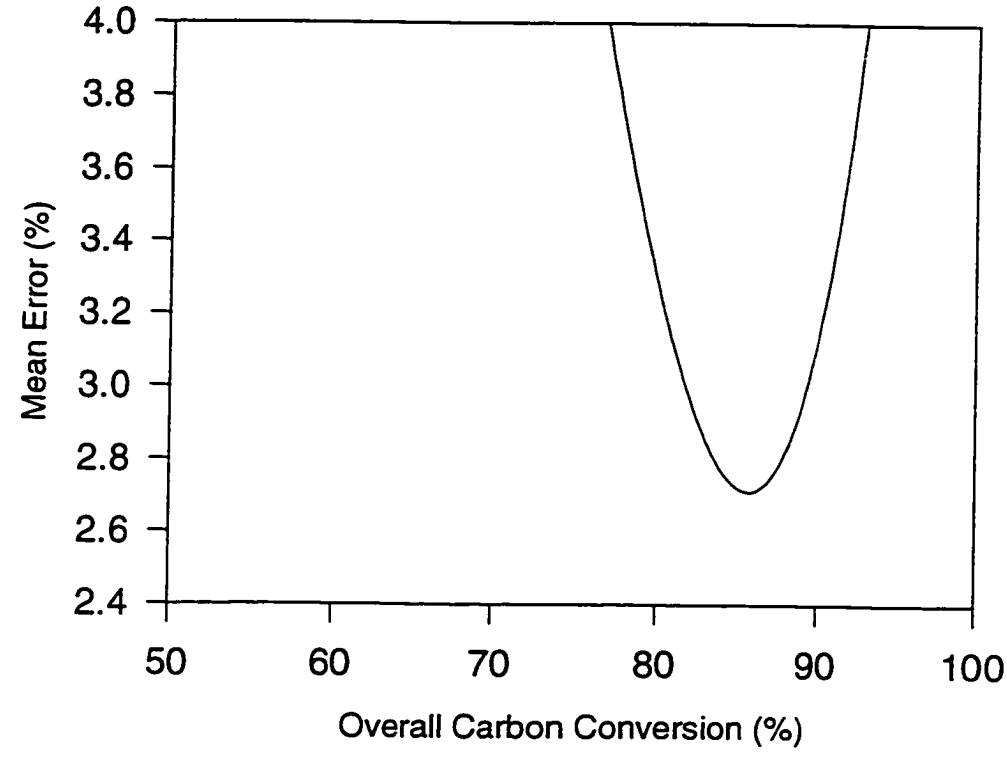

(a) One-Compartment Model

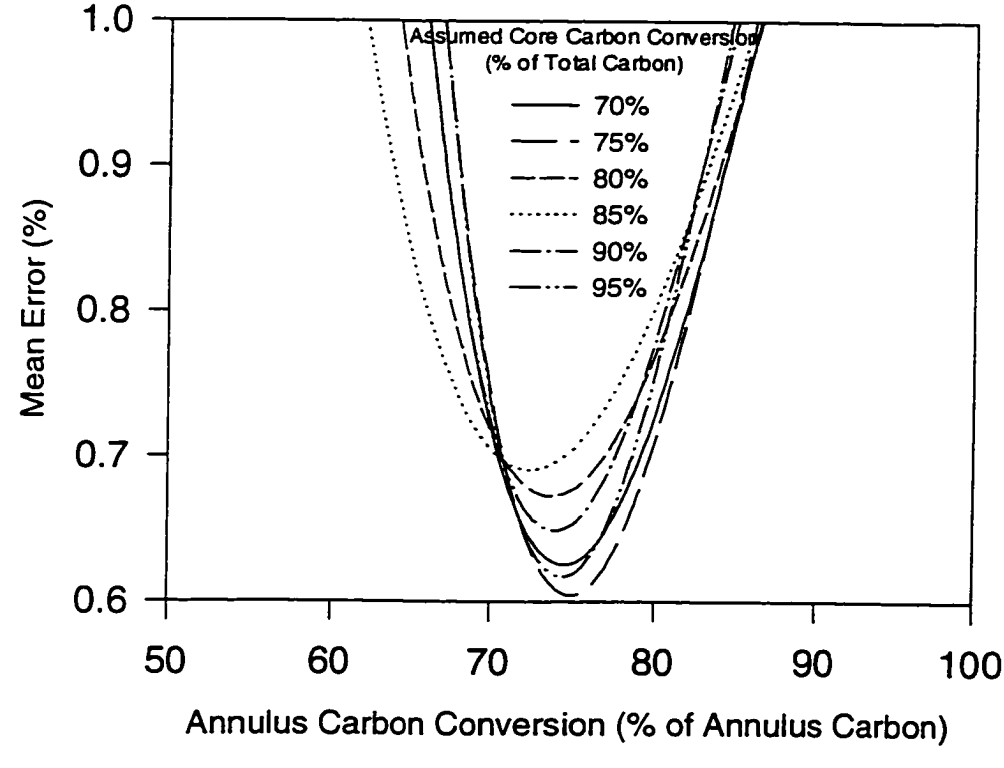

(b) Two-Compartment Model

Figure D-24 Mean error in product gas composition at various carbon conversion ratios and the bed height of 31.5 cm, fluidization velocity of 0.28 m/s and equivalence ratio of 0.35.

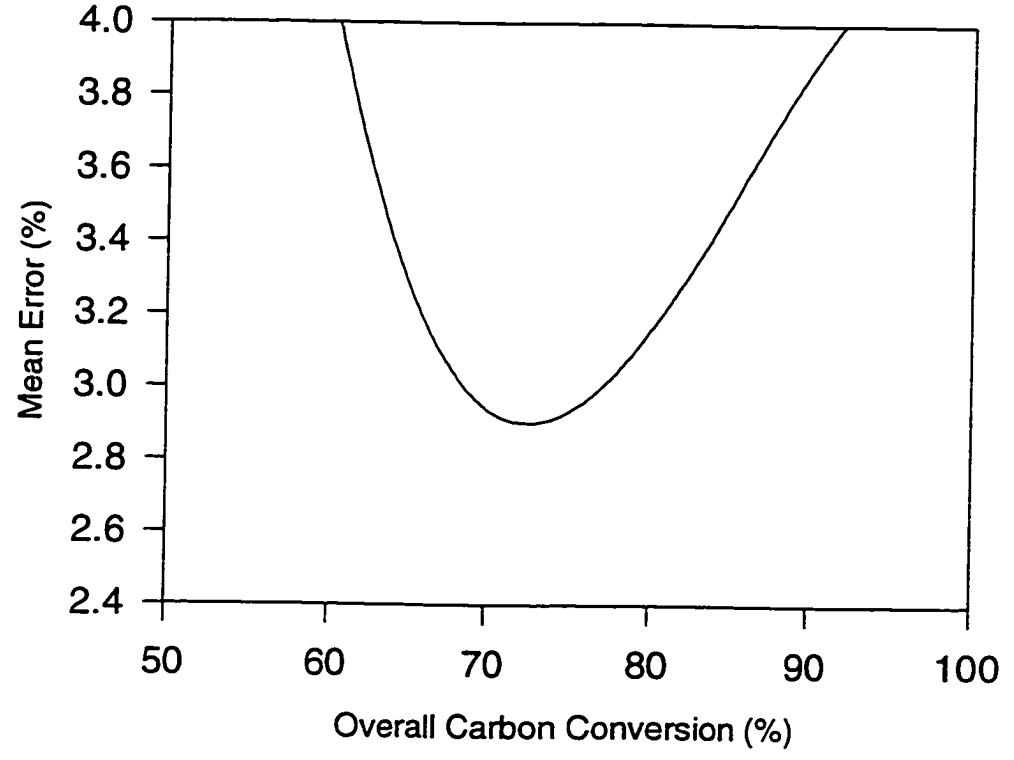

(a) One-Compartment Model

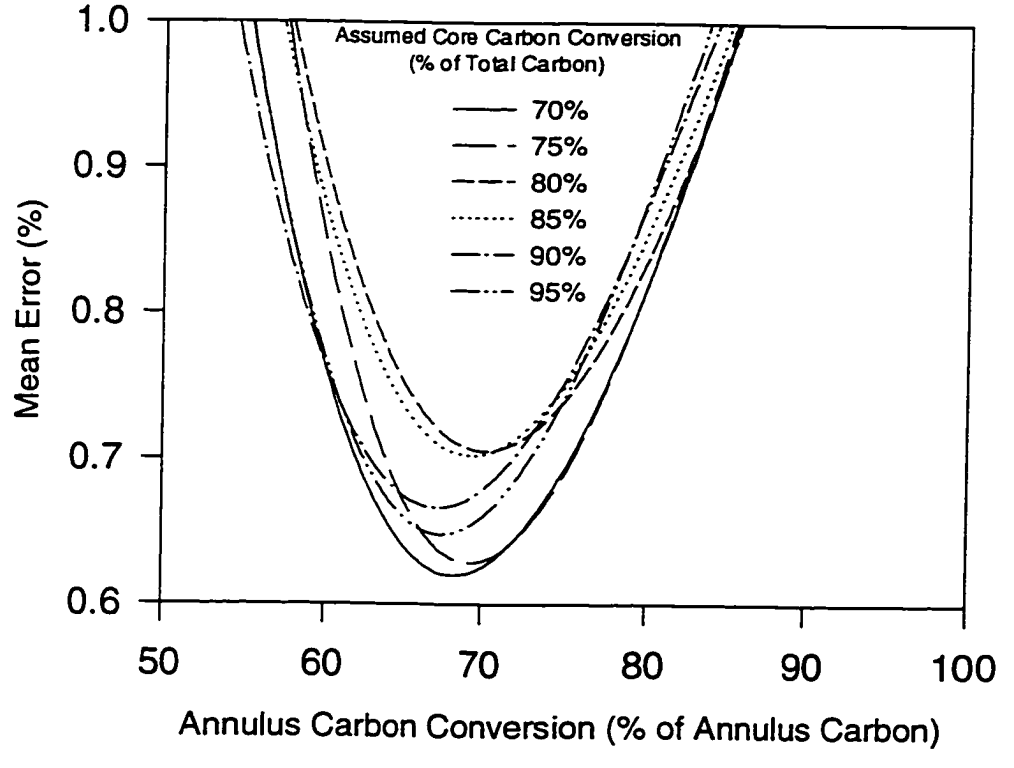

(b) Two-Compartment Model

Figure D-25 Mean error in product gas composition at various carbon conversion ratios and the bed height of 31.5 cm, fluidization velocity of 0.33 m/s and equivalence ratio of 0.25.

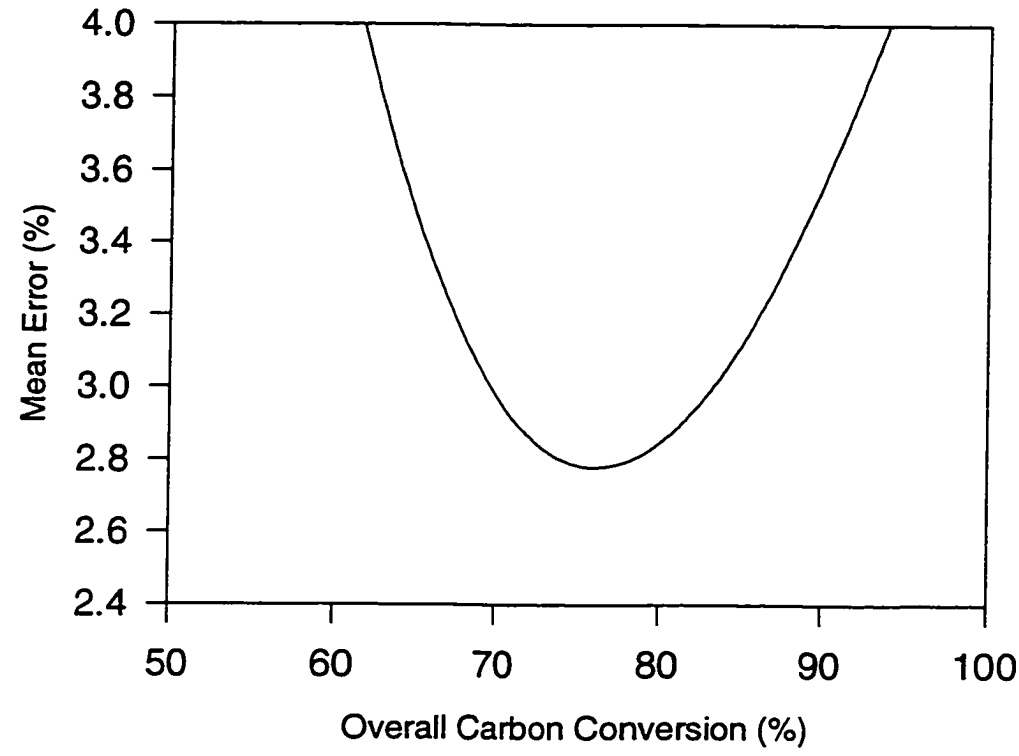

(a) One-Compartment Model

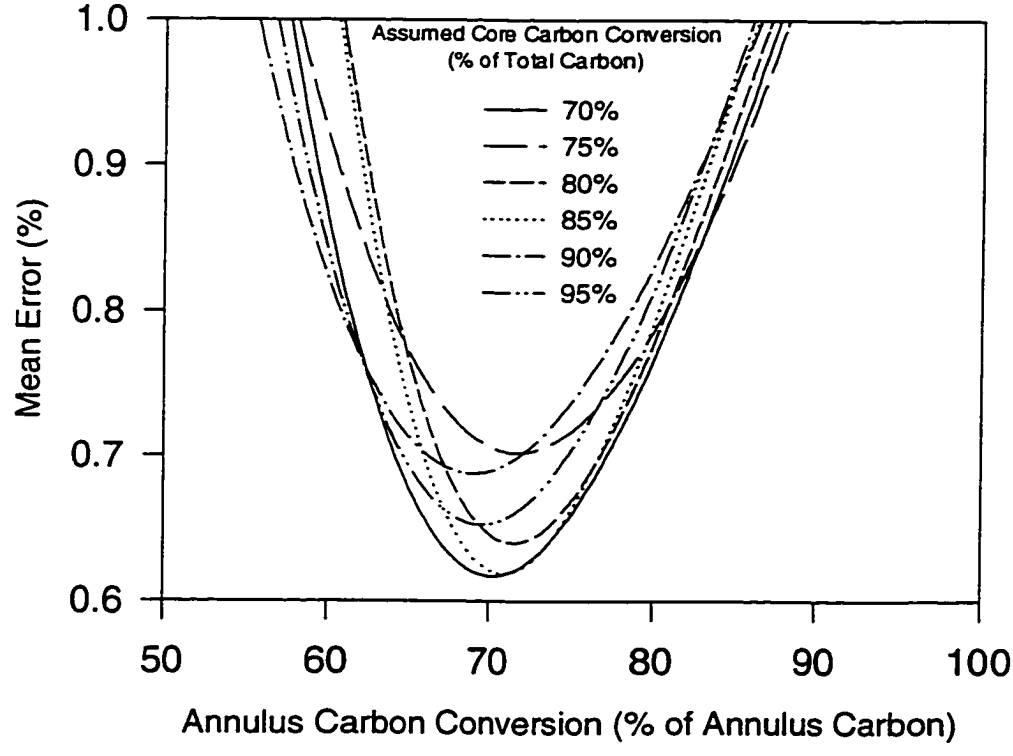

(b) Two-Compartment Model

Figure D-26 Mean error in product gas composition at various carbon conversion ratios and the bed height of 31.5 cm, fluidization velocity of 0.33 m/s and equivalence ratio of 0.30.

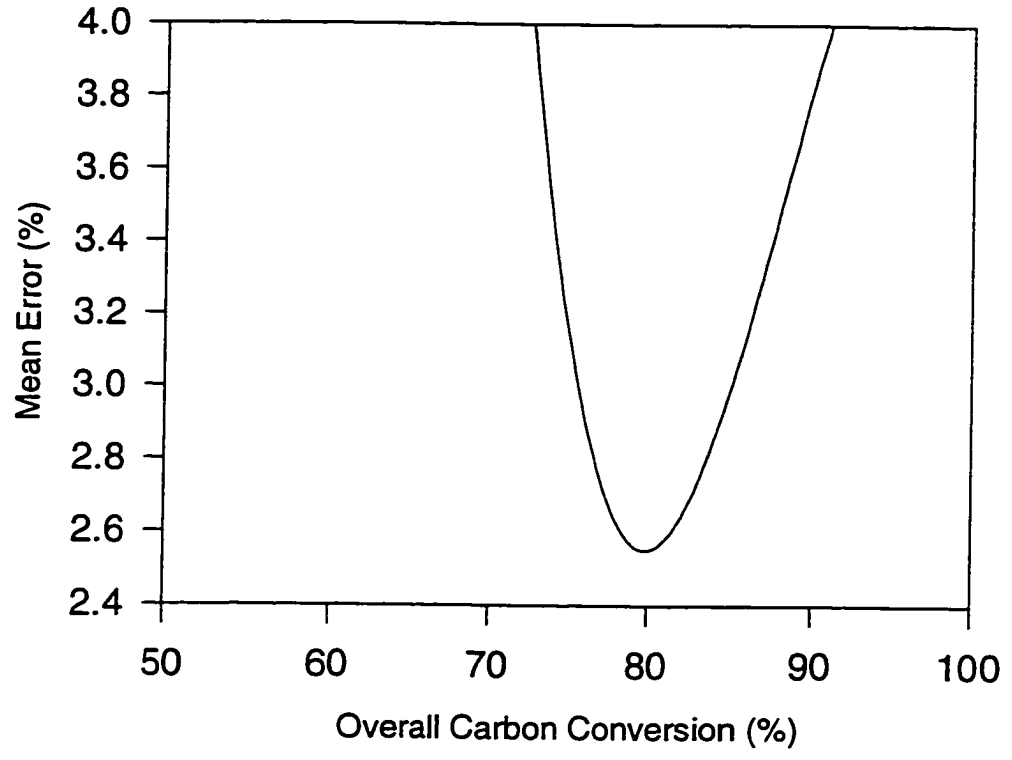

(a) One-Compartment Model

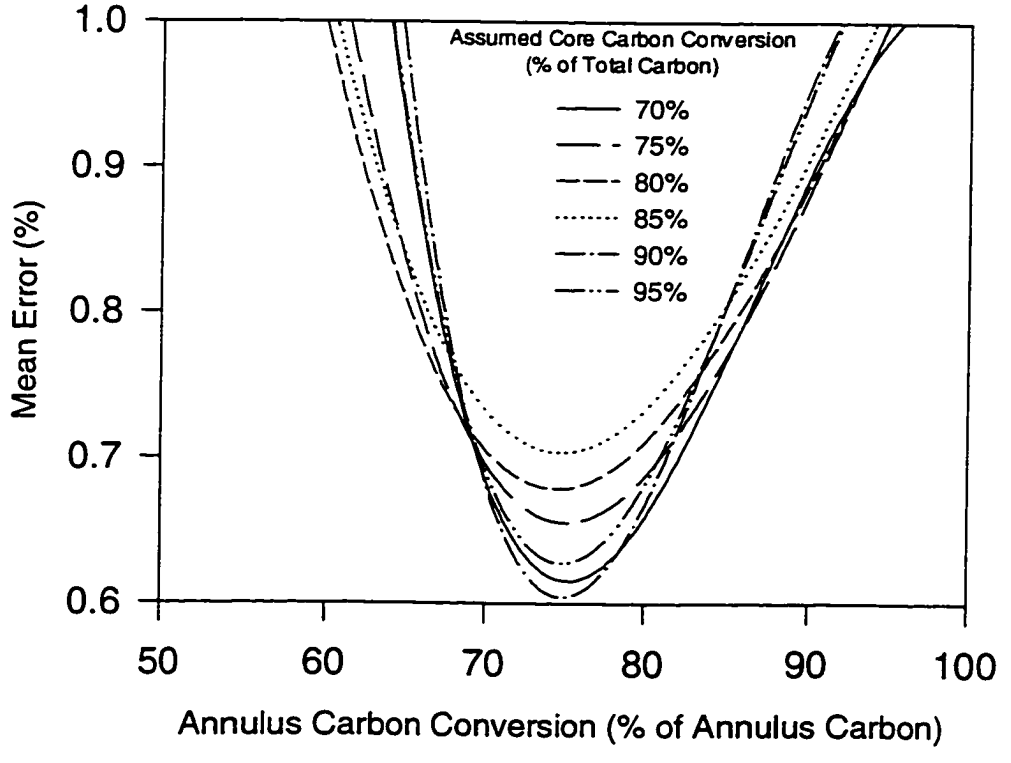

(b) Two-Compartment Model

Figure D-27 Mean error in product gas composition at various carbon conversion ratios and the bed height of 31.5 cm, fluidization velocity of 0.33 m/s and equivalence ratio of 0.35.

IMAGE EVALUATION
TEST TARGET (QA-3)

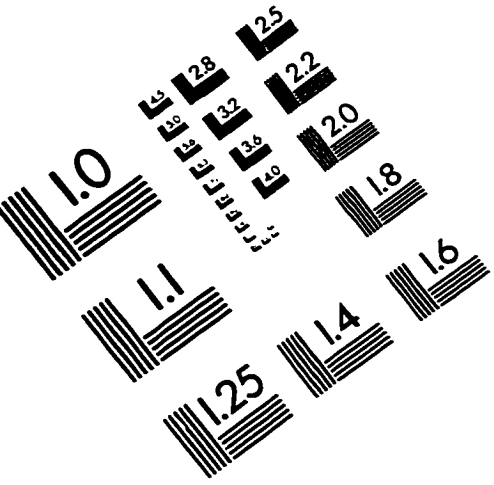

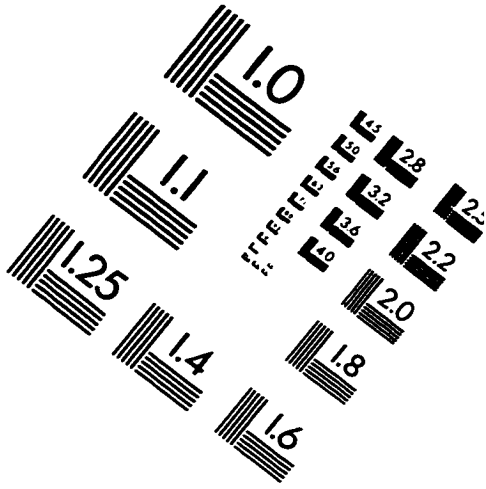

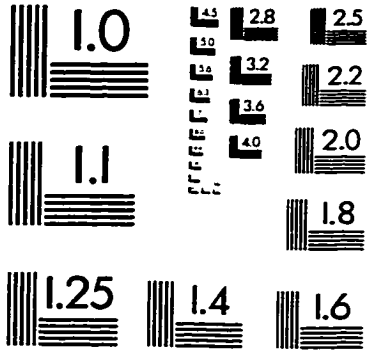

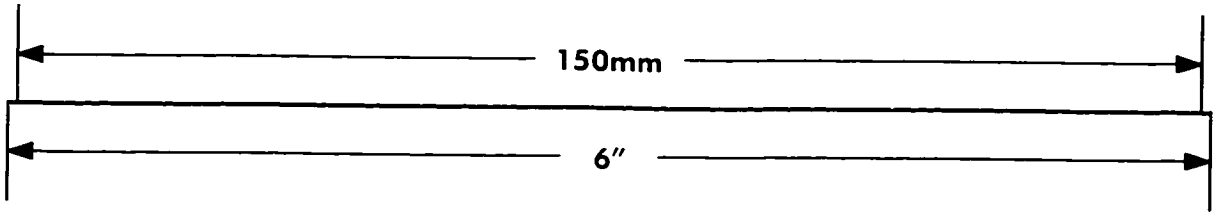

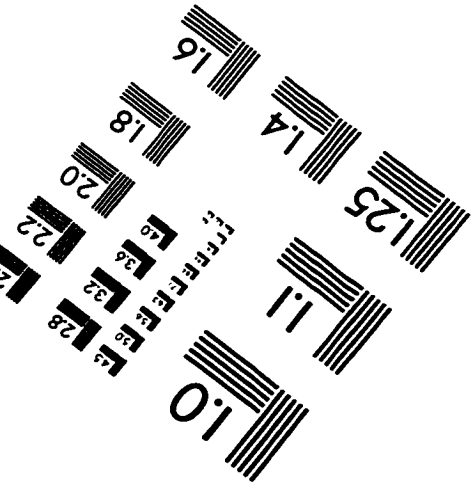

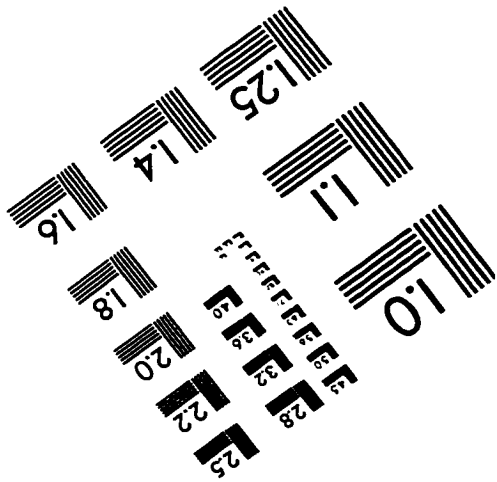

APPLIED IMAGE . Inc
1653 East Main Street
Rochester, NY 14609 USA
Phone: 716/482-0300
Fax: 716/288-5989